VOLUME II

annual progress report

AUTOMOTIVE LIGHTWEIGHTING MATERIALS

FREEDOMCAR AND VEHICLE TECHNOLOGIES PROGRAM

Less dependence on foreign oil today, and transition to a petroleum-free, emissions-free vehicle tomorrow.

U.S. Department of Energy
Energy Efficiency and Renewable Energy
Bringing you a prosperous future where energy is clean, abundant, reliable, and affordable

FreedomCAR & Fuel Partnership

21st CENTURY TRUCK PARTNERSHIP

U.S. Department of Energy
Office of Vehicle Technologies
1000 Independence Avenue S.W.
Washington, DC 20585-0121

FY 2006

Progress Report for Automotive Lightweighting Materials Volume II

Energy Efficiency and Renewable Energy
Office of Vehicle Technologies

Edward Wall
Program Manager, Office of Vehicle Technologies

Rogelio Sullivan
Advanced Materials Technologies Team Leader

Joseph Carpenter
Technology Area Development Manager

October 2007

CONTENTS

Volume I

CONTENTS (CONT.)

Volume II

CONTENTS (CONT.)

Volume II (Cont.)

3. LOW-COST CARBON-FIBER

A. Low-Cost Carbon Fiber from Renewable Resources

Project Contact: F. S. Baker, N. C. Gallego, A. K. Naskar
Oak Ridge National Laboratory (ORNL)
Post Office Box 2008
Oak Ridge, TN 37831-6087
(865) 241-1127, fax: (865) 576-8424; e-mail: bakerfs@ornl.gov

Technology Area Development Manager: Joseph A. Carpenter
(202) 586-1022; fax: (202) 586-6109; e-mail: joseph.carpenter@ee.doe.gov

Expert Technical Monitor: Philip S. Sklad
(865) 574-5069; fax: (865) 576-4963; e-mail: skladps@ornl.gov

---

Contractor: Oak Ridge National Laboratory
Contract No.: DE-AC05-00OR22725

Objective

- Carbon-fiber-resin composites could greatly decrease the weight of passenger vehicles resulting in substantial increases in fuel efficiency. However, carbon fiber is currently too expensive for large-scale use in production vehicles. This project will demonstrate methods for the use of new precursor materials, largely based on renewable resources, which decrease cost and increase availability of carbon fiber that meets the performance and price requirements of the automotive market. The project goal is to identify at least one precursor formulation, comprising both renewable and recycled materials, which could be used to produce industrial-grade carbon fiber at a cost in the range of $3-5 per pound. In addition to precursor, cost savings will also be achieved through improved processing methods and more efficient energy utilization.

Approach

- Provide the data needed to scale-up process steps to industrial levels and to consistently achieve desired fiber properties on an industrial scale.
- Develop the technical knowledge base required to support production of lignin-based carbon-fiber precursor feedstock on an industrial scale, comprising:
  - Lignin isolation and purification to obtain the appropriate lignin properties and degree of purity.
  - Spinning technology, including die structure, plasticizers, nucleating agents and spinning conditions.
  - Oiling and sizing technology.
  - Selection of appropriate copolymer(s), including polyesters and polyolefins.
  - Plasma treatment and sizing technology to make the fiber compatible with selected resin systems.
  - Properties and economics of lignin isolation/purification, carbon-fiber processing and composites.
- Scale and transfer the technology for the production of carbon-fiber precursors from lignin blend feedstock:
  - Evaluate melt-extrusion properties of lignin-based feedstock at increasing scale using near-industrial equipment that can be readily obtained by fiber manufacturers.
  - Evaluate production of carbon fiber using research and pilot-scale production lines.

  - Evaluate mechanical and composite compatibility properties of graphitized lignin-based fibers.
  - Collaborate with partners to evaluate, define, and develop process metrics, economics, and standards.
- Transfer technology and intellectual property for the production of lignin-based carbon fibers to industry.

Accomplishments

- Proof-of-concept demonstration of the melt extrusion of 28-filament tows of lignin-based fibers was made. This validated selected compositions, processing methods, and testing technologies. It also provided a basis for developing a better understanding of the process improvements required for large-scale manufacture of lignin-based, carbon-fiber precursor material.
- Significant amounts of 28-filament tow were successfully spun at the University of Tennessee, Knoxville (UTK), using a two-step process. No sticking problems were apparent and fiber diameter was reduced from ~ 45 microns to ~15 microns with an apparent improvement in mechanical properties.
- Preliminary data indicate that carbon-fiber yields of 50% are feasible, consistent with lignin carbon content.
- Preliminary evaluation of a plasma surface treatment (plus silanation) of lignin-based carbon fibers indicated a significant improvement in fiber-resin bonding compared to conventional carbon fibers.
- Small epoxy-resin composites made using carbon fibers produced from 28-filament lignin-based fiber tow exhibited target composite mechanical properties.
- Identified sources of volatiles within lignin and developed purification methods which selectively remove residual carbohydrates, one source of volatiles, in a single process step.
- Developed potential process technologies for the production of low-salt-content (low-ash) lignin.
- Developed preliminary specification for lignin precursor and demonstrated bench-scale methods to produce lignin meeting the specification.

Future Direction

- Processes for production of industrial-quality carbon fibers from lignin feedstocks will be developed. Work will include:
  - Establishment of lignin isolation conditions that achieve the target lignin specifications with respect to contaminant content (salts, carbohydrates, and particulates) and an appropriate molecular weight.
  - Identification of pretreatment and spinning process conditions which remove volatiles both prior to and, if necessary, during precursor-fiber production.
  - Selection of plasticizers, nucleating agents, and copolymers for melt spinning of lignin-based precursor fibers.
  - Design of spinning dies to provide the best internal structure of the fiber.
  - Development of techniques for spooling and oiling lignin-based precursor fibers at each step.
  - Identification of methods for surface treatment of lignin-based carbon fibers to improve compatibility with relevant resin systems (particularly critical for chopped-fiber composites).
- Collaborate with industrial, government, and academic partners to:
  - Address raw-fiber production issues (lignin, preconsumer recycled polymers, plasticizers, spinning and winding technologies, process scale-up).
  - Demonstrate carbon-fiber production from lignin-based multifilament tow using a pilot-scale industrial process line.
- Transfer the low-cost carbon-fiber production technology to industry.

Introduction

The use of carbon-fiber/resin composites would greatly reduce the weight of passenger vehicles, resulting in substantial increases in fuel efficiency. However, carbon fiber is presently too expensive and too limited in production capacity to support large-scale use in production vehicles. To address these impediments to the commercial use of carbon fiber in the automotive industry, this project is directed to the development of methods for the production of carbon-fiber feedstock from high-volume, low-cost materials based on renewable resources and recycled materials. The goal is the development of technologies which will reduce precursor and processing costs, and which could be implemented to produce low-cost carbon fiber on a scale sufficient to support its large-scale use in passenger vehicles. Use of renewable and recycled materials also decreases sensitivity of carbon-fiber cost to changes in petroleum production and energy costs.

Proof-of-concept production of single fibers from a variety of natural, renewable, and recycled materials available in high volume was demonstrated. Single fibers, melt-spun from blends of Kraft hardwood lignin (an inexpensive, high-volume, wood-pulping byproduct) and small amounts of routinely recycled polyolefins and polyesters, could be processed using conventional stabilization (oxidizing atmosphere), carbonization, and graphitization (inert atmosphere) furnace technologies to yield carbon fibers. Carbon-fiber mechanical properties improved when the fibers were stretched during thermal treatment. Graphite content, as measured by x-ray diffraction, increased with increasing temperature of treatment. Carbon-fiber yield from the lignin-based feedstocks was ~ 50%. Physically, the fibers were dense, smooth-surfaced, and uniformly round.

Larger quantities of a lignin-polyester (recycled) feedstock were melt-spun as a multifilament tow (4-28 fibers) using a 27-mm-diameter twin-screw Leistritz extruder at UTK to meet a September 2003 composite preparation and testing milestone. This Leistritz machine is the smallest member of a line of commercial melt extruders, and can be used to obtain data to design larger-scale melt-spinning equipment. Meeting the milestone showed that: 1) lignin-polyester blend can be melt-extruded as a small tow using near-commercial-scale melt-spinning equipment; 2) resin-fiber composites made using the graphitized lignin-polyester based carbon-fibers exhibited normal fracture patterns; and 3) very smooth-surfaced, lignin-polyester-based carbon fibers can be plasma treated and silanated to provide good fiber/resin adhesion.

Analysis of the samples obtained indicated that bubbles and inclusions were the major flaws in the lignin-polyester-based carbon fibers. Flaws are known to decrease the strength of carbon fibers and are typically the initiation point for fiber breakage. Inclusions were typically natural particulates associated with wood and the pulping process; namely, sand, clay, and cellulose fibers. Bubbles were caused by water trapped in carbohydrates co-precipitated with lignin during conventional processing of lignin for commercial products. Methods were developed to mitigate these problems. Additionally, methods for controlling salt content in the fibers and for pre-filtering black liquor prior to lignin isolation were developed.

Project Deliverables

Goal: By the end of this multi-year program, production of carbon fibers from one or more economically-feasible and environmentally-friendly precursors will be demonstrated, and the transfer of production technologies and related intellectual property to industry initiated.

In fiscal year (FY) 2004, major milestones, including the initial tests of the effect of lignin molecular weight on fiber properties were completed on time.

FY 2005 milestones included development of a lignin feedstock specification that will facilitate industrial production of carbon-fibers meeting program goals (5/2005) and establishment of basic rheology for extruding and winding lignin fiber bundles with improved handling characteristics (9/2005).

FY 2006 milestones included the acquisition, installation, and commissioning of melt-spinning equipment for production of small lignin-fiber tows and initiation of work to identify the critical factors

that control the rheology of lignin and its melt spinnability.

Also in FY 2006, the concept of a greenfield plant was proposed (in a white paper) in which wood, or other appropriate biomass, would be pulped under conditions specifically designed to optimize the properties of lignin isolated from the plant, with minimal purification, for production of low-cost carbon fiber meeting the economic and engineering targets for automotive use. Lignin would be the primary plant by-product; cellulose would be sold for conversion into other value-added products, most notably ethanol fuel for vehicles.

FY 2007 milestones comprise development of a viable process for purification of lignin on a commercial scale, identification of conditions for melt spinning and rewinding of small fiber tows of lignin produced from both hardwood and softwood (with appropriate plasticizers and copolymers), and the production of lignin-based carbon fiber with near-target mechanical properties for composite testing.

Planned Approach

Production of industrial-grade carbon fibers from a radically new type of feedstock requires the parallel development of diverse technologies, including: processes for feedstock isolation and purification and blending with plasticizers and copolymers; identification of conditions for satisfactory melt spinning and handling of the precursor fiber; thermal processing of the precursor fiber into carbon fiber; surface treatment/sizing of the carbon fiber; and demonstration of carbon-fiber quality and suitability for use in composite materials.

First priority was placed on developing cost-effective, environmentally-friendly, precursor-fiber preparation and thermal-processing conditions. Carbonization of lignins, which typically do not contain aromatic nitrogen, does not result in the cyanide emissions typical in the processing of acrylic fibers. Appropriate lignins can also be melt-spun or dry-spun, which eliminates the petrochemical solvents used in producing raw acrylic fiber.

Use of conventional thermal-processing techniques, such as hot-stretching and controlled-atmosphere treatment, will be evaluated to improve the properties and yield of carbon-fiber from the lignin feedstock, as well as advanced processing technologies for reduced-cost carbon-fiber production.

Industrial partners have worked with project staff on the selection of polymers to blend with lignin, strategies for production of cleaner (purer) lignin, and spinning of precursor fiber. In the later stages of the project, quantities of lignin-based carbon-fiber tow sufficient for composite fabrication will be produced using a pilot-scale fiber production line.

Transfer of project technology, including intellectual property, is planned.

Lignin Feedstock Quality

Lignins are inexpensive, high-volume by-products of the pulp and paper industry. More recently, they have also been isolated on relatively small scales from biomass-conversion operations, notably ethanol production. Several different processes produce lignin streams from which carbon fibers could be potentially manufactured, including: 1) alkaline pulping of wood (Kraft and soda); 2) ethanol production from wood and other biomass; and 3) organosolv pulping (currently not practiced commercially). In the Kraft and soda processes, liquid streams (“black liquor”) containing lignin are concentrated and burned to both provide process energy and to facilitate recovery/recycling of the pulping chemicals. The ORNL research work has been focused on alkaline pulping liquors because these represent about 80% of the total domestic pulping industry.

Historically, only two Kraft mills worldwide have isolated dry lignin for commercial sale as chemicals, but all Kraft pulp mills could, in principle, isolate lignin as a potential precursor material for carbon-fiber production. This is accomplished by acidification of black liquor to form a loose gel which is recovered as a precipitate, washed, and dried. This material, and chemical modifications thereof, are marketed for use in many high-volume applications, including dyestuff dispersants, asphalt emulsifiers, concrete additives, lead-acid battery

plate extenders, soil micronutrients, and metallurgical mold releases. These applications are, however, relatively insensitive to the presence of contaminants such as particulates, cellulose fibers, water, volatile, and inorganic pulping chemicals entrained during lignin precipitation.

Production of a cost-effective, industrially-feasible, lignin-based, carbon-fiber feedstock will require the development of processes to remove salts, particulates, and volatiles from the crude lignin isolated from conventional pulping operations. The lab-scale methods developed at ORNL, which typically involve purification of the liquid streams from which lignin is recovered, are discussed below. Using these methods, it proved possible to produce very high-quality lignins from alkaline pulping liquors.

It is also possible to extract low-salt-content, low-volatile-content lignins using novel pulping technologies that are emerging on a commercial scale. Novel biomass-derived lignins produced by project partners were evaluated for potential use as carbon-fiber precursor materials.

Evaluation of Purified Lignins from Conventional Alkaline Pulping

Alkaline pulping technologies, which include Kraft pulping ($NaOH + Na_2S$) and soda pulping (NaOH), dominate domestic production of pulp for use in paper products. In alkaline pulping, wood chips are contacted with the alkaline solution and cooked at high temperature and pressure. At the end of the cooking cycle, a lignin-rich stream, "black liquor," is separated from the wood pulp. Black liquor is concentrated by evaporation and burned to recover the pulping chemicals (>99% recovery) and to provide energy for the pulping and paper production operations (some mills include power co-generation, providing a net energy gain).

Because the process uses wood chips, alkaline pulping is a year-round industry, with the potential of providing a large volume of lignin for use as carbon-fiber feedstock. To put this into perspective, approximately 10% of the lignin passing through alkaline pulping operations, could, if used for carbon-fiber production, supply enough carbon fiber to replace approximately half of the ferrous metals used in passenger transport vehicles.

It is important to keep in mind, however, that pulp and paper mills operate under demanding economic and environmental standards. For example, mills must meet Environmental Protection Agency Cluster Rule emission and effluent standards. To apply the technology developed in this project to the production of enough purified lignin to support widespread automotive use of carbon-fiber, the lignin isolation/purification process technology must be tailored to mill needs.

Commercial lignin products isolated from black liquor typically contain a variety of solid materials (sand, diatoms, cellulose fibers) and chemicals (salts, carbohydrates, wood extractives). In order for this lignin to be used as a feedstock for production of carbon fibers, which are typically <10 micron in diameter, solids >1 micron in diameter must be removed. This can be accomplished by micron-scale filtration of the black liquor prior to lignin isolation. Additionally, carbohydrates, which sorb water, can be precipitated and removed by filtration prior to precipitation of the lignin itself. Using commercial filter media, selectively precipitated and coagulated carbohydrates can be removed from alkaline pulping liquors in a single step.

Thermogravimetric analysis (TGA) curves for desalted, carbohydrate-stripped Kraft and low-sulfur soda hardwood lignins are shown in Figure 1, revealing that these lignins exhibited low volatiles content (<5% weight loss at 250°C). Furthermore, as shown by the solution nuclear magnetic resonance (nmr) spectroscopy data in Figure 2, the carbohydrate-stripped Kraft and soda hardwood lignins contained only very small amounts of residual carbohydrate material.

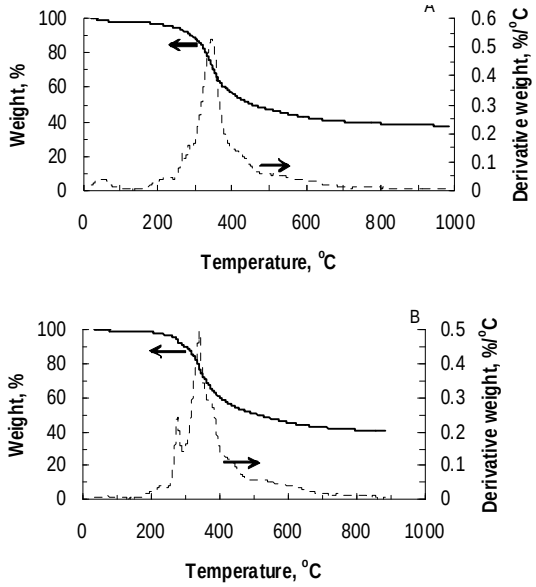

Figure 1. Thermogravimetric analyses of desalted, carbohydrate-stripped soda-anthraquinone (A) and Kraft (B) hardwood lignins.

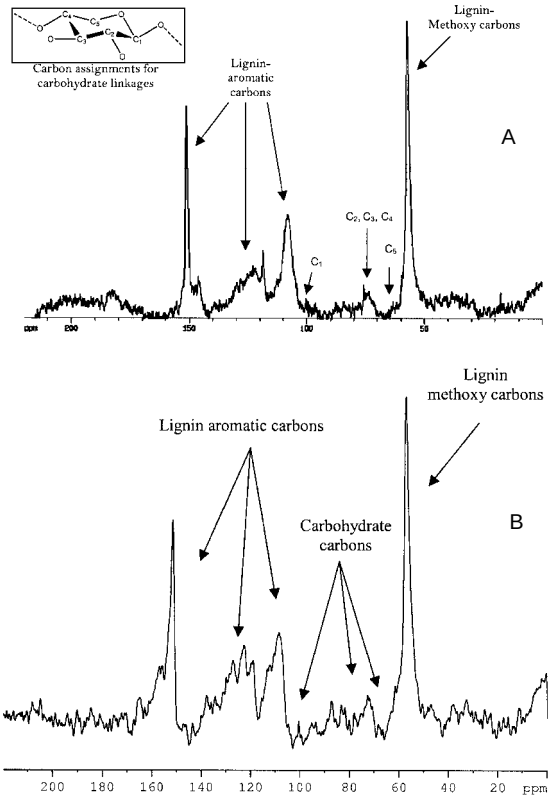

Figure 2. Nuclear magnetic resonance spectra of desalted, carbohydrate-stripped Kraft (A) and soda-anthraquinone (B) lignins.

Biomass Lignins from Ethanol Production

One of the emerging processes for production of ethanol from biomass involves: 1) pretreating the biomass by alkaline or organosolv pulping; 2) hydrolyzing the cellulose fibers to sugars; and 3) fermenting the sugars to ethanol. The mills are being deployed to meet Kyoto treaty requirements for production of fuels and chemicals from biomass. Operators of these mills are interested in developing markets for the significant quantities of lignin by-product which they currently produce. Although this process is not being tested in domestic bioethanol plants, increasingly high petroleum prices could make these biomass ethanol processes attractive in the US. Woody biomass wastes have good year-round availability. A fraction of the ethanol produced from the cellulose pulp is used in the pulping process, and the overall process energy is supplied by burning part of the lignin precipitated during ethanol recovery and recycle.

Granit, a project partner, started pulping-based ethanol production mills this year, and is already able to supply about 10,000 tons/year of lignin, i.e., enough precursor material to support the equivalent of 20% of the worldwide production capacity of carbon fiber. Similarly, Lignol Innovations is constructing an ethanol-organosolv pulping test facility in which conversion of wood residues, such as sawdust and insect-damaged trees, to alcohol is being evaluated. Deployment of this biomass technology is accelerating because the ethanol fuel produced from the process plays a key part in Kyoto treaty compliance strategies for many countries. In the US, it would provide an attractive opportunity for reuse of smaller or older, non-profitable pulp mills. Because the lignins in biomass feedstocks, such as grass or flax, are different in composition and chain length from those typical of wood-derived lignins, their basic properties have been evaluated in this project.

In Figure 3, TGA curves are shown for three lignins derived from biomass ethanol production: Sarkanda grass (“Ecobind 100SA140”); flax (“Ecobind100FA”); and a Lignol Innovations experimental lignin produced from softwood sawdust. From the TGA curves and data in Table I, it is apparent that the Lignol softwood lignin showed potential as carbon-fiber feedstock, at least on the

Table 1. Ash and volatiles in biomass lignins.

Lignin	Ash, %	Volatiles, %
Lignol Innovations	0.2	3
Flax	0.6	10
Sarkanda grass	3	8

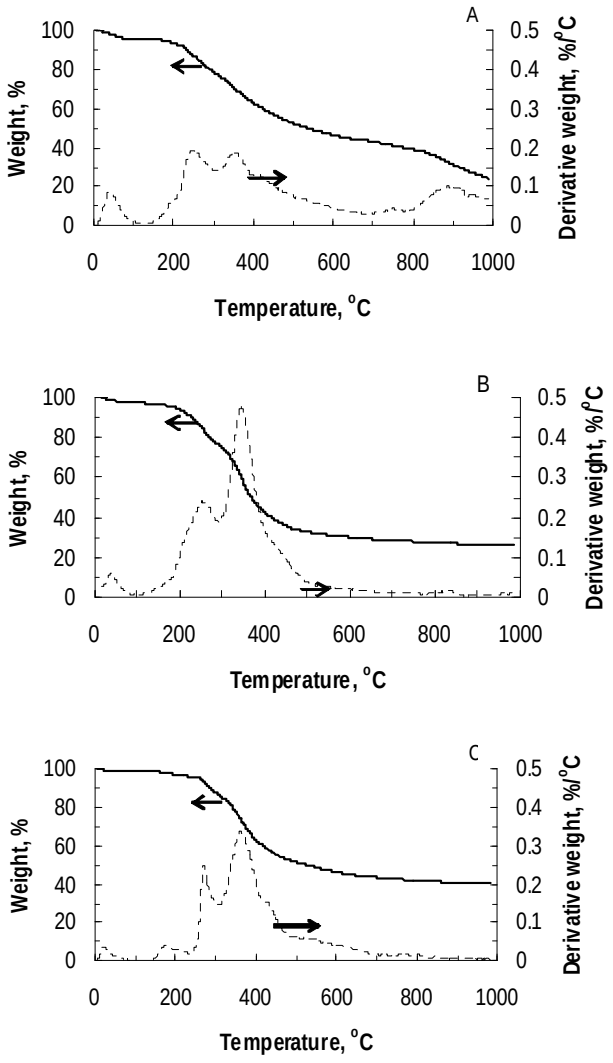

Figure 3. Thermogravimetric analyses for Sarkanda grass (A), flax (B), and Lignol Innovations (C) lignins (derived from biomass ethanol production).

basis of its low volatile content (3%) and low ash content (0.2%), which almost met the target specification (0.1%). The grass and flax lignins exhibited higher volatile contents of 8 and 10%, respectively, about twice the target specification of <5%. Both also exhibited lower residual carbon contents (< 30% at 1000°C) compared to commercial Kraft hardwood lignin (40%). In keeping with commercial alkaline-pulped softwood lignin products, the Lignol softwood lignin exhibited a carbon content of ~40%. Furthermore, as shown by the nmr spectroscopy data in Figure 4, the Lignol experimental softwood lignin contained very low levels of residual carbohydrate.

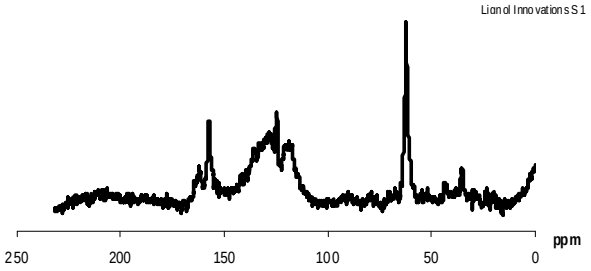

Figure 4. Nuclear magnetic resonance spectra of Lignol Innovations ethanol organosolv lignin.

A major difficulty associated with biomass lignins would be variability in lignin properties due to changes in either the type or condition of biomass feedstock to the pulp mill. Additionally, some biomass feedstocks, such as rice straw, contain significant concentrations of insoluble inorganic materials, such as silicates.

The ash content of the Sarkanda grass lignin was 3%, comparable to that of commercial Kraft hardwood lignin products. Almost all of this ash material could be removed as base-insoluble, filterable particulates. The flax lignin exhibited a lower ash content of 0.6% and, as already noted, the Lignol experimental softwood lignin exhibited a notably low ash content of 0.2%, which would facilitate its purification for use as a carbon-fiber feedstock. Microscopic examination revealed that the particulates in all three of the biomass-ethanol lignins predominantly comprised cellulosic residues from the pulped biomass.

Biomass-lignin production technology is, for the most part, being developed outside of the US as part of the effort to meet Kyoto treaty compliance goals. However, the low cost and potentially high volume of ethanol production from pulped wood wastes and annual biomass could drive the use of these two technologies into the US market. Additionally, both the Granit and Lignol processes could be adopted by Mexican or Canadian companies with near-border plants. Furthermore, the technologies could be

retrofitted into older or smaller pulp mills, which would significantly increase the availability of domestic commodity lignin.

Solvent Extraction Lignins

Although fractions of commercial lignins are soluble in some solvents, carbohydrates and salts are relatively insoluble in both alcohols and ketones. Therefore, MeadWestvaco (MWV), a project partner, felt that it should be possible to produce low-salt, low-carbohydrate lignins by solvent extraction of commercial dry lignin. Several such lignin samples were produced for evaluation.

The ash and volatiles contents of these materials are shown in Table 2. As shown by the TGA data in Figure 5, there was considerable variation in the thermogravimetric behavior of the different solvent-extracted lignins evaluated. Although most of the samples showed relatively high volatile contents at temperatures well below probable melt-spinning temperatures, the LPX-8377-OID sample exhibited low volatile content (4% at 250°C) and a high carbon content (40% residue at 1000°C). Nuclear magnetic resonance spectra of the samples also showed considerable variation in carbohydrate content, with the LPX-8377-OIA sample exhibiting particularly low carbohydrate content.

Ash and particulate levels in the solvent-extracted samples were also variable. As expected for this lignin source, most of the samples had ash levels around or below 1%. However, the LPX-8377-61-M sample exhibited a high ash content of 2.6%, but nevertheless still comparable to that of commercial lignin products.

With optimization, solvent-extracted lignins could potentially be useful carbon-fiber feedstocks or feedstock constituents.

Table 2. Solvent-extracted lignin ash and volatiles content.

Lignin	Ash, %	Volatiles, %
LPX-8377-OID	0.3	11.2
LPX-8377-61-M	2.6	14.5
LPX-8377-OIA	0.2	8.5
LPX-8393-48	0.6	9.2
LPX-8393-49	0.2	8.6
LPX-8393-50	0.1	2.5
LPX-8393-49	0.1	4.6

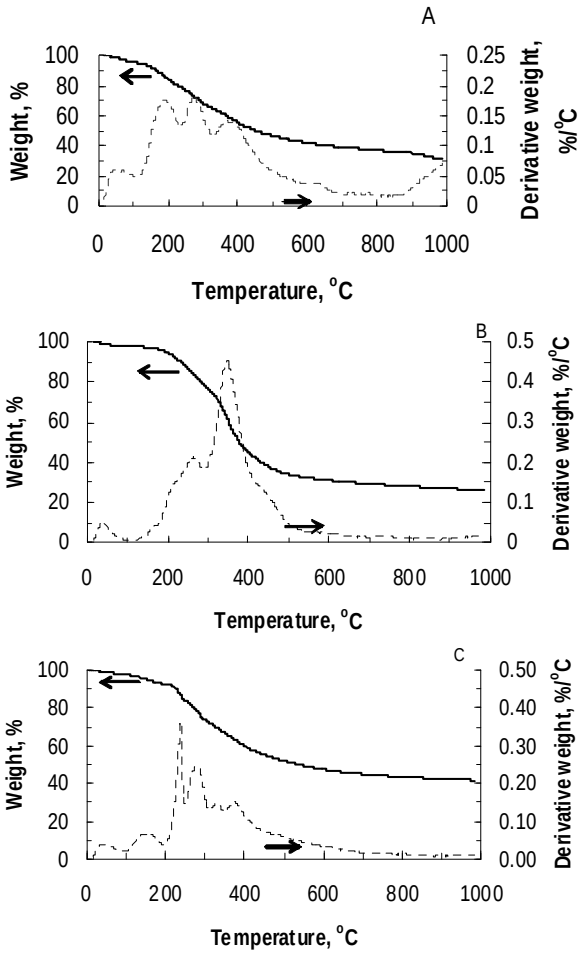

Figure 5. Thermogravimetric analyses of solvent-extraction lignins LPX-8377-61-M (A), LPX-8393-48 (B), and LPX-8377-OID (C).

Lignin Specification

Industrial partners requested that ORNL develop an initial specification for lignin to be used as a precursor material for the production of carbon fibers. The preliminary specifications established are based on data for commercial pitch-based carbon fiber and on the requirements for the twin-screw extrusion of textile fibers, such as polyesters, at 250°C. The lignin specifications comprise: < 1000 ppm ash, < 500 ppm non-melting particulates (e.g., cellulosic fibers), <5% volatiles by 250°C, and the removal of all particulates >1 micron in size.

The volatiles and non-melting particulate content requirements were developed to match the standard requirements for high-temperature textile melt spinning. The specifications for ash and particulates

contents were set on the basis of early pitch-fiber data, with the objective of minimizing inclusions and defects which weaken carbon fibers. These specifications have been met with lignins purified at ORNL using a bench-scale process.

With increasing experience and better understanding of the factors that influence lignin melt-spinning, the specifications will be extended to include relevant physical and chemical properties of lignins deemed suitable for carbon-fiber feedstocks.

Future Direction

Production of lignin-based multifilament tow (28 filaments) and successful use of this material in small resin-fiber composites was demonstrated in FY 2003. The project was re-proposed and extended to permit evaluation of methods for producing high-quality, lignin-based feedstocks for low-cost production of automotive carbon-fiber-reinforced resin and matrix composites.

Having established proof-of-concept, the project staff is systematically addressing the technical issues required to produce industrial-grade, lignin-based carbon fiber at prices and properties meeting automotive need. Because domestic lignins evaluated by this process are derived from alkaline (Kraft and soda) pulping, a major concern has been the need to develop an understanding of the levels and types of contaminants in the lignins which are detrimental to multifilament spinning. This work has recently been complemented with efforts to develop cost-effective, scaleable process technology for selective removal of carbohydrates, non-melting particulates, and salts from lignin.

Using project-developed technologies, it has been possible to consistently produce bench-scale quantities of purified lignin material which meets the preliminary specifications. The specifications will be upgraded and broadened as requirements for a satisfactory precursor material are better defined, e.g., to include physical and chemical properties relevant to blending and melt-spinning.

The techniques for precipitation and purification of lignin are expected to evolve and improve. The goal is an industrially-practicable method which permits one-step removal of better than 90% of the hemicellulose carbohydrate in black liquor prior to lignin precipitation. The carbohydrate material isolated by this means could potentially be reused in paper manufacture if only small amounts of flocculants are used and if the carbohydrate structure is preserved. Incorporating the recovered carbohydrate material (hemicellulose) into paper would enhance the mechanical properties of the paper, as well as offset lignin cost. Alternatively, the hemicellulose carbohydrate could be returned to the black liquor recovery boiler for energy and chemical recycle.

Efforts in fiscal year 2007 will be focused on the development and demonstration of a commercially-viable process for the production of lignin-based precursor material meeting the specifications established for carbon-fiber production. Working in partnership with Pacific Northwest National Laboratory (PNNL) and MWV, a combinatorial chemistry approach will be used to screen a large permutation of process conditions to establish the most cost-effective means of producing purified, melt-spinnable lignin on a commercial scale (See 3.B). Economic analyses will be an integral part of the effort to ensure that the lignin could be produced at a cost consistent with the target for finished carbon fiber. In addition to establishing commercially-viable lignin processing technology, the deliverable from the proposed PNNL/ORNL/ MWV program of work is several hundred pounds of on-spec lignin precursor material that can be used to produce carbon-fiber tow for composite testing (in mid FY 2008).

Studies on biomass-derived lignins will continue, but with reduced emphasis. Biomass utilization is an emerging business, and it is still too early to gauge its potential for commercial success. Nevertheless, if the Granit and Lignol processes for ethanol production from biomass materials are commercially successful, worldwide production of dried biomass lignin could increase by more than 50,000 tons per year, each year. On the downside, shipping costs could be too high for its cost-effective use as a carbon-fiber precursor material. In this context, the major question is whether and to what extent pulp-based biomass ethanol production will become commercially feasible in the US, as well as near-border areas of Mexico and Canada.

Die designs for spinning of lignin-based fibers will be further evaluated. Initial test data indicated that the high-shear dies similar to those used for spinning pitch-based feedstocks create a more uniform internal structure in the raw fiber. Spinning parameters, including rheology of the blend, will be optimized for multifilament production.

Production techniques that provide high-quality, handleable, spoolable, raw, lignin-based fiber are required, and will be evaluated. The techniques include selection and evaluation of plasticizers and nucleating agents, raw-fiber coatings and oils, and spooling.

Following carbonization/graphitization of the lignin-based fiber, the carbon fiber must be surface-treated and sized to increase its compatibility with a given resin system. Fiber-resin compatibility is particularly critical in automotive applications, because the current program plan calls for use of chopped, rather than woven or wound fiber.

As the project work progresses and challenges are resolved, project partners expect to become increasingly involved in scaling-up the processes with respect to lignin production and purification, and to melt-spinning and thermal processing of the fibers.

Partnerships

A number of partners have been instrumental in helping to develop the lignin-based carbon-fiber technology. During the early part of the project, North Carolina State University spun a variety of lignin-polymer blends into single fibers, which were used for the initial feasibility evaluations. Similarly, UTK produced significant quantities of multifilament tow for project use.

The participation of several wood-pulping and biomass companies greatly improved project access to a variety of different lignin materials. Since its inception, the project has benefited from the participation of MWV, which provided hundreds of pounds of softwood and hardwood lignin products for project use, including a wide variety of research lignins. MWV is currently the only producer of lignin products derived from alkaline pulping (specifically the Kraft process), and has recently produced a ten-ton batch of hardwood lignin specifically for use in the program to develop a low-cost carbon-fiber production process.

Later, in FY 2004, the project attracted interest and participation from three other pulp and paper companies: Weyerhaeuser, Granit, S.A., and Lignol Innovations. The participation of these companies broadened the variety of lignins available to the project, including biomass-derived lignins which exhibit lower volatile contents. In late FY 2006, ORNL entered into a formal CRADA with Weyerhaeuser to evaluate experimental soda-pulped lignins for carbon-fiber production.

Summary and Conclusions

The project was re-proposed in FY 2003 and, in FY 2004, re-tasked to focus on larger-scale production of carbon-fiber feedstock. Relationships with MWV, Eastman Chemical Company, and Granit, S.A. were formalized. A third forest-products company, Weyerhaeuser, informally furnished samples of black liquors from which lignins were isolated for melt-spinning evaluation.

Evaluation of MWV's hardwood lignin demonstrated the feasibility of producing precursor fibers by melt-spinning, furthermore, that carbon fibers could be produced from the lignin fiber, and that the carbon fibers could be successfully surface treated and used to prepare small resin composites. However, it was clear from an examination of the carbon fibers that the contaminants inherently present in commercial Kraft lignin products had to be reduced. This was necessary to both improve melt-spinnability of the lignin precursor fiber and to decrease contaminant levels (particulates and volatile materials) in the carbon fibers themselves, which contaminants caused small defects that adversely impacted mechanical properties.

During this period, purification technologies were demonstrated on a lab-scale. Carbohydrate, in the form of cellulosic polysaccharides coprecipitated with lignin, was found to contribute significantly to evolution of gas during lignin-fiber spinning and also to production of char if held for long periods above 200°C. Carbohydrate-stripped lignins showed significantly reduced volatile evolution between 150 and 250°C.

Initial technical evaluations indicate that the carbohydrates recovered prior to lignin separation and purification could be simply incorporated into cellulose pulp with significant increases in tensile and burst indices of the paper (+15%). Recovery of this carbohydrate, primarily hemicellulose, could provide a significant revenue stream to partially offset the cost of lignin purification.

Additionally, preliminary specifications were established for lignin precursor suitable for melt-spinning into fiber. The specifications, which define acceptable levels of ash, particulates, and volatiles, were based on a combination of the specific requirements for spinning lignin-fiber tow and the specifications used for commercial production of pitch-based carbon fibers. Small amounts of lignin purified on a bench-scale consistently met the specifications.

Overall, using a combination of desalting and carbohydrate-stripping techniques, it has been possible to significantly improve, by >75%, the strength and stiffness of lignin-based carbon fibers produced as single filaments. A 7 kg batch of purified Kraft hardwood-lignin material was produced in FY 2006 to support further efforts to demonstrate multifilament spinning and rewinding.

The project was re-tasked in FY 2006 to focus on the development of a program to demonstrate a commercially-viable process for purification of lignin and the installation and commissioning of processing capability to melt-spin lignin-fiber tows in-house (at ORNL, Figure 6), an essential pre-requisite for identification of thermal processing conditions for production of carbon-fibers for composite testing. To support this effort, MWV produced a ten-ton batch of hardwood lignin to meet the precursor material needs of the project through FY 2007 (an effort which necessitated a dedicated pulping run in the paper mill).

Figure 6. New melt-spinning equipment.

In response to a request from the Automotive Composites Consortium (ACC), a white paper was written on the concept of a greenfield plant specifically for the production of lignin from wood, or other appropriate biomass, pulped under conditions specifically tailored to optimize the properties of lignin for low-cost carbon-fiber production. The cellulose by-product from the plant would be converted into other value-added products, most notably ethanol fuel for vehicles.

Efforts in FY 2007 will be focused on two key aspects: 1) development and demonstration of a commercially-viable process for the production of lignin-based precursor material meeting the specifications established for carbon-fiber production, and 2) demonstration of melt-spinning of small tows of lignin fiber, rewinding into larger tows, and thermal processing of the precursor fibers into carbon fiber. Both parts of the work will be undertaken in collaboration with PNNL and MWV, in which selected lignin materials produced in the PNNL combinatorial chemistry approach will be evaluated at ORNL for melt-spinnability and processing into carbon fibers. Both hardwood and softwood lignins will be evaluated in these respects. To help establish melt-spinning conditions and identify plasticizing agents for this purpose, notably for softwood lignin, fundamental measurements will be made with respect to rheological and relevant thermodynamical properties of the lignins.

Presentations/Publications/Patents

(FY 2005/2006)

"Evaluation of lignin from alkaline-pulped hardwood black liquor," A.L. Compere; W.L. Griffith; C.F. Leitten, Jr.; and J.M. Pickel. May 2005. ORNL/TM-2005/88.

"White Paper: Greenfield plant for production of lignin precursor material for manufacture of low cost carbon-fiber," F. S. Baker. Sept. 2, 2006.

Invention Disclosures

"Method for Improving Separation of Carbohydrates from Wood Pulping and Wood or Biomass Hydrolysis Liquors"; William L. Griffith, Alicia Compere, and Carl F. Leitten, Jr., July 19, 2005. Elected for application on August 16, 2005. Patent application drafted by outside counsel; filing pending. Lab Docket No. 1300001598.

"Rendering Lignin Melt Spinnable," Claude C. Eberle, Frederick S. Baker, and Christopher J. Janke. April 21, 2006. Lab Docket Number 1300001741.

"Melt-Spun Carbon-fiber Precursors Containing Lignin – Supplemental to ID 0968"; Alicia Compere, Carl F. Leitten, Jr., and William L. Griffith. June 30, 2006. Lab Docket No. 1300001772.

B. Improved Lignin Purification/Recovery Process for Carbon-Fiber Applications

Co-Principal Investigator: James F. White
Pacific Northwest National Laboratory (PNNL)
902 Battelle Blvd., Richland, WA 99352
(509) 372-5053; fax: (509) 372-6507; e-mail: jim.white@pnl.gov

Co-Principal Investigator: Bert DelliColli
MeadWestvaco Corporation, Specialty Chemicals Division
P.O. Box 118005, Charleston, SC 29423
(843) 746-8305; fax: (843) 746-8165; e-mail htd1@meadwestvaco.com

Technology Area Development Manager: Joseph A. Carpenter
(202) 586-1022; fax: (202) 586-1600; e-mail: joseph.carpenter@ee.doe.gov

Expert Technical Monitor: Philip S. Sklad
(865) 574-5069; fax: (865) 576-4963; e-mail: skladps@ornl.gov

---

Contractor: Pacific Northwest National Laboratory
Contract No.: DE-AC06-76RL01830

Objective

The project objective is to develop an economically-viable and technically-sound process for the purification of lignin to make it acceptable as a raw material for the manufacture of low-cost carbon fiber (CF).

Lightweighting the USA car and light-truck fleet for better fuel efficiency is a current DOE objective. The substitution of stamped steel panels and other body and interior parts with strong, yet lightweight and resilient carbon-fiber-reinforced plastic (FRP) parts can contribute significantly to this objective. Unfortunately, current processes for manufacture of CF are costly, and produce CF at well above the established target cost of under $5.00/lb needed for vehicle lightweighting.

A considerable portion of the cost of current CF is borne by the expensive synthetic polymers that are the normal raw materials. Lignin, as a byproduct of the pulp and paper industry, is an attractive alternate and potentially low-cost raw material for CF. Unfortunately, today's standard means of recovering lignin from paper-mill streams is not able to yield lignin with the levels of acceptable purity and physical properties for fast and economically-viable melt-spinning and eventual conversion to carbon fiber.

This project is tasked with developing and demonstrating at the lab-scale effective means to isolate, recover and purify pulp-mill-derived lignin with properties acceptable for its use as a raw material for CF. Initially, this effort is focused on hardwood lignin from Kraft black liquor and eventually will be extended to softwood lignin from Kraft black liquor. The purity targets that have been set for lignin by prior CF work at ORNL (see 3.A) serve as a guideline. However, we will also use a preliminary test for melt-spinnability (via a fiber-draw test) as a guideline for determining early-success potential. We will also examine other physical properties including melt index (MI) and dynamic viscosity. These physical properties are also expected to be a key to a material's ability to be processed economically into CF whose properties are acceptable for use in CF-reinforced car and truck parts.

Approach

- Evaluate the MeadWestvaco (MWV) concept of differential removal of impurities and lignin precipitation as a process route to achieving the desired level of lignin purity and properties for carbon-fiber application.

- Evaluate post-pulping processes to remove carbohydrate from lignin (using appropriate representative Kraft black liquor(s).
- Screen and determine optimal process variables for the selected process.
- Scale selected process and the optimized conditions to 300 cc and or to 1-liter batch level, or larger as appropriate, to verify process and determine overall material balance and perform preliminary assessment of adaptability to a continuous process.

Accomplishments

- Purchased MI instrument for lignin product characterization. Set up instrument and accomplished operator training and baselining with commercial polymers.
- Successfully addressed environmental, health and safety (EH&S) issues. This included standard operating procedures and safety reviews of instrumentation and autoclave equipment and approved procedures for disposal of waste and recycle materials.
- Developed approved material-handling, characterization and processing procedures.
- Developed procedures for thermogravimetric analysis (TGA), differential thermal analysis (DTA) and differential scanning calorimetry (DSC) of samples to determine moisture, ash and melting-range behavior.
- Established and validated a preliminary "fiber-draw" test to assess the ability of lignin samples to be successfully melt-spun.
- Determined that existing PNNL dynamic mechanical analysis (DMA) instrumentation can adequately measure lignin sample melt viscosity under shear, another property that is deemed key to predicting its ability to be melt-spun into fiber.
- Begun combinatorial, high-throughput experiments with well-per-plate format to assess post-pulping processes. Selected several leads for further evaluation.
- Performed a preliminary evaluation of the MWV differential process for lignin clean-up.
- Performed an evaluation of % loading and methods of incorporation for one recommended type of plasticizer / rheology control agent to aid in lignin melt-spinning. Selected an appropriate loading and incorporation method. (Prior efforts by others have suggested that lignin must be plasticized in order to be effectively melt-spun.)
- Via the cooperative research and development agreement (CRADA) partner, established a technical-service type arrangement with a USA university to perform single-fiber melt-spin tests on samples that appear successful in preliminary testing.

Future Direction

- Development of technology capable of delivering hardwood lignin to the desired purity level.
- Selection of one of three best-apparent technologies for hardwood-lignin recovery and scaling these to a level suitable for validation and to provide sufficient material for single-fiber melt-spin tests at a university.
- Extension of hardwood-lignin recovery methods to the development of technology capable of delivering softwood lignin to the desired purity level.
- Selection of one of three best-apparent technologies for softwood-lignin recovery and scaling these to a level suitable for validation and to provide sufficient material for single-fiber melt-spin tests at a university.
- Delivery of 5 kilograms of the desired purified lignin for melt-spinning evaluations.

Introduction

Carbon fiber derived from lignin-based feedstock offers the potential for meeting the aggressive cost goals established by FreedomCAR for structural applications of carbon fiber. However, the critical requirement for successful development of a lignin-based carbon fiber is the ability to purify the lignin feedstock effectively so that it can be melt-spun and processed at attractive rates into a viable carbon fiber having the required physical and mechanical properties. Effective purification of lignin requires the removal of insoluble particulates, salts and undesirable carbohydrate fragments, which adversely affect the melt-spinning and overall fiber processing. In order to meet current cost targets it is essential that a practical purification process be compatible with current Kraft pulping operations as Kraft lignin is the largest practical source of lignin for the near future. It is also essential that the general lignin purification scheme be easily adaptable to both hardwood and softwood lignin. Longer term, the process must also be able to handle lignin from other renewable sources and processes other than those based on Kraft-type technology.

MWV, the project's cost-sharing CRADA partner, has developed a relatively untested and unrefined concept for lignin purification/recovery that has potential to meet the required purity levels in a cost-effective, environmentally-suitable manner. In addition, the MWV process concept is compatible with existing pulp-plant layout and function, which is a key requirement for early implementation of high-purity lignin for carbon fiber.

The most deleterious lignin components are perceived to be easily volatilized, lignin-bound carbohydrate fragments, along with inorganic salts, insoluble and non-melting materials. MWV's conceptual process is expected to remove these undesirable components very early in the lignin recovery process and also can be retrofitted into a conventional pulp mill design. Early experimental evidence suggests that this concept, although simple, is likely to be more complex and difficult to accomplish successfully than initially believed.

Approach

The overall project approach is multifold, including use of high-throughput, combinatorial methods at PNNL for fast screening and discovery. Bench-scale experiments at 300 cc to 1-liter levels to validate, verify and refine leads, found via high-throughput methods, are also planned. Scale-up to pilot-size and beyond as appropriate will also be conducted to provide confidence in the process and to provide material for single- and multiple-fiber melt-spinning evaluation and also carbonization tests. Initially, the project plan involved various tasks properly described as preparatory, including acquisitions, personnel training and items related to EH&S. This was followed by experimental recovery of lignin via various physical means and also experimental evaluations of a variety of chemical treatments. Ultrafiltration of the black liquor (BL) was also briefly examined.

Fundamentally, we are starting with lignin at the black-liquor stage, that is, when it is closest to the form in which it is first removed from the wood. Prior CF development work with lignin has used material that had already been recovered, isolated, subjected to some degree of purification and dried. Since lignin can have significant reactivity before and during drying, we think that beginning at the BL stage allows us to intercept lignin and process it more effectively before undesirable and irreversible changes take place.

Results

Early accomplishments include the acquisition, set-up, personnel training, a safety review and standard operating procedures (SOP) approvals of a Tinius-Olsen Melt Index testing machine. We have evaluated and validated this instrument with several commercial polymers with known ability to be melt-spun and blown into films.

We have also set-up and validated a preliminary test to very simply evaluate a new material's potential ability for melt-spinning. This preliminary test, known as the "fiber-draw" test is modeled closely after a test designed and successfully used by some staff at Clemson University for determining if a given sample is likely to be suitable for melt-spinning. The "fiber-draw" test apparatus is contained inside a N-filled glove box as lignin is often perceived to be reactive with air. The test is quite simple in concept. A sample is placed in a small aluminum pan on a hot plate whose surface

temperature may be accurately controlled and changed. As the sample temperature is raised by increasing the hot plate's surface temperature, a visual indication of possible melting or softening can be observed. When melting or softening behavior is seen, a sharp-pointed pin is touched to the sample and slowly removed. If a long, uniform, thin fiber can be drawn from the sample as the pin is removed while the sample transitions through a melting or softening stage, then the sample is considered to have good potential for melt-spinning. Figure 1 shows the "fiber draw" behavior of M-50 pitch, a material known to have good melt-spinning behavior. Note the relatively nice looking long fibers drawn from the melted pitch contained in the pan.

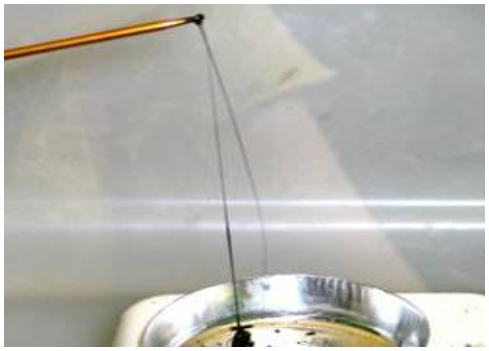

Figure 1. M-50 Pitch fiber-draw test.

Other early activities included staff training on a TGA-DSC apparatus used to determine melting points or melting ranges and also weight loss vs. temperature in inert or air atmosphere.

Experimental work for recovering lignin from hardwood BL is using a commercial BL obtained from the MWV Kraft pulp mill in Charleston SC. We found that most particulate matter and the tall oils could be removed in a single centrifuging step after appropriate pH adjustments. The liquid remaining after this treatment contained about 14% lignin along with dissolved inorganic salts and other organics. Simple precipitation of this lignin followed by washing to remove the inorganic salts and soluble organics followed by vacuum drying, did not yield a particularly good fiber draw test (see Figure 2). The "clumps" and "nodules" on the drawn fibers are indicative of poor melt-spin behavior and are consistent with earlier work which established the need to plasticize the lignin prior to melt-spinning, regardless of its purity.

Figure 2. Precipitated lignin.

Figure 3. Pc-1369 lignin.

As a comparison, Figure 3 shows the fiber-draw test result with unprocessed PC-1369 which is a commercial grade of hardwood lignin shown in past ORNL studies not to be suitable for melt-spinning. The PC-1369 and also the lignins shown in Figures 2 and 4 contain the preferred plasticizer/rheology control agent; but, note the very severe degree of clumping and poor fiber formation in Figure 3 which suggests quite poor melt-spin behavior for PC-1369.

However, Figure 4 shows a fiber-draw test that appears positive for a lignin sample that was obtained from high-throughput screens to evaluate various other BL pretreatments before precipitation, washing and vacuum drying. An approach such as this in combination with a suitable plasticizer is expected to ultimately produce the desired result, an easily melt-spinnable, lignin-based precursor to carbon fiber.

These results appear to be worth following up. Thus, a series of follow-up tests are planned for next quarter at both the 20 mls combi level and at a larger bench-scale. Note that high-throughput combinatorial screens are performed in the PNNL combi system using a 6-well plate. The capacity of each well is about 20 mls. Only a few grams of lignin can be recovered from these screens, about enough to do only TGA-DSC and a fiber draw test.

Figure 4. Fiber draw-test Experimental combi lignin.

Conclusions

Initial experimental results suggest that the conceptual MWV differential recovery / purification process may require a more complex approach than originally anticipated.

PNNL combinatorial studies and corresponding fiber-draw tests have suggested post-pulping process modifications that may provide alternatives that have promise for leading to a lignin product acceptable for melt-spinning. These require further evaluation. They also probably can be integrated into a typical Kraft pulp mill. This and several related methods are presently slated for further evaluation and scale-up to bench-level in the next two quarters at both combi and larger-scale levels.

Presentations/Publications/Patents

None in FY 2006.

C. Advanced Stabilization of PAN Fiber Precursor

Principal Investigator: Felix L. Paulauskas
Oak Ridge National Laboratory (ORNL)
PO Box 2008, Oak Ridge, TN 37831-6053
(865) 576-3785; fax: (865) 574-8257; e-mail: paulauskasfl@ornl.gov

Project Manager, Composites: C. David Warren
Oak Ridge National Laboratory
P.O. Box 2008, Oak Ridge, TN 37831-6065
(865) 574-9693; fax: (865) 576-4963; e-mail: warrencd@ornl.gov

Technology Area Development Manager: Joseph A. Carpenter
(202) 586-1022; fax: (202) 586-1600; e-mail: joseph.carpenter@ee.doe.gov

Expert Technical Monitor: Philip S. Sklad
(865) 574-5069; fax: (865) 576-4963; e-mail: skladps@ornl.gov

Principal Team Members:
Christopher J. Janke, ORNL
Cliff Eberle, ORNL
Daniel Sherman, Atmospheric Glow Technologies
Professor Amod Ogale, Clemson University
Professor Roberto Benson, University of Tennessee
Dr. Marshall Cleland, IBA-RDI
Rick Galloway, IBA-RDI

Contractor: Oak Ridge National Laboratory
Contract No.: DE-AC05-00OR22725

Objectives

- Develop an improved technique for stabilizing carbon-fiber precursor with increased line speed and reduced carbon-fiber cost.
- Verify that finished fiber properties satisfy automotive and heavy-vehicle manufacturers' requirements.
- Conduct a preliminary evaluation of the cost impact of the new stabilization technique.
- Integrate the stabilization module into an advanced technology pilot-line.

Approach

- Investigate thermochemical, ultraviolet, and electron-beam processing stabilization routes.
- Select one of the aforementioned stabilization routes for detailed equipment and process development.
- Develop fiber-handling protocols for continuous processing.
- Conduct parametric studies to correlate processing parameters and fiber properties.
- Characterize fibers to confirm that they satisfy program requirements.

- Develop equipment and process specifications for a prototypical stabilization module to be implemented in a subscale, advanced-technology pilot-line.

Accomplishments

- Demonstrated that thermochemically-stabilized fibers can be plasma oxidized.
- Demonstrated that electron-beam-stabilized fibers can be plasma oxidized.
- Discovered that ultraviolet irradiation of polyacrylonitrile (PAN) precursor fibers produces relatively high gel fraction in < 2 minute residence time.
- Preliminary cost estimate completed for electron-beam stabilization.

Future Direction

- Complete feasibility investigation of ultraviolet stabilization route.
- Sufficiently investigate all routes to establish reasonable basis for evaluation of metrics including throughput and cost estimates.
- Select one stabilization route for detailed development.
- Conduct parametric studies and fiber characterization to better understand process effects and the processing window and to quantify fiber properties.
- Design an advanced stabilization module for an advanced-technology pilot-line.

Introduction

The purpose of this project is to investigate and develop a technique to rapidly and inexpensively stabilize a PAN precursor. New processing techniques are being developed for the purpose of reducing the cost of carbon-fiber conversion. Previous and ongoing research at ORNL has demonstrated that plasma processing shows great promise for inexpensively and rapidly oxidizing, carbonizing, and graphitizing polymer precursors to convert them to carbon fibers. However, the precursor needs to be lightly stabilized, or cross-linked, before it is exposed to plasma-generated oxidative species. Stabilization and oxidation together are estimated to represent ~ 18% of the cost of commercial-grade carbon fiber[1]. A rapid, inexpensive, and robust stabilization technique is needed to complement the aforementioned advanced process modules, and enable the development of an integrated advanced-technology conversion line that converts polymer precursor fibers into carbon fibers at significantly lower cost than conventional conversion technology.

This project therefore intends to develop an advanced stabilization module that integrates with other advanced fiber-processing modules to produce inexpensive carbon fiber with properties suitable for use by the automotive industry. Critical technical criteria include (1) ≥ 25 Msi tensile modulus and ≥ 1.0% ultimate strain in the finished fiber; (2) uniform properties along the length of the fiber tow; (3) repeatable and controllable processing; (4) and significant unit cost reduction compared with conventional processing.

Project Deliverable

At the end of this project, the project team will have demonstrated satisfactory PAN precursor-fiber stabilization with line speed exceeding (or residence time less than) that typical of conventional carbon-fiber conversion lines. The project deliverable is a process specification from which advanced stabilization equipment can be scaled to develop an operational stabilization module for a subscale, multiple- large-tow, advanced-technology pilot-line.

Technical Approach

The researchers are investigating three prospective PAN-precursor-fiber stabilization routes: electron-beam processing, thermochemical processing, and ultraviolet processing. All three routes are based on discoveries previously made in other carbon-fiber

projects, and each appears to offer certain advantages. After initial feasibility studies, the researchers will select the most promising route for detailed process development, with the principal criteria for selection being mechanical properties and finished fiber cost. The preferred route will then undergo detailed parametric studies to characterize the process and develop the processing recipe.

Progress

Electron-Beam Processing

Initial electron-irradiation experiments were conducted at the Radiation Dynamics Inc. Long Island facility in late 2005. Several precursor tows are shown in Figure 1. The precursors on the glass frame were electron irradiated followed by brief heat treatment at a temperature below conventional stabilization temperature. The top precursor was not irradiated, but was heat treated at the same condition as the others. In all cases of irradiation, significant darkening is observed, suggesting that cross-linking has occurred during irradiation.

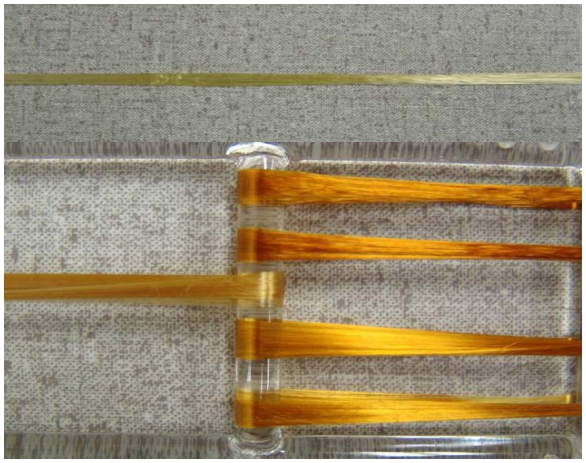

Figure 1. Lower 5 tows were irradiated followed by brief heat soak. Top tow was not irradiated but subjected to identical heat soak.

The precursor density increases only negligibly during electron irradiation, but advances rapidly thereafter upon brief post-treatment at the right conditions.

Differential scanning calorimetry (DSC) results, an example of which is shown in Figure 2, indicate that electron irradiation lowered and spread the exothermic peak, and moved the curve slightly to

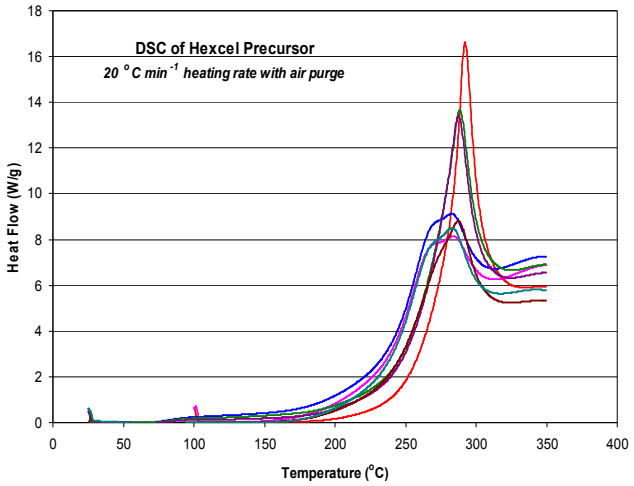

Figure 2. DSC results for electron-irradiated PAN precursor. Highest peak is virgin precursor; others are after irradiation at various conditions.

the left. This was expected to lower the onset of exothermic reaction and to cause greater heat generation at temperatures below the baseline curve, but overall to make the reaction more controllable by reducing the impact of the narrow and steep exothermic peak. However, electron-irradiated precursor could not be processed using the oxidation conditions established for conventionally-stabilized precursor. A parametric investigation of oxidation parameters was initiated and acceptable operating parameters have been identified, but considerably more work is needed in this area. Electron-beam-stabilized fibers were subsequently plasma oxidized, satisfying a mid-year project milestone. In the last half of fiscal year (FY) 2006, initial DSC characterization was repeated and many more DSC runs were made using new equipment at ORNL's Center for Nanophase Materials Sciences. The project team planned and prepared for a new set of irradiation experiments scheduled in October 2006.

Electron-beam-stabilized precursor has been converted to finished fibers by a range of process combinations, and the results compared in Figure 3.

All of the conversions, even by fully-conventional means, were conducted at low carbonization temperature and without the benefit of fiber tensioning, tow spreading, or controlled stretching in any of the conversion stages; hence, the fiber mechanicals are expected to be low compared to those of corresponding commercial fibers. In fact,

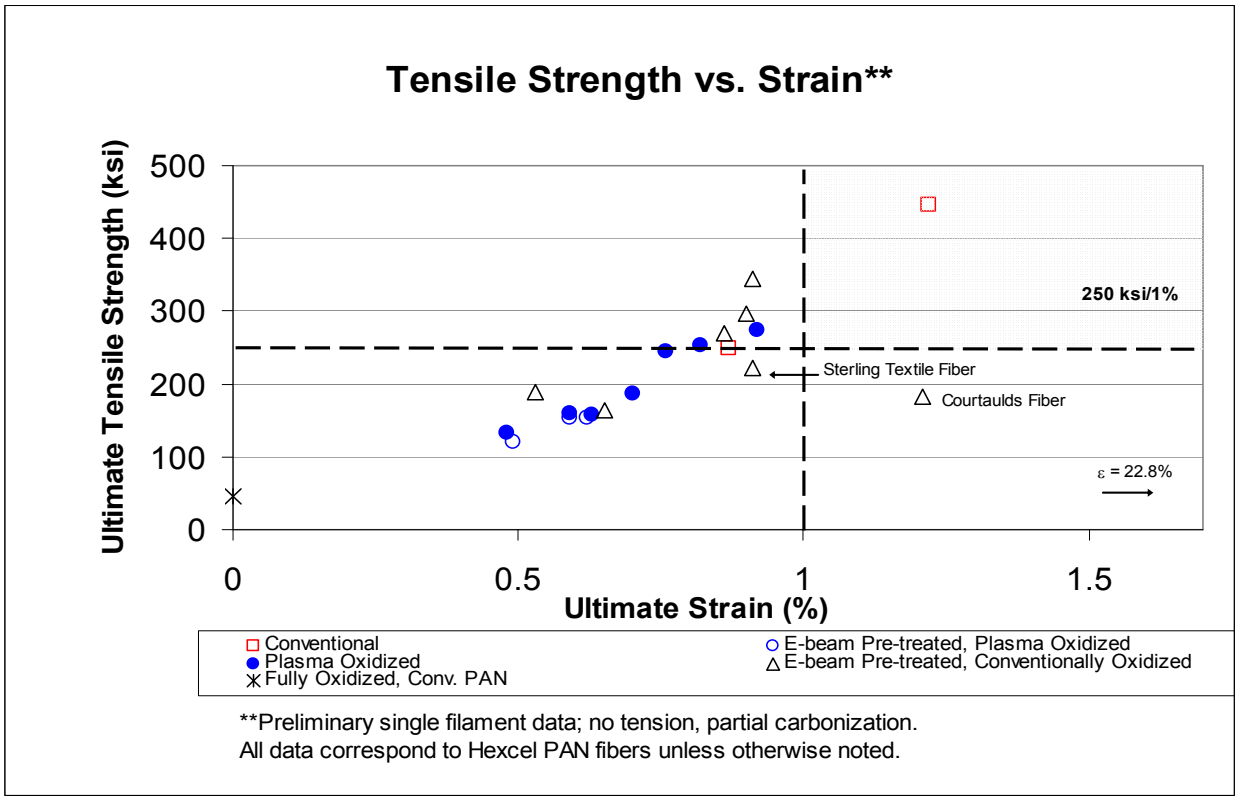

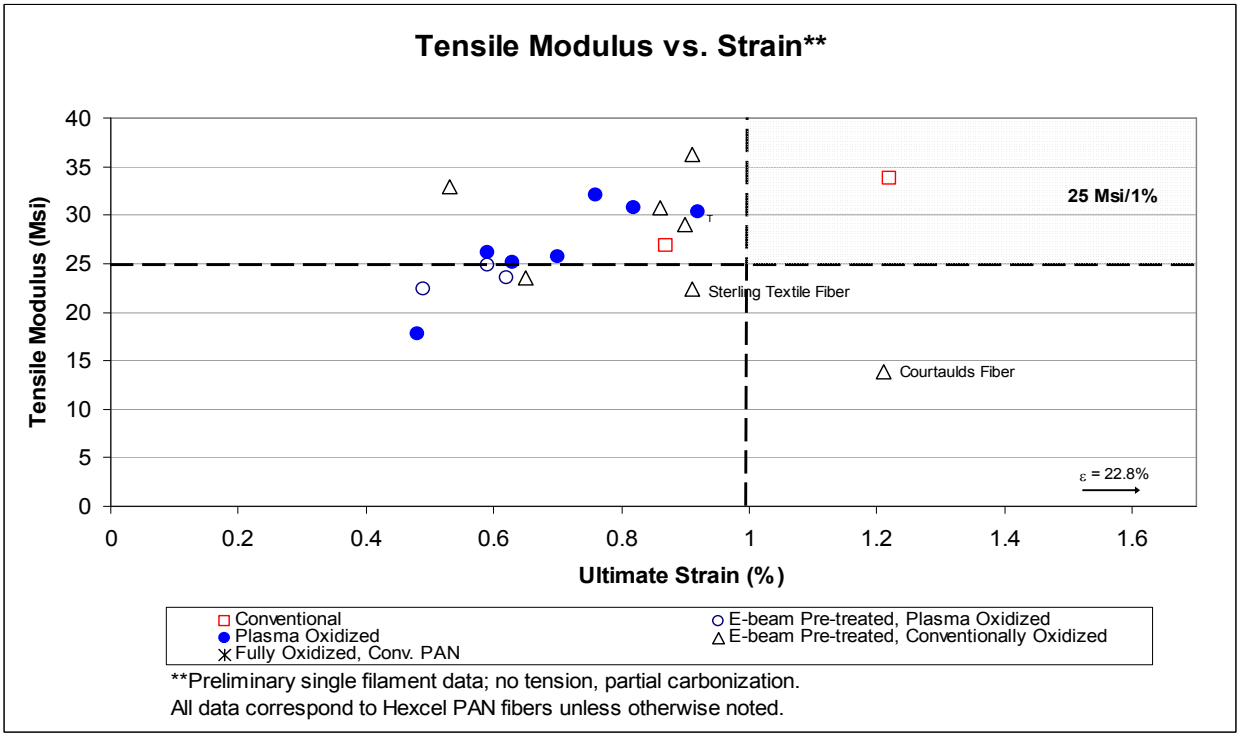

Figure 3. Mechanical properties of first electron-beam-stabilized fiber specimens (tested by single- filament tensile-strength method). Conventional data points were thermally shocked and thermally ramped, respectively.

several of the advanced-technology specimens exhibit a tensile modulus exceeding the 25 Msi requirement. The strain is generally somewhat below the 1% requirement. It is noteworthy that the electron-beam-stabilized samples, even those that were subsequently plasma oxidized, exhibit mechanicals that are not far below those of the thermally-converted fibers. This gives us confidence that the property targets are well within reach. Electron-beam-stabilized fibers will be carbonized at correct temperature and tension after commissioning a high-temperature tube furnace in the second quarter of FY 2007.

Electron-beam irradiation equipment and protocols are relatively mature in other industries, with high reliability and throughputs. One can extrapolate from a well-established experience base to estimate parameters such as availability, throughput, and cost per unit of dose delivered to the product. The major challenges appear to be the interfacing of electron-beam-stabilization and plasma-oxidation processes, and the high capital cost of electron beams. The unit capital cost drops precipitously with increasing scale, and a single high-power beam may be able to serve several production lines. But this will make it necessary to provide "surge capacity" that isolates the beam from downstream processes so that a single-point failure will not disrupt the operation of several fiber production lines. Early analysis suggests that electron-beam stabilization will not be cost-effective for low-production-volume conversion factories, but if system-compatibility issues can be successfully resolved, it is likely to be very attractive for high-volume factories. It may be preferable to electron-beam stabilize at the precursor factory, immediately after precursor spinning, rather than in-line at the conversion factory. This could potentially address the scaling economics. Current metrics are shown in "spider chart" format in Figure 4.

Thermochemical Processing

Stabilization was found to be needed before plasma oxidation because virgin precursor could not with stand the reactive oxidative species generated by plasma. When virgin precursor is exposed to the plasma-generated chemistry, significant exothermic heating occurs fairly rapidly, resulting in interfilamentary adhesion and tow rigidity.

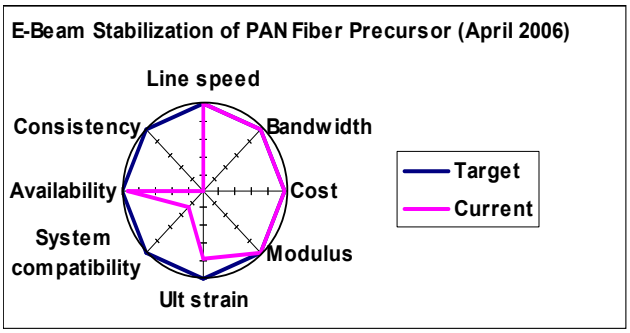

Figure 4. "Spider chart" showing current estimates of electron-beam-stabilization metrics.

Thermochemical stabilization, using some modification of thermal and/or chemical conditions experienced in plasma oxidation, appears to potentially offer a rapid stabilization route.

Thermochemical stabilization was investigated and shown to be technically viable. Virgin precursor was thermochemically treated in the oxidation reactor. The researchers demonstrated the capability to thermochemically stabilize virgin precursor in about 30% less residence time than that required for conventional stabilization. Thermochemically-stabilized fiber was subsequently plasma oxidized, satisfying a mid-year milestone. The researchers are continuing to investigate thermochemical-stabilization parameters with the hope of further reducing the residence time. It is currently too early in the thermochemical stabilization investigation to estimate cost or other metrics.

Other (non-plasma) thermochemical stabilization routes will be conceived and/or reviewed in early FY 2007, and further investigated if they are deemed to offer sufficient merit.

Ultraviolet Processing

Ultraviolet processing potentially offers the combination of high line speeds with low capital cost. The chemistry is generally similar to that of electron-beam processing, but very often ultraviolet requires a photoinitiator that would not be needed for electron-beam cross-linking. One of the major challenges is whether ultraviolet irradiation can deliver uniform cross-linking throughout the tow, with acceptable residence time.

The ultraviolet processing development is being conducted at Clemson University with ORNL providing technical consultation and direction. Clemson's experimental ultraviolet equipment is shown in Figure 5. It utilizes a mercury lamp, with a conveying system to move the material through the temperature-controlled irradiation zone.

Figure 5. Experimental ultraviolet equipment.

Virgin precursor and ultraviolet-irradiated precursor (absent photoinitiator) are shown side-by-side in Figure 6. As shown, a few minutes of ultraviolet irradiation can produce significant color change.

The gel fraction (fraction of material remaining solid in dimethyl sulphoxide solvent) of ultraviolet-irradiated material was measured to be ~ 41%, compared to ~1% for virgin precursor, > 90% for oxidized PAN fiber, and > 99% for finished carbon-fiber. DSC results, shown in Figure 7, show reduction and a slight broadening of the exothermic peak ("UV + thermal" trace). The sample is irradiated at elevated temperature. The purely thermal stabilization, i.e., the stabilization that would occur due only to heat at the temperature in the ultraviolet chamber, is shown by the "thermal" trace in Figure 7. The "thermal" trace approximately duplicates the "as received" trace, suggesting that there is virtually no thermal stabilization component at the irradiation conditions. This indicates that the thermal component alone is insufficient, i.e., the ultraviolet irradiation component is needed to achieve the "UV + thermal" results.

To evaluate the uniformity of cross-linking, DSC measurements were made on different parts of the tow. Figure 8 shows the DSC results, indicating that

Figure 6. Virgin PAN precursor fibers, at left, exposed to increasing ultraviolet dose, at right.

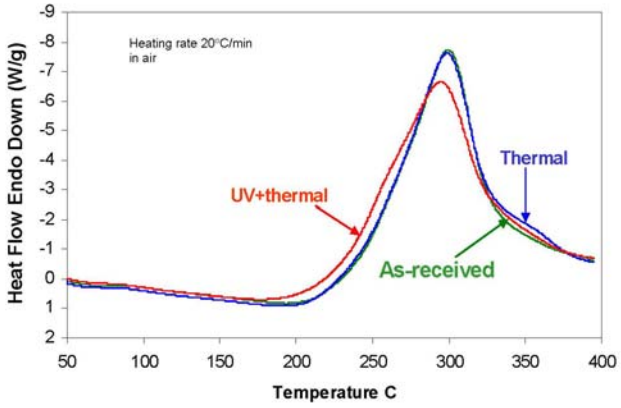

Figure 7. Ultraviolet stabilization DSC (in air) results for Courtaulds precursor.

there is significant cross-linking variability across the tow. The fiber surfaces are damaged by soaking in a 50% solution of sulfuric acid. Figure 9 shows micrographs showing the damage.

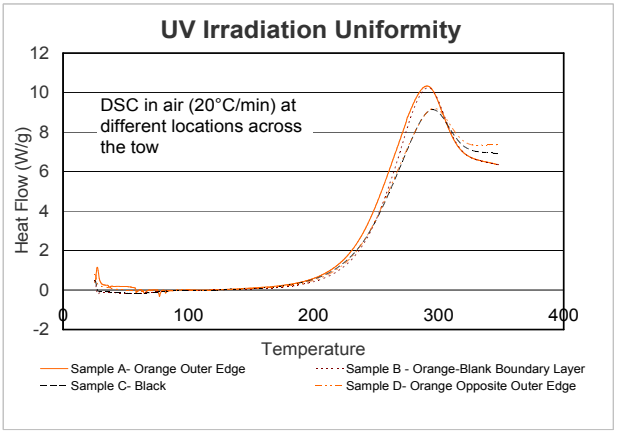

Figure 8. DSC scans of UV-stabilized fibers taken from different locations across the tow.

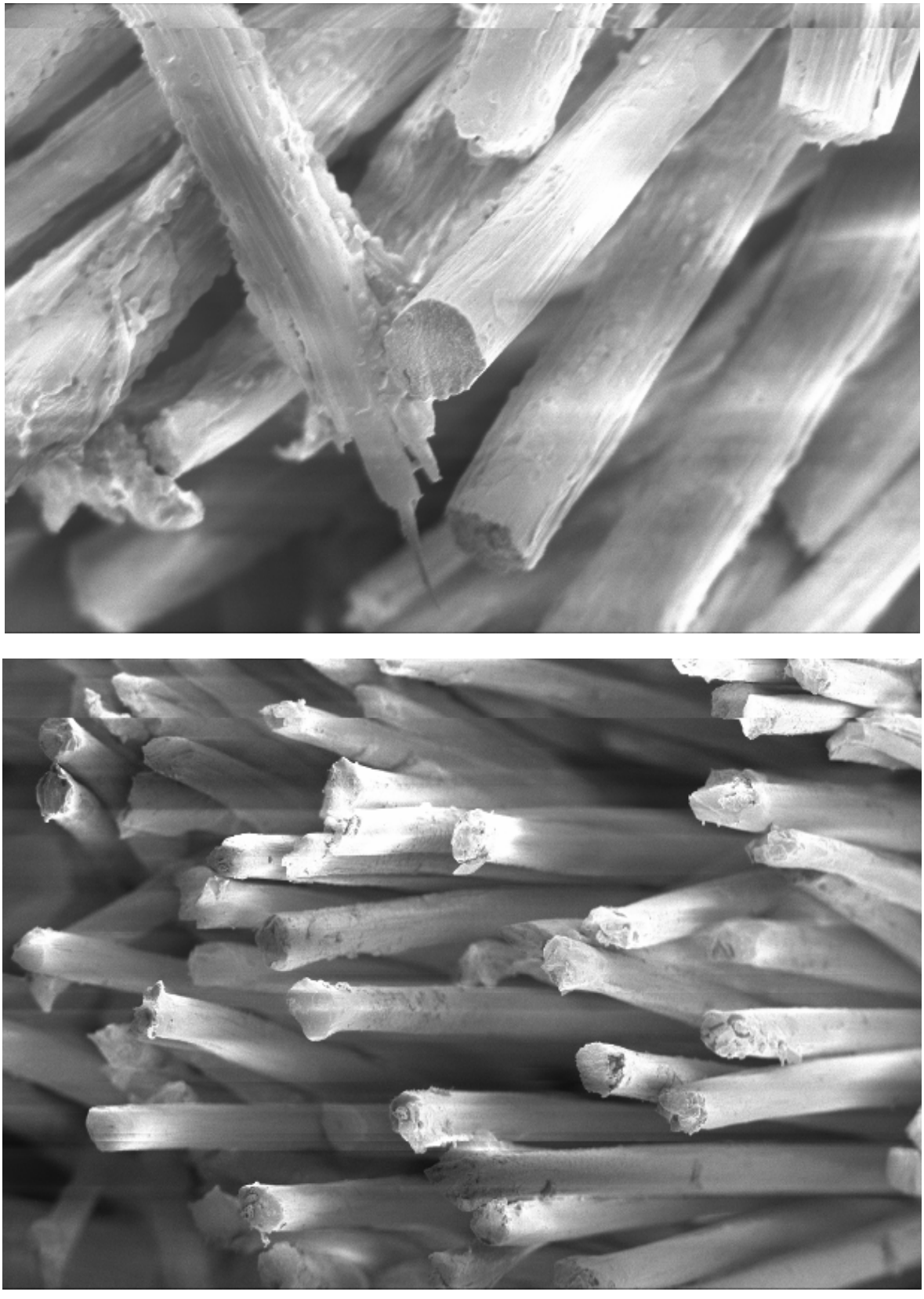

Figure 9. Micrographs of UV-irradiated fibers after acid soak. Top – nominal dose; bottom – 3X nominal dose.

This damage indicates that surface cross-linking is inadequate to protect the underlying polymer from the acid. The low level and variability of cross-linking cause concern, but it is not presently known how dense or uniform the cross-linking must be. Clearly there is some effect of cross-linking, as virgin precursor, when subjected to the same acid treatment, will show significant damage in just minutes. Light cross-linking at the fiber's surface may be sufficient to prepare the fiber for plasma oxidation, and some tow nonuniformity is probably acceptable. The fibers must be tested in the oxidation reactor to determine whether they are sufficiently cross-linked.

To date, there has been no attempt to plasma oxidize ultraviolet-stabilized fibers. This will be done in FY 2007. Ultraviolet-stabilization metrics also have not yet been evaluated. The results to date have raised issues of concern, but on the whole have been encouraging. Considerably more work is needed to determine whether ultraviolet processing is a viable stabilization route.

Future Direction

Early FY 2007 will be devoted to continuing parallel studies of the proposed stabilization routes, with down-selection to a single route in mid to late 2007.

Patents and Publications

Two patents were filed, as follows:
F.L. Paulauskas, T.L. White, and D.M. Sherman, "Apparatus and method for oxidation and stabilization of polymeric materials," application # 11/344,573, filed January 2006; and

F.L. Paulauskas and D.M. Sherman, "Apparatus and method for stabilization or oxidation of polymeric materials," application # 11/391,615, filed March 2006.

A paper by S.M. White, J.E. Spruiell, and F.L. Paulauskas, entitled "Fundamental Studies of Stabilization of Polyacrylonitrile Precursor, Part 1: Effects of Thermal and Environmental Treatment," was presented at the spring SAMPE conference in Long Beach, CA.

Education

Educational institutions participating in this project include Clemson University and the University of Tennessee (UT). A Clemson post-doctoral researcher is conducting ultraviolet-processing studies under the direction of Professor Amod Ogale. UT materials-science graduate students are providing characterization support to the project under the guidance of Professor Roberto Benson.

Partners

ORNL gratefully acknowledges the following partners that have made valuable contributions to this project:

- Atmospheric Glow Technologies – plasma equipment design and processing (subcontract)
- Automotive Composites Consortium – programmatic and technical direction (complimentary)
- Clemson University – ultraviolet process development (subcontract)
- Hexcel Corporation – raw materials and technical consultation (complimentary)
- Radiation Dynamics Inc. – irradiation analysis, protocols, and beam time (complimentary)
- TohoTenax America – raw materials and technical consultation (complimentary)
- University of Tennessee – characterization (subcontract).

Conclusions

Three prospective processing routes to lightly stabilize polymer precursors in an advanced carbon-fiber conversion line are under investigation. Electron-beam processing and thermochemical processing have been shown to be technically feasible, and the early results from ultraviolet processing are surprisingly good. It appears likely that there will be multiple good options from which to choose an advanced stabilization route. Down-selection is scheduled in mid- or late-FY 2007.

[1] S.M. Cohn and S. Das, "A Cost Assessment of Conventional PAN Carbon-fiber Production Technology." Energy Division, Oak Ridge National Laboratory, TN (1998)

D. Advanced Oxidation of PAN Fiber Precursor

Principal Investigator: Felix L. Paulauskas
Oak Ridge National Laboratory
P.O. Box 2008
Oak Ridge, TN 37831-8048
(865) 576-3785; fax: (865) 574-8257; e-mail: paulauskasfl@ornl.gov

Project Manager, Composites: C. David Warren
Oak Ridge National Laboratory
P.O. Box 2008, Oak Ridge, TN 37831-6065
(865) 574-9693; fax: (865) 576-4963; e-mail: warrencd@ornl.gov

Technology Area Development Manager: Joseph A. Carpenter
(202) 586-1022; fax: (202) 586-1600; e-mail: joseph.carpenter@ee.doe.gov

Expert Technical Monitor: Philip S. Sklad
(865) 574-5069; fax: (865) 576-4963; e-mail: skladps@ornl.gov

Participants:
Kenneth D. Yarborough, ORNL
Professor Joseph Spruiell, University of Tennessee, Knoxville
Daniel Sherman, Atmospheric Glow Technologies

Contractor: Oak Ridge National Laboratory
Contract No.: DE-AC05-00OR22725

Objectives

- Develop an improved technique for oxidizing carbon-fiber precursor with increased line speed, reduced carbon-fiber cost, and reduced equipment footprint.
- Verify that finished fiber properties satisfy automotive requirements.
- Conduct a preliminary evaluation of the cost impact of the new oxidation technique.
- Integrate the oxidation module into a prototypical conversion line.

Approach

- Develop a plasma process for oxidation using atmospheric-pressure plasma.
- Develop fiber-handling protocols for continuous processing.
- Conduct parametric studies and perform diagnostics to correlate processing parameters and fiber properties.
- Characterize fibers to confirm that they satisfy program requirements.

Accomplishments

- Developed stable protocol for oxidation of conventionally “pre-stabilized” 3k polyacrylonitrile (PAN) precursor tow with atmospheric-pressure plasma using a continuous process at 0.05 m/min line speed at mid-year, increased to 0.15 m/min by year end.

- Fully oxidized "pre-stabilized" fiber in atmospheric-pressure plasma with approximately 3X reduction in residence time of conventional oxidation.
- Demonstrated plasma oxidation of electron-beam-stabilized and thermochemically-stabilized PAN precursor.
- Carbonized fibers after plasma oxidation and measured mechanical properties.
- Designed, constructed, and commissioned a six-zone reactor that permits parametric control in each zone independently of process parameters in the other processing zones.
- Submitted two patent applications.

Future Direction

- Continue refining the reactor design and processing protocols to achieve high-speed, multiple-large-tow, continuous, plasma oxidation process.
- Refine oxidation recipe and equipment design to interface with stabilization techniques under development.
- Acquire and implement new diagnostic tools. Conduct parametric studies and fiber characterization to better understand process effects and the processing window and to quantify fiber properties.
- Conduct rate-effect studies and update cost analysis.
- Investigate oxidation of alternative precursors.

Introduction

The purpose of this project is to investigate and develop a plasma processing technique to rapidly and inexpensively oxidize PAN precursor fibers. Oxidation is a slow thermal process that typically consumes over two-thirds of the processing time in a conventional carbon-fiber conversion line. A rapid oxidation process could dramatically increase the conversion line throughput and appreciably lower the fiber cost. A related project (see 3.E) has already demonstrated the potential for greatly increasing line speed in the carbonization and graphitization stages, and rapid stabilization techniques are being developed (see 3.C), but the oxidation time must be greatly reduced to effect fast conversion. This project intends to develop plasma oxidation technology that integrates with other advanced fiber-conversion processes to produce inexpensive carbon fiber with properties suitable for use by the automotive industry. Critical technical criteria include (1) ≥ 25 Msi tensile modulus and ≥ 1.0% ultimate strain in the finished fiber; (2) uniform properties over the length of the fiber tow; (3) repeatable and controllable processing; (4) and significant unit cost reduction compared with conventional processing.

Project Deliverable

At the end of this project, the researchers will have developed an advanced oxidation process with residence time much less than that typical of conventional carbon-fiber conversion lines. The advanced oxidation process will be sufficiently well understood and documented that the team can commence scaling it to develop a multiple-large-tow oxidation module for an advanced-technology pilot line.

Technical Approach

The researchers are investigating PAN precursor fiber oxidation using nonequilibrium, nonthermal plasma at atmospheric pressure. Plasma processing is believed to enhance oxygen diffusion and chemistry in the PAN oxidation process. Atmospheric-pressure plasma provides better control over the thermal environment and reaction rates than does evacuated plasma, in addition to eliminating the sealing problems accompanying evacuated-plasma processing. Various fiber characterization tools and instruments are used to conduct parametric studies and physical, mechanical, and morphological evaluations of the fibers to optimize the process.

Atmospheric-Pressure Plasma Processing Results

Exposure to plasma products at or near atmospheric pressure provides superior thermal control because the gas flow should convectively heat or cool the fibers. This is deemed particularly important to avoid fiber melting from exothermic reactions. However, the short mean-free-path and life-span of the chemically reactive species at atmospheric pressure presents another set of challenges principally associated with finding a process recipe that delivers high process stability and short residence times.

In ORNL's conventional pilot line, which represents the baseline process, PAN stabilization and oxidation occur in four successive furnaces in air, at temperatures increasing from about 200 to 250°C. Although there is not a precise transition from stabilization to oxidation, in general, one can consider stabilization to occur in the first furnace and (chemical) oxidation in the last three, so in this project the researchers are working to reproduce the conversion advancement from the last three furnaces. The advancement from the first furnace is being addressed in the parallel advanced stabilization project (see 3.C).

At the end of fiscal year (FY) 2005, the researchers demonstrated complete oxidation, starting with a "pre-stabilized" precursor, at a continuous processing line speed of 0.05 m/min. In the first half of FY 2006, the researchers continued to refine the reactor design, instrumentation, control, and processing protocols to further reduce residence time and increase the process stability. At the end of this period ~3X reduction in oxidation residence time was achieved in a single-zone reactor (one input point and one exit point for reactive species) designed for ~ 0.05 m/min line speed. By the end of FY 2006, a six-zone reactor was constructed and commissioned, enabling independent control of the chemical inputs in each zone. This reactor is designed for a line speed up to ~ 0.3 m/min in a single pass, but the transport system also readily allows repeated passes to enable higher line speeds. By the end of FY 2006, the researchers had conducted experiments at ~ 0.15 m/min line speed for a single, 3k tow.

During FY 2006, single fibers were carbonized after plasma oxidation, and their mechanical properties measured. The results are shown in Figure 1. Despite the lack of fiber tension, tow spreading, or controlled stretching during conversion, and the low-temperature carbonization, plasma-oxidized fibers were generally about 25 Msi tensile modulus (25 Msi requirement) and ≥ 0.5% ultimate tensile strain (1.0% requirement). These values exceed expectations at this stage of the investigation and inspire confidence that the required properties will be exceeded.

Interfacing the oxidation module to other modules received significant attention during this reporting period. As illustrated in Figure 2, the module interfaces may not occur at the same degree of advancement (marked by increasing density in the conventional process) for conventional and advanced-technology production lines. It was previously reported that plasma oxidation produces a lower radial oxidation gradient in the fiber. Plasma-oxidized fibers generally do not exhibit the "hollow core" structure that is common in conventionally-oxidized fibers. Because plasma-oxidized fibers have a partially oxidized core, earlier onset of carbonization may be possible (i.e., at lower fiber density), as illustrated by the uncertain location of the oxidation-carbonization interface in Figure 2. This would likely reduce the overall conversion residence time. Furthermore, the processing protocols in every module are sensitive to the prior processing history. For example, the researchers found that the oxidation protocols developed for conventionally-stabilized fibers did not work for electron-beam-stabilized fibers, and it was necessary to modify the oxidation process parameters significantly when oxidizing electron-beam-stabilized fibers. Acceptable oxidation process recipes were developed for all stabilization routes run through plasma oxidation thus far.

Plasma oxidation shows great promise. A number of principal metrics has been developed to measure forward progress, and will no doubt be refined as the researchers continue to grow their understanding of technology development and deployment. The researchers' best estimate of current status vs. target metrics is shown in "spider chart" format in Figure 3, and tabulated in Table 1.

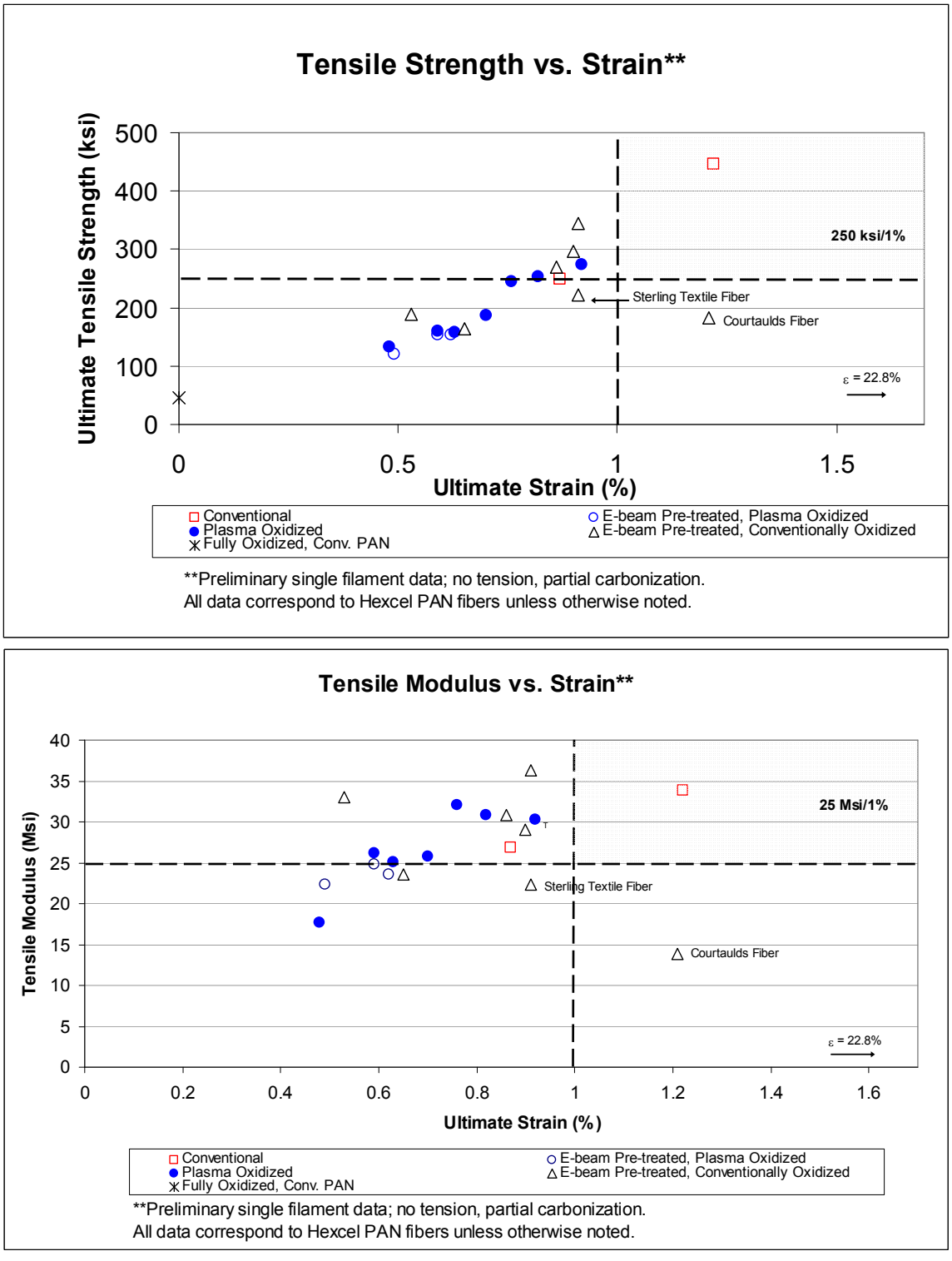

Figure 1. Mechanical properties of carbon fibers stabilized and oxidized by various routes, then conventionally carbonized at low temperature. There was no tensioning, controlled stretching, or tow spreading during conversion. Conventional data points are for thermally-shocked and thermally-ramped heating protocols.

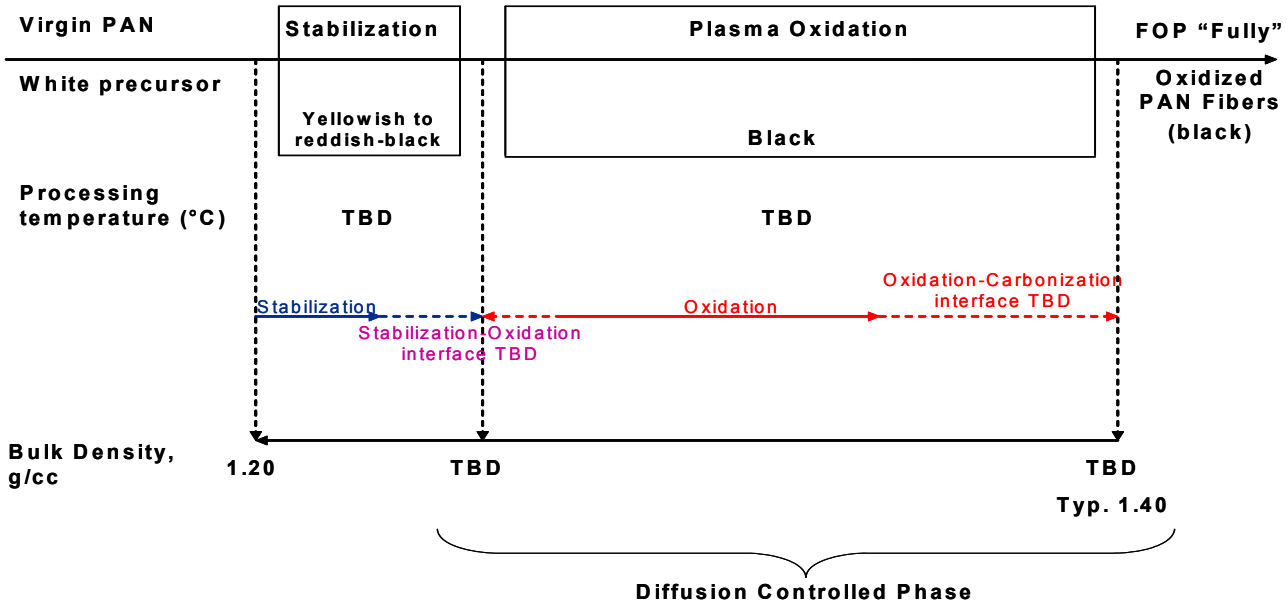

Figure 2. Schematic representation of stabilization and oxidation modules. Conventional module interfaces are represented by the vertical dotted lines. As shown by the horizontal arrows, the interface locations may change with advanced technology.

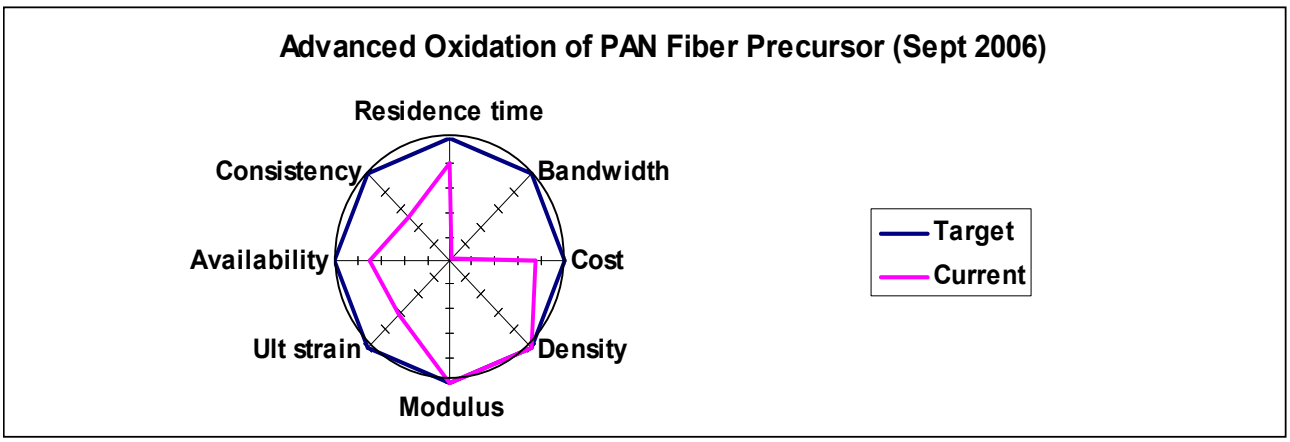

Figure 3. "Spider chart" showing current estimates of plasma oxidation metrics.

Table 1. Current estimates of plasma oxidation metrics.

Parameter	Target	Current	Conventional
Residence time	15 minutes	30 minutes	~ 90 minutes
Bandwidth	350k filaments*	3k filaments	Order 10M filaments
Cost	$0.40 ($3/lb)	~ $0.60†	~ $1.20†
Density	1.38 - 1.40	1.38	1.38 - 1.40
Modulus	25 Msi	25 Msi	30 – 35 Msi
Ultimate strain	≧1.0%	0.63%	~ 1.5%
Up time	~ 95%	~ 70%‡	~ 85%
Consistency (1 - 3*COV)*100	≥ 90%	~ 50%**	~ 90%

* Based on seven-tow pilot line
† Estimated from cost modeling reports
‡ "Rough order of magnitude" estimate

For patent protection and export control reasons, equipment and process parameters are not published, but they are periodically disclosed to the relevant program managers in oral briefings.

Future Direction

During FY 2007, the project focus will be on parametric studies with improved diagnostics and interfacing the oxidation module to the evolving stabilization module. The researchers will also carbonize plasma-oxidized fiber under more rigorous conditions (tension and temperature) to validate its mechanical properties. Oxidation-carbonization interface investigations will commence if progress on other tasks and budget permit. In future years, the project team will fully address the oxidation-carbonization interface and commence scaling studies to increase line speed, tow size, and bandwidth.

Patents and Publications

Two patents were filed, as follows: F.L. Paulauskas, T.L. White, and D.M. Sherman, "Apparatus and method for oxidation and stabilization of polymeric materials," application # 11/344,573, filed January 2006; and

F.L. Paulauskas and D.M. Sherman, "Apparatus and method for stabilization or oxidation of polymeric materials," application # 11/391,615, filed March 2006.

A paper by S.M. White, J.E. Spruiell, and F.L. Paulauskas, entitled "Fundamental Studies of Stabilization of Polyacrylonitrile Precursor, Part 1: Effects of Thermal and Environmental Treatment," was presented at the spring SAMPE conference in Long Beach, CA.

Education

The materials characterization has been conducted in partnership with the University of Tennessee's (UT's) materials science department. UT graduate students were engaged to provide characterization support to the project.

Partners

ORNL gratefully acknowledges contributions to this project by Hexcel and TohoTenax America. Both have generously provided raw materials and offered technical consultation. Additionally, technical and programmatic consultation has been provided by the Automotive Composites Consortium.

Conclusions

Plasma oxidation of PAN fibers continues to progress toward the goal of reducing the cost of carbon-fiber manufacture. To date, the researchers have reduced oxidation residence time by ~ 3X compared to conventional oxidation. Plasma-oxidized fibers were carbonized and the mechanical properties checked, with good results considering the level of rigor applied and the current stage of process development. A six-zone reactor was commissioned with higher line speed and control of

chemistry inputs to each zone independent of chemical conditions in other zones. Continuous oxidation was conducted at 0.15 m/min line speed. The plasma oxidation process was modified to enable interfacing with advanced stabilization technologies; module interfacing is expected to be a significant task for the remainder of the program. Major metrics were developed and good progress was made toward satisfying those metrics.

E. Low-Cost Carbon-Fiber Manufacturing Using Microwave Energy

Principal Investigator: Felix L. Paulauskas
Oak Ridge National Laboratory (ORNL)
Oak Ridge, TN 37831-8048
(865) 576-3785; fax: (865) 574-8257; e-mail: paulauskasfl@ornl.gov

Project Manager, Composites: C. David Warren
ORNL
P.O. Box 2008, Oak Ridge, TN 37831-6065
(865) 574-9693; fax: (865) 576-4963; e-mail: warrencd@ornl.gov

Technology Area Development Manager: Joseph A. Carpenter
(202) 586-1022; fax: (202) 586-1600; e-mail: joseph.carpenter@ee.doe.gov

Expert Technical Monitor: Philip S. Sklad
(865) 574-5069; fax: (865) 576-4963; e-mail: skladps@ornl.gov

Principal Team Members:
Timothy S. Bigelow, ORNL
Terry L. White, ORNL
Kenneth D. Yarborough, ORNL
Professor Roberto Benson, University of Tennessee

Contractor: Oak Ridge National Laboratory
Contract No.: DE-AC05-00OR22725

Objective

- Investigate and develop a microwave-assisted technical alternative to carbonize and graphitize polyacrylonitrile (PAN) based precursor.
- Prove that carbon fiber with properties suitable for use by the automotive industry can be produced inexpensively using microwave-assisted plasma (MAP) processing.
- Demonstrate that MAP processing can produce acceptably uniform properties over the length of the fiber tow.
- Show that for specified microwave input parameters, fibers with specific properties may be controllably and predictably manufactured using microwave furnaces.
- Demonstrate the economic feasibility for producing approximately 30-Msi modulus fibers at a significant cost reduction relative to those produced conventionally.

Approach

- Demonstrate the ability to deliver high fiber mass throughput by increasing line speed and tow count.
- Conduct parametric studies on the continuous carbon-fiber processing pilot unit to continually improve the system design, process parameters, and fiber properties.
- Characterize MAP-processed carbon fibers to confirm that they satisfy program requirements.
- Continually evaluate, develop, and characterize “spin-off” technology, hardware, and ideas that improve upstream or downstream processing, or facilitate more efficient utilization of fiber.

Accomplishments

- Completed MAP relocation and re-assembly of equipment.
- Restarted MAP carbonization line after relocation and re-assembly.
- Validated improved energy distribution in reactor.
- Carbonized three large tows, satisfying property requirements and a major milestone, at > 1 m/min line speed.

Future Direction

- Integrate into advanced technology, subscale carbon-fiber pilot conversion line and address remaining technical issues.
- Develop partnership(s) to commercialize the technology.

Introduction

The purpose of this project is to investigate and develop a microwave-assisted technical alternative to carbonize and partially graphitize PAN precursor. The project is to prove that carbon fiber with properties suitable for use by the automotive industry can be produced inexpensively using MAP processing. It is to be demonstrated that MAP processing can produce acceptably uniform properties over the length of the fiber tow. The project is also to show that, for specified microwave input parameters, fibers with specific properties may be controllably and predictably manufactured using microwave furnaces. Lastly, but most importantly, this project is to demonstrate the economic feasibility for producing fibers with tensile modulus ≥ 25 Msi and ultimate tensile strain ≥ 1.0% at a significant cost reduction below those produced conventionally.

Project Deliverables

At the end of this project, a continuous, multiple-tow, scalable, high-line-speed, MAP carbon-fiber prototype unit will have been developed, constructed, and tested. The MAP hardware will subsequently be integrated into an advanced-technology pilot line. Appropriate industry briefings will be conducted to facilitate commercialization of this economically-enabling technology.

Facility Relocation

In fiscal year (FY) 2005, the carbon-fiber conversion laboratory and associated equipment was moved from the Y-12 site to the ORNL main campus. Completion of equipment reassembly, installation, and checkout was completed in early FY 2006.

Processing

Changes were made to the reactor to improve its reliability and power distribution, and decrease reflected power. The improved power distribution yielded a 4X increase in the plasma volume in the reactor, enabling substantially higher line speed. Figure 1 shows the MAP system during operation, with the glow indicating good local power density along the entire reactor length. Experimental operations resumed and operational testing was performed in the first half of FY 2006. At the request of the Automotive Composites Consortium (ACC), two one-lb. spools of pre-oxidized, 50k tow were single-tow MAP carbonized and short sample lengths were delivered to ACC researchers for characterization. ORNL also characterized samples of this fiber. Physical and mechanical properties are shown in Table 1. Wide angle x-ray scattering morphology data are shown in Figure 2, and include data for Zoltek's Panex® 33 fiber, indicating that MAP-carbonized fiber morphology compares favorably with that of commercial-grade fibers.

The latter half of FY 2006 was principally dedicated to experimental operations targeted toward achieving 3-tow operation at a line speed ≥ 1 m/min. The first experiments were conducted with one tow to perform system debugging during carbonization. Then we began to push toward the milestone. We experienced several process and equipment failures as we extended the limits of our operational experience. Some of these failures, such as broken

Figure 1. Latest version of MAP reactor during operation.

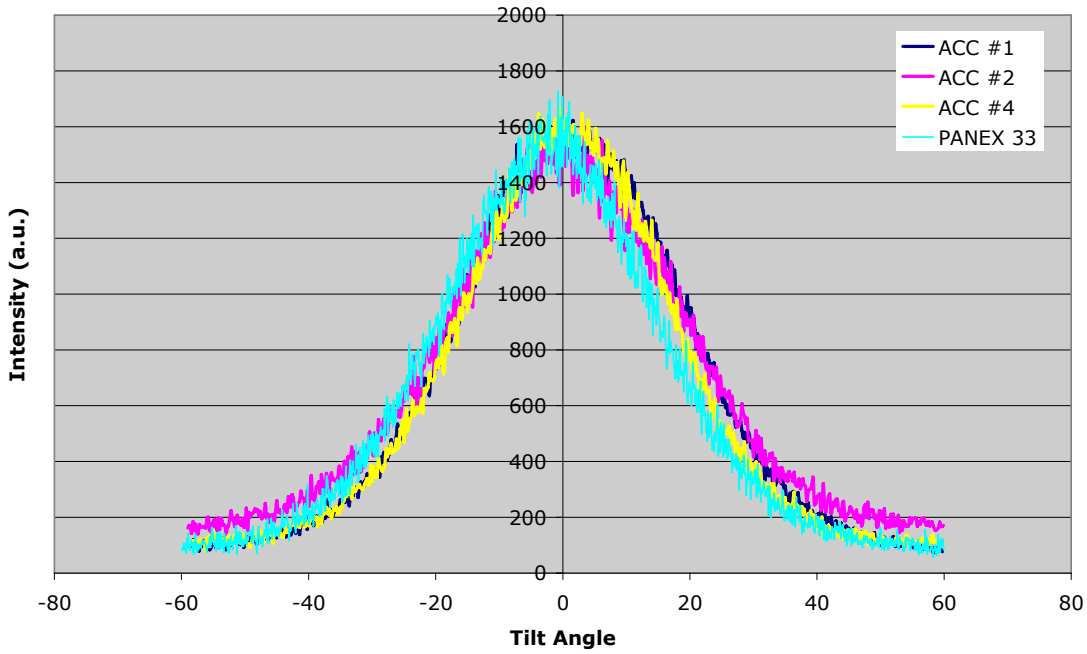

Figure 2. Crystal tilt angle in fibers delivered to ACC.

reactor tubes, caused considerable delays. Nevertheless, we were able to resolve all of the problems and ran the system with three large tows, at ~ 1.1 m/min, for a period of about one hour, in August 2006.

Mechanical properties of the finished fibers from the milestone run are shown in Table 2. These data were measured using untreated, unsized, large tows made into 50k broom straws. There is a clear pattern of changing properties from tow to tow; this is because the tows are not equidistant from the microwave inlet. This is easily resolvable by a simple geometrical reconfiguration. Otherwise, the mean properties are quite satisfactory, especially considering that the absence of surface treatment and sizing should slightly reduce the strength and strain properties. The high variability is expected at this point in the development program. Reducing the variability will be a necessary part of future work.

The current estimated status against established metrics is shown in Figure 3. These metrics are based on limited experience operating the new reactor design, and should improve with further experimentation and increased operational experience.

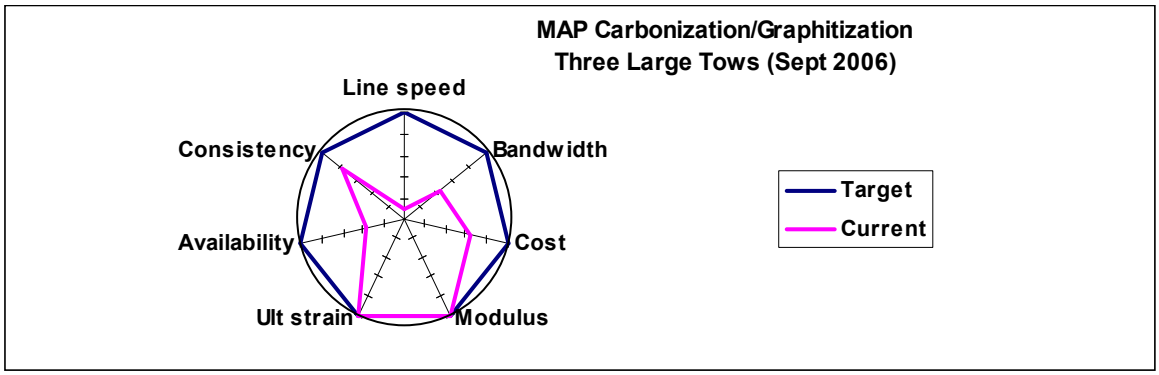

Figure 3. "Spider chart" showing estimated current status vs. metrics.

Future Direction

Remaining technical issues that need to be addressed include improved reactor sealing methods and/or atmospheric-pressure operation, reactor materials, reduced variability of finished fiber properties, as well as continued scale-up of both tow count and line speed, and integration with other conversion modules.

Patents and Publications

Patent application # 11/270,065, co-invented by T.S. Bigelow, F.L. Paulauskas, and T.L. White, and entitled "System to Continuously Produce Carbon Fiber via Microwave-Assisted Plasma Processing," was filed in November 2005. It describes the design details of the MAP carbonization system.

A paper by F.L. Paulauskas, T.L. White, and J.E. Spruiell, entitled "Structure and Properties of Carbon Fibers Produced Using Microwave-Assisted Plasma Technology, Part 2," was presented at the spring SAMPE conference in Long Beach, CA.

Education

The materials characterization has been conducted in partnership with the University of Tennessee's Materials Science Department. Graduate students provided characterization support to the project under the guidance of Professors Roberto Benson and Joseph Spruiell.

Conclusions

After relocation of the MAP carbonization system to ORNL's main campus in late FY 2005, it was re-assembled and operationally tested in early FY 2006. Checkout tests indicated a much improved power distribution and plasma volume. At their request, fiber samples were provided to ACC for evaluation. Fiber conversion experiments were conducted in the last half of FY 2006. Experiments culminated in 3-tow operation at 1 m/min line speed to produce mechanically-competent fibers. This satisfied the project's end-of-year milestone. Future work includes scale-up and resolution of a small number of key technical issues.

Table 1. Physical and mechanical properties of fibers provided to ACC.

	Production Date	Approx. Production Line Speed	Final Density (pycnom.)	Calculated Tow Area	Calculated Filament Diameter	Tow Linear Electrical Resistance	Electrical Resistivity	Mechanical Properties (based on single filament tests)			Comments
								Modulus	Ultimate Tensile Strength	Elongation at Break	
		in/min	g/cm^3	$10^{-2}cm^2$	μm	Ω/ft (10^{-2} Ω/cm)	10^{-3} Ω-cm	Msi	Ksi	%	
ACC #1	5/4/2006	36	1.8472	2.376	7.77	7.0 (22.966)	5.46	22.4	437	1.70	
ACC #2	5/9/2006	36	1.7912	2.342	7.72	4.5 (14.764)	3.46	26.0	410	1.46	
ACC #3	5/11/2006	36	1.8244	2.335	7.71	7.5 (24.606)	5.75				Due to the similarities to ACC #1, no mechanical evaluations were performed.
ACC #4	5/11/2006	36	1.7884	2.323	7.69	3.4 (11.158)	2.59	28.2	382	1.28	

Table 2. Mechanical properties of 50k tows that were MAP carbonized in 3-tow, 1 m/min milestone run.

		3 Tow MAP Single Filament Test *Broom Straw Test* *			CONVENTIONAL		Program Goals
		Tow 1	Tow 2	Tow 3	Zoltek Panex 33	Fortafil F3(C)	
Production Line Speed	(in/min)	44	44	44	-	-	-
Modulus**	(x 10^6 lb/in^2)	28.5 ***27.7 ± 0.6***	25.2 ***25.2 ± 1.5***	24.5 ***23.0 ± 0.7***	26.1	31.1	**25**
Ultimate Strength	(x 10^3 lb/in^2)	432 ***303 ± 27***	448 ***280 ± 33***	375 ***272 ± 30***	408	485	**250**
Elongation at Break	(%)	1.44 ***1.08 ± 0.10***	1.59 ***1.10 ± 0.12***	1.44 ***1.16 ± 0.14***	1.5	1.5	**1.0**
Production date:		08/17/06					

* 50k broom straw without fiber surface treatment or sizing

** modulus increases with applied load for broom-straw tests, measurements reported at ε = 0.2 – 0.6 %

F. Carbon-Fiber Systems Integration

Principal Investigator: Felix L. Paulauskas
Oak Ridge National Laboratory
P.O. Box 2008 MS 6053, Oak Ridge, TN 37831-6053
(865) 576-3785; Fax: (865) 574-8257; e-mail: paulauskasfl@ornl.gov

Project Manager, Composites: C. David Warren
Oak Ridge National Laboratory
P.O. Box 2008, Oak Ridge, TN 37831-6065
(865) 574-9693; fax: (865) 576-4963; e-mail: warrencd@ornl.gov

Technology Area Development Manager: Joseph A. Carpenter
(202) 586-1022; fax: (202) 586-1600; e-mail: joseph.carpenter@ee.doe.gov

Expert Technical Monitor: Philip S. Sklad
(865) 574-5069; fax: (865) 576-4963; e-mail: skladps@ornl.gov

Principal Team Members:
Kenneth D. Yarborough, ORNL
Timothy S. Bigelow, ORNL
Stanley C. Forrester, ORNL
C. David Warren, ORNL
Cliff Eberle, ORNL

Contractor: Oak Ridge National Laboratory
Contract No.: DE-AC05-00OR22725

Objectives

- Develop a subscale, modular test facility for demonstrating advanced carbon-fiber conversion technology.
- Integrate advanced-technology conversion modules into a functional and reliable system.
- Validate system process models and system inputs into cost analyses.
- Provide a capability for developing and testing conversion protocols for new polymer precursors.
- Provide the capability to produce small quantities of finished carbon fiber.
- Demonstrate advanced conversion technology to prospective commercialization partners.

Approach

- Procure and install a subscale, conventional carbon-fiber pilot-line.
- Construct a prototypical advanced-technology carbon-fiber line using equipment and process specifications developed in other carbon-fiber conversion projects.
- Locate the advanced technology and conventional lines adjacent to each other, highly instrument them for process characterization, and equip them with versatile fiber transport equipment.
- Develop a small tube-furnace system for developing and evaluating conversion processes for prospective precursor fibers available in quantities of a few grams or less.

Accomplishments

- Completed acceptance testing for conventional pilot-line.
- Measured conventional pilot-line emissions and determined necessary emission controls/containment for sustained operation.
- Completed partial upgrade of conventional pilot-line, constructed some equipment for future installation and designed carbon-proofing and automation systems.
- Completed installation and commenced experimental operation of microwave-assisted-plasma (MAP)-carbonization advanced-technology module.
- Commenced design and specification of a precursor evaluation system.

Future Direction

- Complete conventional pilot-line upgrades and validation, and update safety basis for sustained operation.
- Add capability to develop and evaluate conversion processes for precursor fibers available in gram quantities; evaluate alternative precursors and develop conversion protocols for selected precursors.
- Procure, install, and commission other advanced-technology modules when the processes and equipment designs are sufficiently mature.
- Perform precursor studies and parametric process studies.
- Investigate and demonstrate stable operating envelope, as well as system reliability, availability, and maintainability.
- Develop partnership(s) to commercialize the technology.

Introduction

The purpose of this project is to integrate advanced carbon-fiber technology developed in the ALM efforts. The project encompasses the acquisition and operation of conventional conversion technology for benchmarking and validation; integration of advanced-technology conversion modules into a functional system; and developing and/or evaluating conversion protocols for prospective precursors.

A small pilot facility will be designed specifically for processing tows of commercial-grade (large-tow) fiber, but will be sufficiently versatile that it can potentially process some higher-strength fibers. It will be designed to process a variety of polymer precursors; it may be adaptable to pitch precursors (this would require equipment and process modifications), but that is not a project requirement.

The heart of the pilot-scale conversion facility will be two adjacent, subscale, carbon-fiber conversion lines. One line will be based on conventional pre-treatment, conversion, and post-treatment processes and the other will embody advanced-technology processes. The facility will be highly instrumented for characterizing fiber properties and process parameters. It will also be highly modular and will be equipped with versatile tow-transport equipment so that tows can be routed through any combination of conventional- and advanced-technology conversion, pre-treatment, or post-treatment modules. The system-integration line will be capable of running a single tow or any number of tows up to its maximum capacity, which will be at least five 50k tows. The integration line may eventually be mated with upstream or downstream processes. The facility is shown schematically in Figure 1. Essential advanced-technology modules are stabilization, oxidation, and carbonization. Optional advanced-technology modules include graphitization, surface treatment, advanced instrumentation and control, and downstream processing. The integration line will use conventional pre-treatment, sizing, and fiber-transport equipment.

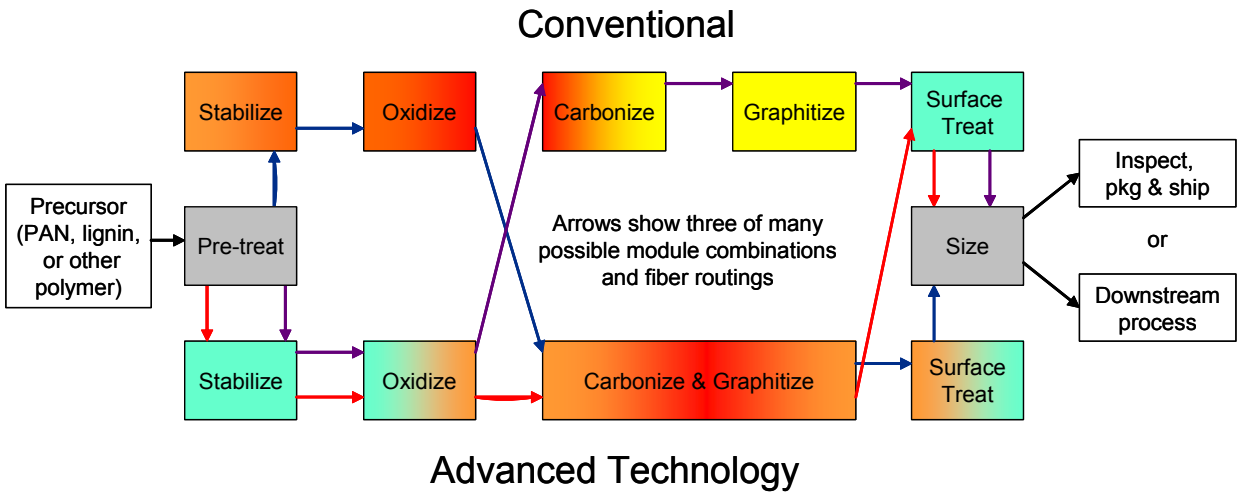

Figure 1. Schematic of carbon-fiber pilot-lines.

New precursor-development projects initially produce much smaller quantities of precursor fibers than are required by the aforementioned pilot- lines. Therefore, a tube-furnace system will be assembled for evaluating small quantities of prospective precursors and developing their conversion protocols.

Project Deliverables

At the end of this project, advanced-technology modules will have been assembled into a functional, prototypical, carbon-fiber conversion line with 5 – 10 large-tow capacity, and alternative precursor-conversion protocols will have been developed and/or evaluated. The following tasks will have been completed:

- confirm that advanced-technology conversion modules work together as a functional system;
- determine interfaces to optimize system
- cost and performance;
- determine and/or characterize system processing envelope, utility requirements, effluent streams, etc.;
- demonstrate system process control, stability, repeatability, scalability, safety, and reliability/availability/maintainability;
- investigate system fault tolerance and response;
- evaluate alternative precursor fibers and
- develop conversion protocols for selected precursors;
- scale alternative precursor tow sizes and validate their conversion at the pilot-scale; and
- validate that cost and technical targets were achieved.

Completion of these tasks should sufficiently demonstrate the advanced-technology's value, robustness, and scalability to convince an industrial partner to commercialize it.

Current Status

Conventional Pilot-Line

In fiscal year (FY) 2006, the conventional pilot-line was cleaned, serviced, and operationally tested. Acceptance test data are shown in Table 1. Acceptance data were slightly lower than the commercial-fiber baseline, but were considered quite good for a short first run; therefore, ORNL accepted ownership of the equipment. Figure 2 shows the conventional pilot-line installed at ORNL.

The previous owner of the pilot-line did not find it necessary to automate its operation. They run a 24/7 production facility, so it is quite simple for production operators to make manual adjustments to the pilot-line during its startup, operation, and shutdown. In contrast, ORNL research is a single-shift operation. Therefore, automation is necessary to enable safe and effective single-shift operation of the conventional pilot-line. Operational and environmental testing indicated the need for

Table 1. ORNL acceptance test data for conventional pilot-line.

Property	Parameter	Acceptance Run	Baseline*
Tensile modulus, Mpsi	Mean	30.4	28.7
	Standard deviation	0.90	0.71
	Design basis**	27.7	26.6
Ultimate strain, %	Mean	1.12	1.20
	Standard deviation	0.10	0.08
	Design basis	0.81	0.97
Ultimate strength, kpsi	Mean	349	364
	Standard deviation	34.3	22.0
	Design basis	246	298

* Baseline is commercial-grade fiber, tested at ORNL

** Design basis is mean less three standard deviations

Figure 2. Conventional pilot-line installation at ORNL.

modifications to the exhaust system, gas-purging system, and control system, in addition to "carbon proofing" to protect nearby electronics and high voltage electrical equipment. Modifications made in FY 2006 included:

- steam heat for tow pre-treatment (the pilot-line seller initially undersized the steam generator, so this required two iterations);
- chilled-water cooling for furnace seals at fiber inlets to and exits from the furnaces;
- addition of carbon-particulate filtration in the exhaust system; and
- improved purge-gas manifolding.

The project team designed and constructed or acquired, for future installation,

- sizing squeeze rolls,
- sizing dryer,
- ozone generator for ozone surface treatment, and
- ozone monitoring equipment.

The project team initiated carbon-proofing, as well as upgrades to the purge-gas delivery system, control system, and exhaust system; the necessary hardware for these modifications will be procured and installed in FY 2007. High-speed winder acquisition was planned to commence in FY 2006, however, budget reductions delayed acquisition by a year. Winder specifications were developed in FY 2006. The microwave-assisted plasma (MAP) carbonization module (see 3.E) was prepared for integration with other modules. Advanced oxidation parameters were found to depend on the advanced stabilization route (see 3.C). Therefore, the advanced stabilization-oxidation interface, and the respective process parameters were experimentally investigated (see 3.D).

Advanced-Technology Pilot-Line

The MAP carbonization module is the base module for the advanced-technology integration line. Other modules will be added to it later. It is now in place and operational. The MAP carbonization milestone of three-tow operation at 1 m/min was satisfied in FY2006; hence, the MAP unit is now ready for integration. The project team will continue scaling and maturing the MAP carbonization technology under integration and/or other future projects.

Several high-speed winders and tensioners are needed to support operation at the bandwidth (number of tows) and range of speeds targeted for the conventional and advanced-technology lines. Specifications have been drafted, but the capital procurement is scheduled for FY 2007 and beyond, per funding availability.

Metrics have been established for the systems-integration project. They are shown in "spider chart" form in Figure 3. Current status, as expected very early in the project, is well off the target for most metrics.

Precursor Evaluation System

Due to its size, the aforementioned pilot facility requires ≥ 1k tows, preferably many meters long. The tensioning system is not sufficiently precise to handle tows smaller than 1k without breaking them. Startup time for the conventional pilot-line graphitization furnace is about 20 hours, so restringing and restarting after tow breakage requires many hours. This is incompatible with the

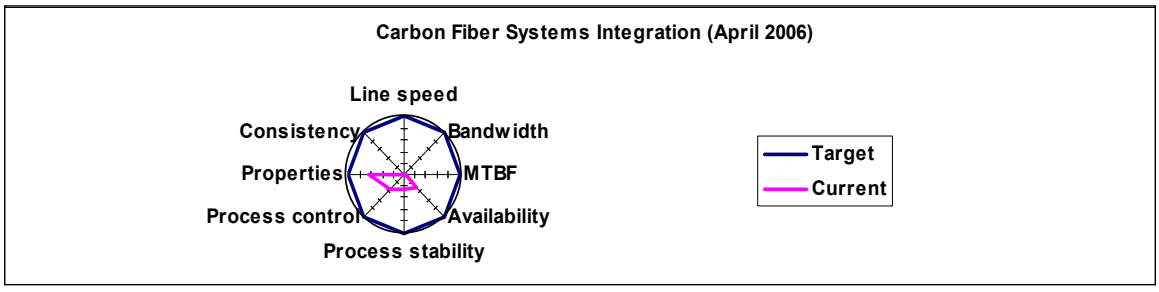

Figure 3. "Spider chart" showing carbon-fiber systems-integration metrics and estimated current status.

need for inexpensive, fast-turnaround, precursor evaluations. New precursor-development projects need many intermittent trials on very small tows, as they initially extrude one or a few filaments in short lengths for initial testing. The conventional pilot-line is not amenable to this kind of operation; therefore, a compact tube-furnace system with precision tensioners will be assembled for evaluating prospective precursors and developing their conversion protocols. The tube-furnace system will have rapid start-up/shutdown capabilities and will be capable of heat-treating short lengths of single filaments or any number of filaments up to approximately 3k tow size. Controlled tension can be applied to tows larger than approximately 10 - 20 filaments. Smaller tows can be "restrained" to provide some tension. Short fiber lengths can be readily transported through the system on trays or similar compact carriers. During FY 2006, the researchers commenced designing and specifying the tube-furnace system. It is expected to become operational in the second quarter of FY 2007.

Future Direction

During FY 2007, conventional pilot-line modifications and the advanced-technology pilot-line design and procurement will continue. The conventional and advanced-technology pilot-lines will be carbon-proofed (to better protect proximate electronic and high-voltage equipment), and conventional pilot-line operation will be automated. The researchers will investigate methods for resolving sealing and materials issues on the MAP carbonization advanced-technology module. Researchers plan to commence investigating the oxidation-carbonization interface, specifically addressing whether it is possible to carbonize fibers at a reduced oxidation level. Major procurements will include special fiber-handling equipment (a capital procurement) for the conventional and advanced-technology pilot-lines; furnaces, controllers, and transporters/tensioners for the precursor-evaluation system; and instruments that can be used for *in-situ*, real-time measurement of temperatures, gas compositions, etc. at various points in the advanced conversion processes. If lignin precursor fibers become available, a lignin-conversion process will be developed. If work is initiated on textile-based precursors, the researchers will optimize the textile-PAN conversion protocol; convert textile-based materials in the conventional pilot-line; and distribute finished textile-PAN tows to the three domestic automotive OEMs.

Conclusions

The development of a "carbon-fiber systems-integration" facility for testing and demonstrating new carbon-fiber manufacturing technology is underway. A conventional carbon-fiber pilot-line has been installed and tested. Modifications are underway to enable sustained, automated operation of the conventional pilot-line. An advanced-technology pilot-line will be constructed next to the conventional pilot-line, with capability to utilize any combination of conventional and advanced-conversion processes provided by the two adjacent lines. The MAP carbonization module is the first advanced-technology module and has been installed adjacent to the conventional pilot-line. MAP carbonization scaling is underway to increase line speed and bandwidth. Advanced stabilization and oxidation projects are developing modules that will be installed in the advanced-technology pilot-line in future years. A precursor evaluation system is being developed to evaluate conversion protocols for lignin and other alternative precursor fibers. Metrics have been established against which progress toward system integration and commercialization can be evaluated.

Presentations/Patents/Publications

None.

4. POLYMER COMPOSITES R&D

A. Development of Manufacturing Methods for Fiber Preforms (ACC 040[i])

Principal Investigator: Patrick Blanchard
Ford Motor Company, Research and Innovation Center
P.O. Box 2053, MD 3135 RIC, Dearborn, MI 48121-2053
(313) 390-6230; fax: (313) 390-0514; e-mail: pblanch3@ford.com

Principal Investigator: Jeff Dahl
Ford Motor Company, Research and Innovation Center
P.O. Box 2053, MD 3135 RIC, Dearborn, MI 48121-2053
(313) 845-1039; fax: (313) 390-0514; e-mail: jdahl@ford.com

Project Manager: C. David Warren
Oak Ridge National Laboratory (ORNL)
P.O. Box 2009, Oak Ridge, TN 37831-8050
(865) 574-9693; fax: (865) 574-0740; e-mail: warrencd@ornl.gov

Technology Area Development Manager: Joseph A. Carpenter
(202) 586-1022; fax: (202) 586-1600; e-mail: joseph.carpenter@ee.doe.gov

Expert Technical Monitor: Philip S. Sklad
(865) 574-5069; fax: (865) 576-4963; e-mail: skladps@ornl.gov

---

Contractor: U.S. Automotive Materials Partnership
Contract No.: DE-FC05-95OR22910

Objective

- Develop and demonstrate new fiber-preforming processes to decrease cost, increase manufacturing rates and improve reproducibility of large preforms for composite molding.
- Develop the thermoplastic programmable powdered preform process (TP-P4) concept as a high-volume composite manufacturing process for thermoplastic composite materials.
- Develop low-cost carbon-fiber rovings with reduced individual bundle size.

Approach

- Investigate materials, process equipment, and tooling technology to further reduce the cost and enhance the quality of chopped-fiber preforms.
- Explore the extension of automated preforming technology to make preforms with a thermoplastic matrix.
- Investigate heating methods for thermoplastic composite blanks manufactured using the TP-P4 process.
- Perform cost analysis to determine the economic benefits of the TP-P4 process technology.

Accomplishments

- Completed preliminary processing studies to establish feasibility of the TP-P4 process.
- Completed a business assessment of the TP-P4 process technology.

Future Direction

- Further develop P4 process technology to accommodate rapid cycle times in support of high-volume production.
- Continue cost modeling of process concepts to determine business rationale for migration of process technology to the OEM supply base.

Introduction

This project has focused on the development of the P4 process, a fully-automated robotic preforming process. A prototype, two-station manufacturing cell was designed, fabricated and installed at the National Composites Center (NCC) in Kettering, Ohio. This equipment is currently being utilized to support preforming and material development efforts within the Automotive Composites Consortium (ACC).

During this reporting period, the facilities at NCC were used primarily in support of new process developments for a derivative of the conventional P4 process. The new process makes use of commingled yarn for subsequent hot-flow compression molding. Preliminary investigations were conducted to determine the feasibility of the process. The sections that follow, describe the results from these studies.

Thermoplastic P4 (TP-P4)

Equipment Capability: The existing P4 processing equipment, originally designed for preforming of glass fiber materials, has been adapted to enable manufacture of thermoplastic composites. However, the capability of this equipment is limited in terms of cycle time and hence throughput capacity. Regardless of these limitations, processing parameters have been developed to allow manufacture of components in the order of 700 mm x 700 mm, while maintaining minimal process interruptions. Process yield, measured by part weight, is currently 1500 g/min, although attempts have been made to increase this to 5000g/min. However, from a commercial perspective the low material output would ultimately lead to increased capital investment for high-volume production. By way of example, for a vehicle liftgate panel, the cell will currently support 1 part every 7.5 minutes. If the target cycle time for this component is 45 s, this translates to either 10 lines of process equipment or a ten-fold increase in material throughput capability for a single cell. This prompted a re-design of the cell with the objective of accommodating the higher throughput capabilities.

As part of the design process, a manufacturing cell layout was developed for production of the liftgate inner panel described above. Process simulation software was used to account for the dynamics of the process and resultant cycle times. The surface area of the liftgate was calculated as 1.5 m^2. All analyses were conducted assuming a final part thickness of 3.0 mm with an areal density of 4500 g/m^2.

From the process simulation studies, the following conclusions can be made:

- For a 1.5 m^2 part surface area, a 45 s cycle time is achievable from a single cell.
- Material throughput for the TP-P4 cell would need to be capable of 20 kg/min to meet the target cycle time.

Based upon these results, a more detailed cell specification has been developed. Several equipment manufacturers have also been contacted regarding the feasibility of designing and building a unit to meet these specifications.

TP-P4 Tooling*:* Experimental studies to date have been conducted on an existing flat-panel tool (700 mm x 700 mm). The size of this tooling limits the size of parts used for basic material characterization and process development. Therefore, a new tool, measuring 1500 mm x 2250 mm, has been designed for larger components. This tool will allow development of thermoplastic composite components such as the liftgate inner panel. It will also be used for extended testing of TP-P4 manufacturing cell to validate process robustness. Fabrication of this was completed in quarter four (Q4) of 2006.

TP-P4 Process Cost Modeling: To evaluate the economic merits of the TP-P4 process technology, a cost modeling contract was awarded to the EPFL in Lausanne Switzerland. The statement of work developed included a comparison with competing composites-based processes. In total, seven different competing technologies were compared to the TP-P4 option and its derivatives. Table 1 provides a summary of the conventional process technologies that were compared to a proposed TP-P4 manufacturing cell. In parallel to identification of competing process technology, target applications were selected in order to establish the complete manufacturing process. Two components were selected: a liftgate inner, based upon a concept developed for a General Motors (GM) sport utility vehicle; and a rear seat frame from a Chrysler minivan. It was anticipated that the size and complexity differences for these parts would yield an insight into the suitability of the TP-P4 process for a broad range of components. However, this report provides a summary restricted to the liftgate analysis as the seat-back modeling remains on-going. A computer-assisted design (CAD) rendering of the liftgate geometry is shown in Figure 1.

Table 1. Process comparison used to evaluate the thermoplastic P4 process.

Conventional Composites Technology
Direct LFT Injection
Indirect LFT Injection
Direct LFT Compression
GMT Compression
GMTex compression
Hybrids
Direct LFT Compression + fabric over-molding
Direct LFT Injection + fabric over molding

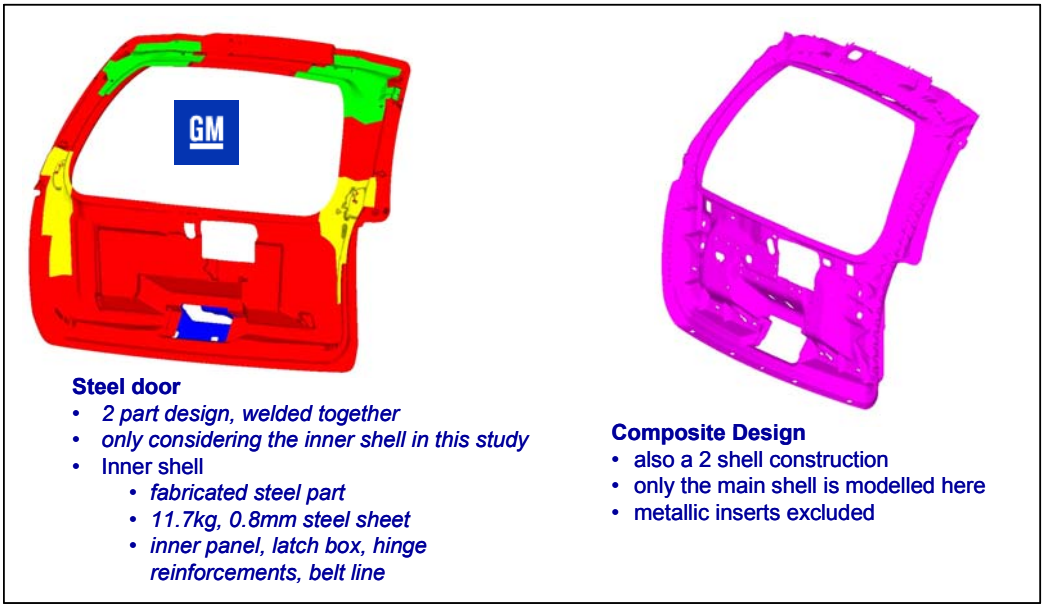

Figure 1. CAD rendering of steel liftgate and composite concept.

Based upon the intrinsic material properties and individual process characteristics, mass assumptions were developed for the different composite options. As material price is typically a major contributor to overall piece price, considerable effort was made to assign realistic targets for each process. However, as the scope of the cost analysis was limited to a screening study, no structural analyses were performed. For example, the part manufactured in glass mat thermoplastic (GMT) was assumed to weigh 6.6 kg, whereas further weight reductions were forecast based upon the increased fiber loading (60%wt vs. 40%wt) offered by the TP-P4 manufacturing route. This resulted in an assumed part mass of 5.1 kg. Table 2 also describes the effect of hybrid processing on part mass. In these cases, processes were combined to allow over-molding of structural composite inserts. The columns labeled "upper" and "lower" indicate the limits applied to sensitivity analysis; however, this detail is not included in this report. Once the process options and part dimensions had been defined, process layouts were developed for each cost analysis.

Table 2. Dimension and mass assumptions of liftgate designs.

Lift gate			
part X,Y, Z (for machine bed size etc)	1.5m width, 1.1m high, 250mm deep		
part projected area (for tonnage calculations)			
max part thickness	5mm		
min part thickness	3mm, 2.5mm ribs		
ribs	2.5mm		

Weight assumptions, (kg)	baseline	upper	lower
Part mass in steel	11.7		
Part mass in GMT	6.6	6.7	6.5
Part mass in GMTex 4-1/GMT	6.2	6.6	6.0
Part mass in TP-P4 random 60% gf	5.1	5.2	5.0
Part mass in TP-P4 random 60% gf + GF/PP 40 LFT hybrid	5.1	5.8	5.1
Part mass in TP-P4 random 40% gf	6.6	6.7	6.4
Part mass in GF/PP 50 celestran (IM)	6.4	6.6	6.3
Part mass in GF/PP 40 direct LFT	6.6	6.7	6.5
Part mass in Tw-40 indirect	6.6	6.7	6.5
Part mass in Twintex 4/1 fabric + GF/PP 40 LFT hybrid	5.0	5.1	4.9

In summary, the analysis suggests that for large components that do not require the strength and modulus benefits of TP-P4, either of the direct-feed processes will offer a cost advantage. However, the potential weight savings may still remains a key consideration. In cases where typical direct long-fiber thermoplastic (D-LFT) injection or compression properties are insufficient, the TP-P4 process can be combined as a hybrid process to offer a low-cost and lightweight solution. Furthermore, for structural parts that typically require GMT materials, the TP-P4 option is considered a cheaper and lighter alternative.

It should be noted, that while the above analysis justifies continued research into TP-P4 process development, several basic process assumptions need to be demonstrated. In particular, technical feasibility of the high-throughput TP-P4 cell has still to be proven. Furthermore, final selection of an appropriate heating method for TP-P4 materials is still outstanding. Therefore, while the future TP-P4 process capabilities that were included in the model are considered realistic, considerable technical work is required to develop a robust and repeatable process.

TP-P4 Materials Characterization: A series of specimens was extracted from 18" x 18" flat plaques manufactured using the TP-P4 process. The main objective of this exercise was to establish baseline performance as a reference to determine future improvements in materials performance.

Tensile Specimens: Procedures listed in ASTM D638 were followed in fabricating the tensile specimens, which were 216 mm (8.5 inch) in length and 19mm (.75 inch) wide. The "neck down" region was 12.7 mm (.50 inch) wide at the center. Specimens were sectioned by using a diamond-blade

band saw, while the "necked down" region was milled using a high-speed router. Fine filling was used to reduce potential stress risers that could influence specimen data. All tensile specimens were tested on an MTS Sintech 30/G load frame with a RenewTm interface Works 4.0 data acquisition software. A 30,000 lb. load cell was calibrated and used in conjunction with a two-inch longitudinal extensometer.

Compression Specimens: Procedures listed in the ASTM D3410 were followed in fabricating the compression specimens, which were 127 mm (5.0 inch) in length and 12.7 mm (.5 inch) wide. The specimens were sectioned using a diamond-blade band saw. Fine filling was used to reduce potential stress risers that could influence specimen data. All compression specimens were tested on an MTS 810 load frame and microconsole with Test Works 2.1 data acquisition software. A 10,000 lb. load-cell cartridge was used in conjunction with a 5.0-inch-stroke cartridge. The Ford Motor Company version of the standard IITRI lock-down compression fixture was used for testing.

Flexural Specimens: Procedures listed in the ASTM D790 were followed in fabricating flexural test specimens, which were 127 mm (5.0 inch) in length and 25 mm (1.0 inch) wide. The specimens were sectioned using a diamond-blade saw. Fine filling was used to reduce potential stress risers that could influence specimen data.

Results

Property measurements of TP-P4 blanks are shown in Figures 3 to 7. These values appear to be in line with other commercial alternatives. However, a further series of tests will be performed to determine any additional benefit to the retention of fiber length in process blanks. At present, blanks have been processed using 75-mm-long fibers, which is an order of magnitude higher than other compression-molding processes.

TP-P4 Preheating Studies

The TP-P4 process can result in a lofted composite charge that exhibits some rigidity and handling strength. However, under these circumstances, the heating cycle within the TP-P4 process is often insufficient to create good wetting of the fiber reinforcement bundles and overall charge consolidation. This presents a new challenge regarding establishing a suitable means of heating the TP-P4 material prior to molding. Hence, a series of investigations was conducted on materials processed under a wide variety of process conditions using infrared (IR), forced-air and convection ovens.

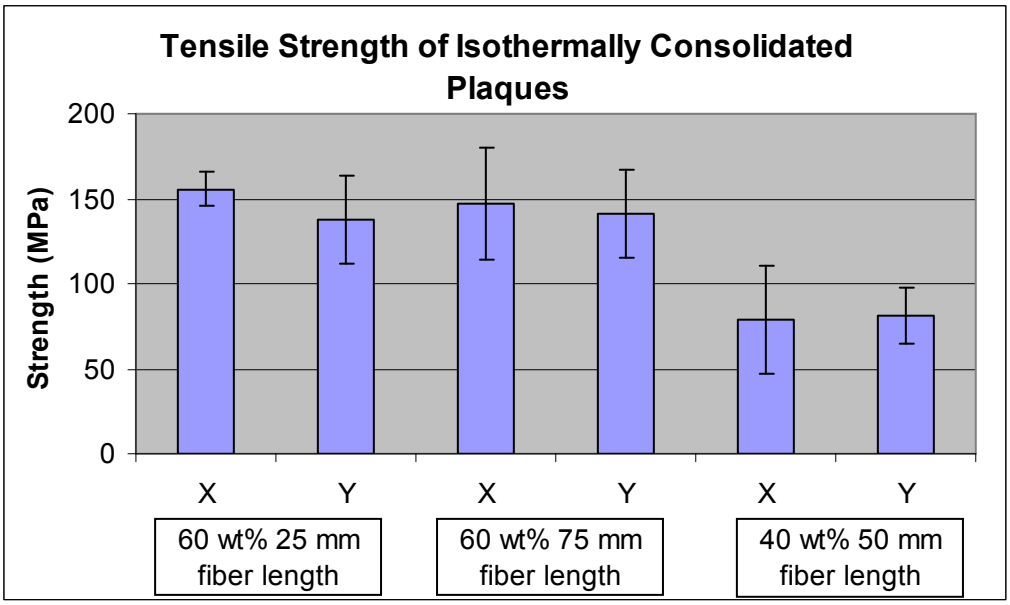

Figure 3. Tensile test results for isothermally-consolidated TP-P4 blanks.

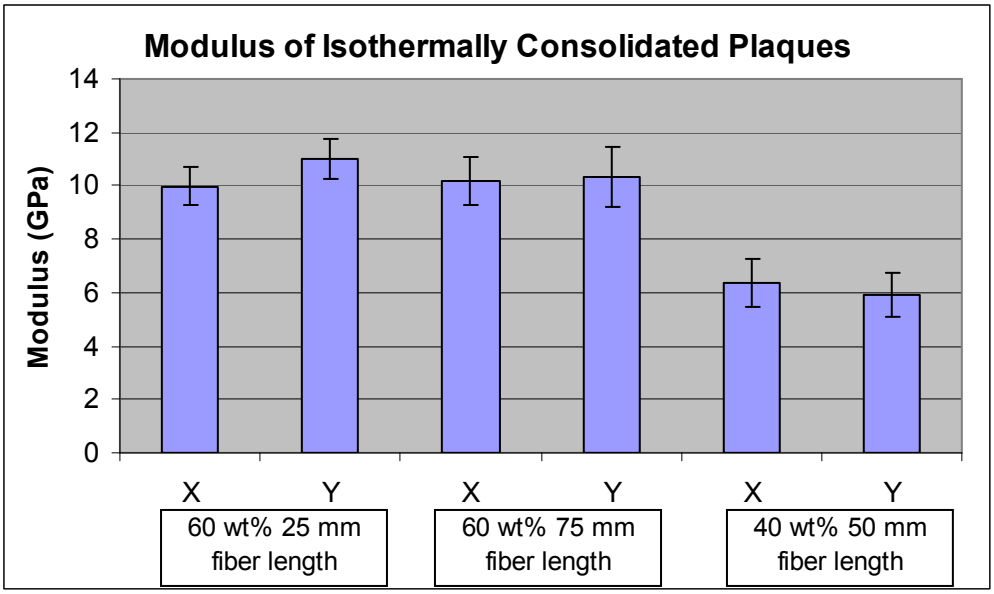

Figure 4. Tensile modulus results for isothermally-consolidated TP-P4 blanks.

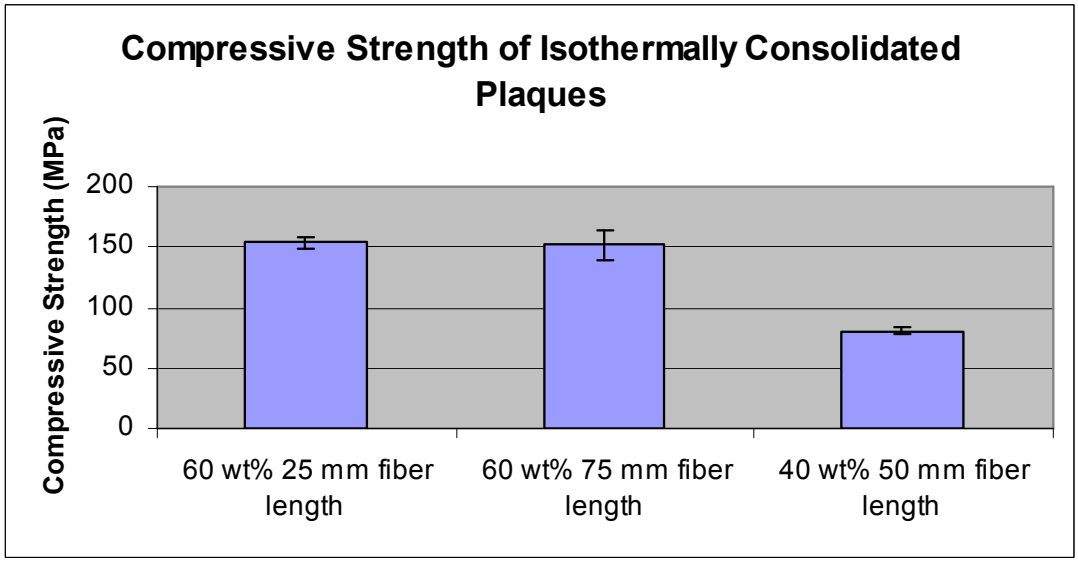

Figure 5. Compressive strength test results for isothermally-consolidated TP-P4 blanks.

The main objective of the study was to determine the most appropriate material form and heating method for TP-P4 materials processed under different conditions.

Experimental Methods: Heating studies were performed on TP-P4 materials processed to a range of consolidation levels.

TP-P4 blanks of ~50% void content were heated with an IR oven to determine optimum time and temperature profiles for future design-of-experiment (DoE) studies. The heated samples were nominally 100 mm wide and 381 mm long. Low-porosity samples (< 5%) of thickness 3.5, 4, 5 and 6 mm were also examined. The samples were fitted with three J-type thermocouples positioned approximately at the center of thickness. Temperature histories were recorded

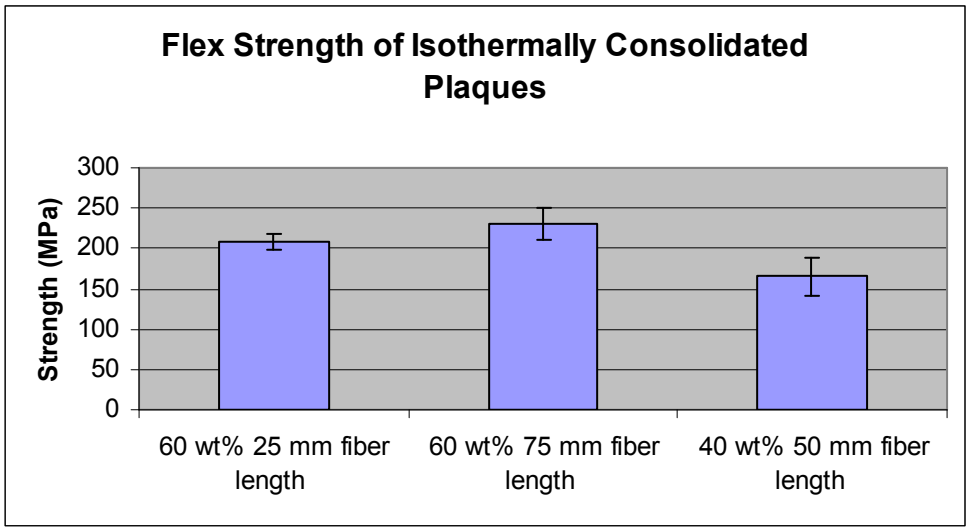

Figure 6. Flexural strength test results for isothermally-consolidated TP-P4 blanks.

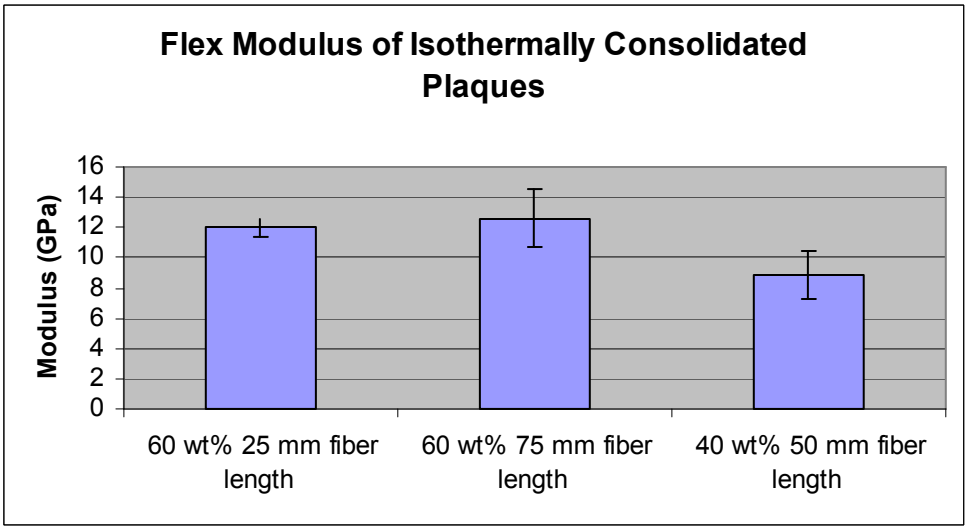

Figure 7. Flexural modulus test results for isothermally-consolidated TP-P4 blanks.

during heating trials to determine the heat-up rates of materials in either a consolidated or unconsolidated state.

Sample Manufacture: The TP-P4 materials were comprised of 60% wt. fiberglass and 40% wt. polypropylene (PP), and manufactured using equipment installed at the NCC.

Preheating Options: Several preheating options were identified such as a free convection, infrared (IR) and forced-air convection.

Free-convection studies were performed using a Fisher Scientific- ISOTEMP® 800 Series, model 13-247-838F (medium) oven. It provides a temperature range from 50°C to 325°C in 1°C intervals. A small ventilator made the temperature relatively uniform in the oven, but did not give extensive air circulation.

The RR-heating studies were performed using a Krelus IR-heating oven with six upper zones and six lower zones, each individually controlled. Each zone contains 2kW, 9.1A IR medium wave units. The forced-air preheating study was performed with an Ernst Reinhardt GmbH, forced-air convection oven

based at the EPFL. The following parameters were used:
convection: 45m^3/min
2m^3 operating volume
oscillating tray (for more homogeneous preheating)
oven set temperature: 230°C

Results and Discussion

For materials consolidated to a porosity level of approximately 43%, rapid heating of the material could be achieved. Hence, there appeared to be no further benefit to creating material blanks of increased consolidation. However, unconsolidated blanks were more difficult to heat as highlighted in Figure 8.

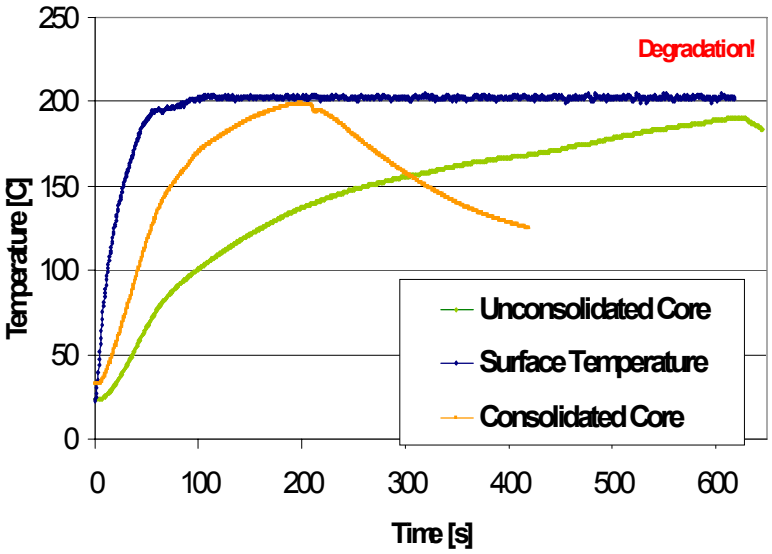

Figure 8. Comparison of core temperatures for unconsolidated and consolidated 3.5 mm blank (202°C setpoint).

Although a free-convection oven is a low-flux density method of heating, as opposed to IR heating, degradation was observed in all TP-P4 samples tested in this oven because of the

extended heating times required. Comparisons between unconsolidated and consolidated heating curves in a free-convection oven can be seen in Figure 9.

Figures 10 and 11 show that rapid heating can be achieved using the forced-air oven. For these tests, 2 mm blanks were heated to 180°C within 2.1 to 2.3 minutes whether using consolidated or unconsolidated blanks. However, as Figure 12 and 13 indicate, with thicker blanks such as 6 mm, the differences in heating times are significant between unconsolidated and consolidated blanks. The cores of unconsolidated 6 mm blanks heated to 180°C in 16.5 minutes compared to 14.8 minutes for consolidated blanks. In summary, the difference between heating times for cores of blanks thicker than 4 mm are greater than those of thinner blanks. However, the likelihood of needing to heat blanks of such thickness is remote. The results do prove that thinner blanks, such as 2 mm, can be heated in forced-air ovens without first being consolidated. Such practice would eliminate the need for any consolidation equipment and associated costs.

Conclusions

In conclusion, the forced-air convection oven provides the most optimum heating environment to heat TP-P4 blanks. This conclusion is based upon reduced material degradation while maintaining rapid heating times. Although IR ovens are commonly used to preheat thermoplastic material blanks, there is increasing interest and use of forced-air and impingement ovens as their surface flux levels are much lower and they exhibit increased uniformity of heat. In practice, it may be optimum to heat TP-P4 materials in a combination IR/forced-air

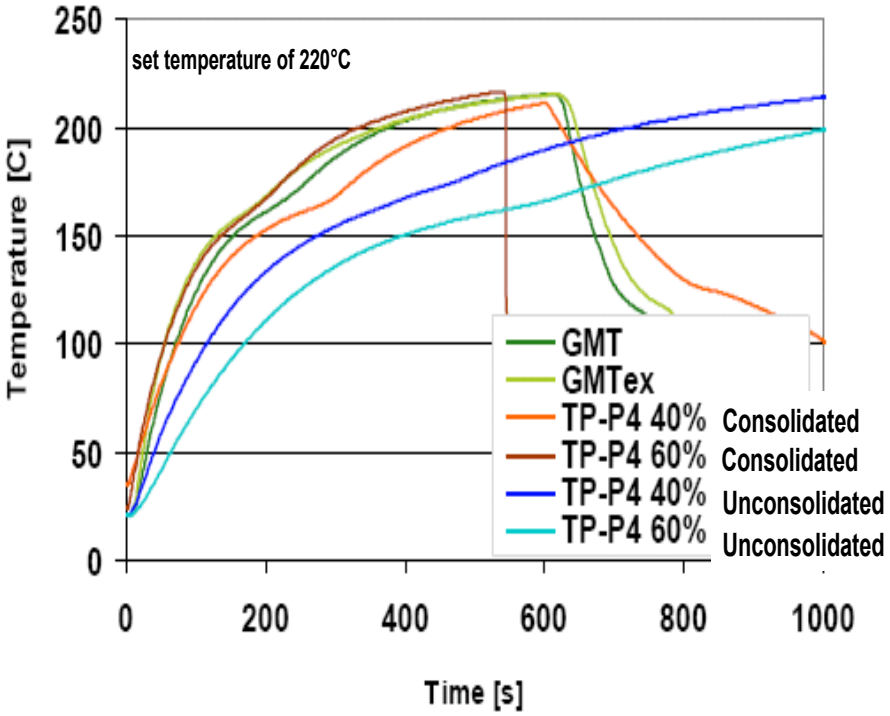

Figure 9. Temperature histories of unconsolidated and consolidated blanks heated in a free-convection oven (standard GMT is included as a comparison).

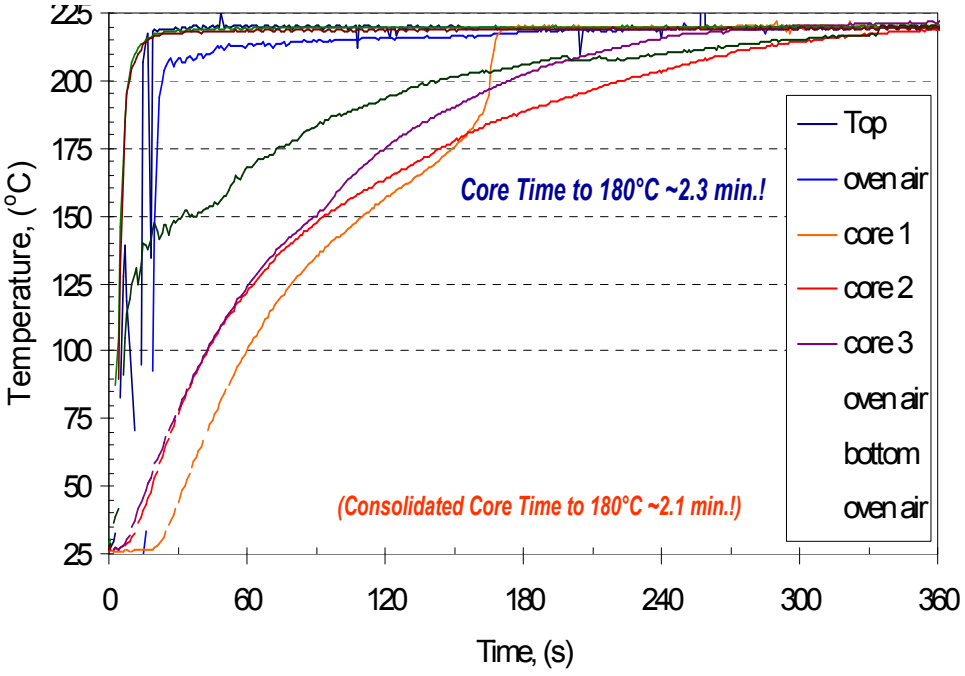

Figure 10. Temperature histories for unconsolidated 2 mm sample (forced-air oven, 220°C, 50% fan speed).

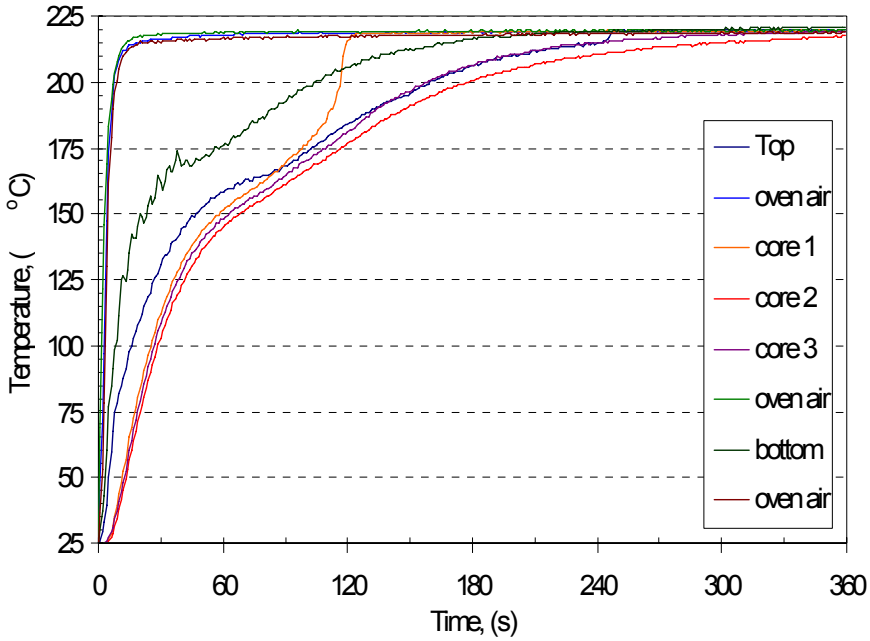

Figure 11. Temperature histories for consolidated 2 mm sample (forced-air oven, 220°C, 50% fan speed).

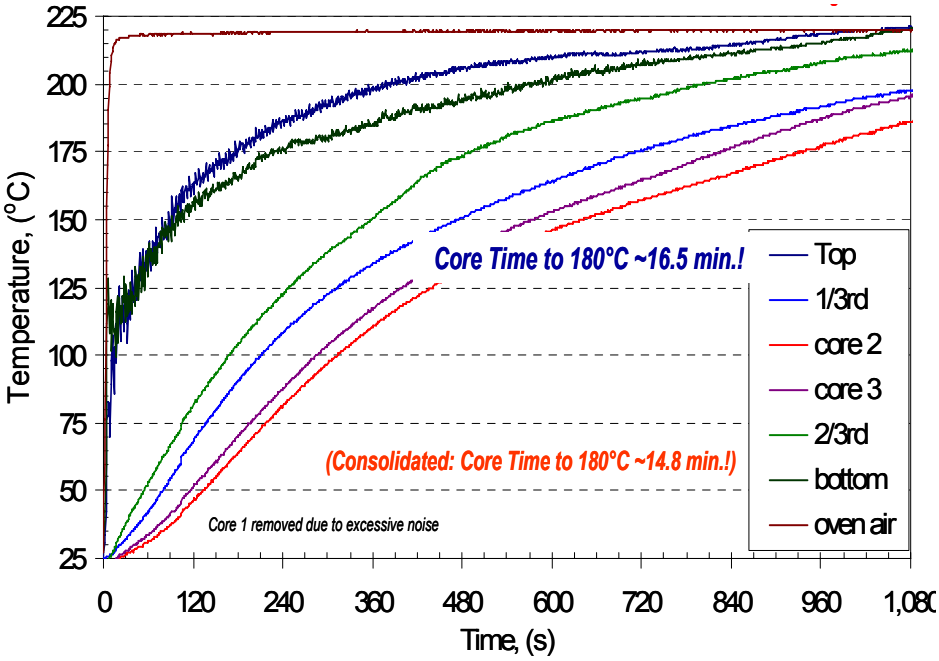

Figure 12. Temperature histories for unconsolidated 6 mm sample (forced-air oven, 220°C, 50% fan speed).

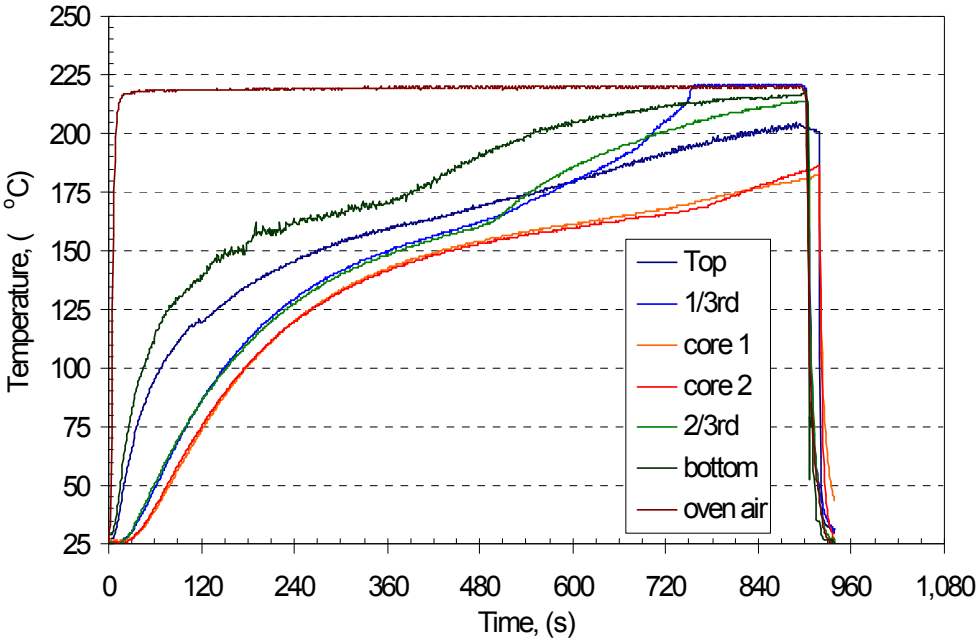

Figure 13. Temperature histories for consolidated 6 mm sample (forced-air oven, 220°C, 50% fan speed).

oven, such as an indexing conveyor type oven with an initial IR-heating station which then indexes the blank into a pressure-differential type forced-air oven until the core temperature is achieved.

Free-convection ovens are not feasible for production of unconsolidated or consolidated blanks due to the excessive time at temperature causing significant degradation to the surfaces before the core reached a set temperature.

If an upper limit of blank thickness is set to 2 mm thickness or less, it appears that a forced-air oven works well and that the level of blank consolidation does not inhibit heating rates.

Carbon-Fiber Roving Development - Toho Tenax Carbon Fibers

The research program with Toho Tenax to develop carbon fiber rovings more amenable to the P4 preforming process has been terminated. Toho Tenax was unwilling to continue with this research program.

[i] Denotes project 040 of the Automotive Composites Consortium (ACC), one of the formal consortia of the United States Council for Automotive Research (USCAR), set up by the "Big Three" traditionally USA-based automakers to conduct joint pre-competitive research and development.

B. Development of Next-Generation Programmable Preforming Process

Principal Investigator: Robert E. Norris, Jr.
Oak Ridge National Laboratory (ORNL)
P.O. Box 2008, Oak Ridge, TN 37831-6053
(865) 576-1179; fax (865)-574-8257; e-mail: norrisrejr@ornl.gov

Field Project Manager, Composites: C. David Warren
ORNL
P.O. Box 2008, Oak Ridge, TN 37831-6065
(865) 574-9693; fax: (865) 576-4963; e-mail: warrencd@ornl.gov

Technology Area Development Manager: Joseph A. Carpenter
(202) 586-1022; fax: (202) 586-1600; e-mail: joseph.carpenter@ee.doe.gov

Expert Technical Monitor: Philip S. Sklad
(865) 574-5069; fax: (865) 576-4963; e-mail: skladps@ornl.gov

---

Contractor: Oak Ridge National Laboratory
Contract No.: DE-AC05-00OR22725

Objectives

- Develop the next-generation of low-cost fiber-preforming technologies based on programmable, robotic-controlled, directed chopped-fiber processes for the application of
  - low-cost carbon fiber
  - reinforced thermoplastics
  - hybrid glass-carbon
- Develop supporting technologies required to successfully implement the process technology including
  - preform characterization (e.g., permeability, areal density uniformity)
  - perform-process modeling for process effects analysis
- Conduct parametric process studies to investigate fundamental process effects and establish process-property relationships.
- Conduct requisite molding investigations—experimental and through modeling—to elucidate relationship between preform characteristics and moldability.

Approach

- Establish a base-research, programmable, robotic preforming system for which advanced capabilities (e.g., new chopper designs) can be developed and evaluated.
- Establish a highly-instrumented and controlled research molding capability to isolate and investigate the effects of process variables on moldability and mechanical properties.
- Develop new severing technology to facilitate the implementation of low-cost-carbon-reinforced thermoplastics, and hybrid glass-carbon products.
- Benchmark and implement process modeling into experimental work to guide parameter selection and to provide tools for longer-term implementation of preforming and related technologies.

Accomplishments

- Completed construction and installation in ORNL composite laboratories of a 750-ton, intelligent-leveling research press and general-purpose experimental mold to support evaluation of preforming process advances as reflected in actual composite articles. Completion of acceptance testing and installation of this equipment fulfilled an ORNL/DOE "Critical Outcome" milestone for this fiscal year (FY).
- Completed required laboratory floor structure and utilities up-grades to accommodate the equipment as described above.
- Completed checkout and began implementation of radial-flow permeability measurement system and associated controls and data acquisition systems specifically configured for the ORNL-developed sensor system. Demonstrated consistency and repeatability of measurements that compare with literature values.
- Initiated actual experimentation to validate earlier estimated requirements to demonstrate feasibility of laser severing technology. Although initial experiments were impeded by apparent surface ionization of the carbon fiber using the parameters necessary for severing at the maximum rates envisioned, severing was demonstrated using both pulsed- and continuous-waveform laser exposure at less aggressive rates.
- Previously-developed general modeling approach was expanded to include a new algorithm that made possible quick simulation of tens of thousands of fibers, new algorithms for fast void discovery, an initial model for shaped substrate, and an initial model for mat compression.
- Obtained various combinations of fibers and binders to establish materials baselines for comparison with previous and ongoing programmable powdered perform process (P4) work (see 4.A) being conducted by the Automotive Composites Consortium (ACC) and to be used in establishing glass baseline for related permeability-test implementation.
- Initiated chopping experiments with glass tows fully impregnated with polypropylene (PP) using the Directed Reinforced Fiber Technology (DRIFT®) process and TwinTex commingled glass and PP fibers.

Future Direction

- Complete integration of injection/compression press and general purpose mold (procured during FY 2006) with associated heating system (deferred until FY 2007 due to budget reductions). Evaluate programmatic benefits versus costs and risks of refurbishing an existing injection machine for Structural Reaction Injection Molding (SRIM) to complement current focus on other molding technologies and implement if justified.
- Conduct permeability measurements on preforms made by simulated split-tow products of varying tow size.
- Evaluate preform process models relative to physical preform characteristics and expand model capability as resources permit.
- Initiate preforming experiments utilizing hybrid combinations of carbon and glass fiber to evaluate potential advantages of combining these materials to achieve performance and/or economic benefits. Continue preforming studies with various product forms incorporating reinforcement and thermoplastic-matrix materials "co-processed" through the preforming machine including forms with low-cost carbon fiber as available.
- Construct and test through-thickness permeability rig as funding and other resources permit.
- Advance bench-top studies of advanced severing technology to determine technical feasibility of utilizing equipment that can be practically adapted and implemented for this application within one to three years. Initiate complementary investigation of cutting tribology issues to determine if alternative materials and techniques might improve variations of current severing technologies.

Introduction

Polymer-matrix composite materials offer a number of benefits in "lightweighting" of automotive and heavy vehicles, including greater stiffness and strength per unit weight than conventional materials, easier formability, less corrosion susceptibility, the ability to tailor properties to specific load requirements, and enhanced noise and vibration damping. However, widespread implementation of carbon-fiber composites, which offer among the greatest mass savings potential, requires lower-cost materials and processes than are currently available. Advanced preforming processes offer opportunities to facilitate the widespread use of carbon composites.

Robotic-controlled, programmable, directed-fiber preforming processes have demonstrated exceptional value for rapidly preforming large, glass-reinforced, automotive composite structures. Due to their unique features and flexibility, and to their inherently low scrap rate, they are among the most viable candidate processes for making affordable carbon-fiber preforms for a variety of structural automotive components. The ACC has implemented the P4 with glass fibers very successfully in its truck box program—Focal Project 2 (FP2). Original equipment manufacturers (OEMs) have transferred the technology to commercial applications such as the General Motors (GM) Silverado pickup box and the Aston Martin Vanquish body-side.

Analyses have indicated a potential for greater than 60% mass savings for a carbon-fiber-intensive body-in-white (BIW) under the assumption of a thickness design constraint of 1.5 mm. The analyses also indicate the potential of saving an additional 15% if the thickness constraint is reduced to 1 mm; unfortunately, evidence suggests that 1.5 mm may be a practical limit for liquid molding. However, thermoplastics preforms, in which the matrix and fiber are both deposited in the preforming step, offer a potential path to obtaining thinner sections, and consequently additional mass savings as well as greater potential for recyclability. Hybrid-fiber preforms offer another potential benefit in terms of economics and property enhancement and may be a good route for actually introducing more carbon fiber to automotive applications.

Preforming Developmental Approach

The objective of this project is to advance directed-fiber preforming processes to effect a further reduction in vehicle mass—relative to glass-fiber composites—while maintaining the economical advantages of net-shape preforming. The project is pursuing three focus areas corresponding to three materials systems: reinforced thermoplastics, carbon fiber, and hybrid glass-carbon fiber. Each focus area consists of four main tasks concentrating on 1) materials developments, including introduction and evaluation of alternative and/or new fiber product forms and binders; 2) machine developments, particularly new severing technology; 3) process developments, for example, to control areal-density uniformity and preform anisotropy; and 4) development of supporting technologies such as modeling and preform characterization techniques. Furthermore, this project will undertake to develop sufficient understanding of fundamental aspects of the process and their effect on preform quality and mechanical properties in the molded part. As such, this project will support, augment, and facilitate the current and future research activities undertaken in related ACC projects (see 4.A and 4.D).

A preforming system, which will serve as the base for hardware and associated technology developments was completed and installed in the polymer composites laboratories at ORNL in the second quarter of FY 2005. Several combinations of fibers and binders have been obtained to establish materials baselines for comparison with previous and ongoing P4 work being conducted by the ACC and to be used in establishing glass baseline for related permeability test implementation. This machine is currently being used to build preforms for evaluation utilizing the various forms of glass reinforcement and glass fiber commingled with thermoplastic fiber to serve as the matrix. Smaller amounts of carbon fiber have been processed as well as glass impregnated with thermoplastic resin utilizing the DRIFT® process.

ORNL has been working at a low level with Polycomp (inventor of DRIFT®) and Fiberform (a

key licensee) to evaluate possibility of chopping the DRIFT® product form in the ORNL preforming machine. Polycomp made sample quantities of glass-impregnated polypropylene using a 2400 tex glass tow which had been processed into a ribbon about 0.2 inch wide and .035-inch thick. As expected, the ribbon handles more like a solid strip of plastic than a pliable fibrous tow and does not cut as easily as the glass tow, even with scissors. In initial trials, ORNL was able to get some of the material through the preformer chopper, but with only very small amounts cut before beginning to break blades in the chopper.

Plans are to make some more DRIFT® samples in FY 2007 using a smaller tow size (probably about 1150 tex, which is about the size of the current TwinTex product) in order to get a thinner ribbon. Once it has been established that the material can be rapidly chopped using the existing rotating blade configuration or one similar to that currently in the preforming machine, we will work to establish more optimum material forms and chopper configurations that might be economically feasible for implementation. Fiberform has also put ORNL in touch with a cutting equipment supplier who has developed cutting equipment for them in the past. With related equipment experience provided by the supplier, we will be able to better address alternative means for processing the DRIFT® materials form.

Procurement of a Press and Mold for Composites Evaluation

Key to being able to demonstrate the advances achieved in preforming technology is the ability to demonstrate that these advances translate into improvements in actual representative composites. The best way to effect this demonstration is through adequate evaluation of the preform itself as well as full consolidation of the preform and resin in a composite in the manner in which this would be accomplished in actual composite manufacturing.

During the last fiscal year, efforts were initiated to identify the most appropriate equipment necessary to do this on a research basis. ORNL staff worked with members of the ACC's Processing Group to quantify process equipment requirements and initiate activities necessary to procure a research press, general purpose mold, and injection machine. These requirements were turned into formal requests for quotes (RFQs) for designing and building these systems, which were issued to companies that had been identified through ORNL and ACC interactions as having potential to meet or exceed all performance targets. The intelligent-leveling press was specified to accommodate various molds and molding processes and to be instrumented above routine standards in order to provide more process details in experimental research. Nominal pressing capacity is 750 tons. The general-purpose plaque mold is specified for instrumented experiments using SRIM, compression molding of reinforced thermoplastics, and sheet molding compound (SMC) processes. This equipment will allow ORNL to demonstrate preform advances while further investigating advances in the various molding processes themselves.

During FY 2006, the bid package reviews for the press and mold were completed and formal contracts placed with Williams White of Moline, Illinois, for the press and Service Mold of Windsor, Ontario, for the mold. Although originally a portion of this process, procurement of an injection machine has been deferred due to higher than expected bid costs and less current focus on the SRIM process. Programmatic benefits for utilizing an existing, older model SRIM machine having capacities close to those identified as targets for the procurement process are being evaluated versus costs and risks for possible refurbishment and upgrade to employ when SRIM capabilities are needed. Acceptance testing for the mold was conducted at a test facility contracted by Service Mold in Windsor, Ontario, in May while acceptance testing for the press was conducted at Williams White in June; both activities were supported by ACC representatives. Although minor issues were observed during the testing of both pieces of equipment, in general, the reviews were considered quite positive and shipment to ORNL upon implementation of minor adjustments was authorized for both. After completion of these adjustments, both press (Figure 1) and mold (Figure 2) were shipped to ORNL and installed in July and August.

Figure 1. Intelligent-leveling, 750-net-ton, Williams White injection/compression press installed in ORNL composite processing laboratory.

As part of planning for installation of the press in the ORNL composites laboratories, an engineering study was conducted to determine structural needs for operation of the new equipment. Although the facility was originally designed to accommodate heavy processing equipment, this particular press presents a loading scenario that is larger statically and significantly larger dynamically than the equipment envisioned when the facility was designed. Beyond structural capacity, vibration from the dynamic loading to the floor was a major concern due to highly sensitive equipment in the vicinity. Accordingly, the engineering study determined that the floor needed to be reinforced well above current capacity. Adding supporting members to the existing floor was determined to be impractical structurally and other modifications would also be necessary for the vibrations. The result of this study is the design of new flooring to accommodate the press which required tear out of the existing floor and excavation to nearby bedrock. The floor was replaced by an isolated structural base

Figure 2. General-purpose flat-plaque mold for SRIM, SMC, and thermoplastics.

and new three-foot concrete slab as shown in Figures 3 and 4. In addition to the structural modifications, necessary utilities were provided to the new equipment as part of this activity.

Due to budget reductions during FY 2006, plans to procure and install a heat-transfer system for the mold have been deferred until FY 2007.

Permeability Measurements

It has been found that injection-compression offers distinct advantages over injection-only liquid molding for the infiltration of high-volume-fraction preforms. Both the in-plane permeability and the through-thickness permeability affect the moldability of the part. Accordingly, development of two novel research instruments was commissioned in order to provide experimental data to characterize the three-dimensional permeability of the fiber-mat preform.

During this fiscal year, work on the development of the in-plane rig (see Figure 5) with a flow capacity of 0.33 gpm and a fluid capacity of 2 gallons was completed and checkout testing conducted. The test rig can be operated in either constant-flow or constant-pressure mode under feedback control. Maximum pressure and fluid viscosity are 100 psi and 5 poises, respectively. Both platens are

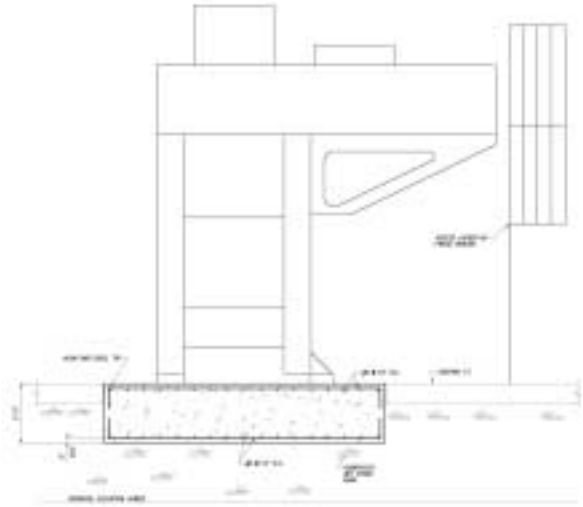

Figure 3. Floor up-grade required to accommodate ORNL press.

Figure 4. Site preparation for press installation.

instrumented with sensors—a total of 218 sensors—to monitor the flow-front with resolution of 0.25 in.

A data acquisition and control system was developed by ORNL based on National Instruments' PXI hardware and LabVIEW software.

Stand-alone program modules have been written to evaluate sensor performance, to conduct the permeability experiments, to analyze the collected data and calculate permeability value, and to review the experiment at reduced speed. The modules that

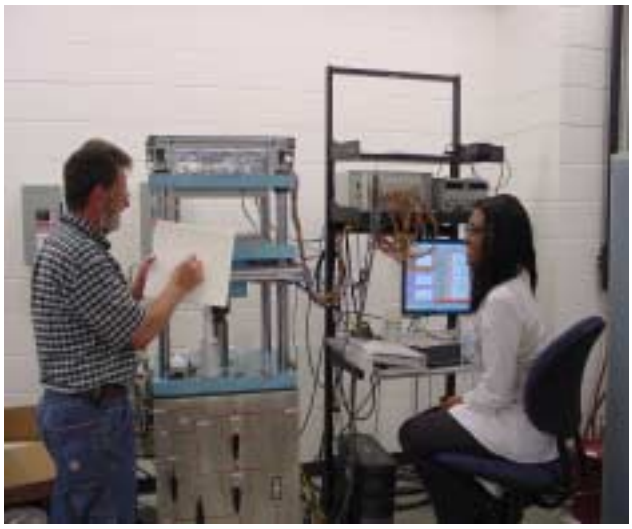

Figure 5. Radial-permeability test rig showing associated data acquisition and monitoring station.

monitor the sensors have been developed for both conductor and thermocouple-based sensors evaluated for this rig.

An analysis module that takes the elliptical flow front and calculates the in-plane components of the permeability sensor has been developed from expressions provided by Professor Richard Parnas. Full characterization of the analysis module has now been completed following resolution of sensor reliability and accuracy issues and a variety of preforms are currently being evaluated. Consistency and repeatability of measurements that compare with literature values has been demonstrated with standard commercially available preform materials (Figure 6). Characterization of permeability for developmental preforms versus process parameters is being conducted as materials and resources permit. A limited amount of testing has also been conducted on some natural-fiber preforms fabricated by a small business under a DOE Small Business Innovative Research (SBIR) grant as shown in Figure 7.

A through-thickness rig has also been designed and fabrication of a portion of the hardware has been completed. Maximum pressure and viscosity are the same as the in-plane rig. Due to the change in focus and budget reduction, resources have been redirected and further development and implementation of this system deferred.

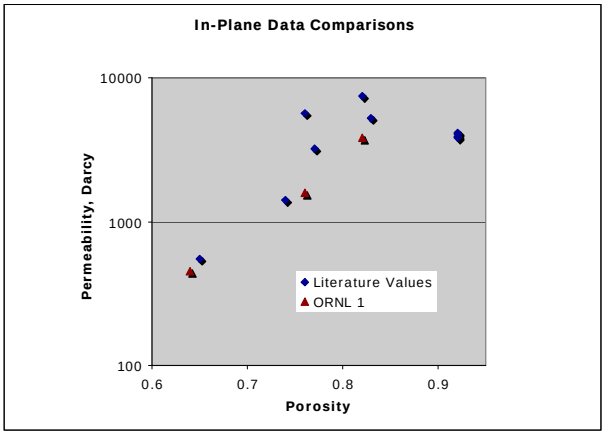

Figure 6. Permeability test data showing comparison with various continuous- strand mats.

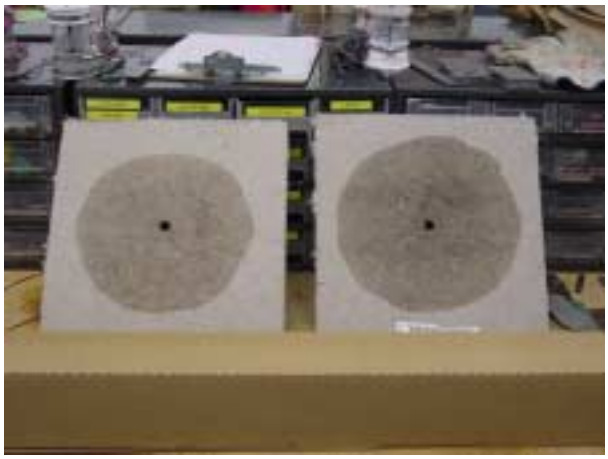

Figure 7. Natural-fiber preforms tested for a SBIR partner.

Fiber-Severing Technology

Due to significant differences in the physical properties of various reinforcement fibers as well as their available product forms, chopping technology that has been successful for glass fibers systems has demonstrated less-satisfactory results for the carbon-fiber products that are currently available. It is expected that similar results will occur for reinforced thermoplastics and hybrid glass-carbon products. Accordingly, consideration is given in this project to identifying alternative severing technology. A literature and patent search was undertaken to assess promising technologies for bench-top investigation. Possibilities identified include mechanical-based, laser-based, CO_2 pellet, liquid nitrogen, water-jet, and ultrasonic. Based on the information available in the literature and

consideration of project-team experience in related activities, laser-based choppers appear to offer the most promise.

During this period, initial effort to identify laser types and projected power levels required to sever carbon-fiber tows in sizes close to those likely to be employed in performing, was expanded to actually demonstrate the potential for laser severing. A neodymium:YAG laser system was set up in the laboratory and experiments with a carbon-fiber tow were conducted at the bench-scale to evaluate feasibility. Calculations based on the enthalpy of vaporization of carbon indicated that the laser identified for this work should be able to comfortably deliver the energy required to sever a large carbon-fiber tow (roughly 50,000 filaments) at about 1,000 cuts per second, which would represent a tow traveling at close to the maximum velocity as would be encountered in the ORNL chopper and chopped at a rate sufficient to yield a 0.5-inch cut length. Initial trials were conducted using laser-processing parameters thought to be representative of pulse time length, pulse physical shape, and delivered energy required to sever at this rate. However, at these conditions, we were unsuccessful in getting the necessary power delivered into the entire fiber bundle to effect severing. It appeared that the surface of the outer fiber ionizes and prevents further energy deposition and penetration into the bundle. Additional experiments were conducted with this same laser using a variety of laser power levels and with alternative environmental conditions to determine if the "ion cloud" could be mitigated by immersing the fiber with different inert gases or if the cloud could be quickly dispersed by a large flow rate of these gases being drawn across the fiber at the point of laser impact. Again, these efforts were unsuccessful in producing more than minimal severing of the outer fibers.

In order to determine if laser severing might be possible at somewhat different regimes that might not match our aggressive requirements directly, but possibly still adaptable to work in this area, we conducted experiments using a continuous-wave CO_2 laser as well as an excimer laser and a more tunable (and slower pulse rate) neodymium:YAG laser. With all three of these systems, we were able to demonstrate severing of carbon fiber, although none has yet been accomplished at the rates described above, which would be representative of the most aggressive cases we had thought possible with the original neodymium:YAG laser. At the time of this report, we are continuing work with the more tunable neodymium:YAG laser as its associated operating environment offers us the most flexibility in terms of controlling the process and more thoroughly investigating the cutting mechanisms we have encountered.

If successful with one of the alternative systems, these results will be utilized to define the more-detailed laser parameter and control requirements in order to be able cleanly sever a moving carbon-fiber tow at the speeds required for utilization in the P4 system. Initial work will continue to be done in static tests to determine beam width, power levels versus time, and other necessary information before moving to low-speed tests, and then tests at speeds more representative of actual fiber deposition rates. With this background, plans are to then scale up the hardware for on-machine experimentation and demonstration. In addition to severing carbon fiber, future work will address other reinforcing fibers, as well as fibers used as binders, and blends of reinforcing and binder fibers.

ORNL plans to continue initial evaluation of laser severing and to initiate a more basic study of mechanical chopping in FY 2007 for various materials forms. It has been mentioned earlier that plans are being developed to evaluate modifications to the chopper equipment with respect to processing the DRIFT® materials. With a better understanding of chopping mechanics and developing experience with varying blade designs, blade materials, and cutting mechanisms, we will be able to better address a variety of cutting issues associated with carbon fibers specifically as well as with other materials and material blends.

Modeling of Fiber Deposition

A C-based program is under development to analyze the effects of process variables on preform characteristics. The program will be used to evaluate preforms in terms of measures such as fiber run length, fiber connectivity, distribution of voids, etc.

When correlated with permeability data and areal-density measurements, the program will provide an understanding of the effects of process variables on resulting preforms and their "moldability." Recent advancements to the program have included continued enhancement of the previously-developed general modeling approach by addition or improvement of many of the capabilities. Examples of these enhancements include correlation of processing parameters with density variations, and improved models for fiber deformation. Work is in progress towards mat compression, consolidation, surface roughness, models for fiber splitting, tow fiberization, deposition variations, and deposition on variable geometry substrates. Also underway is conversion of the model to more widely available platforms to facilitate more widespread utilization and correlation with processing experience. A core portion of this model has been ported for internal evaluation. Further development of the model will be continued as program data are available to support model expansion and verification.

Summary and Conclusions

The Development of Next-Generation Programmable Preforming Process effort will continue to build on past development and application of directed-fiber preforming processes, namely, those of the P4, to extend the process to new material systems. Developments are expected to facilitate the use of low-cost carbon fiber, reinforced thermoplastics, and glass-carbon hybrid materials as effectively as is the current state-of-the-art with glass. Utilizing these materials is expected to lead to further reductions in vehicle mass in a more cost-competitive scenario than is currently possible. A preforming system, which will serve as the base for hardware and associated technology developments, was completed and installed in the polymer composites laboratories at ORNL in the second quarter of FY 2005. This machine is currently being used to build preforms for evaluation utilizing various forms of glass reinforcement and glass fiber commingled with thermoplastic fiber to serve as the matrix. Smaller amounts of carbon fiber have been processed as well as glass impregnated with thermoplastic resin utilizing the DRIFT® process.

Also during FY 2006, fabrication and installation of a complementary advanced research press and general-purpose plaque mold were completed providing the requisite equipment necessary to demonstrate the advances achieved in preforming technology through actual experimental composite manufacturing.

Development has been completed and testing is in progress utilizing a novel permeability rig designed to characterize the preforms resistance to in-plane resin flow during the molding process.

Initial fiber-severing experiments were conducted utilizing a neodymium:YAG laser system set up in the laboratory for static cutting of a carbon-fiber tow. Although initial trials were unsuccessful in severing carbon fiber at all using a laser system and process parameters that had been estimated as meeting the most aggressive of project requirements, subsequent trials using three alternative systems have demonstrated that carbon fiber can indeed be severed via laser exposure. Additional experiments with these alternative laser systems are being conducted to determine beam width, power levels versus time, and other necessary information representative of actual fiber-severing requirements for preforming and related processes.

Modeling of the fiber-deposition process continues through the development of an in-house code. The program will be used to evaluate preforms in terms of measures such as fiber run length, fiber connectivity, distribution of voids, etc. Results will be correlated with permeability data and areal-density data to assess the effect of process parameters on preform quality as well as the mechanical properties of molded parts. Work is underway to provide availability of the model to operate on a standard desktop "Windows" platform and a core portion of this model has been produced for internal evaluation.

Collectively, the technology under development in this project will advance low-cost processing on two fronts. First, it will provide the opportunity to employ additional materials in the net-shape preforming process, which is expected to lead to additional mass reduction and/or better performance. Second, it will provide the requisite

tools to evaluate the effect of process parameters on the utility and performance of preforms and molded parts.

C. High Volume Processing of Composites (ACC 115[i])

Principal Investigator: Becky Joitke
DaimlerChrysler NA, Advance Vehicle Engineering
CIMS 489-00-00, 1030 Doris Road, Auburn Hills, MI 48326
(248) 754-9761; fax (248) 754-9720; e-mail: rlj@daimlerchrysler.com

Technology Area Development Manager: Joseph A. Carpenter
(202) 586-1022; fax: (202) 586-1600; e-mail: joseph.carpenter@ee.doe.gov

Expert Technical Monitor: Philip S. Sklad
(865) 574-5069; fax: (865) 576-4963; e-mail: skladps@ornl.gov

---

Contractor: U.S. Automotive Materials Partnership
Contract No.: DE-FC-59OR22545

Objective

- Develop and demonstrate high-volume manufacturing (molding) processes to produce lightweight composite automotive components.
- Expand the scope of the Automotive Composites Consortium (ACC) composite efforts into the thermoplastic area.

Approach

- Benchmark current thermoplastic processes.
- Develop and study high-volume composite manufacturing processes within approved research efforts.
  - Develop manufacturing processes for carbon-fiber SMC body panels amenable to cost-effective high-volume applications.
  - Investigate compatibility of natural-fiber reinforcements with polymer systems for structural and semi-structural applications.
  - Develop understanding of soy-based polymers in conjunction with glass and carbon-fiber reinforcements.
  - Investigate DRIFT technology with various fiber reinforcements in polymer systems for structural and semi-structural applications, including partnership with the ORNL carbon-fiber line.
  - Acquire tooling necessary for the support of ACC115 research programs.

Accomplishments

- Provided process support for the duration of Focal Project 3, B-Pillar molding (ACC080, see 4.D).
- Preliminary experiments with carbon-fiber SMC completed with Meridian Automotive Systems and sample benchmarking plaques submitted for testing.
- Injection-molding plaque tool completed and undergoing final preparation for starting work on thermoplastic characterization database.
- Compression molding plaque tool complete and supporting ACC040 (see 4.A) investigations.
- Completed investigation into acquiring 3000T press to be used in development work.
- Technology benchmarking in Germany and Switzerland, January 2006.

Future Direction

- High-volume processing of lightweight structural thermoplastic composites.
  - Characterize panels fabricated with Fiberforge® technology and proceed with optimizing the polymer systems to enhance performance and appearance.
  - Participate in DRIFT® investigations at ORNL relative to testing and processing optimization.
- Carbon-fiber SMC body panels for exterior and interior applications:
  - Continue working with fiber and resin suppliers to develop properties, improve repeatability, and optimize manufacturability within cost and supply constraints.
- Natural-fiber reinforcements and soy-based polymers:
  - Characterization results will be used to refine testing methods for determining durability properties of natural-fiber composite systems.
  - Optimize fiber-surface treatments and polymer systems to minimize the moisture absorption of natural-fiber composite systems.
- Provide process support to Focal Project 4, Composite Underbody/Seat (ACC007).
  - Utilize the injection-molding and compression-molding plaque tools to manufacture composite plaques for material characterization and development of a thermoplastic reference database.

Introduction

The purpose of this project is to develop the high-volume composite molding technologies germane to automotive production. The direction of ACC115 is to collaborate with suppliers to develop low-cost, high-volume molding processes compatible with the material property and processing requirements of the automotive industry.

Four processing investigations are under way. 1) Collaboration with Fiberforge® was initiated to determine the feasibility of robotic placement of uni-directional fiber tapes in desired orientations, to produce locally-reinforced blanks at high speed. 2) DRIFT®, a patented pultrusion process, is being studied for its ability to support the project objectives and its compatibility. This work is being conducted at ORNL. 3) A program has been initiated to resolve issues with producing carbon-fiber SMC body panels for exterior and interior applications. Finally, 4) natural fibers and soy-based polymers are being studied for their compatibility with current systems, and their physical characteristics, with the intent of adding the desired feature of sustainability to the other objectives.

To support these initiatives, purchase of two plaque tools, one for compression molding and one for injection molding, was completed in FY 2006. These molds can be used at various suppliers and national laboratories to create plaques for mechanical testing using various thermoplastics and reinforcements. The compression molding tool was delivered 4Q 2005. The injection tool was completed at the end of FY 2006. In addition, purchase of a new compression-molding press was proposed to support the research needs of existing and future projects being pursued by the ACC working groups.

An investigation was completed on securing a new compression-molding press for the purposes of supporting the research objectives.

Fiberforge®

In the Fiberforge® process, unidirectional tapes are robotically placed to enhance structural performance of specific areas of the components produced. Initial meetings have been held with Fiberforge® to develop a work plan, roles and responsibilities, and a cost analysis. Plaques made via the Fiberforge® process, utilizing nylon 6 (PA6) with carbon-fiber reinforcement, have been submitted to the ACC Materials Working Group for analysis and characterization.

DRIFT®

In FY 2005, ACC115 began work in conjunction with ORNL to address the compatibility of Directly Reinforced Fiber Technology (DRIFT®) with low-cost carbon-fiber program objectives. DRIFT® is a patented pultrusion process by which tapes, chips, pellets, sheets, or woven fabrics are produced, which then are capable of feeding a variety of molding processes.

As part of its Advanced Preforming Initiative, ORNL has been working at a low level with Polycomp (inventor of DRIFT®) and Fiberform (a key licensee) to evaluate possibility of chopping the DRIFT® product form in the ORNL preforming machine. Polycomp made sample quantities of glass-impregnated polypropylene using a 2400 tex glass tow which had been processed into a ribbon about 0.2 inch wide and .035-in thick. As expected, the ribbon handles more like a solid strip of plastic than a pliable fibrous tow and does not cut as easily as the glass tow, even with scissors.

In initial trials, ORNL was able to get some of the material through the preformer's chopper, but with only very small amounts were cut before blades began to break in the chopper. Plans are to make more samples in FY 2007 using a smaller tow size (most likely 1150 tex, which is about the size of the current TwinTex® product) in order to get a thinner ribbon. Once it has been established that the material can be rapidly chopped using the existing rotating blade configuration or one similar to that currently in the preforming machine, work will proceed on optimizing material forms and chopper configurations that might be economically feasible for implementation. ORNL plans to continue initial evaluations of laser severing and to initiate a more basic study of mechanical chopping in FY 2007 for various materials forms.

Fiberform has also put ORNL in touch with a supplier of cutting equipment with whom Fiberform has worked in the past. With a better understanding of this background and related equipment experience provided by the supplier, ORNL will be able to better address alternative means for processing the DRIFT® material form.

Longer-term and perhaps more importantly, ORNL continues working with Polycomp and Fiberform towards putting a prototype DRIFT® line at the end of a low cost carbon-fiber pilot line to evaluate and demonstrate technical and economic potential for various automotive applications of the DRIFT® process.

More definitive work plans are being developed for collaboration in both broad application of DRIFT® with carbon fiber as well more specifically with utilization in preforming equipment. Objectives would include optimizing the fiber types, percentages, and types of polymer systems to achieve needed levels of mechanical performance and appearance. Important process characteristics such as low warpage and reduced material system cost will be explored. Test specimens and components will both be tested for characterization and durability for use in structural and semi-structural applications.

Carbon-Fiber SMC

The objectives of this work are to develop high-performance, cost-effective, carbon-fiber SMC materials and associated processing techniques for high-volume automotive components. The technical emphasis is to optimize properties, improve consistency of the properties, and to optimize the manufacturability of the compound. The project assumptions are that the material could be used for all current structural and Class-A SMC applications; that the current SMC compounding, molding processes, and equipment can be utilized; and that the thickness of the new materials will be in the range of 1.0 to 3.0 mm. In addition to the technical issues and constraints, there are the business challenges of the carbon-fiber cost, the limited supply of carbon fiber, and the disinclination of the carbon-fiber suppliers to cooperate on research, perhaps due to the low-cost requirement of the automotive industry.

A few preliminary experiments have been done using Hexcel A54C1925 and split-tow Toho XO502 carbon fibers with Meridian Automotive Systems' vinyl ester resin. The results suggested that fiber format and sizing could have a strong influence on short-beam shear properties and styrene solubility. Additional effort has subsequently been made to

arrange the cooperation of carbon-fiber suppliers (Toho Tenex, Toray, and Zoltek) and resin suppliers (AOC, Ashland, and Reichhold). For benchmarking, sample plaques of Meridian's in-house structural carbon-fiber SMC using Toray T700 fibers have also been prepared for physical and mechanical testing through the Automotive Composites Consortium.

Natural Fibers and Biocomposites

A DOE project titled "A Fundamental and Applied Investigation of Kenaf-Based Fiber/Polymer Composites as Potential Lightweight Materials for Automotive Composites," at ORNL and Mississippi State University was started in FY 2006. The ACC was assigned to the project as an industry partner. The project kick-off was accomplished and project objectives were established.

Project objectives are listed below:

- Investigate the compatibility of natural-fiber reinforcements with polymer systems, for usage in exterior and interior applications of both structural and semi-structural purpose.
- Optimize fiber-surface treatments and polymer systems to enhance compatibility and performance, as well as minimize moisture absorption.
- Develop an economical, automated, high-throughput fiber retting process.
- Improve natural-fiber composite properties by the addition of inexpensive, nanoscale additives and/or excellent interfacial bonding.

Ashland Chemical Soy Resin Project

Test plaques utilizing a commercially-available, soy-based resin, reinforced with glass and carbon fiber, were compression-molded at Ashland Chemical. The test plaques were fabricated for a direct comparison with petroleum-based resin systems that have identical reinforcement percentages. The characterization was conducted by the ACC. Tensile and compression results are shown in the following charts. Tensile stress results shown in Chart #1 for glass-reinforced composite indicated the petroleum-based and soy-based plaques performed similar with little anisotropy. Carbon-fiber results indicated the petroleum-based plaques performed better with a noticeable difference in anisotropy. Tensile-modulus results shown in Chart #2 for glass-reinforced composite indicated the petroleum-based and soy-based plaques performed similar with some anisotropy. Carbon-fiber results indicated the petroleum-based plaques performed much better in the 0^{o} direction and better in the 90° direction. Tensile strain-to-failure results shown in Chart #3 indicated higher strain-to-failure values for glass reinforced composite when compared to carbon fiber, which was expected. Compression-stress results shown in Chart #4 for glass-reinforced composite indicated the petroleum-based and soy-based plaques performed similar. Carbon-fiber results indicated the petroleum-based composite performed better with lower variability.

Additional testing for shear, density, fiber and void content, dynamic mechanical analysis (DMA), coefficient of linear thermal expansion (CLTE) and moisture absorption for the soy and petroleum-based plaques still remains to be completed.

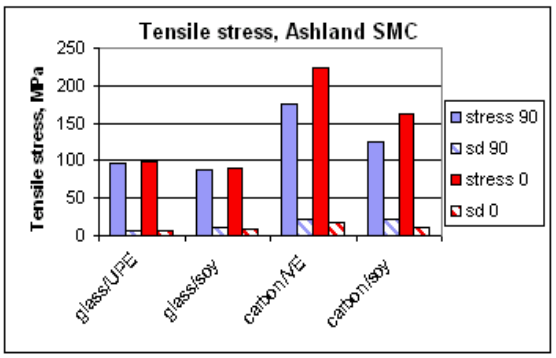

Chart 1. Tensile Stress, Petroleum vs. Soy Resins.

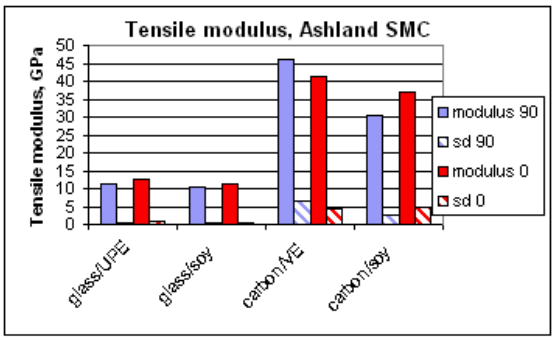

Chart 2. Tensile Modulus, Petroleum vs. Soy Resins.

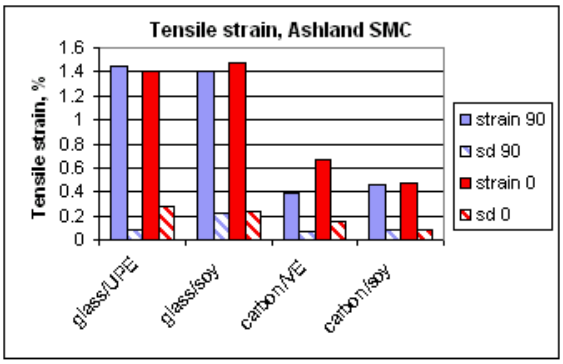

Chart 3. Tensile Strain, Petroleum vs. Soy Resins.

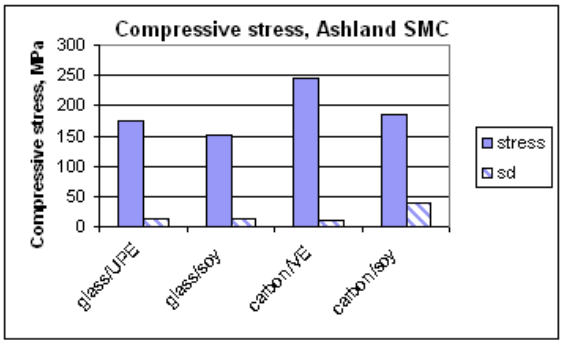

Chart 4. Compressive Stress, Petroleum vs. Soy Resins.

Tool Acquisitions

One of the obstacles identified with studying the consistencies of processing various materials has been the inability to make test plaques. To address this concern, the ACC Board of Directors approved the proposals to build an injection-mold plaque tool, and a compression molding plaque tool.

Each tool was designed to produce a 610 mm X 610 mm (24" x 24") plaque using a wide variety of materials and be capable of multiple thicknesses. The individual tools can be shipped to various molders to compare samples made from the same tool but with optimum process conditions. In addition, pressure sensors and thermocouples were specified for several positions in each tool so that process data can be collected and compared between trials in a consistent fashion. Tool-commissioning trials are complete and the final sign-off occurred November 15th 2005.

The injection-molding tool was designed by a team of ACC members and incorporated many "lessons learned" on prior projects. The stringent requirements included options of producing test panels from 2.0 mm to 5.0 mm in thickness in increments of 0.5 mm, easy access to multiple sensors at prescribed positions, and capability of withstanding high clamp forces without flashing. The full requirement list is available on VROOM*.

The injection plaque tool completed runoff in late September. The tool will be a significant part of the Material Working Group's thermoplastic database development.

ACC Compression-Molding Facility

Purchase of a new compression-molding press has been proposed to support the research needs of existing and future projects being pursued by the ACC working groups. With this objective, a new press facility was proposed for installation at the North Central Campus of Emerging Technologies (NCC-ET). This satellite of the National Composite Center was considered a suitable location for both logistical and infrastructure reasons. Hence, during 2006 extensive discussions were held with the proprietors of the NCC-ET facility and Dieffenbacher, the proposed press manufacturer. The scope of the overall facility capabilities was also extended to include a proposed collaboration with the German institute, Fraunhofer, ICT.

*Available only by authorization

The total project cost for USAMP and NCC equipment purchases and building modifications was estimated at $4M.

Although approvals were secured through USAMP for the project to go forward, several key events in 2006 ultimately prompted a cancellation. The first main issue emerged following an attempt to secure the purchase of the main press unit. The press manufacturer stated several objections to the USAMP purchase order terms and conditions. After many months of protracted discussions, an impasse was reached and the USAMP order for the press was cancelled. Instead, the NCC offered to purchase the press and rent time to the Automobile Composites Consortium on an as-needed basis. However, the NCC failed to secure financing for such a project and by the end of September, the ACC members made a decision to cease further activity related to the new press facility. Therefore, for the time being, the ACC has decided to continue supporting process investigations by attempting to rent access to equipment within the tier supply base.

European Benchmarking Trip

In line with the objective of benchmarking current plastics processes, a group of seven members from the ACC Board of Directors and the ACC115 working group spent a week in January 2006 touring companies and educational sites in Europe to gather information about the state of the plastics industry. Europe is widely considered to be the seat of automotive plastics innovation, particularly within the thermoplastics area, as the economic forces for lightweight vehicles are stronger in Europe than in the United States.

An aggressive five-day agenda took the team to 7 different suppliers and 2 academic research sites. Valuable contacts were made and opportunities for further processing research were discussed; a summary of the visits and technologies was presented in the semi-annual report.*

Conclusions

ACC115 explores different approaches to the high-volume processing of composites. Four processing programs are in progress, each with the objective of researching ways to save weight in automobiles, at the volumes unique to the industry. Carbon-fiber SMC research is progressing slowly against constraints of cost and supply. Natural fibers and biocomposites C. ACC115[2]-- also hold future possibilities of less reliance on petrochemicals and greater recyclability. DRIFT® and Fiberforge® work continues; basic characterization is in progress and applications will be considered. Acquisition of new equipment specifically owned by ACC will speed research by eliminating time needed to move tools between suppliers, and will also provide the benefit of reducing variation in the test results.

---

[i] Denotes project 115 of the Automotive Composites Consortium (ACC), one of the formal consortia of the United States Council for Automotive Research (USCAR), set up by the "Big Three" traditionally USA-based automakers to conduct joint pre-competitive research and development.

D. Automotive Composites Consortium Focal Project 3 Composite-Intensive Body Structures (ACC 080[i])

Principal Investigator: Stanley A. Iobst
GM Research & Development
MC 480-106-710
30500 Mound Road
Warren, MI 48090-9055
(586) 986-1223; fax: (586) 986-1207; e-mail: stanley.a.iobst@gm.com

Field Project Manager, Composites: C. David Warren
Oak Ridge National Laboratory (ORNL)
P.O. Box 2009, Oak Ridge, TN 37831-8050
(865) 574-9693; fax: (865) 576-4963; e-mail: warrencd@ornl.gov

Technology Development Manager: Joseph Carpenter
(202) 586-1022; fax: (202) 586-6109; e-mail: joseph.carpenter@ee.doe.gov

Expert Technical Monitor: Philip S. Sklad
(865) 574-5069; fax: (865) 576-4963; e-mail: skladps@ornl.gov

---

Contractor: U.S. Automotive Materials Partnership (USAMP)
Contract No.: DE-FC26-02OR22910

Objectives

- Design, analyze, and develop the technology to build a composite-intensive, body-in-white (BIW), offering a minimum of 60% weight savings over steel at a cost close to that of steel, while meeting manufacturing, assembly, and performance targets.
- Provide a focus for bringing together technology developed by each of the Automotive Composites Consortium (ACC) working groups through emphasis on carbon-fiber-reinforced composites and the use of hybrid materials, faster manufacturing processes, design optimization including crashworthiness, and rapid joining methods.

Approach

- Optimize the design and complete the finite element analysis (FEA) for the carbon-fiber-composite BIW (Phase 1).
- Build one part of the BIW (the B-pillar portion of the body-side) to demonstrate high-volume processing methods (Phase 2).
- Develop and model a structural test for the B-pillar.

Accomplishments

- B-pillar preforming pattern for the Hexcel 12x3K carbon-fiber was developed.
- Carbon-fiber-reinforced B-pillars have been preformed, molded, and bonded.
- Flow modeling studies for the full body-side model with carbon-fiber were completed for multiple injection ports.
- Several new ACC programs being bubbled up for potential full-fledged projects

---

Introduction

The ACC Focal Project 3 (FP3) is intended to be a design and processing study to develop a cost-effective manufacturing scenario for carbon-fiber-intensive composite vehicle structures. All of the materials, manufacturing processes, and fabrication and assembly methods to be considered in this project are to be consistent with the following overall objectives:

- High-volume production techniques (>100,000 units per year)
- Cost parity with equivalent steel structures
- Overall 60% mass reduction relative to steel BIW structure
- Structural performance equivalent to or better than that of a steel structure
- Dimensional tolerance equal to or better than that of steel

The current stage of the project is the development of the manufacturing processes necessary to produce the body side. This work was done with the B-pillar (a portion of the FP3 body-side design shown in Figure 1) preform and molding tooling. The preliminary preform development with glass fiber was completed earlier. The preforming and molding trials with carbon fiber are now also completed. A run of carbon-fiber B-pillars has been prepared for bonding and structural testing. The structural reaction-injection molded (SRIM) injection/compression mold-filling model was extended to multiple injection ports.

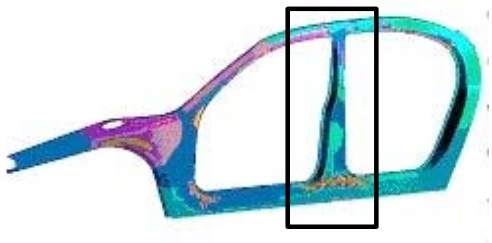

Figure 1. B-pillar portion of body side is outlined.

New Program Bubble-up

Several new efforts are in preliminary development as potential new focal projects, and brief summaries of each will be given.

- Bond-line read-through
- Structural-composite underbody
- Lightweight, low-cost composite seat

B-Pillar Preforming Development

Final preforming development efforts were completed on the ACC P4 (see 4.A) machine using the original B-pillar preform tooling. Previous preforming efforts were conducted using revised tooling in which the 'B' surface is the preform deposition surface and the 'A' surface is the consolidation surface. Although the preform and molding tool compatibility issue was addressed with the revised preform tooling, the inverse orientation of the deposition surface (relative to the original tooling) created additional issues during the material deposition process, which turned out to be more intractable than the original reason for changing the tooling.

The preforming optimization proceeded with many delays due to servo errors, robot-cabling problems, a fiberglass type change (which altered deposition patterns) and issues involving the SRIM molding press. However, the necessary maintenance was performed and preform development was resumed. The type of glass fiber used for the pre-carbon optimization was changed to Owens Corning (OC) 905 from OC 433. The 905 has a slightly different sizing applied, causing it to spray differently. This difference in sizing led to further modifications of programs already made specifically for the type 433 glass. The SRIM molding press, which provided molding performance feedback to the preforming process, was also down for maintenance. However, the issues were resolved and molding has commenced.

After completion of optimization with glass fibers, the decision was made to manufacture carbon-fiber preforms once an overall fiber volume fraction of 40% was achieved with glass fibers and at least a few preforms could be successfully molded. While the latest programs were modified to optimize the spraying of glass fibers, further modifications to the programs were made once the material was changed to carbon fiber.

Since a commercial-grade, low-cost carbon fiber was not available at this stage of the program, the Hexcel 12x3K fiber used in the earlier plaque program was used for the B-pillar preforms. Overall, the target fiber volume fraction of 40 % was achieved using carbon-fiber; however, difficulty in molding completely- filled carbon-fiber preforms at this fiber volume fraction led to molding preforms with only 35 % overall fiber volume fraction for most of the final test pieces.

The Hexcel 12x3K roving is not a regular production material, and thus issues with the carbon-fiber spools were encountered, such as knots which get clogged in the feed tubes and variations in density. Both are possibly due to inconsistencies in sizing application. A large amount of carbon fiber was wasted due to the knots interrupting the deposition routines.

Extensive areal-density sampling was performed on one set of B-pillar inner and outer preforms. The sampling was accomplished with 25 mm or smaller cutouts, which exacerbates the variation in fiber density measurement. The data from these two preforms indicate high variability of fiber volume. An example is given in Figure 2, which shows the fiber content in the different regions of the outer preform. The shallower inner preform was easier to produce and had a lower fiber variation across the part.

Even though the preforms were not fully optimized, a run of carbon-fiber preforms was made with the current process capability. Figure 3 shows carbon-fiber preforms ready for molding. Issues with the carbon-fiber spools, such as knots and variability in sizing, continued to be an ongoing problem. Also, cycle times could be further reduced as current total cycle times for inner and outer B-pillars remain

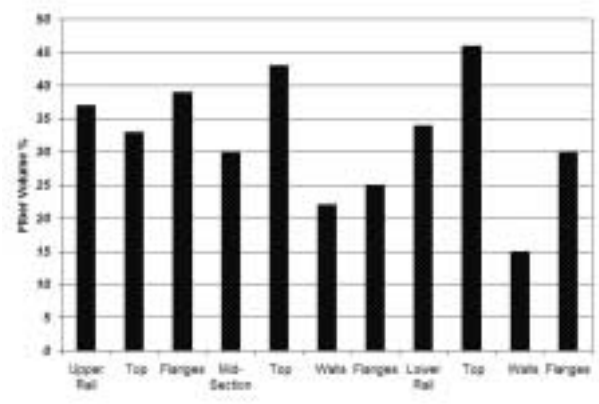

Figure 2. Variation in fiber volume across different regions of the B-pillar outer preform.

Figure 3. Carbon-fiber B-pillar preform, outer and inner views.

at 6 min. 34s and 8min. 35s, respectively. The total fiber spraying times are 3min. 30s and 5min. 47s for inner and outer B-pillar routines, respectively.

B-Pillar Molding Development

The preliminary preforming and molding development work with the glass preforms was a prolonged activity since both the preforming and molding were difficult processing conditions due to the complicated part geometry. There was also a limited supply of the carbon fiber, so it was deemed necessary to have processing conditions as well defined as possible with glass before changing to carbon. The difficulty in processing the available carbon fiber was discussed above. The combined factors of the limited personnel available for preforming and the poor yield of preforms meant

that there was only a limited amount of additional preform development with the carbon fiber. The preforms were not perfect, but were deemed satisfactory for molding. Figure 4 shows carbon-fiber preforms in the molding tool.

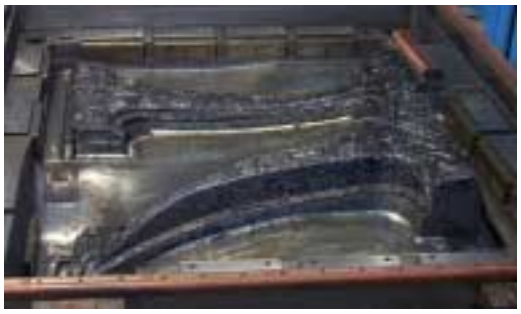

Figure 4. Carbon-fiber B-pillar preforms in the SRIM mold.

Preliminary molding runs indicated that there was better success in molding preforms at 35 volume % than at 40%. It was decided that most of the program objectives could be demonstrated with the 35% preforms and to not consume the additional resources that would have been necessary to complete the 40% preform development. The completed B-pillar inner and outer panels are shown in Figure 5.

Even with the 35% preforms, it was necessary to go to maximum press tonnage, 1000 tons, to completely fill the parts. This tonnage was necessary to get the resin to the far ends of the parts. There were occasional small dry areas where the variability in fiber deposition caused areas of low permeability in the preforms. These were primarily in the thicker rail sections. These observations are consistent with the fiber distribution data that show the preforms to be heavy on the flat areas and lighter on the walls and flanges. Thus, most of the resin flow is through the heavier portion of the preform. This also indicates that, with a more uniform fiber distribution, this part should fill at 40% fiber volume. A part of the complexity and long narrow aspect ratio of the B-pillar would probably require a flow leader, a runner cut into the mold cavity surface, to assist resin flow to desired areas.

The B-pillar has demonstrated a number of issues to consider were this effort to continue to full body-side. In addition to the flow leader, the injection points should be in the thicker sections of the part. This would reduce the amount of resin that has to flow through constricted areas of the preform. With the B-pillar there was only a limited choice of where to position the injection point. The full body side would have more flexibility in selecting injection-port locations. The flow modeling, discussed below, addresses molding the full body side. Also, the resin seals around the cavity must be designed in such a way that they do not hinder removing the molded part from the tool.

Figure 5. Molded carbon-fiber B-pillar.

B-Pillar Bonding

Bonded assemblies were fabricated to be tested and provide experimental data to validate the structural models created in this project.

Bonding of B-pillar inner and outer panels preformed and molded using carbon-fibers was completed at EMC^2 in Sterling Heights, MI. Two sets of panels were bonded first to confirm the bonding parameters. Six sets were then bonded for subsequent torsion and bending tests. A bonded assembly of carbon-fiber B-pillars is shown in Figure 6.

Figure 6. Carbon-fiber assembly in heated bonding fixture.

All six bonded parts were coordinate-measuring-machine (CMM) checked after bonding in 32 locations along the bond-line and 23 locations on the outer surface. One part fell within the dimensional tolerance (±1.0mm) in all locations. The locations that fell outside of the specified tolerance on the other parts were primarily along the center of the B-pillar and were slightly outboard of design intent.

Flow Modeling

Professor Suresh Advani of the University of Delaware developed a flow model for the molding of carbon-fiber preforms by the injection-compression process used in FP3 (see also 4.L). The flow model is a design tool to assist in optimizing the location of the injection points for body-side tooling. The intention was to develop and confirm a flow model with the B-pillar and then extend it to the full body side. The body-side flow model was completed earlier for a single injection point, and is now extended to multiple injection points.

The mold filling of the full body side was modeled in a similar fashion to the B-pillar. At the start of the injection step, the mold is assumed to be partially open, with a gap between the preform and the upper mold half. The resin is injected into this gap and is initially pooled on top of the preform. In the compression step, the mold is fully closed, which then forces the resin completely through the preform, filling out the part.

The filling dynamics, including the last area to fill and the cavity pressure, were modeled for several locations of multiple injection points. This was not an optimization, since with the decision to not produce the full bodyside, there was no justification for a large expenditure of resources for a rigorous optimization. Instead, several case studies were presented to show the effect of using different injection points. An example of the case study is shown in Figure 7 above. The upper chart shows the filling profile with three injection points marked by the arrows. The adjoining dark areas indicate the initial resin pools, and the circles show the last points to fill. The lower chart is the corresponding pressure prediction, with the circle indicating the

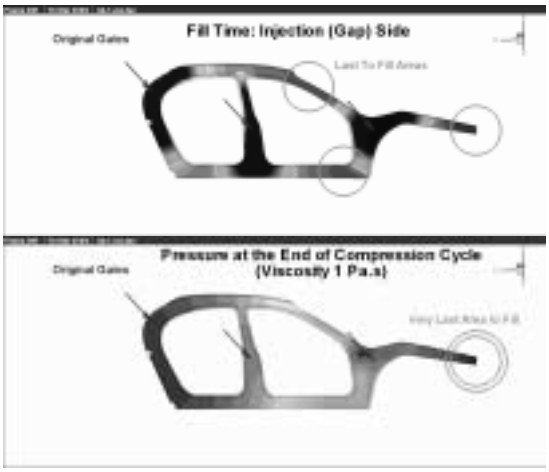

Figure 7. Mold-filling model case study; arrows indicate resin ports, circles are last-to-fill areas, and double circle is lowest-pressure area at fill completion.

position of the lowest pressure in the cavity at completion of fill.

Biocomposites and slurry preforms

Another focus area for reducing vehicle mass is biocomposites. Biocomposites encompass both natural fibers for reinforcement, and using resins based fully or partly on natural products.

One of the major challenges of working with natural fibers is that processing the fibers into composites, either fully formulated or as preforms for liquid molding, is not developed in a cost-effective manner that will yield the volumes needed for automotive production. We are working with Materials Innovation Technologies, Hendersonville, NC, and Advanced Process Technology, Columbia City, IN, to evaluate a slurry process for making preforms. This slurry process is currently used to make speaker cones for audio systems, and is well developed for the uniformity and process speed necessary for that market. The requirements for the automotive market, however, require different fibers, as well as much heavier preforms.

We have evaluated preforms made of carbon-fiber, glass fiber and hemp fiber with this technology, and have found it to be promising. This provides an alternate process for our current fibers, and means for processing fibers which cannot pass through the P4 system. A recent molding trial used commercial

urethane resin, as well as a soy-based resin. Processing was successful, in spite of initial concerns about permeability. Material property evaluation is underway.

B-Pillar Summary

The successful preforming and molding of carbon-fiber B-pillars has been demonstrated. The injection/compression mold-filling model is completed and an alternative preforming technology was investigated. The carbon-fiber distribution by the P4 process is not yet at the uniformity needed for production, but the process feasibility has been demonstrated. The carbon-composite B-pillars were successfully bonded, and these assemblies will be subjected to structural testing shortly. Even though the demonstration batch was molded at 35% fiber volume, much of the resin flow was actually through sections of preform which were above 40% fiber volume. Thus, with improved fiber uniformity, it is expected that preforms of 40% fiber volume would be successfully molded.

Bond-Line Read-Through

A new effort was established to develop a tool to predict bond-line read-through (BLRT) in adhesively-bonded joints was established in FY 2006. This effort consists of three phases:

- Phase 1: Identify a measurement tool capable of objectively quantifying the severity of BLRT
- Phase 2: Experimental evaluation of the contribution of various factors on the creation of BLRT
- Phase 3: Development of an analytical tool to predict BLRT during the design phase.

A better understanding of this defect will allow OEMs to establish minimum material gage specifications based on structural criteria rather than on appearance criteria.

Phase 1

Four imaging systems with the potential to provide the needed objective data for quantifying BLRT were identified. Three of these systems were "structured light" systems. One was a laser scanning system. A preliminary evaluation of each was conducted and the Ondulo system from Visuol Technologies, Metz, France was found to be the most promising. Consequently, this system was selected for a more in-depth evaluation.

For the in-depth evaluation of the Ondulo system, Meridian Automotive Systems provided a number of decklid assemblies that the plant felt exhibited varying amounts of read-through. The entire decklid was primed and then cut in half. One half of each decklid was painted with a black basecoat/clear-coat automotive paint system. The ACC Joining team visually evaluated these parts prior to the Ondulo trial and found it very difficult to see any defects. Nevertheless, four painted decklid halves and two primed decklid halves were selected for evaluation with the system.

This evaluation showed that the Ondulo system was able to image BLRT below the visible limit. This is a positive result since it will allow the team to identify what factors contribute to the creation of BLRT even if the contribution cannot be seen with the unaided eye. Example of Ondulo image is shown in Figure 8.

Unfortunately, the methodologies normally used to quantify defects in this system resulted in numerical values that did not correlate to the team's visual assessment of the severity of the defect in the images.

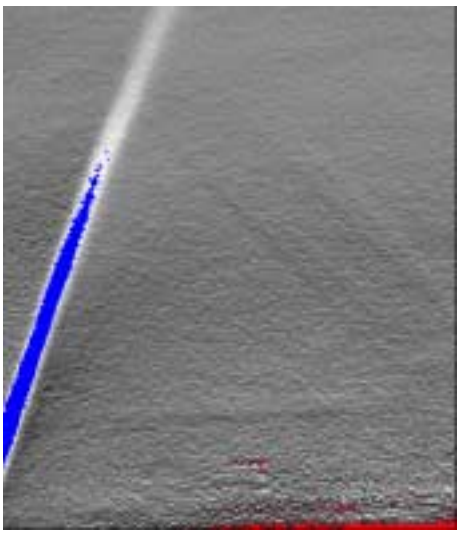

Figure 8. Curvaturemap for primed decklid #3.

A second trial was completed at Meridian Automotive System's Shelbyville, IN manufacturing plant with the intent of creating parts with more visible defects on the parts. Defects were visible in these parts, but not until after the bonded parts had been primed. Even though the severity of the defects was greater and the difference between the severities of the defects was greater, the existing methods for quantifying defects still did not produce values that corresponded with our visual assessment.

Visuol Technologies was then contracted to identify an appropriate metric given the data available in the images. The Joining team created a set of fifty panels that cover the spectrum of BLRT severity from not visible to very visible. The set included "as-bonded", primed, and painted panels. The images of these panels will be used to derive the parameters that influence the apparent severity of the defect.

BLRT was visible on the primed plaques and the painted black plaques. Those two sets of panels were visually ranked by thirty people to provide baseline "visual assessment" data. The imaging and analysis of those images will be completed in FY 2007.

Phase 2

Once a measurement tool is available to quantify the severity of BLRT, experiments can be completed to determine the root causes of this defect. The team generated a list of forty-one potential sources of BLRT. The list was then reduced by designating certain factors as noise factors and by prioritizing the list. The team discussed how best to evaluate the effect of the various factors. A flat outer panel was determined to be sufficient for this work, but no existing inner-panel tool was found that meets the project's needs. Consequently, a project-specific inner-panel tool was designed. The construction of the inner-panel tool was contracted to JATCO Machine & Tool Co., Inc in Pittsburgh, PA after a competitive bidding process. The tool construction is now underway.

Structural Composite Underbody

A new effort being developed to take advantage of the learnings from FP3 is the structural composite underbody. The objective is the design, analysis, and fabrication of a structural-composite underbody, as well as the joining of this underbody to the rest of the vehicle. This is targeted to be part of the USAMP Multi-Material Vehicle (MMV) project, and will follow the MMV goals for cost and mass as they are established. The primary research outcomes of this project will be:

- A 2 ½ minute cycle time (100k upa, 2-shift operation)
- Developing methods of joining and assembly of the underbody to the vehicle

A large, rear-wheel-drive vehicle has been selected as the donor vehicle for the MMV, including this underbody. Phase 1 of this effort is the selection of the materials and processes for the underbody. This involves:

- the development of a design concept, including a means of joining and assembly
- the preliminary design of the concept using a limited number of material and process systems
- the selection of a material and process system based on
  - manufacturing considerations
    - Is there a way forward to get to 2 ½ minute cycle time?
    - Is joining and assembly feasible in a manufacturing environment?
  - compatibility with MMV goals, including mass and cost
  - technical cost model analysis

Phase 2 will be full design, incorporating other components of the MMV, based on the donor vehicle.

Phase 3 will be fabrication of the underbody and assembly to the donor-vehicle structure.

Phase 1 had progressed with analysis of the current steel underbody, and selection of a design concept. This preliminary design is shown in Figure 9. This design concept makes use of ribbed sections, and

will address attachment via weld-bonding to the front and side rails. Our analysis is now showing that strain will be a major factor in the performance of a composite material in this application, so we are developing an experimental program aimed at increasing the strain of our material options. This will target design of fabric reinforcements, as well as alternative fibers such as Kevlar or Spectra.

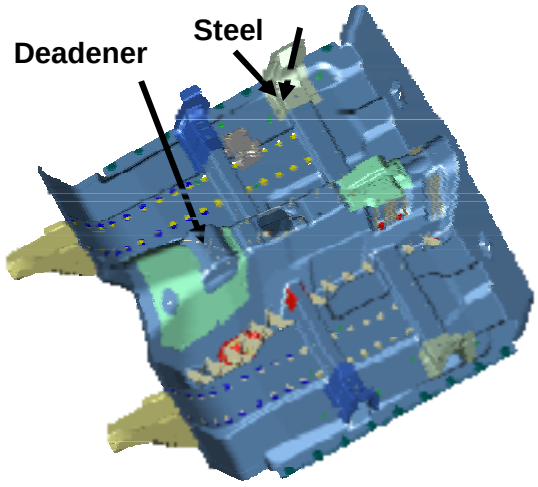

Figure 9. Top view of the preliminary design concept for the composite underbody.

Lightweight, Low-Cost Composite Seat

This is a new effort started in January of 2006. The primary objective is to develop materials, processes and designs to yield a light-weight, low-cost composite seat structure. A team has been established and a set of assumptions has been created.

On a vehicle level, 2nd-row, outboard, stand-alone seats are the target applications for the composite. Comparator seats from each of the OEMs have been selected: Land Rover LR3, Chrysler Town & Country Stow N Go, and the GMT-800 (Suburban). Manufacturing volumes of up to 200k upa will be designed for.

On a structural level, only the back frame, cushion frame, and the pivoting recline/folding joint will be included in the scope of the effort. The structure will include provisions for mounting a conventional carry-over headrest and will be designed for inclusion of a seat-integrated restraint. The mechanisms and stanchions that mount the seat to the floorpan of the vehicle will not be included. These components are quite vehicle specific due to the variations in floorpan geometry and in desired articulation of the seats for fold-flat and easy entry.

On a materials level, the effort will investigate predominately glass-fiber-reinforced composites due to cost considerations, but will consider local reinforcement with carbon-fiber and other materials including metal reinforcements. Both thermoset and thermoplastic matrix material will be included.

This effort intends to further the understanding and state of research in several areas. In the design arena, it will seek additional parts- integration opportunities by investigating structural-appearance composites. Opportunities exist in folding seats since the seat back becomes a load floor in the folded position. This load floor is very often trimmed with an additional panel over the structural seat-back that provides both an acceptable appearance as well as abrasion and wear resistance. The goal is to integrate the appearance, wear, and abrasion resistance into the structural seat-back, thus eliminating pieces. There is also opportunity to integrate many of the current plastic trim covers into the structure of the seat.

Hard-point design will also be advanced. The pivoting joint between the seat-back and the cushion will require the use of a steel recliner mechanism and will need to be a bolted connection for trimming, assembly and repair. This will require innovative design of the bolted joints in the composite structures due to the high loads that these joints must carry, particularly when the seat-integrated restraint is included.

In the materials arena, the use of oriented fibers for local reinforcement will need to be developed at the high volumes required for the seat application. Hybrid materials of glass and carbon-fiber reinforcement with also need to be developed.

Comparison seat teardowns and testing have been have been preformed by MSX International, Auburn Hills, MI. As an example of non-destructive load testing, Figure 10, details the first static load case

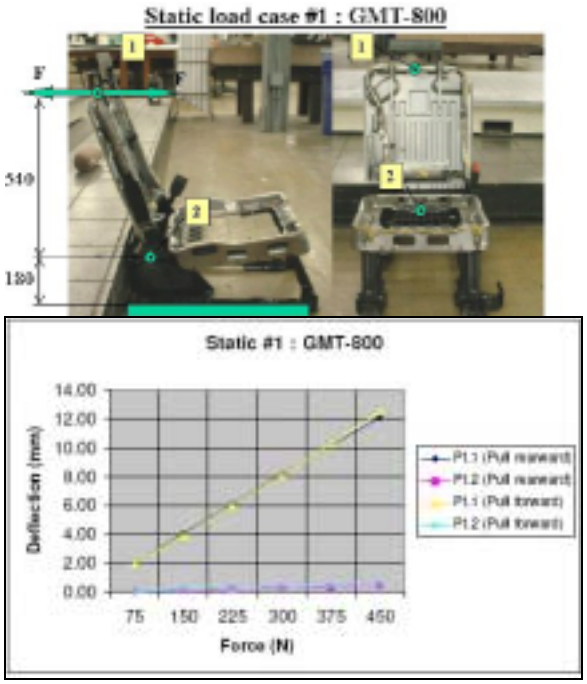

Figure 10. Test setup and example data from comparator seat testing.

where a series of loads were applied to the seat-back and deflections were measured at the top and bottom of the GMT-800 (Suburban) seat-back. Altair Engineering, Troy, MI, applied these load cases to the current seat design, Figure 11, generated by Chelexa Design, Taylor, MI. Three materials, a carbon-fiber composite, a long-glass polypropylene and a glass-fiber SMC, at a uniform thickness of 5 mm, were compared to the load case results, with the carbon-fiber composite being too stiff and the glass-fiber SMC and long-glass polypropylene not stiff enough. The seat design is being modified by Chelexa Design for each of the three materials to obtain the best weight savings.

Figure 11. Design status of composite seat structure.

Publications

Stanley Iobst, Xinran Xiao, Libby Berger, Jeff Dahl, and Dan Houston, "Fabrication and Structural Modeling of the Automotive Composites Consortium B-Pillar," presented at SAMPE, Long Beach, May 4, 2006.

[i] Denotes project 080 of the Automotive Composites Consortium (ACC), one of the formal consortia of the United States Council for Automotive Research (USCAR), set up by the "Big Three" traditionally USA-based automakers to conduct joint pre-competitive research and development.

E. Interphase Analysis and Control in Fiber-Reinforced Thermoplastic Composites

Principal Investigator: Jon J. Kellar
Department of Materials and Metallurgical Engineering
South Dakota School of Mines and Technology
501 E. St. Joseph Street
Rapid City, SD 57701-3901
605-394-2343, fax: 605-394-3369; e-mail: jon.kellar@sdsmt.edu

Technology Area Development Manager: Joseph A. Carpenter
(202) 586-1022; fax: (202) 586-6109; e-mail: joseph.carpenter@ee.doe.gov

---

Contractor: South Dakota School of Mines and Technology
Contract No.: DE-FG02-04ER46117

Objectives

- Develop the science underlying the formation and effects of transcrystalline regions in carbon-fiber-reinforced thermoplastic-matrix composite systems.
- Exploit the understanding developed from the research described above to allow controlled tailoring of the interphase transcrystallinity for specific applications.
- Analyze processing parameters in new thermoplastic-matrix composite technologies, specifically the DRIFT (**D**irect **R**einforcement **F**abrication **T**echnology, Southern Research Institute/University of Alabama-Birmingham) and the P4 (**P**rogrammable **P**owered **P**reform **P**rocess, Department of Energy (DOE)/Oak Ridge National Laboratory (ORNL)) processes.
- Generate composites with tailored interphases for specific applications of laminates produced by the DRIFT and P4 processes in the FreedomCAR and other DOE initiatives in lighter weight vehicles.

Approach

- Choose matrix materials relevant to the FreedomCAR and DOE automotive lightweighting materials initiatives.
- Characterize the chosen matrix materials with respect to mechanical properties and crystallinity.
- Determine the thermodynamic and practical adhesion between the chosen matrix materials and carbon fibers. The carbon fibers will be both sized and unsized.
- Identify and control the presence and size of transcrystalline regions in the matrix material adjacent to the carbon fibers.
- Manufacture laminates using the DRIFT and P4 processes having controlled transcrystalline regions.
- Perform mechanical testing, including tensile testing, impact testing and indentation testing of the laminates having controlled interphases.

Accomplishments

- Calibrated carbon-fiber resistive-heating unit for PAN- and pitch-based fibers.
- Measured the maximum shear stress, debond load and friction coefficient for pitch-based carbon fibers having different transcrystalline layer thicknesses. Thicker transcrystalline layers increased all three quantities by 25-50%.

- Measured the transcrystalline layer thicknesses at 2, 7, 15 and 50ºC/minute cooling rates and determined the variability (~20%) of the transcrystalline layer thickness.
- Developed an analytical model for determining carbon-fiber temperature during resistive heating.
- Measured the tensile properties, including Young's modulus, Poisson's ratio and yield strength, of neat polypropylene.
- Developed a sample preparation procedure for examining the transcrystalline interphase regions of thermoplastic polymer beads melted onto carbon fibers.
- Completed building of a tabletop Mini-DRIFT system.
- Principal investigator Dr. Kellar and co-PI Dr. Kjerengtroen visited ORNL to discuss this project.

Future Direction

- Thermodynamic and practical adhesion measurements of thermoplastic polymer matrices with carbon fibers having various (including no) sizings will continue.
- Mechanical property determination of matrices and fibers will continue. Much of this work will be performed at SDSM&T, but some single-fiber testing work may be performed at ORNL.
- Measurement of the extent of transcrystalline regions in test pieces will be continued using an upgraded atomic-force microscope accessory.
- Laminates will be manufactured using the miniature-DRIFT apparatus developed in this research.
- Static and dynamic mechanical testing of DRIFT laminates made under controlled conditions leading to specific transcrystalline region thicknesses will be performed.
- Develop a mathematical model to predict the behavior of transcrystalline regions of carbon fibers/thermoplastic-matrix composites during a continuous manufacturing process.

Introduction

Over the past decade considerable effort has been expended to develop a new generation of vehicles that are lighter and more fuel-efficient than today's vehicles. In addition, these vehicles should retain crashworthiness and be of relatively low cost. Targets include reduction in overall weight of approximately 40%, primarily achieved through lighter body and chassis materials. Polymer-matrix composites (PMCs) have reached this target with a potential weight savings of 70%. At the current time, PMC technology has, in general, been deemed too costly, as carbon-fiber- based PMCs can cost ten times as much as steel parts. Some of this increased cost is due to the high price of carbon fibers and some due to limitations in the manufacturing process. Many of the problems in the manufacturing process are caused or exacerbated by lack of fundamental scientific knowledge of the interactions between the fibers and matrix materials.

This research is of significance to the DOE ALM in that it will help develop the necessary science base to allow more complete exploitation of PMCs having thermoplastic matrices. Traditionally, these materials have trailed the use of PMCs having thermosetting matrices, because of processability issues stemming from the low viscosity and wetting of the thermoplastic-matrix material. In addition, thermoplastic matrices are generally less strong and less stiff than thermoset matrices. This liability is further compounded by the fact that most fiber reinforcements associated with thermoplastic-matrix PMCs are of fairly short length, mainly because of the processing limitations mentioned earlier. This latter aspect is relevant because short -fiber reinforcements do not carry load as well as long- or continuous-fiber reinforcements. From the automotive perspective, short-fiber-reinforced PMCs are, therefore, most utilized in non-structural components. Further comparisons between thermoplastic- and thermoset-matrix PMCs are warranted here to highlight the focus of this

research project, namely, the role of the interface/interphase region between the fiber and the matrix.

The development of the interphase in thermoplastic PMCs is quite different from that of thermosetting matrices, which tend to be amorphous in nature. Rather, in thermoplastic PMCs, the interphase development is generally due to nucleation and growth of crystallites from the fiber surface rather than actual chemical reactions within the interphase. The interphases formed in these systems are termed transcrystalline regions, reflecting their dependence upon the thermoplastic crystallinity. There has been much speculation in the literature as to the cause for the formation of the transcrystalline region and its role in bulk composite properties. Several conclusions can be reached. First, the transcrystalline region can grow in size to tens of microns, depending upon such parameters as fiber type, morphology and fiber surface treatments such as sizings. Second, the transcrystalline region can significantly affect properties such as the strength and impact resistance. Also, in some cases, different types of transcrystalline interphases may be formed. For instance, both α and β transcrystalline regions were produced around natural fibers in polypropylene-matrix composites. These regions could be altered by inclusion of maleic anhydride in the polypropylene or on the fiber.

With respect to these novel processing routes, two examples are of particular interest to this research. The first is a low-cost process to produce continuous reinforcing fibers with thermoplastic matrices, called the **D**irect **R**einforcement **F**abrication **T**echnology (DRIFT) developed by the Southern Research Institute (SRI) and now located at the University of Alabama-Birmingham (UAB). PMCs produced by this continuous-fiber technology could serve as metal replacements in structural applications, specifically for the automotive industry. Keys to optimal utilization of the DRIFT process are fiber wetting and, ultimately, adhesion of the thermoplastic matrix. Traditionally, sizings are applied to the fibers to help prevent abrasive damage, and assist with lubrication. A major component of the sizing is a coupling agent that aids in wetting, adhesion and hydrothermal stability of the composite. Research conducted in this program utilizes thermoplastic-matrix PMCs produced by UAB or in-house using the DRIFT process.

The second novel processing route of interest is the **P**rogrammable **P**owered **P**reform **P**rocess (P4). While the P4 technology does allow control over fiber length, its main potential benefit is its ability to circumvent previous PMC process limitations through robotic control. To our knowledge, no fundamental analysis of PMC interphases formed by the P4 technology has been undertaken.

This research program builds upon a multi-disciplinary effort with a strong background in interphase analysis and control in thermosetting PMC systems, and applies this experience to new thermoplastic-matrix PMC systems. The research investigates model systems deemed of interest by members of the Automotive Composites Consortium (ACC) as well as samples at the forefront of PMC process development (DRIFT and P4 technologies). Finally, the research investigates, based upon the fundamental understanding of the interphases created during the fabrication of thermoplastic PMCs, the role the interphase play in key bulk properties of interest to the automotive industry.

Project Deliverables

This research will provide a better understanding of the science, particularly with respect to adhesion, of thermoplastic matrices with fiber reinforcements. The adhesion data will be used to identify processing parameters for thermoplastic-matrix composites to tailor transcrystalline interphase formation. Transcrystalline interphases are often quite large (>10 microns) and can be stronger and stiffer than the matrix material or tougher and with greater work of fracture than the matrix. In addition, this work will produce composite samples using new processing technologies and the scientific knowledge gained with respect to adhesion and interphase formation. These test protocols are important to possible end uses for the tailored PMCs in automotive applications.

Accomplishments

Research accomplishments during the past year occurred in two primary areas: interphase formation

conditions and effect of transcrystallinity on composite performance. Progress in each of the two areas is described below.

Interphase Formation Conditions

Interphase formation conditions have been investigated in three primary areas: adhesion, mechanical property determination and extent of crystallinity as a function of formation conditions.

Adhesion: Thermodynamic-adhesion research has been mainly focused on extending the recently-developed fiber resistive-heating apparatus to the use of pitch-based fibers, while practical adhesion has been studied through microindentation testing of model composite systems.

Thermodynamic Adhesion: Thermodynamic adhesion, in this work, is primarily concerned with the measurement of the contact angle of polymer beads on fibers of interest. The melting of beads on carbon and subsequent control of cooling rate is necessary for understanding of the effect of transcrystallinity on the thermodynamic adhesion. To manufacture the beads in a manner similar to the DRIFT process, a technique to resistively heat the carbon fibers has been developed. Currently, this system has been calibrated and a variety of fibers tested to determine the reproducibility of fiber heating and of the resistivity (at 20°C) and temperature coefficient. Figure 1 shows a graph of the data obtained for several PAN-derived, carbon fibers and several pitch-based, carbon fibers. Literature values for carbon are also shown[1,2]. As shown in Figure 1, the data for the various fiber types exhibit relatively small levels of variation, as the coefficients of variation for both the resistivity (at 20°C) and the temperature coefficients are less than 11.5% for both fiber types. Compared to the literature values, both fiber types exhibit smaller magnitude temperature coefficients (16-19 µohm*m for PAN fibers and 13-15 µohm*m for pitch-based fibers) and larger resistivity at 20 ºC (-2.5 to –3 x 10^{-4} K^{-1} for PAN fibers and –1 to –2 x10^{-4} K^{-1} for pitch-based fibers). The resistivity of carbon given in the literature varies from about 3-60 µohm*m depending upon the crystal structure and the presence of impurities[1,2]. Only one literature value for the temperature coefficient was found. The importance of these data for this work is that pitch-based carbon fibers have the smallest temperature coefficient, which will increase the imprecision of determining the fiber temperature during resistive heating from about 2°C for PAN-based carbon fibers to about 7°C for pitch-based, carbon fibers.

Interphase regions are known to significantly affect the mechanical properties, such as strength and impact resistance, in thermoplastic composites. Generally, both the temperature and the rate of change in the temperature, affect the formation of transcrystalline regions during manufacturing processes. Thus, analyzing thermal behaviors of the transcrystalline regions during heating and cooling processes is important in understanding the mechanisms of formation/growth of the transcrystalline regions. To better understand these thermal behaviors, a model was developed.

A nonlinear differential equation was obtained by applying an energy balance principle on a finite element of the carbon-fiber model. The model was then discretized and the corresponding difference equation was coded by Matlab. A negligible temperature gradient along the fiber was observed, except at the very end regions, close to the electric poles. Therefore, conduction along the wire could be neglected. Because the time to reach the steady-state temperature is less than 200 msec, transient temperature effects can also be neglected. In addition, the natural convective heat-transfer term can be neglected, because its value is far less than that of the radiation heat-transfer term. Thus, the applied electric energy is balanced only by the radiation heat-transfer term and can be approximated further into an algebraic steady-state-temperature equation in terms of the input supply voltage as shown by Equation 1. In Equation 1, V_s is the applied voltage, r is the fiber radius and L is the length of the carbon fiber, while σ and ε are

$$\frac{2\sigma\varepsilon(T^4 - T_\infty{}^4)}{r} + \frac{V_s{}^2}{L^2\rho_e[1+\alpha(T-T_\infty)]} = 0 \qquad (1)$$

the Stefan-Boltzmann constant and the emissivity, respectively. Finally, T is the temperature of the fiber and T_∞ is the air temperature.

Equation 1 was solved by a root-finding algorithm. This equation shows how the temperature of a carbon fiber (T) can be controlled by adjusting the input electric voltage. However, predicting the temperature is significantly affected by the uncertainty of input parameters such as electric resistivity (ρ_e) and the temperature coefficient of resistivity (α) of the carbon fiber. The values for these parameters measured in this work are shown in Figure 1. Currently, no technique has been found to directly measure the surface temperature of the heated carbon fiber; thus, the temperature is approximated by melting thermoplastic polymers with a known melting temperature.

Practical Adhesion: To measure the practical adhesion, model unidirectional composite samples were manufactured by compression molding a thin, polypropylene/pitch-based carbon-fiber laminate at 205°C at 0.3 tons pressure for 30 minutes to erase the thermal history of the PP. After the melting hold time, the samples were cooled at 2°C/minute using the press-cooling ability and at ~50°C/minute using dry ice applied to the top and bottom mold surface. As will be shown in the *Extent of Crystallinity as a Function of Formation Conditions* section, these cooling rates produced different thicknesses of transcrystalline regions around the fibers, about 100 µm thick for 2°C/minute and 20 µm thick for 50°C/minute.

These samples were prepared for practical adhesion (microindentation) testing so that the total thickness was about 76 µm. A thin sample such as this was necessary for push-through microindentation testing. Individual fibers were located and indented using a force ramped from 0 to 60 mN over 30 seconds and held at the

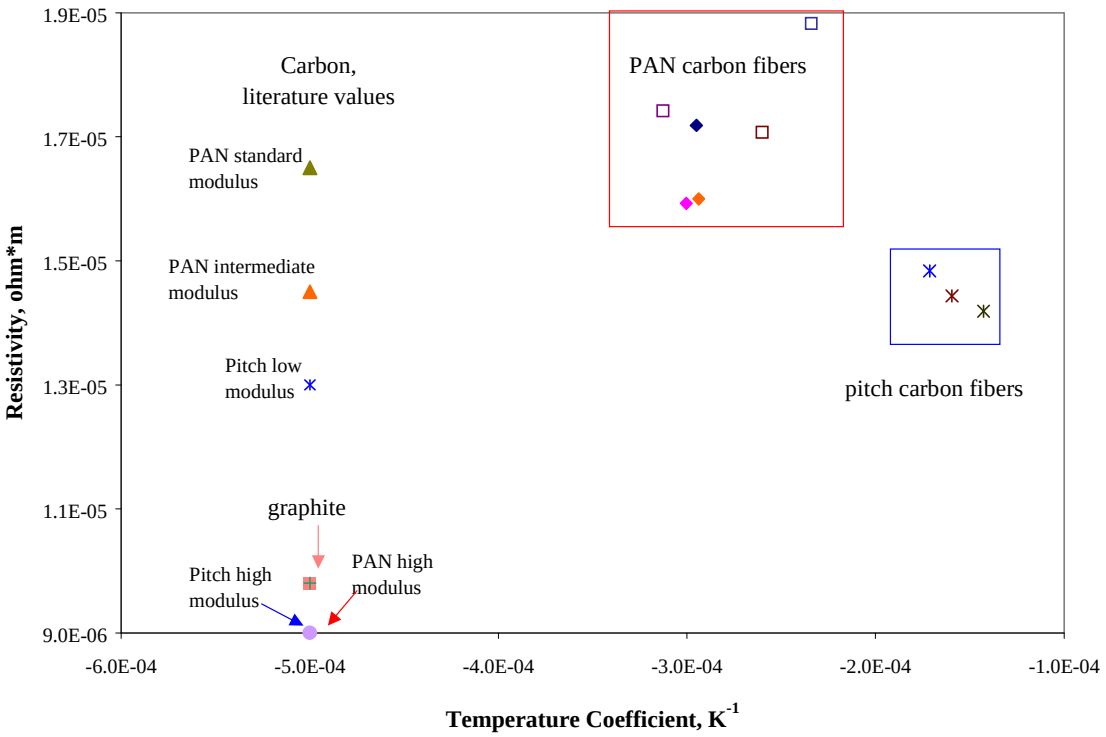

Figure 1. Temperature coefficient and resistvity at 20°C determined for the fibers used in this work compared to literature values1,2 for various types of carbon.

maximum value for 10 seconds. Unloading occurred over the same time range as did loading. For the cooling rates examined, at least 15 fibers were debonded.

There are typically four different regions of the load-displacement curve. Stage I is the initial loading of the fiber. In this stage, the indenter goes from no contact to full contact with the fiber surface, making this region non-linear since the contacted area of the tip is increasing with the load. Stage II is the linear sample-loading segment. The fiber and matrix are deflecting under load with no relative motion between the two. Stage III is the crack-initiation and debonding region of the curve. The initial part is where the mode II crack initiates at the fiber/matrix interface. The crack grows to an unstable state until the entire fiber is completely debonded from the matrix. Stage IV is the region where the fiber is sliding along the interface. The debond load was calculated for each test performed. Also, the maximum shear stress (MSS) was calculated from shear-lag theory and the slope of Stage II. Finally, the post-debonding behavior was modeled using a sliding-friction model.

Table 1 contains a comparison of the microindentation data for the two cooling rates. The more rapidly cooled sample, having a larger transcrystalline layer thickness (100 μm vs. 20 μm), exhibits a greater MSS (37% greater) and debond load (46.5% greater). Theses differences are statistically significant at the 90% level. Further, discussion of this can be found in reference 3.

Mechanical Property Determination: The tensile properties of pure polypropylene have been studied during the research period just finished. The polypropylene samples were manufactured using a Wabash press with stops to ensure a sample thickness of 2.9 mm. The specimens were heated at 5°C/minute to 200°C, held at this temperature for 10 minutes, then cooled at 10 °C/minute. Following cutting the samples to ASTM D638, Type I sample size specifications, strain gauges were affixed to determine the Poisson's ratio and tensile tests were performed according to ASTM D638 with a rate of 5 mm/minute leading to specimen failure in approximately 1 minute. Figure 2 shows a typical stress-strain curve for these samples. At the strain rate utilized, the Young's modulus shows in Figure 2 is 1950 MPa, while the average Young's modulus found was 2130 ± 350 MPa. The yield strength was also found from the stress-strain curve and the mean yield strength found was 7.0 ± 2.3 MPa. Finally, the mean Poisson's ratio was determined to be 0.326 ± 0.018.

Also, on certain samples, strain gauges were placed on both the top and bottom of the specimen. Little difference was observed between the two sides of the sample indicating that the top and bottom of the tensile samples were in the same state of tension.

Extent of Crystallinity as a Function of Formation Conditions

To investigate the extent of crystallinity as a function of formation conditions in greater detail, research efforts were directed towards two areas: 1. transcrystalline layer formation and 2. sectioning polypropylene beads on carbon fibers perpendicular to the long fiber axis.

Transcrystalline Layer Formation: Experiments were conducted to examine transcrystalline layer formation during cooling. These experiments used a hot stage mounted on a polarized microscope stage Two thin layers of polypropylene with a small number of fibers sandwiched between the layers were placed in the hot stage and heated to approximately 200°C for 10 minutes. After this hold, the stage was slowly cooled at various rates and the crystallization recorded with a video

Table 1. Microindentation test data.

	Maximum Shear Stress, MPa	Debond Load, mN	Friction Coefficient
2°C/minute	0.37±0.13	38.7±12.5	<0.2
50°C/minute	0.27±0.05	26.4 ± 5.8	<0.1

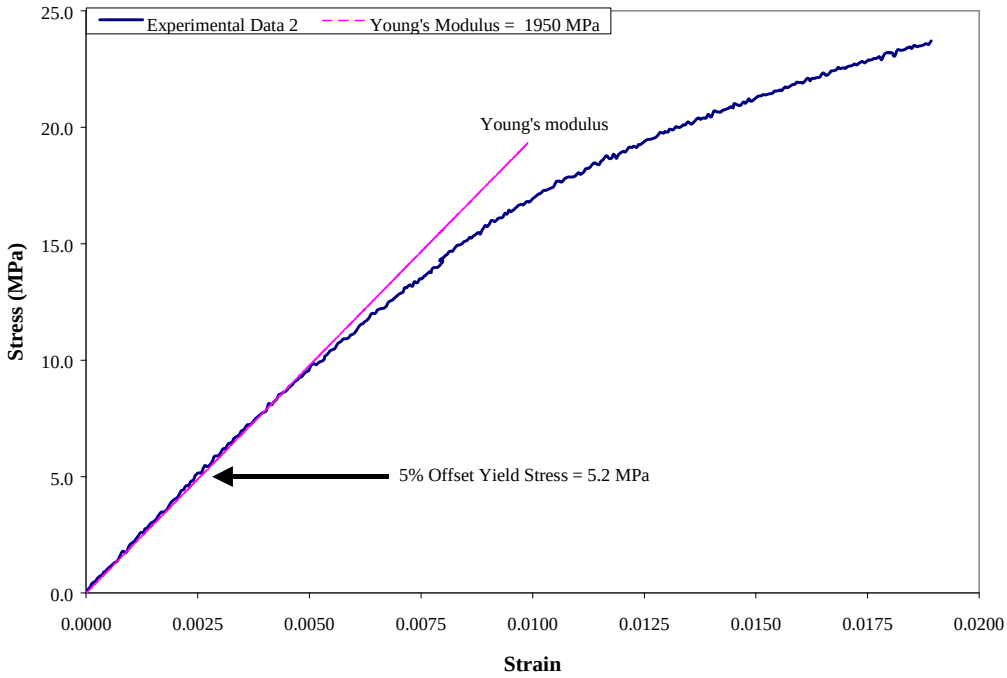

Figure 2. Typical stress-strain cuve of polypropylene tested at 5 mm/minute.

camera mounted to the polarized microscope. Following examination of the transcrystalline layer by video, the samples were microtomed and etched using a potassium permanganate/sulfuric acid/orthophosphoric acid etchant. Figure 3 shows scanning electron microscope micrographs of the etched samples. As seen in Figure 3, the transcrystalline layers were quite variable in thickness. This had been observed previously, and was quantified from the video micrographs taken in this research for a PP/pitch-based carbon-fiber system. The mean transcrystalline layer thickness was 3.3 times the fiber diameter (~10 μm) or about 30-35 μm. The standard deviation of measurements is 0.7 times the fiber diameter, giving a coefficient of variation of about 20%. From Figure 3 and similar figures not shown in this report, the thicknesses of the transcrystalline layer were estimated. The slow-cooled (2°C/minute) samples exhibited a significantly larger transcrystalline layer thickness (~100 μm) than the other three cooling rates all of which exhibited approximately 20-μm-thick transcrystalline layers.

Sectioning polypropylene bead: To obtain samples suitable for atomic-force-microscopic examination of polypropylene beads, sectioning of the bead perpendicular to the fiber long axis was necessary. Bead sectioning was accomplished by embedding the bead and fiber in an epoxy matrix then polishing the resultant cylinder until the bead was reached. Once the bead was found, polishing with 5 μm Al_2O_3 for 2 minutes, then 1 μm Al_2O_3 for 1 minute and 0.3 μm Al_2O_3 for 1-5 minutes was used to yield a surface suitable for atomic force microscopy (AFM).

Initial AFM interrogation of the region surrounding the carbon fiber is shown in Figure 4. In Figure 4, a 10.5 μm x 10.5 μm region is shown in both height (left image) and phase (right image). The fiber is clearly observed, but no obvious transcrystalline layer was observed in this case as the transcrystalline layer is expected to be larger than the area studied. The efficacy of the sample-preparation procedure is shown in the less than 500-nm-height difference over the whole of the sample.

Effect of Transcrystallinity on Composite Performance

Research on the effect of transcrystallinity on composite performance has centered on developing a miniature DRIFT machine. The goal of this

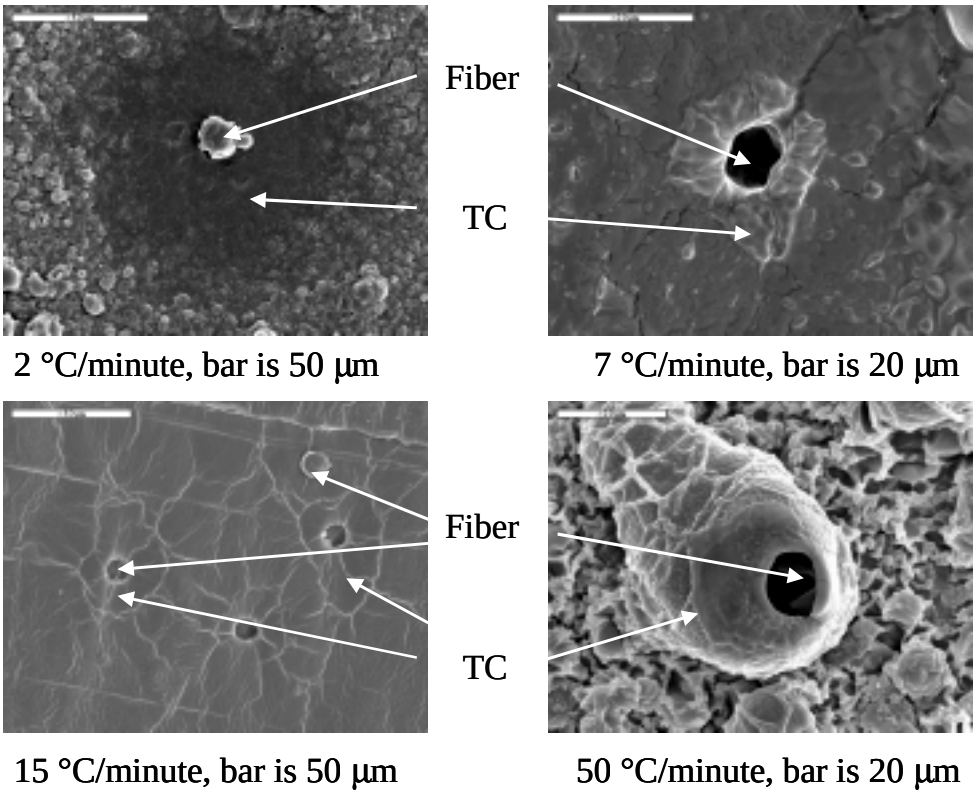

Figure 3. Transcrystalline regions developed around pitch-based, carbon fibers at various cooling rates. TC indicates transcrystalline region. In some cases, the fiber regions indicated on the graph are places where fibers had been pulled out of the surface during sample preparation.

Mini-DRIFT research was to develop a system for producing lab-scale, thermoplastic-composite prepreg samples using the DRIFT process. The DRIFT process is a procedure for making continuous-fiber prepreg materials. It specifies that a continuous-fiber reinforcement material be drawn through a molten resin after being heated beyond the temperature of the resin. While in the resin, a shear is applied to the reinforcement material leaving substantially no voids in the prepreg material (Patent Number: 5,911,932). One of the goals of this aspect of this research is to control and monitor operating parameters and their effects on fiber wetting and material properties. The parameters to be controlled include: fiber draw speed, fiber tension, fiber preheat temperature, resin temperature, and prepreg cooling. The Mini-DRIFT machine consists of four main components: a fiber feed/tensioning system, a furnace, an impregnation tool, and a cooling unit. Flexibility to allow for processing different materials was a major design goal. The system allows different roving sizes and temperature ranges. Due to limited laboratory space, components were selected and/or designed to be compact. The fiber feed/tensioning system, the furnace, and the cooling system are attached to two industrial carts to permit portability and storage. The system produces a continuous tape of prepreg material that can then be processed, likely by compression molding, into the desired sample type for testing. Compared to the UAB system, the Mini-DRIFT system is much better controlled, allowing samples with better-understood history to be manufactured. This understanding will lead to less ambiguity in the determination of the effects of processing parameters on the final product.

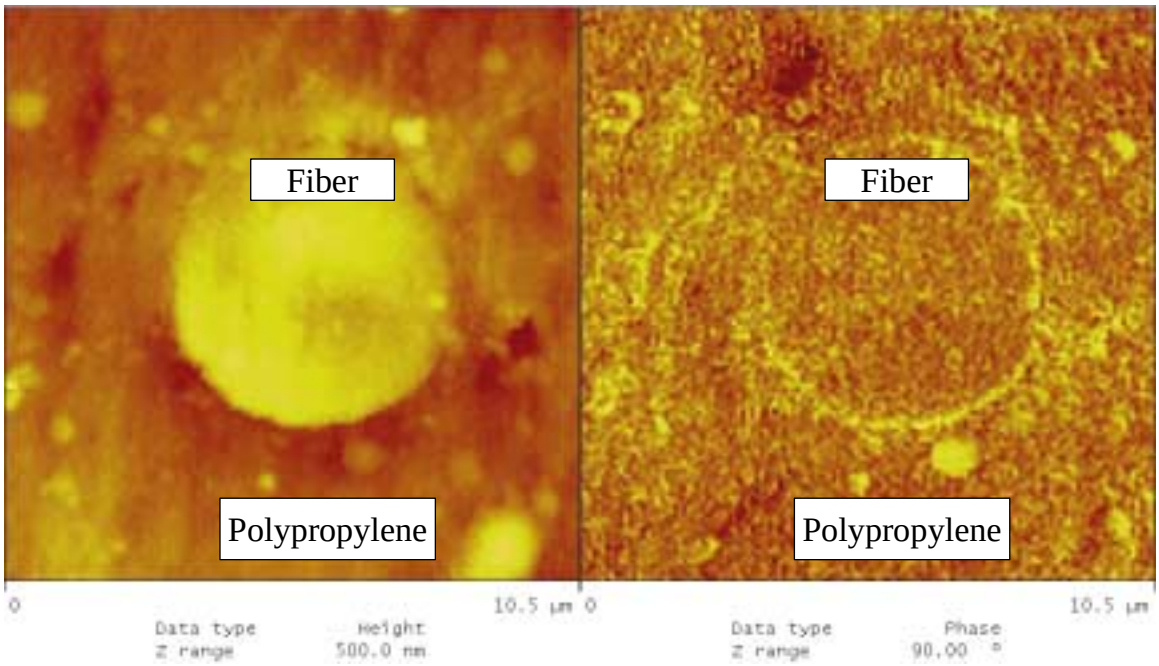

Figure 4. Atomic force micrograph of a polypropylene bead containing a carbon fiber encased in epoxy. The left image is a height image (500 nm maximum height), while the right image is a phase image (90° maximum phase change).

Summary

Highlights of our 2006 research include:

1. Calibrated carbon-fiber resistive-heating unit for PAN- and pitch-based fibers.

2. Measured the maximum shear stress, debond load and friction coefficient for pitch-based carbon fibers having different transcrystalline layer thicknesses. Thicker transcrystalline layers increased all three quantities by 25-50%.

3. Measured the transcrystalline layer thicknesses at 2, 7, 15 and 50 ºC/minute cooling rates and determined the variability (~20%) of the transcrystalline layer thickness.

4. Developed analytical model for determining carbon-fiber temperature during resistive heating.

5. Measured the tensile properties, including Young's modulus, Poisson's ratio and yield strength of neat polypropylene.

6. Developed a sample preparation procedure for examining the transcrystalline interphase.

7. Regions of thermoplastic polymer beads melted onto carbon fibers.

8. Completed building of a tabletop Mini-DRIFT system.

Presentations/Publications/Patents

1. "Characterization of Transcrystalline Zones by Atomic Force Microscopy" L. Nielsen, W. Cross, L. Kjerengtroen and J. Kellar, 2006 South Dakota EPSCoR Conference, Rapid City, SD September 2006.

2. "Transcrystallinity Effects in Polypropylene Matrix Composites" S. Nielsen, W. Cross, R. McGlothlin, J. Kellar and L. Kjerengtroen, 2006 South Dakota EPSCoR Conference, Rapid City, SD September 2006.

3. Bickett, S.J., "Investigation Of Transcrystallinity In Fiber Reinforced Thermoplastic Composites," Masters of Science

Thesis, South Dakota School of Mines and Technology, 2006.

References

1. "Resistivity of Carbon, Graphite", http://hypertextbook.com/facts/2004/AfricaBelgrave.shtml, *The Physics Factbook*, edited by Glenn Elert, 2004, accessed December 11, 2006.

2. "Resistivity and Temperature Coefficient at 20 C," http://hyperphysics.phy-astr.gsu.edu/HBASE/Tables/rstiv.html, *HyperPhysics*, Carl R. Nave, 2005, accessed December 11, 2006.

3. Bickett, S.J., "Investigation Of Transcrystallinity In Fiber Reinforced Thermoplastic Composites," Masters of Science Thesis, South Dakota School of Mines and Technology, 2006.

F. Durability of Carbon-Fiber Composites

Dan J. Naus (Principal Investigator), J. M. Corum, L. Klett, R. L. Battiste
Oak Ridge National Laboratory (ORNL), P.O. Box 2008
Oak Ridge, TN 37831-8056
(865) 574-0657; FAX: (865) 574-6098; e-mail: nausdj@ornl.gov

Technology Area Development Manager: Joseph A. Carpenter
(202) 586-1022; fax: (202) 586-1600; e-mail: joseph.carpenter@ee.doe.gov

Expert Technical Monitor: Philip S. Sklad
(865) 574-5069; fax: (865) 576-4963; e-mail: skladps@ornl.gov

---

Contractor: Oak Ridge National Laboratory
Contract No.: DE-AC05-00OR22725

Objective

- To develop experimentally-based, durability-driven design guidelines to ensure the long-term (15-year) integrity of representative carbon-fiber-based composite systems that can be used to produce large structural automotive components. Durability issues being considered include the potentially degrading effects of cyclic and sustained loadings, exposure to automotive fluids, temperature extremes, and low-energy impacts from such events as tool drops and kickups of roadway debris on structural strength, stiffness, and dimensional stability.

Approach

- Characterize and model the durability behavior of a progression of three representative carbon-fiber composites, each with the same thermoset urethane matrix but having a different reinforcement preform: (1) continuous fiber, ±45° crossply; (2) continuous fiber, quasi-isotropic; and (3) random chopped fiber.
- Replicate on-road conditions in laboratory tests of each composite to generate durability data and models.
- Subsequently shift focus to suitable thermoplastic composites, for which durability issues are generally more significant.
- Develop and publish durability-based design criteria for each composite.

Accomplishments

- Completed durability assessment of a quasi-isotropic carbon-fiber-reinforced thermoplastic material.
- Completed program review with ACC representatives.
- Completed and published durability-driven design criteria document on carbon-fiber-reinforced PPS material suitable for automotive structural applications

Future Direction

- Investigation developing durability-driven design criteria documents for thermoset and thermoplastic fiber-reinforced composite materials has been completed.

Introduction

Before composite structures will be widely used in automotive applications, their long-term durability must be assured. The Durability of Carbon-Fiber Composites project at ORNL was established to develop the means for providing that assurance. Specifically, the project is developing and documenting experimentally-based, durability-driven design criteria and damage-tolerance assessment procedures for representative carbon-fiber composite systems to assure the long-term (15-year) integrity of composite automotive structures. Durability issues being considered include the potentially degrading effects of cyclic and sustained loads, exposures to automotive fluids, temperature extremes, and incidental impacts from such things as tool drops and kick-ups of roadway debris. Research to determine the effect that these environmental stressors and loadings have on structural strength, stiffness, and dimensional stability is being conducted. The project is carried out in close coordination with the ACC.

The approach to investigating durability initially was to address a progression of thermoset composites, each of which had the same urethane matrix:

- reference $[\pm 45]_{3S}$ crossply composite,
- $[0/90/\pm 45]_S$ quasi-isotropic composite, and
- randomly-oriented chopped-carbon-fiber composite.

Characterization of the first two continuous-fiber composites has been completed, and design criteria documents published. In mid-FY 2002, the focus turned to chopped-carbon-fiber composites. Characterization of the randomly-oriented chopped-carbon-fiber composite was completed in FY 2003 and the durability-based design criteria report published. In FY 2003 investigation of carbon-fiber-reinforced thermoplastic materials for structural automotive applications was initiated.

All experimental activities investigating the initial thermoplastic material have been completed and the final report providing durability-based design criteria has been completed and published.[1] Contained in the following sections is a description of the quasi-isotropic carbon-fiber-reinforced thermoplastic material (T material) and a summary of results obtained for this material including a comparison to a previously-investigated quasi-isotropic thermoset carbon-fiber composite (Q material).[2]

Material Description

The T material consisted of a polyphenylene sulfide (PPS) thermoplastic matrix reinforced with 16 plies of carbon-fiber unidirectional tape, $[0°/90°/+45°/-45°]_{2S}$. The carbon fiber was Hexcel AS-4C and was present in a fiber volume of 53% (60%, by weight). Nominal plaque thickness of the T material was 2.9 mm.

The Q material had a 40% volume fraction and a Baydur 420 IMR urethane matrix. Carbon-fiber reinforcement for the Q material was a $[0/90/\pm 45]_S$ layup of continuous, 6K tow, aerospace-grade fibers. Nominal plaque thickness of the Q material was 2 mm.

Elastic and Creep Properties for Design Analysis

In-plane elastic constants for the quasi-isotropic thermoplastic composite (T material) are listed in Table 1, where they are compared with the quasi-isotropic thermoset composite (Q material) values. The T material stiffness is about 13% larger than the Q material value at room temperature, and it is slightly less affected by an increase in temperature to 120°C than is the Q material. Prior thermal cycling had a small effect on the T material. After 25 thermal cycles between -40° and 120°C the

Table 1. Elastic constants.

Temperature (°C)	Elastic modulus, E (GPa)	Poisson's ratio, ν
Quasi-isotropic thermoplastic composite (T material)		
23	36.5	0.29
120	35.7	0.30
Quasi-isotropic thermoset composite (Q material)		
23	32.4	0.31
120	29.8	0.34

tensile strength increased 9.2%, compressive strength decreased 8.4%, and shear strength increased 6.6%. With respect to the Q material, the tensile strength decreased 6.6%, the compressive strength increased 19.7%, and shear strength decreased 3.4%. The loss in shear stiffness was more significant for the Q material (25.1%) than for the T material (4.2%).

A few prior mechanical loadings within the allowable stress range degraded the modulus of elasticity slightly for both materials. For the T material there was no loss of stiffness during the first load cycle, but the stiffness decreased slightly with succeeding load cycles reaching a maximum of about 4% during the last load cycle. Both the T and Q materials exhibited no degradation in ultimate tensile strength during the final load cycle to failure. However, larger numbers of cyclic loads, within the design-allowable cycle numbers, can lead to a gradual stiffness loss. There was no indication that the limit of 10% loss of stiffness over the design-allowable life (reflection of damage accumulation under cyclic loading) would be exceeded in either quasi-isotropic composite.

The bounding effect of fluids on elastic modulus was the same for both the thermoplastic and thermoset quasi-isotropic composites — a reduction of 4%.

Time-dependent tensile creep strains at room-temperature were significantly less in the T material than they were in the Q material. This is illustrated in Table 2 by the time-dependent creep strains predicted to result from the application of a 60 MPa stress for 5000 h.*

Time-dependent creep strain for this condition is about 14 times larger at room temperature in the Q material than in the T material. At 120°C, the factor jumps to 37.9 using the information in Table 2.

Table 2. Time-dependent tensile creep strains due to a stress of 60 MPa applied for 5000 h at room temperature.

Composite	Creep strain (%)	Temperature multiplication factor at 120°C
T material	0.000981	1.7
Q material	0.014684	4.3[a]

[a]The actual stress-dependent factor is 2.9 for 60 MPa, but a single bounding factor of 4.3 was used in Ref. 2.

At room temperature, compressive creep is the same as tensile creep for both the quasi-isotropic composites. At 120°C, compressive creep is about six times the predicted tensile creep for the T material. For the Q material, the factor ranges from 8 to 18 for the stresses examined. In either case, compressive loadings at 120°C should be carefully considered in design.

A single creep-strain multiplication factor of 2.2 is recommended to account for fluid effects in the T material. The corresponding factor for the Q material was 1.7.

Allowable Stresses for Static Loadings

The basic time-dependent allowable-stress quantity used for the T material was the same as that used for the Q material except that the design factor on creep rupture strength was changed from 0.8 to 0.67.

$$S_t \leq \begin{cases} S_0 \\ 0.67\,\sigma_r\ (\text{T material}); 0.8\,\sigma_r\ (\text{Q material}) \end{cases}$$

Here, S_t is the time-dependent allowable stress applicable to tensile stress components, S_0 is the short-time (time-independent) allowable stress, σ_r is the average creep-rupture strength, and S_r is the minimum creep-rupture strength corresponding to time t. Representative values of S_t are tabulated in Table 3 for both the T and Q materials. The room-temperature S_0 value for the T material is 169% of the value for the Q material. This percentage increases to 200% at 120°C, so the short-time strength of the T material is degraded less by

* The 60-MPa stress level is below the allowable stress levels, even at 120°C.

temperature than is that of the Q material. At 5000 hours, the corresponding percentages are 160% and 200%, so temperature has about the same affect on both materials.

Table. 3. Tensile S_t values in air (MPa).

Temperature (°C)	Time		
	0 h	**5000 h**	**15 years**
Quasi-isotropic composite (T Material)			
23	327	311	302
120	314	284	279[a]
Quasi-isotropic composite (Q Material)			
23	194	194	194
120	157	142	130[a]
[a] Unrealistic condition.			

Prior mechanical loads, thermal cycles, and fluid exposure each degrade the allowable stress, S_0. Bounding relations for the T material are summarized and compared with the corresponding reductions for the Q material in Table 4.

Table 4. Bounding strength reductions.

Effect	Strength reductions (%)	
	Quasi-isotropic composite (T Material)	**Quasi-isotropic composite (Q Material)**
Prior loads	4	15
Prior thermal cycles	3	7
Fluid exposure	35	0

For tensile biaxial stress states, the maximum principal-stress theory is recommended for design with both composites. The principal-stress theory is also recommended for compressive and other nontensile biaxial stress states for the Q material. However, the maximum shear strength criterion is recommended for the T material for compressive and other nontensile biaxial stress states. For these latter stress states, the stress is limited to the quantity S_t*, which is based on short-time compressive strength and compressive creep-rupture results. Representative S_t* values for the T material are tabulated and compared with Q material values in Table 5.

The T material allowables in Table 5 are reduced 26% by fluid exposure at room temperature, and 35% at 120˚C. These are much larger than the values used for the Q material.

Table 5. S_t* (MPa) allowable stresses applicable to nontensile biaxial stress states.

Temperature (°C)	Time		
	0 h	**5000 h**	**15 years**
Quasi-isotropic composite (T Material)			
23	175	134	125
120	93	52	46[a]
Quasi-isotropic composite (Q Material)			
23	130	130	130
120	76	17	10[a]
[a] realistic condition.			

Allowable Stresses for Cyclic Loadings

Two room-temperature design fatigue curves were developed for the T material. The first curve is directly applicable to all cycles having a positive mean stress. The second curve is applicable to all cycles having a zero or negative mean stress. The governing stress parameter is $S = \sqrt{S_{max} \times S_a}$, where S_{max} is the maximum stress reached in the cycle, or in the case of a compressive cycle, the absolute value of the minimum stress, $|S_{min}|$, and S_a is the alternating-stress component. To account for the effect of temperature and fluid effects, stress-reduction factors are provided.

Table 6 compares representative allowable maximum cyclic stresses for tensile cycling for the T material with the corresponding stresses for the Q material. At room temperature, the allowable cyclic tensile stress at 10^8 cycles for the T material is 22% greater than that for the Q material. The percentage is 106% at 120°C.

Table 6. Allowable maximum cyclic stresses for tensile cycling (R = 0).

Temperature (°C)	Maximum stress (MPa)	
	10^2 cycles	10^8 cycles
Quasi-isotropic composite (T material)		
23	379	192
120	292	163
Quasi-isotropic composite (Q material)		
23	267	157
120	259	79

Bounding fluid effects multiplication factors for the two materials are tabulated in Table 7. The T material factors are somewhat lower than are those for the Q material.

Table 7. Bounding fluid multiplication factors for allowable cyclic stresses.

Composite	10^2 cycles	10^8 cycles
T material	0.85	0.77
Q material	0.92	0.98

Simplified Summary of Allowable Stresses

As a way of further simplifying and summarizing the allowable design stresses for static and cyclic loadings, Table 8 gives the key allowable stress values for various conditions as percentages of the average room-temperature ultimate tensile strength (UTS) value —551 MPa for the T material and 336 MPa for the Q material. The table shows that while the two sets of values are fairly similar, temperature and time had a greater relative effect on the Q material than they did on the T material.

A strain limit of 0.3 to 0.4% has often been used, at least for glass-fiber composites for design of composite automotive structures.* The strain limit is intended to cover all effects. For the T material, strain limits of 0.3 and 0.4% correspond to elastic stresses of 19% and 26% of the average room-temperature UTS, respectively (the corresponding values for the Q material are 29 and 39%, respectively). Comparison of the 19% and 26% stress levels for the T material with the allowable values in Table 8 shows that the 0.3% strain limit covers all the listed conditions, while the 0.4% limit covers all conditions except 10^8 cycles at 120°C with fluid effects. For the Q material, the strain limits would cover all the realistic conditions except for high-cycle fatigue at 120°C.

Table 8. Key allowable tensile stresses, expressed as a percentage of average room-temperature UTS[a].

Stress allowable	Without fluid effects		With fluid effects[b]	
	23°C	120°C	23°C	120°C
Quasi-isotropic composite (T material)				
S_0 (0 h)	59	57	54	52
S_t				
5000 h	56	52	52	48
15 years	55	51[c]	52	48[c]
S_{max} (R = 0)				
10^2 cycles	69	53	59	45
10^8 cycles	35	30	27	23
Quasi-isotropic composite (Q material)				
S_0 (0 h)	58	47	54	44
S_t				
5000 h	58	42	54	40
15 years	58	39[c]	54	36[c]
S_{max} (R = 0)				
10^2 cycles	79	77	73	71
10^8 cycles	47	24	46	23

[a] T material UTS_{avg} = 551 MPa; Q material UTS_{avg} = 336 MPa.
[b] Prior loads and prior thermal cycling reductions are not included in these values.
[c] Unrealistic condition.

Damage Tolerance Evaluation

For specific low-energy impacts such as roadway kickups, tool drops, and load drops in a pickup box, experimentally-derived correlations are given for (1) estimating the damage area from the mass and velocity of the impacting object and (2) determining, from the estimated damage area, the resulting degradation in strength. While these correlations are clearly tied to the specific sizes and geometries of the impacted plate specimens and of the specimens used for mechanical property evaluations, it is thought that they do provide useful information. This is particularly true when

* In the aerospace industry, fixed wing and rotocraft composite structures have been successfully designed to operate at strains up to 0.4%.[2]

comparing the relative response of two different composites.

Table 9 gives the predicted impact damage areas that were obtained from design curves that had been developed for four representative combinations of impactor mass and velocity for the quasi-isotropic thermoplastic composite (T material), the quasi-isotropic thermoset composite (Q material), and the ±45° crossply laminate.[3] The latter continuous-fiber thermoset composite is added to the comparison because it has roughly the same thickness (3.2 mm) as the T material, whereas the Q material was thinner (2 mm vs. 2.9 mm). With one exception, the damage areas for the T composite are larger than those for the other two composites. As observed from the impact tests, the T material had a greater propensity to delaminate than did the previous composites.

Table 9. Damage areas in mm^2 from design curve.

Mass (kg)	Velocity (m/s)	Quasi-isotropic Comp. (T Mat'l)	Quasi-isotropic Comp. (Q Mat'l)	±45° Cross-ply
11.52	0.8	178	168	72
11.52	1.3	350	891	338
0.0227	22.4	321	168	84
0.0227	36.4	911	891	396

The T material is somewhat more damage tolerant than the Q material. For both composites, 76.2-mm-wide mechanical property specimens containing the impact damage area were cut from impacted plate specimens. The T material specimens were used for both tension and compression tests. Only compression tests were performed for the Q material. Typical strength-reduction ratios from the lower-bound curves that had been developed are tabulated in Table 10.

Table 10. Estimated strength-reduction ratios caused by impact damage.

Damage area (mm^2)	Strength-reduction ratio	
	T material	Q material
100	0.71	0.60
500	0.51	0.45

Conclusions

Recommended durability-based design properties and criteria for a quasi-isotropic carbon-fiber reinforced thermoplastic composite for possible automotive structural applications have been developed. The composite consisted of a polyphenylene sulfide (PPS) thermoplastic-matrix (Fortron's PPS – Ticona 0214B1 powder) reinforced with 16 plies of carbon-fiber unidirectional tape $[0°/90°/+45°/-45°]_{2S}$. The carbon fiber was Hexcel AS-4C and was present in a fiber volume of 53% (60%, by weight). The study was guided by (1) the need to establish criteria that could be readily integrated into the existing automotive structural design process and (2) by the fact that it was not feasible to experimentally examine all possible combinations of conditions. Thus, simplifications, assumptions, and extrapolations were necessary, as is often the case when definitive design guidance must be provided. The criteria were based upon four categories of data: (1) short-time tensile, compressive, shear, and uniaxial and biaxial flexure; (2) cyclic fatigue; (3) time-dependent creep and creep rupture; and (4) prior load effects. In all categories, except for the fourth, the effects of temperature and of two bounding fluids - distilled water and a 70% methanol/30% distilled water windshield washer fluid - were established. From these tests, properties and correlations for elastic and creep design analyses were generated, a biaxial-strength criterion was chosen, time-dependent allowable stresses for static loadings were developed, and limits for cyclic loadings were established. The resulting criteria are summarized in Table 8 for key conditions. The allowable stresses in the table are expressed as a percentage of the average room-temperature UTS of 551 MPa. These allowables vary from 59% of the UTS for short-time loadings at room temperature in air, to 35% for 10^8 cycles at room temperature in air, to 23% for 10^8 cycles at 120°C with fluid effects.

It was not possible to examine all possible combinations of conditions in establishing the allowables reflected in Table 8, and while it is believed that the allowables would lead to an adequate design, some areas should be further examined. In particular, it is suggested that the effects of compression and biaxial stresses in creep

and the effects of biaxial and mean stresses in fatigue may require further attention. How do the criteria presented here compare with past design practice for glass-fiber composite automotive structures? A commonly used "rule-of-thumb" has been a strain limit of about 0.3%. For the quasi-isotropic carbon-fiber-reinforced thermoplastic composite, this strain limit corresponds to an elastically-calculated stress of 19% of the average room-temperature UTS. Comparison of this value with the allowables in Table 8 shows that the 0.3% strain limit covers all listed conditions.

References and Publications

1. D.J. Naus et al., Durability- Based Design Criteria for a Quasi-Isotropic Carbon-Fiber-Reinforced Thermoplastic Automotive Composite, ORNL/TM-2006/011, Oak Ridge National Laboratory, Oak Ridge, Tenn., April 2006.

2. J.M. Corum et al., *Durability-Based Design Criteria for a Quasi-Isotropic Carbon-Fiber Automotive Composite*, ORNL/TM-2002/39, Oak Ridge National Laboratory, Oak Ridge, Tenn., March 2002.

3. J.M. Corum et al., *Durability-Based Design Properties of Reference Crossply Carbon-Fiber Composite*, ORNL/TM-2000/322, Oak Ridge National Laboratory, Oak Ridge, Tenn., April 2001.

G. Composite Crash-Energy Management (ACC100[i])

Principal Investigator: Richard Jeryan
Ford Research and Innovation Center
2101 Village Road
MD3137 SRL
Dearborn, MI 48124-2053
(313) 594-4903; fax: (313) 337-5581; e-mail: rjeryan@ford.com

Field Project Manager: C. David Warren
Oak Ridge National Laboratory (ORNL)
P.O. Box 2009, Oak Ridge, TN 37831-8050
(865) 574-9693; fax: (865) 574-4963; e-mail: warrencd@ornl.gov

Technology Area Development Manager: Joseph Carpenter
(202) 586-1022; fax: (202) 586-1600; e-mail: joseph.carpenter@ee.doe.gov

Expert Technical Monitor: Philip S. Sklad
(865) 574-5069; fax: (865) 576-4963; e-mail: skladps@ornl.gov

---

Contractor: U.S. Automotive Materials Partnership (cooperative agreement) Automotive Composites Consortium (ACC) Energy Management Working Group
Contract No.: DE-FC05-02OR22910

Objective

- Experimentally determine the effects of material, design, environment, and loading on macroscopic crash performance to guide the design and the development of predictive tools.
- Determine the key mechanisms responsible for crash-energy absorption and examine microstructural behavior during crashes to direct the development of material models.
- Develop analytical methods for predicting energy absorption and crash behavior of components and structures.
- Conduct experiments to validate analytical tools and design practices.
- Develop and demonstrate crash design guidelines and practices.
- Develop and support design concepts for application in demonstration projects.

Approach

- Conduct experimental projects to increase understanding of the global and macro influences of major variables on crash performance.
- Use the data from these experiments to create crash intuition, guidelines, and rules-of-thumb and data for the validation of analysis developments.
- Conduct microscopic experimental characterization to define the mechanisms that occur during and as a result of the crash process.
- Develop and validate analytical design tools to predict structural crash performance based on both phenomenological and micro-mechanical approaches to material and crash-mechanism modeling.

Accomplishments

- A study of the static and dynamic behavior of composite crash was completed to experimentally determine the microstructural factors that lead to decreased dynamic tube-crush energy absorption.
- The average strain energy release rate, G_{Ic}, was obtained in Mode I testing of adhesive joints under static and dynamic loading. Tests showed the effects of mixed loading modes on fracture-energy values.
- A study of structural concepts to improve the energy absorption of sandwich panels showed that the effectiveness of the improvements is highly dependent on the type of core material and somewhat less dependent on the type of fiber facesheet reinforcement.
- Experimental adhesive lap-joint data were used to develop theoretical and numerical tools that describe non-self-similar progression of cracks without specifying an initial crack. A cohesive-decohesive zone model was adopted to represent the degradation of the material ahead of the crack tip. This model unifies strength-based crack initiation and fracture-mechanics-based crack progression.
- A rate-dependent plasticity model for triaxially-braided composites was incorporated into the current predictive tool, along with an implementation of the Tsai-Hahn fiber-bundle theory as applicable to braided composites, to account for the effect of a critical damage area (CDA).
- Tests of 30º, 45º, and 60º triaxially-braided square and circular tubes were completed. The experimental data were obtained for test speeds of 1 m/s and 4 m/s. A predictive algorithm has been developed as a vectorized user material (VUMAT) subroutine for use with the commercial software ABAQUS® and is being validated.
- Kink banding in axial tows was investigated as another phenomenon that contributes to post-peak softening in braided composites. All models investigated included several degrees of tow misalignment. Stress-strain plots for such models show snap-back behavior which is dependent on misalignment degree.
- The study of multiscale modeling methods included the verification of the proposed framework against benchmark computational models. The verification of the multiscale simulation toolkit was completed. The proposed multiscale fracture model was verified against the direct homogenization method and significant improvements in computational performance were demonstrated.

Future Direction

- Continue the development and validation of both micro-mechanical and phenomenological analytical design tools to predict structural crash performance.
- Expand micro-mechanical approaches to model material and crash mechanisms and explore novel multi-scale approaches.
- Expand focus on design tools suitable for use with random chopped carbon-fiber-reinforced composites.
- Continue the characterization of the energy-absorption mechanisms of carbon-fiber-reinforced composites.
- Characterize the critical physical parameters required for analytical model development. Develop test methods to obtain the stress-strain response beyond the peak stress of the materials and expand the current experimental methods to more fully characterize the dynamic material and physical properties needed to advance the modeling capability.
- Determine the effects of manufacturing features and environmental and loading factors, e.g., minor field damage, abrasion, fatigue, and cumulative effects, on the macroscopic crash performance of carbon and carbon/glass hybrid reinforced composites. These results will establish design guidelines and guide the development of predictive tools.
- Develop relationships to implement analytical tools for commercial use.

Introduction

The purpose of the Composite Crash-Energy Management project is to develop and demonstrate the technologies required to apply production-feasible structural composites in automotive crash and energy-management applications. Efforts within the project are intended to understand the mechanisms of polymer composite crash, develop analytical tools for use in vehicle design, and build a knowledge base for the vehicular application of lightweight polymer composites. The projects relate to materials, molding and assembly process and design configurations that are useful in realistic applications. Design-analysis methods will be developed that can be used at several different steps in the design process. These steps require different levels of precision and speed of use and the appropriate tools are expected to include both micro-mechanical and phenomenological approaches.

Static vs. Dynamic Performance

This effort's objectives are to experimentally determine the microstructural factors and behaviors that lead to decreased energy absorption when crushing tubes dynamically. In this study, the strain-rate effects of a braided carbon-fiber composite are investigated at the material- specimen level. The goal is to determine the source of rate effects using specimen-level tests and develop experimental methods by which candidate materials for energy absorption can be evaluated for their rate sensitivity. The results of this study will be used to develop and enhance analytical models that will need to take into account rate-sensitive material behavior.

The effort has been completed and a final report drafted. The study conclusions include:

1. Static 3-pt bending fracture tests (Mode I) showed that the average fracture energy is the best variable for characterizing the "fracture behavior" of carbon-fiber braided materials. It was found that the fracture energy is influenced by the local microstructure.

2. Low-velocity impact tests showed that two "crack systems" were present during crack propagation, i.e., a primary crack in the matrix and a retarded secondary crack within the fiber-bridging zone.

3. The low-velocity impact fracture energies were found to be lower than the static fracture energy for both the Hetron and Epon matrix composites. It was found that under static loading conditions, the extent of the bridging zone was larger and contained a great deal of fiber pullout. In addition, the primary crack was found to be wavy in its trajectory during static loading. Macro- and micro-scopic examination showed that the biased tows pull out of the matrix during crack propagation under static loading. Under impact conditions, the biased tows break cleanly and show less fiber pullout.

4. A comparison of the *in-situ* properties of the Hetron and Epon composites was made. This included a procedure to extract *in-situ* properties from basic specimen-level tests. The results showed that even though the virgin material properties between these resins are similar, the *in-situ* behavior that is observed from composites made from these materials is different. For example, the fracture toughness of the Hetron was about eight times larger than the Epon.

5. Off-axis compression tests used to characterize the shear stress-strain response showed that the shear response in Epon was lower than the Hetron composite. This is an indicator of why there is a difference in the fracture toughness.

6. In addition, the Hetron composite contained 3.6 times more voids than the Epon, especially at the center of the tows. There were also residual tensile stresses in the Hetron composite that led to more cracking in the biased tows. These two factors also led the Hetron composite specimens to absorb more fracture energy.

7. Mode II fracture tests were also carried out under static and dynamic conditions. The Mode II fracture toughness values were found to be insignificant when compared to the Mode I data. The conclusion is that during crushing, the energy dissipation due to interlaminar cracking within the tube walls is insignificant when compared to the corner cracking energy (Mode I).

8. A discrete cohesive zone model (DCZM) was developed and used through ABAQUS® as a subroutine. Simulations using DCZM were used to study Mode I fracture in the braided composites. Using the material's orthotropic properties along with a one-parameter plastic material model, fracture toughness, and the specimen geometry, the DCZM simulations were found to be in close agreement with experimental values.

9. The DCZM model is a simple tool for characterizing the corner cracking of tubes that explicitly takes into account the fracture energy of the materials in question. As such, it is recommended that codes that are intended to be used for tube crushing utilize the material fracture energy, especially if gross cracking is present, as in the case of tubes.

Impact Performance of Bonded Structures

The objectives of this effort are to (1) evaluate the performance of bonded structures under crash loads; (2) examine the influence of bond design concepts, impact velocity, and other material issues; and (3) fabricate new molding tools to produce simulated automotive structures.

The scope is a combined computational and experimental study of the dynamic response and fracture of an adhesively-bonded, automotive sub-structural component under impact loading. The approach consists of characterizing the dynamic fracture of the adhesive material from falling- wedge drop-tower tests of bonded beam-type specimens under various mode mixities. Numerical constitutive models of the adhesive are developed and validated from the drop-tower tests. The structural sub-component selected is a 4 in. by 4 in. square, composite material tube fabricated by adhesively bonding the overlap of two U-sections. Axial impact tests of the composite tubes are being conducted at ORNL. The numerical constitutive model of the adhesive has been implemented in the LS-DYNA software package to simulate the tube crush tests. Comparison between test results and those from numerical simulation are being used to assess the computational modeling methodology.

Experimental work:

Mode I fracture testing has been successfully completed using the standard double-cantilever beam (DCB) specimen geometry. Results from both quasi-static and various dynamic rates are presented. Driven-wedge test results have been analyzed and compared with Mode I DCB test results in order to establish a correlation among testing procedures. Additionally, a finite-element (FE) analysis has been conducted in order to establish correction factors for shear and root rotation at the crack front associated with the short crack lengths observed in the driven-wedge test. Mixed-Mode I/II tests were completed for both quasi-static and dynamic loading conditions utilizing the asymmetric double-cantilever beam (ADCB) and single-leg bend (SLB) specimen geometries. A Mode III test fixture has been designed in order to aid in the full characterization of the PL-731SIA adhesive and to develop a full three-dimensional fracture envelope for the adhesive.

Mode I Testing Results

Results show that the average strain-energy release rate (SERR), G_{Ic}, for 11-ply and 36-ply DCB specimens range from an average of 2800 J/m^2 and 2460 J/m^2, respectively, under quasi-static loading conditions to an average of 1060 J/m^2 and 700 J/m^2, respectively, at an applied loading rate of 1 m/s. These average values take into account cohesive fractures within the adhesive layer only, as delamination within the composite adherends has been observed in some specimens. Stick-slip behavior is still present and is thus resulting in very few data points per specimen. On average, two to three fracture events are observed along the length of each 300 mm test specimen under quasi-static loading conditions, while as many as five fracture events have been recorded at higher loading rates. It should also be noted that 20-ply specimens have been tested at various loading rates; however, only about 10% of the fracture events have been observed within the adhesive layer, while the remainder have been observed to propagate into the composite adherends resulting in interlaminar fractures. Figure 1 illustrates the relationship established between the Mode I fracture energy, G_{Ic}, and the applied loading rate.

Mixed-Mode I / II Testing Results:

Initial Mode I DCB dynamic fracture testing was conducted using a servo-hydraulic test machine capable of achieving test velocities up to 1 m/s. This particular machine was outfitted with a 2.5 kip strain gage-based load cell. All data acquisition software for this machine was developed in-house by engineers at ORNL using National Instruments LabVIEW software. A lightweight slack adaptor was developed in-house from standard off-the-shelf components (#2 Morse Taper) to allow the test machine to reach maximum velocity prior to applying any load to the test specimens.

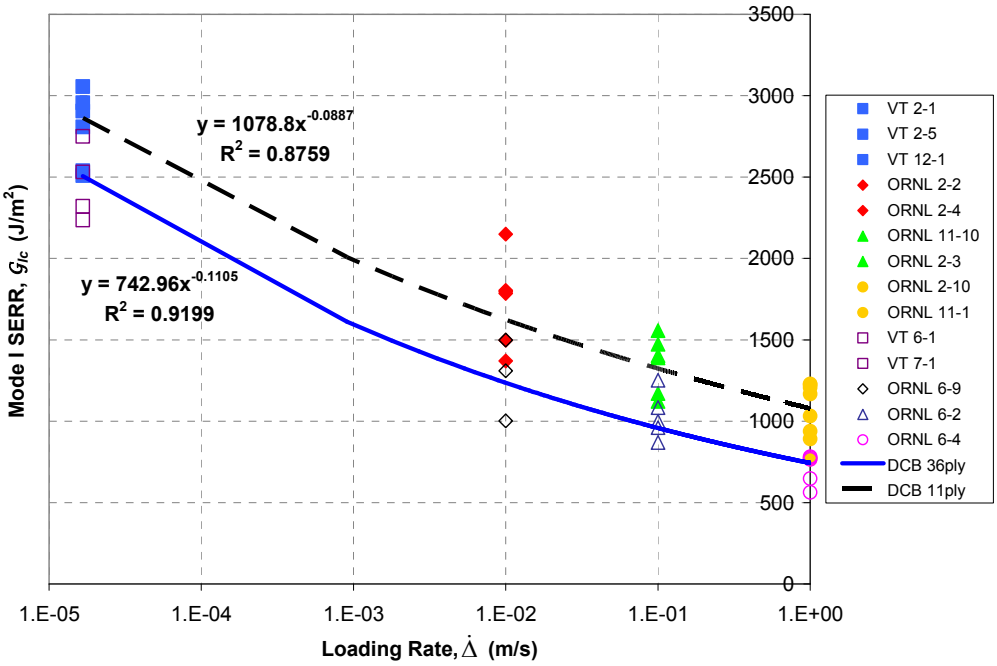

Figure 1. Mode I SERR, G_{Ic}, vs. applied loading rate for 11 and 36-ply bonded composite specimens. Note: filled symbols = 11-ply specimens and unfilled symbols = 36-ply specimens.

The remaining dynamic tests (mixed-Mode I/II and Mode II) were conducted using a custom designed MTS servo-hydraulic test machine at ORNL outfitted with a 500-lb. piezoelectric load cell and improved slack-adaptor design. This machine is capable of achieving test velocities up to 18 meter/second. A high-speed imaging system was used for monitoring crack propagation during all dynamic test events.

From the ADCB tests it was observed that, with the addition of even a small Mode II component, the total mixed-Mode I/II fracture energy values, $G_{I/IIc}$, are an average of about 50% lower than those observed under pure Mode I loading conditions. This was believed to be the case due to the fact that the fracture surfaces of the asymmetric specimens showed that the crack was driven to the interface, thus resulting in lower total fracture energies. Another important aspect of these tests was that many more data points per test specimen were obtained because of the interfacial failure, thus allowing for a more complete mode-mixity characterization. When compared with a maximum of three to four data points per specimen for the Mode I tests, as many as twelve to fifteen data points were recorded for several of the ADCB tests. In conjunction with the ADCB tests, SLB specimens were utilized to help further characterize the mixed-mode fracture behavior of this particular material system. Symmetrically-bonded composite specimens were utilized for this aspect of the study, resulting in a fixed level of mode-mixity. Although the fracture surfaces were similar to those observed from the ADCB tests, only a limited number of data points could be gathered from the SLB tests, with roughly

five data points per specimen being recorded. Figure 2 provides a complete summary of the ADCB and SLB test results.

Computational Work:

The computational work continued on providing support to the experimental work done on lap joints at ORNL. Using experimental data obtained from standard fracture-test configurations, theoretical and numerical tools are developed to mathematically describe non-self-similar progression of cracks without specifying an initial crack. A cohesive-decohesive zone model, similar to the cohesive zone model known in the fracture mechanics literature as the Dugdale-Barenblatt model, is adopted to represent the degradation of the material ahead of the crack tip. This model unifies strength-based crack initiation and fracture-mechanics-based crack progression.

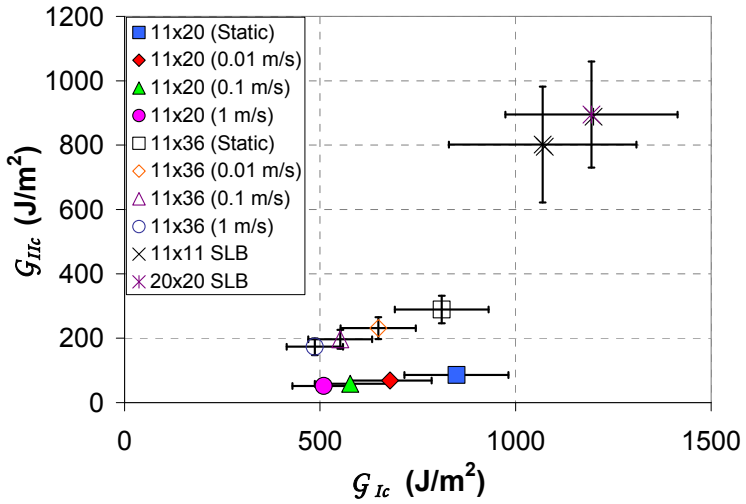

Figure 2. Summary of ADCB and SLB mixed-mode fracture tests.

The cohesive-decohesive zone model is implemented with an interfacial surface material that consists of an upper and a lower surface that are connected by a continuous distribution of normal and tangential nonlinear elastic springs that act to resist either Mode I opening, Mode II sliding, Mode III sliding, or a mixed mode. The initiation of fracture is determined by the interfacial strength and the progression of the crack is determined by the critical energy release rate. The adhesive is idealized with an interfacial surface material to predict interfacial fracture. The interfacial surface material is positioned within the bulk material to predict discrete cohesive cracks. The interfacial surface material is implemented through an interface element, which is incorporated in ABAQUS using the user-defined element (UEL) option.

A procedure is established to formulate a rate-dependent model based on experiments carried out on compact tension test specimens. The rate-dependent model is incorporated into the interface element approach to capture the unstable crack growth observed in experiments under quasi-static loading conditions. The compact tension test gives the variation of the fracture toughness with the rate of loading; this information is processed and a relationship between the fracture toughness and the rate of the opening displacement is established. The cohesive-decohesive zone model is implemented through a material model to be used in an explicit code (LS-DYNA). Dynamic simulations of the standard test configurations iii for Mode I (DCB) and Mode II (End Load Split) are carried out using the explicit code. Verification of these coupon tests leads to the crash analysis of realistic structures such as the square composite tube. Analyses of bonded and unbonded square tubes were completed. These tubes show a unique fracture mode that has been captured in the analysis. Disadvantages of the interface element approach are well documented in the literature. An alternative method, known as the

Extended Finite- Element Method (XFEM), is implemented here through an eight-noded quadrilateral plane-strain element. The method, based on the partition-of-unity, is used to study simple test configurations like the three-point bend problem and a double-cantilever beam. Functionally-graded materials are also simulated and the results are compared to the experimental results available in the literature.

Performance of Novel Sandwich Composites

The objective of this effort is to investigate the viability and crashworthiness of novel sandwich composite concepts for automotive applications. It addresses topics such as wrinkling, face-sheet de-bonding, Poisson's effects and core-skin property mismatch, load rate effects, impact damage modes and energy absorption, to mention a few. The research work being performed at the University of Utah is split into three phase-specific objectives as has been noted in earlier reports.

Phase II work that was completed during the dates outlined involved testing of the four sandwich configurations shown in Table 1. The focus of the current phase during this timeframe was on the following:

Structural testing

- Development and understanding of structural-level concepts for energy absorption.
- Structural impact testing.
- Necessary improvements to test fixture to help progressive crushing of sandwich panels.

Damage evolution testing

- Mixed mode testing of the sandwich panels to determine critical strain-energy release rates.

Table 1. Sandwich Configurations Used in Phase II Study.

	Facesheet	Core
1	Woven Carbon Epoxy	Balsa Wood
2	Woven Carbon Epoxy	Polyurethane Foam
3	P4 Carbon-Epoxy	Balsa Wood
4	P4 Carbon-Epoxy	Polyurethane Foam

The development of structural-level concepts was completed and involved a study of beveled ends, embedded notches, stitches and improvements to the test fixture to obtain progressive, high energy-absorbing fracture mechanisms. The findings show that the effectiveness of the structural-level concepts is highly dependent on the type of core material (balsa vs. foam) and somewhat less dependent on the type of facesheet (woven vs. P4). The structural impact testing involved the edgewise impact tests of 280 x 280-mm sandwich panels. These structural impact tests were completed using the Test Machine for Automotive Crashworthiness (TMAC) facility at ORNL (see 8.B). Figure 3 shows a summary of the improvements made in energy absorption due to progressive crushing as a result of adding features in the core as well as improvements made to the test fixture.

The damage evolution testing was completed and involved the Mixed Mode tests of the sandwich configurations shown in Table 1. As reported earlier, the Mode-I (DCB), Mode-II (ENF) had already been completed on these panels. The mixed-mode test is illustrated in Figure 4. Stable crack growth was achieved in this test, as in the other two fracture tests, thus enabling the measurement of an initiation and propagated values of the critical strain-energy release rate.

Phase III involves development of finite-element modeling methodologies for damage progression, effects of geometric/material alterations on damage progression and energy absorption with a view toward the implementation of closed-form analytical models to address specific deformation modes. This phase is currently underway.

Energy Absorption of Triaxially-Braided Composite Tubes

The objective is to develop a predictive tool for crush analysis of triaxially-braided composite

structures based on a smeared micromechanics model utilizing shell elements. A smeared micromechanics model developed under an earlier contract was extended to dynamic analysis. The project answers questions pertaining to the basis of the mathematical representation of the energy absorbing mechanisms, unit-cell size relative to the FE size, rate effects, stress-concentration effects on load-sustaining ability, objectiveness of damage-evolution assumptions, and micro-mechanics application to shell FEs.

The smeared micro-mechanics unit-cell model code has been rewritten to improve its computational efficiency. A rate-dependent plasticity model was incorporated into the code, along with an implementation of the Tsai-Hahn fiber-bundle theory as applicable to braided composites, to account for the effect of a critical damage area (CDA). The numerical results after accounting for CDAs are shown in Figure 5 for the case of a static crush of a 45º braided coupon with a hole and in Figure 6 for the case of dynamic crush of a 45° square tube. These simulations are accomplished on one-eighth of the tube model assuming symmetric boundary conditions. Tests were conducted both at the TMAC facility at ORNL and at Stanford University to generate crush data for both circular and square tubes. This was done in order to collect experimental data to help establish a better correlation between the numerical code and tests. Tests included 30°, 45°, and 60° tubes with the crush being initiated by 1/4th-and 5/16th-inch fillet radius steel plugs in the square and circular tubes, respectively. The tubes used for the experiments are shown in Figure 7. The experimental data were obtained for test speeds of 1 m/s and 4 m/s.

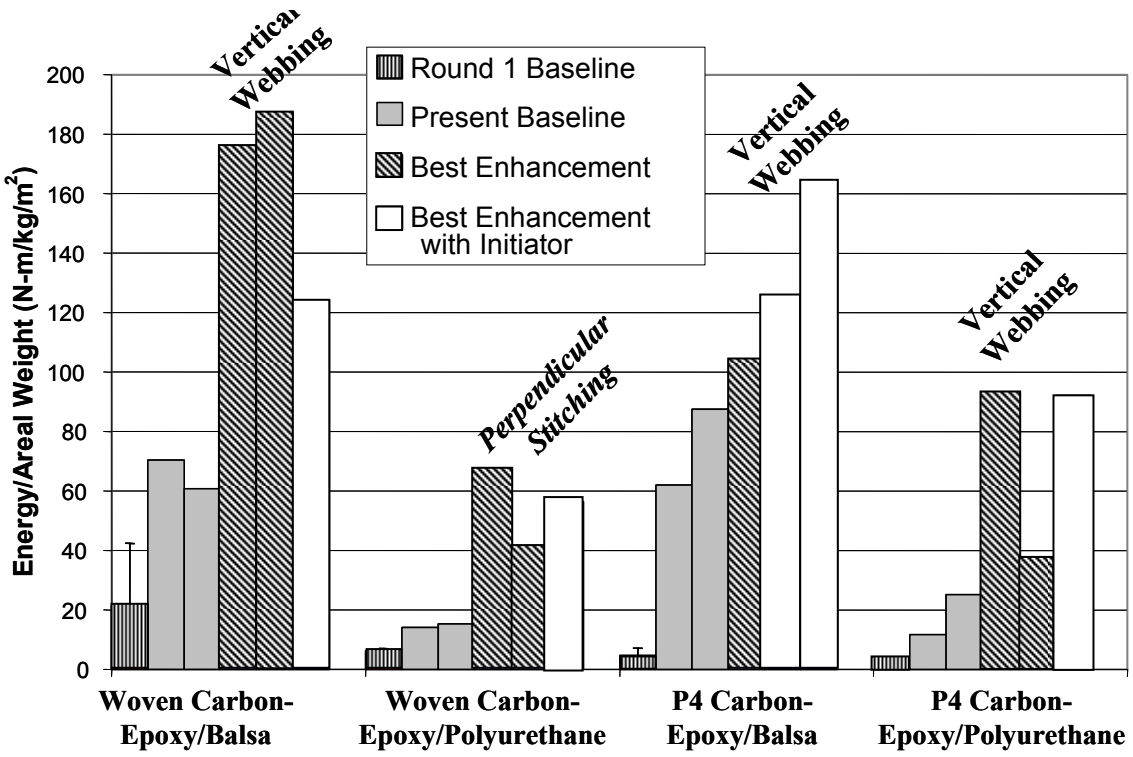

Figure 3. Energy absorption improvements from design modifications.

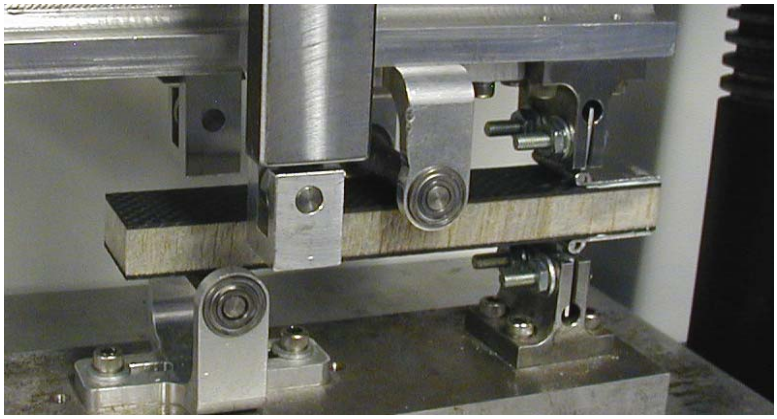

Figure 4. Mixed-mode bending (MMB) test.

The code has been developed as a VUMAT subroutine for use with the commercial software ABAQUS®. The code is currently being tested for validity against the crush of a full tube as opposed to a symmetry model used by the developer.

Post-Peak Response Characterization of Two-Dimensional Triaxially-Braided Composites

The objectives of this effort are: 1) computationally demonstrate post-peak softening (PPS) observed with single unit-cell structural models on multi-cell structural models; 2) computationally investigate how the hierarchy of damage/fracture modes and the number/arrangement of unit cells affect PPS predictions; 3) computationally investigate how the variation in degree of imperfection in the micro-architecture affects the derived structural properties of the 2D triaxially-braided composite (2DTBC); 4) experimentally test multi-unit cell structural specimens in order to reflect, refute, or support the finding of the above objectives.

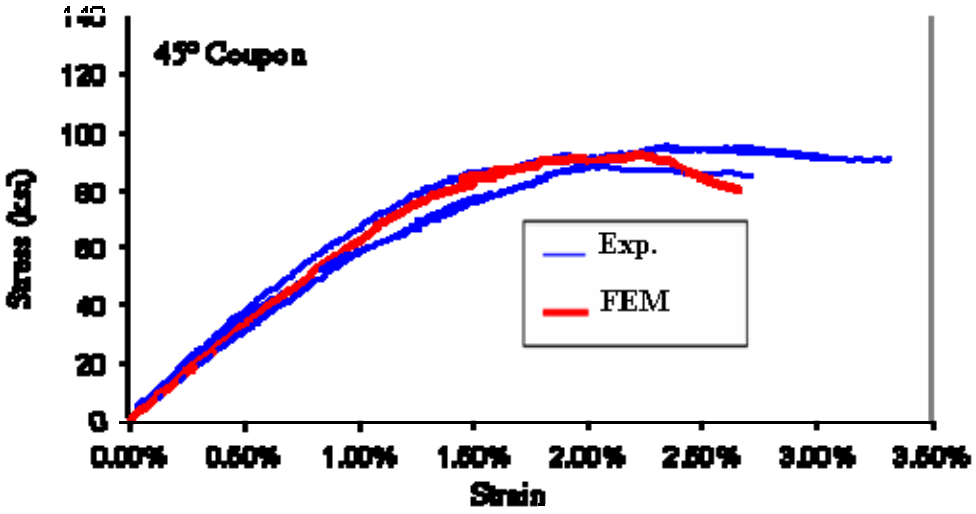

Figure 5. Comparison between test and numerical analysis showing the effect of implementing a critical damage area (CDA).

In this effort, scalability of macroscopic structural stress-strain relations in 2DTBC will be investigated and studied. Computational models will be employed to demonstrate PPS observed with single-unit cell structural models on multi-cell unit structural models. The results of such analyses are directly applicable to the development of structural properties of 2DTBC for large-scale FE simulations that are needed to assess energy absorption in 2DTBC structural components. Using laser extensometer and speckle photography for full-field strain measurements, experimental tests to measure PPS on single- and multi-cell 2DTBC will be performed. Further, computational models that incorporate cohesive zones (CZ) within the cell in order to capture experimentally-observed tow/matrix separation will be developed and analyzed including the effect of CZ on PPS. Finally, the computational analyses will be carried further in order to study and characterize the effects of measured architecture imperfections on the single-unit-cell and multi-cell structural stress-strain properties of 2DTBC, including the effects of different types and distribution of imperfection on PPS.

The primary resin materials (Hetron and Epon) were experimentally characterized by measuring their pure (virgin) properties, performing coupon tension tests (with different tow orientations), and then using data-reduction techniques to back-calculate *in-situ* material properties. Compression tests on coupons were also performed in the transverse direction (which are matrix-dominated).

It was found that *in-situ* matrix properties differ from pure matrix properties, and hence, the *in-situ* properties (not pure) should be used for subsequent FE analyses, Figures 8 and 9. Since axial fiber tows are the dominant load-carrying component, statistical scanning electron microscopy (SEM) in conjunction with photo-stitching techniques were performed on the Hetron- and Epon-based composites. From the detailed specimen preparation and subsequent SEM images, it was found that unwetted regions inside the tows need to be accounted for (e.g., in FE analysis) by a reduction in tow cross-sectional area and/or material constants. Such regions which reduce the fiber volume fraction exist in the Hetron-based composite and are usually associated with micro-cracking. Note that Hetron typically exhibits an approximately 10% shrinkage during curing. However, detailed SEM images of Epon-based composite show that the tows are fully wetted and micro-cracks are minimal (typically,

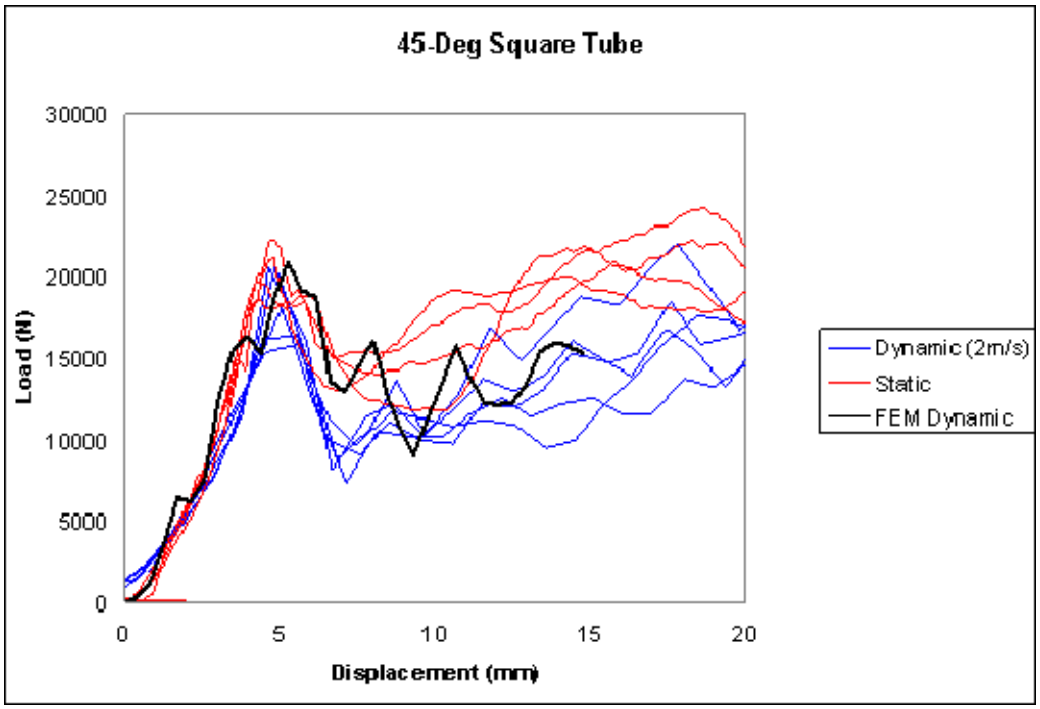

Figure 6. Comparison between test and numerical analysis for the dynamic crush of a 45° square tube.

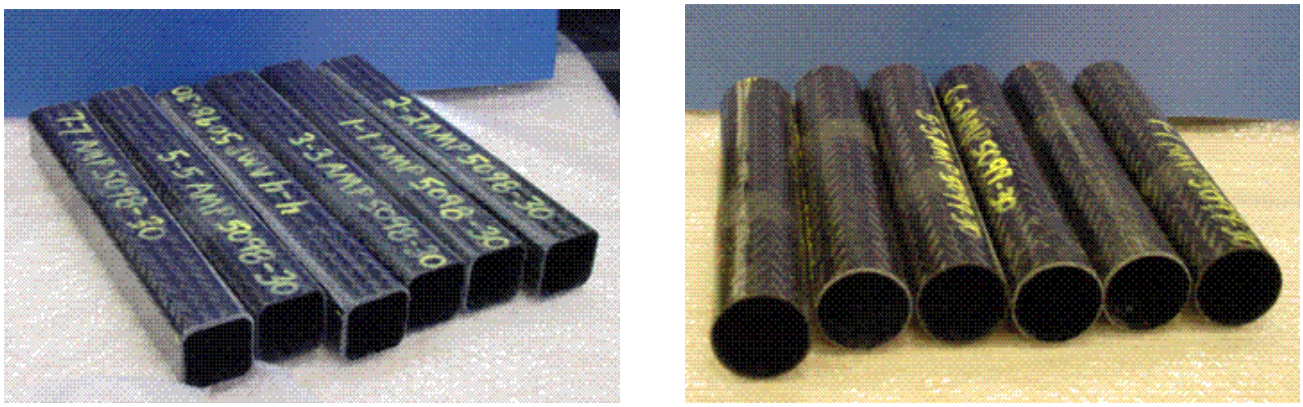

Figure 7. Square and circular tubes used for the dynamic tests at ORNL.

Epon exhibits little or no shrinkage while curing). Such a difference might explain (at this stage in the study) the higher energy-absorption capacity of the Hetron-based system as compared with the Epon-based one as reported in the literature. To investigate this voids effect, two detailed FE models of a fiber tow were developed; one does not include any voids, while the other has the core cut out resulting in a tow resembling an undulated thick cylinder. Eigen analyses were performed and subsequent response analyses (with 6% imperfections—scaled with respect to eigenmodes) showed that an appreciable reduction in the maximum Plateau stress can be caused by including such tow voids. However, FE analyses showed that as the number of RUCs increase, the effect of voids on peak-stress reduction deceases.

Detailed FE models have been developed for one RUC for both material systems (Hetron and Epon).

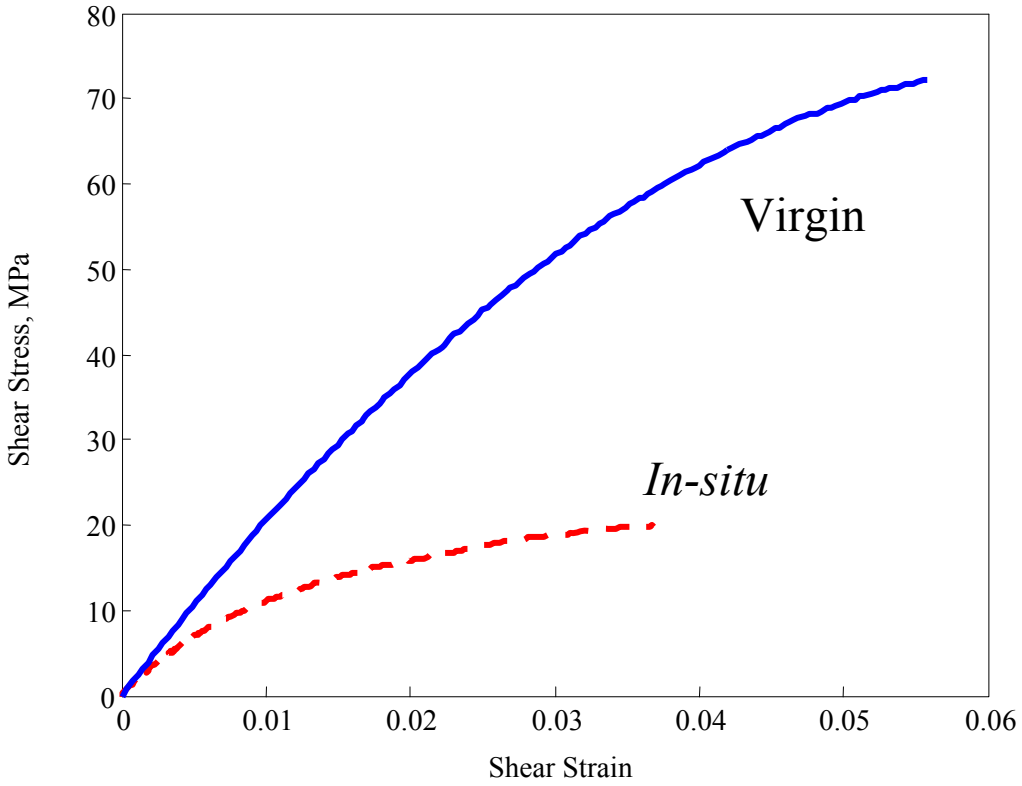

Figure 8. Shear stress vs. shear strain for pure (virgin) matrix (solid line) and the corresponding *in-situ* matrix (dashed line).

The RUC model (which is based on the real geometry) was analyzed using a new method in order to obtain the *(in-situ)* stress state of the matrix within a braided textile composite. It was found that, when performing RUC-based analysis, it is important to recognize volume consolidation processes occurring during manufacturing. For example, when an enlarged cross-sectional image of a multi-layered braided composite is analyzed, and the "theoretical" boundaries of adjacent RUCs (within this images) are marked, one notices that some RUCs are overlapping. To account for this fact in subsequent analyses, a computer program was developed to analyze the image and calculate the "actual" axial fiber tow area. Based on the latter, the actual fiber volume fraction is recalculated, and the axial fiber tow modulus within one RUC is adjusted.

An imperfection analysis study on one RUC was performed using finite-element analysis (FEA). The geometric imperfection was derived from the eigen modes of the RUC with the imperfection amplitude used as a parameter. Nonlinear geometry and nonlinear material properties were included. The analyses demonstrated the imperfection-sensitivity character of this material/structural system.

It was found that when a plasticity model is used, the Mises stress within the matrix element (in the RUC) has already reached the maximum value specified by the plasticity curve. This results in an artificial stiffening of the matrix. Because inelastic behavior is associated with work-loss, the team has suggested the development and employment of a Schapery-like, thermodynamically-based theory

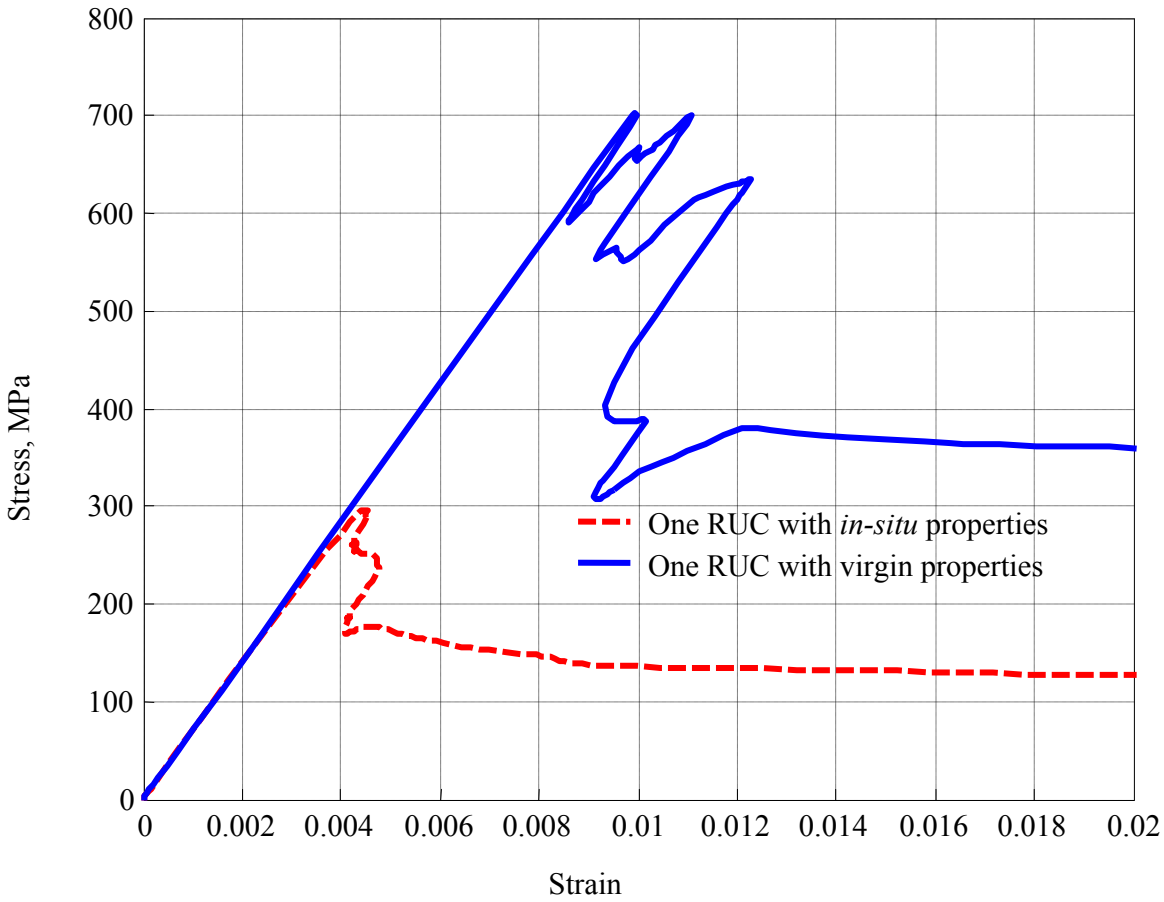

Figure 9. Finite-element analysis results for compressive stress vs. strain for one representative unit cell (RUC) using pure (virgin) matrix properties (solid line), and the corresponding *in-situ* matrix properties (dashed line).

(ST) to characterize the progressive (inelastic) damage. Such an approach requires the definition of internal state variables (ISV). Further, the above methodology (based on Schapery) will encompass mechanism-based damage/fracture modeling in order to model degradation at both the micro- and macro-(structural) levels. A mathematical model was developed, and several laboratory tests were carried out on coupon specimens. Using the stress-strain test data, the ISV were extracted for RUC damage modeling. Such information was then incorporated directly into a FEA code so that ISVs (implicit to the constitutive law) are automatically calculated during analysis execution.

In previous studies, fiber tows were treated as elastic, which is an approximation since the matrix influences the transverse tow properties. To improve the model, an orthotropic deformation theory featuring an elastic-plastic formulation was derived and implemented. Several models for one RUC (with different imperfection amplitudes—as previously described) were analyzed in which the effects of tow plasticity were investigated. It was found that such effects on such simplified models are not significant and are significantly less dominant than tow-void inclusion.

More detailed FE models were developed which included multiple RUCs (4, 9 and 16 RUCs). Such models introduced various new modeling challenges including how to preserve edge/boundary conditions, imperfections and periodicity. In addition to uniform global imperfection, a local imperfection was added so that the "center column" of the fiber tows would bulge out more than the neighborhood cells. Convergence computational studies were carried out and trends of convergence started to appear between the 1, 4, 9 and 16 RUCs. Figure 10 shows the preliminary results for the 1, 4, 9 and 16 RUCs with 6% imperfections. For models including 9 RUCs or more, the computational resources become significant and model execution time becomes large.

Kink banding in axial tows was also investigated as another phenomenon that contributes to post-peak softening in braided composites.

Since tows can include tens of thousands of fibers, simplified (but detailed) 3D FE models were developed which included fibers within a matrix (modeled using matrix *in-situ* properties). Two tow models were developed, one with isotropic fiber properties and another with orthotropic fiber properties. All models included several degrees of tow misalignment. Stress-strain plots for such models show snap-back behavior which is dependent on misalignment degree. For larger misalignment (approx. 1 deg.) the stress-strain relation resembled an almost elastic-perfectly plastic behavior (with some decreasing plateau stress). Figure 11 shows the preliminary results for an orthotropic fiber-tow kinking model with different misalignments.

Investigations into fiber-kinking modes were carried out. The FEA predictions showed qualitative agreement with tests when damaged zones, predicted by model, are compared with images taken of the damaged test specimens. Such agreement provided additional confidence in the modeling methodologies and predictive capabilities.

Lateral Impact Study

The objective of this effort is to achieve a fundamental understanding of the energy-absorbing mechanisms in triaxially-braided composites subjected to lateral bending and impact. A combined experimental and analytical approach has been planned and implemented for this purpose. The analytical study has applied the smeared micro-mechanics material model previously developed in this project, available as a user sub-routine with ABAQUS®. Following a correlation study based on a simple test coupon, a specimen representative of an automotive component subjected to bending impact loads will be evaluated.

The overall study involves three distinct phases: 1) smeared micro-mechanics material model of composite strips under lateral bending, 2) validation of the model using experimental data, and 3) extension of the model for designing automotive components. Phase I of the project has been completed with the modeling and analysis of a [0° 80k / ±45° 12k] triaxially-braided carbon-fiber composite strip subjected to off-axis compressive loading and Phase II was previously reported. Further work on Phase III has not occurred due to personnel changes.

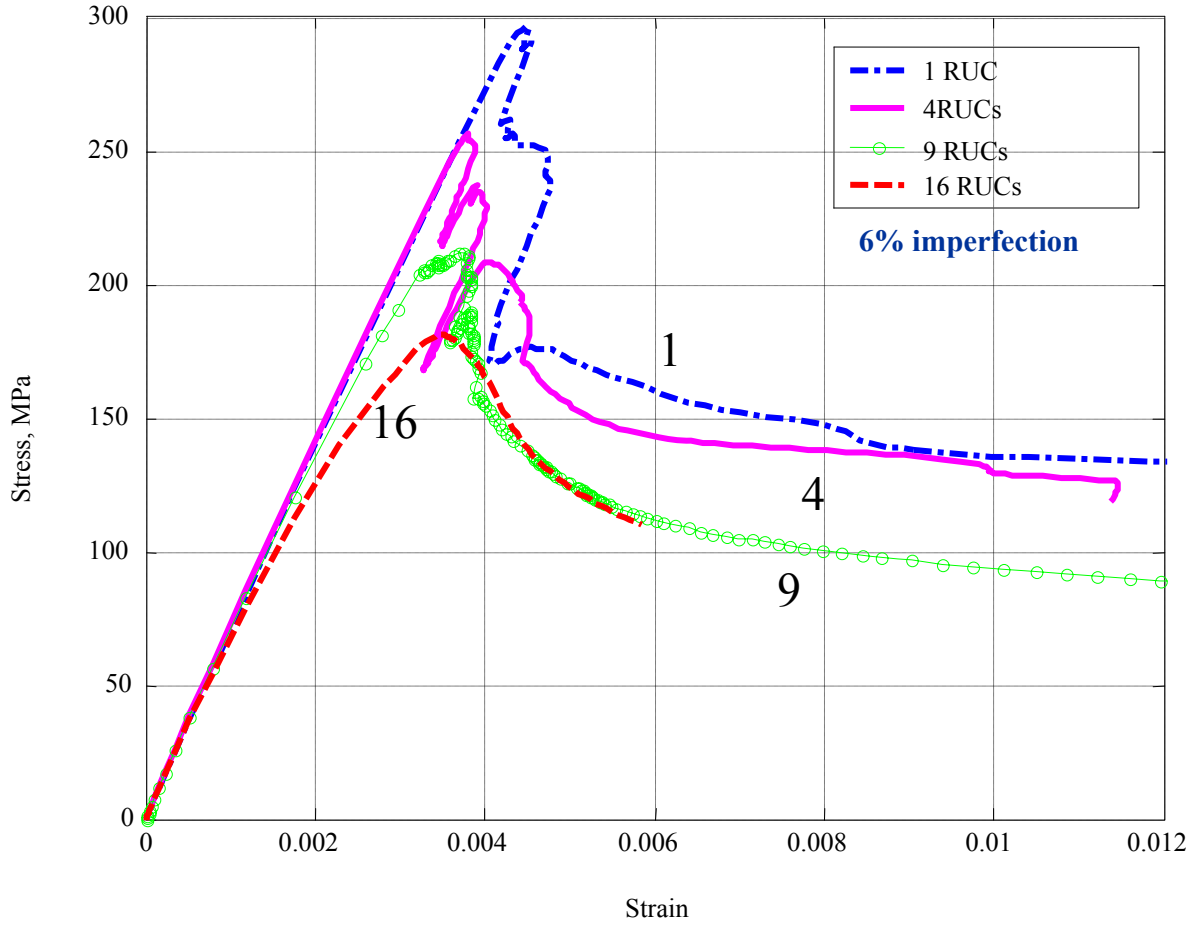

Figure 10. Preliminary FEA results for the 1, 4, 9 and 16 representative unit cells (RUCs) with 6% imperfections.

Multiscale Modeling for Crash Prediction of Composite Structures

The objective of this work is to develop a material model that considers microstructural aspects of damage and an efficient multiscale modeling tool that is able to predict dynamic crush response of automotive composite structures at an affordable computational cost. Five tasks of the research were proposed to accomplish the goal: (1) development of a multiscale computational framework for the crash analysis of polymeric composites,
(2) implementation of the framework into ABAQUS Explicit, (3) verification of the proposed framework against benchmark computational models,
(4) calibration using experimental data, and
(5) validation of the proposed simulation capabilities against composite tube specimens' behavior under crushing loads.

Tasks (1) and (2) were completed and presented in previous reports. The current research efforts have been focused on completing tasks (3) and (4). Task (3), verification of the multiscale simulation toolkit, was completed. A direct homogenization method based on the classical nonlinear homogenization theory was implemented and compared to the fixed- and variable-reduced-order models. The fixed-point reduced-order-model was developed and verified earlier. A variable-point reduced-order model was developed and verified against direct homogenization. The computational performance of the variable-point reduced-order model is documented in Table 2 and clearly shows the computational advantages of the multiscale methodology developed over the classical nonlinear homogenization approach.

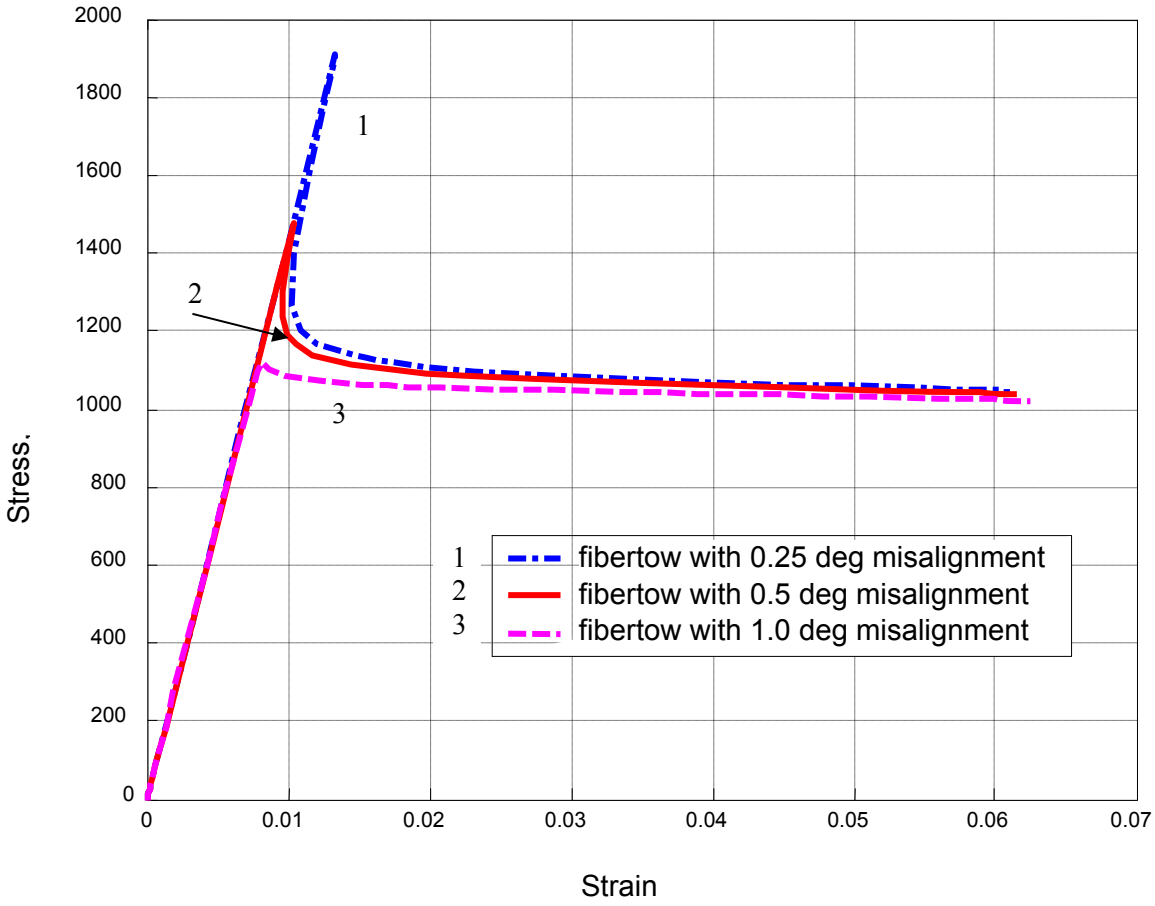

Figure 11. Preliminary results for an orthotropic fiber-tow kinking model with different misalignments.

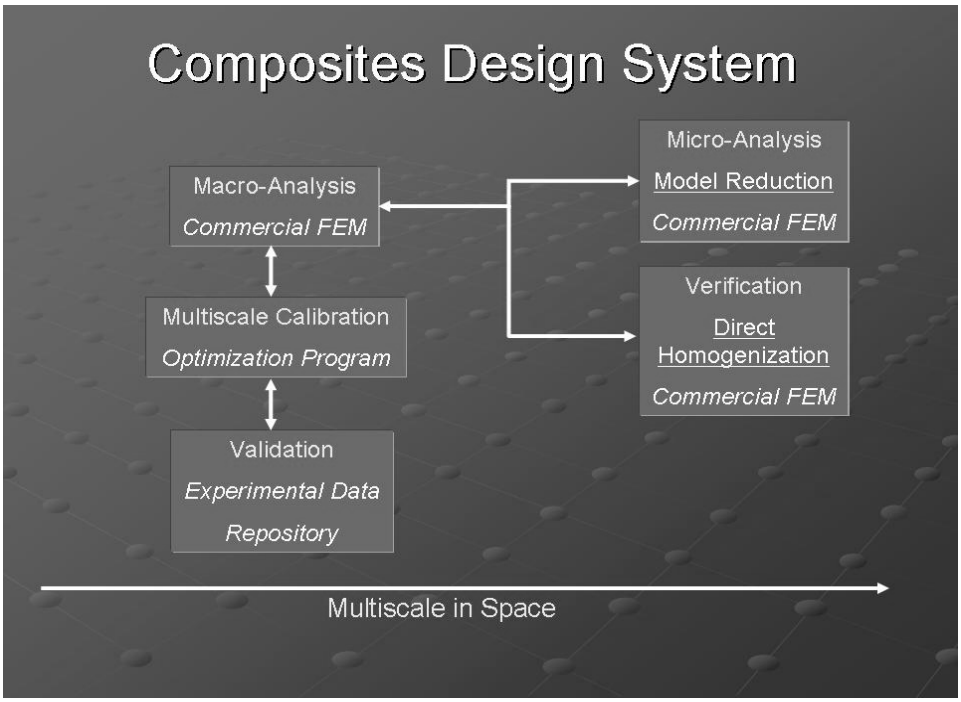

Figure 12. Components of the Crash Prediction Design System.

For Task (4), a calibration strategy was developed for the evaluation of the material properties associated with the elastic and failure behavior of the composite microconstituents and interfaces. The calibration toolkit, Figure 12, developed permits incorporation of various experiments into the experiment simulator repository. In the multiscale simulation toolkit developed, an objective function is automatically created based on the available experiments, and model failure parameters are identified using optimization techniques with minimal user interference.

Table 2. Simulation performances of the variable point reduced order multiscale model and comparison to fixed point reduced order model and direct homogenization.

Model	# of incr.	# of iter.	total CPU time
Fixed 0+1 point	32	57	~1 min.
Fixed 0+5 point	32	122	~3 min.
Variable pt.	**32**	**109**	**~5 min**
Fixed 0+10 point	32	112	~25 min.
Direct homogenization	9	81	~ 6 days

The calibration strategy was integrated with ABAQUS and used for the calibration of the braided composite architecture provided by the ACC. The braided composite unit-cell shown in Figure 13 consists of three phases: axial tows, bias tow and matrix. It was constructed using ABAQUS/CAE. The general guidelines for preparing arbitrary unit cells with ABAQUS/CAE were developed. The elastic properties for microconstituents were calibrated based on the chord moduli from the tensile and compressive tests provided by ACC and Reference 1. The calibrated values are summarized in Table 3. The failure parameters of the 1+4-point reduced-order model were calibrated based on three types of tests: tensile test to failure, compression test to failure and short-beam three-point bending to failure. The resulting predictions of the moduli and strengths compared with experiments are summarized in Tables 4 and 5.

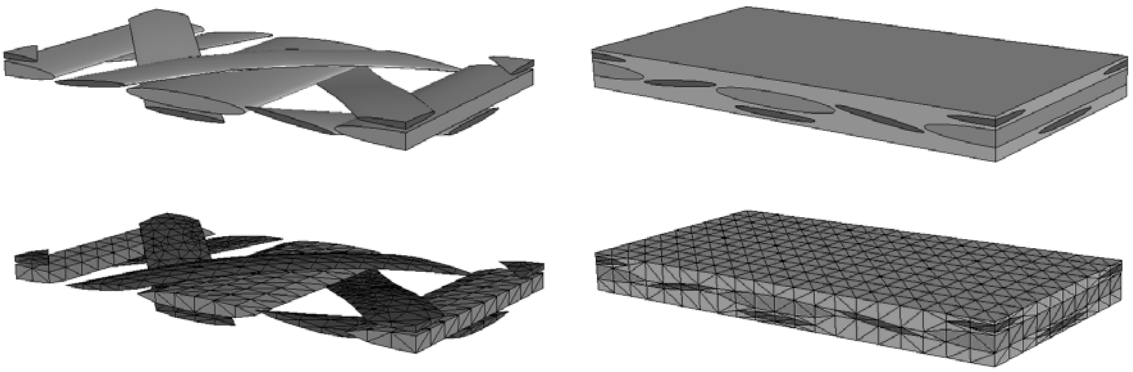

Figure 13. The unit-cell model for braided composite.

Table 3. Calibrated elastic properties of micro-constituents for the braided composite.

	Axial Tow					Braider Tow					Matrix	
X1=XA	E11	E22	G12	v12	v23	E11	E22	G12	v12	v23	E	v
(GPa) for E & G	218	15.3	9.9	0.36	0.3	218	15.3	9.9	0.37	0.3	3.57	0.35

Table 4. The comparison of the overall moduli between experiments and simulations.

(GPa)	Experiment*	Simulation(relative error)
$\overline{E}_A$	60.3 ± 2.95	60.29 (0.009%)
$\overline{E}_T$	8.7 ± 0.24	8.70 (0.13%)

Table 5. The comparison of the strengths between experiments and simulations.

(MPa)	Experiment	Simulation
Tensile Strength	654 ±66.7	663
Compressive Strength	376 ± 29.4	370.5
Short-beam Strength	43.1 ±2.33	41.3

The next phase will focus on incorporation of rate effects into the multiscale reduced-order model, calibration of additional parameters corresponding to rate effects (completing Task 4) and validation of the simulation capabilities developed against the experimental data on braided composite tubes in a drop test (completing Task 5).

Summary

The Composites Crash-Energy Management project develops and demonstrates technologies that are used to apply production-feasible structural composites in automotive crash and energy-management applications. Efforts within the project are intended to understand the mechanisms of polymer composite crash, develop analytical tools for use in vehicle design, and build a knowledge base for the vehicular application of lightweight polymer composites. During FY 2006, in the experimental projects,

- The contract to study the static and dynamic behavior of composite crash was completed and a final report drafted. This study's objectives were to experimentally determine the microstructural factors and behaviors that lead to decreased energy absorption when crushing tubes dynamically.
- Results of Mode I testing of adhesive joints show that the average strain energy release rate, G_{Ic}, for 11-ply and 36-ply DCB specimens range from an average of 2800 J/m^2 and 2460 J/m^2, respectively, under quasi-static loading conditions to an average of 1060 J/m^2 and 700 J/m^2, respectively, at an applied loading rate of 1 m/s. These average values take into account cohesive fractures within the adhesive layer only, as delamination within the composite adherends has been observed in some specimens.
- Adhesive sample tests showed that, with the addition of even a small mode II component, the total mixed-Mode I/II fracture energy values, $G_{I/IIc}$, are an average of about 50% lower than those observed under pure Mode I loading conditions.
- A study of structural concepts to improve the energy absorption of sandwich panels was completed and included the use of beveled ends, embedded notches, stitches and improvements to the test fixture to obtain progressive, high energy-absorbing fracture mechanisms. The findings show that the effectiveness of the structural improvements is highly dependent on the type of core material (balsa vs. foam) and somewhat less dependent on the type of fiber facesheet reinforcement (woven vs. random P4).

In the analytical studies,

- Analyses of adhesive lap joints were conducted to support the experimental studies at ORNL. Using experimental data obtained from standard fracture test configurations, theoretical and numerical tools were developed to mathematically describe non-self-similar progression of cracks without specifying an initial crack. A rate-dependent model was incorporated into the interface element approach to capture the unstable crack growth observed in adhesive-joint experiments under quasi-static loading conditions.
- A rate-dependent plasticity model for triaxially-braided composites was incorporated into the current predictive tool, along with the implementation of the Tsai-Hahn fiber-bundle theory, to account for the effect of a critical damage area (CDA).
- Tests of 30°, 45°, and 60° triaxially-braided square and circular tubes were completed at test speeds of 1 m/s and 4 m/s. A predictive algorithm was developed as a vectorized user material (VUMAT) subroutine for use with the commercial software ABAQUS® and is being validated.
- The development and employment of a Schapery-like thermodynamically-based theory (ST) to characterize the progressive, inelastic damage is continuing. The proposed formulation shows several relationships between internal state variables and the energy of the system, as well the relation between instantaneous moduli in damaged state and virgin state.

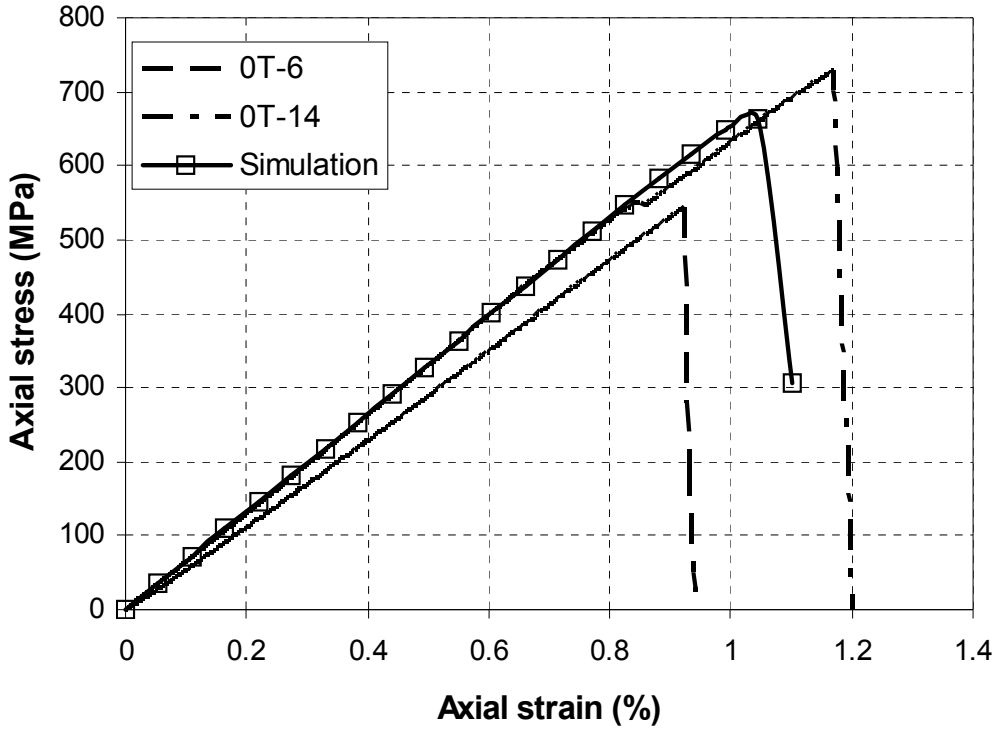

Figure 14. The stress-strain curve for tensile test.

- As part of the study of post-peak behavior, a computer program is being developed to calculate internal state variables from stress-strain test data. This program is incorporated directly into a FE analysis code so that ISVs implicit to the constitutive law are automatically calculated during a finite-element analysis.
- Kink banding in axial tows was also investigated as another phenomenon that contributes to post-peak softening in braided composites. All models included several degrees of tow misalignment. Stress-strain plots for such models show snap-back behavior which is dependent on misalignment degree.

- The study of multiscale modeling methods included the verification of the proposed framework against benchmark computational models. The verification of the multiscale simulation toolkit was completed. The proposed multiscale fracture model was verified against the direct homogenization method and significant improvements in computational performance were demonstrated.

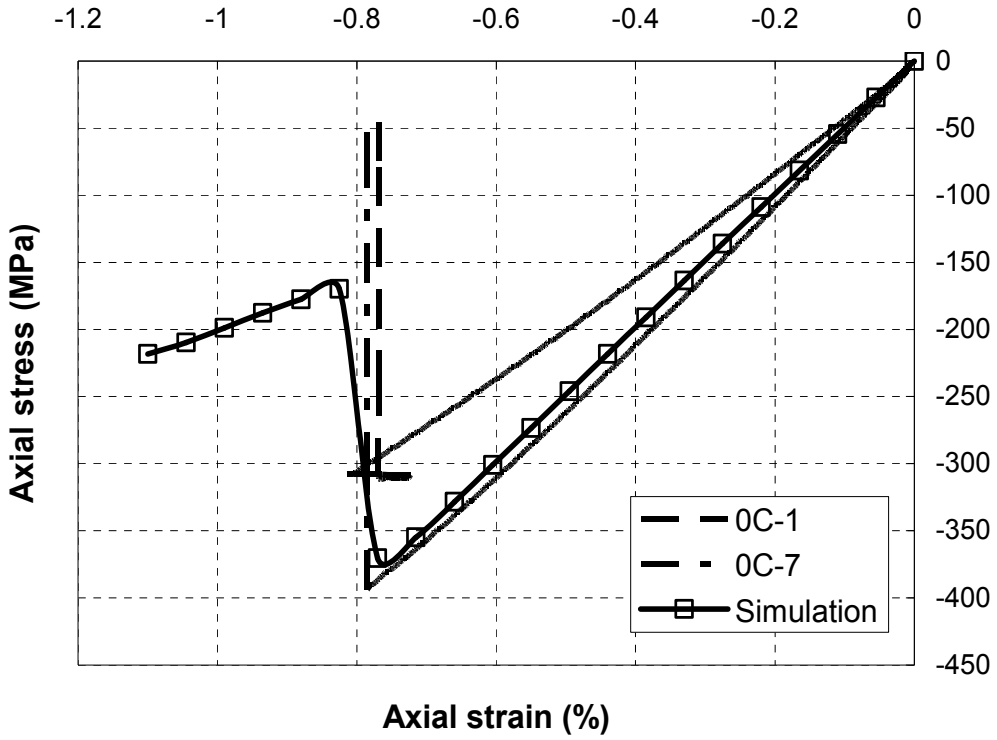

Figure 15. The stress-strain curve for compressive test.

References

1. S. J. Beard. 2000. Energy Absorption of Braided Composite Tubes. Thesis. Stanford University.

Further Related Bibliography

1. Brimhall, Thomas J. "Friction Energy Absorption in Fiber Reinforced Composites." Ph.D diss., Michigan State University, 2005.

2. Salvi, Amit G.; Waas, Anthony M.; Caliskan, Ari, Rate-Dependent Compressive Behavior of Unidirectional Carbon Fiber Composites Polymer Composites, Aug 2004, v 25, n4, pp. 397-406.

3. Salvi, Amit G.; Waas, Anthony M.; Caliskan, Ari, Specimen Size Effects in the Off-axis Compression Test of Unidirectional Carbon Fiber Tow Composites, Composites Science & Technology, v64 n 1, January 2004, pp. 83-97.

4. Kapania, Rakesh K., Makhecha, Dhaval P., Johnson, Eric R., Simon, Josh, Dillard, David A., Modeling Stable And Unstable Crack Growth Observed In Quasi-Static Adhesively Bonded Beam Tests. IMEC204-59765. Proceedings of IMECE'04, 2004 ASME International Mechanical Engineering Congress and Exposition, Anaheim, California, USA, November 13-16, 2004

5. Joshua C. Simón, David A. Dillard, Eric R. Johnson, Characterizing the Impact Fracture Properties of Structural Adhesives, Presented at the 27th Annual Meeting of Adhesion Society, Wilmington, NC, USA, February 15-18, 2004.

6. Flesher, N. D. *Crash-energy Absorption of Braided Composite Tubes*. Dissertation. Stanford University. Department of Mechanical Engineering. December 2005. 160 pp.

7. Flesher, N.D.; Chang, F-K. Modeling the Response of Braided Composites with Stress Concentrations. 11th US-Japan Conference on Composite Materials. September 9-11, 2004. Yonezawa, Japan.

8. Flesher, N.D.; Chang, F-K. Effect of Cross-Section Configuration on Energy Absorption of Triaxially Braided Composite Tubes. 18th Annual Technical Conference American Society for Composites. Oct. 19-22, 2003. University of Florida.

9. Van Otten, A. L., N. S. Ellerbeck, D. O. Adams, C. L. Nailadi, K. W. Shahwan, *Evaluation of Sandwich Composites for Automotive Applications,* Proceedings of the 2004 SAMPE Conference, Long Beach, California.

10. Flesher, N.D., Cheng, W. Evaluation of STCrush for Characterization of Crushing Behavior of Composite Tubes. 10th US-Japan Conference on Composite Materials. September 16-18, 2002. Stanford University.

11. Quek SC, Waas AM, Shahwan KW and Agaram, V. Compressive response and failure of braided textile composites: Part 2 - computations, Int J.Nonlinear Mech. 39 (4): 650-663, June 2003.

12. Quek SC, Waas AM, Shahwan KW and Agaram, V. Compressive response and failure of braided textile composites: Part 1 - experiments, Int J. Nonlinear Mech. 39 (4): 635-648, June 2003.

13. Quek, S C, A M Waas, K W Shahwan, and V Agaram, Analysis of 2D Flat Triaxial Braided Composites, Int.J. Mechanical Sciences, 45 (6-7): 1077-1096, 2003.

14. Quek SC, Waas AM, Micromechanical Analyses of Instabilities In Braided Glass Textile Composites, AIAA J, 41 (10): 2069-2076 Oct. 2003

15. Cagler, O. and Fish, J. *Eigendeformation-Based Reduced Order Homogenization.* Submitted to Computer Methods in Applied Mechanics and Engineering

16. D. Xie, A. Salvi, and A. Waas , A Caliskan, "Discrete Cohesive Zone Model to Simulate Static Fracture in Carbon Fiber Composites" 46th AIAA/ASME/ASCE/AHS/ASC Structures, Structural Dynamics & Materials Conference Apr 18-21, 2005, Austin, TX (AIAA-2009-2320).

[i] Denotes project 100 of the Automotive Composites Consortium (ACC), one of the formal consortia of the United States Council for Automotive Research (USCAR), set up by the "Big Three" traditionally USA-based automakers to conduct joint pre-competitive research and development.

H. Crash Analysis of Adhesively-Bonded Structures (CAABS)

Principal Investigator: J. Michael Starbuck
Oak Ridge National Laboratory (ORNL)
P.O. Box 2009, Oak Ridge, TN 37831-8048
(865) 576-3633; fax: (865) 574-8257; e-mail: starbuckjm@ornl.gov

Project Manager, Composites: C. David Warren
Oak Ridge National Laboratory
P.O. Box 2008, Oak Ridge, TN 37831-6065
(865) 574-9693; fax: (865) 576-4963; e-mail: warrencd@ornl.gov

Technology Area Development Manager: Joseph A. Carpenter
(202) 586-1022; fax: (202) 586-1600; e-mail: joseph.carpenter@ee.doe.gov

Expert Technical Monitor: Philip S. Sklad
(865) 574-5069; fax: (865) 576-4963; e-mail: skladps@ornl.gov

---

Contractor: Oak Ridge National Laboratory
Contract No.: DE-AC05-00OR22725

Objectives

- Develop a comprehensive experimental and analytical methodology to analyze and design adhesively-bonded automotive composite structures to sustain axial, off-axis, and lateral crash/impact loads.
- Determine the rate sensitivity of bonded tubes to crush-through experiments on the Oak Ridge National Laboratory (ORNL) Test Machine for Automotive Crashworthiness (TMAC. See 8.B).
- Determine influence of critical joint design parameters, for example, bond length, bond thickness, and fillet, on specific energy absorption.

Approach

- Coordinate with the bonded-joint experimental and analytical efforts undertaken in the Automotive Composites Consortium (ACC) project "Composite Crash Energy Management." (See 4.G)
- Select a substrate, adhesive, and representative subcomponent joint geometry for evaluation.
- Characterize substrate material, adhesive material, and coupon-level joints under static and dynamic loads.
- Build and test unbonded and bonded rail components under static and dynamic crush loads.
- Correlate experimental results with analytical results by developing finite-element-based tools with appropriate material models and progressive damage algorithms.
- Enhance the understanding of joint performance by conducting full-field deformation measurements.

Accomplishments

- Completed static and dynamic tests at five different velocities on both unbonded and bonded tubes using TMAC.
- Designed and fabricated test fixtures for conducting dynamic fracture-toughness tests.
- Completed bulk adhesive dynamic fracture-toughness tests at rates above 1 meter/second.

- Completed static and dynamic Mode I, Mode II, and mixed-mode fracture-toughness tests.
- Installed high-rate equipment for conducting coupon-level dynamic tests at crosshead rates up to 18 meters/second.

Future Direction

- Complete Mode III fracture toughness tests at static and dynamic rates.

Introduction

The objective of this project is to develop a comprehensive experimental and analytical methodology to analyze and design adhesively-bonded automotive composite structures to sustain axial, off-axis, and lateral crash loads. This direct-funded project is closely aligned with the experimental and analytical efforts undertaken by the Automotive Composites Consortium (ACC) for adhesively-bonded composite substrates. The focus of this work, however, is restricted to the adhesive-joint issues. The key to the methodology development is the understanding of how critical joint design parameters, for example, bond length, bond thickness and fillet, affect the energy absorption. Recent investigations at ORNL have provided valuable insight toward the understanding of composite joint performance and composite crashworthiness. The next logical step is determining the correlation between measurable adhesive-joint parameters and their influence on the structure to dissipate energy and ultimately predict crashworthiness for a particular composite design.

Experimental tasks include material testing under quasi-static and dynamic loads for substrates, adhesives, and joints; strain-rate sensitivity studies; fracture-toughness testing; and test method development as required. These experimental results will provide the building blocks for model developments—first at the coupon level, then progressing in complexity to component level. Correlation with experimental results will provide the basis for which the analytical developments, including development of constitutive laws, materials models, damage algorithms, and new finite elements will be made. Structural tests are conducted on the new intermediate-rate TMAC at ORNL (see 8.B).

Approach and Results

The technical approach involves both experimental and analytical tasks. There are four main tasks:

Task 1—Materials Selection and Screening,
Task 2—Material Characterization,
Task 3—Component Testing, and
Task 4—Computational Tools Development.

Task 1 was completed and reported on in the FY 2002 annual report. The selected chopped-carbon-fiber prepreg material system was characterized from flat plaques provided by the vendor. Discussions with the vendor led to an overly optimistic view of the suitability of the material for this project. Additionally, delays in receipt of the material from the supplier resulted in consideration of a carbon-fiber sheet molding compound (SMC). Both materials were unsatisfactory due to processing difficultly and material variability. As a result of the variability in the initial material screening tests and difficulty in fabricating tubes with this material, the substrate material was changed to a carbon-fiber braided system. The woven-fabric prepreg comprises T300B carbon fiber with a tow size of 3K and 42% (by weight) epoxy resin.

Task 2 was initiated during FY 2002 and has been a continuing effort through FY 2006. This task focuses on determining the rate dependencies, if any, for mechanical properties of the bulk adhesive, substrate, and coupon-level joints.

Task 3 started in FY 2004 with preliminary tests to determine if the selected composite tube geometry would provide for a stable progressive crush behavior instead of global buckling. The geometry for the tube was 100 mm by 100 mm square with a 3-mm wall thickness and a 300-mm length. A 45-degree bevel was used for the triggering mechanism. These tests showed that a progressive

crush failure mechanism was achievable using this geometry. Therefore, the required unbonded and bonded tubes needed for the remainder of the project were procured from Pacific Composites. These tubes were then tested on TMAC at five different velocities during FY 2005 and FY 2006.

Task 4, the development of computational tools, was subcontracted to Virginia Tech under ACC Cooperative Agreement funding.

Bonded and Unbonded Tube Tests

The matrix for the tube testing consisted of crushing at different velocities tubes having different bond widths (BWs) and bond thicknesses (BTs). The test velocities were 5 mm/sec, 50 mm/sec, 100 mm/sec, 500 mm/sec, and 5000 mm/sec. The bond-line thicknesses were either 0.5 mm or 1.0 mm and the bond width or tube overlap was either 25 mm or 50 mm. Figure 1 shows the test results in terms of the specific energy absorbed (SEA) as a function of test velocity. A snapshot of one of the bonded tubes being crushed at 5000 mm/sec is shown in Figure 2. The results in Figure 1 show a significant decrease in SEA as a function of loading rate with the largest reduction seen to occur below the 500 mm/sec rate. Also, the unbonded or complete tubes are seen to have the highest SEA compared to the bonded tubes. The effect of bond width appears to be negligible but there does appear to be a slight effect of bond thickness with the thinner bond having slightly higher SEA's.

Bulk Adhesive Fracture Toughness

A key parameter in the development of computational models under Task 4 was the rate-sensitive fracture toughness of the bulk adhesive. Miniature compact-tension (CT) specimens were machined from hockey-puck-shaped adhesive castings. Quasi-static and dynamic fracture toughness tests were conducted on the bulk adhesive using an 8-mm-thick specimen per the geometry specified in ASTM D5045-99.

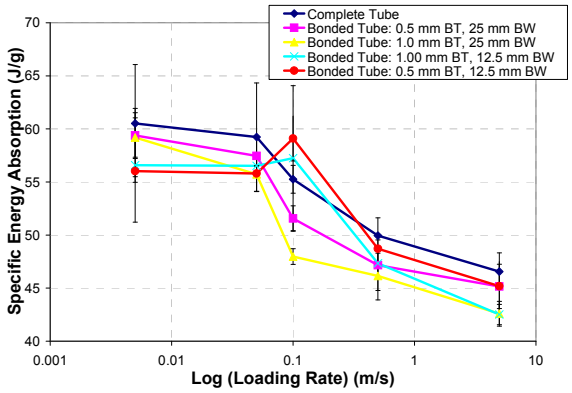

Figure 1. Measured tube SEA as a function of cross-head rate.

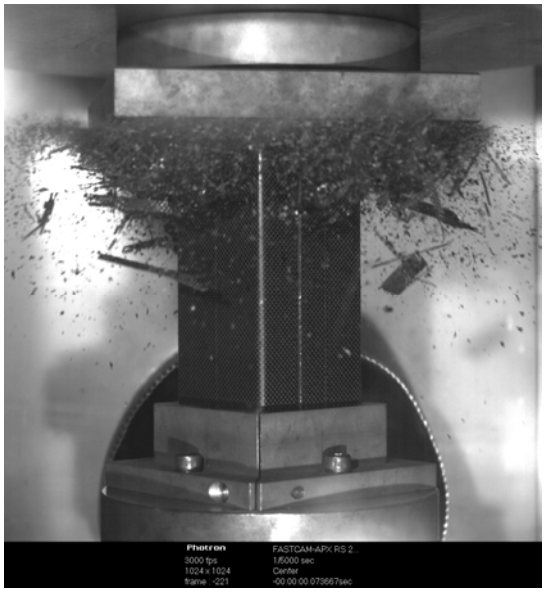

Figure 2. Bonded tube tested at 5000 mm/sec.

Fracture-toughness tests of the bulk adhesive were conducted at room temperature on a conventional closed-loop servo-hydraulic machine at rates ranging from 10^{-6} to 1 m/s. The load frame was equipped with a commercial slack adaptor or lost-motion device. Checkout tests were completed and it was determined that the target velocities could be achieved prior to the load application. However, at rates of 0.5 and 1 m/sec, it was difficult to accurately detect the relatively small loads generated by the test specimen because of contributions from the momentum of the 4 kg commercial slack adapter. Hence, a much smaller and lighter slack adapter was fabricated in-house. Fracture-toughness tests were successfully repeated at various rates from 10^{-6} to

1 m/sec with three specimens tested at each rate. The new setup included a smaller load cell, a shorter and simplified load train between the load cell and specimen, and reduced weight on the specimen because of the lighter adapter.

Even with the new setup, there was some question about the validity of the 1-meter/second test results. This was due to using a strain-gage load cell for measuring force. The new 18-meter/second test machine came on-line which uses a piezoelectric load cell. Therefore, some of the CT tests were repeated using the new test machine. The piezoelectric load cell should eliminate any inertia effects associated with the higher velocity test rates. Additionally, a new lightweight slack adaptor was designed and fabricated to provide a means for the actuation of the high-rate test machine to reach maximum velocity prior to engaging the test specimens. Results obtained from this study provide a much more accurate depiction of the behavior expected under such high rates of strain for the adhesive system in question.

Results show that the average fracture toughness, K_{Ic}, for the bulk adhesive CT specimens range from an average of $2.5 \pm 0.1\ MPa\sqrt{m}$ under quasi-static loading conditions to $1.7 \pm 0.01\ MPa\sqrt{m}$ at an applied loading rate of *1 m/s*. Furthermore, when converted from fracture toughness to strain-energy release rate (SERR), G_{Ic}, the corresponding average values ranged from $2260 \pm 180\ J/m^2$ under quasi-static loading conditions to $1015 \pm 7\ J/m^2$ at an applied loading rate of *1 m/s*. These average values take into account only those tests that were in compliance with the ASTM D5045-99 test standard. A full summary of the CT test results is presented in Table 1 while Figure 3 illustrates the relationship established between the Mode I fracture toughness, K_{Ic}, and the applied loading rate.

It is believed that the characterization of the performance of both the bulk adhesive and bonded composite joint specimens is best completed by looking at a local crack-tip loading rate, $d\sqrt{\mathcal{G}}/dt$, instead of a global loading rate, $\dot{\Delta}$. This conclusion was established based on the difference in stiffness among the bulk adhesive CT and the 11-ply, 20-ply, and 36-ply bonded composite joint specimens, both in the standard Mode I double-cantilever beam (DCB) configuration, as well as the newly-developed driven-wedge (DW) specimen geometry by Virginia Tech. With the newly obtained CT results, a correlation could be established between the bulk adhesive and bonded composite joint specimens as a function of local crack-tip loading rate, as illustrated in Figure 4.

Table 1. Summary of Mode I CT Test Results.

Rate (m/s)	K_{Ic} (Mpa*m$^{1/2}$)	$\mathcal{G}_{Ic}$ (J/m^2)
1.70E-05	2.5	2256
1.70E-04	2.3	1959
0.01	1.8	1191
0.1	1.9	1334
0.3	1.9	1335
1	1.7	1014

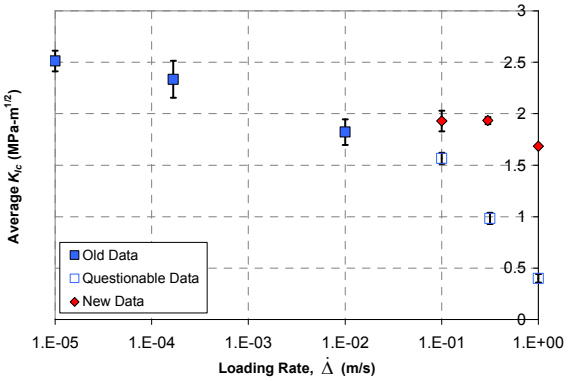

Figure 3. Mode I fracture toughness, K_{Ic}, vs. applied loading rate for bulk adhesive CT specimens.

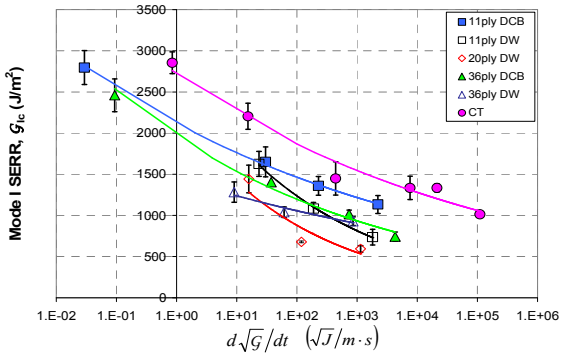

Figure 4. Complete summary of Mode I fracture results correlation.

DMA Results

Virginia Tech completed a dynamical mechanical analysis (DMA) test to verify the value for the glass transition temperature, T_g, for the SIA (Sovereign Specialty Chemicals) adhesive. Additionally, this test was conducted in an attempt to determine whether or not the Time Temperature Superposition Principle (TTSP) was applicable to the material system in question. A single-cantilever bend specimen was utilized for this study, and was subjected to a full frequency sweep from *0.1 – 20 Hz* over a temperature range of *-100 – 160°C*. Specialized rheology software was utilized for constructing a master curve in order to generate shift factor data to be used in the future for determining accurate frequency steps according to TTSP in order to conduct sub-ambient fracture tests relating to previously conducted high-rate experiments.

Results from the DMA test provide conclusive evidence that suggests a glass transition temperature of roughly *130°C*. This was determined from a tan(δ) versus temperature, *T*, curve, and is illustrated in Figure 5. Additionally, the generated shifted-frequency master curve was used to develop shift factors that can be used to relate temperature to frequency, thus corresponding to applied loading rate. In other words, the generated data can provide information that will allow for the sub-ambient testing of bonded composite joints that will directly correspond with tests conducted under high applied loading rates or at least this is the expected relationship. This will not only provide an accurate characterization of materials, but it will also provide a much easier means for completing such experiments. Figure 6 illustrates the final master curve that was generated with the specialized rheology software.

Conclusion

Material characterization tests were completed on bulk adhesive specimens and carbon-fiber woven-fabric adhesive joint specimens. A key parameter for the modeling efforts being conducted at Virginia Tech was the determination of the rate-sensitive fracture-toughness for the bulk adhesive. This was accomplished for Mode I by conducting compact-tension tests at different loading rates. These tests were conducted on the new 18 meter/second high-rate test machine in addition to tests previously conducted on a conventional servo-hydraulic machine. A new piezoelectric load cell was used in combination with a refined slack adaptor in an attempt to refute test results obtained from previous experiments conducted at high test velocities. These previous results were believed to be suspect due to inertia effects associated with the strain- gage-based load cell utilized in those experiments. Furthermore, additional DMA tests have been conducted on the SIA bulk adhesive in an attempt to determine whether or not the principle of TTSP can be used for future tests in order to virtually eliminate the need for high-rate testing. The results presented in this report illustrated that this concept is entirely possible.

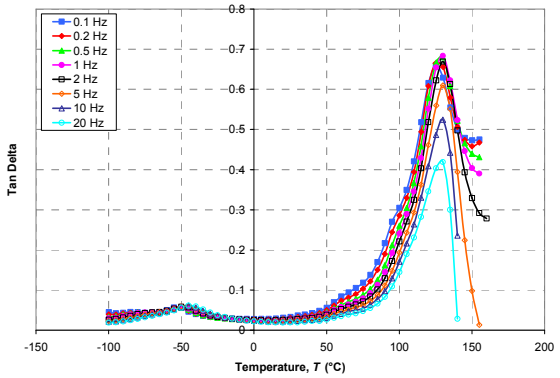

Figure 5. Tan δ vs. temperature curve generated from SIA adhesive DMA test.

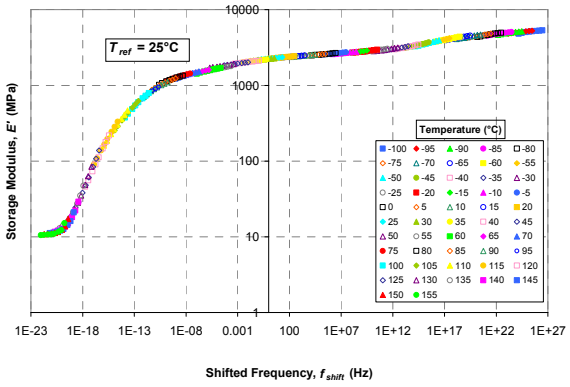

Figure 6. Shifted frequency vs. storage modulus for SIA adhesive DMA specimen.

To validate analytical models and to quantify the effect that an adhesive joint has on specific-energy absorption, a series of progressive crush tests on composite tubes were conducted using TMAC. Tests on bonded and unbonded tubes were completed at loading rates of 5, 50, 100, 500, and 5000 mm/sec. The SEA's were calculated and the results showed a decrease in SEA with loading rate for both the unbonded and bonded tubes. This trend is similar to that seen in previous ACC composite tube crush data, where the majority of the decrease in SEA appears to occur below the 500 mm/sec velocity.

Presentations/Publications/Patents

"The Effect of Rate on the Fracture of an Automotive Adhesive," presented at the 29th Annual Meeting of the Adhesion Society, Jacksonville, Florida, February 19-22, 2006.

"Using a Driven Wedge Technique for Characterizing Fracture Resistance of Adhesives Exhibiting Pronounced Slick-Slip Behavior," presented at the 29th Annual Meeting of the Adhesion Society, Jacksonville, Florida, February 19-22, 2006.

"Crashworthiness of Adhesively Bonded Composite Structures and Their Strain-Rate Sensitivities," presented at the Society for Experimental Mechanics Annual Conference on Experimental and Applied Mechanics, June 4-7, 2006, St. Louis, Missouri.

I. Engineering Property Prediction Tools for Tailored Polymer Composite Structures

Principal Investigator: Ba Nghiep Nguyen
Pacific Northwest National Laboratory (PNNL)
902 Battelle Boulevard, P.O. Box 999, MS: K5-22, Richland, WA 99354
(509) 375 3634; Fax: 509-375 673; e-mail: Ba.Nguyen@pnl.gov

Principal Investigator: James D Holbery
PNNL
902 Battelle Boulevard – P.O. Box 999 – MS: K5-22, Richland, WA 99354
(509) 375 3686; Fax: 509-375 6736; e-mail: James.Holbery@pnl.gov

Principal Investigator: Vlastimil Kunc
Oak Ridge National Laboratory (ORNL)
P.O. Box 2009, Oak Ridge, TN 37831
(865) 574 8010; Fax: 865-574-0740; e-mail: kuncv@ornl.gov

Technology Area Development Manager: Joseph A. Carpenter
(202) 586-1022; fax: (202) 586-1600; e-mail: joseph.carpenter@ee.doe.gov

Expert Technical Monitor: Philip S. Sklad
(865) 574-5069; fax: (865) 576-4963; e-mail: skladps@ornl.gov

---

Contractors: Pacific Northwest National Laboratory, Oak Ridge National Laboratory
Contract No.: DE-AC06-76RL01830, DE-AC05-00OR22725

Objective

- Enable the optimum design of lightweight automotive structural components using injection- molded long-fiber-reinforced thermoplastic (LFT) composites.

Approach

Phase I: Technical feasibility assessment

- Perform a technical assessment of current process models and computational methods for short-fiber polymer injection-molded composites in order to determine their accuracy, limitations and potential applications to LFTs.
- Identify the research directions needed to develop process and constitutive models for LFTs.
- Understand and examine the LFT emerging microstructure, characterization techniques and material processing.
- Characterize fiber orientation in LFT samples.
- Examine the molding behavior of glass and carbon fibers.

Phase II: Research and development

Develop an integrated approach that links process to structural modeling allowing the optimum design of LFT composite structures. This work includes:

- development of process models for LFTs that allow simulations of LFT structures in order to predict flow-induced fiber orientation and other microstructural features,
- development and implementation of LFT constitutive models for structural finite-element analyses that make use of the composite microstructure predicted by process modeling. These constitutive models will predict the composite thermoelastic properties and its nonlinear behaviors due to damage, fatigue, creep and impact,
- development of characterization methods for LFT materials,
- injection-molding of larger samples and complex geometries,
- experimental testing to determine the model parameters and to validate the process and constitutive models.

Accomplishments

- Long-fiber materials have been specified and procured from MTI Thermoplastics with either glass fibers (GF) or carbon fibers (CF) in a polypropylene (PP) matrix. The materials include 40% by weight GF in a PP matrix (i.e., 40%GF/PP), 31%CF/PP, and 31%Ni-Coated CF/PP. These weight percents give a common volume fraction of approximately 20%.
- In conjunction with Delphi Automotive, parts have been injection molded in three geometries under specific test conditions. These samples, molded from both CF/PP and GF/PP materials, were subsequently analyzed for both fiber orientation and mechanical properties.
- A technical assessment of the current process models for discontinuous fiber composites was conducted that provided insight on their limitations and applicability to LFTs.
- Numerical simulations of LFT injection molded samples were carried out using the current models to predict the fiber orientations. The predicted orientations were compared with the experimental data to assess the accuracy of the current models applied to LFTs.
- Computational models have been developed to predict the thermoelastic properties of LFTs. These models account for fiber length and orientation distribution in addition to the constituents' thermoelastic properties.
- A comprehensive website was developed to collect all data, publications, and updates for the program participants.
- Experimental methods for measuring fiber orientation and fiber length in LFTs were evaluated.
- Fiber orientation was evaluated for a set of specimens using a University of Leeds (Leeds) system.
- Measurements from Leeds system were validated via manual measurement.
- Fiber-length measurement techniques for glass and carbon fibers were developed.
- Method for separation of long carbon fibers was developed.
- Mechanical tests were performed to assess mechanical properties of LFT samples.

Future Direction

- Develop a material characterization matrix to obtain composite constitutive parameters for model input
- Develop process and property prediction models for LFTs
- Further develop non-destructive techniques to determine fiber orientation, fiber length, and fiber attrition in molded parts
- Procure materials and subsequently mold test samples with selected Tier 1 molder
- Develop orientation models for implementation in the Moldflow software for improved simulation of LFT composites.

Introduction

Recently, injection-molded long-fiber thermoplastics (LFTs) have generated great interest within the automotive industry as these materials can be used for structural applications in order to reduce vehicle weight. However, injection-molding of these materials poses a great challenge because of two main reasons: (i) no process models for LFTs have been developed that can be used to predict the processing of an LFT part, and (ii) no experimental characterization methods exist to fully characterize the as-formed LFT microstructure to determine the fiber orientation and length distributions and fiber dispersion that are critical for any process model development.

This report summarizes the work conducted during fiscal year (FY) 2006 that includes (i) the assessment of current process modeling approaches, (ii) experimental evaluation of LFT microstructure and mechanical properties, and (iii) the computation of thermoelastic properties using the measured and predicted orientation distributions as well as the measured fiber-length distribution. Our objective is two-fold. First, it is necessary to assess current process models and characterization techniques in order to determine their capabilities and limitations, and the necessary developments for LFTs. Second, before modeling the nonlinear behaviors of LFTs, it is essential to develop computation tools for predicting the elastic and thermoelastic properties of these materials.

Assessment of Current Process Modeling Approaches

During FY 2006, we assessed process models for fiber-reinforced injection-molded thermoplastics in order to determine the limitations and applicability of these models to predict the as-formed composite microstructure. The details of this study are presented in [1-2]. First, the concentration regimes were examined to facilitate the understanding of different types of fiber-fiber interaction that can occur for a given fiber volume fraction. Basically, there are three concentration regimes which are the dilute, semi-concentrated (or semi-dilute), and concentrated regimes [3].

After the formulation of the fiber suspension flow problem and the simplification leading to the Hele-Shaw approach, the interaction mechanisms were examined. In general, fiber-fiber interactions can be classified into two categories: *hydrodynamic interaction* [4] and *mechanical interaction* [5]. Hydrodynamic interactions are hydrodynamic in nature and include *short-* and *long-range interactions* [4, 6]. The long-range hydrodynamic interaction results as a fiber is placed in the disturbance flow field of other fibers. The short-range hydrodynamic interaction is due to the lubrication forces and torques. At high concentrations, mechanical interactions due to direct fiber-fiber contacts and Coulomb friction occur [7-8].

Depending on the concentration regimes, both hydrodynamic and mechanical interactions do occur in injection-molded short-fiber-reinforced thermoplastic (SFT) and LFT systems. For SFTs, Folgar and Tucker [9] added a diffusion term to the Jeffrey's dilute solution in order to represent the randomizing effect of the fiber-fiber interaction in concentrated suspensions. This term hence depicts the hydrodynamic interactions. Later, Advani and Tucker [10] recast the Folgar-Tucker equation in terms of the fiber orientation tensor components as:

$$\frac{DA_{ij}}{Dt} + \frac{1}{2}(\omega_{ik}A_{kj} - A_{ik}\omega_{kj}) = \frac{1}{2}\kappa(\dot{\gamma}_{ik}A_{kj} + A_{ik}\dot{\gamma}_{kj} - 2\dot{\gamma}_{kl}A_{ijkl}) + 2C_I\dot{\gamma}(\delta_{ij} - 3A_{ij}) \quad (1)$$

where A_{ij}, A_{ik}, and A_{kj} are the components of the second-order orientation tensor, and A_{ijkl} is the fourth-order orientation tensor. δ_{ij} is the identity tensor, and ω_{ik} and ω_{kj} are the components of the vorticity tensor. $\dot{\gamma}_{ik}$, $\dot{\gamma}_{kj}$, and $\dot{\gamma}_{kl}$ are the components of the rate of the deformation tensor whose scalar magnitude is $\dot{\gamma}$. κ and C_I are material constants; κ depends on the fiber aspect ratio *r*, and C_I is called the interaction coefficient. If $C_I = 0$ and, $\kappa = (r^2 - 1)/(r^2 + 1)$, Eq. (1) is then Jeffrey's equation for the motion of a rigid ellipsoidal shape fiber in a Newtonian solvent. This

is strictly valid for dilute suspensions in which the fiber-fiber interaction is absent or negligible.

Recent experience with SFTs suggests that the rate of orientation in concentrated fiber suspensions is slower than the standard model prediction (Eq. (1)), and thus the *SRF* (strain reduction factor) factor has been introduced to improve the agreement between prediction and experiment [11-12]:

$$\frac{DA_{ij}}{Dt} + \frac{1}{2\,SRF}(\omega_{ik}A_{kj} - A_{ik}\omega_{kj}) = \frac{1}{SRF}[\frac{1}{2}\kappa(\dot{\gamma}_{ik}A_{kj} + A_{ik}\dot{\gamma}_{kj} - 2\dot{\gamma}_{kl}A_{ijkl}) + 2C_I\dot{\gamma}(\delta_{ij} - 3A_{ij})] \quad (2)$$

One problem arises in Eq. (2) if $SRF \neq 1$, namely it does not necessarily give the same answer in every coordinate system. To overcome this issue, in this report, a new model, called the *reduced strain closure RSC* model, was used that can be applied to all flows and coordinate systems. Next, the establishment of the rheological constitutive equation was studied. A constitutive relation is necessary to relate the stress in the suspension to the rate of deformation, the fiber orientation state and the suspension parameters such as the fiber volume fraction, the fiber aspect ratio, and the viscosity of the suspending liquid. As the compressibility of the suspending liquid and the fibers are negligible, the total stress σ_{ij} is separated into an hydrostatic contribution from the pressure *P* plus a contribution from the suspension defined as the *extra stress*, τ_{ij} [3]:

$$\sigma_{ij} = -P\delta_{ij} + \tau_{ij} \quad (3)$$

where

$$\tau_{ij} = 2\eta(\dot{\gamma},T)\dot{\gamma}_{ij} + 2\eta(\dot{\gamma},T)N_p A_{ijkl}\dot{\gamma}_{kl} \quad (4)$$

$\eta(\dot{\gamma},T)$ is the suspension viscosity which is in general a function of the strain rate and temperature *T*. N_P is defined as the particle number and is a dimensionless parameter dependent on the fiber volume fraction and aspect ratio. If N_P is equal to zero, Eq. (4) is the constitutive relation of a generalized Newtonian fluid in which the stress field is assumed not to be dependent on the orientation state. This is the assumption for using a decoupled flow/orientation approach.

The coupled and decoupled flow/orientation approach was also reviewed. In a decoupled approach, the fluid-flow problem is first solved as if the fibers were not present, and the resulting kinematics (i.e., velocity field) is used to compute the fiber orientation. On the other hand, in a coupled problem the flow and orientation equations must be solved simultaneously. To date, the coupled approach has not been implemented in commercial finite-element software packages.

This section applies the current capabilities to computationally predict fiber orientation for three different LFT materials, using two different mold geometries: an *end-gated strip* and a *center-gated disk*. In order to compute the orientation state for an injection-molding operation, the equations of balance of mass, momentum, and energy must be solved so that a velocity field can be computed. A program named ORIENT was used to solve the velocity profile and the orientation in the above-mentioned geometries [11]. ORIENT uses the Hele-Shaw approximation for solving for the velocity field in mold-filling operations where the velocity solution is decoupled from the orientation solution.

Table 1 provides a concise summary of each of the samples molded. The sample code identifies each material as "PNNLwxyz." The letter "w" identifies each material; "x" indicates either fast or slow injection speeds; y corresponds to the sample thickness in mm (all samples with orientation measurements were 3 mm thick); and z indicates the part geometry (D or I, indicating a disk or ISO plaque). Material A has a polypropylene matrix with a 40% weight fraction of glass fibers. Material B is a polypropylene matrix with 31% weight fraction of carbon fibers, and material C is the same as material B, with the exception that the carbon fibers are nickel-coated. The center-gated disk is 177.8 mm in diameter, while the ISO plaque is 90 mm long and 80 mm wide. Moldflow, Inc (Ithaca, NY) performed a complete evaluation of materials A and C and supplied the appropriate rheological and thermal properties.

Table 1. Summary of materials, injection speed, and mold geometry for each of the studied samples.

Sample Code	Material	Injection Speed Setting		Geometry
		Fill Speed	Fill Time [s]	
PNNLAF3D	A	Fast	0.65	Disk
PNNLAS3D	A	Slow	4.79-4.18	Disk
PNNLAF3I	A	Fast	0.48	ISO Plaque
PNNLAS3I	A	Slow	3.33	ISO Plaque
PNNLBF3D	B	Fast	0.67-0.81	Disk
PNNLBS3D	B	Slow	4.93-4.96	Disk
PNNLCF3D	C	Fast	0.67	Disk
PNNLCS3D	C	Slow	4.99-5.01	Disk
PNNLCF3I	C	Fast	0.475-0.480	ISO Plaque
PNNLCS3I	C	Slow	3.69-3.73	ISO Plaque

The properties of material B were assumed to be equivalent to those of material C. In order to compare the predicted and measured orientations, each of the samples presented in Table 1 were analyzed at three regions denoted A, B, and C. For the ISO plaques, region A was centered near the inlet at x = 15 mm, region B was centered approximately half-way down the length of the plaque at x = 45 mm, and region C was closer to the end of the plaque, centered at x = 75 mm. Each of the regions was located centrally in the cross-flow direction. For the center-gated disk, region A was located near the inlet at r = 6 mm, region B was at r = 34 mm, and region C was closer to the edge of the disk at r = 64 mm, where r is the radius of the disk. Each of the samples was 3 mm thick.

Orientation measurements were preformed by ORNL staff at GM using a Leeds image analysis system developed by Hine et al. [12]. The important orientation descriptors are the orientation tensor elements A_{11}, A_{22}, A_{33}, and A_{31}. A_{11}, A_{22}, and A_{33} range between 0 and 1. Figures 1-4 illustrate the orientation tensor components at region B for some of the selected samples.

Experimental Evaluation of LFT Microstructure and Mechanical Properties

The experimental effort was focused on development and validation of procedures for fiber-orientation and fiber-length measurements and on providing measurements of these quantities in molded samples at specific locations. Thermo-elastic properties were measured at identical locations to allow correlation of mechanical properties to local material microstructure.

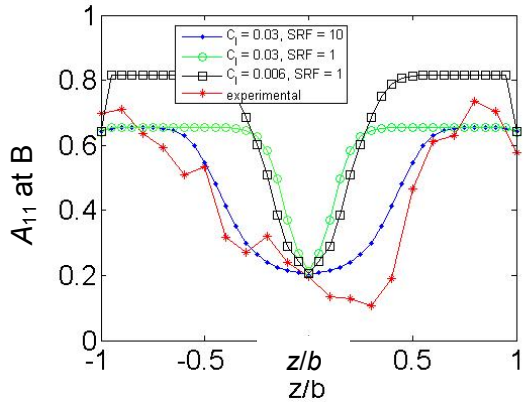

Figure 1. A_{11} vs. non-dimensional thickness coordinate z/b for PNNLAF3I.

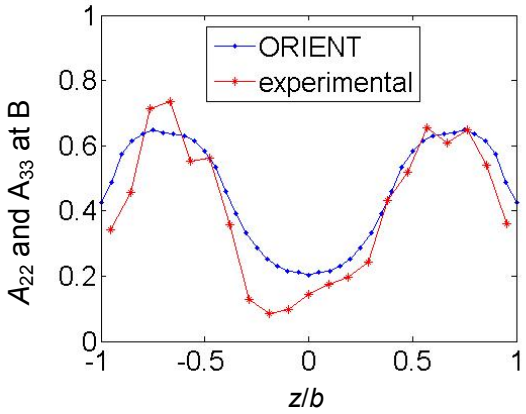

Figure 2. A_{11} vs. non-dimensional thickness coordinate z/b for PNNLAS3I at region B. SRF = 30 and C_I = 0.03.

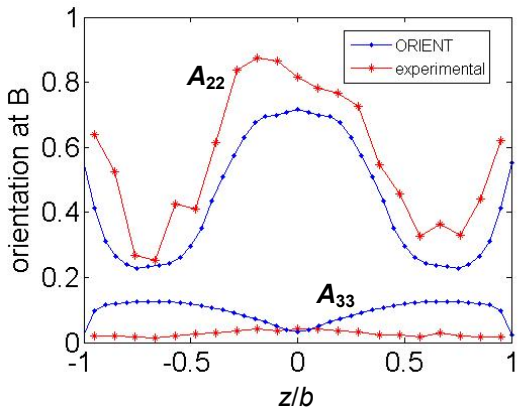

Figure 3. A_{22} and A_{33} vs. non-dimensional thickness coordinate *z/b* for PNNLAS3I at region B. *SRF* = 30 and C_I = 0.03.

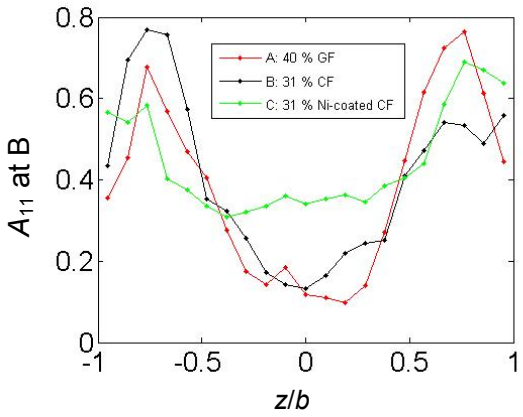

Figure 4. Experimental A_{11} vs. *z/b* at region B for all three materials. The samples were slow-filled disks.

For fiber-orientation measurements, tensile, ISO and disk samples were sectioned. Specimens were mounted in a resin and polished. Glass specimens were etched and sputter coated with gold to increase contrast between fibers and matrix.

Polished samples were analyzed using an optical system developed by University of Leeds. This system collects an array of digital images from a cross-section of a sample and performs assembly of these images. Fibers are assumed to be straight cylinders, therefore, the cross-sections of fibers in a given plane should be visible as ellipses. The Leeds system distinguishes fibers from matrix through thresholding and ellipses are fitted to the thresholded image. Fiber orientation is determined based on the ratio and size of minor and major axes of ellipses fitted to the image. Leeds analysis was performed in three locations on all specimens, with the exception of 6-mm-thick ISO bars. Voids in these samples prevented meaningful analysis.

The system assumes that fibers are straight and that ellipses can be fitted to a cross-section of each fiber crossing the plane. These long fibers were not counted in the Leeds analysis, therefore raising the question about the accuracy of the measurement. Discounting "in-plane" fibers is particularly damaging to the accuracy of fiber-orientation measurement, because the number of "in-plane" fibers is significantly smaller compared to fibers crossing the plane at greater angles. The Leeds system also tends to fit ellipses to clusters of fibers, rather than to separate fibers. This phenomenon was particularly pronounced for specimens with Ni-coated carbon fibers.

The fiber orientation obtained from the Leeds system was further scrutinized due to the reasons outlined above. Representative samples for glass-, carbon- and Ni-coated-carbon-filled materials were imaged at ORNL and analyzed at University of Illinois. Figure 5 shows comparison of Leeds and manual measurement for orientation tensor components for Ni-coated-fiber-filled specimen CS3I, which was expected to have large measurement errors. Only 1/6th of the sample was re-measured; however, good match between the data is already apparent. The same manual measurement on larger portions of AS3I and BF3D samples resulted in closer match of the Leeds results. Good match for all three specimens examined manually

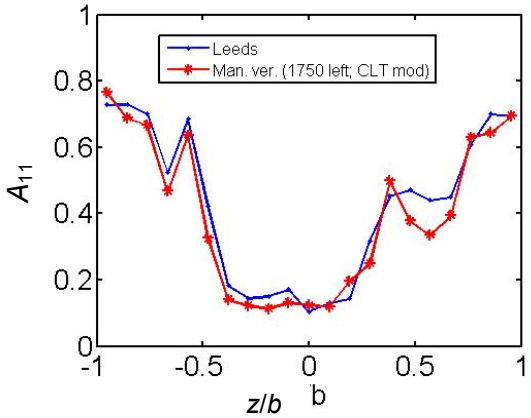

Figure 5. Comparison of Leeds and partial manual measurements for A_{11} (PNNLCS3I).

indicates that the Leeds system measures ellipse cross-sections with acceptable accuracy.

Preliminary burn-off tests revealed a wide range of fiber lengths present in molded samples. Standards and measurement techniques developed for short-fiber-reinforced plastics could not be used due to the wide range of fiber lengths and the tendency of the long fibers to bend. Procedures have been developed for fiber-length measurement of glass- and carbon-filled LFTs. The procedures consist of identical major steps; however, the execution of these steps differs due to different physical properties of glass and carbon fibers. These are the steps of fiber-length measurement:

1. composite coupon isolation
2. constrained removal of matrix material
3. fiber-sample isolation
4. filament dispersion
5. imaging and individual filament-length measurement

The size of a coupon cut out from a specimen must be large enough to prevent measurement of cut fibers. Materials examined in this project were molded with initial nominal fiber length of 12 mm, therefore, the distance of the center of the section - the location of interest - from any edge must be 12 mm or more.

The composite coupon is placed in an aluminum sheet-metal form whose inside dimensions correspond to the shape and area dimensions of the coupon. The sheet-metal form provides restraint at the edges of the coupon during the matrix-removal step, which was performed via burn-off. The form and its contents are sealed at the top and bottom with aluminum-foil lids. The form-height dimensions are greater than the coupon thickness to provide for some expansion of the fibers during matrix burn-off. This expansion is believed to facilitate the separation and spreading of the filaments during the dispersal step that follows later in this procedure.

The fiber-sample-isolation step involves isolating the central fibers of the residual fiber mass for subsequent collection and characterization. The process involves inserting the needle attached to a hypodermic syringe loaded with a liquid epoxy through the center of both the top and bottom lids of the aluminum form containing the fiber. The needle is withdrawn from the form and through the fiber stack while dispensing the epoxy through the needle at a constant rate. The continuous stream of epoxy results in approximately cylindrical column of resin that extends through the entire thickness of the fiber stack. The number of fibers collected from the specimen is proportional to the epoxy plug volume (diameter of the cylinder). Factors that control the volume include the resin's viscosity, the needle gage and the withdrawal rate of the needle through the fiber stack. The resin injection is conducted with the aid of an actuator for better control of uniform epoxy deposition. After injection, the epoxy is allowed to gel at room temperature and the resin is subsequently cured. Filaments in the vicinity of the epoxy are thereby bonded in-situ to the epoxy cylinder. The bonded fibers are extracted by removing the fiber stack with epoxy plug from the aluminum form, manually shaking the specimen and short blasts of low-pressure air. Figure 6 is a photograph of an extracted carbon fiber-and-epoxy plug specimen. Long and shorter fibers are visibly attached to the plug specimen along its length.

Figure 6. Extracted carbon fiber-and-epoxy plug specimen.

A major portion of development effort was devoted to the technique of long-carbon-fiber separation. Long carbon fibers exhibit the tendency to form filament clumps, therefore preventing measurement of individual filament length. A number of unsuccessful trials involving liquids and various chemicals did not result in an acceptable technique. Mechanical methods usually caused breakage of the filaments.

The newly developed dispersal process relies on a corona field provided from a high-frequency generator to create fields of static charge in the vicinity of the carbon filaments and a substrate surface. In this case, the substrate is a ply of paper supported on a notebook pad of paper that is approximately 6-mm thick. The paper stack is elevated by supports so that the corona field from the tip of the high-frequency generator can be applied from beneath. A portion of the residual fiber clumps are placed on the paper and the high-frequency generator is switched on to generate the corona field beneath the paper stack As the paper and carbon filaments acquire static charge, two phenomena occur that aid in separation and dispersal of the carbon filaments. One is that the carbon filaments seem to repel each other and, when the residual fiber mass is sufficiently small, fly apart and disperse. The other is that the carbon fibers are attracted to the charged substrate and tend to adhere to the paper so long as the corona field is applied. The procedure for dispersal therefore involves gently moving the residual fiber clumps across the paper surface while generating the statically-charged fields in their vicinity with the high-frequency generator. The carbon filaments from the clumped fiber mass gradually are "shed" from the outside of the clump and onto the paper. This shedding process occurs with the smallest filaments first, leaving the longer filaments to be dispersed later in the process. Manipulation of the clumps is done manually. Wooden sticks from cotton swabs work well for this purpose as well as insulating the operator from electrical shocks.

As-is, the carbon-fiber-dispersal technique is rudimentary, but effective. A little art and technique on the part of the operator is required to effectively disperse all of the fiber clumps and, depending on circumstances (clump size, fiber length distribution, etc.), some strategies work better than others. Some care is required to avoid breaking the filaments during manipulation. Applying the corona field directly to the carbon fibers themselves will induce arcing that is definitely damaging to the fibers. The technique becomes less effective as the paper substrate becomes loaded with dispersed filaments, so changing the paper at regular intervals is recommended.

Following dispersal, a layer of clear adhesive-backed laminating film is applied over the dispersed carbon filaments and the copier printer paper substrate. The laminating film fixes the fibers in place to the paper so they cannot shift, re-combine, fly away, etc. These laminated sheets can then be transported, stored for future reference, etc. Digital images of the carbon filaments are scanned through the clear laminating film and into a computer file for later analysis.

The ease of glass-fiber dispersion depends on proper amount of expansion during the first constrained burn-off. Complete constraint results in an entangled mass of fibers of approximately original sample thickness because glass fibers anneal at burn-off temperatures. Attempting to separate fibers from this entangled state is impractical. Constraint-free burn-off would result in dislocation of fibers, thereby preventing subsequent isolation of a representative sample. Identical steps for fiber-sample separation can be followed. Dispersion of glass fibers is performed on glass Petri dishes by gently tapping the dish. The fibers exhibit affinity for the glass surface. As in the case of carbon-fiber separation, the short fibers adhere to the surface first. Petri dishes with dispersed glass fibers can be scanned using a regular scanner. Traditionally, multiple images were collected from a microscope with an x-y stage and then joined. The use of a scanner considerably simplifies and shortens the measurement process. It is also possible to consider the use of automated image-analysis software for fiber-length evaluation, as problems with imperfectly-joined images are eliminated.

Fiber-length distribution is currently determined by manually measuring the fiber length of fibers using the Image J software. Presently-available automated software packages can not cope with typical LFT bent fibers and multiple fiber ends in the same location. A prototype software package capable of length measurement of approximately straight fibers and identification and isolation of problematic measurements is under development.

Mechanical tests were performed on all specimen geometries and materials. Elastic properties corresponding to certain locations considered for fiber-orientation and fiber-length measurements were obtained. Carbon-fiber-filled specimens did not

perform as expected and poor fiber-matrix interface is suspected based on scanning electron microscope images showing no resin residue present on carbon fibers after fracture. Preliminary measurements of the coefficient of thermal expansion were performed. Processes active within the material at elevated temperatures resulted in highly non-linear thermal expansion. Therefore, the results of these measurements are not conclusive at this time.

Three students from Virginia Polytechnic Institute, University of Illinois and University of Tennessee actively participated in developing experimental techniques and performing measurements while working at ORNL.

Computation of LFT Thermoelastic Properties

Computation of LFT elastic properties: The measurement of fiber lengths in LFT samples shows that the actual fiber-length distributions (FLDs) are unsymmetrical and exhibit a shape having a sharp peak in the short fiber range and a long "tail" towards the long fiber range (> 1mm). The Weibull's distribution that contains two shape parameters named "*b*" and "*c*" can be used to represent such a distribution. The Weibull's probability distribution function is given by:

$$f(l) = \frac{c}{b}\left(\frac{l}{b}\right)^{c-1} e^{-\left(\frac{l}{b}\right)^{c}} \qquad (7)$$

where *l* is the fiber length. The stiffness matrix of a unidirectional (UD) fiber composite containing a fiber length distribution (e.g. represented by Eq. (7)) is then computed as:

$$C_{ijkl} = \frac{\int_0^\infty C^*_{ijkl}(l/d) f(l)\, dl}{\int_0^\infty f(l) dl} \qquad (8)$$

where $C^*_{ijkl}(l/d)$ is the stiffness matrix of the UD fiber composite having the aspect ratio *l/d*. In this work, the Eshelby-Mori-Tanaka method [13-14] was applied to compute $C^*_{ijkl}(l/d)$, and after the calculation of C_{ijkl} using Eq. (8), the elastic stiffness of the actual composite in which the fiber orientation was achieved after injection molding was computed using the orientation averaging method [10]:

$$\begin{aligned}\overline{C}_{ijkl} &= B_1\, A_{ijkl} + B_2(A_{ij}\delta_{kl} + A_{kl}\delta_{ij}) + \\ &B_3(A_{ik}\delta_{jl} + A_{il}\delta_{jk} + A_{jl}\delta_{ik} + A_{jk}\delta_{il}) \\ &+ B_4\delta_{ij}\delta_{kl} + B_5(\delta_{ik}\delta_{jl} + \delta_{il}\delta_{jk})\end{aligned} \qquad (9)$$

where the coefficients B_i (i = 1, 5) are related to the stiffness components of the UD transversely isotropic composite (Eq. (8)). The results are illustrated for the moduli E_{11}, E_{22} and E_{33} in Figures 7(a-c) for the PNNLAF3D material (location B), respectively. On these figures are presented the results obtained using one and two Weibull's FLDs, and also those obtained using the average fiber length (1.42 mm). The results based on one Weibull's FLD are very close to the values based on the use of two Weibull's distributions. This shows that it is not necessary to closely capture the experimental distribution with two Weibull's fits, and the results based on the average fiber length constitute a fair approximation of the values obtained by the use of one or two Weibull's FLDs.

Computation of thermal expansion coefficients: The Eshelby-Mori-Tanaka approach to predict the elastic properties of fiber composites can be extended to compute the thermal expansion coefficients (CTEs) of these materials. The key idea is to incorporate the thermal strain in the governing equations to first obtain the CTEs for the UD fiber composite [15]:

$$\boldsymbol{\alpha}_c = \boldsymbol{\alpha}_m + \frac{f\,(\boldsymbol{\varepsilon}^* + \boldsymbol{\alpha}^*)}{\Delta T} \qquad (10)$$

where *f* is the fiber volume fraction, ΔT is the temperature change; $\boldsymbol{\alpha}_c$ and $\boldsymbol{\alpha}_m$ are the CTEs of the UD fiber composite and matrix material, respectively. $\boldsymbol{\varepsilon}^*$ is defined as the eigenstrain and $\boldsymbol{\alpha}^*$ is the strain resulting from the mismatch of CTEs of the constituents. Next, the CTE solution $\overline{\alpha}_{ij}$ for the actual random fiber composite is determined from the CTEs and stiffness of the UD fiber composite, the second and fourth-order orientation tensors using the *aggregate averaging method* [16]:

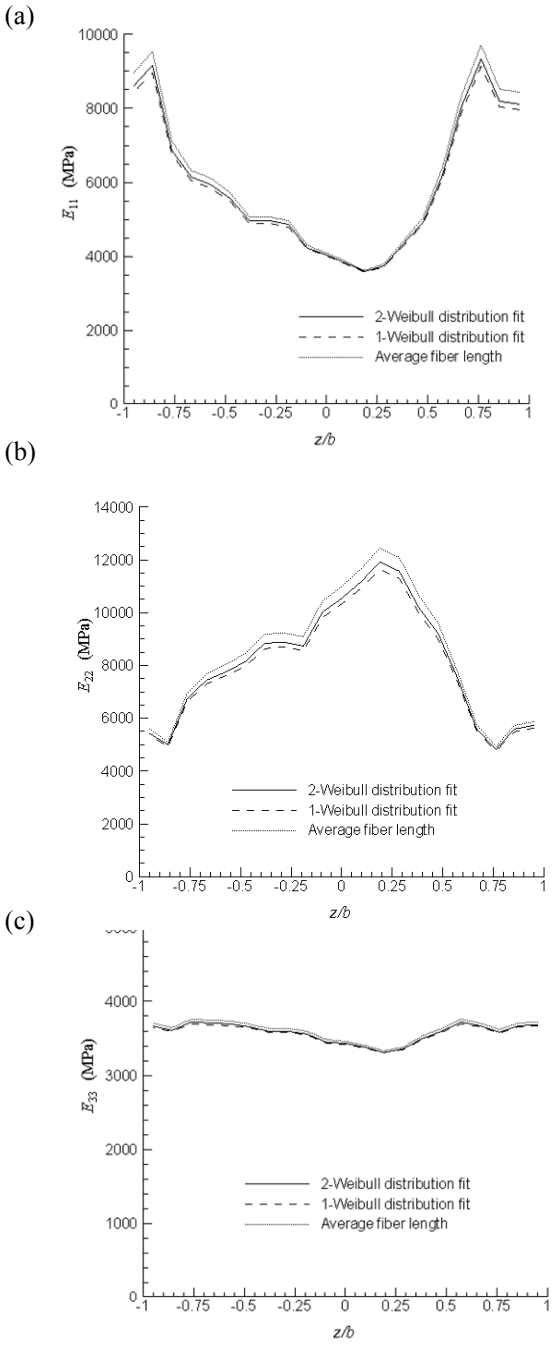

Figure 7. Moduli (a) E_{11}, (b) E_{22}, and (c) E_{33} predicted along the specimen thickness direction (PNNLAF3D, location B).

$$\overline{\alpha}_{ij} = \overline{C}^{-1}_{ijkl}\hat{\alpha}_{kl}$$
$$\hat{\alpha}_{ij} = \left\langle C_{ijkl}\alpha^{c}_{kl} \right\rangle = \hat{\alpha}_1 A_{ij} + \hat{\alpha}_2 \delta_{ij} \quad (11)$$

where $\hat{\alpha}_1$ and $\hat{\alpha}_2$ are related to the CTEs of the UD fiber composite. The model to compute CTEs of LFTs has been implemented in the homogenization procedure using the Eshelby-Mori-Tanaka framework. Results will be presented in the next report.

Conclusions

During this year our efforts were focused on the technical assessment of current process models, computational capabilities, and experimental methods that enable us to address the issues arising in LFTs. The feasibility assessment phase has been successfully completed. In addition, computational models and tools have also been developed to predict the thermoelastic properties of LFTs. These models account for fiber orientation and length distributions. The following conclusions have been drawn:

- LFT microstructure possesses a skin/shell/core layered structure as observed in SFTs. However, flow-direction alignment in the shell layers is significantly lower in the LFT samples than in SFTs.
- In addition to the fiber orientation, there are emerging variables for LFTs which are fiber length distribution, fiber volume fraction, fiber curvature, and orientation clustering.
- The current fiber orientation and constitutive models can adequately predict the fiber orientation, suspension viscosity in dilute and semi-concentrated regimes. However, these models have limitations to capture the fiber orientation in concentrated regimes. This is true for both short- or long-fiber systems.
- The Hele-Shaw assumption for flows in thin cavities applies to both short- and long-fiber systems.
- The best fits of the RSC model to LFT fiber orientation data show that the SRF value for carbon fibers is higher than the SRF value for glass fibers. This suggests that fiber stiffness plays a role in determining SRF.

- Neither the standard fiber orientation model nor the new RSC model can predict fiber orientation in LFT samples to the level of accuracy needed for predictive engineering.
- The fundamental limitation of the fiber orientation model seems to reside in the interaction term. This term needs to be improved to account for the rotation of long fibers and the anisotropic character of the fiber-fiber interaction which cannot be adequately represented by an isotropic rotary diffusion term.
- The data for Ni-coated carbon fiber is more erratic than for uncoated carbon fiber. Thus, we have not established that Ni-coated carbon fiber is a direct substitute for uncoated carbon fiber in terms of fiber orientation behavior.
- The Leeds system provides accurate measurement of fiber cross-sections.
- Long carbon fibers can be separated using corona field of static electricity.
- Validation of the thermoelastic property prediction tool will be achieved by comparing the predicted moduli with the corresponding experimental values.

References

1. B.N. Nguyen, J.D. Holbery, V. Kunc (2006). "Property Prediction Tools for Tailored Polymer Composite Structures." FY06 semi annual report.

2. B.N. Nguyen, J.D. Holbery, M.T. Smith, V. Kunc, R.E. Norris, J. Phelps, C.L. Tucker III (2006). "Assessment of Current Process Modeling Approaches to Determine Their Limitations, Applicability and Developments Needed for Long-Fiber Thermoplastic Injection-Molded Composites." PNNL internal report No. PNNL-16236.

3. C.L. Tucker III and S.G. Advani (1994). "Processing of Short-Fiber Systems." In: Flow and Rheology in Polymer Composites Manufacturing, S.G. Advani, Ed., Elsevier Science, 147-202.

4. M. Rahnama, D.L. Koch, and E.S.G. Shaqfeh (1995). "The Effect of Hydrodynamic Interactions on the Orientation Distribution in a Fiber Suspension Subject to Simple Shear Flow." *Phys. Fluids*, 7(3): 487-506.

5. C. Servais, J.-A.E. Manson, and S. Toll (1999). "Fiber-Fiber Interaction in Concentrated Suspensions : Disperse Fibers." *J. Rheol.*, 43(4), 991-997.

6. M. Djalili-Moghaddam and S. Toll (2005). "A Model for Short-Range Interactions in Fiber Suspensions." *J. Non-Newtonian Fluid Mech.*, 132: 73-83.

7. F. Folgar and C.L. Tucker III (1984). "Orientation Behavior of Fibers in Concentrated Suspensions." *J. Reinf. Plast. Comp.*, 3:98-119.

8. S.G. Advani and C.L. Tucker III (1987). "The Use of Tensors to Describe and Predict Fiber Orientation in Short-Fiber Composites." *J. Rheol.*, 31 (8):751-784.

9. H.M. Huynh (1999). Improved fiber orientation predictions for injection-molded composites. Master's thesis, University of Illinois, Urbana, IL.

10. J.H. Phelps and C.L. Tucker III (2006). "Assessing Fiber Orientation Prediction Capability for Long-Fiber Thermoplastic Composites." Technical Report submitted to PNNL, University of Illinois at Urbana-Champaign.

11. R.S. Bay and C.L. Tucker III (1992). "Fiber Orientation in Simple Injection Moldings. Part I: Theory and Numerical Methods. *Polym. Compos.*, 13:317-331.

12. P.J. Hine, N. Davidson, R.A. Duckett, A.R. Clarke, I.M. Ward (1996). "Hydrostatically Extruded Glass-Fiber-Reinforced Polyoxymethylene. I: The development of Fiber and Matrix Orientation." *Polym. Compo.*, 17:720-729.

13. J.D. Eshelby (1957). "The determination of The Elastic Field of An Ellipsoidal Inclusion and Related Problems." *Proc. Royal Soc. London*, A 241:376-396.

14. T. Mori, K. Tanaka (1973). "Average Stress in Matrix and Average Elastic Energy of Materials with Misfitting Inclusions." *Acta Metall.*, 21:571-574.

15. Y. Takao Y, M. Taya M (1985). "Thermal Expansion Coefficients and Thermal Stresses in an Aligned Short Fiber Composite with Application to A Short Carbon Fiber/Aluminum." *J. Applied Mechanics*, 52:806-810.

16. C. Camacho, C.L. Tucker III, S. Yalvac, R.L. McGee (1990). "Stiffness and Thermal Expansion Predictions for Hybrid Short-Fiber Composites". *Polym. Compos.*, 11:229-239.

Presentations and Publications

Experimental Methods to Evaluate Fiber Length and Orientation Distribution of Long Glass Fibers in Injection Molded Thermoplastics, Gregorio Velez-Garcia, Vlastimil Kunc, Fiber Society Conference, October 10-12, 2005, Knoxville, TN.

J. Simulation of Injection Molding of Thermoplastics Reinforced with Short and Long Fibers

Principal Investigator: Donald G. Baird
Virginia Polytechnic Institute and State University
Department of Chemical Engineering
Blacksburg, VA 24061
(540) 231-5998; fax: (540) 231-2732; e-mail:dbaird@vt.edu

Co-Principal Investigator: Peter Wapperom
Virginia Polytechnic Institute and State University
Department of Math
Blacksburg, VA 24061
(540) 231-7252; e-mail:pwappero@vt.edu

Technology Area Development Manager: Joseph A. Carpenter
(202) 586-1022; fax: (202) 586-1600; e-mail: joseph.carpenter@ee.doe.gov

Expert Technical Monitor: Philip S. Sklad
(865) 574-5069; fax: (865) 576-4963; e-mail: skladps@ornl.gov

---

Contractor: Virginia Polytech Institute and State University
Contract No.: DMI-052918

Objective

- Improve predictions of fiber orientation in thermoplastics during injection and compression molding by:
  - using a theory that couples fiber orientation with the flow field and incorporates the effects of fiber interaction and the viscoelastic behavior of the suspending medium.
  - incorporating the frontal flow region (which is dominated by extensional flow) into the finite-element simulation.
- Evaluate predicted-orientation distribution by comparing results to glass-fiber orientation found in injection-molded parts produced using basic mold geometries (end- and center-gated parts).

Approach

- Conduct shear and extensional, steady and transient rheological studies on glass-fiber-filled polypropylene (PP) and polybutylene terephthalate (PBT) systems in which fibers of various lengths (length: 0.2 - 11 mm, diameter: 12.5 microns) are used to asses the effects of both fiber length and the viscoelastic nature of the matrix on the transient rheology.
- Determine the relationship between fiber-orientation distribution and the nonlinear rheological behavior in shear flow.
- Identify the limitations of Doi theory for concentrated systems of rigid-rod molecules in a Newtonian suspending medium to represent the rheology and associated orientation distribution of glass fibers in a non-Newtonian matrix by comparing model predictions to experimental observations.
- Modify theory to address the limitations.

- Define and evaluate specific rheological tests to determine the material parameters in the constitutive equation which are unique and give consistent results when used in numerical simulations.
- Develop a finite-element-method simulation program capable of using multiple constitutive equations to simulate mold filling in injection molding, including the extensional flow kinematics of the advancing front region.
- Assess the performance of the simulation by comparing predicted fiber orientation against values determined experimentally from injection-molded samples containing fibers of varying length and of different matrix viscosity and viscoelasticity.
- Further assess the performance of the model by comparing the model predictions for fiber orientation to that of experimental findings for a tubular element (runner), an end-gated plaque, and center-gated disk injection-mold geometries.

Accomplishments

- Composite Materials: Various glass-fiber-filled composite materials were produced relating to the dilute, semi-dilute and concentrated concentration regimes with both polypropylene and polybutylene matrices.
- Rheology: Rheological characterization of the short-glass-fiber composites was performed, including intermittent stress growth/relaxation tests to elucidate the stress contribution of the fiber, matrix, and flow field on the transient evolution of fiber orientation. Rheological characterization of the long-glass- fiber composite has been initiated.
- Model: A constitutive relation is currently being developed that incorporates stress contributions from the fiber and the viscoelastic suspending medium. Model predictions compared to rheological data suggests a term accounting for fiber interaction in the evolution equation for fiber motion is needed.
- Simulation: A computer simulation of mold filling in injection molding is being developed. Currently, the program is capable of performing simulations with the discontinuous Galerkin finite-element method for 2-D flows using the Hele-Shaw approximation.
- Injection molding: Center-gated disks of polypropylene containing long glass fibers were injection molded and determination of fiber orientation within these samples was initiated with Oak Ridge National Laboratory (ORNL) using x-ray tomography. End-gated plaques of incrementally increasing size “short-shots” have been made and characterization of the advancing front has been initiated.
- Equipment design: A sliding-plate rheometer has been designed and is 80% completed. The sliding-plate rheometer is being fabricated primarily for the purpose of performing unbiased and reproducible rheological experiments on long-glass-fiber-filled polymeric fluids. In addition, the rheometer with be used in tracking the transient evolution of long-fiber orientation upon startup and cessation of shear flow.

Future Direction

- Accurately characterize the rheological behavior of the long-glass-fiber-filled polypropylene composite samples.
- Establish the relationship between the fiber-orientation distribution and the nonlinear rheological behavior in shear for short- and long-fiber composites.
- Extend the model to incorporate fiber interaction in the equation governing fiber motion.
- Determine a protocol for attaining unique material parameters for the model.
- Extend the numerical technique to track the frontal flow to an axisymmetric coordinate system.
- Determine the impact on the fiber orientation of the Hele-Shaw approximation when compared to simulations including the fontal flow and compare with experimental results.

Introduction

Glass fibers have been used for decades to improve the mechanical, thermal and isolative properties of polymers. These property improvements are highly dependent on the orientation distribution of the fiber. This makes it desirable to not only be able to predict the flow behavior of the composite fluid but the orientation distribution of the fiber within the fluid or melt generated during processing. Previous work on modeling glass-fiber-composite melts has primarily been accomplished by using a decoupling method, where the flow field is calculated using a purely viscous constitutive equation and the fiber orientation is post-calculated. The primary objective of this project is to improve on current simulated predictions of fiber orientation during processing of composite fluids and, hence, the ability to predict stiffness and part dimensional stability.

Materials

Three commercially-available, glass-fiber-filled composites have been chosen for this study: a 30 wt% short-glass-fiber-filled polybutylene terephethalate (commercial name Valox 420), a 30 wt% short-glass-fiber-filled polypropylene (commercial name RTP 105), and a 40 wt% long-glass-fiber-filled polypropylene (commercial name VLF 8017 cc). Three additional fiber concentrations relating the dilute, semi-dilute, and concentrated concentration régimes were made for each of the short-glass-fiber-filled composites by diluting the 30 wt% composite with the neat suspending medium. The following table outlines all the samples.

Table 1. Composition of the various composite materials that is used in this research.

	Mass fraction	Volume fraction	Aspect ratio	Concentration regime
PBT-Valox	0.3	0.1766	~29	concentrated
PBT-C	0.0842	0.044	~29	concentrated
PBT-SD	0.04071	0.0208	~29	semi-dilute
PBT-D	0.00287	0.00144	~29	dilute
SGF-PP-105	0.3	0.1288	~35	concentrated
SGF-PP-C	0.0809	0.0295	~35	concentrated
SGF-PP-SD	0.03884	0.01375	~35	semi-dilute
SGF-PP-D	0.001869	0.000646	~35	dilute
LGF-PP	0.4	0.187	~375	concentrated

Rheological Behavior

Subsequently, we outline the pertinent rheological behavior, in shear flow, exhibited by glass-fiber-composite fluids as it will aid in the discussion on model development. When the steady-state rheology of a suspension is compared to its neat counterpart, it typically has an enhanced Newtonian plateau and can exhibit a shear-thinning behavior at lower shear rates than the neat resin. At high shear rates the viscosity curves typically merge. In some cases, typically at very high fiber loading, the suspensions can exhibit yield-like behavior, the point being that the steady-state viscosity can be predicted with a number of shear-rate-dependent empiricisms, i.e., Carreau-Yasuda model. Conversely, the transient shear rheology of fiber suspensions is typically easily distinguishable from that of a neat resin. For example, when a sample with an isotropic fiber orientation is subjected to a stress growth upon inception of steady-shear-flow test, the sample will exhibit a large stress overshoot in both the shear stress and the normal stress differences. This is believed to be a result of the fiber aligning itself in the principal flow direction. Once aligned, the stresses reach a steady state. Hence, the transient rheological behavior is coupled with the fiber orientation and being able to model the evolution of orientation is imperative for correctly predicting the rheology.

A key aspect of this research is to be able to determine the cause of the enhanced rheological properties of glass-fiber-filled composites compared to the virgin matrix. If it is possible to separate the contributions from the fiber, matrix, and their interaction, then it is much easier to correctly model the behavior**.** One way to do this is to look at intermittent stress growth/relaxation behavior. This is accomplished by imposing a constant strain rate on the material until a steady state is reached in the stresses, and then the displacement is stopped and the stresses are allowed to relax for some period of time, after which the flow (constant strain rate) is turned on again. This gives insight to the evolution of the fiber orientation in the composite.

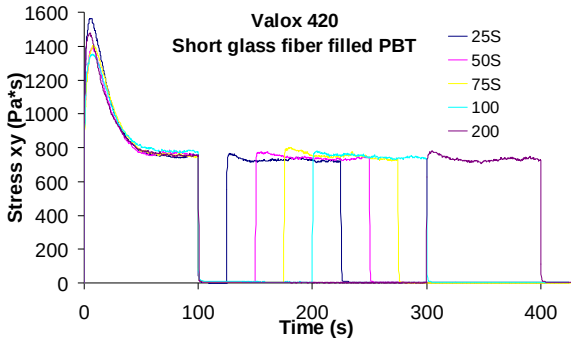

Figure 1. Intermittent stress growth/relaxation tests performed on the 30 wt% short-glass-fiber-filled PBT.

As seen in Figure 1, the initial stress overshoot is roughly double the steady-state value. This phenomenon is attributed to the random orientation of the glass fibers in the sample, which upon flow, orient themselves in the flow direction where a steady-state value is reached. An interesting observation is that this large peak does not reappear after the composite is allowed to relax, even after long periods of time. This is attributed to the fibers holding their position and staying oriented. As a note, it is believed with a highly viscoelastic polymer matrix, the recoiling of the polymer chain upon relaxation of flow could slightly affect the fiber orientation, but this has yet to be confirmed.

Model Development

To capture both the effects of the fiber and the non-Newtonian suspending medium in an approach where the flow is coupled with the fiber orientation, we propose an additive scheme, where the total extra stress is equal to a sum of contributions from the fiber and the suspending medium. In the model, the contribution of the fiber is calculated using a special form of the Doi theory for concentrated rigid-rod molecules. As a note, because the Doi theory was developed for rigid rods, we will synonymously use the term “rods” to refer to glass fibers in our real system. The contribution from the suspending medium is captured using a multi-mode viscoelastic constitutive relation.

We begin with the simple framework that the total extra stress is equal to the sum of the contribution to the stress tensor from the rods and the matrix as follows:

$$\underline{\underline{\tau}}_{\text{total}} = \underline{\underline{\tau}}_{\text{rods}} + \underline{\underline{\tau}}_{\text{matrix}} \cdot \qquad (1)$$

Rod contribution to the stress. The starting point for the development of the contribution of the rods to the extra stress is Doi’s molecular theory for mono-disperse rod-like molecules suspended in a Newtonian fluid. The Doi theory for rod-like molecules consists of two components. The first calculates the rod-orientation distribution and its evolution under external forces. The second post calculates the stress tensor which is a function of the rod orientation. In both, the quadratic-closure approximation is used. The rod orientation within the system is characterized by the deviatoric form of the orientation order parameter tensor ($\underline{\underline{S}}$), and is defined as

$$\underline{\underline{S}} = \left\langle \underline{u}\underline{u} - \frac{1}{3}\underline{\underline{\delta}} \right\rangle \qquad (2)$$

where $\underline{u}$ is a unit vector parallel to the axis of a rod, $\underline{\underline{\delta}}$ is the unit tensor, and the brackets $\langle$--$\rangle$ represent the ensemble average over the distribution function.

In simple shear flow, the time evolution of $\underline{\underline{S}}$ is equal to the contributions from Brownian motion, $\underline{\underline{F}}(\underline{\underline{S}})$, plus the contribution from the macroscopic flow field, $\underline{\underline{G}}(\underline{\underline{\nabla v}}, \underline{\underline{S}})$:

$$\frac{\partial \underline{\underline{S}}}{\partial t} = \underline{\underline{F}}\left(\underline{\underline{S}}\right) + \underline{\underline{G}}\left(\underline{\underline{\nabla v}}, \underline{\underline{S}}\right) \quad . \tag{3}$$

The Brownian motion contribution is dominant in the case of rod-like molecules or in the case where the rods are on the length scale where the effect of Brownian motion is a contributing factor and is defined by:

$$\underline{\underline{F}}\left(\underline{\underline{S}}\right) = -6\overline{D}_r\left[\left(1-\frac{U}{3}\right)\underline{\underline{S}} - U\left(\underline{\underline{S}}\cdot\underline{\underline{S}} - \frac{\underline{\underline{\delta}}}{3}\underline{\underline{S}}:\underline{\underline{S}}\right) + U\underline{\underline{S}}\left(\underline{\underline{S}}:\underline{\underline{S}}\right)\right] \tag{4}$$

where U is a phenomenological parameter representing the interaction potential of the system, and $\overline{D}_r$ is the average rotational diffusivity. The $\underline{\underline{F}}\left(\underline{\underline{S}}\right)$ quantity acts as a randomizing potential and is most easily understood by using the model to predict interrupted stress growth behavior. During stress relaxation, $\underline{\underline{F}}\left(\underline{\underline{S}}\right)$ causes the rod orientation to relax or randomize, as one would expect for suspensions of rod-like molecules. For systems of glass fibers, the $\underline{\underline{F}}\left(\underline{\underline{S}}\right)$ term is very small and can be neglected. The $\underline{\underline{G}}\left(\underline{\underline{\nabla v}}, \underline{\underline{S}}\right)$ component is defined by

$$\underline{\underline{G}}\left(\underline{\underline{\nabla v}}, \underline{\underline{S}}\right) = \frac{1}{3}\left[\underline{\underline{\nabla v}} + \left(\underline{\underline{\nabla v}}\right)^t\right] + \left[\underline{\underline{\nabla v}}\cdot\underline{\underline{S}} + \left(\underline{\underline{\nabla v}}\cdot\underline{\underline{S}}\right)^t - \frac{2}{3}\underline{\underline{\delta}}\underline{\underline{\nabla v}}:\underline{\underline{S}}\right] - 2\left(\underline{\underline{\nabla v}}:\underline{\underline{S}}\right)\underline{\underline{S}} \tag{5}$$

where $\underline{\underline{\nabla v}}$ is the velocity gradient. Equations (3, 5) represent six coupled ordinary differential equations that can be solved numerically for the time evolution of orientation for a known velocity profile.

The Doi theory states that the stress contribution from the rods is equal to the sum of an elastic component ($\underline{\underline{\tau}}_E$) and a viscous component ($\underline{\underline{\tau}}_V$):

$$\underline{\underline{\tau}}_{rods} = \underline{\underline{\tau}}_E + \underline{\underline{\tau}}_V \quad . \tag{6}$$

$\underline{\underline{\tau}}_E$ comes entirely from the Brownian potential and the contribution to the stress from the rods is very small. The viscous dissipation of energy of the rods is given by

$$\underline{\underline{\tau}}_{rods} = \underline{\underline{\tau}}_V = -A\left(\underline{\underline{\nabla v}}\cdot\underline{\underline{S}}\right)\left(\underline{\underline{S}} + \frac{\underline{\underline{\delta}}}{3}\right) . \tag{7}$$

A is a constant theoretically equal to $ck_bT/2D_r$, where *c* is the concentration of rods, k_b is Boltzman's constant, and *T* is temperature in Kelvin. For modeling purposes, we choose to fit the parameter *A* to transient-stress growth data.

Matrix contribution to the stress: A key concept behind the model is that the contribution from the rods to the stress primarily occurs while the rods are changing their orientation. After the rods have reached a steady-state in their orientation, their contribution to the stress is at a minimum. However, the enhanced steady-state rheology and the viscoelastic properties can be predicted by superimposing the rod contribution onto a viscoelastic constitutive relation fit to the bulk steady-state rheology. In this approach the contribution to the extra stress of the matrix is captured using a multi-mode viscoelastic constitutive relation. For the model predictions in the paper, we chose to use the Phan-Thien Tanner equation (PTT).

Model Prediction

The Doi theory equations that make up the rod contribution to the total extra stress (equations 3, 5, and 7) are similar in structure and in what they predict to Dinh and Armstrong. The model predicts $\underline{\underline{\tau}}_{rods} \to 0$ at long times or at steady-state. However, the model predicts a transient stress contribution when the initial orientation of $\underline{\underline{S}}$ is different from the steady-state value of $\underline{\underline{S}}$. This can be seen graphically in Fig. 2, for a random initial $\underline{\underline{S}}$ at a shear rate of 1 s^{-1}.

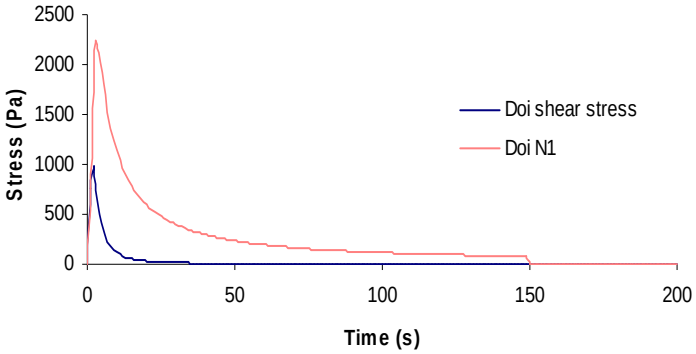

Figure 2. Modified Doi theory prediction for the contribution of the rods to the extra stress. Prediction is for a shear rate of $1s^{-1}$.

The model predicts the steady-state shear rheology to the degree of accuracy of the multi-mode PTT model. The ability of the model to predict the transient shear rheology of a suspension is generally summarized in Figure 3. Figure 3 is a graph of the experimental data for the short glass fiber filled PP in an interrupted stress growth test. Beginning with an isotropic fiber orientation, the sample was subject to a constant rate of deformation, 1 s^{-1}. After 150 seconds the flow was stopped and the stresses were allowed to relax. After another 75 seconds the flow was reapplied and the stresses were recorded. As expected, initially the sample exhibited a large stress overshoot that decayed to a steady state. As previously mentioned, this is believed to be a result of the rods rotating to align themselves in the principle flow direction. Subsequent to the overshoot , a steady state in the stresses was reached which is believed to coincide with a steady state in the rod orientation. When the flow is removed, the stresses relax. However, when the flow is reapplied at the same shear rate, the overshoot does not reoccur. This is a typical result where particles, for which Brownian motion can be neglected, are suspended in a fluid in which particle sedimentation is negligible. It is believed to be a result of the rods maintaining their orientation during the stress relaxation. Hence, when the flow is reapplied, the stress immediately grows to its previous value because the rod orientation has not changed. When the model is set to the same test conditions, i.e., initial random fiber orientation subject to interrupted stress growth shear flow, it predicts the transient response fairly well. First, it can predict the magnitude of the stress overshoot but slightly under-predicts the breadth of time the overshoot takes to decay. The steady-state plateau and the

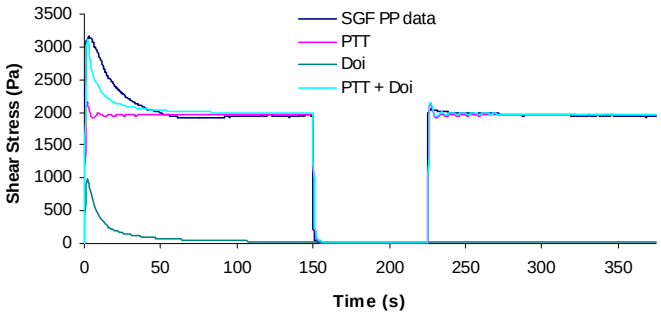

Figure 3. The shear stress vs. time for an interrupted stress growth test. Short-glass-fiber (SGF) PP data is the experimental data for a short-glass-fiber-filled PP. PTT and Doi are the separate model predictions for the 7-mode PPT and the modified Doi theory respectively. The PTT+Doi is the addition of the three stress contributions. Prediction is for a shear rate of $1s^{-1}$.

relaxation dynamics are dominated by the multi-mode PTT model resulting in a good model prediction. Interestingly, when the flow is reapplied in the model, it also does not predict a reoccurring overshoot.

The primary normal stress difference (N_1) exhibits a similar behavior to the shear stress. The model is capable of predicting the steady-state N_1 to the degree of accuracy of the multi-mode PTT model. The model prediction of the transient shear stress can be seen in Figure 4, which is graph of N_1 vs. time for the short-glass-fiber PP suspension at a shear rate of $1s^{-1}$. N_1 initially exhibits a large overshoot that decays to a steady-state. The model does predict an overshoot in N_1 but not of the magnitude seen experimentally.

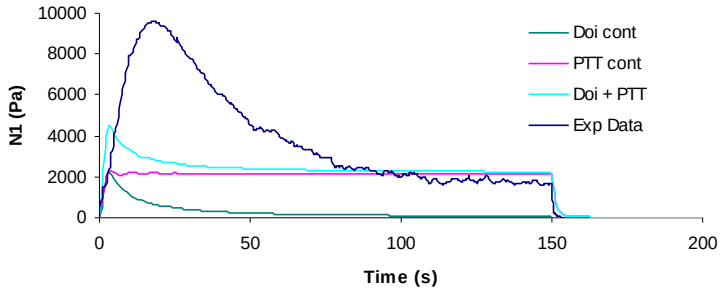

Figure 4. The primary normal stress difference vs. time for a stress growth/relaxation test. PTT and Doi are the separate model predictions for the 7-mode PPT and the modified Doi theory, respectively. The PTT+Doi is the addition of the three stress contributions. Prediction is for a shear rate of $1s^{-1}$.

The inability of the model to predict breadth of time in the shear stress overshoot and the magnitude of the first normal stress overshoot is believed to be a result of a deficiency in the equation governing rod motion. Currently, the equation is developed for dilute suspensions of rods and does not account for interaction between the fibers. We have initiated the formulation of such an equation that includes fiber interaction.

Simulation

The simulation of mold-filling in injection molding will be completed in two phases. Phase 1: a discontinuous Galerkin finite-element method code will be developed for 2-D using the Hele-Shaw approximation, which treats the flow as being dominated by shear flow. Phase 2: the code will be adapted to incorporate the kinematics of the frontal region which has been shown to be dominated by extensional flow and plays a major role in controlling fiber orientation on the part surface. It is also noted that the quadratic decoupling approximation in the Doi theory will be modified to a Bingham approximation for the frontal flow region.

Currently, Phase 1 of the computer simulation has been completed. A discontinuous Galerkin finite-element method has been implemented for multiple constitutive equations including Doi theory and various viscoelastic models. A simple and stable numerical technique to track the frontal flow in simulations of fiber-filled suspensions has been developed and implemented. The method tracks the frontal motion along spines at the moving front.

The location of the frontal surface at a new time level is obtained along spines (lines of constant height) and a particle tracking technique. At every spine, first the position of the particle is determined that arrives at the spine in a time interval Delta t. The second step of the method determines the new position in the direction of the spine. Preliminary tests have shown that the above method is stable and predicts a surface without oscillations. The accuracy of the method has been tested for a Newtonian fluid and compared with results in the literature.

Injection-Molded Samples/Fiber Orientation Analysis

Long- and short-glass-fiber samples have been injection molded into a center-gated die (thickness: .5 cm, diameter: 11 cm). A series of increasing diameter "short shots" has been completed to look at the development of the advancing front and the evolution of fiber orientation in the mold-filling process. Currently we are in contact with Vlastimil Kunc from ORNL to use x-ray tomography and the "Leeds method" to look at fiber orientation in the long glass fiber and short glass fiber samples, respectively. (See 4.I.)

Conclusions

Our research efforts to complete the project objectives correlate with the time-line for project completion. In recap of our efforts: Various short- and long-glass-fiber composite have been made. The short-glass-fiber-filled composite materials have been rheologically characterized. A sliding- plate rheometer has been designed and is under production to rheologically characterize the long-glass-fiber composite. A modified form of the Doi theory that accounts for the non-Newtonian nature of the suspending medium and the interaction between the fiber is currently being developed. Phase 1 of the computer simulation has been completed and Phase 2 has been initiated.

Presentations

1. D.G. Baird, A.P.R. Eberle, and P. Wapperom, "Transient Rheology of a Polypropylene Melt Reinforced with Long and Short Glass Fibers," 77th Annual Meeting of The Society of Rheology, October 16-20, 2005, Vancouver BC, Canada (2005).

2. A.P.R. Eberle, D.G. Baird, "Transient Rheology of a Polypropylene Melt Reinforced with Long and Short Glass Fibers," AIChE Annual Meeting, October 30-November 4, 2005, Cincinnati, OH (2005).

3. A.P.R. Eberle, D.G. Baird, and P. Wapperom, "Modeling the Transient Rheology of a Polypropylene Melt Reinforced with Long and Short Glass Fibers," SPE ANTEC Annual Meeting, May 7-10 2006, Charlotte, NC (2006).

4. A.P.R. Eberle, G.M. Velez, D.G. Baird, and P. Wapperom, "Modeling Polymer Melts Containing Long and Short Glass Fibers: Part I Transient Rheology," 78th Annual Meeting of The Society of Rheology, October 2006, Portland, Maine (2006).

5. A.P.R. Eberle, G.M. Velez, D.G. Baird, and P. Wapperom, "Modeling Polymer Melts Containing Long and Short Glass Fibers: Part I Transient Rheology," AIChE Annual Meeting, San Fransisco Ca, USA November (2006).

6. G.M. Velez, A.P.R. Eberle, D.G. Baird, and P. Wapperom, "Modeling Polymer Melts Containing Long and Short Glass Fibers: Part II the Simulation of Injection Molded Parts," AIChE Annual Meeting, San Fransisco Ca, USA November (2006).

7. P. Wapperom, G.M. Velez, A.P.R. Eberle, and D.G. Baird, "Numerical Simulation of Polymer Melts Containing Short and Long Fibers," Workshop on Numerical Methods for non-Newtonain Flows, Rhodes Greece, June (2007).

8. A.P.R. Eberle, G.M. Velez,, D.G. Baird, and P. Wapperom, "Rheology and Flow Simulation of Polymer Melts Containing Glass Fibers," European Polymer Congress (EPC) Annual Meeting, Portoroz, Slovenia, July (2007).

Publications

1. Aaron P.R. Eberle, Donald G. Baird, and Peter Wapperom, "Modeling the Transient Rheology of a Polypropylene Melt Reinforced with Long and Short Glass Fibers at Small Deformation Rates", *SPE Proceedings of the 64th Annual Technical Meeting,* 52, 2315-2319 (2006).

2. D. Baird and A. Eberle, "Modeling The Rheology And Orientation Distribution Of Short Glass Fibers Suspended In Polymeric Fluids: Simple Shear Flow", *Proceedings of the 65th Annual Technical Conference,* Cincinnati, OH,

May 6-11, Society of Plastics Society of Plastics Engrs. 2823-2827(2007).

3. A.P.E. Eberle, D.G. Baird, and P. Wapperom, "The Rheological Properties of Non-Newtonian Fluids Containing Glass Fibers: A Review of Literature", *Ind. Eng. Chem. Res.* Submitted for publication.

K. A Hierarchical, Structure-Oriented and Stochastic Approach to Model Liquid Molding Processes

Principal Investigator: Thanasis D. Papathanasiou
Department of Chemical Engineering
University of South Carolina
Columbia, SC 29208
(803) 777-7219; fax: (803) 777-6245; e-mail: papathan@engr.sc.edu

Technology Area Development Manager: Joseph A. Carpenter
(202) 586-1022; fax: (202) 586-1600; e-mail: joseph.carpenter@ee.doe.gov

National Science Foundation (NSF) Monitor: Mary Lynn Realff
This project was jointly funded by NSF and DOE
(703) 292-7088; fax: (703) 292-9056; e-mail: mlrealff@nsf.gov

---

Contractor: University of South Carolina Research Foundation
Contract No.: DMI-0522221

Objective

- To develop models for the hydraulic permeability of fibrous media, taking explicit account of the underlying microstructure and its variability.

Approach

- Our approach is computational. A large number of simulations have been carried out, using a parallel implementation of the Boundary Element Method (BEM), in microstructures consisting of ~600 fiber cross-sections placed within a containing unit-cell by a Monte Carlo (MC) procedure. This allows a direct and unambiguous correlation between the hydraulic permeability (K) and the microstructure of the fiber arrays.

Accomplishments

- We carried out an extensive investigation of Stokes flow across a large number of unidirectional, random fiber arrays generated by a Monte-Carlo procedure.
- This numerically-intensive task was accomplished by developing and running an in-house parallel BEM code on a distributed-memory parallel computer.
- The transverse permeability (K) of systems consisting (each) of 576 fibers, calculated in the porosity range $0.45<\phi<0.90$ by averaging over 20 random realizations at each porosity value, was computed.
- The microstructural characteristics of the model fiber distributions were analyzed and the mean nearest inter-fiber spacing ($\langle\delta_1\rangle$) was identified as a parameter that correlates with the numerical estimates of (K). Specifically, we found that (K) is a statistical function of $\langle\delta_1\rangle$, with its average behavior ($\langle K\rangle$) expressed by $\ln\left(\langle K\rangle / K_{hex}\right)/ n = \ln\left(\langle\delta_1\rangle/\delta_{hex}\right)$, where ($n$) is a linear function of porosity and K_{hex} and δ_{hex} are known functions of porosity. The deviation of (K) from this average behavior is related to the variability of the underlying microstructure, as expressed by the variance of (δ_1).

Future Direction (for the next calendar year)

- Continue to develop codes that simulate microstructure, and to test/propose metrics that quantify microstructural features such as fiber clustering.
- Continue to investigate the effects of microstructure on the permeability of unidirectional fibrous media, using the previously developed two-dimensional (2D) parallel boundary element codes. Specifically, the effects of non-uniform inter-tow and intra-tow fiber packing and random fiber clustering will be studied.
- Start to implement a parallel boundary element code for solving three-dimensional (3D) Stokes flow problems.
- Start to implement the Fast Multipole Boundary Element Method (FMBEM). The FMBEM for solving 2D potential flow problems has been applied to study the barrier improvement factor in flake-filled membranes.

Introduction

Viscous flow through fibrous media is a problem of long-standing interest in engineering due to its importance in the manufacturing and process industries. With specific reference to manufacturing of lightweight materials, flow through fibrous media is of direct relevance to several composites-forming operations such as liquid molding, pultrusion and autoclave processing. To numerically model flow through fibrous preforms, nodal permeability values must be specified at points dictated by the domain discretization method; the accuracy in the provided permeability data is critical to successful modeling. For this purpose, permeability measurement techniques suitable for fibrous media similar to those used in liquid molding have been developed. However, these measurements are known to be subject to large uncertainties, caused by structural variations and/or deformation of the preform during the experiment but also by the non-uniformity of real fiber beds [1-3]. Indeed, ordered fiber packing geometries are rare, while fiber packing disorder, fiber bundling and fiber size variations are typical in fiber preforms. Therefore, in parallel with the development of more accurate and faster permeability testing methods, a great deal of effort has been devoted to developing models that would predict the permeability of a fibrous preform based on knowledge of its structure. In recent years, this has prompted many authors to investigate the effects of fiber size variation, imperfect fiber lattice and perturbed fiber positions on the transverse permeability of non-regular fiber arrays, either analytically or numerically [4-6]. Random fiber arrays are, in principle, well-suited for analysis using effective medium approaches. Work in this area [7-9] has produced results that are valid at the dilute (high porosity, ϕ) limit but questionable in the porosity range of interest to composites manufacturing, e.g. $0.4 \leq \phi \leq 0.7$. For example, Spielman and Goren's theory [8] gives highly unrealistic predictions for $\phi < 0.6$. The same problem has been addressed numerically by Sangani and Yao using a multipole collocation method [10] and by Ghaddar using a parallel finite-element approach [11]. CPU speed and memory storage limitations allowed these studies to consider only small systems, consisting of no more than 25 fibers, and mean permeability values were obtained by averaging results over a number of configurations. As a result, the 'noise' in the obtained data was high and the effect of sample size (in terms of its influence on the spatial statistics of the fiber population as well as in terms of the influence of the boundary conditions on the obtained averages) unclear.

Currently, no correlation exists between the permeability of random fiber arrays and any geometrical characteristic other than porosity; what has emerged is a firm realization of the fact that random fiber arrays do exhibit widely scattered permeability values. This state of affairs makes optimal design of fiber preforms impossible. Investigating the possible existence of structure-permeability correlations in disordered fiber arrays is therefore of obvious importance and the focus of this work. Due to the disordered nature of the fiber distributions we are addressing, large representative unit cells are required to produce sound statistics. This necessitates numerical solution of large systems, typically too large for a single workstation, and, in addition, detailed description of the flow geometry – both in terms of meshing and microstructural quantification. These are the two

principal difficulties in such a direct modeling approach. The difficulty associated with generating a mesh on complex, multiply-connected domains has greatly limited the use of domain methods such as the finite element method. To ease the task of mesh generation, we adopt the Boundary Element Method (BEM), which requires discretization of only domain boundaries. A parallel implementation of the BEM for distributed-memory parallel computers has been used in order to overcome the difficulties associated with CPU time and memory storage. A large number of simulations in large unit cells, each containing ~576 fibers, with varied porosity and varied degrees of local fiber aggregation were carried out. The spatial statistics of the fiber distributions, namely the mean nearest inter-fiber distance, were quantified.

Problem Formulation

We consider a fibrous medium composed of long cylindrical fibers with their axes oriented perpendicular to the direction of bulk flow. The computational unit cell represents a plane cut normal to the fibers' axes. As our focus is on the effect of the spatial distribution of fibers, these are of the same size. A typical unit cell is shown in Fig. 1. The porosity of the system is $\phi = 1 - N_f \pi R^2 / A$, where N_f is the number of fibers, R is the fiber radius and A is the area of the unit cell. The random configuration of fibers is generated by a Monte-Carlo procedure.

The governing equations for slow viscous Newtonian flow across the fibrous medium are the Stokes equations:

$$\nabla \cdot \mathbf{u} = 0 \qquad \text{on } \Omega \qquad (1)$$

$$\mu \nabla^2 \mathbf{u} = \nabla p \qquad \text{on } \Omega \qquad (2)$$

Here u, p, μ and Ω denote the velocity vector, pressure, viscosity and the 2D flow domain, respectively. Equations (1)-(2) can be cast into boundary integral representations involving boundary velocities and tractions only. This technique is well established. Using fundamental solutions, the boundary integral equations are usually written as:

$$c_{ij}(x_p) u_j(x_p) = \int_\Gamma u_{ij}^*(x_q, x_p) t(x_q) d\Gamma - \int_\Gamma t_{ij}^*(x_q, x_p) u_i(x_q) d\Gamma \qquad (3)$$

where u_{ij}^* is the Stokeslet representing the fluid velocity at x_p in the i^{th} direction due to a point force at x_q in the j^{th} direction and t_{ij}^* is the analogous singularity for tractions.

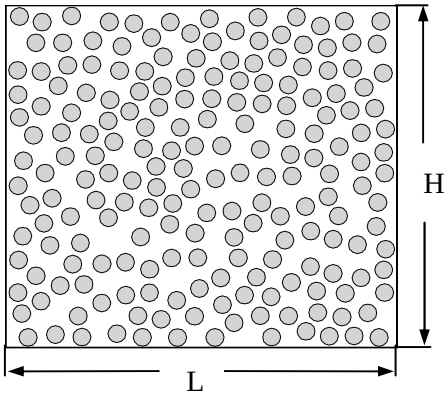

Figure 1. Model geometry used to represent a crossection of a unidirectional array of randomly placed fibers.

Quadratic elements were used to discretize Eq.(3), providing second-order approximations for both geometry and field variables. After discretization, the resulting system of linear equations is usually represented as $[\mathbf{H}]\{\mathbf{u}\} = [\mathbf{G}]\{\mathbf{t}\}$, where $\{\mathbf{u}\}$ and $\{\mathbf{t}\}$ contain two complete sets of both known and unknown nodal velocity and tractions, respectively; and [**H**] and [**G**] are influence-coefficient matrices whose elements are either non-singular or singular integrals. The non-singular integrals were typically evaluated by *10*-point Gauss quadrature. The singular integrals were worked around by the well-known assumption of rigid-body motion, and the weakly singular integrals were evaluated by Gauss-Laguerre quadrature with the aid of coordinate transformation. To prevent the deterioration of accuracy of numerical quadrature in non-singular integrals, the ratio of the closest distance between two nodes at different elements to the element size should be kept above a certain value. In the worst case, the closest distance between two nodes at different elements is equal to the minimum allowable nearest inter-fiber spacing δ_{min}. Therefore, the discretization of fiber surfaces should be finer when δ_{min} gets smaller. In this study, the smallest value of δ_{min} is one tenth of the fiber radius (R). We typically used 24~36 nodes per fiber. This translates to a distance-to-element ratio of 0.25 for less than

10^{-5} error according to an empirical error bound. It was observed that further refinement did not change the results significantly. Also specific to the problem setup, there is one additional unknown of traction at each corner node. This has been treated using the stress balance method.

The main (inherent) shortcoming of the BEM is that its application results in dense and non-symmetric coefficient matrices. In the two-dimensional cases studied here, there are two unknowns for each node, plus four extra unknowns of traction at corner nodes because of the imposed boundary conditions, which result in $2\times(N_f \times M_f + 4 \times M_b + 4)$ degrees of freedom, assuming M_f is the number of nodes per fiber and M_b is the number of nodes per unit cell edge. The amount of computational work can exceed the capability of a workstation easily as the number of fibers in the unit cell increases. The bottleneck is the main memory (RAM) that can be used (for example, a simulation involving 576 randomly placed fibers results in a system with about 32,000 degrees of freedom and requires about *8* Gb of storage using double precision arithmetic). For this reason, it is desirable to implement the BEM on a distributed-memory parallel computer. In this study, we implemented a parallel boundary-element code which exploits the coarse parallelism in the different phases of the BEM, namely, matrix assembly, solution and post-processing. The solution of the dense linear system is the most time-consuming part in the BEM. In our study the implementation of the L-U decomposition algorithm in ScaLAPACK is achieved using a two-dimensional block-cyclic data-decomposition scheme. This is scalable in the sense that the memory efficiency is N^2/np, where *N* is the global matrix size and *np* is the number of processors used. Our code was written in FORTRAN with function calls to BLACS, ScaLAPACK and MPI libraries.

Microstructure Generation and Quantification

The fiber distributions considered by this study were generated using a Monte-Carlo (MC) procedure, which is similar to the method described in Torquato's monograph [12] for generating an equilibrium ensemble of hard disks. The MC process starts with a fixed fiber packing arrangement (square array in our case) and proceeds by randomly and sequentially perturbing the fiber locations. The microstructures generated in this manner are primarily governed by the choice of porosity ϕ and the minimum allowable inter-fiber distance δ_{min}. The latter, defined as the closest distance between fiber surfaces, is the mechanism used to prevent fibers from overlapping during the MC process. Additionally, the unit-cell boundaries act like rigid walls to restrict fibers inside the cell. Such a MC process generates a random field which is short-range correlated. Typical fiber distributions generated in this manner are presented in Fig. 2, with differences in ϕ and δ_{min}.

It is evident that small values of δ_{min} result in patterns showing local (small-scale) fiber aggregation while large values of δ_{min} lead to more or less uniform distributions that show only small deviations from a hexagonal lattice. The effect of δ_{min} on fiber aggregation is more pronounced when the porosity is large. By varying δ_{min}, a spectrum of fiber distributions can be generated at the same porosity level, ranging from locally aggregated to homogeneous.

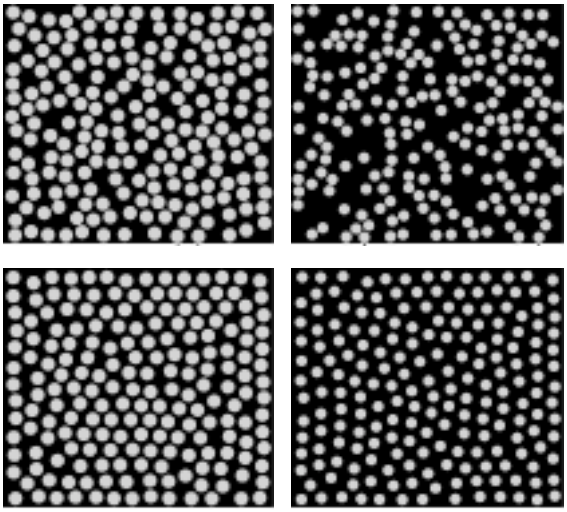

Figure 2. Sample geometries created by the Monte-Carlo process. They exhibit differing degrees of local aggregation. From top left clock-wise (ϕ,δ_1) = (0.5,0.1R); (0.7,0.1R);(0.7,1.0R); (0.5,0.4R).

The possible range of δ_{min} is determined by numerical considerations (at the low end) and by porosity (at the high end). Specifically, the smallest

value of δ_{min} was taken to be one tenth of fiber radius (R) to ensure accurate integrations as well as to avoid excessive CPU time, as explained previously. In spite of the artificiality of this choice, we found that when δ_{min} is given small values, the resulting fiber distributions appear similar to the ones we have observed in several liquid-molded or pultruded unidirectional composites. Prior to any analysis, it is necessary to quantify the microstructure of the fiber distribution first. In this effort, we have investigated the use of the nearest inter-fiber spacing whose statistics differ between different fiber arrangements. For each fiber one can find a number of 'neighbors', which are assigned with a subscript (i) in such a way that the nearest one corresponds to i=*1* and the others are in ascending order according to relative distances. Thus, the near-neighbor distances are the center-to-center distances from the reference fiber k to its neighbors, which are denoted as $\{d_i^k\}$. The nearest-neighbor distance for a reference fiber k is therefore the minimum in this distance set, i.e., $d_1^k = \min\{d_i^{(k)}\}$. For a population of fibers, the mean nearest-neighbor distance is denoted as $\langle d_1 \rangle$, which is simply an arithmetic mean. This metric is frequently used to indicate the degree of local heterogeneity in spatial point patterns. At each level of (ϕ), smaller values of $\langle d_1 \rangle$ are associated with disordered patterns, while larger $\langle d_1 \rangle$ indicate a homogeneous arrangement. By subtracting the fiber diameter D, d_1^k is translated to δ_1^k, which is the closest spacing between the reference fiber (k) and its neighbors. Because δ_1^k is more relevant to fluid space, we will use δ_1^k in correlating the microstructure of a fiber array to its permeability in the rest of this paper. We will also refer to the arithmetic mean of { δ_1^k, k=1…N_f} as the mean nearest inter-fiber spacing, denoted as $\langle \delta_1 \rangle$.

As is the case in experimental measurement of permeability in fiber preforms, the stochastic nature of the fiber distribution leads to scatter in the computed permeability data. In the present study, a number of random realizations (N_r) were generated for each class of fiber distributions characterized by ϕ and $\langle \delta_1 \rangle$ (or δ_{min}), and the permeability values were computed for the resulting unit cells. The average permeability and its standard deviation are then computed as:

$$\langle K \rangle = \frac{1}{N_r} \sum_i^{N_r} K_i \tag{4}$$

$$\sigma(K) = \frac{1}{N_r - 1} \sqrt{\sum_i^{N_r} \left(K_i - \langle K \rangle\right)^2} \tag{5}$$

A representative flow field is shown in Fig. 3 below.

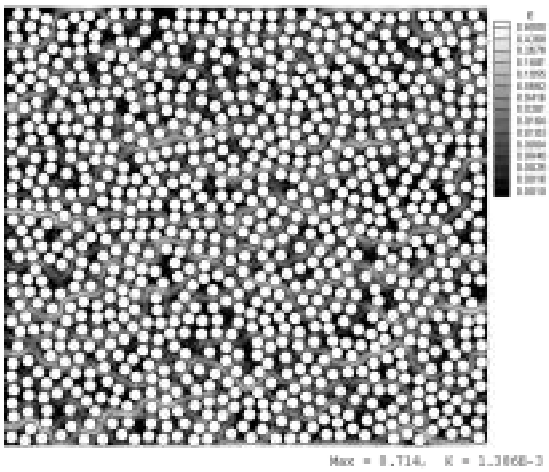

Figure 3. Fluid speed contours for Stokes flow across a unidirectional fiber array consisting of 900 fibers at ϕ=0.50. Flow is horizontal.

Results

The use of porosity alone is not sufficient to explain the scatter in the permeability of random fiber arrays, whether calculated numerically or determined by experiment. The objective of this study is to link the transverse permeability of random fiber arrays to the geometrical characteristics of these arrays. To do so, the dimensionless permeability data are plotted against $\langle \delta_1 \rangle$/R in Fig. 4. A correlation between K and $\langle \delta_1 \rangle$ is evident. In the porosity range $0.45<\phi<0.7$ it appears that decreasing $\langle \delta_1 \rangle$ or equivalently, moving from a homogeneous system to ones progressively showing higher local aggregation, results in a permeability reduction. This trend is more pronounced at lower porosities (ϕ = *0.45, 0.5*). This permeability reduction, as a result of non-uniformity in fiber distribution (quantified by the Morishita index in that case) was also reported in a recent study [13].

At higher porosities, an opposite trend is shown: at $\phi>0.7$ as $\langle\delta_1\rangle/R$ decreases (below ~1.0 for $\phi=0.8$) the permeability seems to increase. It is necessary to point out that large-scale clustering (in which cluster dimensions are comparable to unit-cell dimensions) does not occur in our systems because of the hard-core distribution statistics implicit in the MC procedure used for microstructure generation.

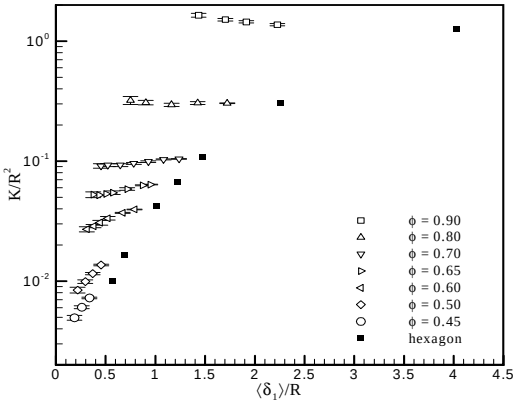

Figure 4. Dependence of dimensionless permeability (K/R^2) on the mean nearest inter-fiber spacing, $\langle\delta_1\rangle/R$. The symbols are mean values and the error bars represent standard deviations ($\pm\sigma$) in each ensemble of data. Each ensemble of data contains *20* runs on geometries of similar spatial statistics. Also shown are permeability values of the hexagonal arrays at each porosity.

The surprisingly good fit between $<\delta_1>$ and (K) can be qualitatively explained by the fact that, in the absence of large-scale clustering, the flow resistance around each fiber is governed by the narrowest gap separating it from its neighbors. The whole system can then be viewed as a network of flow paths connected in parallel as well as in series. The resistance of each component in the network is determined by the narrowest gap, which is included in the statistics of the inter-fiber spacing (see earlier section). It is therefore not surprising that such a clear correlation exists between $\langle\delta_1\rangle$ and $<K>$.

In the porosity range of practical interest to composites manufacturing ($0.45<\phi<0.70$), Fig. 4 suggests that the functional form which describes the relation between $\langle\delta_1\rangle$ and K should be:

$$\frac{K}{R^2}=\left(\frac{\langle\delta_1\rangle}{R}\right)^n f(\phi) \qquad (6)$$

where the exponent n is a function of ϕ as evidenced by the different slopes of the data sets corresponding to different porosities. In seeking a functional form for $f(\phi)$ in Eq.(6), we recall that Eq.(6) should reduce to existing models for the transverse permeability when the fiber array becomes uniform. When the array approaches a uniform hexagonal array, $\langle\delta_1\rangle$ should equal the inter-fiber spacing of a hexagonal array (δ_{hex}) and the corresponding permeability will be K_{hex}, which is known to be only a function of porosity. For example, at the low porosity limit, K_{hex} and δ_{hex} are given by Eq. (7):

$$K_{hex}=\frac{2}{9\pi\sqrt{3}}\left(\frac{\delta_{hex}}{R}\right)^{5/2}R^2 \qquad (7a)$$

$$\delta_{hex}=2\left(\sqrt{\frac{1-\phi_{\min}}{1-\phi}}-1\right)R \qquad (7b)$$

where $\phi_{min}=1-\pi/\left(2\sqrt{3}\right)$, is the porosity at maximum packing for a hexagonal array. To be asymptotically correct, the form of $f(\phi)$ should therefore be:

$$f(\phi)=\left(\frac{R}{\delta_{hex}}\right)^n\frac{K_{hex}}{R^2} \qquad (8)$$

and thus Eq.(6) yields:

$$\frac{K}{K_{hex}}=\left(\frac{\langle\delta_1\rangle}{\delta_{hex}}\right)^n \qquad (9)$$

We attempted to scale the computational results of Fig. (4) as suggested by Eq. (9). The result is presented in Fig. 5, in which each data point corresponds to one simulation, characterized by one set of values (ϕ, $\langle\delta_1\rangle$). As expected by the dependence of the exponent n on ϕ, this scaling does not collapse the data onto one single master curve. Fitting the data as a power function gives the lowest estimate of $n=0.164$ at $\phi=0.7$ and the highest estimate $n=0.628$ at $\phi=0.45$. It is interesting to note that a plot of n versus ϕ suggests a linear relationship

$n=\alpha+\beta\phi$. Therefore an overall correlation between K and $\langle\delta_1\rangle$ for random fiber arrays can be written as:

$$\frac{K}{K_{hex}} = \left(\frac{\langle\delta_1\rangle}{\delta_{hex}}\right)^{\alpha+\beta\phi} \qquad (10)$$

where the constants α and β are determined from a least square fit as $\alpha = 1.51 \pm 0.06$ and $\beta = -1.93 \pm 0.10$. It goes without saying that the linear relationship $n = \alpha+\beta\phi$ can only be considered applicable in the indicated range of ϕ and $\langle\delta_1\rangle$.

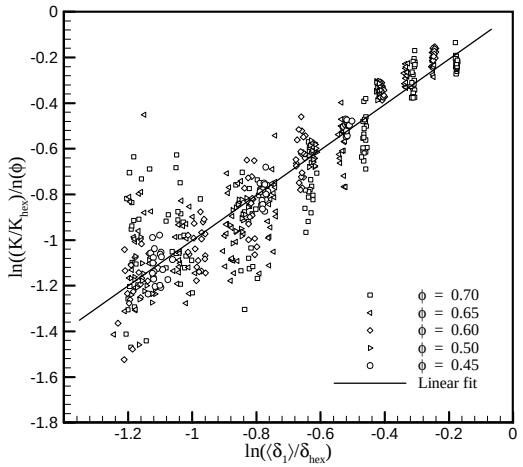

Figure 5. The correlation between permeability and the mean nearest inter-fiber spacing in the porosity range [0.45, 0.70]: plot of $\ln(K/K_{hex})/n$ versus $\langle\delta_1\rangle/\delta_{hex}$. Each data point in the graph is the result of one simulation. The linear fit in Fig. 5 has a slope of (*0.994± 0.018*) and an intercept of (*-0.008±0.01*).

Taking logarithms in both sides of Eq. (10) results in:

$$\ln(K/K_{hex})/n(\phi) = \ln(\langle\delta_1\rangle/\delta_{hex}) \qquad (11)$$

The computational data for (K), transformed according to Eq. (11), are plotted in Fig.5. A solid line in Fig.5 indicates the least square fit of the data set to a linear model with slope around unity (*0.994± 0.018*) and intercept (*-0.008±0.01*) very close to zero, exactly as anticipated from Eq.(11). It seems that Eq.(11) predicts the correct average behavior, as the data are indeed shown to be distributed randomly around an average log-linear relationship. In the studied ranges of ϕ and $\langle\delta_1\rangle$, the permeability follows, on average, Eq. (11), with a scatter that is inversely proportional to $\langle\delta_1\rangle$. Additionally, the scatter of the permeability values around the mean trend is also related to the variance (σ^2) of δ_1, or, in other words, to the non-uniformity of the underlying microstructure. Relating the known statistics of (δ_1) to the obtained statistics of (K) is of great practical interest and we are working in this direction.

Conclusion

We carried out an extensive investigation of Stokes flow across a large number of unidirectional, random fiber arrays generated by a Monte-Carlo procedure. This numerically-intensive task was accomplished by developing and running an in-house parallel BEM code on a distributed-memory parallel computer. The transverse permeability (K) of systems consisting (each) of 576 fibers, calculated in the porosity range $0.45<\phi<0.90$ by averaging over 20 random realizations at each porosity value, was computed. Following this, we point out the need to consider some measure of the underlying fiber spatial statistics as an additional parameter affecting permeability. The microstructural characteristics of the model fiber distributions were analyzed and the mean nearest inter-fiber spacing ($\langle\delta_1\rangle$) was identified as a parameter that correlates with the numerical estimates of (K). Specifically, we found that (K) is a statistical function of $\langle\delta_1\rangle$, with its average behavior ($\langle K\rangle$) expressed by $\ln(\langle K\rangle/K_{hex})/n = \ln(\langle\delta_1\rangle/\delta_{hex})$, where ($n$) is a linear function of porosity and K_{hex} and δ_{hex} are known functions of porosity. The deviation of (K) from this average behavior is related to the variability of the underlying microstructure, as expressed by the variance of (δ_1).

References

1. Parnas, R.S., Flynn K.M. and Dal-Favero M.E. "A Permeability Database for Composites Manufacturing," Polym. Compos. 18(5):623-633, 1997.

2. Skartsis, L., Kardos, J.L. and Khomami, B. "Resin flow through fiber beds during composite manufacturing processes. Part I: Review of Newtonian flow through fiber beds," Polym. Eng. Sci. 32(4):221-230, 1992.

3. Astrom, B.T., Pipes, R.B. and Advani, S.G. "On flow through aligned fiber beds and its applications to composites processing," J. Compos. Mater. 26(9):1351-1373, 1992.

4. Papathanasiou, T.D. and Lee, P.D. "Morphological effects on the transverse permeability of arrays of aligned fibers," Polymer Composites 18(2):242-253, 1997.

5. Cai, Z. and Berdichevsky, A.L. "Numerical-simulation on the permeability variations of a fiber assembly," Polym. Compos. 14:529-539, 1993.

6. Lundstrom, T.S. and Gebart, B.R. "Effect of perturbation of fiber architecture on permeability inside fiber tows," J. Compos. Mater. 29(4):424-443, 1995.

7. Howells, I.D. "Drag due to the motion of a Newtonian fluid through a sparse random array of small fixed rigid objects," J. Fluid Mech. 64:449-475, 1974.

8. Spielman, L. and Goren, S.L. "Model for predicting pressure drop and filtration efficiency in fibrous media," Env. Sci. Technol. 2:279-287, 1968.

9. Koch, D.L. and Brady, J.F. "The effective diffusivity of fibrous media," AIChE J. 32(4):575-591, 1986.

10. Sangani, A. S. and Yao, C. "Transport processes in random arrays of cylinders. II. Viscous flow," Phys. Fluids 31(9):2435-2444, 1988.

11. C.K. Ghaddar, "On the permeability of unidirectional fibrous media: a parallel computational approach," Phys. Fluids 7(11):2563-2586, 1995.

12. S. Torquato, "Random Heterogeneous Materials," 1st edition, Chap. 12:273-277, Springer-Verlag, 2001.

13. Bechtold, G. and Ye, L. "Influence of fibre distribution on the transverse flow permeability in fibre bundles," Compos. Sci. Technol. 63:2069-2079, 2003.

L. Simulation of Compression Resin-Transfer-Molding Process for Manufacturing Net-Shape Structures

Principal Investigator: Suresh G. Advani
Department of Mechanical Engineering
University of Delaware
Newark, DE 19716
(302) 831-8975; fax: (302)-831-8525; e-mail: advani@me.udel.edu

Technology Area Development Manager: Joseph A. Carpenter
(202) 586-1022; fax: (202) 586-1600; e-mail: joseph.carpenter@ee.doe.gov

---

Contractor: University of Delaware
Contract No.: DMI-0521789

Objective

- The principal objective in this phase is to build fundamental understanding of flow-compression coupling in CRTM process and to identify the issues to be addressed in the subsequent analytic, experimental and numerical work.

Approach

- We extended, streamlined and analyzed the existing approach to model compression resin-transfer molding (CRTM). The scheme was utilized to analyze several parts with certain degree of success, but two drawbacks were revealed: low computational performance and limited accuracy. To answer these concerns, extended problem descriptions which include fiber-tow saturation and preform deformation were developed to be implemented in future modeling efforts.

Accomplishments

- An existing RTM simulation package was utilized to model the CRTM process with limited success and some parametric studies were performed. The approach was streamlined and most limitations (such as the requirement that the compression is kinematically driven) were alleviated.
- New governing relations for the general liquid composite molding (LCM) and, in particular, for CRTM have been developed and implemented in a simple numerical scheme. The scheme is currently being tested and, if successful, will be implemented in a finite-element-based simulation and will overcome the limitations of the current modeling approach.

Future Direction

The following tasks are planned:

- Verify the current model by comparison with laboratory experiments.
- Study the influence of processing and material parameters – including multiple constitutive relations – using the current solution as well as the extended model which is currently being tested.
- Develop and experimentally validate the numerical simulation of CRTM based on the extended model to address processing of complex, large-scale structures.

Introduction

All liquid composite molding (LCM) processes require one to place a fibrous preform inside the mold. The mold is sealed and a liquid resin (typically a thermosetting resin, due to its low viscosity) is injected to saturate the preform. The fibers in the preform and the preform itself are usually stationary or may undergo slow and infinitesimal deformations during the injection process. Next, the resin is allowed to cure. During the curing process, the resin cross-links and hardens. Once the resin has sufficiently solidified, the mold is opened and the part is removed. Two commonly used techniques in this process are RTM and vacuum-assisted resin-transfer molding (VARTM), but there are several other processes of interest, such as RTM "Light" and the subject of this report, CRTM. Figure 1 schematically compares these processes.

In all these variations, the flow of the resin through the preform is important. If particular sections of the preform remain dry after the injection is complete, the resulting void will seriously compromise the composite properties. This may, for example, happen if the inlets or vents are poorly placed. As it is not possible to visualize the resin flow inside a closed mold, this created a need to simulate the filling process using a science-based process model. For conventional RTM process, many reliable computer simulation tools have been established and validated with experiments [1-14]. They have been used to verify designs and, more recently, for the purposes of process optimization and control [15-20]. When other LCM variations in the process are involved, the modeling tools are scarce and RTM tools are usually adapted [21-22], though the results are sometimes not quite satisfactory. In this report, we analyze the adaptation of RTM modeling package to CRTM modeling.

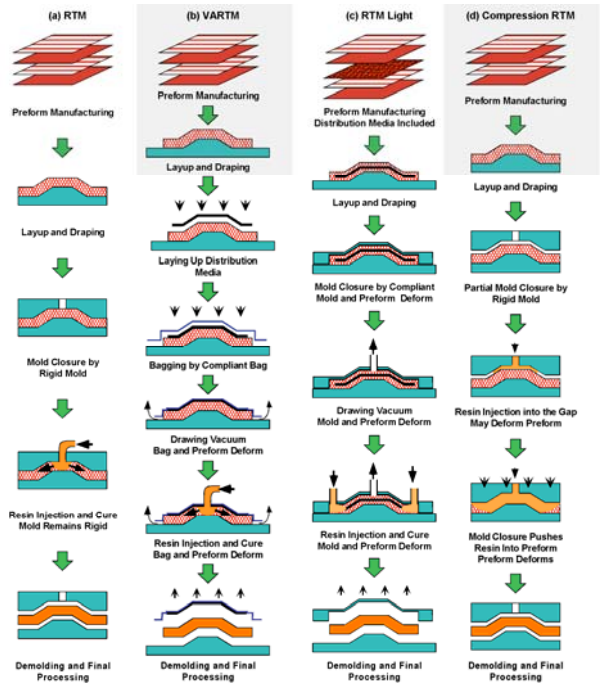

Figure 1. Comparison of several important LCM variations which includes CRTM.

CRTM Process

Traditionally, LCM processes are considered for small- to medium-production batches. The major limit to adaptation of this process to large-scale production is its cycle time. This may be overcome with a new process variation, CRTM, in combination with near-shape preform manufacturing, particularly the programmable powdered preform process (P4). This process combines resin injection into a preform in a partially-open mold, subsequently closing the mold to squeeze the resin into the preform and simultaneously compacting the preform to increase the fiber volume content, which is necessary for structural components. This process offers the potential to manufacture moderately-sized structures in a few minutes while preserving the advantages of RTM, namely, net-shape manufacturing of complex curvatures with class A surface finish.

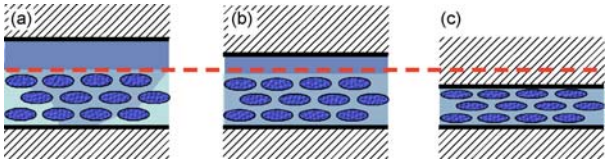

Figure 2. Three stages of CRTM process.

The resin flow in the CRTM process is more complex than any other LCM variations. It exhibits three distinct stages which are shown in Figure 2. All of the phases can be modeled as flow through porous media under different boundary and initial conditions.

The three stages are:

1. resin injection into the narrow gap between the mold platen and the fiber preform in the mold,
2. closing of the gap while squeezing the resin into the preform without direct contact between the movable tool part and the perform, and
3. compaction of the preform by the mold platen along with continuing resin impregnation.

Note that individual stages may overlap in time depending on tool geometry and kinematics. Also, a single composite structure may be undergoing different phases in different regions. For the sake of simplicity, we assume that these three stages follow each other. This assumption may be relaxed if necessary.

Stage 1: Resin Injection into the Narrow Gap

In the first stage, the resin is injected into the gap between the movable mold part and preform (Figure 2 (a)). It can readily spread through the gap, as its permeability is much higher than that of the preform. It also penetrates into the preform. This is analogous to the flow in traditional VARTM. In CRTM, the gap plays the role of the flow-enhancement layer known as the distribution media. As there is a pressure gradient across the preform thickness, the preform will undergo stress (compaction) to ensure equilibrium. However, the injection pressure is usually not particularly high to induce the resin to flow in the gap and hence one can neglect this compaction.

Stage 2: Closing the Gap

In the second stage (Figure 2 (b)), the resin injection is switched off and the mold platen moves to close the gap. The gap filled with the resin serves as a continuous resin source to impregnate the rest of the dry preform. The gap between the preform and the mold platen reduces as the mold closes and the resin is displaced and forced into the preform and in the unfilled regions of the gap. As the gap thickness reduces, so does its permeability. However, pressure increases, accelerating the resin flow into the preform. In this phase, as the resin pressure is higher, we expect higher deformation of the preform due to the pressure gradients, even though there is no mold-preform contact. For low-pressure compression molding one could assume that this physical phenomenon does not influence the flow significantly, but experimental verification of this assumption is highly desirable.

Stage 3: Preform Compaction

In the final stage (Figure 2 (c)), the gap between the preform and the mold platen vanishes, and the mold wall comes in contact with the preform and compresses the preform directly. Consequently, the resin is forced from already-filled regions which serve as a resin source to impregnate the unfilled regions in the mold. The preform compaction can be described reliably if the mold kinematics are known. Then, the volume fraction, permeability, etc. of the preform can be predicted at any time during this stage. A notable exception to this rule is the case when the force required for compression is known, instead of the mold kinematics. The coupling between the mold closure and the pressure field would not significantly complicate the modeling if one could predict the stresses in the preform. These could be combined with known resin pressure using the Terzaghi equation [23]. Unfortunately, the stress/deformation relation of preforms is not well mapped despite a fair amount of research in this field [24-35].

Process Model

All three stages of the CRTM process described above are similar to other RTM variations as they represent a pressure-driven flow in porous medium. This should allow one to create a modeling algorithm utilizing the existing, well-developed RTM modeling software. We will show below an iterative scheme that is able to model the process and undeniably useful for researching the process but could be made efficient by modifying the governing equations.

RTM Modeling

First, we should briefly examine the traditional RTM modeling approach. The resin flow into a thin, closed-mold cavity can be represented as flow through porous media, usually with negligible inertial effects due to the high viscosity of the resin [3]. To describe the physics of such a flow one usually uses the Darcy's law

$$\langle \mathbf{v} \rangle = -\frac{\mathbf{K}}{\eta} \cdot \nabla p \quad (1)$$

and the continuity equation

$$\nabla \cdot \langle \mathbf{v} \rangle = 0 \quad (2)$$

to formulate the governing equation. Here $\langle \mathbf{v} \rangle$ is the volume-averaged flow velocity, ∇p is the pressure gradient in the impregnating fluid, and η is the viscosity of the fluid. The positively-definite tensor **K** describes the permeability of the fibrous porous media. The continuity equation reflects the fact that no preform deformation takes place.

Substitution of equation (1) in the continuity equation (2), results in the following governing equation:

$$\nabla \cdot \left(\frac{\mathbf{K}}{\eta} \cdot \nabla p \right) = 0 \quad (3)$$

This equation is usually solved to provide the pressure field for a given configuration. Flow velocity is then computed from equation (1) to provide description of the flow. Modeling flow of the viscous liquid into the mold involves a moving boundary. There are several ways to numerically simulate the filling process [1-14]. In our package, LIMS (Liquid Injection Molding Simulation), we utilize the common finite-element/control volume (FE/CV) solution scheme described elsewhere [3, 9, 36].

Challenge of Deformable Preform

The conservation of mass, equation (2), assumes that the porous medium does not deform. Once the control volume associated with the porous medium starts changing during the flow, a new source term appears in this equation. For modest deformation, one can use infinitesimal volumetric strain rate $\dot{\varepsilon}$ and a coordinate system fixed to the porous media:

$$\nabla \cdot \langle \mathbf{v} \rangle = -\dot{\varepsilon} \quad (4)$$

The infinitesimal strain can be replaced by other strain measure as needed. The rigorous evaluation of the deformation field requires a known stress-strain relation in the fibrous preform and evaluation of this stress field. This is impossible to accomplish within a RTM modeling package as one would need to couple the flow computation with stress/strain analysis (of poorly characterized material). One can, however, make several acceptable assumptions to simplify the solution:

1. The preform deforms through the thickness only.
2. The preform deforms uniformly through the thickness.
3. The preform does not deform without tool contact.

The first assumption is true for most variations of LCM which deform the preform. The second assumption relies on use of similar material in all layers of the preform and limited through-the-thickness pressure gradient. The last assumption is generally tied to the second one and depends on pressure gradient through the thickness not deforming the material (at least not significantly). With these assumptions, we can replace the strain rate by the rate of change of preform thickness *h(**x**,t)*. For linear strain it is:

$$\nabla \cdot \langle \mathbf{v} \rangle = -\frac{\dot{h}(\mathbf{x},t)}{h_0(\mathbf{x})} \quad (5)$$

where h_0 is the original preform thickness, before the mold platen starts compressing it. Utilizing Darcy's law, we can obtain the governing elliptic partial differential equation (PDE) for pressure as follows

$$\nabla \cdot \left\langle \frac{\mathbf{K}(h)}{\eta} \cdot \nabla p \right\rangle = \frac{\dot{h}(\mathbf{x},t)}{h_0(\mathbf{x})} \quad (6)$$

This equation looks similar to those for compressible preforms [21, 22]. However, the thickness variation is generally known as a function of time (and location) from the kinematics of the tooling. Note that even if the compaction force is prescribed in lieu of the closing speed, the closing direction is known; but, we will return to this case later. This means that neither the source term on the right-hand side, nor the permeability value K on the left-hand side is coupled with the unknown pressure

field. The pressure field is related only to the fluid pressure averaged over the pores. Thus, we still have a linear partial differential equation (PDE) for pressure, only its coefficients are transient. Note that the compressive force cannot be evaluated unless an additional constitutive model is introduced for preform stress-strain relations.

Note that if the linearized deformation is not acceptable, one can replace the right-side term in (6) with a more appropriate one.

The usual, explicitly-integrated, quasi-static solution of the RTM flow [3] may be modified to solve equation (6) using the following steps:

1. At a particular time step, the filled region represents the solution domain. Permeability and the rate of deformation are known. The rate of deformation allows one to compute the source term on the right side of equation (6) and set these as injection rates at filled nodes. Then, the equation is solved to determine the pressure. Flow rates are determined using Darcy's law and current permeability values. The flow is advanced accordingly by explicit time integration over a selected time step to include more filled control volumes in the solution domain just like in traditional RTM modeling [3].

2. Thickness is changed accordingly to the compaction rate and new permeability values are computed.

At this point, we should return to the case of prescribed compression force and unknown compression rate. As equation (6) is linear in pressure and closing rate, one can evaluate the necessary strain rate as follows:

1. Estimate the closure rate and evaluate the pressure field.

2. Compute the total force from resin pressure and compare it to the prescribed force minus whatever force is exerted by the compressed preform.

3. Multiply the closing rate by the ratio, recompute pressures, and advance the flow as described above.

This approach is restricted to linearized strain and preform stress/strain behavior to elastoplastic.

Permeability and Deformation

Besides creating the "source" effect, preform deformation also changes the preform properties necessary to compute pressure field and flow, most importantly, the permeability and porosity (fiber volume fraction).

The dependence of permeability on the fiber volume fraction K*(vf)* has been studied for various cases, but there seems to be no generally accepted, physically meaningful formula. The Karman-Kozeny equation

$$\mathbf{K}\left(v_f\right) = \mathbf{k}\frac{\left(1-v_f\right)^3}{v_f^2} \qquad (7)$$

is commonly being used for this purpose, often as a curve-fitting tool, because of its simplicity. The results are usually acceptable, though it may be possible to achieve a better fit using other formulas in individual cases [37].

Modeling CRTM with RTM Simulation Package

A sensible approach to the solution of equation (6) would require one to rewrite the solution package. The conventional RTM modeling packages do not allow one to change the part volume. Additionally, the solution is optimized for constant permeability and limited number of inlets [9]. Moreover, a brand new approach would allow one to relax the assumptions of uniform deformation through the thickness of the preform.

While a new solution is desirable and quite feasible, it is possible to simulate CRTM filling using the existing RTM simulation code, assuming that:

1. Preform properties such as permeability and porosity may be changed during the simulation execution.

2. There is no limit for the number of inlets.

It is not even necessary for the simulation code to modify parameters and set inlets on its own; an external program can be used to accomplish this. Our simulation does have the capability to evaluate and change material properties within the simulation and to set/close inlets as needed due to the scripting capability. This makes it possible for us to adopt this package to address CRTM flow under the above mentioned assumptions.

We decided to model the preform as a three-dimensional, porous solid with fixed dimensions. Three stages are modeled independently. A two-dimensional model is inadequate as the gap on top of the preform makes the flow three dimensional [36]. Dynamically-changing dimensions are a fact of the CRTM process, but cannot be implemented in the package. Instead, the thickness is tracked independently and porosity is adjusted to simulate the actual part volume. This does not correspond to either the original preform or to the compacted final part. Note that the preform is being compressed only in the third phase of the process, i.e., any deformation caused by resin pressure in previous phases is neglected. The permeability is modified according to Karman-Kozeny equation (7).

In phases I and II, the channel on top is modeled similarly as a standard distribution medium in VARTM, using two-dimensional elements [36, 38]. The only change relative to the way this model is used in VARTM for distribution media is that the equivalent permeability of the gap is approximated from the equations for creeping (lubrication) flow in a narrow channel of given height (thickness) as

$$K_{xx} = K_{yy} = \frac{h^2}{12} \qquad (8)$$

This is obviously acceptable only if the thickness of the gap h is much smaller than the in-plane dimensions of the part. The thickness, h, is constant in the first stage, and then it continuously varies during the stage 2 from its original value to zero. The permeability of the gap must be modified accordingly. In the last phase, the gap is non-existent, which can be accomplished by setting its thickness and permeability to zero.

The mold is assumed to be rigid and its motion is described by the vector of its velocity **v**, with the displacement x(t). These values are known throughout the process. If the compression load is specified, it can be handled as described above. The model for all three stages is summarized in Figure 3.

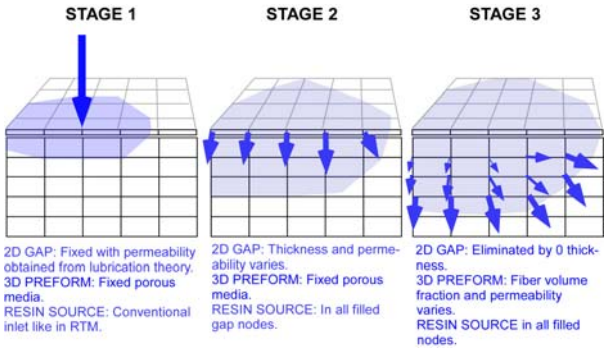

Figure 3. Modeling the three stages of CRTM process.

Modeling Algorithm: Stage 1

In the first stage, the mold is fixed. Resin is injected into the channel on top of the preform and is simulated as ordinary VARTM injection with distribution medium of thickness h, fiber volume fraction of 0 and permeability as described by Equation (8).

The simulation at this stage can predict the time required for injection of a required volume of resin, which is known as the final part dimensions and fiber volume fraction are known in advance. This is trivial if the simulation uses flow-rate control, but the simulation provides the flow rates at inlet(s) in any case, such as constant pressure or even mixed inlets. These can be integrated to provide the volume of resin injected during a certain time period.

The only assumption made at this stage is that the preform itself does not deform as the pressure continues to build. Since the resin pressure will cause some deformation, this may reduce the modeling accuracy by a certain degree, though the pressure build-up in the gap in this stage is likely to be small.

Modeling Algorithm: Stage 2

In this stage, the upper mold platen moves with speed **v**, while there is no resin injection into the mold and the injection gate is closed. If force is

prescribed, one might evaluate **v** simply, as no forces in preform are involved at this stage. The thickness of the gap changes with time. Every saturated node in channel represents a control volume. The change of thickness in this area results in resin source that is applied at that node. This value might change with each time step. Even if the mold speed is constant, one still has to set new "inlets" in newly-filled control volumes with every time step. One also has to obtain the new thickness before each step and update the permeability in the channel whose gap is reducing due to the closure of the mold platen (equation 8) and update each gap element. The process is straightforward, but one must be careful to prevent generating elements with negative thickness of the channel due to the round-off error.

The only assumption made here is that the preform itself does not deform as the pressure builds. At this stage, this assumption might be more questionable, as higher resin pressure is expected and this could deform the preform. One could eliminate this error if we had the compaction data by following these steps: (i) compute the through-the-thickness deformation at each location, (ii) adjust the dimensions of the gap accordingly, (iii) adjust the properties of preform and (iv) create a flow source in the filled preform that is being compressed. The last two points are examined below in Stage 3.

Additionally, we neglected the partially-filled volumes as sources. The fill-factor of these volumes should be updated as they get compressed and, if it reaches unity, the flow source should be introduced for that element. This results in net loss of resin volume during the simulation. This simplification may be alleviated at a cost of implementation complications. The accuracy is also affected by the explicit time integration over finite time steps, though this error should go to zero with mesh refinement.

Modeling Algorithm: Stage 3

In this phase, there is no resin being injected and no gap to provide a preferential flow path. The resin source is the preform itself that is being deformed by compaction. We cannot easily change the "thickness" of three-dimensional (3D) elements, but we can modify their properties to reflect the correct porosity and permeability [36].

The preform thickness and the normal (through-the-thickness) direction in the preform is not immediately obvious in three-dimensional meshes and one needs to perform substantial book-keeping to determine these values and to track them.

Then, we need to create the flow-rate gates in every filled control volume of the domain (Figure 3). In each time step, the closing speed **v** may change and one must set new inlets in the volume(s) just filled and modify the ones filled previously.

The deformation is "averaged" through the thickness, assuming that the deformation is uniform through the thickness. This assumption is fully justifiable only if the preform is fully saturated through the thickness. Otherwise, through-the-thickness pressure and saturation gradients will cause variations in deformation and deformation rates. However, to alleviate this problem one would need to solve a coupled elasto-visco-plastic deformation problem in the three-dimensional preform.

Also, the change of fill-factors in partially-saturated volumes in the preform was not accounted for during the previous stage. This introduces a small inaccuracy in the mass conservation of resin.

The entire modeling approach is summarized in the flowchart presented in Figure 4. The most important difficulty encountered with this model lies in the fact that the performance of the simulation is drastically reduced compared to the conventional RTM modeling. For realistic parts, it is formidable to conduct a parametric study or to try to optimize the injection.

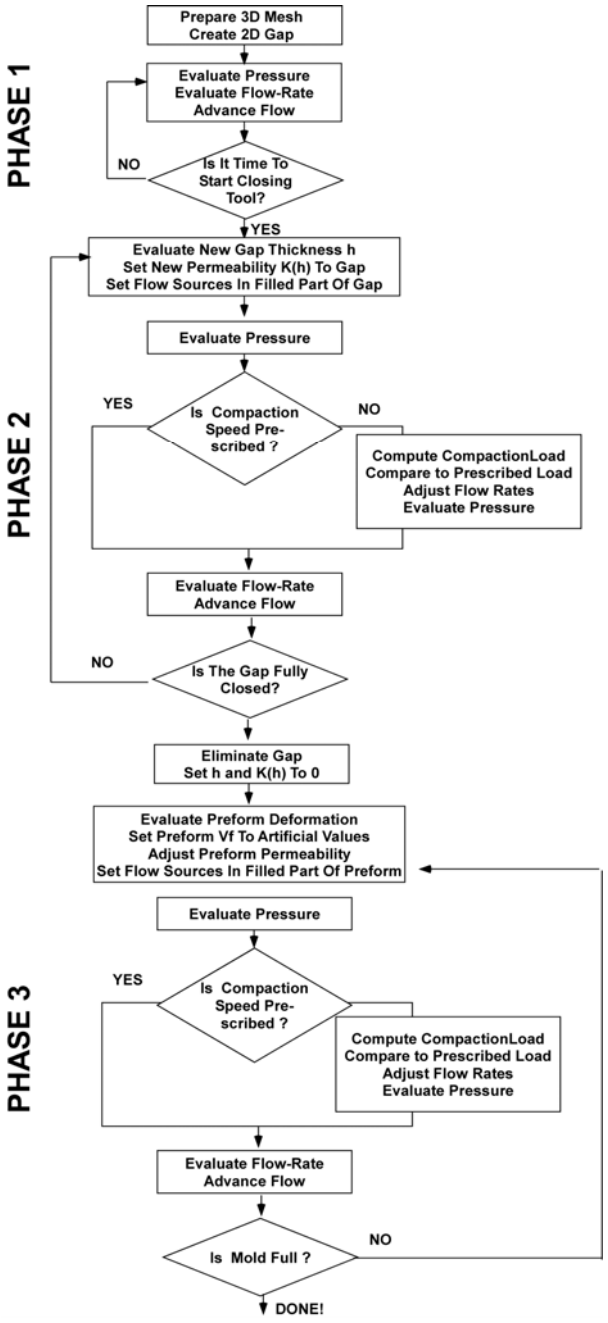

Figure 4. Simulating CRTM by RTM modeling package: The Flowchart.

Results and Discussion

Figure 5 shows the mesh used for the simulation of CRTM filling of a circular test part using LIMS. The radius of the part is 75 mm, the original material thickness is 10 mm and the original fiber volume fraction is 25%. In-plane permeability of the material at this fiber volume fraction is $7.40.10^{-10}$ m^2, the through-the-thickness permeability is $2.50.10^{-11}$ m^2. The in-plane permeability varies with the Kozeny-Karman equation (7). The material data correspond to those measured for a P4 preform. Only one quarter of the part is modeled because of symmetry.

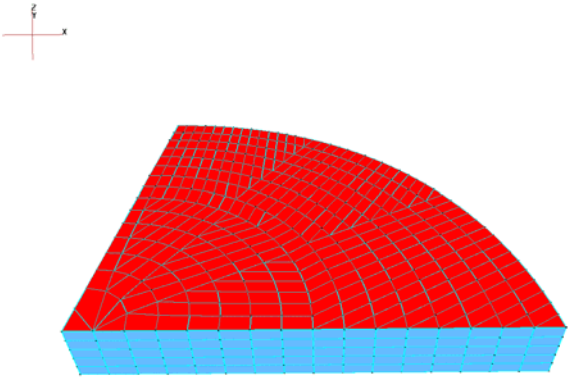

Figure 5. Mesh used for simulation of circular test part manufactured using CRTM.

For this mesh, the simulation takes only several minutes to execute, allowing one to conduct parametric studies varying the material parameters. The most obvious parameter to study is the original thickness of the gap. If the gap thickness is too large, the compression cycle will be extended as closing the gap takes time. If the thickness is too small, the injection cycle might get extended as the resin is effectively injected (with limited pressure) into the preform which has only limited permeability, creating a process close to RTM. Figure 6 shows the flow patterns during the injections with gradually reduced gap thickness.

The filling time goes from almost a minute for 5 mm gap to 35 s for 2.5 mm to 27 s for 1.25 mm gap. However, once the gap size decreases further to 0.625 mm, the fill time jumps to 35 s and the flow starts developing three-dimensional character.

Modeling complex, practical parts is quite feasible. Unfortunately, the time required for a single simulation run is increased to days, or at least many hours. This complicates the use for optimization purposes or even most parametric studies. We have simulated the process for I beams and full-body panels which involve thousands of nodes with this methodology to demonstrate the capability of the simulation. However, the simulation took over 52 hours and requires an expert to write the script to

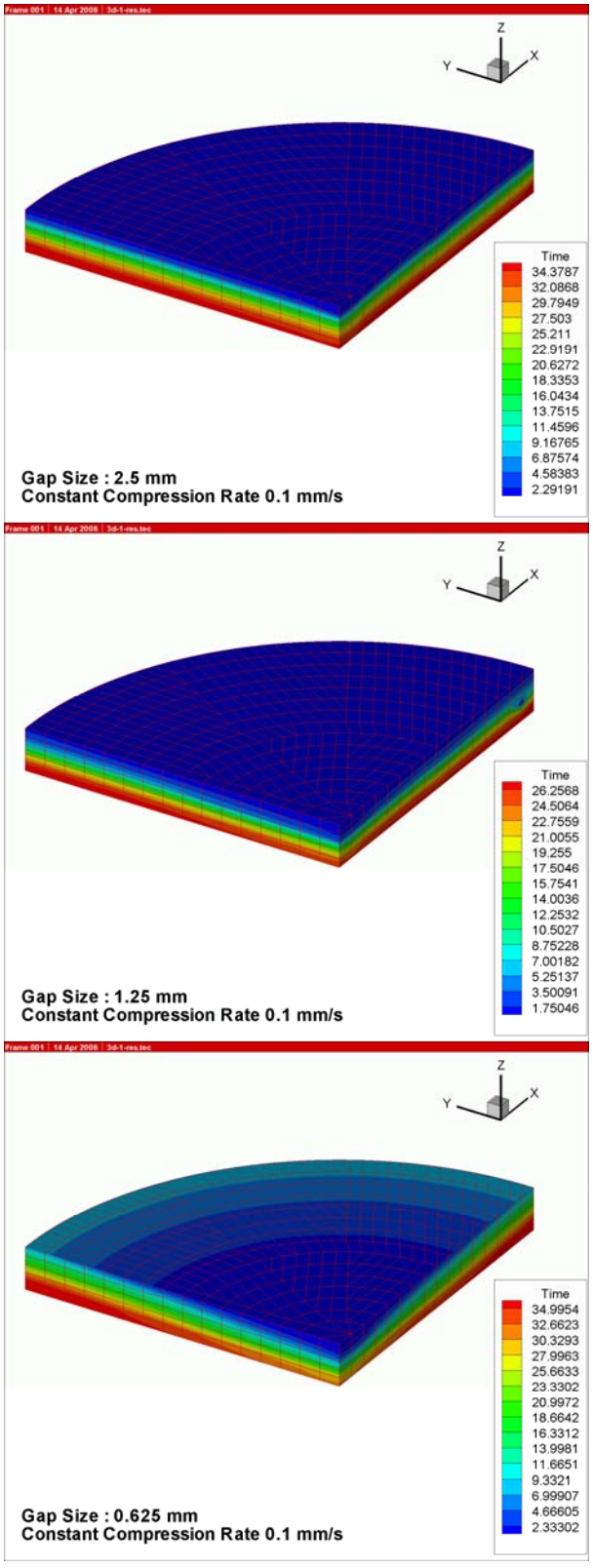

Figure 6. Filling of the test part with CRTM and varying original thickness of gap. The same shade of grayscale indicates regions filled at the same time.

manage the three phases. Hence, our objectives will be to develop efficient algorithms to speed up the calculations as we can do for RTM (of the order of minutes) and to develop a user-friendly interface to make it truly useful for Industry

Discussions and Conclusions

It was demonstrated by adapting the existing RTM simulation software that one can model and simulate CRTM process with certain success, although experimental comparisons are yet to be carried out. This modeling capability is useful to provide some insight into process parameters and, in absence of better models, it may even be used to model injection into complex structure.

However, there are two drawbacks of this methodology that cannot be overcome by an evolutionary approach based on the current solutions. First, the assumption of uniform deformation is uncertain, but it can be overcome only by a different system of governing equations that includes the preform deformation. Second, the computational performance is not quite satisfactory and it is certainly not adequate for the task of process design and optimization in industrial settings. A novel approach is needed to provide industry-strength modeling capability for CRTM process. Discretization of the governing equation system and development of a solver rather than adding many correctional steps to an existing RTM solver will help overcome these shortcomings and are planned for the future.

Acknowledgements

The authors gratefully acknowledge partial support provided by the National Science Foundation under Grant DMI-0521789 and the Department of Energy/National Energy Technology Laboratory.

References

1. C.A. Hieber, S.F. Shen, “A finite element/finite difference simulation of the injection mold filling process,” J. Non-Newtonian Fluid Mech. 7, pp. 1-31, (1980).

2. T.A. Osswald, C.L. Tucker, Polymer Eng. & Sci. 28, pp. 413-420, (1988).

3. M. Bruschke, S.G. Advani, "Finite Element/Control Volume Approach to Mold Filling in Anisotropic Porous Media," Polymer. Composites 11, pp. 398-405, (1990).

4. R.W. Lewis, A.S. Usmani, J.T. Cross, "Finite Element Modeling of Mold Filling," Finite Elements in the 90's, ed. by E. Onate, J. Periaux and A. Samuelsson, Springer-Verlag/CIMNE, Barcelona, (1991).

5. V.R. Voller, Y.F. Chen, "Prediction of Filling Times of Porous Cavities," International Journal Numerical Methods 10, (1995).

6. N.D. Ngo, R.V. Mohan, P.W. Chung, K.K. Tamma, "Recent Developments Encompassing Non-Isothermal/Isothermal Liquid Composite Molding Process Modeling/Analysis: Physically Accurate, Computationally Effective, and Affordable Simulations and Validations," Journal of Thermoplastic Composite Materials 6, pp. 493-532, (1998).

7. F. Trochu, R. Gauvin, D.-M. Gao, "Numerical Analysis of the Resin Transfer Molding Process by the Finite Element Method." Advances in Polymer Technology 12(4), pp. 329-342, (1993).

8. B. Minaie, Y.F. Chen, A.M. Mescher, "A Methodology to Obtain a Desired Pattern During Resin Transfer Molding," Journal of Composite Material, 14, pp. 1677-1692, (2002).

9. R.S. Maier, T.F. Rohaly, S.G. Advani, K.D. Fickie, K.D. "A Fast Numerical Method for Isothermal Resin Transfer Mold Filling," International Journal of Numerical Methods in Engineering 39, (1996).

10. M.K. Kang, W.I. Lee, J.Y. Yoo and S.M. Cho, "Simulation of Mold Filling Process During Resin Transfer Molding," Journal of Materials Processing and Manufacturing Science, 3, pp. 297-313, 1995.

11. W.B. Young, "Three-Dimensional Nonisothermal Mold Filling Simulations in Resin Transfer Molding," Polymer Composites, 2, pp. 118-127, 1994.

12. O. Mal, A. Couniot and F. Dupret, "Non-Isothermal Simulation of the Resin Transfer Moulding Process," Composites Part A: Applied Science and Manufacturing, 1-2, pp. 189-198, 1998.

13. M. V. Bruschke and S. G. Advani, "A Numerical Approach to Model Non-isothermal, Viscous Flow with Free Surfaces through Fibrous Media," International Journal of Numerical Methods in Fluids, 19, pp. 575-603 (1994).

14. P. Simacek and S.G. Advani, "Approximate numerical method for prediction of temperature distribution in flow through narrow gaps containing porous media," Computational Mechanics, v 32, n 1-2, September, pp. 1-9 (2003).

15. M.Y. Lin, M.J. Murphy, H.T. Hahn, "Resin transfer molding process optimization," Composites: Part A 31, pp. 361-371, (2000).

16. R. Mathur, B.K. Fink, S.G. Advani, "Use of Genetic Algorithms to Optimize Gate and Vent Locations for the Resin Transfer Molding Process," Polymer Composites 2, pp. 167-178, (1999).

17. E.M. Sozer, S. Bickerton, S.G. Advani, "Use of Sensors and Simulations for Strategic Control of Liquid Composite Mold Filling Process," SME Technical Paper, Composite Manufacturing and Tooling 2000, (2000).

18. B.Y. Kim, G.J. Nam, J.W. Lee, "Optimization of Filling Process in RTM Using a Genetic Algorithm and Experimental Design Method," Polymer Composites, 1, pp. 72-86, (2002).

19. S. Bickerton , H.C. Stadtfeld , K.V.Steiner, S.G.Advani, "Design and application of actively controlled injection schemes for resin-transfer molding," Composites Science and Technology, v 61 n11, pp. 1625-1637 (2001).

20. D.R. Nielsen, R. Pitchman, "Closed-loop Flow Control in Resin Transfer Molding Using Real-time Numerical Process Simulation," Composite Science and Technology, 2, pp. 283-298, (2002).

21. Acheson, Jeffrey A.; Simacek, Pavel; Advani, Suresh G., "The implications of fiber compaction and saturation on fully coupled VARTM simulation" Composites Part A: Applied Science and Manufacturing, v 35, n 2, February, pp. 159-169 (2004).

22. Correia, N.C., Robitaille, F., Long, A.C., Rudd, C.D., Simacek, P. and Advani, S.G., "Use of Resin Transfer Molding Simulation to Predict Flow, Saturation and Compaction in the VARTM Process," Journal of Fluids Engineering, Vol 126, March, pp. 1-6 (2004).

23. Terzaghi, K., and Peck, R. B., "Soil Mechanics in Engineering Practice," 2nd, ed., John Wiley & Sons, New York (1967).

24. Carnaby, G.A. and Pan, N. "Theory of Compression Hysteresis of Fibrous Assemblies," Textile Research Journal 27 (1989).

25. Batch, G.L. and Macosco, C.W. "A Model For Two-Stage Fiber Deformation In Composite Processing," 20th Internationa SAMPE Technical Conference, 1988 (1988).

26. Komori, T., Itoh, M. and Takaku, A. "A Model Analysis of the Compressibility of Fiber Assemblies," Textile Research Journal 10, pp. 567-574 (1992).

27. Hearle, I.W. and Shanahan, W.J. "11-An Energy Method for Calculations in Fabric Mechanics; Part I: Principles of the Method," Journal of Textile Institute 4, pp. 81-91 (1978).

28. Shanahan, W.J. and Hearle, I.W. "12-An Energy Method for Calculations in Fabric Mechanics; Part II: Examples of Application of the Method to Woven Fabrics," Journal of Textile Institute, pp. 93-100 (1977).

29. Simacek, P. and Karbhari, V. M., "Notes on the Modeling of Preform Compaction: I - Micromechanics at the Fiber Bundle Level," Journal of Reinforced Plastics and Composites 1, pp. 86-122 (1996).

30. Karbhari, V. M. and Simacek, P. "Notes on the Modeling of Preform Compaction: II - Effect of Sizing on Fiber Bundle Micromechanics," Journal of Reinforced Plastics and Composites 8, pp. 837-861 (1996).

31. Gutowski, T.G. and Dillon, G., "The Elastic Deformation of Lubricated Carbon Fiber Bundles: Comparison of Theory and Experiments," Journal of Composite Materials 16, pp. 2330-2347 (1992).

32. Cai, Z. and Gutowski, T., "The 3-D Deformation Behavior of A Lubricated Fiber Bundle," Journal of Composite Materials 8, pp. 1207-1237 (1992).

33. A.A. Somashekar, S. Bickerton and D.B. Bhattacharya, "Non-elastic Effects during Compression of Fiber Reinforcements," International Conference on Flow Processes in Composite Materials, FPCM 7, 413-418 (2004).

34. T. Kruckenberg and R. Patton, "Compaction of Dry and Lubricated Reinforcements," International Conference on Flow Processes in Composite Materials, FPCM 7, 425-436 (2004).

35. P.A. Kelly and R. Umer, "Modeling the Viscoelastic Behavior of Fiber Reinforcing Fabrics," International Conference on Flow Processes in Composite Materials, FPCM 7, 443-446 (2004).

36. Simacek, P. and S.G. Advani, "Desirable Features in Mold Filling Simulations for Liquid Molding Processes," Polymer Composites, 25, pp. 355-367 (2004).

37. Bruschke, M., Advani, S.G., "Flow of generalized Newtonian fluids across a periodic array of cylinders," Journal of Rheology, 37(3), pp. 479-498 (1993).

38. Modi, D., Simacek, P., Advani, S.G., "Numerical Issues in Mold Filling Simulations of Liquid Composites Processing," Proceedings of 10th US-Japan Conference on Composite Materials (2002).

M. Incorporating Higher-Order Tensors in the Computation of Polymer Composite Mechanical Properties

Principal Investigator (PI): Douglas E. Smith
University of Missouri at Columbia
E2411 Lafferre Hall / MAE Dept., Columbia, MO 65211
(573) 884-6552; fax: (573) 884-5090; e-mail: smithdoug@missouri.edu

Technology Area Development Manager: Joseph A. Carpenter
(202) 586-1022; fax: (202) 586-1600; e-mail: joseph.carpenter@ee.doe.gov

Participants: David A. Jack and Elijah C. Caselman, University of Missouri at Columbia

---

Contractor: University of Missouri at Columbia
Contract No.: NSF Grant DMI-0522694

Objective

- Develop a predictive capability that incorporates higher-order orientation tensors to evaluate mechanical properties of short- and long-fiber-reinforced polymer composites.

Approach

- Development of a model for predicting mechanical properties from higher-order orientation tensors derived from flow simulations or measurements that are not limited by the material symmetry requirements imposed by current models.
- Development of an automated three-dimensional (3D), voxel-based, finite-element modeling technique that may be used to predict the effective mechanical properties of short- and long-fiber suspensions.
- Integration of micro-computerized-tomography (micro-CT)-derived fiber reconstructions to illustrate the applicability of the proposed approach on production hardware to be obtained from industry or DOE.
- Statistical assessment of mechanical property calculations to address sampling issues associated with using the proposed averaging techniques.
- Demonstration of the proposed methodology on an industrially-relevant polymer-composite product where flow simulation software is to be provided by Moldflow Corporation.

Accomplishments

- Derived an analytical relationship between elastic mechanical properties and fiber-orientation tensors for statistically-independent short fibers, including both the property's mean and variance.
- Evaluated mechanical properties using existing property models from simple melt-flow simulations that employ 4^{th}- and 6^{th}- order-tensor closures.
- Developed Monte Carlo method for computing mean and variance of elastic properties of short-fiber composites from fiber-orientation-distribution functions.
- Evaluated mechanical properties of short-fiber composites via Monte Carlo sampling procedure, validating analytical approach developed as part of this project.

- Developed a 3D, voxel-based, finite-element model using a representative volume element (RVE) and related periodic boundary conditions for predicting elastic material properties of short- and long-fiber polymer composites.

Future Direction

- Continue verification work for 3D, voxel-based, finite-element procedure for fiber-reinforced polymer composites.
- Continue develop an automated procedure for defining 3D finite-element models of a representative cell that may be used with analytically-derived fiber-orientation-distribution functions, or fiber-orientation states obtained from micro-CT measurements.
- Compute elastic mechanical properties from 3D, voxel-based, finite-element model for short- and long- fiber composites.

Introduction

The purpose of this project is to develop a predictive capability that incorporates higher-order orientation tensors to evaluate mechanical properties of short- and long-fiber-reinforced polymer composites. To realize this goal, the project will develop a computational methodology to predict elastic mechanical properties from orientation tensors of second- and fourth-order which are computed during melt-flow simulations. The micromechanics of both short- and long-fiber suspensions will be simulated with a voxel-based finite-element modeling approach, so that the mechanical properties of randomly-oriented fiber samples can be computed. Simulated fiber- orientation states, as well as those obtained from micro-CT scans will serve as input. Finally, fiber- orientation states from industrially-relevant products will be evaluated with the new methodology to assess its applicability for complex geometries.

This report provides a brief description of the three-year project, a predictive method for mean and variance of elastic properties using higher-order tensors, Monte Carlo validation, and new results from our 3D, voxel-based, finite-element approach.

Project Deliverables

The primary deliverable of this research will be a relationship between higher-order (i.e., fourth) orientation tensors and the elastic mechanical properties for short- and long-fiber suspensions. An assessment of the variability of mechanical properties among fiber-orientation states will be provided, along with a computational procedure for evaluating the same properties for a specific orientation state. A final report will be generated to communicate the functional form of the mechanical properties and the relevant model parameters for specific examples studied.

Background

Orientation tensors are used extensively to represent the stochastic nature of polymer- composite fiber suspensions in a form that is suitable for large-scale melt-flow simulations. Orientation-tensor research over the past two decades has advanced the state-of-the-art related to polymer composites; however, the use of tensors today is still basically the same as it was when these methods were first developed nearly twenty years ago. In addition, the application of orientation tensors to long-fiber composites is nearly non-existent.

The continued advancement of our basic understanding of short- and long-fiber-reinforced polymer composites is critical in numerous industries including consumer products and automotive which rely heavily on the low cost, design flexibility, and superior performance offered by these materials. A major focus of the National Science Foundation / US Department of Energy / American Plastics Council-sponsored workshop[1] co-organized by the PI in June, 2004 was the need for the US automotive industry to incorporate more fiber-reinforced polymer composites in the design of

[1] See http://web.missouri.edu/~smithdoug/nsf/index.htm for workshop information.

future vehicles to reduce the weight, emissions, and fuel consumption.

For example, a specific goal of the 2010 FreedomCAR is to reduce the weight of an automotive structure by 50% for the same cost and durability as seen in today's products. The key to meeting these objectives is a comprehensive predictive engineering approach that is capable of accurately simulating critical attributes associated with the design of both the product and its manufacturing process. In this approach, a critical link that connects the computation of materials processing attributes with the prediction of a composite product's performance is the evaluation of structural mechanical properties from melt flow predictions.

Given the dramatic increases in affordable computing over the past decade, and the anticipated demands on our predictive capabilities for composite materials over the next decade, it is now time to reconsider assumptions that compose today's fiber-orientation models. For example, limiting fiber-orientation predictions to solving for only the second-order orientation tensor components in an effort to reduce computational effort may not be necessary. This project will provide a higher-order approximation to more accurately describe suspension mechanics for complex flow fields such as those where both shear and elongational velocity gradients exist in all three different planes.

Evaluating Elastic Properties from Orientation Tensors

One task of this research is to develop a formulation for computing short- and long-fiber- composite elastic properties from orientation tensors. Here we consider the expected value of the elasticity tensor $\langle C_{ijkl} \rangle$ defined in terms of the orientation distribution function $\psi(\mathbf{p})$ as

$$\langle C_{ijkl} \rangle = \int_S Q_{pi}(\mathbf{p}) Q_{qj}(\mathbf{p}) Q_{rk}(\mathbf{p}) Q_{sl}(\mathbf{p}) \overline{C}_{pqrs} \psi(\mathbf{p}) d\mathbf{p}$$

where **p** is a unit vector in the fiber direction as shown in Figure 1. In this calculation, $\overline{C}_{pqrs}$ is the underlying unidirectional compliance tensor for a single fiber (computed using the Mori-Tanaka, Halpin-Tsai, or similar inclusion model) and $Q_{ij}(\mathbf{p})$ is a rotation tensor that rotates the unidirectional components into a selected coordinate system. Elasticity tensor components may be computed in this manner for various orientation-distribution functions. However, when $\psi(\mathbf{p})$ is written in terms of the Fourier basis functions such as those given in Advani and Tucker[2], it can be shown that $\langle C_{ijkl} \rangle$ reduces to the well-known result

$$\begin{aligned}\langle C_{ijkl} \rangle = {} & B_1(a_{ijkl}) + B_2(a_{ij}\delta_{kl} + a_{kl}\delta_{ij}) \\ & + B_3(a_{ik}\delta_{jl} + a_{il}\delta_{jk} + a_{jl}\delta_{ik} + a_{jk}\delta_{il}) \\ & + B_4(\delta_{ij}\delta_{kl}) + B_5(\delta_{ik}\delta_{jl} + \delta_{il}\delta_{jk})\end{aligned}$$

where a_{ij} and a_{ijkl} are the 2nd- and 4th-order fiber-orientation tensors, δ_{ij} is the identity tensor, and the constants $B_1 - B_5$ are computed from $\overline{C}_{pqrs}$.

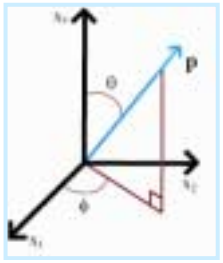

Figure 1. Coordinate system defining fiber direction with the unit vector p(θ,ϕ).

This derivation shows that when the elastic properties are computed as the volume-averaged result of unidirectional fibers weighted by the orientation-distribution function, the highest-order orientation tensor that contributes is the fourth. In this case, sixth- and higher-ordered orientation tensors do not define to the composite's elasticity tensor. What is important to note about this result is that the equations above implicitly assume that each fiber that composes a_{ij} and a_{ijkl} does not interact when stresses are imposed on the fiber-matrix structure. While the effect of fiber interaction has received much attention in melt-flow analyses, little

[2] S. Advani and C.L. Tucker, Jn. of Rheology, vol. 31, no. 8, pp. 751-784, 1987.

effort has been devoted to understanding its role on elastic response of these composites. The elastic response of a high volume-fraction short-fiber composite, as well as long-fiber composites, is expected to be influenced by structural fiber-fiber interaction.

The variance σ^2_{ijkl} of the elastic properties may be computed in a similar manner by taking the second moment of the rotated unidirectional compliance tensor about the mean given as

$$\sigma^2_{ijkl} = \oint_{S^2} \left(Q_{qi}(\mathbf{p}) Q_{rj}(\mathbf{p}) Q_{sk}(\mathbf{p}) Q_{tl}(\mathbf{p}) \overline{C}_{qrst} - \left\langle C_{ijkl} \right\rangle \right)^2 \psi(\mathbf{p}) d\mathbf{S}$$

For relatively simple $\psi(\mathbf{p})$, an analytical result for variance may be obtained by integrating the above equation. This has been performed as part of this research for several distribution functions. These results are beyond the scope of this report, but may be found elsewhere[3]. It is important to note here that while the mean value of the elasticity tensor $\left\langle C_{ijkl} \right\rangle$ contained orientation tensors through 4th order, the variance σ^2_{ijkl} is a function of orientation tensors through 8th order. Therefore, to use the result described here, analytical or approximate values of the 2nd-, 4th-, 6th- and 8th-order orientation tensors are required.

Monte Carlo Simulation

A Monte Carlo simulation method was developed to validate analytical results for the mean and variance obtained above for the elastic properties of a short-fiber composite. The Monte Carlo calculations included an Accept-Reject algorithm to obtain a set of fiber orientation angles for any given orientation distribution that is described by an orientation-distribution function or set of orientation tensors. The mean and variance of the compliance matrix are computed in these Monte Carlo simulations using a discrete form of the continuous equations given above for $\left\langle C_{ijkl} \right\rangle$ and σ^2_{ijkl}.

Several example Monte Carlo calculations have been performed to verify the analytical forms described above. Consider the fiber-orientation-distribution function

$$\psi(\theta,\phi) = \tfrac{9}{4\pi} \sin^8\theta \cos^8\phi$$

where θ and ϕ describe the fiber angle as shown in Figure 1. Figure 2 illustrates the form of this distribution function which is highly aligned in the x_1 direction. The figure also shows a representative volume of fibers with a volume fraction of 10% that were generated for the Monte Carlo simulations. Computed results for C_{1111} are shown in Figure 3 for 10^8 Monte Carlo simulations where matrix and fiber properties are taken from Tucker and Liang[4] and the volume fraction is 10%. As shown in the figure, this component of the compliance tensor varies between a predictable lower and upper bound with a linear probability distribution.

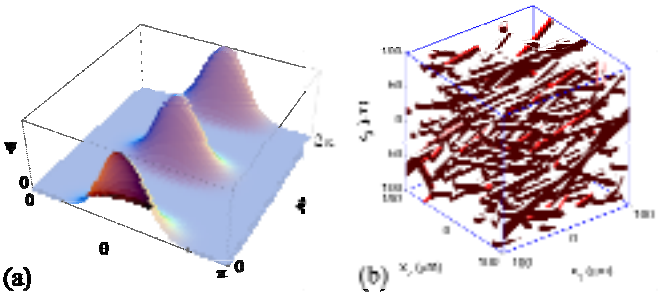

Figure 2. Fiber-orientation-distribution function used in example calculations (a) and a representative sample set of fibers (b).

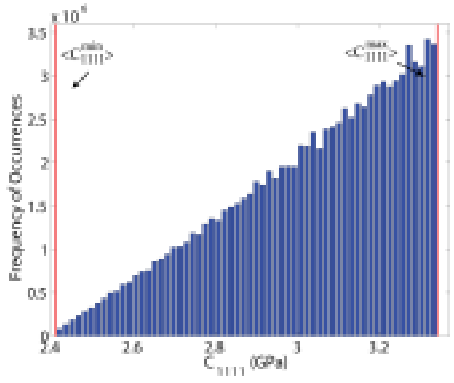

Figure 3. Histogram from Monte Carlo calculations for C_{1111} using 10^8 fiber occurrences.

[3] D.A. Jack and D.E. Smith, Jn. of Composite Materials, Accepted for Publication, 2007.

[4] C.L. Tucker and E. Liang, *Comp. Science and Technology*, vol. 59, pp.655-671, 1999.

Of more practical use is the predicted distribution and related statistical properties for multiple sets of fibers since we are typically interested in the elastic properties of a material point which can vary from part to part. To this end, we apply the Central Limit Theorem to compute the statistical nature of multiple sets of fibers such as that shown in Figure 2b. Figure 4 shows the results of 10^6 sets of fibers where each set contains 101 fibers. As predicted by the Central Limit Theorem, the results become normally distributed. Also shown is the analytically-evaluated normal distribution function obtained by applying the Central Limit Theorem to the analytical mean and variance equations given above. The figure clearly shows that the analytical form that we have derived for the statistical properties of fiber suspensions is verified through our Monte Carlo simulations.

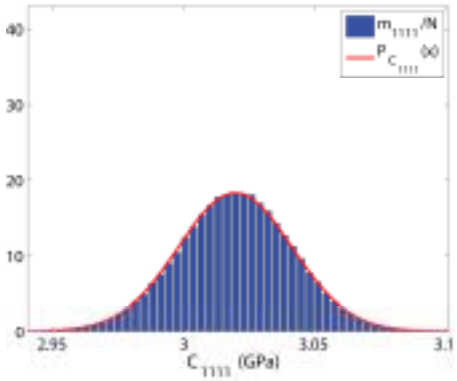

Figure 4. Histogram and normal probability distribution function for C_{1111} using 10^6 fiber sets.

Monte Carlo simulations have also been performed to predict the statistical behavior of the complete compliance tensor for both simple analytical fiber-orientation distributions and for distributions that arise during polymer melt flow. The latter are evaluated from numerical simulation of the fiber-orientation-distribution function evolution. In all cases, our analytical results are validated with Monte Carlo-simulation results. This work is the first to consider the statistical nature of short-fiber composite elastic properties at this level of detail.

Three-dimensional Finite-Element Analysis for Evaluating Mechanical Properties

All of the calculations described above are restricted to short-fiber composites, and explicitly assume that the stress state around each fiber is not influenced by its neighbors. To address these shortfalls, a 3D finite-element modeling technique is being developed that will be used to gain a better understanding of the effect of fiber-fiber interaction in the elastic solid. Our approach is to use a voxel-based finite-element model to represent a characteristic elastic unit within the composite structure. Properties of each point within the model will be based on fiber distributions obtained analytically, or through experimentally-derived procedures, making it possible to include short- and long-fiber composites in the analysis. To reduce the number of degrees-of-freedom in these 3D finite-element simulations, a custom element has been developed that can incorporate a large number of sampling (or Gauss) points within its domain, and thus provide a more refined spatial definition without increasing the number of degrees of freedom.

This modeling approach is being implemented in the general-purpose finite-element program ABAQUS using a user-defined element. RVEs (see e.g., Figure 2b) are defined by a uniform grid of 3D elements where the elastic properties of each Gauss point are defined by its spatial location in relationship to the position of the fibers. The number of Gauss points is increased within each element to provide the required spatial refinement. Unique elemental shape functions have been created to increase the complexity of the displacement field in each element so that elements which contain both matrix and fiber are not over-constrained by the more traditional bi-linear response. In addition, periodic boundary conditions are implemented so that both axial and shear loads may be accurately applied to the RVE. A fitting procedure has also been developed to compute elastic properties from multiple RVE runs where constraints are imposed to enforce a desired material symmetry.

Figure 5 shows a finite-element model of a single fiber embedded in a polymer matrix that has been used to validate our calculation procedure. The

dimensions and material properties for this model are taken from Xia, et al.[5] who provide both simulation and experimental results for comparison. Figure 6 shows a voxel-based finite- element model of the same geometry where contours are provided to indicate the fiber's location. Note that this plot simply shows element- by-element values, and thus does not provide insight into the spatial refinement with each element that is included with our multiple-Gauss- point approach. Both of these models were loaded in axial tension in each of the coordinate directions in addition to various shear-loading conditions.

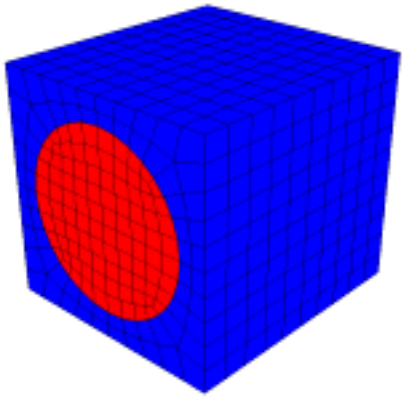

Figure 5. Two-material RVE finite-element model as defined by Xia et al.[5].

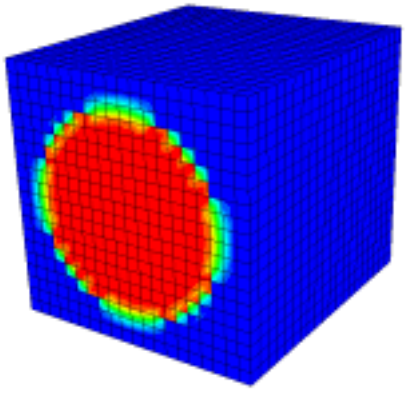

Figure 6. Voxel-based finite-element model of RVE with contours illustrating elements that contain fiber, matrix, or both.

[5] Z. Xia, Y. Zhang, and F. Ellyin, *Solids and Structures*, vol. 40, pp. 1907-1921, 2003.

Table 1 compares engineering elastic constants obtained from the models in Figures 5 and 6 with values provided by Xia et al.[5]. It can be seen that our two-material model (see e.g., Figure 5) provides results that are nearly identical to Xia's results which compare well with experimental data as reported in their paper. Table 1 also shows that results obtained with our voxel finite-element model agree quite well with the two-element models. These latter results are computed with ten elements in each of the *x*, *y*, and *z* directions where the elements have six Gauss points in each direction.

In other simulations, we have been able to obtain similar agreement with results provided by Tucker and Liang[4] who model a more complicated short-fiber composite sample. Other runs have been performed to establish limits on the number of elements and Gauss points that will be needed for modeling RVEs with smaller fibers (such as that shown in Figure 2b).

Table 1. Elastic properties computed from two-material and voxel-based finite-element models (moduli in GPa).

Elastic Constants	Xia et al.[5]	Two-mat'l model (Fig. 5)	Voxel-based model (Fig. 6)
E11	214	214.4	216.1
E22	143	143.7	147
E33	143	143.7	147
G12	54.2	53.9	56.4
G23	45.7	45.4	45.6
G13	54.2	53.9	56.4
v12	0.195	0.195	0.194
v23	0.253	0.253	0.244
v13	0.195	0.195	0.194

Conclusions

This research project focuses on the prediction of elastic mechanical properties from higher-order fiber-orientation tensors. As part of this work, the expression for computing elastic properties form fiber-orientation tensors is verified and shown to ignore fiber-fiber interaction. In addition, the role of higher-order tensors on mechanical property prediction when using this approach is explored. Finally, results of a 3D, voxel-based finite-element modeling procedure have been shown to be in good agreement with more conventional FE approaches.

Presentations/Publications/Patents

1. D.A. Jack and D.E. Smith, 'Elastic Properties of Short-Fiber Polymer Composites, Derivation and Demonstration of Analytical Forms for Expectation and Variance from Orientation Tensors', Accepted for publication in *Jn. of Composite Materials*, 2007.

2. D.A. Jack and D.E. Smith, 'A Statistical Method to Obtain Material Properties from the Orientation Distribution Function for Short-fiber Polymer Composites', IMECE2005-81263, Proceedings of ASME IMECE'05, Orlando, Florida, Nov. 5-11, 2005.

3. D.A. Jack and D.E. Smith, 'Mechanical Properties from the INV6 Closure for Short-Fiber Suspensions', SPE ANTEC 2006, Charlotte, North Carolina, May 7-11, 2006.

4. Jack, D.A. *Advanced Analysis of Short-Fiber Polymer Composite Material Behavior with Higher-order Orientation Tensor Closure Methods*. PhD thesis, University of Missouri - Columbia, December 2006.

5. D.E. Smith, M.T. Grimshaw, and D.A. Jack, 'Incorporating Higher Order Tensors in the Computation of Polymer Composite Mechanical Properties', Poster presentation at the *2006 NSF Design, Service and Manufacturing Grantees and Research Conference*, St. Louis, Missouri, July 24-27, 2006.

N. Linking Process-Induced Properties to Thermoplastic-Matrix Woven-Fabric Composites Performance

Principal Investigator: James A. Sherwood
Department of Mechanical Engineering
University of Massachusetts Lowell
One University Avenue
Lowell, MA 01854
(978) 934-3313; fax:(978) 945-5701; e-mail: James_Sherwood@uml.edu

Co-Principal Investigators: Julie Chen, Larissa Gorbatikh
Department of Mechanical Engineering
University of Massachusetts Lowell
Lowell, MA 01854
(978) 934-2992; fax (978) 934-3048; e-mail: Julie_Chen@uml.edu

Technology Area Development Manager: Joseph A. Carpenter
(202) 586-1022; fax: (202) 586-1600; e-mail: joseph.carpenter@ee.doe.gov

Expert Technical Monitor: Philip S. Sklad
(865) 574-5069; fax: (865) 576-4963; e-mail: skladps@ornl.gov

---

Contractor: University of Massachusetts Lowell
National Science Foundation Contract No. DMI-0522923, jointly funded by NSF and DOE

Introduction

Modeling of the in-service performance of thermoplastic-matrix woven-fabric-reinforced structural composites – e.g., damage tolerance, crashworthiness, vibration – is currently inadequate for parts of any geometric complexity because of the inability of existing performance models to capture the true deformed material properties. As a result, lightweight composite materials are utilized inefficiently or not at all; alternatively, extensive experimental trial and error or design of experiments must be conducted to develop a satisfactory product. The key to addressing this barrier is to provide a direct link between part geometry, material selection, process conditions, process-induced local properties, and part performance, allowing informed feedback to the design process.

Fiber-reinforced thermoplastic composites have a variety of applications including structural components in automotive, aerospace, marine, infrastructure and recreation industries. The main advantage of these composites over metals is their high specific strength. They also have other beneficial properties including low thermal expansion and good corrosion resistance when compared to metals. Woven fabrics offer many other advantages when compared to metals in terms of deformation capabilities, including dimensional stability, good conformability, and deep-draw shapability. Compared to nonwoven-fabric composites, the woven-fabric composites provide more balanced properties, higher impact resistance, easier handling and lower fabrication cost, particularly for parts with complex shapes.

The objective of this research is to utilize an integrated analytical, experimental, and numerical effort to attain a fundamental understanding of two governing physical phenomena – interlayer (fabric-fabric) friction and interconnected through-thickness and in-plane compaction. The former is important in multiple-layer and multiple-step forming, both needed for industrial processes. The latter is a critical factor affecting the final part thickness, void content, fiber orientation, and fiber distribution – all are important for structural stiffness and damage

tolerance. To validate and further demonstrate the capabilities of the integrated structure-process-performance design tool, the model will be used to identify critical process and material parameters for one particular performance model – damage tolerance. The funding for this research has only been available for six months, so the results reported here are very limited.

In Section 2, a combined inter-tow friction model, developed in a previous NSF-funded research program (DMII-0331267), based on the equilibrium equations of the unit cell of a balanced plain-weave glass/polypropylene woven fabric is extended to account for fiber compaction. To accomplish this extension of the model, fiber-compaction experiments have been completed and the results are reported here.

In Section 3, the design of a 3rd-generation friction-testing apparatus is presented. Previous research efforts used a constant-displacement control device to load the undeformed fabrics during the friction testing. While the information learned in these tests was invaluable in developing a fundamental understanding of the tool-fabric behavior, the 3rd-generation friction-testing apparatus will be a load-control device and will yield an even deeper fundamental understanding of the friction mechanisms by being able to study inter-layer friction between fabrics and tool/fabric friction on undeformed and deformed fabrics.

Analytical Modeling of the Shear Behavior of Woven-Fabric Composites

Trellis shear is considered the main deformation mode during the stamping process of woven-fabric composites [1]. Thus, the formability of woven-fabric composites is primarily a function of the shear properties of the woven fabric. Therefore, analytical models to obtain the shear properties of woven-fabric composites are very important for using the finite-element method for the modeling of the thermostamping process and for the designing of new fabrics.

A unit-cell model, which included (1) the key shear-deformation-resistant mechanisms, (2) the friction between the warp and weft yarns at every crossover, and (3) the lateral compaction between adjacent yarns, was developed by Liu *et al*. [2,3] to predict the shear properties of woven fabrics for the thermostamping process. In the model, some yarn parameters such as the yarn-to-yarn coefficient of friction μ, the fiber contact frequency ratio β, and the ideal maximum fiber volume fraction V_a, were chosen to develop an empirical model to fit the experimental data. Validation of those parameters is necessary to complete the unit-cell model.

The maximum yarn-fiber volume fraction V_a is an ideal limit to which fibers in a yarn can be compacted. As the yarn-fiber volume fraction approaches this maximum value, the stiffness in the transverse direction increases dramatically to approach the stiffness of the solid fiber material. According to the packing theory of uniform sizes of fibers, square packing corresponds to V_a of $\pi/4$ (or 0.785), and hexagonal packing results in a value of $\sqrt{3}\pi/6$ (or 0.907). Because the diameters of the polypropylene and glass fibers are different in the commingled polypropylene/glass yarn, the square packing theory is modified for the commingled fibers, and the obtained V_a equals to 0.813 [4].

In the plane-strain compression tests, 50-mm-long fiber bundles were placed in the channel fixture as shown in Fig. 1. A compressive force was applied perpendicular to the axial direction of the fibers (call this the z direction) using an Instron machine at a rate of 0.042 m/sec. Load and extension data were logged on a data-acquisition computer so that stress and strain in the z direction could be calculated. Because the transverse compliance can be also calculated in the fiber bundle model as a function of β, regression of the experimental data will give the mean value of β. In Fig. 2, the predicted and experimental values of the yarn transverse compliance S_{22} are compared for various values of β. The experimental results are obtained from the plane-strain compression tests for five layers of yarns as described by [5]. From Fig. 2, it can be seen that the values of β are in the range from 150 to 175 for the commingled polypropylene and glass yarns.

To investigate the sensitivity of the model to the yarn input parameters such as the maximum fiber volume fraction V_a, the fiber contact ratio β and the yarn-to-yarn coefficient of friction μ, a parametric

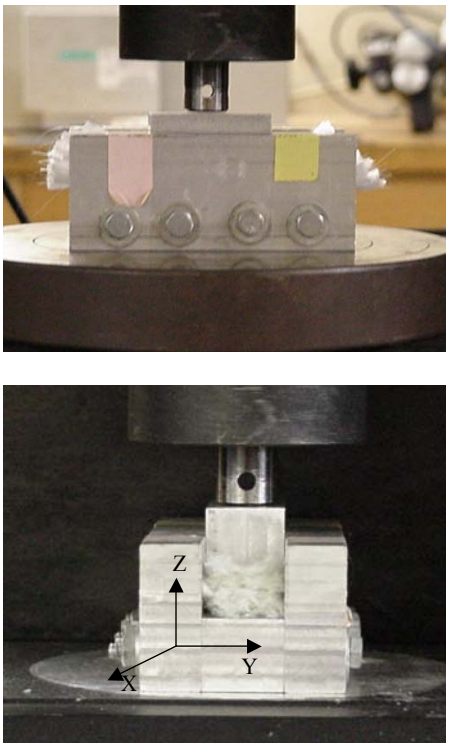

Figure 1. Plane-strain compression test fixture [5].

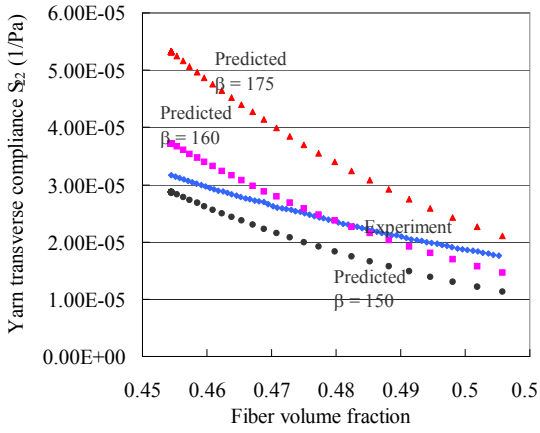

Figure 2. Comparison of the values of S_{22} obtained from the plane-strain compression tests and the fiber bundle modeling [5].

study was conducted. To separate the individual contributions from friction and lateral compaction, intermediate models were studied separately, i.e., the lateral compaction resistant moment was set to be zero to study the coefficient of friction, while in the study of β and V_a, the friction resistant moment was set to be zero in the equilibrium equation.

Fig. 3 shows the results of the simulation of β varying from 150 to 175. In the figure, it can be seen that as the value of β decreases, the shear load increases. The loads increase because at relatively low values of β, the yarn stiffness in the transverse direction increases due to increased fiber bending. As shown in Fig. 4, decreasing the value of V_a has a similar effect because, with relatively low values of V_a, yarn stiffness in the transverse direction increases due to decreased space for compaction.

Thus, with the main parameters all validated, the developed analytical model can be used to predict the shear properties of woven-fabric composites and reduce or eliminate the need for curve fitting of fabric-level experimental data.

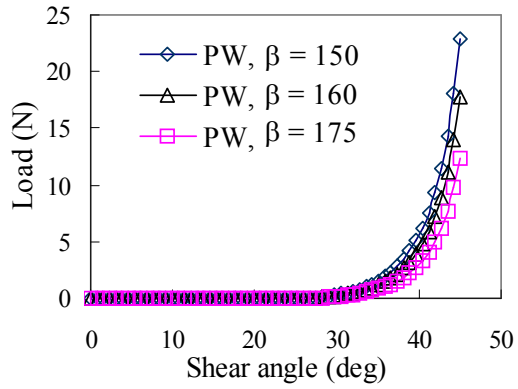

Figure 3. Simulation of the fiber contact frequency ratio.

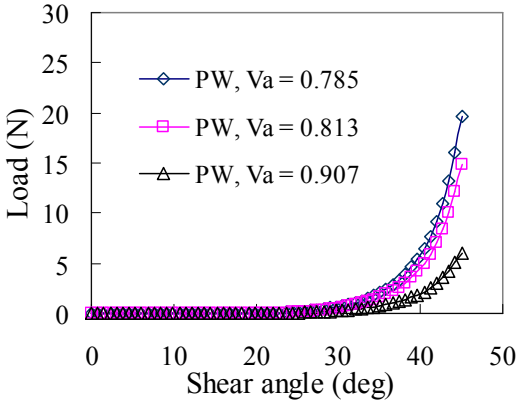

Figure 4. Simulation of the maximum fiber volume fraction.

Friction Behavior Composite between the Metal Tool and the Woven-Fabric and Inter-Layer Shear

Past research has led to advances in a user-defined friction subroutine for use in finite-element applications. The Stribeck curve (Fig. 5 [6]) and the Hersey number, *H*, (Eqn. 1) were used to predict the friction coefficient for the ranges of velocities and normal forces studied.

$$H = \frac{\eta \cdot U}{N} \qquad (1)$$

where η is the viscosity, U is the fabric velocity and N is the normal force.

The results of the study conducted by Gorczyca [7] showed that the velocity of the fabric, tool temperature, and applied normal force have the greatest effects on the friction coefficient. From these results she developed a model that relates the friction coefficient to the Hersey number, shown in Eqn. 2:

$$\mu = (6.1191 \cdot H + 0.2718) - \mu_{\upsilon} \qquad (2)$$

where μ_{υ} is a scaling term included for the effects of the tool temperature.

The results from testing such fabrics will be analyzed for their applicability to the relationship between the coefficient of friction and the Stribeck curve, as developed by Gorczyca [7,8] and Chow [9]. The design of a 3rd-generation friction-testing apparatus aims to overcome past limitations, and to enhance the characterization of not only the commingled glass-polypropylene plain-weave fabric, but also other types of fabrics involved in an international benchmarking study, as shown in Fig. 6.

Previous research focused on the static coefficient of friction [7-9]. The method of normal force application used in that research was displacement controlled. It was found that during a typical friction test the normal force applied to the fabric surface decreases, as shown in Fig. 7.

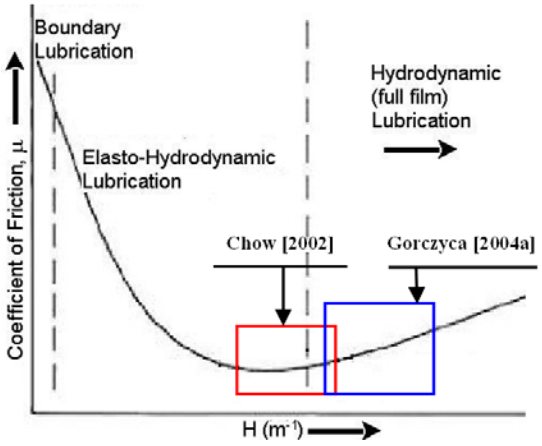

Figure 5. The Stribeck Curve and areas of interest pertaining to current research [6].

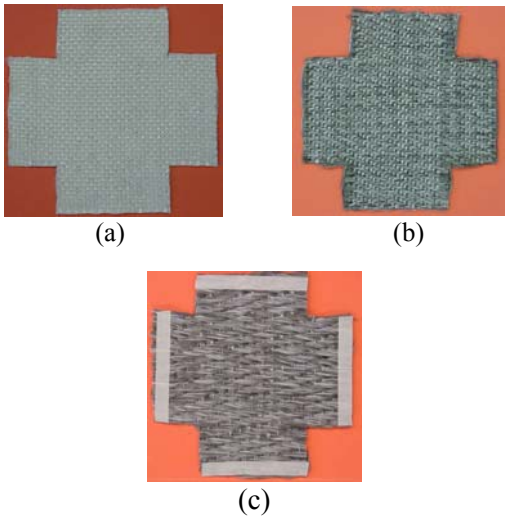

Figure 6. Fabric used during international benchmark activity: (a) Balanced plain weave (PW); (b) Balanced twill weave (TW); (c) Unbalanced twill weave (UTW).

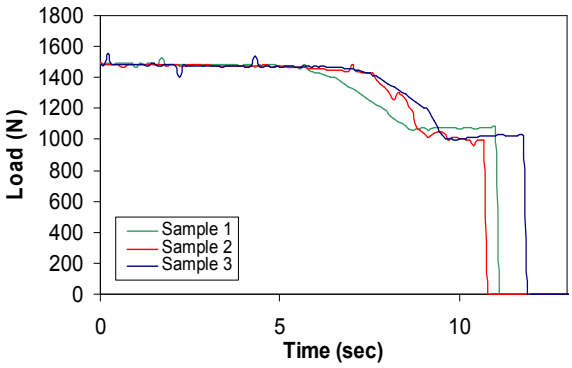

Figure 7. Normal force decrease over time for displacement controlled test of commingled glass-polypropylene plain-weave fabric.

For the tests shown in Fig. 7, the initial applied load was approximately 1500 N. The applied normal force dropped by approximately 400 to 450 N over the duration of the test. The mechanisms behind this decrease in normal force are fabric nesting and tow compaction. The fabric tows adjust their position as the adjacent layers of fabric nest, tow undulation decreases and fibers compact due to the combination of heat and pressure. Any one or more of these mechanisms causes a slight change in the displacement necessary to maintain the desired normal force.

Due to the drop in normal force, only the static coefficient of friction, which is the value obtained at the first instant of fabric movement, can be reliably quantified. Understanding the dynamic coefficient of friction may lead to a model that more accurately represents the frictional relationship by encompassing the behavior over the entire duration of the thermostamping process. To gain the ability to determine the dynamic coefficient of friction, a force- or pressure- controlled application mechanism is being constructed. The force-controlled mechanism consists of a pneumatic air-spring actuator and a closed-loop control algorithm to continuously monitor and regulate the magnitude of force applied to the fabric surface throughout the duration of the test.

Further considerations in the development of test criteria involve investigating the effects of tow orientation on the friction coefficient. During the thermostamping process, as the punch draws the fabric into the die, the tows rotate to assume the shape of the mating members due to the restrictions placed by the binder ring. This mechanism is referred to as trellis deformation and is shown in Fig. 8.

For the stamping of a hemisphere with a plain-weave fabric (as shown in Fig. 8) the tows are initially oriented 90° from one another, and this angle decreases as the part is stamped. The significance of the effect of tow orientation will be investigated for possible incorporation into the friction subroutine of the finite-element analysis of woven-fabric composite forming behavior.

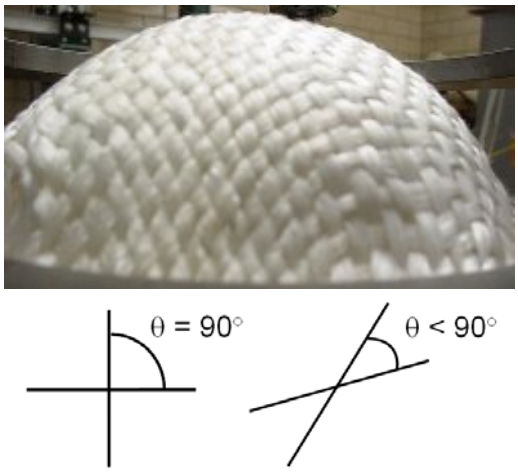

Figure 8. Trellis deformation of a stamped hemisphere.

Additional considerations for the 3rd-generation friction-testing apparatus include the development of a stand-alone test machine. The limiting factor for the current mechanism that withdraws the fabric from between the pressure plates is its dependence on the Instron testing machine. In addition, integrating all fabric movement into one test apparatus will minimize travel time from the oven, therefore reducing any cooling effects as the fabric is transferred. Fig. 9 shows a schematic of the complete proposed 3rd-generation friction-testing apparatus.

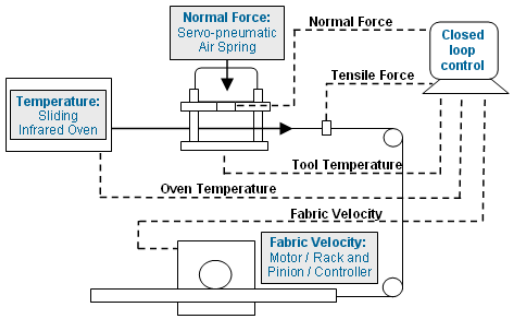

Figure 9. Schematic representation of the 3rd generation friction test apparatus.

Conclusions

Yarn and fiber parameters were investigated and their ability to model the compaction behavior of commingled fibers has been demonstrated by their influence on the resulting shear load-deformation curve. A new friction-test apparatus is under development with a load-control method to apply the normal force to the surface of the fabric,

allowing the dynamic coefficient of friction to be quantified. The new design will overcome past limitations identified by previous research and enhance characterization of tool-fabric and fabric-fabric friction coefficients. The analysis of the friction interface will also be extended to the effects of tow orientation as well as to the analysis of the fabrics involved in an international benchmark study. These research tasks are enhancing the fundamental understanding of the mechanical behavior of the commingled fiberglass/ polypropylene woven fabrics and the development of a design tool linking the process-induced properties to the modeling of the in-service performance of thermoplastic composites. To validate and further demonstrate the capabilities of the integrated structure-process-performance design tool, the model will be used to identify critical process and material parameters for one particular performance model – damage tolerance.

Acknowledgements

The authors would like to thank the NSF Division of Design, Manufacture, and Industrial Innovation (DMI #0522923) and Ford Motor Company (Dr. Patrick Blanchard) for their support of this research. The letter of support from General Motors for the grant proposal is also appreciated. The contributions of Dr. Lu Liu, UMass-Lowell graduate and post doc, and MSME candidate Lisa Gamache are appreciated.

References

1. A.E. Long, C.D. Rudd, M. Blagdon, and P. Smith, "Characterizing the processing and performance of aligned reinforcements during perform manufacture," *Composites Part A,* vol. 27A, pp. 247-53, 1996.

2. L. Liu, J. Chen, X. Li, and J.A. Sherwood, "A two dimension macro-mechanics shear model of woven fabrics," *Composite Part A*, vol. 36, pp. 105-114, 2005.

3. L. Liu, J. Chen, J. Gorczyca, and J. Sherwood, "Modeling of friction and shear in thermostamping of composites – part II," *Journal of Composite Materials*, vol. 38, pp. 1931-1947, 2004.

4. L. Liu, J. Chen, and J. Sherwood, "Analytical model of shear of 4-harness satin weave fabrics," American Institute of Physics Proceedings 712, 8th NUMIFORM Technical Conference, June 13-17, Columbus, OH, 2004.

5. A. Bulusu, Modeling of Architecture and Deformation of Dry Woven Fabrics during Shear, MS Thesis, Department of Mechanical Engineering, University of Massachusetts Lowell, Lowell, MA, 2001.

6. I.M. Hutchings, Tribology: Friction and Wear of Engineering Materials, CRC Press, Ann Arbor, MI, 2002.

7. J. Gorczyca, A Study of the Frictional Behavior of a Plain-Weave Fabric during the Thermostamping Process, Doctoral Dissertation, Department of Mechanical Engineering, University of Massachusetts Lowell, Lowell, MA, 2004.

8. J. Gorczyca, J. Sherwood, L. Liu, L. and J. Chen, "Modeling of friction and shear in thermostamping of composites – part I," *Journal of Composite Materials*, vol. 38, pp. 1911-1929. 2004.

9. S. Chow, Frictional Interaction between Blank Holder and Fabric in Stamping of Woven Thermoplastic Composites, MS Thesis, Department of Mechanical Engineering, University of Massachusetts Lowell; Lowell, MA, 2002.

O. Comparative Determinations of Orientation in Injection-Molded Thermotropic Liquid-Crystalline Copolyester (TLCP) Plaques

Principal Investigator: Robert A. Bubeck, Ph.D.
Michigan Molecular Institute
1910 West St. Andrews Road
Midland, MI 48640
(989) 832-5555; fax: (989) 832-5560; e-mail: bubeck@mmi.org

Principal Investigator: Wesley R. Burghardt, Ph.D.
Department of Chemical & Biological Engineering
Northwestern University
2145 Sheridan Road, Room E136
Evanston, IL 60208
(847) 467-1401; fax: (847) 491-3728; e-mail: w-burghardt@northwestern.edu

---

Contractor: Northwestern University and Michigan Molecular Institute
Contract No.: #0521823

Introduction

Thermotropic liquid-crystalline polymers (TLCPs) combine the virtues of superior tensile properties with the ability to injection mold with very easy flow through the spontaneous ordering of molecules. These attributes are keys to the use of these materials in high-performance electrical connectors for which the attainment of high physical properties in one dimension is a key requirement. A critical processing issue is the development of high anisotropy during TLCP processing. Although the concurrence of high tensile properties and high directional orientation is of great benefit in fiber spinning, severe anisotropy can be a plague in obtaining balanced properties in net-shape injection-molded parts. The rigid nature of the mesogenic segments in TLCP molecules usually leads directly to a high orientational bias favoring the direction of flow with injection molding and other directional processing of thermotropes [1,2]. Upon recrystallization, the high molecular orientation often leads to very favorable properties in the direction of orientation and lower physical properties in the transverse direction.

Characterizations were previously performed for the direction of greatest strength in relatively narrow injection-molded tensile bars fabricated from Celanese VECTRA® 6-hydroxy-2-naphthoic acid/ 6-hydroxyben-zoic acid (HBA/HNA) type-copolyesters by Dreher, et al. [3] These researchers showed that tensile modulus increases linearly with the Hermans orientation function. Molding a plaque or other part with a broad aspect ratio, however, will incur much greater flow complexity and, therefore, more complex states of orientation. Shear flow dominates near the surface while transverse stretching dominates near the mid-plane, [4] resulting in bimodal cross-ply orientation, as schematically shown in Figure 1. Depending upon thickness, a "skin/core" structure also results with a high molecular alignment in the "skin" that may be maximized in a direction different from that in the "core." Shear asserts increasing dominance with decreasing sample thickness. Accordingly, the emphasis in this study concerns the molding of plaques under a systematic set of conditions and thicknesses, and then characterizing the resulting bimodal orientations. Near-edge x-ray absorption fine structure (NEXAFS) was used to determine the molecular orientation in the near surface (2 nm deep). Two-dimensional wide-angle x-ray scattering (2-D WAXS) in transmission was used to determine *average* orientations of the "skin" and "core" layers and their directions of greatest magnitude by performing, when necessary, deconvolution of the scattering associated with the bimodal contributions from the "skin" and "core" layers. The results from NEXAFS and 2-D WAXS were then compared to define the state of orientation in the plaques.

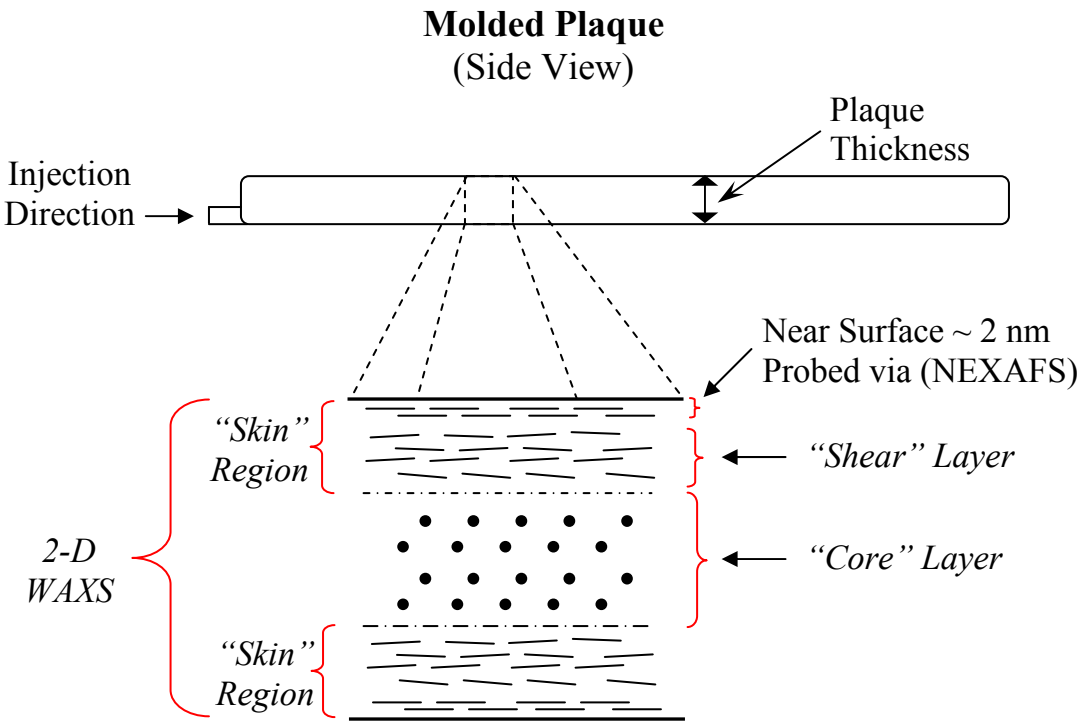

Figure 1. Idealized representation of an injection-molded plaque cross-section illustrating the various levels of morphology present along the plaque thickness direction. 2-D WAXS in transmission averages structural information through the sample thickness while NEXAFS probes molecular orientation over depths of 2 to 3 nm in the near surface layer.

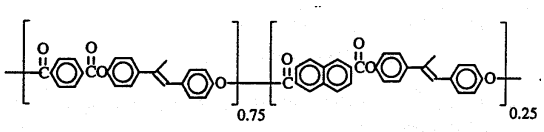

Figure 2. Copolyester of 4, 4'-dihydroxy-α-methylstilbene (DHαMS).

Experimental

Materials and Fabrication: The TLCP utilized in this study is a copolyester containing 4,4'-dihydroxy-α-methylstilbene (DHαMS) as the mesogen and a terephthalate/isophthalate/2,6–naphthalenedicarboxylate molar ratio of 65/10/25.[5] The chemical structure for the TLCP based upon DHαMS is shown in Figure 2. Sample plaques were fabricated using a Boy 30T2 injection-molding machine with which both melt and mold temperatures were readily controlled. The plaques fabricated for the results presented in this paper measure 76 mm x 76 mm and were molded with a coat-hanger gate. An insert mold with polished faces was utilized permitting the fabrication of plaques of various thicknesses from 0.8 mm to 3.2 mm. Polymers with molecular weights of about 35,000 g/mol were evaluated. Usually "fast" fill times of 1 s were utilized, but some additional molding performed at a "slow" 5 s. It was ascertained that the samples required surface cleaning to remove contaminants before the NEXAFS examination. The cleaning was performed using a 1% solution in de-ionized water of Alconox Liqui-Nox® cleaning agent with a Bransonic 220

ultrasonic cleaner for a duration of 10 min. Both the initial presence of contaminants and their effective removal were verified for selected samples by atomic-force microscopy (AFM) using a Topometrix 2000 AFM.

Near-Edge X-ray Absorption Fine Structure Determinations of Surface Orientation: As is apparent from the previous discussion, the contribution to the orientation of the skin layer is difficult to deconvolute from that of the core of a molding. Plummer et al. [6] and Dreher and coworkers [3] attempted to qualitatively determine the skin orientation in TLCP moldings using WAXS of microtomed layers. Layer orientation in injection-molded plaques of 6-hydroxy-2-naphthoic acid/6-hydroxybenzoic acid (HNA/HBA) (58 mol % HBA and 42 mol % HNA) random type copolyesters was determined by Pirnia and Sung [7] using Fourier transform infrared (FT-IR) attenuated total reflection (ATR) dichroism. This technique enabled these researchers to determine relative orientation encompassing a depth of material 5 μm below the sample surface. Using measured dichotic ratios to calculate the orientation parameter, the skin, intermediate layers and core were characterized for a series of samples cut from positions along injection-molded plaques by progressively removing material by milling. An alternate, less laborious, and less intrusive means, however, of determining surface orientation with a much smaller "footprint" (~1 mm^2) presents itself in the form of NEXAFS.

NEXAFS is a synchrotron source soft x-ray spectroscopy technique that is sensitive to the orientation of phenyl groups in the direction of melt flow via the intensity, I, of the partial electron yield (*PEY*) of Auger electrons of 1s → π* transition of the C=C bonds in the C K edge. The technique using *PEY* is sensitive to the top 2 nm of a surface. The orientation is determined through a series of measurements of the C K edge spectrum over a range of incident angles, θ, (20°, 30°, 40°, 55°, 60°, 70°, 80°, and 90°) of a monochromated linearly-polarized ultarviolet (UV) beam relative to the sample surface. This technique has been successfully used to determine the orientation of LC alignment on rubbed polyimide substrates by Stöhr and Samant [8] and by Pattison et al. [9] The NEXAFS was performed on the NIST/Dow Soft X-ray Materials Characterization Facility, U7A, at the National Synchrotron Light Source, Brookhaven National Labs. Using the technique of Stöhr and Samant, the *PEY* intensity *I(θ)* is predicted to take the form:

$$I(\theta) = A + B\sin^2\theta \qquad (1)$$

regardless of the degree of orientation. Based on the method by Kramer recently published by Pattison et al., [9] the molecular orientation parameter, $S_{Surface}$, was calculated using:

$$S_{Surface} = \left(1 - \frac{2(A+B)}{A + \frac{B}{6P}(3P-1)}\right) \qquad (2)$$

where, *P* is the beam polarization (0.85 in this case).

2-D WAXS Data and Analysis Procedure of Injection-Molded Plaques: An orientation map for each plaque type was determined by 2-D WAXS performed at 20 keV (0.62 Å) for multiple positions on the samples using the 5BM beam line of the DuPont/Northwestern University/Dow Collaborative Access Team at the Advanced Photon Source of Argonne National Lab. An incident x-ray beam with a 1-mm-diameter size was used. A Mar CCD detector was used to collect 512 x 512 pixel raw x-ray scattering patterns with 15-second exposures. The WAXS patterns were obtained in positions corresponding to the grid shown in Figure 3. Although this information is very useful, there are significant bimodal contributions from both the core and the skin in the WAXS patterns obtained for the thicker plaques, examples of which are shown in Figures 3 and 4.

Details of the data analysis techniques employed are given by Rendon, et al. [10] The following section contains a simplified summary. The 2-D WAXS patterns usually indicate the presence of two discrete populations of orientation: one parallel to the flow direction and the other transverse to the flow direction. As evidenced in all of the patterns, nematic crystalline peaks always diffract perpendicular to the orientation direction. Scans made along this horizontal region of the plaque suggest the dominance of transverse-orientation modes relative to shear-flow modes manifested by

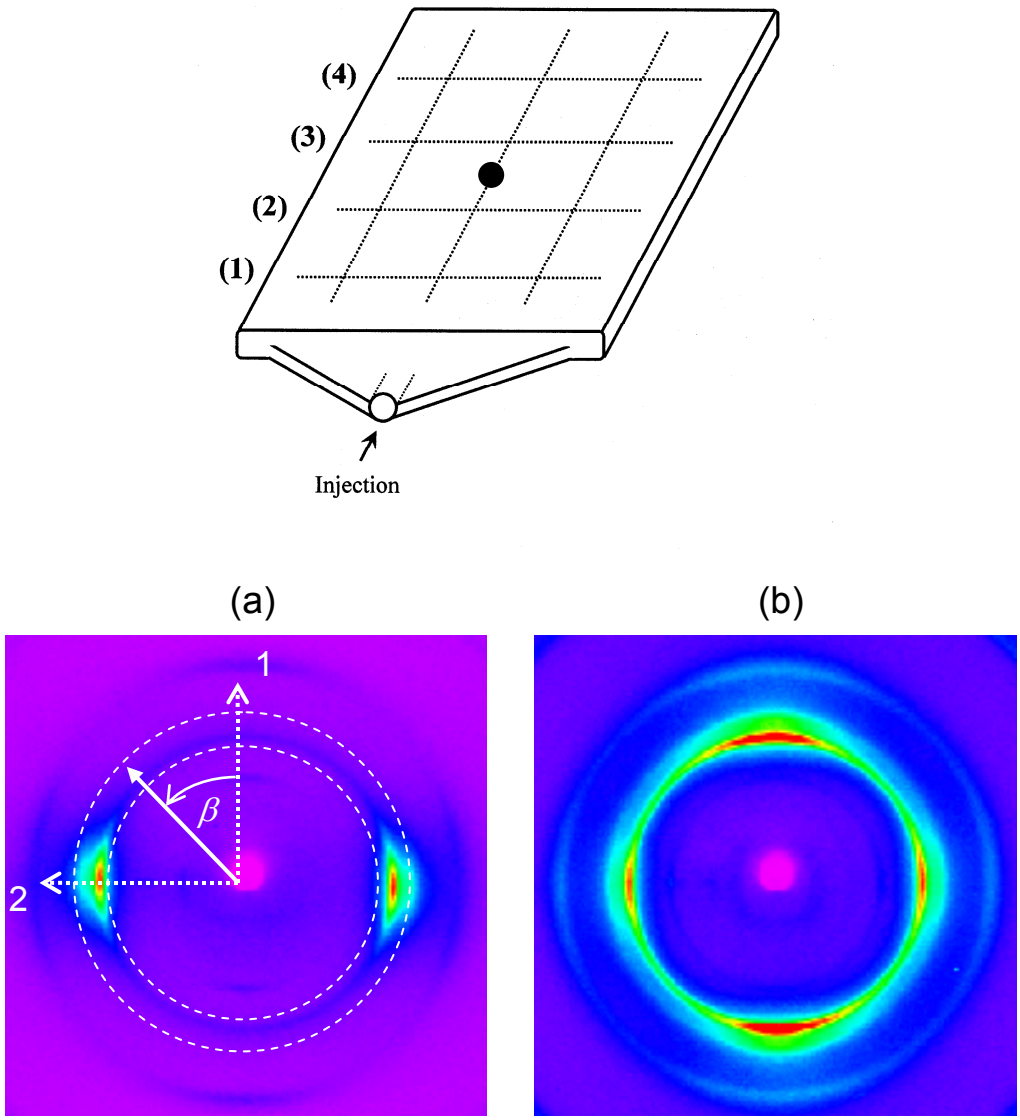

Figure 3. Physical orientation of an injection-molded plaque along with two representative 2-D WAXS patterns taken for a centerline position of a: (a) 0.8-mm-thick molded plaque showing uniaxial contribution to the orientation due to shear flow and a (b) 3.2-mm-thick plaque showing bimodal orientation populations due to shear and extension. The arrow indicates the principal direction of flow. The plaque examples were processed at constant fast fill time of 1 s with melt and mold temperatures of 270°C and 45°C, respectively. The overlays in (a) define the coordinates and range of the scattering wave vector, q, used for the extraction of azimuthal scans; β is the azimuthal angle measured away from the vertical filling direction. Dotted lines indicate the path locations where 2-D WAXS measurements were performed 15 mm apart.

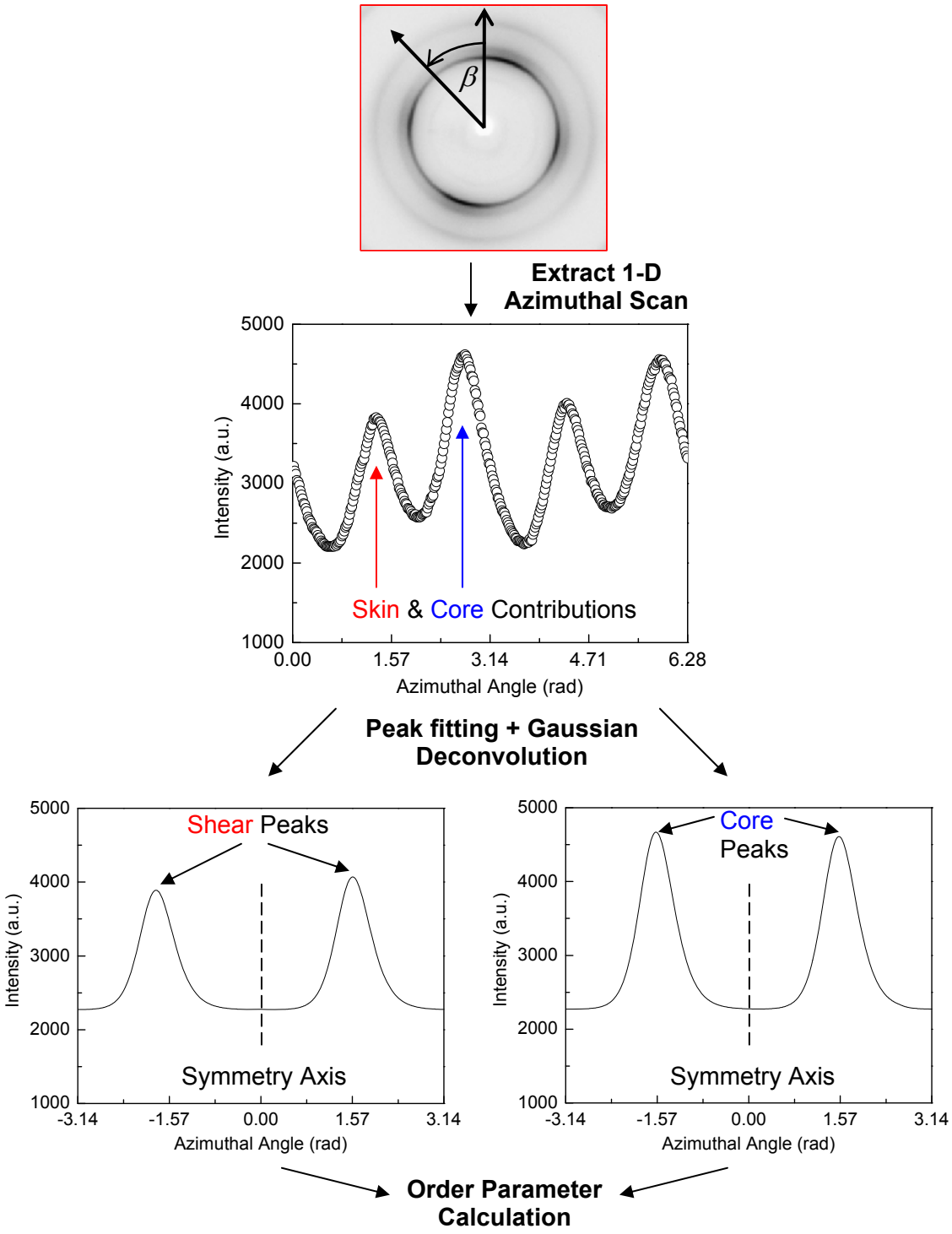

Figure 4. Data analysis procedure used to extract azimuthal intensity scans describing the scattering contributions due to shear ('skin') and extension ('core'). Two $I(\beta)$ scans are extracted from a single 1-D 'bulk' sample azimuthal scan via a Gaussian deconvolution of azimuthal intensity peaks. Resulting scans are subsequently processed to compute S_{Shear} and S_{Core}.

strong crystalline peaks, which are indicative of higher degrees of molecular orientation. Away from the centerline position, the bimodal character switches direction indicating that the transverse mode has rotated relative to molecular orientation at the centerline.

An assumption of uniaxial orientation is not appropriate when studying complex flow kinematics where both shear and extensional flows occur across the entire thickness of the sample. In order to obtain a quantitative measure of orientation, azimuthal intensity scans were extracted from 2-D scattering patterns at the scattering vector *q* location of the nematic crystalline peaks. Because of the crystalline nature of the peaks, selecting a relatively narrow *q* range of intensity was sufficient in maximizing the intensity available for computing azimuthal scans. Background subtraction was performed on the WAXS patterns for each plaque. The baseline correction values correspond to the lowest value of intensity observed for the experiment with the highest degree of molecular orientation. Each measurement is an average of all structure levels that the beam encounters when passing through the thickness of the plaque or slit-flow channel in the case of steady isothermal flows.

Quantitative determination of skin, core, and bulk degrees of molecular orientation in molded plaques involved computing order parameters from azimuthal intensity scans extracted from 2D WAXS patterns collected in transmission. Because 1D azimuthal scans contain information averaged through the entire plaque sample thickness, 'skin' and 'core' contributions to the orientation must be computed separately, as shown in Figure 5. Herman's order parameters that reflect the localized *skin* contribution to the bulk molecular orientation are computed from 1D azimuthal intensity scans that only contain peak information due to *shear flow*. Similarly, localized *core* contributions to the bulk molecular orientation are computed from azimuthal scans which only contain peak information due to transverse extension. These azimuthal scans are generated by applying a Gaussian deconvolution method (using a software platform known as Peakfit®) to the original 'bulk' azimuthal intensity scan that effectively generates two different sets of intensity peaks (i.e., two new azimuthal scans) each containing information from either shear or transverse modes of orientation. Having done this, it is assumed that the uniaxial orientation to compute the corresponding order parameters can be based upon the Herman's convention, viz.,

$$S = \tfrac{1}{2}\left(3\cos^2\beta - 1\right) \qquad (3)$$

where the limit of perfect orientation this quantity yields a value of 1 and 0 indicates a randomized orientation state. The procedures are described further by Bubeck and co-workers [11].

Atomic force microscopy of plaque surfaces: AFM examinations were performed using a Topometrix 2000 in oscillating mode on the surfaces of a selected number of DHαMS copolyester plaques. Confirmation via AFM of the benefit of ultrasonic surface cleaning of surfaces intended for NEXAFS has already been mentioned in this section. Given that NEXAFS is a surface-spectroscopy technique, knowledge of the surface topology of the plaques does prove useful. The AFM revealed two principal topological features on the plaque surfaces: a fine texture on the order of 1 nm in height, and a much broader feature in the form of corrugations with low gradient slopes on the order of 8 nm in height and 200 nm in width at the base. The broad corrugations are aligned in the principal direction of flow. Neither feature was deemed likely to significantly interfere with the NEXAFS measurements.

Results and Discussion

An example of a set of NEXAFS C K edge spectra for the surface skin of an injection molded plaque is shown in Figure 5. The spectra were measured as a function of incident angle of the UV beam relative to the sample surface. The sample was cut from the middle of the vent-end edge of a plaque molded with a melt temperature of 245ºC and a mold temperature of 45ºC. The π (C=C) peaks from the in-plane C=C bonds are minimized when the polarized UV beam is perpendicular to the surface and the complementary σ orbital peaks are correspondingly maximized. This result is consistent with molecular alignment in the plane of the plaque skin. The intensity of the $\pi^*(C{=}C)_1$ peak varies linearly with $\sin^2$ of the incident angle, θ, an example of which is shown in Figure 6. Using the resulting intercept *A*

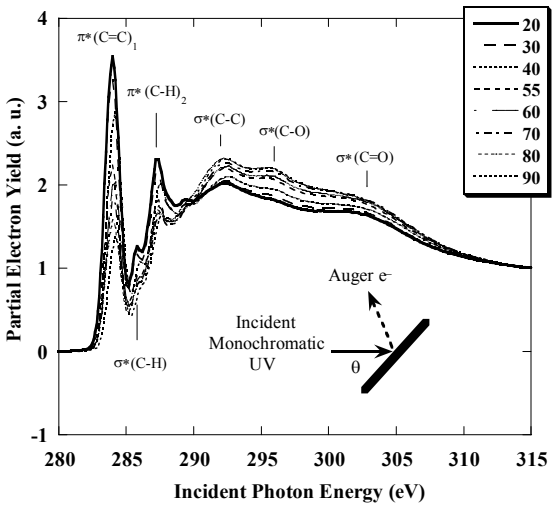

Figure 5. Representative NEXAFS C K edge spectra for a DHαMS copolyester plaque surface. Spectra collected at varying angle of incident beam relative to the surface. Beam polarization is aligned with the direction of maximum orientation. Process parameters: melt temperature = 290°C, mold temperature = 45°C.

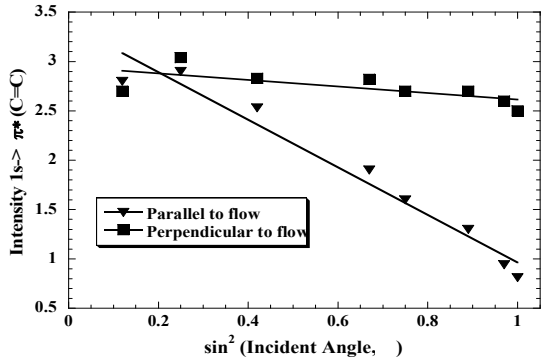

Figure 6. Analysis of C=C π* absorption intensity dependence on incident angle, from which molecular order parameter in surface region may be extracted. Angular dependence of resonance is shown parallel and perpendicular to the principal direction of shear flow at the surface. Beam polarization was aligned parallel and, then, perpendicular to the principal flow direction to obtain the two sets of data.

and slope B of $I(\theta)$ versus $\sin^2\theta$ using equations 1 and 2 permits the determination of molecular order parameter, $S_{Surface}$. The nearly flat slope for the case of orientation perpendicular to the flow direction indicates that the surface orientation of the molecules in the plane is predominantly nematic uniaxial. Order parameters derived from the NEXAFS analyses were found to be greatest along the centerline of the plaques and typically range from about 0.70 to 0.85 depending on position and processing conditions. The most consistent results are obtained for very smooth surfaces that retain the polish finish of the mold faces and when the 20° incident angle spectrum is omitted from the calculation of $S_{Surface}$.

The following discussion of results proceeds from relatively simple cases of flow-induced surface orientation along sample center lines in plaques that are coat-hanger gated to the more complex cases involving orientation states away from the centerline and with a narrow gate. The plaques are 72 mm x 72 mm and were injection-molded with a tool fitted with a "coat-hanger" gate, which permits a relatively even flow of polymer into the mold. This configuration was chosen in order to study less complex filling conditions and to be a source of plaques from which tensile samples with relatively simple orientation states could be machined and mechanically characterized. The mechanical data for these plaques has been reported elsewhere. [12] Tensile modulus and fracture stress were found to obey a 'universal' correlation called an anisotropy factor (*AF*) derived from 2-D WAXS measurements of molecular orientation projected onto the axis of the tensile specimens.

NEXAFS examination made along the center line of four plaques is reported in terms of molecular orientation of the near-surfaces. The effect of mold temperature on surface orientation is shown in Figures 7a and 7b for two melt temperatures. At a melt temperature of 290°C, orientation parameter $S_{Surface}$ ranges from about 10 to 20 percent more for a 45°C mold temperature than for a 90°C mold temperature – a result which is consistent with what one might expect as a result with more rapid cooling and crystallization derived from the colder mold. If a more unusual melt temperature of 245°C is chosen at the low end of the melting transition, then the relative orientations obtained for the same two mold temperatures reverse their ranking for retained surface orientation. The higher mold temperature is required to obtain relatively uniform orientation for the four plaque positions, particularly on the gated end (Position 1).

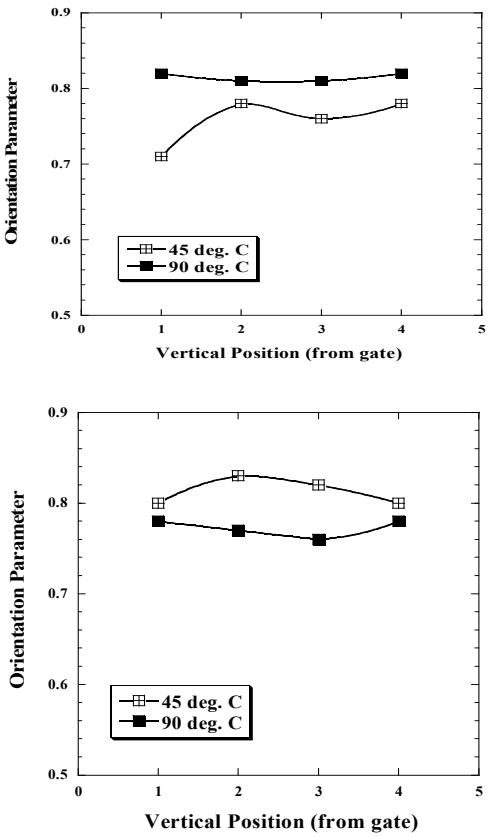

Figure 7. A comparison of orientation parameters *S* for two mold and two melt temperatures derived from the NEXAFS method as a function of vertical position from the gate in the centerline of two 1.6 mm thick injection molded 76 mm x 76 mm DHαMS plaques. (a) Conditions: 290°C melt temperature; 45°C and 90°C mold temperatures. (b) Conditions: 245°C melt temperature; 45°C and 90°C mold temperatures. The numbered positions correspond to those indicated in Figure 3.

Results obtained off from the centerline for a series of six plaques are covered in the following discussion. Figure 8 consists of an example 2-D WAXS pattern for one of the plaques (plaque no. 1), a surface orientation map derived from the 2-D WAXS, and a plot of slope *B* versus azimuthal angle derived from multiple NEXAFS measurements taken at the position indicated aside from the center line. The molecular orientation parameter $S_{Surface}$ is indicated for the maximum slope. The position is nearly equidistant between the gate and vent edges and the centerline and the side edge. Arrows in the 2-D WAXS pattern indicate scattering contributions due to "skin" shearing kinetics and mid-plane extension in the "core" associated with melt flow. The surface orientations obtained by 2-D WAXS are shown in a surface orientation map of the plaque and the angle of maximum surface orientation is indicated. The processing conditions and thicknesses, and values of corresponding values of *S*, as determined by 2-D WAXS and NEXAFS, are summarized in Table 1. Also included are: the azimuthal rotation angle ϕ_{max} associated with the maximum surface molecular orientation from NEXAFS; and the azimuthal angle ϕ_{max} indicative of the average orientation direction in the "skin" region, as determined by WAXS.

The results for plaques nos. 1 and 2 are tabulated for nearly identical processing conditions (45°C mold temperature, 1.6 mm plaque thickness, and 1 s fill time), the only difference being the melt temperature (290°C versus 270°C). The nominal peak melting point for the TCLP was 290°C in a broad melting range of 240°C to 300°C. The principal loss of orientation associated with the 20°C decrease in melt temperature was realized in the core where extensional flow dominates. Corresponding decreases in mechanical properties in the direction of maximum orientation have also been observed with the decrease in melt temperature. The molecular orientation on the near-surface $S_{Surface}$ about 2 to 3 nm deep decreased slightly (0.80 vs. 0.76) with the melt temperature decrease while S_{Shear} was more greatly affected (0.55 vs. 0.48), reflecting the fact that the WAXS results from orientation averaged over a much greater thickness into the sample than does NEXAFS.

Halving the thickness for plaque no. 3 to 0.8 mm and maintaining a melt temperature of 270°C resulted in an overall increase in S_{Shear} from 0.48 to 0.66, but no change in molecular orientation $S_{Surface}$ at the near-surface. The orientation in the core S_{Core} became essentially equivalent with S_{Shear} because the filling flow in general at the thickness is dominated by shear. The molecular orientation at the near surface (2 nm to 3 nm deep) was observed to decrease slightly from 0.76 to 0.74. Doubling the thickness for plaque no. 4 from 1.6 mm to 3.2 mm resulted in a sharp decrease in the molecular orientation of the "skin," but with much less influence on the near surface orientation. Shear flow

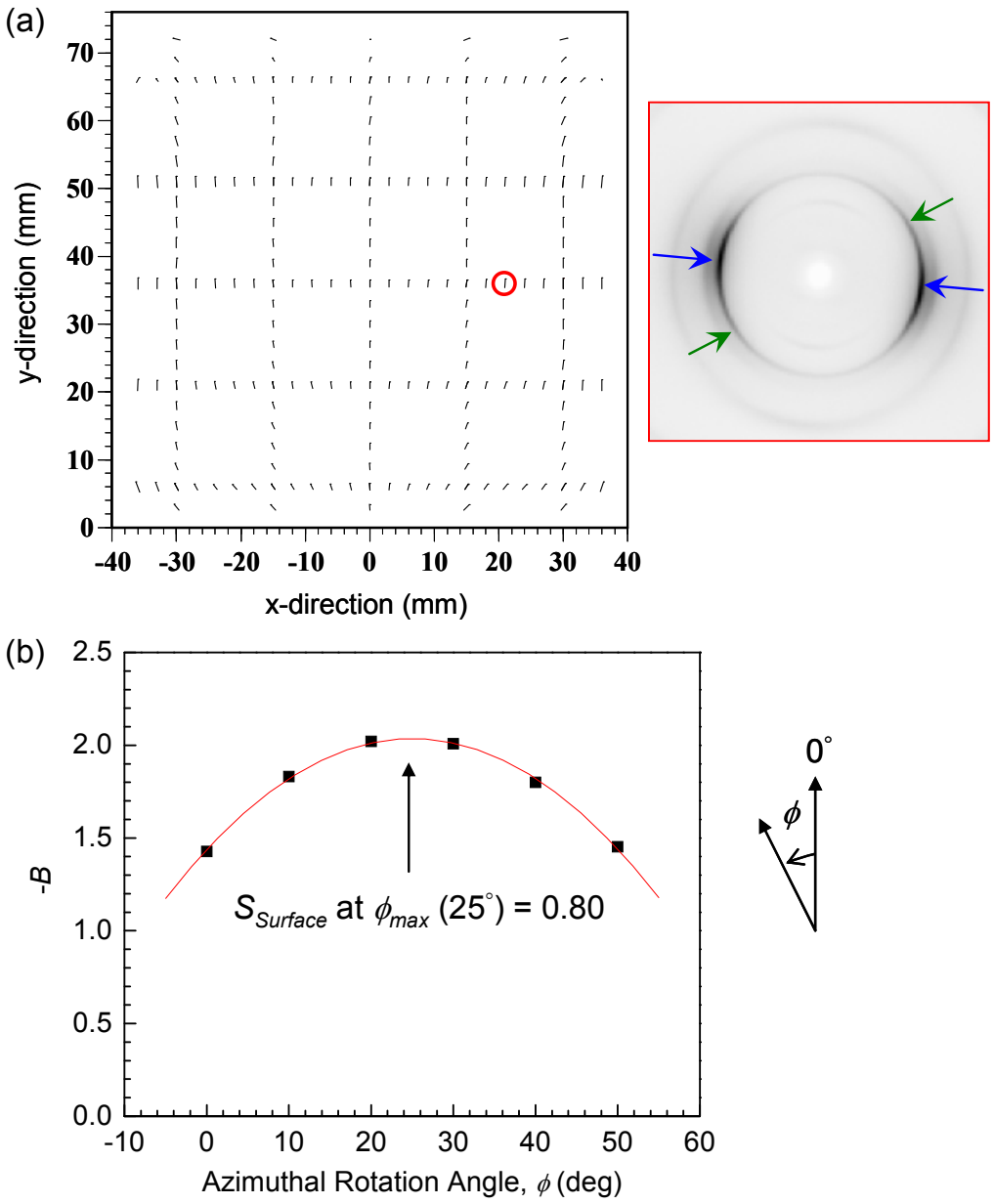

Figure 8. WAXS and NEXAFS characterization of an example 1.6 mm thick DHαMS plaque. (a) Vector plot representation of molecular orientation using the second-moment tensor description of anisotropy and the average orientation direction (See Refs. 10 and 12). The x-ray pattern was collected at the specified sample position (on vector plot) where WAXS and NEXAFS measurements were performed. *Blue* arrows in the x-ray pattern indicate scattering contribution due to "skin" shearing kinematics and *green* arrows indicate scattering contribution due to mid-plane extension in the "core." (b) Plot of the slope from $I(\theta)$ given in Equation 2 versus azimuthal rotation angle, ϕ. Maximum surface orientation ($S_{surface}$ = 0.80) was found for the example at ϕ_{max} = 25°. The sample was extracted from a plaque processed at 1 s fill time with melt and mold temperatures of 290°C and 45°C, respectively.

Table 1. Summary of molding conditions and resulting orientation parameters for 76 mm x 76 mm injection-molded plaques. [a]Near-surface molecular order parameter obtained by NEXAFS computed using Equations 1 and 2. [b]Order parameter obtained by WAXS describing the shear (or skin) contribution to the orientation. [c]Order parameter obtained by WAXS describing the core contribution to the orientation. [d]Azimuthal rotation angle associated with the maximum surface molecular orientation from NEXAFS. [e]Azimuthal angle indicative of the average orientation direction in the skin region as determined by WAXS.

Plaque No.	Thickness (mm)	T_{melt} (°C)	T_{mold} (°C)	Fill rate (s)	$^{a}S_{Surface}$	$^{b}S_{Shear}$	$^{c}S_{Core}$	$^{d}\phi_{max}$ (deg)	$^{e}\beta_{max}$ (deg)
1	1.6	290	45	1	0.80	0.55	0.24	25.0	20.0
2	1.6	270	45	1	0.76	0.48	0.17	15.0	10.0
3	0.8	270	45	1	0.76	0.66	N/A	19.3	15.0
4	3.2	270	45	1	0.74	0.22	0.28	12.9	8.0
5	3.2	290	90	5	0.71	0.50	0.24	7.3	2.0
6	3.2	245	90	5	0.71	0.29	0.27	19.5	14.0

has much less influence for the thicker mold and time for cooling to the point of crystallization is longer, which both mitigate against maximizing orientation.

The data for plaques nos. 5 and 6 set up a comparison of the effects of two melt temperatures (290°C and 245°C, respectively) at slower fill times of 5 s. The mold thickness was 3.2 mm and melt temperature was 90°C in both cases. While the near-surface molecular orientation $S_{Surface}$ remained constant, the molecular orientation in the core S_{Core} and shear S_{Shear} (which reflect the result

of flow and the average orientation deeper into the plaque) decreased by about 40% for the lower melt temperature. This comparison is an illustration of where obtaining enhanced flow at the optimum melting point trumps the relative time to crystallize the TLCP in the interior. Although the *magnitude* near-surface molecular orientation $S_{Surface}$ remained constant, its *direction* of greatest magnitude shifted by about 12 deg.

For every case, the molecular orientation of the near-surface $S_{Surface}$ varied far less than the changes in orientation associated with S_{Shear}. This result is most likely associated with the fact that the material at the mold surface is the first to crystallize. The directions of maximum orientation for $S_{Surface}$ and S_{Shear}, as indicated by the azmuthal angles ϕmax and βmax, always coincided well.

The range of values for molecular orientation $S_{Surface}$ reported here are similar in kind and magnitude to those reported by Pirnia and Sung using the surface-specific technique of FT-IR ATR dichroism. [7] The sampling depth for the IR technique is about 5 μm, whereas with NEXAFS the depth is under 3 nm. We have obtained similar data by a very similar FT-IR method on samples for which 2-D WAXS and NEXAFS data have also been obtained. As one might expect, the values of *S* obtained by IR are close, but typically about 5% less than by NEXAFS.

Future work will entail characterizations of the state of orientation using a 6-axis sample manipulator for positions distanced from the centerline. The ability to rotate the sample azimuthally will enable the accurate determination of surface orientation in the regions of high bimodal complexity with more efficiency than by the individual rotation of small samples cut from plaques. The orientation results shall be utilized in processing models (e.g., Moldflow®, Folgar-Tucker) to predict the optimum processing conditions for the fabrication of net-shape parts. Process optimization of TLCPs can lead to a means of fabricating structural components with less weight. Through the National Science Foundation, the United States Council for Automotive Research and DOE are helping to fund this research with the reduction of vehicle weight as an ultimate goal.

Summary

The influences of molding parameters and mold thickness on the anisotropy, skin-core morphology, and mechanical properties of injection-molded DHαMS copolyester TLCP were studied. The

contributions of shear and extensional flows on the bimodal orientational character of the moldings were characterized by a combination of 2-D WAXS and NEXAFS.

1. The maxima for molecular orientation $S_{Surface}$ obtained by NEXAFS for the near-surface were found to be in the 0.7 to 0.8 range for all cases.

2. Mold thickness was found to influence S_{Skin} and S_{Core} obtained from 2-D WAXS much more strongly than melt temperature within the nominal processing range of 270°C to 300°C.

3. Correlation of the directions for the maxima of $S_{Surface}$ (2 mm depth) and S_{Skin} (~0.4 mm depth) was found to be very good.

4. The equivalency of NEXAFS with the FT-IR ATR techniques as measures of surface orientation was found to be good. $S_{Surface}$ is about 5% greater by NEXAFS.

5. NEXAFS has proved to be effective at determining the orientation of the very surface of the skin layer.

Acknowledgements

Thank you, first of all, to my principal collaborators in this work: W. R. Burghardt and S. Rendon (Northwestern University), and L. S. Thomas (MMI). Thanks are extended to J. Quintana and the staff of the DND-CAT of the Advanced Photon Source, Argonne National Labs; and to D. A. Fischer and the staff of Beamline U7A of the National Synchrotron Light Source, Brookhaven National Labs. Funding support from the National Science Foundation and the Department of Energy through NSF Grant DMI-0521771 is gratefully acknowledged.

References

1. A.M. Donald and A.H. Windle, Liquid Crystalline Polymers, Cambridge University Press, Cambridge, 1992.

2. Liquid Crystalline Polymers, E.T. Samulski, ed., National Materials Advisory Board, National Academy Press, USA, NMAB-453, 1990.

3. Dreher, S. Seifert, H.G. Zachman, N. Moszner, P. Mercoli, and G. Zanghellini, J. Appl. Polym. Sci., vol. 67, pp. 531-545, 1998.

4. D.K. Cinader and W.R. Burghardt, J. Polym. Sci.: Part B: Polym. Phys., vol. 37, pp. 3411-3428, 1999.

5. S.E. Bales, R.E. Hefner, R. Singh, The Dow Chemical Co., US Patent 5,614,599, March 25, 1997.

6. C.J.G. Plummer, B. Zulle, A. Demarmels, and H.-H. Kausch, J. Appl. Poly. Sci., vol. 48, pp. 751-766, 1993.

7. A. Pirnia, and C.S.P. Sung, Macromolecules, vol. 21, p. 2699, 1988.

8. J. Stöhr and M.G. Samant, J. Elec. Spectrosc. Relat. Phenom., vol. 98-99, pp. 189-207, 1999.

9. L.R. Pattison, A. Hexemer, E.J. Kramer, P.M. Petroff, and D.A. Fischer, Macromol., 2006, in press.

10. S. Rendon, W.R. Burghardt, A. New II, R.A. Bubeck, L.S. Thomas, Polymer, vol. 45, pp. 5341-5352, 2004.

11. R.A. Bubeck, L.S. Thomas, S.Rendon, W.R. Burghardt, A. Hexemer, and D.A. Fischer, Journal of Applied Polymer Science, vol. 98, pp. 2473-2480, 2005.

12. S. Rendon, W.R. Burghardt, R.A. Bubeck, L.S. Thomas, B. Hart, Polymer, vol. 46, p. 10202, 2005.

5. JOINING

A. Die-Cast Net-Shaped Hole Process Development for Application of Thread-Forming Fasteners

Principal Investigator: Dean M. Paxton
Pacific Northwest National Laboratory (PNNL)
P.O. Box 999, Richland, WA 99352
(509) 375-2620; fax (509) 375-2186; e-mail: dean.paxton@pnl.gov

Technology Area Development Manager: Joseph A. Carpenter
(202) 586-1022; fax (202) 586-1600; e-mail: joseph.carpenter@ee.doe.gov

Expert Technical Monitor: Philip S. Sklad
(865) 574-5069: fax: (865) 576-4963; e-mail: skladps@ornl.gov

---

Contractor: Pacific Northwest National Laboratory
Contract No.: DE-AC06-76RL01830

Objective

- Evaluate the effect of casting variation on clamp load and serviceability when using thread-forming fasteners in die-cast net-shaped holes of aluminum and magnesium alloys.
- Collect in-field data on casting-die hole features and pins during production operations at casting suppliers.

Approach

- Evaluate the effect of hole size and shape variation on clamp load when using a variety of thread-forming fasteners (TFFs) in die-cast net-shaped holes in Al and Mg alloys.
- Evaluate the reusability performance of a variety of TFFs in Al- and Mg-alloy die-cast net-shaped holes when subjected to repeated assembly/disassembly of a single fastener into the same hole.
- Evaluate the extent to which contamination in the form of debris is produced when inserting TFFs into Al- and Mg-alloy die-cast net-shaped holes.
- Collect in-field measurements of the variation in size, shape, and position of casting-die hole features and pins from automotive casting suppliers.

Accomplishments

- Completed testing to evaluate the effect of the hole size and shape when using three different TFF designs in Mg alloy AZ91D and a second TFF design (ALtracs®) in Al alloy A380. Testing of TAPTITE 2000® SP™ fasteners in A380 is also complete and results previously reported.
- Completed testing to evaluate the reusability performance of two TFF designs in Al alloy A380 and four TFF designs in Mg alloy AZ91D.
- Completed an evaluation of contamination created during the sequence of assembly/disassembly of TFFs into die-cast nut specimens of Al alloy A380 and Mg alloy AZ91D.
- Collected in-field measurements from automotive casting suppliers showing minimal variation in casting-die hole features and pins during production operations.

Future Direction

- Objectives for this project have been completed. Project participants are actively seeking a manufacturing demonstration project wherein die-cast net-shaped holes could be used to establish production experience of this capability.

Introduction

The focus of this technical-feasibility project was on resolving the highest priority technical challenges associated with application of thread-forming fasteners (TFFs) into die-cast, net-shaped holes in aluminum (Al) and magnesium (Mg) alloys, identified during the initial concept feasibility project completed in 2003. The priority issues were grouped into four technical challenges: (a) casting variation, (b) fastener design, (c) assembly processing, and (d) in-service requirements. The major facets of casting variation are cast hole size, shape, and position, resulting from the thermal, mechanical and metallurgical effects of the die-casting process. Fastener testing is complete to evaluate the effect of hole size and shape on clamp load. The closely related in-service issues of contamination and reusability were also evaluated via fastener testing. In addition, in-field data were collected from casting suppliers on die-pin wear and degradation. A variety of fastener designs, provided by the fastener suppliers, and assembly procedures, were evaluated during the testing. All of the prioritized issues were addressed for both Al alloy A380 and Mg alloy AZ91D during the Phase 1 technical-feasibility project.

Background

Progress has been made in applying TFFs into machined or stamped holes featured in steel automotive applications for general assembly. Use of these fasteners has eliminated the tapping operation, which reduced costs, investment, and improved warranty, while delivering better joint properties within an assembly. Opportunities exist to reduce costs. By using TFFs with net-shaped holes in lightweight castings, the drilling operation and associated equipment investment is eliminated without sacrificing joint performance. Potential applications for using TFFs in cast components are numerous and include powertrain (transmissions, engines, and rear axles), chassis, (control arms, suspensions) and body structures that utilize large castings (inner doors, lift gates, under-hood attachments and supports). Expanding the use of lightweight materials is the driver behind this project. Progress in applying the concept to Al castings has been minimal and even less with Mg. Successful development of this idea in cast products will expand the use of lightweight materials due to the proven benefits already achieved in the existing applications.

Approach to Hole Size and Shape Variation Testing

Holes in die castings are created by the use of steel pins inserted in specific locations in the die block. The potential exists for the dimensions of the die pin to change in size (diameter), or shape (taper), because of the repeated contact with the molten metal filling the die cavity. Molten Al tends to dissolve some alloy constituents of the steel and this dissolution is a function of temperature. Thus, if dissolution were to occur, it would be most prevalent at the leading end of the pin, which is the hottest, due to the large die block acting as a heat sink. In addition, exposure to molten Al and Mg can result in soldering of the alloys onto the pin, which is then cleaned with an Emory cloth. Repeated application of this mechanical cleaning process can result in further removal of pin material, thereby changing the diameter of the pin. Both of these changes, in time, have the potential to cause variation in the desired size and shape of the resulting hole in the die casting. The purpose of this hole-size and -shape test matrix was to determine the impact of variations from nominal hole size (diameter) and shape (taper) on the resulting clamp load, when using a TFF. The matrix for this testing includes three different tapers and up to three increments of larger and smaller hole diameters.

Clamp load was determined using the LabMaster Fastener Evaluation Test Cell. The nut-runner was programmed to drive the fasteners to failure and the Labmaster software recorded clamp load, input torque, and failure torque versus time and angular

rotations of the fastener for each test. The failure mode was noted at the end of the test (break the fastener or strip the threads). Thirty tests, each combination, have already been completed and reported for TAPTITE 2000® SP™ fasteners in A380. Testing was completed at each combination of size and shape for ALtracs® coated with Magni 565 in Al alloy A380 and for ALtracs®, Mag-form®, and Remform® F, all coated with ZinKlad in Mg alloy AZ91D.

Results for Holes Size and Shape Variation Testing

PNNL completed 15 tests at each combination of size and shape for each fastener design in Mg alloy AZ91D. Torque-tension testing was completed for the ALtracs®, Mag-form® and Remform® F in Mg. The ALtracs® fastener shows minimal effect of size or shape on resulting clamp load at failure of the fastener, except for the 0.5° hole with the largest diameter where some fasteners stripped, as shown in Figure 1.

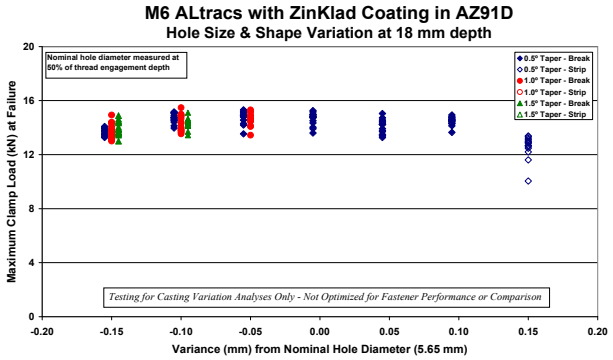

Figure 1. Torque-tension test results for size and shape matrix using ALtracs® in AZ91D.

The Mag-Form® showed a consistent clamp load over the range of size or shape variation, with similar data presented in Figure 2. The Remform® F fastener shows a minimal effect of size and shape on most combinations of size and shape; however, a broad range of clamp load was observed at the smallest hole size.

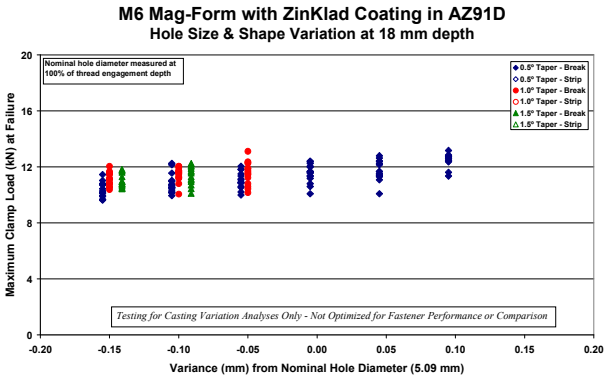

Figure 2. Torque-tension test results for size and shape matrix using Mag-Form® in AZ91D.

Approach to TFF Reusability Testing

The reusability test evaluated the capability of a fastener to maintain clamp load after repeated installation of the same fastener into the same hole. To achieve this, the clamp load, at a target input torque, was measured for 14 consecutive rundowns of a single fastener into a die-cast nut specimen. For a given fastener design, the target input torque was experimentally determined to be the torque required to generate 9 kN of clamp load. This clamp-load target was also established experimentally as the load generated by installing a machine screw at 11 Nm of input torque, which is a common assembly specification range (10-12 Nm) for M6 fasteners. After 14 consecutive rundowns, the torque limit was removed and the fastener tested to failure. Clamp load and input torque at failure, as well as the failure mode, were recorded to conclude the test.

Results for Reusability Testing

Reusability testing was completed for TAPTITE 2000® SP™ and ALtracs® fasteners coated with Magni 565 in Al alloy A380. Three hole shapes were evaluated for each fastener and include: 1.0° taper, 0.5° taper and 0° taper (drilled hole) for comparison. Figure 3 shows the average of the clamp load and corresponding input torque for a total of 15 tests conducted using the ALtracs® fastener at each of the three hole shapes (1.0°, 0.5° and 0.0°). Clamp-load retention is 100% after 14 rundowns of the same fastener and the same hole and the fastener broke in all cases on the 15th rundown with no torque limit. These results indicated no change in clamp-load magnitude or retention over the range of hole shapes tested.

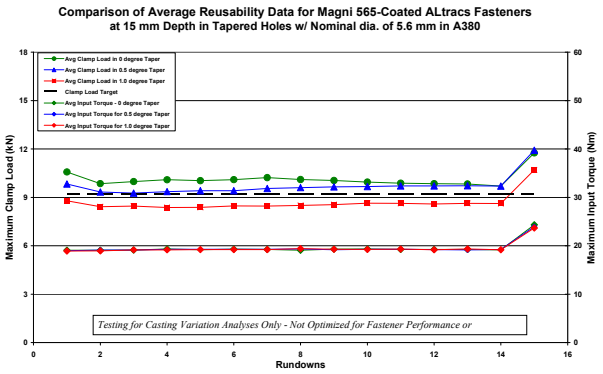

Figure 3. Reusability results for a range of hole shapes (taper) using ALtracs® fasteners in A380.

For Mg alloy AZ91D, reusability testing was completed for ALtracs®, Mag-form®, Magtite®, and Remform® F all coated with ZinKlad. Similar to the Al alloy, three hole shapes were evaluated for each fastener 1.0°, 0.5° and 0° tapers. Figure 4 shows average reusability data for the Magtite® design. Clamp-load retention for this fastener is nearly 100% and the fastener broke in all cases on the 15th rundown with no torque limit. Similar results were achieved for the ALtracs®, Mag-Form® and Remform® F designs in AZ91D with nearly 100% clamp-load retention at breaking of the fastener when tested to failure.

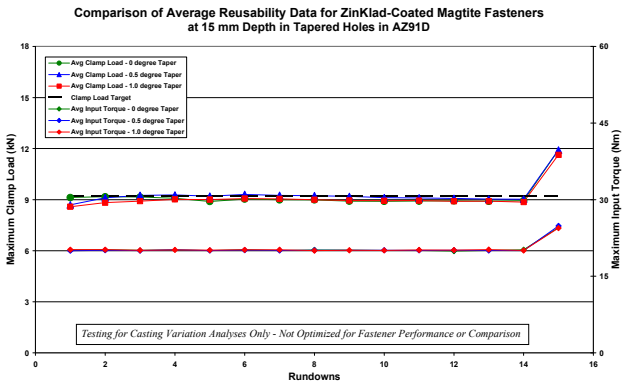

Figure 4. Reusability results for a range of hole shapes (taper) using Magtite® fasteners in AZ91D.

Approach to TFF Contamination Testing

PNNL investigated the extent to which contamination in the form of debris is generated while using TFFs in Al- and Mg-alloy die-cast net-shaped holes during this technical-feasibility project. The approach to this test was to collect and weigh any debris generated during installation of the fastener during the reusability test. Debris was cumulatively weighed using an electronic balance after the 1st, 2nd and 5th rundowns. Samples of collected debris were analyzed using a scanning electron microscope (SEM) equipped with an energy-dispersive spectrometry (EDS) detector to determine the composition of the debris collected.

Results for TFF Contamination Testing

Debris was collected during six reusability tests for TAPTITE 2000® SP™ and ALtracs® fasteners for each of the 1.0°, 0.5°, and 0° tapers, and for three machine screws in tapped holes. All fasteners were coated with Magni 565. Both TFFs generated measurable amounts of debris with drilled holes generating slightly more debris, in each case, as shown in Figure 5. The machine screw generated minimal amounts of debris during the sequence of rundowns.

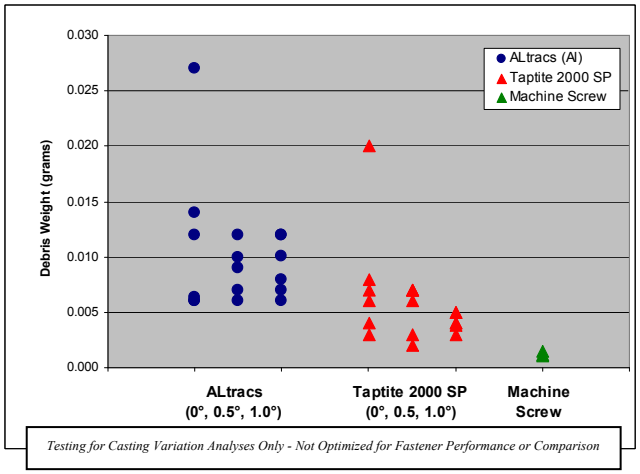

Figure 5. Contamination results for a range of hole shapes (taper) TAPTITE 2000® SPTM and ALtracs® fasteners in A380.

SEM analysis of samples of the debris showed that, in both cases, the debris composition matched the A380 alloy, with small amounts of coating deposits smeared on some pieces of debris. For the AZ91D alloy, debris was also collected during nine reusability tests, for ALtracs®, Mag-Form®, Remform® F and Magtite® fasteners, all coated with ZinKlad coating, for each of the 1.0°, 0.5° and 0° tapers, and for three machine screws in tapped holes. Figure 6 shows the amount of debris collected from these five fasteners. The ALtracs®, Mag-Form®, and Remform® F fasteners showed measurable amounts of debris, with drilled holes generating slightly more

debris in each case. The Magtite® fasteners and machine screws generated minimal amounts of debris during the sequence of rundowns.

SEM analysis of samples of the debris showed that, in all cases, the debris composition matched the AZ91D alloy, with small amounts of coating deposits smeared on some pieces of debris.

Approach to TFF In-Field Casting Variation Data

In-field data from various casting suppliers was collected to analyze and determine capability, and to identify practices for achieving minimal variation in size, shape, and position of as-cast holes. Hole-position data were measured daily on selected castings.

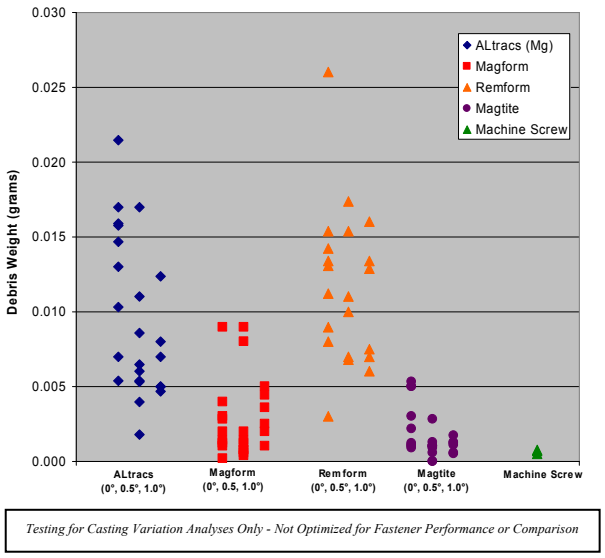

Figure 6. Contamination results for a range of hole shapes (taper) ALtracs®, Mag-Form®, Remform® F, and Magtite® fasteners in AZ91D.

Results for In-Field Casting Variation Data

In-field data were collected from automotive casting suppliers for analysis and comparison to laboratory test data. The in-field data and laboratory test-cell data were compared to identify best practices and to determine gaps for further technical development.

Instead of measuring actual cast holes, the approach selected was to measure the core pins that made the holes. Core pins were measured before dies were put back into service from major maintenance overhauls. Most dies are taken out of service every 20,000 to 40,000 cycles for routine maintenance and core-pin replacement. The same core pins were removed and measured, after the dies were removed from service, for the next major maintenance overhaul. Three typical automotive casting dies were included in the study, ranging in size from a pump-body casting, a transfer-case casting, to a transmission-case casting.

Figure 7 shows the measurements from the pump body casting. The pins were in service for 29,724 shots and experienced a maximum dimensional change of 0.05 mm.

Pump Body after 29,724 shots

PIN #	LOCATION	ORIG. DIA.	FINAL DIA.	VARIATION	
6	A	0.257 inch.	0.257 inch.	0.000 inch.	0.00 mm
	B	0.226 inch.	0.226 inch.	0.002 inch.	0.05 mm
	C	0.204 inch.	0.209 inch.	0.002 inch.	0.05 mm
6	A	0.257 inch.	0.257 inch.	0.000 inch.	0.00 mm
	B	0.227 inch.	0.226 inch.	0.001 inch.	0.026 mm
	C	0.204 inch.	0.206 inch.	0.002 inch.	0.05 mm

Figure 7. Diameter measurements from pump body casting die before and after 29,724 shots.

Figure 8 shows the measurements from the transfer-case casting. The pins were in service for 23,108 shots and experienced a maximum dimensional change of 0.025 mm. Figure 9 shows the measurements from the transmission-case casting. The pins were in service for approximately 25,000 shots and experienced a maximum dimensional change of 0.17 mm.

Transfer Case after 23,108 shots

PIN #	LOCATION	ORIG. DIA.	FINAL DIA.	VARIATION	
8	A	0.299 inch.	0.298 inch.	0.001 inch.	0.025 mm
	B	0.287 inch.	0.287 inch.	0.000 inch.	0.00 mm
17	A	0.298 inch.	0.298 inch.	0.000 inch.	0.00 mm
	B	0.288 inch.	0.289 inch.	0.001 inch.	0.025 mm

Figure 8. Diameter measurements from transfer case casting die before and after 23,108 shots.

Transmission Case after 25,000 shots (approx.)

PIN #	LOCATION	ORIG. DIA.	FINAL DIA.	VARIATION
MO1 A	A	5.76 mm	5.62 mm	0.14 mm
MO1 C	A	5.76 mm	5.66 mm	0.10 mm
MO1 D	A	5.76 mm	5.72 mm	0.04 mm
MO1 E	A	5.76 mm	5.72 mm	0.14 mm
MO3	A	6.03 mm	6.01 mm	0.02 mm
MO4	A	8.2 mm	8.03 mm	0.17 mm

Figure 9. Diameter measurements from transfer case casting die before and after ~25,000 shots.

These results were overlaid onto the laboratory results for the TAPTITE 2000® SP™, as shown in Figure 10. As can be seen, the entire set of clamp load outputs under the range of dimensional variation from the core pins are all well above the 9 kN level, which is the design criterion for an M6 fastener. Therefore, it is reasonable to conclude that, based on comparison of available field measurements and laboratory clamp-load tests, it is probable that for properly sized core pins, variation in hole size and shape can provide acceptable clamp loads over the entire maintenance cycle of the core pins without additional cost or effort over the existing process.

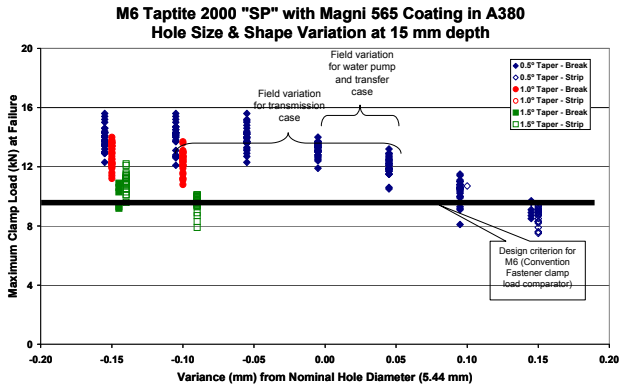

Testing for casting variation analysis only – not optimized for fastener performance or comparison.

Figure 10. Comparison of size and shape testing to in-field casting measurements.

In-field hole position data were collected from the quality system for two castings. Hole position is important because variation in hole position, which results in any amount of shadowing of mating holes, will affect the installation of the fastener. As part of the routine quality inspection process, at least one casting, per shift, per die cavity was measured on a coordinate measuring machine to verify all dimensions are within specification. The position data for a selected cast hole in the pump-body casting and in the transfer- case casting were provided for our analysis during the time frame the shape and size core-pin study was underway. The data provided were hole positions from datum lines in two planes.

The analyses of the dimensional data provided yielded the following results:

Surface	Min.	Max.	Total Var.
Pump Body			
X Dimension	0.037 mm	0.50 mm	0.46 mm
Y Dimension	92.12 mm	92.4 mm	0.20 mm
Transfer Case			
X Dimension	6.2 mm	6.4 mm	0.20 mm
Y Dimension	151.1 mm	151.2 mm	0.10 mm

The adequacy of cast hole position capability will ultimately be determined by the product design requirements and the designers ability to accommodate the position variation in the specific application.

Conclusions

This technical-feasibility project has aimed to resolve the highest-priority issues associated with applying thread-forming fasteners in die-cast net-shaped holes in lightweight alloy castings. The fastener testing results and in-field casting variation measurements can be coupled together to conclude that indeed capability exists to use thread-forming fasteners in as-cast components currently in production today. We assessed this capability using a variety of fastener designs, in both aluminum and magnesium die-casting alloys and by assessing the variation in components produced by multiple casting suppliers.

Future Work

We completed all work on this project. Project participants are actively seeking a manufacturing demonstration project wherein die-cast net-shaped

holes could be used to establish production experience of this capability.

Publications

"*Application of Thread-Forming Fasteners in Net-Shaped Cast Holes in Lightweight Metal Alloys,*" D.M. Paxton, G.J. Dudder, W.C. Charron, T.H. Cleaver, TMS Letters: Lightweight Materials, 2006.

Presentations

"*Application of Thread-Forming Fasteners in Net-Shaped Cast Holes in Lightweight Metal Alloys,*" D.M. Paxton, G.J. Dudder, W.C. Charron, T.H. Cleaver, at the TMS Symposium on Lightweight Materials, March 16, 2006.

"*Use of Thread-Forming Fasteners in Lightweight Alloy Die-Cast Net-Shaped Holes,*" D.M. Paxton, G.J. Dudder, W.A. Charron, T.H. Cleaver, at THERMEC' 2006: International Conference on Processing & Manufacturing of Advanced Materials, July 3-6, 2006.

B. Forming Limits of Weld Metal in Aluminum Alloys and Advanced High-Strength Steels

Principal Investigator: Richard W. Davies
Pacific Northwest National Laboratory (PNNL)
P.O. Box 999, Richland, WA 99352-0999
(509) 375-6474; fax: (509) 375-5994; e-mail: rich.davies@pnl.gov

Technology Area Development Manager: Joseph A. Carpenter
(202) 586-1022; fax: (202) 586-1600; e-mail: joseph.carpenter@ee.doe.gov

Expert Technical Monitor: Philip S. Sklad
(865) 574-5069; fax: (865) 576-4963; e-mail: skladps@ornl.gov

Participants:
Elizabeth V. Stephens and Glenn J. Grant, PNNL
General Motors, DaimlerChrysler, Ford, US Steel, Alcoa, Olympic Controls

---

Contractor: Pacific Northwest National Laboratory
Contract No.: DE-AC06-76RL01830

Objective

- Develop, validate, and disseminate a combined experimental and numerical method to statistically describe and systematically quantify the forming limits of welded aluminum (Al) alloys and advanced high-strength steels (AHSSs).

Approach

- Develop a standard tool for weld process development that will systematically quantify failure probabilities during forming.
- Provide accurate and standardized methods of experimentally characterizing weld-metal formability using unique, but simple, test methods available on the shop floor.
- Provide predictive models for more accurate forming simulations of tailor-welded blanks (TWBs) and hydroforming operations. Predict parts-per-thousand failure rates during production from finite-element analysis (FEA).
- Characterize static/fatigue properties and forming behavior of several weld populations and correlate with statistically-based tool.

Accomplishments

- Incorporated digital image correlation (DIC) or speckle pattern interferometry strain evaluation method to study the details of localization in uniaxial and biaxial testing.
- Completed uniaxial experiments of welded material populations (friction-stir-welded (FSW) AA5182-O to AA5182-O, FSW AA5182-O to AA6111-T4, laser-welded (LW) DP600 to DP600, and LW DQ to DQ steel).
- Completed biaxial experiments of welded-material populations.
- Completed metallography and weld-microhardness measurements of welded-material populations.

- Completed miniature tensile tests of specimens removed from the FSW weld zones of the 5182 and 5182 to 6111 welded-alloy populations.
- Completed probabilistic-based forming-limit predictions for DP600 and AA5182-6111 welded alloys.

Future Direction

- Further investigate a combined forming-limit prediction for DP600 and AA5182-6111 welded alloys.
- Increase focus on biaxial experiments.
- Quantify the combined forming-limit diagram (FLD) using the statistical approach.
- Implement new testing approach for AA5182-O to AA5182-O welded alloys to biaxial limited-dome-height tests.

Introduction

This work is a collaboration effort between DOE, Pacific Northwest National Laboratory (PNNL), a USAMP team of the U.S. Council for Automotive Research (USCAR), US Steel, Olympic Controls and Alcoa. This project will develop, validate, and disseminate combined experimental and numerical methods that systematically quantify the forming limits of weld materials in Al alloys and AHSSs through a combination of experimental and deformation-modeling analyses. This work will enable high-volume, robust deployment of tailor-welded blanks (TWBs), seam-welded tubes, and tailor-welded tubes in emerging materials. Figure 1 is a schematic of the project.

The deformation of weld materials and their limits of formability are important aspects to both TWB and hydroforming technologies. The conventional low-carbon steels used in automotive applications are easily fusion welded using conventional technologies, and suffer no appreciable strength degradation near the weld. Al alloys are more difficult to weld than low-carbon steels due to high conductivity and reflectivity, and low molten viscosity. They have a high propensity for porosity to form during fusion welding, as well as hot cracking and heat-affected-zone (HAZ)-related issues in heat-treatable Al alloys. Many of the AHSSs that are finding increasing application in the automotive industry suffer from degradation of

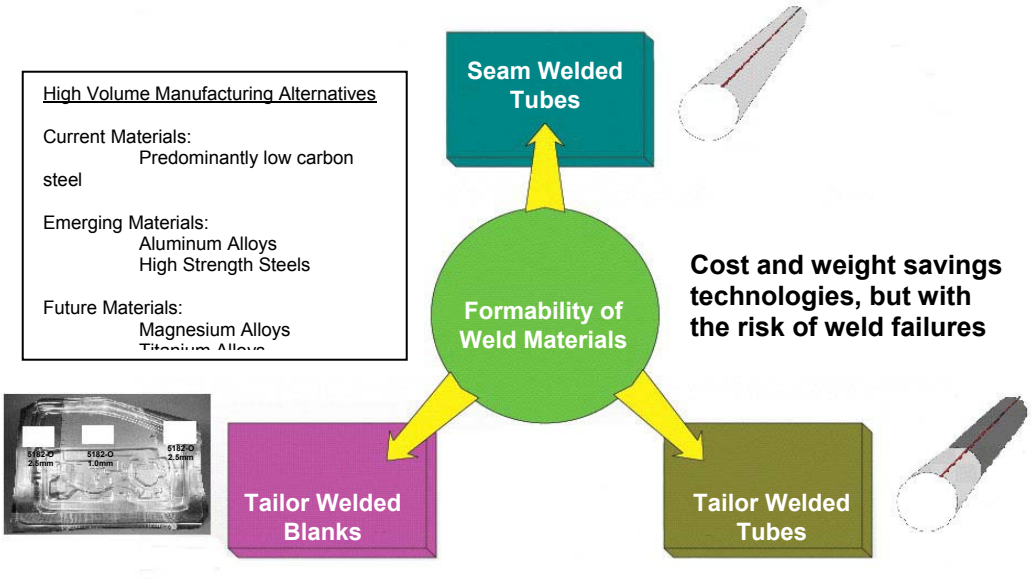

Figure 1. A schematic of the formability-of-weld-materials project.

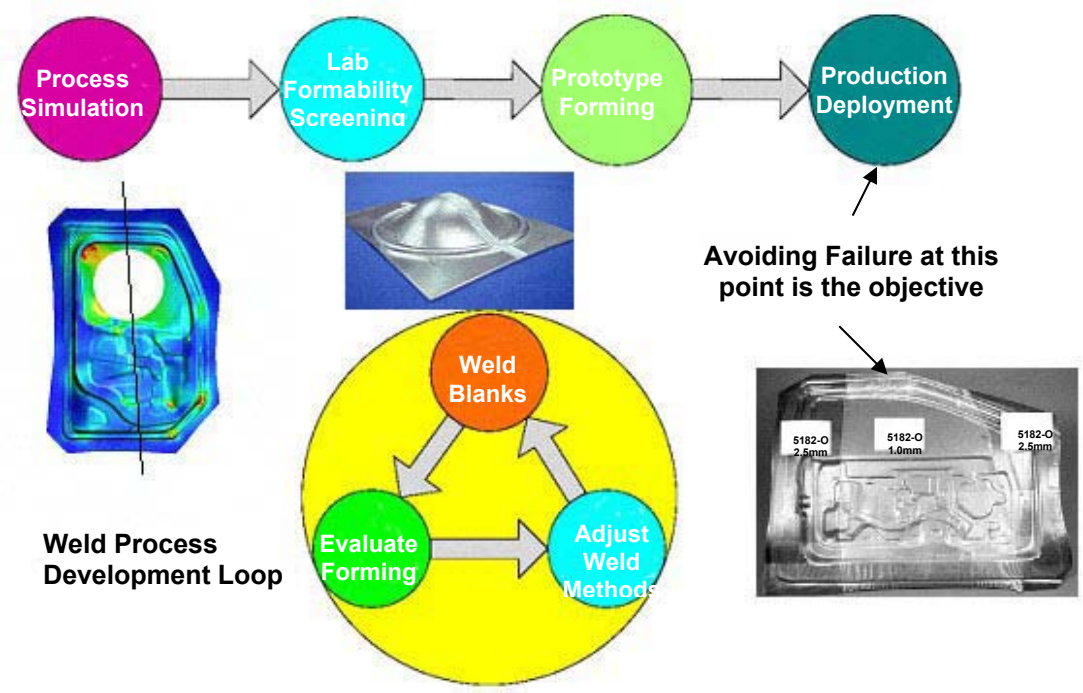

Figure 2. A schematic of the typical manufacturing process development.

strength in the HAZ. Furthermore, nearly all fusion welds suffer from irregular geometries and elevated levels of surface roughness compared to the parent materials, which also influence formability and component performance.

This project will focus on developing a generalized numerical method to predict material-forming limits in weld materials and verifying deformation and forming-limit predictions. The approach will rely on developing standardized test methods for weld-material populations to establish a statistical description of material imperfection and mechanical properties in their weld region, and developing statistically-based forming-limit diagrams or continuum damage models that predict material failure in the weld region.

The project will include numerical model development, validation, and supporting experiments. A number of candidate weld methods will be examined in combination with selected Al alloys and AHSSs. The project materials will include 5000 series and 6000 series Al alloys and relevant AHSSs including high-strength low-alloy (HSLA), transformation-induced plasticity (TRIP), and dual-phase steels. The selection of sheet materials and welding methods will be coordinated with the participating OEMs and will be representative of high-volume, commercially-viable materials and processing technologies.

The deliverables will include a standard procedure for weld-material evaluation coupled with a numerical approach for establishing weld-region forming limits. The results will also allow evaluation and development of candidate weld processes and the interaction between materials and weld parameters. The overall objective is to develop test methods and experimental results to enable wide-spread deployment of weight-optimized TWB and tube hydroforming and to avoid weld failures during production. Figure 2 is a schematic of the typical manufacturing process development.

Experimental Characterization

The experimental characterization of the second program year has focused on incorporating digital image correlation as a strain-evaluation method, continuation of uniaxial testing with the simple geometric specimen design, and biaxial testing. The TWB material combinations evaluated were LW DP600 to DP600, LW DQ to DQ, FSW AA5182-O to AA5182-O, and FSW AA5182-O to AA6111-T4

with greater emphasis on the DP600 and AA5182-6111 welded alloys.

Strain Characterization Utilizing Digital Image Correlation

During this reporting period, digital image correlation (DIC), or speckled pattern interferometry, has been applied for use with uniaxial tests and biaxial limited dome-height formability tests. DIC is a data-analysis method which uses an algorithm to analyze digital image data taken when a sample is subjected to mechanical strain. Displacement and strain are measured. This technique uses white-light speckle correlation, where two similarly speckled images captured by a video camera represent the state of the object before and after deformation. Consecutive images are captured during testing and the image correlation will register a change in surface characteristics as the specimen is affected by stresses imposed upon it. The actual object movement is measured and the Lagrangian strain tensor is available at every point on the surface.

This technique will help us further understand strain localization in a non-homogenous gage such as a weld. We are able to track strain localization and strain variation of the welded parts during forming. For example, Figure 3 illustrates the strain rate results from the DIC analysis during uniaxial testing of a LW DP600 longitudinal specimen. Four levels of deformation are shown. The faint line in the illustrations is the weld. Localization occurs when the local strain rate is much greater than the overall specimen strain rate. In this specimen, as in all the other longitudinal DP 600 specimens, we observe the strain rate localizing in the weld just prior to failure.

Uniaxial Experimental Testing

Continuation of the uniaxial tests occurred this reporting period where rectangular specimens were designed with the weld oriented either longitudinal or transverse to the tensile axis as shown in Figure 4. Thirty longitudinal and thirty transverse specimens were made for each welded TWB material combination. All specimens were etched with square grids to determine the incipient necking condition utilizing optical strain grid analysis (a more

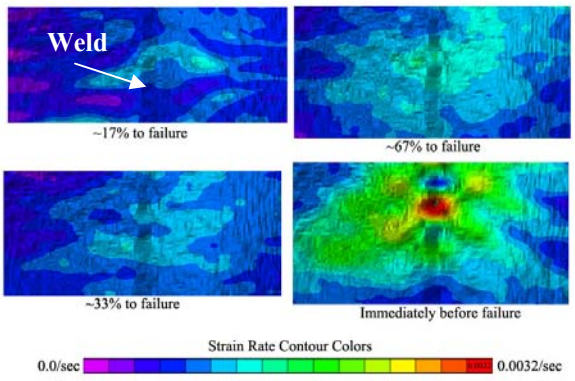

Figure 3. The strain-rate results from the DIC analysis of a longitudinal LW DP600 specimen at four different levels of deformation during uniaxial testing.

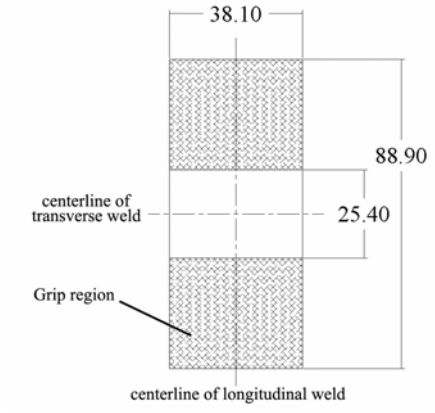

Figure 4. Uniaxial specimen design for longitudinal and transverse specimens. Measurements in millimeters.

conventional method in addition to DIC). All tests were stopped after an 8% drop in load.

Microhardness testing was performed on a cross-section of the LW DP600 weld. The microhardness test measurements show that the weld is considerably harder than the parent sheet with a minimum HAZ (Figure 5). All thirty uniaxial DP600 longitudinal specimens failed in the weld. All thirty of the transverse specimens failed in the thin sheet away from the weld and weld region (HAZ). Localization occurs in the weaker thin sheet. Failure is determined by the weld properties in the longitudinal DP600 welded specimens, where as failure is determined by the properties of the thin parent sheet material in the transverse specimens.

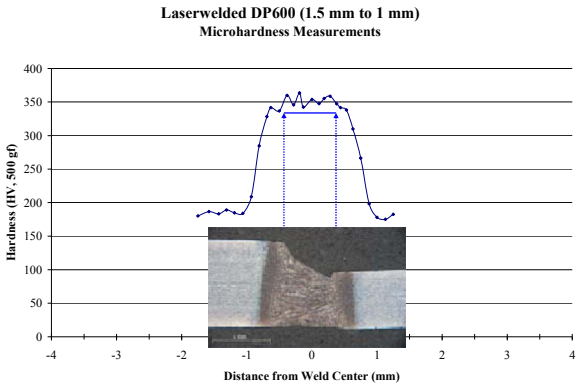

Figure 5. Microhardness test measurements of the DP600 welded alloy.

For the 5182-6111 friction-stir-welded alloys, all thirty longitudinal specimens failed in the weld and twenty-nine of the thirty transverse specimens failed in the HAZ of the thin sheet 6111 material. Miniature tensile tests performed on specimens removed from the weld and weld region indicated the weld material to be a strong, yet less ductile, material in comparison to the parent sheets (Figure 6) and weaker in the HAZ. A depression in strength was observed in the HAZ

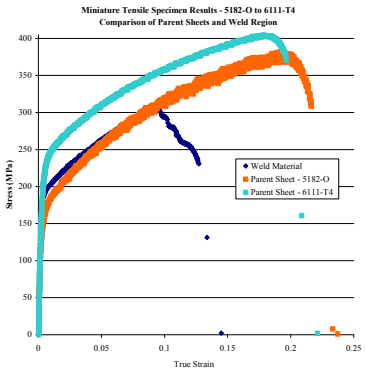

Figure 6. The stress-strain curves of the parent materials and weld material of the 5182-6111 TWB.

In this welded-alloy combination, failure is determined by the weld properties in the longitudinal specimens, where as failure is determined by the HAZ of the thinner 6111 material in transverse specimens.

For the FSW 5182 welded alloys, twenty-nine of the thirty longitudinal specimens failed in the grip region and all thirty transverse specimens also failed in the grip region. Miniature tensile tests performed on specimens removed from the weld and weld region indicated the weld material to be just as ductile and strong as the parent sheet. Minimal mechanical property gradients across the weld and weld region were observed. Further testing approaches need to be investigated.

Biaxial Experimental Testing

Biaxial limited dome-height tests were performed on the DP600 and 5182-6111 welded alloys. Both full domes and 4-inch-wide domes were tested, with a minimum of five specimens tested for each condition. Full dome tests were also conducted on the parent sheet materials for the two TWB combinations. Both optical strain grid analysis and DIC was used to evaluate the specimens. Figure 7 is an illustration of the DIC analysis for a full- dome DP600 welded specimen.

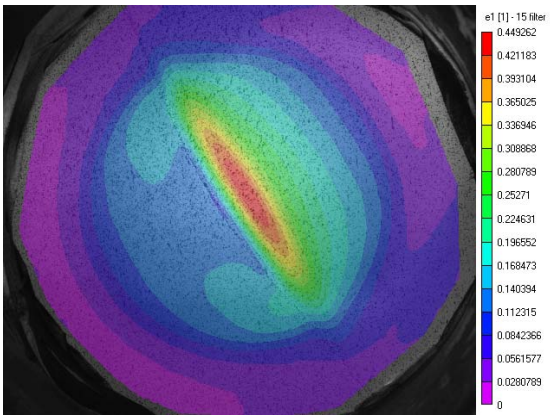

Figure 7. An illustration of the DIC strain data just prior to fracture on a LW DP600 limited dome-height test.

For the DP600 welded specimens, all full-dome biaxial tests failed in the thin sheet parallel to the weld. All 4-inch-width domes failed in the weld, transverse to the weld.

For the 5182-6111 welded specimens, all full-dome biaxial tests failed in the weld; however, two different failure modes were observed. The specimens either failed in the weld, longitudinal to the weld, or failed in the weld, transverse to the weld with the crack propagating into the thin sheet 6111 material. In the 4-inch-width dome tests, all specimens failed in the weld, transverse to the weld.

M-K Method to Predict Formability

Forming-limit diagrams for the DP600 and 5182-6111 TWBs were generated using a Marciniak-Kuczynski (M-K) method approach. The M-K model can track the development of plastic strains in the monolithic sheet and the weld materials under applied external loading. The model also tracks the evolution of imperfections and predicts localization and failure of the specimens.

Theoretical FLDs are generated based on uniaxial tensile results and statistical probability. The level of imperfection *f* that must exist in the specimens in order to describe the formability for each of the thirty longitudinal specimens is determined. A Weibull probability distribution is then applied to describe the longitudinal specimen imperfections and the predicted FLD for the TWBs is generated.

The LW DP600 full-dome biaxial test experiments were compared to the theoretical forming-limit diagram generated. Discrepancies of the model and biaxial experiments were observed, so all test results were combined in a FLD where the strain longitudinal to the weld and the strain transverse to the weld was plotted (Figure 8). The FLD of the parent sheet material (from literature) was also plotted. Figure 8 shows that there is a region in the FLD where the weld will always fail and a region where the sheet will fail. In between is a "gray area" where either the weld or sheet will dictate the failure. A similar methodology was applied to the 5182-6111 welded-alloy population and a similar "gray area" was observed where the weld or HAZ of the thin sheet 6111 material will dictate the failure.

Further investigation of how the FLDs will be suppressed in these "gray areas" is needed including further modification to the forming-limit prediction.

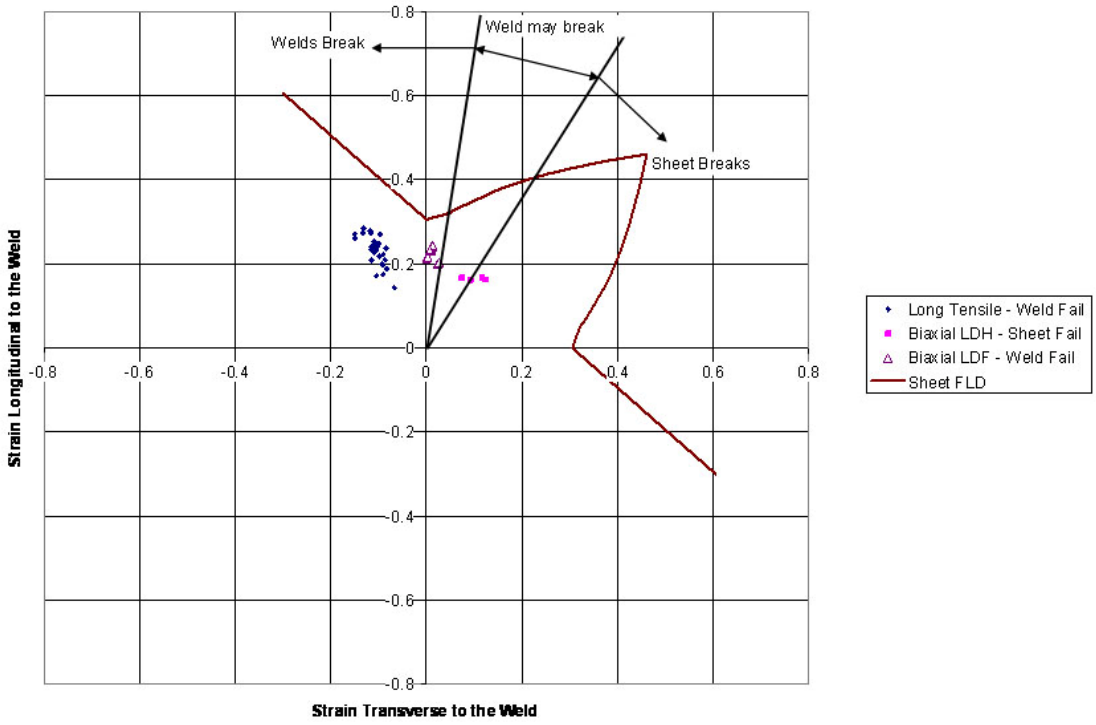

Figure 8. DP600 laser-welded materials combined test results. The FLD for DP600 monolithic sheet is also shown.

Conclusions

From this investigation, the following conclusions were derived:

- In uniaxial tests of LW DP600 specimens, failure is determined by the weld properties in the longitudinal specimens, where as failure is determined by the properties of the thin parent sheet material in the transverse specimens.
- In uniaxial tests of FSW 5182-6111 specimens, failure is determined by the weld properties in the longitudinal specimens, where as failure is determined by the HAZ of the thinner 6111 material in transverse specimens.
- The tensile approach for the FSW 5182 to 5182 welded alloys appeared to be limited for the higher quality welds and a change in testing methodology is needed, possibly to biaxial limited dome height only.
- Further investigation of a combined forming-limit prediction of DP600 and AA5182-6111 welded alloys is needed where the combined FLD is quantified using the statistical approach.

Presentations and Publications

- Davies, RW, et al. 2006. "Forming Limits of DP600 TWBs during Biaxial Stretching." In *IDDRG '2006.*
- "*Forming Limits of DP600 TWBs during Biaxial Stretching*" presented at International Deep Drawing Research Group 2006, Porto, Portugal, June 2006.
- *"Forming Limits of Weld Material in Aluminum Alloys and High-Strength Steels"* presented at United States Automotive Materials Partnership AMD Offsite Annual Review Meeting, Detroit, MI, October 2005.
- *"Forming Limits of Weld Material in Aluminum Alloys and High-Strength Steels"* presented to Industrial Team Advisory Committee, Detroit, MI, October 2005.

C. Impact Modeling and Characterization of Spot Welds

Principal Investigator: Zhili Feng
Oak Ridge National Laboratory (ORNL)
1 Bethel Valley Road, Oak Ridge, TN 37831
(865) 576-3797; fax: (865) 574-4928; e-mail: fengz@ornl.gov

Principal Investigator: Srjdan Simunovic
ORNL
1 Bethel Valley Road, Oak Ridge, TN 37831
(865) 241-3863; fax: (865) 574-7463; e-mail: simunovics@ornl.gov

Technology Area Development Manager: Joseph A. Carpenter
(202) 586-1022; fax: (202) 586-1600; e-mail: joseph.carpenter@ee.doe.gov

Expert Technical Monitor: Philip S. Sklad
(865) 574-5069; fax: (865) 576-4963; e-mail: skladps@ornl.gov

---

Contractor: Oak Ridge National Laboratory
Contract No.: DE-AC05-00OR22725

Objective

- Develop a new, robust spot-weld element (SWE) for modeling various modes of spot-weld failure as a function of impact, welding conditions and materials, while maintaining the current computational efficiency and ease-to-use.
- Develop the implementation procedure to incorporate SWE in crash-simulation FEA codes used by the automotive crash modelers.
- Generate a companion experimental database on the performance of advanced high-strength steel (AHSS) spot-weld behavior under various loading conditions and deformation rates to support and validate the modeling approach.

Approach

- A new SWE and associated constitutive models.
- Modeling and characterization of weld microstructure and property.
- Deformation and failure-behavior testing under different dynamic-loading conditions.

Accomplishments

- Finalized the plan for making weld coupons and dynamic testing.
- Completed literature review on modeling of spot welds.
- Initiated formulation of spot-weld element.

Future Direction

- Develop testing procedures for dynamic testing of spot-weld and produce preliminary data.
- Complete development of SWE to demonstrate its basic characteristics meeting the intended modeling requirements.

- Deliver initial version of the SWE and its implementation procedure.
- Demonstrate SWE-based model.

Introduction

This is a joint program between Oak Ridge National Laboratory (ORNL) and University of South Carolina (USC) sponsored by DOE FreedomCAR and USAMP. It aims at developing a novel and robust spot-weld modeling approach, supported by experimental data that can be implemented in crash simulation FEA codes used by the automotive crash modelers. ORNL's effort focuses on 1) a new, robust, spot-weld finite-element formulation and implementation procedure for modeling various modes of spot-weld failure as a function of impact, welding conditions and materials while maintaining the current computational efficiency; 2) validation of the new crash-modeling approach by component-level crash testing. The companion effort at USC is 1) to perform coupon-level dynamic testing to generate the experiment database of spot-weld performance under different loading modes and strain rates during impact, and 2) work with ORNL to formulate a failure criterion which can adequately deal with the failure-mode changes usually encountered during dynamic loading of spot-welds of high-performance and lightweighting materials such as advanced high-strength steels (AHSS) and aluminum (Al) alloys.

This program was approved in July 2006. Funding was provided to ORNL in August 2006. Therefore, very limited progress has been made in FY 2006. For this report, we will first describe the research needs, the planned technical approach, and the work scope of this research. We will then summarize the progress made in FY 2006.

A primary premise that drives increased use of AHSS in auto-body structures is the drastic improvement in crash performance while reducing the weight. Resistance spot-welding (RSW) is by far the most common joining process used in automotive manufacturing. Typically, there are thousands of spot-welds in a vehicle. Because the separation of spot-welds can affect the crash response of a welded structural component, the static and dynamic behavior of the spot-welds has been one of the critically important considerations in vehicle design and manufacturing.

RSW of AHSS presents unique technical challenges for automotive structure applications. Due to their high carbon and alloying element contents, AHSS are considerably more sensitive to the thermal cycle of welding than the conventional steels used in auto body structures. The higher-grade AHSS (e.g., DP800/1000, TRIP, boron) are more difficult to weld and more susceptible to forming brittle microstructures and solidification-induced defects in the weld region. In addition, heat-affected zone (HAZ) softening can occur. Therefore, RSW of AHSS can very exhibit different structural performance characteristics than the ones made of conventional steels [1-9]. For example, AHSS spot-welds can fail under different failure modes (button pullout, interfacial, or mixed). In addition, impact experiments on joints [7] and structural components (top-hat, double-hat sections) [8, 9] have shown that RSWs have different response under static and dynamic loads. Not only the behavior of RSW in AHSS can be different from that of conventional mild steels [9], the spot-weld structural performance among different AHSS can be drastically different and highly dependent on the grades and types of AHSS [2, 3] (see Figure 1. and Figure 2). Furthermore, there can be considerable variations in microstructure and properties in the weld region for a given type and grade AHSS made by different steel producers, due to the differences in steel chemistry and processing routes employed [5, 6].

In recent years, CAE-based simulation of dynamic (impact) behavior of auto-body structure during crash has become an indispensable tool that enables rapid and cost-effective design and engineering of crash-resistant auto-body structures. Currently, the behavior of spot-welds in FEM impact simulations is usually modeled with a kinematics representation of the joint and the associated constitutive model describing the material-related response of the joint [10]. Currently, the kinematics of the joint are treated as a point connection by means of flexible or

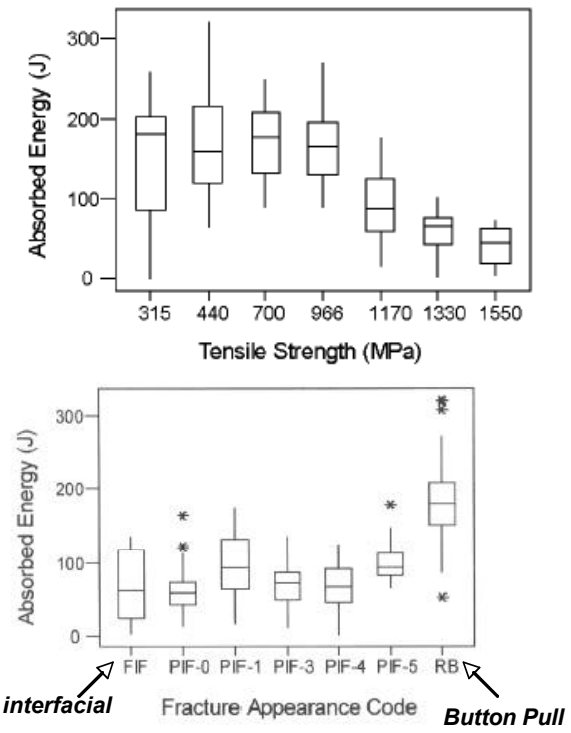

Figure 1. Impact energy in cross-tension test of resistance spot-welds made from different AHSS. After Peterson et al, 2000 [2].

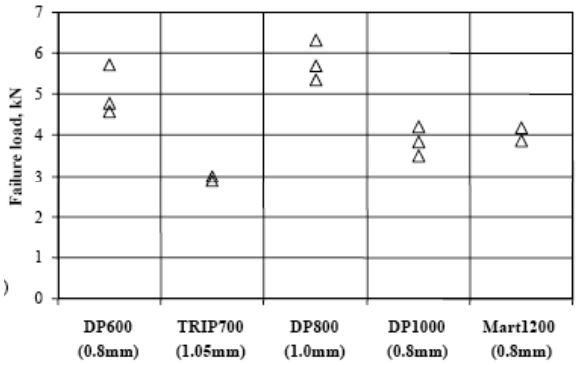

Figure 2. Static failure load in cross-tension test of resistance spot-welds made from different AHSS. After Shi et al, 2003 [3].

rigid (i.e., constrained) links. The sophistication of these beam-link models is limited and can practically involve only force-based laws. Deformation-based criteria require flexible beams or equivalently penalty-based formulations for which the material properties are difficult to assign.

The new constraint-based models [11] allow for independence of connecting FEM mesh topologies, but share similar limitations. The failure models can be derived from purely experimental data [12,13] or can be derived from assumed failure modes [14] fitted to experiments. One of the principal problems with beam-based kinematics models is that the stress and strain distributions in the weld area are not accurately represented. A simple illustration of this drawback is the distribution of through-thickness shear in the shear-lap joint model where nodes of two shells are joined via a beam. As shown in Figure 3, maximum shear stress is expected in reality. However, the shell element theory requires stresses to vanish on the shell surface and, therefore, the resulting stress/strain distributions in the weld area are not accurate.

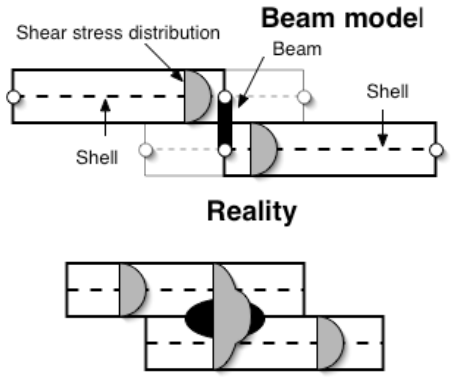

Figure 3. Through-thickness shear distribution in shells in beam RSW model.

It is important to point out that the maximum shear stress in the weld nugget could be the primary stress component causing the interfacial failure of RSW. For RSW in *conventional* steel structures, the dominant failure mode is the button pull-out and the inadequate calculation of the shear stress may not be a major concern in impact simulation of vehicles. On the other hand, for AHSS RSW, accurate determination of the shear stress may be critical because of the reported interfacial failure or mixed interfacial plus pull-out failure mode. The brittle fracture associated with the interfacial failure of the spot-weld is more likely during impact where plastic deformation of the base material may be constrained by large elastic stress field. Compared to a gradual increase in hardness in the HAZ in mild steel RSWs, the AHSS exhibit sharp hardness change [15] that adds to brittleness and notch sensitivity. In addition, the multiple failure modes and the changes in failure modes under different loading conditions require

development of more versatile failure criteria based on the fracture and damage mechanics principles than the resultant force-based ones. From the structural stiffness perspective, the bar and beam models typically yield acceptable accuracy under tension, out-of-plane torsion and bending loads. However, the stiffness models are highly inaccurate for in-plane torsion and shear.

Approach and Work Scope

This program aims at (1) developing a new, robust spot-weld CAE simulation approach that provides the required accuracy of stress distribution to allow for realistic representation of different failure modes and failure mode transition as a function of impact, welding conditions and materials while maintaining the computational efficiency; and (2) a companion experimental database on the performance of RSW in AHSS components during impact. Three major research activities are planned to achieve the above program objectives.

- A new spot-weld-element formulation,
- A strain-rate-sensitive constitutive model incorporating the complex variations of microstructure and property in the RSW,
- Deformation and failure behavior database of AHSS spot-weld under different dynamic-loading conditions.

It is expected that the effort will be divided into two phases. The first phase will be an initial development of the SWE modeling framework and demonstration of the effectiveness of such modeling approach for the steel grades, thickness, and weld conditions selected by the Auto/Steel Partnership (A/SP). The initial development will cover two AHSS grades and one gauge thickness. The deliverables at the end of the first phase will be the initial version of the SWE and its implementation in FEM crash codes. The constitutive models to be used in a SWE will be based on strain-rate-sensitive elasto-plastic fracture and damage mechanics, and incorporate the microstructure changes in the weld region of AHSS. Welding process modeling and weld-microstructure characterization will be used to understand the welding effects. Failure criterion properly dealing with the failure mode changes during impact of AHSS spot-weld will be formulated based on the experimental data and fracture mechanics and damage mechanics principles. Figure 4. shows the organization and relationship among different tasks of the project.

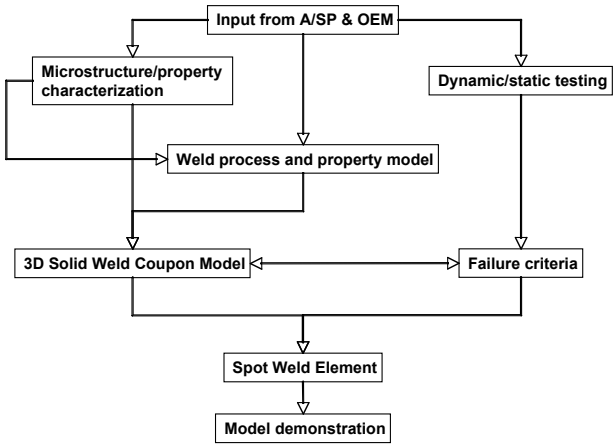

Figure 4. Project plan.

If the initial feasibility phase successfully demonstrates the effectiveness of the new modeling approach, a more comprehensive development phase will follow with the objectives of (1) further refining the SWE formulation and implementation procedure for different types of AHSS and component configurations, (2) more comprehensive component-level testing and model validation, and (3) expanding to other lightweight materials (Al, Mg alloys) and welding processes (weld bonding, friction-stir spot welding, etc).

Progress to Date

Working with the Strain Rate Characterization Committee of the Auto/Steel Partnership (A/SP, a test plan for producing welded coupons and dynamic testing has been finalized. Three steels have been selected: DQSK (IF) baseline mild steel, DP780, and boron steel. All steels sheets will be in the thickness range of 1.0 to 1.2-mm nominal. The dynamic testing will begin with lap-shear and cross-tension configuration. The mixed-loading-mode coupon and fixture design is underway and will be finalized before February 2007. Three different weld-nugget sizes will be made to study the transition of failure modes for each steel under different loading rate conditions. All welds will be made in 2-T stack-up configuration in this phase. The A/SP Strain Rate Characterization Committee will issue a procurement request to welding vendors to produce the welded coupons for dynamic testing using

welding conditions similar to those used in the production environments. All welded coupons will be fabricated before February 2007.

In addition, we have completed a critical review on modeling the spot-welds in automotive crash simulations. The review focused on the current state-of-the-art modeling approaches and their respective characteristics. A letter report is under preparation to summarize the critical review.

Conclusions

This is a new program started in August 2006. Working with the Strain Rate Characterization Committee of A/SP, we have finalized the testing matrix for lap-shear and cross-tension dynamic testing and the specifications to produce the welded testing specimens. The program is on time and on budget.

Presentations/Publications/Patents

None in FY 2006.

References

1. Committee on Automotive Applications (2005), *Advanced High Strength Steel (AHSS) Application Guidelines*, International Iron & Steel Institute.
2. Peterson, W. and Borchelt, J. (2000), *Maximizing Cross Tension Impact Properties of Spot-welds in 1.5mm Low Carbon, Dual-Phase, and Martensitic Steels*, SAE Technical Paper No 2000-2001-26680.
3. Shi, S.G. and Westgate, S.A. (2003), *Resistance Spot-welding of High Strength Steel Sheet (600-1200N/mm^2)*, TWI CRP Report No 767, The Welding Institute.
4. Kuo, M. and Chiang, J. (2004), *Weldability Study of Resistance Spot-welds and Minimum Weld Button Size Methodology Development for DP Steel*, *SAE* Technical Paper No 2004-01-0169.
5. Chiang, J. and Jiang, C. (2004), *Effect of Cooling Rate on Fracture Toughness at the Simulated HAZ of DP600 Steels*. SAE Technical Paper 04M-156.
6. Feng, Z., Chiang, J. and Jiang, C. (2004) *Effects of Steel Chemistry on the Microstructure and Property of DP600 Weld*, MPLUS Program Report, Oak Ridge National Laboratory.
7. Birch, R. S. and Alves, M., *Dynamic Failure of Structural Joint Systems*, Thin-Walled Structures, **36**:(2), 137-154.
8. White, M. D. and Jones, N. (1999), *Experimental Quasi-Static Axial Crushing of Top-Hat and Double-Hat Thin-Walled Sections*, International Journal of Mechanical Sciences, 41:(2), 179-208.
9. Schneider, F. and Jones, N. (2003), *Influence of Spot-Weld Failure on Crushing of Thin-Walled Structural Sections*, International Journal of Mechanical Sciences, **45**:(2), 2061-2081.
10. Xu, S and Deng X, (2004), *An Evaluation of Simplified Finite Element Models for Spot-Welded Joints*, Finite Elements in Analysis and Design, **40**:(9-10), 1175-1194.
11. Palmonella, M, Friswell, M. I., Mottershead, J. E. and Lees, A. W. (2004), *Guidelines for the Implementation of the CWELD and ACM2 Spot-weld Models in Structural Dynamics*, Finite Elements in Analysis and Design, **41**:(2), 193-210.
12. Rusinski, E., Kopczynski, A., and Czmochowski, J. (2004), *Tests of Thin-Walled Beams Joined by Spot-welding*, Journal of Materials Processing Technology, **157-158**:(20), 405-409.
13. Bayraktar, E., Kaplan, D. and Grumbach, M. (2004), *Application of Impact Tensile Testing to Spot-welded Sheets*, Journal of Materials Processing Technology, **153-154**:(10), 80-86.
14. Lin, S-H., Pan, J., Tyan, T. and Prasad, P. (2003), *A General Failure Criterion for Spot-welds under Combined Loading Conditions*, International Journal of Solids and Structures, **40**:(21), 5539-5564.
15. Rathbun, R.W., Matlock, D.K. and Speer, J.G. (2003), *Fatigue behavior of spot-welded high strength sheet steels*, Welding J., 207S-218S.

D. Friction-Stir Spot Welding of Advanced High-Strength Steel

Principal Investigator: Michael L. Santella
Oak Ridge National Laboratory (ORNL)
1 Bethel Valley Road, Oak Ridge, TN 37831-6096
(865) 574-4805; fax: (865) 574-4928; e-mail: santellaml@ornl.gov

Principal Investigator: Glenn J. Grant
Pacific Northwest National Laboratory (PNNL)
902 Battelle Boulevard, P.O. Box 999, Richland, WA 99352
(509) 375-6890; fax: (509) 376-6034; e-mail: Glenn.Grant@pnl.gov

Principal Investigator: Zhili Feng
OR NL
1 Bethel Valley Road, Oak Ridge, TN 37831-6096
(865) 576-3797; fax : (865) 574-4928; e-mail: fengz@ornl.gov

Principal Investigator: Yuri Hovanski
PNNL
902 Battelle Boulevard, P.O. Box 999, Richland, WA 99352
(509) 375-3940; fax: (509) 376-6034; e-mail: Yuri.Hovanski@pnl.gov

Technology Area Development Manager: Joseph A. Carpenter
(202) 586-1022; fax: (202) 586-1600; e-mail: joseph.carpenter@ee.doe.gov

Expert Technical Monitor: Philip S. Sklad
(865) 574-5069; fax: (865) 576-4963; e-mail: skladps@ornl.gov

---

Contractor: Oak Ridge National Laboratory & Pacific Northwest National Laboratory
Contract No.: DE-AC05-00OR22725 & DE-AC06-76RLO1830

Objective

- The primary objective of this project is to develop friction-stir spot welding (FSSW) as a superior method to join advanced high strength steels (AHSSs).
- Phase 1 activities will address the critical questions of whether there are tool materials available that have potential for reasonable life, and whether FSSWs made in high-strength steels are feasible and can develop similar or better mechanical performance than welds made by conventional processes like resistance spot-welding (RSW).
- Phase 2 activities will seek to increase joint strength through a more through investigation into weld process parameters and tool design. This will be accomplished both explicitly using new tools and refined operating parameters and by means of modeling both the process and fundamental conditions applicable to FSSW.

Approach

- The project is a collaborative effort between ORNL and PNNL, and includes an advisory committee with representatives from DCX, Ford, GM, two automotive steel suppliers, and a friction-stir welding tool supplier.
- Lap joints are made and used to correlate tensile shear strength with processing parameters and microstructures.
- Tool durability is evaluated by measuring tool wear after and during test programs and by characterizing the tool strength with changing welding conditions.
- Process modeling will be developed to help define optimum processing conditions and tool geometries.

Accomplishments

- Test programs fabricating spot-welds in DP780 and hot-stamped boron steel (HSBS) were initiated and a wide range of scoping weld parameters was investigated.
- Fabricated coupons were subjected to metallographic examination, hardness testing, and lap-shear tests.
- Metallurgically-bonded areas in the weld nuggets were measured, characterized, and found to be smaller than expected, thus indicating the need for more development work on weld process parameter and tool design.
- Two tool materials, tungsten 25% rhenium (W25Re) and polycrystalline cubic boron nitride (PCBN), and three tool geometries were initially investigated.
- Initial trials show that tool wear in PCBN is low, but tool wear in W25Re is high; however, tool wear and durability are strongly related to weld process conditions.
- Mechanical testing of phase-1 lap-shear coupons in DP780 and HSBS indicate that, while overall strengths weld parameters are in the range of acceptable values defined by the Draft AWS (American Welding Society) Specification for RSW of steel, the specific strength of nearly any condition exceeds the minimum stress condition.
- As tool geometry was found to have a profound effect on joint performance, four new tools were designed, procured and tested for the onset of phase-2 work.
- Several optimum and exploratory weld conditions were used with each of the four new tool designs with marked increase in lap-shear performance.

Future Direction

- Initial phase-1 study has shown joint strengths are at and just below the parameters set in the Draft AWS Specification for RSW of steels. Phase-2 activities will develop higher-strength joints through a more thorough investigation into weld process parameters and tool designs.
- Other factors critical to industrial implementation will be investigated including total spot cycle time, tool wear and robustness as a function of changing weld parameters, tool life, and the process of transferring optimized process parameters to a robotic system.
- Both process and fundamental models will be developed to predict weld performance with changing process conditions.
- Assess the potential for in-process NDE.

Introduction

The technology for implementing friction-stir spot welding (FSSW) of aluminum (Al) in automotive manufacturing environments exists. C-gun-type FSSW heads have been developed and adapted to robotic systems that are now commercially available for FSSW of Al alloys. This project addresses the questions of whether the FSSW process is viable for advanced high strength steels (AHSSs) and whether FSSW has advantages over conventional processes like resistance spot-welding (RSW). Preliminary work on FSSW of AHSS suggests that several

features of the process (fine-grained microstructure in the nuggets of AHSS, potentially higher-strength joints and higher energy absorption in crash, low energy consumption and environmental emissions during manufacturing) may give FSSW cost and energy-saving advantages over RSW. In addition, the process may be viable for lightweight materials that currently have joining problems using conventional techniques (DP1000, Martensitics, hot-stamp boron steels, etc). If this can be accomplished, the FSSW process may be an enabler for more widespread use of the lightweight, advanced and ultra-high-strength materials.

- Important questions remain about effective, economical application of FSSW to AHSS. Critical unknowns to be addressed in this study include:
- Are tool materials available that have potential for reasonable life?
- Are joint strengths comparable to or better than conventional processes?
- Are manufacturing issues appropriate (cycle time, tool wear, process robustness and sensitivity to production variation)?
- Do FSSW joints have any advantage for NDE, or for real-time process control over RSW?
- Are total-life cycle costs appropriate?
- Can the process be modeled and predictive tools developed to aid designers?

If FSSW of high-strength steels can be demonstrated and its advantages over RSW identified, then it may help to accelerate the insertion of lightweight, high-strength materials into automotive body construction to help meet FreedomCAR goals.

Approach

The primary objective of this project is to characterize the responses of AHSSs to FSSW. The project is organized into two phases. Phase-1 activities addressed the critical questions of whether there are tool materials available that have potential for reasonable life, and whether FSSWs made in high-strength steels could develop strengths comparable to those made by conventional processes like RSW. Phase 2 encompasses activities including development of a more detailed process model including weld performance prediction, evaluation of joint microstructures and mechanical properties, assessments of the potential for in-process NDE and establishment of the framework of a design database for spot-friction-welded structures. The project is a 50/50 collaboration between ORNL and PNNL, and it includes an advisory committee with representatives from DCX, Ford, and GM.

Three uncoated high-strength steels were selected for the Phase-1 study: 1) dual-phased steel, DP780; 2) a steel with transformation-induced plasticity, TRIP780; and (3) a hot-stamp boron steel (HSBS) sourced from a Swedish supplier. It was agreed to acquire the material in a thickness of 1.5 mm based both on easy availability from the steel suppliers (Mittal Steel Corp. and Gestamp US Hardtech, Inc) and on the level of interest among OEMs.

Two materials were selected for the friction-stir tools: polycrystalline cubic boron nitride (PCBN) and an alloy of tungsten containing 25 wt% rhenium (W25Re). Both materials are commercially available. Initially, four tool designs, shown in Figure 1, were selected using input from the industry supplier of the PCBN, MegaStir, Inc. The tool design shown in the upper left corner of Figure 1 is considered relatively conventional, having a pin that protrudes from its main body. The main body is referred to as the shoulder region with a diameter of 0.4 inches. The pin itself is a truncated cone with three flats.

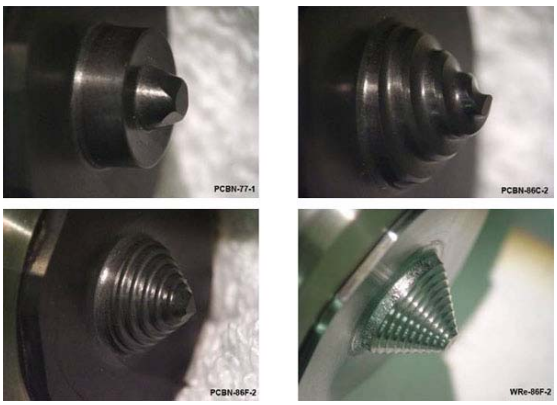

Figure 1. Tool geometries investigated in Phase 1.

The remaining three tools in Figure 1 depict 'shoulderless' tools. The tool in the upper-right corner is designated a coarse spiral and the two lower tools are fine-spiral designs. Both of these tools do not engage the shoulder with the workpiece. This geometry was recommended by MegaStir based on their exploratory work on FSSW. Two tools of each design and material were made and tested during Phase 1 of this study.

Lap joints were made to measure tension-shear strength, and to correlate strength with processing parameters and microstructures. Spot-welds were made by varying the parameters of tool plunge depth and tool plunging rate. In addition to these control parameters, a number of other process variables were recorded for each weld including weld time, spindle torque, normal force, and temperature on the back side of the two-sheet stack-ups.

Joint strength, as measured by lap-shear load, was correlated with these parameters. Joint strengths were also compared with those of resistance spot-welds using data from the Draft AWS Specification for RSW of Steel.

Correlations between weld process parameters, joint strengths, and bonded-area measurements developed throughout phase 1 were used to design new tools for phase-2 initiation. These optimized tools were subjected to similar testing to determine the effect of tool design on joint strength, bonded area and tool life.

Results and Discussion

Published data indicate the variables of plunge depth and weld cycle time are important for determining spot-weld strength in Al alloys. Based on this information, the initial testing plan for the AHSSs was meant to probe this parameter space by plunging to predetermined depths at constant rates, and by including a dwell at the end of each spot-weld program.

The friction-stir machine was used in displacement control during the spot-welding. The plunge depths were selected by considering the geometry of the conventional pin tool and the thickness of the two-sheet stack-ups being used for the welding. The pin extends beyond the plane of the shoulder by about 2.33 mm. The two-sheet stack-up is about 3 mm thick. Consequently, plunging to a depth of 2.3 mm would insert the pin entirely into the stack-up and just start to engage the shoulder of the tool on the surface of the top sheet. Plunging to a depth of 2.9 mm would insert the end of the pin nearly to the bottom surface of the bottom sheet. Based on this reasoning, the plunge depths were varied from 2.3-2.9 mm in 0.1 mm steps. Operating the machine in the displacement mode ensured that the desired final plunge depths were achieved.

Because the friction-stir machine was operated in displacement control, the dwell portions of the welding control programs required special consideration. Using a fixed-position dwell in displacement-control mode would permit the normal load on the tool to decrease due to temperature rise at the dwell position. It was believed that maintaining the loading conditions at the dwell position would promote better bonding. Consequently, incorporation of a dwell was accomplished by creating a two-step welding program that involved first plunging to nearly the full desired depth followed by further plunging the final 0.2 mm of depth at a slower rate. Three initial plunging rates were used: 0.4 mm/s, 2 mm/s, and 3 mm/s. The two secondary plunge rates used were 0.07 mm/s and 0.20 mm/s. These secondary plunge segments produced 'quasi-dwells' of either 1 s or 3 s at the end of each weld program.

Examples of two weld programs are shown in Figure 2. This procedure resulted in 14 individual welding programs at each plunging rate for 42 individual welding conditions. These 42 sets of conditions encompassed total welding times of 1.70-9.75 s. Spot-welds were made using both the conventional tool and the shoulderless tool. Six parameter sets were chosen to produce plunge depths of either 2.3 or 2.9 mm and weld times of 1.70, 2.05, 3.90, 4.35, 6.25 and 9.75 s.

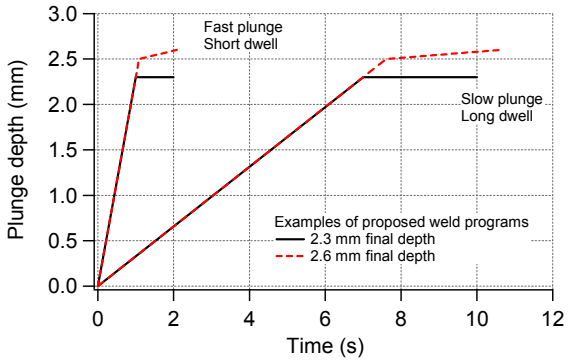

Figure 2. Illustration showing examples of conditions using for friction-stir spot-welding.

Figure 3 shows a representative micrograph of two friction-stir spot-welds in cross-section. These welds show the effects of different plunge depths at the extremes of the test matrix. The key feature of a high-strength joint is the width of the bonded area on each side of the exit hole. The bonded area is that part of the weld where the original surface between the two sheets disappears into the recrystallized and transformed stir zone on each side of the exit hole. Figure 3a shows a weld with a bonded area that is very narrow, due to an insufficient plunge depth. In Figure 3b, the bonded area is much wider indicating a significantly larger area of the joint was transformed, recrystallized, and plastically deformed. The original surface between the sheets has become a fully-mixed interface. Maximizing the bonded area is the goal of the process-parameter development because there is a strong correlation between bonded area and lap-shear strength. This is somewhat different from a resistance spot-weld where outer diameter of the spot is the key feature correlated with strength.

Figure 4 illustrates the shape of the bonded area in a FSSW. If the dimension W_w, the width of the annular bonded area, becomes too thin, then even large-diameter nuggets will fail at low loads because of lack of load-carrying section. This concept may require a different way of evaluating the quality of FSSW on the production floor. Joints that easily meet strength minimums may fail across this annular bonded area, and not by conventional nugget pullout. Inspecting and qualifying FSSW joints will be addressed in phase 2.

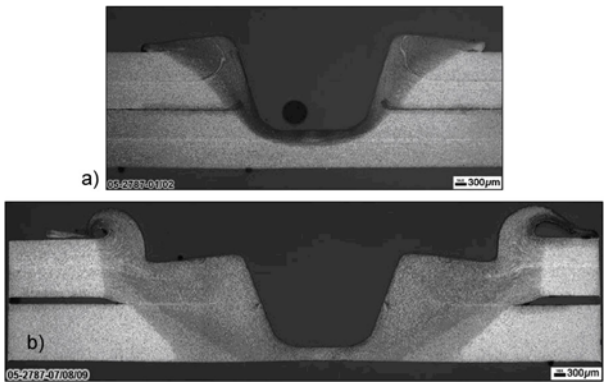

Figure 3. Bonded area is a function of tool design, plunge depth, tool material, shoulder heating, and process parameters (RPM, plunge rate, dwell).

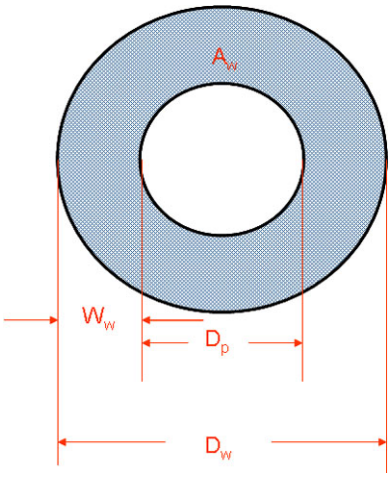

Figure 4. Geometry of the bonded area of a FSSW.

Figure 5 shows the correlation between lap-shear strength and total annular area of the bonded region. The area was calculated by measuring (by optical comparator) the dimensions of the sheared, or pulled-out, weld metal on the surface of a weld coupon after testing. It was assumed that these areas represent the bonded area, although in material cases where the heat-affected zone (HAZ) is weaker than the stir zone, the pull-out or sheared area will include more than just "nugget" material.

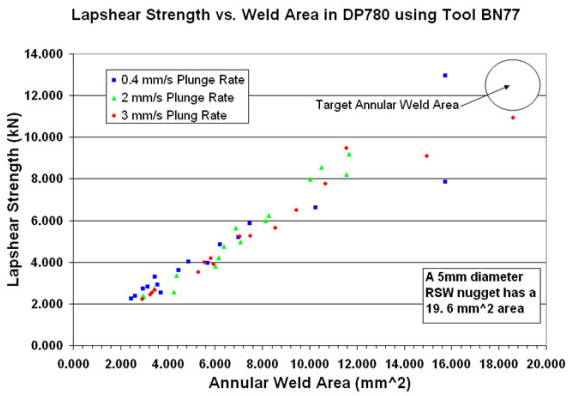

Figure 5. Lap-shear strength vs. annular weld area showing linear relationship.

Data in Figure 5 show a logical linear correlation between bonded area and lap-shear strength. For comparative purposes, a RSW joint with a nugget diameter of 5 mm will have an annular area of 19.6 mm^2. While the data in this graph are from a wide range of process parameters, only a single tool design (smooth-shouldered, smooth pin with three flats) was used. Plots like this allow for process optimization by pointing to operating parameters that lead to larger bonded areas and higher strengths. For example, lap-shear tests that resulted in loads above 10kN occurred in cases where plunge rates were on the high side of tested conditions (3mm/sec) and dwell times were longer (3 sec).

Figure 6 shows the relationship, for a single tool design, between lap-shear strength and total weld time, as defined by the time from tool touch down to retraction. (Also shown is the relationship between strength, plunge rate and dwell time). The figure shows there are process parameters where joint strength over 10 kN can be achieved at weld cycle times of 4 seconds.

Figures 7 and 8 demonstrate unique differences between FSSW and traditional RSW. According to the Draft AWS Specification for RSW of Steel, D8.1M:200X, minimum lap-shear strengths for spot-welds of overlapping 1.5 mm sheets in 780 MPa materials should be 10.4 MPa with an applicable minimum spot size of 19.6 mm^2. While several acceptable FSSW parameters produced lap-shear

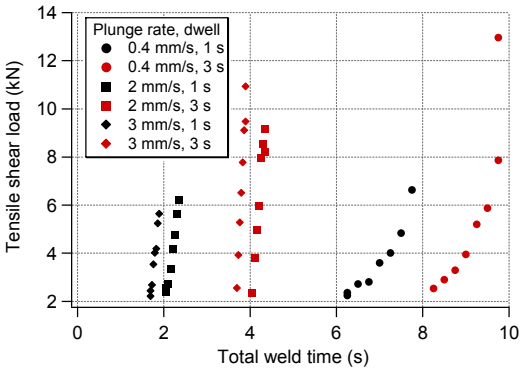

Figure 6. Lap shear strength vs. total weld time for a BN77 three-flat tool.

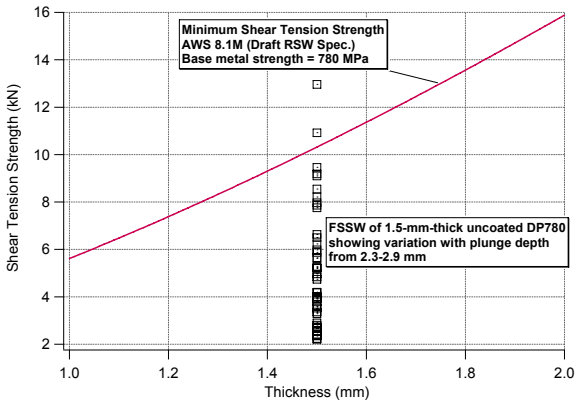

Figure 7. Graph represents data for all process parameters and a single conventional tool superimposed on a minimum strength standard for RSW welds (Draft AWS D8.1M:200X).

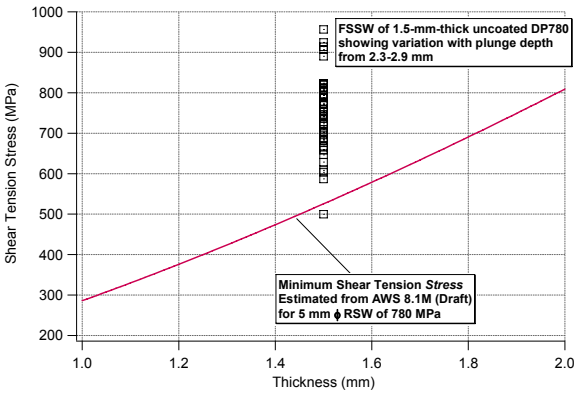

Figure 8. Graph represents specific strength data for all process parameters and a single conventional tool superimposed on a minimum strength/minimum area criteria (Draft AWS D8.1M:200X).

strengths exceeding such a requirement, bonded areas of the friction-stir spot-welds were below the required minimum spot size.

In order to compare the lap-shear response of friction-stir spot-welds to the Draft AWS Specification minimums, specific strengths of each FSSW specimen in DP780 were compared to the standard minimum requirement for 780 MPa steel with 1.5 mm thicknesses. Figure 8 more clearly demonstrates the lap-shear strength comparison of friction-stir spot-welds by factoring in the bonded area data into the specific-strength calculations. While these data shed a positive light on the ability of FSSW to retain a great percentage of the base metal strength, it also illuminates the need for developing tools and parameters that produce a larger bonded region in FSSW joints.

Four new tools were designed with the intent of increasing the overall bonded area of the FSSW. Pin lengths were shortened to force the shoulder to engage deeper into the top sheet, and pin geometry was altered to enhance the mixing characteristics of the tool. Additionally, one tool was chosen with a convex shoulder and short, threaded pin with the intent of mixing a larger region in a shorter duration.

Initial weld trials using the four redesigned tools shown in Figure 9 have provided marked increases in lap shear strengths and bonded areas.

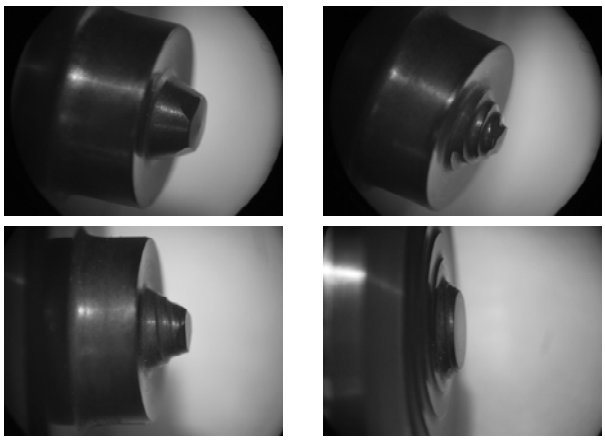

Figure 9. Initial phase 2 tools.

Tool Wear

Several hundred welds have been performed on the PCBN tool shown in the upper left part of Figure 1. No visible wear has occurred on the tool. More detailed and quantified wear studies are currently underway. Tungsten 25% rhenium tools, however, have shown significant wear. It is not yet clear if this is due to incorrect process parameters for this tool material (overload due to different thermal conditions) or if some kind of surface reaction or high friction condition is occurring between the W25Re and the steel base materials. The W25Re is under study for surface reactants currently to see if tool interaction with the work piece is at the core of the wear problem.

Conclusions

Friction-stir spot-welds were made on a two-high stack-up of DP780 and some initial trials on HSBS steel using polycrystalline cubic boron nitride tools. Three tool geometries were initially used, that of a conventional pin tool and two tools with a shoulderless geometry and differing thread pitches. Tool wear appeared negligible. Lap-shear results indicate that reasonable strengths can be obtained and that strength is highly dependent on tool design and process parameter. Phase 2 of this work will continue to investigate new tool designs and parameter development in an effort to increase the bonded area and increase the lap-shear strength. Phase 2 will also include the following scope:

- Other factors critical to industrial implementation will be investigated including total spot cycle time, tool wear and robustness as a function of changing weld parameters, tool life, and the process of transferring optimized process parameters to a robotic system
- Both process and fundamental models will be developed to predict weld performance with changing process conditions
- Assess the potential for in-process NDE
- Establish the framework of a design database for spot-friction-welded structures.

E. Long-Life Electrodes for Resistance Spot Welding of Aluminum Sheet Alloys and Coated High-Strength Steel Sheet (AMD 302[i])

Principal Investigator: Warren Peterson
Edison Welding Institute
1250 Arthur E. Adams Drive
Columbus, OH 43221-3585
(614) 688-5261; fax: (614) 688-5001; e-mail: warren_peterson@ewi.org

Project Manager: Eric Pakalnins
DaimlerChrysler Corporation
Materials Engineering- Welding
800 Chrysler Dr.
CIMS 482-00-15
Auburn Hills, MI 48326-2757
(248) 576-7454; fax: (248) 576-7490; e-mail: ep18@daimlerchrysler.com

Technology Area Development Manager: Joseph A. Carpenter
(202) 586-1022; fax: (202) 586-1600; e-mail: joseph.carpenter@ee.doe.gov

Expert Technical Monitor: Philip S. Sklad
(865) 574-5069; fax: (865) 576-4963; e-mail: skladps@ornl.gov

---

Contractor: U.S. Automotive Materials Partnership
Contract No.: FC26-02OR22910

Objective

- Survey the currently available technology for achieving long electrode life.
- Comparatively test a broad selection of existing and developmental electrode technologies that have technical merit.
- Investigate the electrode wear process through a combination of testing, metallography, and computer modeling.
- Evaluate a “best practice” electrode(s) through beta-site automotive production testing. The goal of these tests is to demonstrate the potential to double electrode life in a production environment through changes to electrode materials and/or geometry.

Approach

- Conduct benchmarking (Phase 1). A review of the open literature, available corporate literature, and interviews of industry experts produced a state-of-the-art report on electrode wear. This phase has been completed.
- Conduct testing (Phase 2). Candidate electrode technologies were screened and in-depth testing of electrodes was performed to help define the mechanism(s) of electrode wear. “Best practice” electrodes for beta-site testing were produced as part of this phase. This phase is complete, except for completion of the beta-site tests.
- Computer modeling (Phase 3). Computer models of the electrode metallurgical and mechanical changes that occur as a result of electrode wear were developed. These models helped to investigate the mechanism(s) of electrode wear and define the best practice electrodes. This phase is complete.

Accomplishments

Accomplishments that have been completed since the last reporting period:

- Completed beta-site tests at the DaimlerChrysler Windsor assembly plant on galvannealed steel.
- Developed procedures for establishing stepper procedures evaluating comparative stepper-based electrode testing in a production environment.
- Established optimum production stepper schedule for "best practice" electrodes – able to double and triple electrode life on actual application.
- Developed procedures for comparing "best practice" electrodes for the DiamlerChrysler beta-site tests.

Future Direction

- All work completed.

Introduction

Resistance spot-welding (RSW) has been heavily adopted by the automotive industry due to its relatively low capital and operating costs and the capacity to support high production rates. RSW is commonly used to weld high-strength steel and aluminum (Al) in vehicle construction. These materials are commonly selected to reduce vehicle weight and thus improve fuel economy and reduce greenhouse gas emissions. However, electrode wear of coated steels and Al continues to be a significant issue. Electrode wear adversely affects the cost and productivity of automotive assembly welding due to reduced weld quality, reliability, and robustness. This mandates increased inspection rates and greater control of welding parameters. Consequently, large potential cost savings and quality improvements are expected from substantial improvements in electrode life.

As technology has developed, few engineering solutions have been successfully introduced into the manufacturing process to manage electrode wear. Weld-current steppers and electrode-cap dressers have been used for many years, but these techniques do not resolve the underlying causes of electrode degradation. More recent efforts to remedy electrode wear have resulted in innovative electrode technologies, such as new material compositions, material inserts at the electrode face, surface-coated electrodes, and nontraditional electrode geometries (P-, G-, and S-nose). The scope of the present investigation is to objectively evaluate existing and developmental electrode material and geometry technologies to improve electrode life in production.

Review of Previous Work on AMD 302

The overall program organization is schematically illustrated in Figure 1. Prior work in AMD 302 covered most of Phases 1 to 3. The current work activities cover the beta-site testing (Phase 2) of electrodes developed from Phases 1-3. The scope of work in AMD 302 has focused primarily on the influence of electrode materials on the electrode life of both Al and high-strength galvanized steels. However, after completing several electrode life tests on Al using a number of electrode materials, no demonstrable plan based on electrode composition was clearly highlighted. Electrode wear in Al occurs through deposition of Al onto the face of the electrode. The factors that contributed to reduce sticking of the tip to the Al sheet during electrode

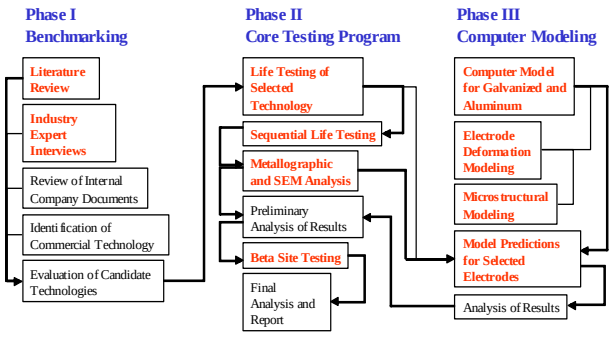

Figure 1. Current activities include production of targeted electrodes and beta-site testing in Phase 2. Work completed in previous phases include: benchmarking, core testing, and computer modeling.

retraction were opposite to those which improved weld-nugget stability. Additionally, this work showed that the solutions to electrode wear involved much more than just a study of alternate electrode materials. As a result, this part of the program was curtailed and additional efforts were focused on the electrode wear mechanism on steel.

Achievement of the program objectives for galvanized steel required a fundamental understanding of how electrode wear occurs. In prior phases of this work, three key processes responsible for electrode wear in RSW have been identified, namely, electrode-face extrusion, gamma-brass deposition onto the steel sheet, and weld-nugget stability. In this program, these three processes have been integrated into a coherent mechanism to describe the weld-nugget failures associated with electrode wear. In summary, the first two wear processes act to enlarge the contact area at the electrode face. This reduces current density and results in an inherent loss of weld-nugget stability in galvanized steels. This mechanism also addresses the phenomenon of pitting and electrode sticking associated with the metallurgical phenomena occurring during electrode wear.

The electrode wear mechanism developed in this program was based on interpretation of standard electrode life and stepper tests performed on several common electrode geometries that were produced from standard and developmental electrode materials. Computer modeling of the two electrode-enlargement processes described above were developed to better understand significant aspects of the phenomenon, such as edge extrusion rate, electrode surface temperature, and brass evolution. This was coupled with information from a detailed metallographic examination of the electrodes at several stages of electrode wear. The metallographic work identified the development, formation rate, and composition of brass alloys and parting layers on the face of the electrodes throughout electrode life. Altogether, this work formed the foundation of the electrode wear mechanism that described spot-weld behavior during electrode life in galvanized steel.

Electrodes Studied in the Beta Test Phase

Two beta-site test locations were identified. The work performed at General Motors has been previously reported. The present report focuses on the beta-site evaluation at DaimlerChrysler. Both sites used the best-practice electrodes based on either reducing the electrode surface temperature or maintaining a high current density by promoting a protrusion, or narrowed conduction path through the workpieces. These two approaches are summarized below:

- **Low Face Temperature Approach** (reduce rate of electrode face enlargement)
  - Internal fins and reduced face thickness
  - Conductive electrode material
  - Balance conductivity, electrical surface resistance, thermal conductance, and high-temperature strength

- **Sacrificial Electrode Approach** (maintain current density by protrusion formation)
  - One-dimensional heat flow, face must be hot to maintain protrusion
  - Selective sticking, deformation, and chemical erosion occur sacrificially to maintain protrusion
  - Protrusion formation produces a high current density in the center of the electrode that promotes nugget stability

The latter approach uses either P-cap or G-cap sacrificial electrode-nose geometry with appropriate material to reduce electrode sticking and maintain the protrusion under high heat conditions.
The candidate electrode materials and geometries considered for beta-site testing are listed in Table 1.

Table 1. Candidate Beta-Site Test Electrodes.

Material	Electrode Design	Beta Site Test Material	Approach
CuZr	E-cap w/internal fins	HDG	Low Temperature
CuZr	B-cap w/internal fins	GA, HDG	Low Temperature
M material	E-cap	GA, HDG	Low Temperature
M material	B-cap	GA, HDG	Low Temperature
M material	G-cap	GA, HDG	Sacrificial
Al_2O_3 ODS	P-cap	GA, HDG	Sacrificial

GA = Galvannealed
HDG = Hot-Dip Galvanized

Due to corporate preferences, the electrode geometries used in the beta-site tests were limited to 16-mm body diameter B-nose cap designs with 4.8-mm flat faces. Both conventional CuZr and an experimental alloy, Alloy M, were evaluated in these tests. The CuZr electrodes incorporated fins to increase surface area and facilitate heat transfer at the water cooling channel. The electrodes made from both materials used reduced face thickness (6-7 mm) to further enhance heat flow.

DaimlerChrysler Windsor Assembly Plant Beta-site Test Results

The DCX beta-site tests were performed on a non-safety-critical part with easy equipment access and good plant support. The joint combination was 0.66- mm galvannealed DQ steel welded to 1.2-mm galvannealed 350-MPa steel. A stationary pedestal-type AC welder was used with robotic part manipulation. 11 welds are made per part at a welding rate of about 30 welds per minute (wpm). The electrodes were replaced once per shift. The initial stepper schedule produced about 3400 welds before electrode replacement. The standard electrodes were composed of dispersion-strengthened copper (DSC) core with a CuZr body and used a similar B-nose design with standard face thickness (10 mm).

The original stepper-based weld schedule at the DaimlerChrysler Windsor Assembly Plant was:

- Electrode force: 330 lbf
- Weld time: 14 cycles
- Hold time: 2 cycles
- Initial Current: 9000A
- Stepper Slope: 2A/weld for 1000 welds, 1.5A/weld for 1500 welds, 1A/weld for 1500 welds

This schedule produced a current of approximately 15.5 KA after one shift. Initial observations of the standard production processing of the beta-site test application showed that every weld was made at expulsion for at least the first 2500 welds.

Weld quality during the beta-site trials was primarily monitored through periodic component teardowns. Ultrasonic testing was available, but the equipment was out of service during many of the early weld trials at the facility. Without frequent non-destructive testing, visual detection of expulsion was the method used to verify the presence of a weld.

However, maintaining expulsion accelerates electrode wear and increases the stepper slope rate. Thus, with greater expulsion frequency, higher stepper slopes are expected, limiting the effective electrode stepper life. Alternately, lower current-stepper slopes reduce the rate of electrode face enlargement, but endanger weld quality if the stepper slope is insufficient to maintain the minimum weld size. While undersized welds are acceptable in the laboratory to determine the need to increase weld current, they are unacceptable for assembly operations. Additionally, operating current values vary due to differences in materials, prior processing, and setup practice. Therefore, production weld currents must be maintained high enough to produce acceptable welds under most normal production conditions. These factors tend to favor high operating weld-current levels and steeper stepper slopes.

Selection of the appropriate stepper slope also involved operating below the upper limit of the transformer and scheduling the opportunities to exchange electrode sets. At the DaimlerChrysler site, the opportunities to change the electrodes for this part occurred during lunch breaks and shift changes. Historically, electrode changes for this application have been made on each lunch break. The goal of the AMD 302 project was to double electrode life in production. However, doubling the electrode life in a 3-shift operation would result in changing the electrodes every other shift. In order to reduce confusion, DCX personnel suggested changing the electrodes twice daily or every shift and a half. Alternately, the electrodes could be changed once per day.

The maximum stepper rates to achieve a 1½- and a 3-shift electrode change are 0.75 amp/weld and 0.35 amp/weld, respectively. This is based on 3400 welds per shift, initial current, and upper operating current limit of the transformer. Based on the initial trials, a decision was made to change the electrode sets twice daily. This meant that the

electrodes should be fully capable of reaching two shifts during the weld set-up testing.

The first stage of stepper development during these trials was to reduce the initial operating current and stepper slope. A weld schedule suitable for producing welds over 1½ shifts (average 0.75 amp/weld) during the beta-site testing with the M electrode material was:

- Electrode force: 380 lbf
- Electrode geometry: B-cap with 4.8-mm flat face on 16-mm body diameter
- Electrode material: M electrode
- Weld time: 10 cycles
- Hold time: 2 cycles

Different combinations of stepper slopes were evaluated to extend these results through a full second shift. The stepper rate was divided into three portions:

- 0.65 amp/weld for 2500 welds
- 0.76 amp/weld for 2500 welds
- 0.85 amp/weld for 2500 welds

The increasing stepper slope values maintained the appropriate current density as the electrode face size increased.

Acceptable electrode life performance was based on maintaining weld quality during the stepper campaign using the prescribed stepper schedule developed for doubling electrode life.

Experience on this project showed that if the weld-current was able to sustain low numbers of expulsions per part, then weld quality was significantly improved compared to the original welding practices. Conversely, if the number of expulsions per part decreased using the prescribed stepper schedule, then weld quality deteriorated.

DCX Beta-site Production Trials

A graphical summary of the 12-hour production weld trials performed on the M Alloy, CuZr Finned, and original DSC electrodes are given in Figures 2 to 4. These plots show moving averages of the number of welds exhibiting expulsion per 11 welds made per part. This expulsion rate is plotted against the number of assemblies made during the trials. While the numbers of assemblies per shift varied, the average number of assemblies between electrode changes was approximately 550.

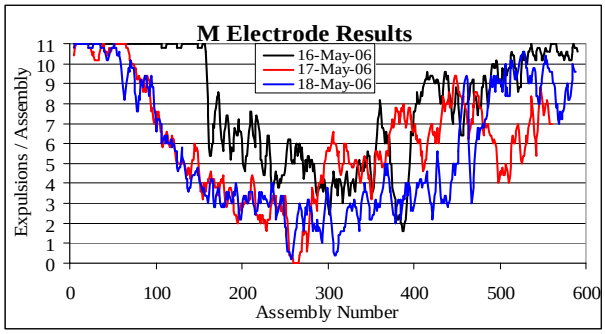

Figure 2. The average number of expulsions per part (11 welds maximum) plotted against the number of assemblies (parts) made for the 12-hour trials on the reduced face thickness B-cap M electrode.

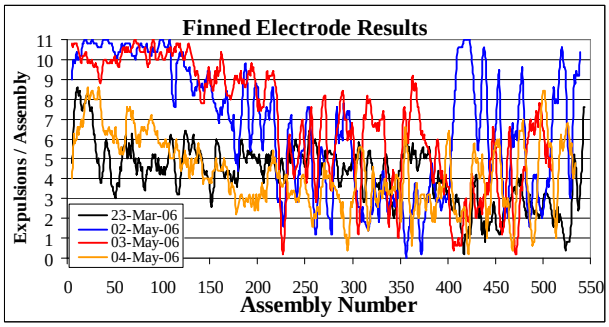

Figure 3. The average number of expulsions per part (11 welds maximum) plotted against the number of assemblies (parts) made for the 12-hour trials on the reduced face thickness B-cap CuZr Finned electrodes.

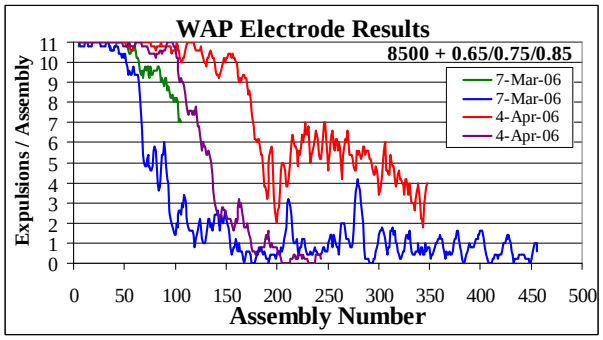

Figure 4. The average number of expulsions per part (11 welds maximum) plotted against the number of assemblies (parts) for the 12-hour trials on the original DaimlerChrysler electrodes.

The M Alloy and the CuZr Finned electrodes successfully passed weld-quality requirements using the prescribed stepper schedule during six 12-hour production weld trials. The original DSC electrodes were unable to maintain consistent weld quality during the 12-hour trials and these tests were terminated. This demonstrated the improvement in electrode life using the best-practice electrodes.

The success of the finned caps at the DCX beta-site promoted a further reduction in stepper slope in an effort to produce a 24-hour weld trial. The stepper rate was divided into three portions:

- 0.35 Amp/weld for 5000 welds
- 0.40 Amp/weld for 5000 welds
- 0.45 Amp/weld for 5000 welds

This stepper schedule was successfully used on the finned caps over three shifts as shown in Figure 5.

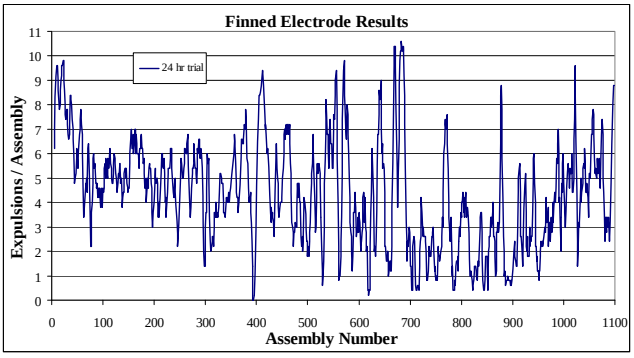

Figure 5. The average number of expulsions per part (11 welds maximum) plotted against the number of assemblies (parts) made for a 24-hour trial on the reduced face thickness B-cap CuZr Finned electrodes.

Metallographic Evaluation of the Electrodes

The working surface of the electrodes was photographed prior to metallurgical sectioning to examine the electrode surface and cross-section in a manner similar to that done in previous phases. Similar to other phases of the program, these results showed that recrystallization occurred at the face of the CuZr electrodes producing softening at room temperature. Conversely, the M Alloy and DSC (original DCX) electrodes maintained a fibrous grain structure with slight softening occurring on the M Alloy electrode at room temperature.

Observations of the electrode face showed that the CuZr electrodes had a smooth surface appearance with minor pitting. Conversely, the M Alloy and DSC electrodes exhibited rough surface appearances with extensive central pitting. In addition, the M Alloy electrode showed surface cracking. The brass alloy distribution and layer thicknesses were similar to those from the GM tests with exception of the original DSC and the 24-hour finned electrodes. These two electrodes had much thicker parting layers at test termination.

These observations confirmed that chemical erosion (dissolution and deposition of brass onto the workpiece) is a very significant component of the electrode wear process.

Benefits of Improved Electrode Life

Improvements in electrode life reduce the number of electrodes and labor associated with electrode replacement. Improved electrode life improves process robustness and can result in a reduced-frequency weld-quality inspection. In addition, the lower stepper rates associated with improved stepper schedules require less energy on a per-day basis. This latter point is illustrated in Figure 6 showing total energy for the M Alloy and Finned electrodes relative to the original DSC electrodes. The M Alloy reduces energy consumption by 6% while the Finned electrodes provide an 18% reduction relative to the DSC electrodes.

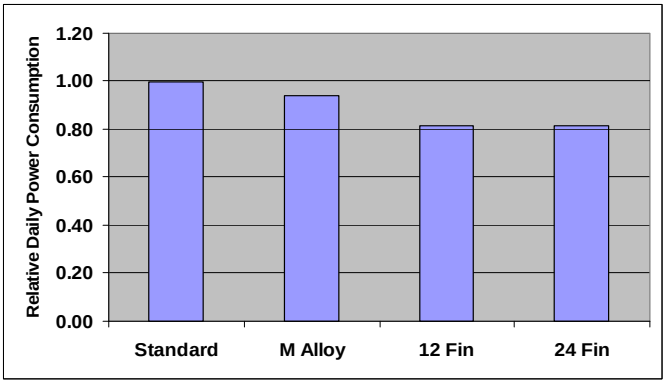

Figure 6. The relative daily power costs for the M Alloy and Finned electrodes relative to the original DSC electrodes used on the beta-site application plotted against the number of number of hours.

Conclusions

The work performed in the beta-site phase of AMD 302 has shown that the stepper performance of the "best practice" varieties of electrodes met the project expectations of doubling and potentially tripling electrode life on galvannealed steel in a production environment. Significant results from the beta-site tests include:

1. The stepper slope for galvannealed steel is much lower and more repeatable than the slopes produced on hot-dip-galvanized steel.
2. The "best-practice" electrodes developed from previous phases of this work may be machine and application dependent. Specifically, these electrodes are strongly influenced by the volume of cooling water.
3. Increasing stepper-slope schedules maintain current density as the cap face increases in size.
4. Evolutionary operation-type experimental plans were used to develop optimized stepper schedules in production.
5. The CuZr Finned electrode provided up to 24-hours (3 shifts) of electrode life under production conditions.
6. The M Alloy electrode provided 2 shifts of useful electrode life under production conditions.
7. The original electrodes at the DCX beta-site were unable to maintain a consistent performance for a 2-shift extension of electrode life.
8. The significant role of chemical erosion was shown in electrode face enlargement for specific electrode materials.
9. Improved electrode life results in significant cost savings due to power reduction, improved process robustness, and electrode replacement costs.

Presentations/Publications/Patents

2003. Gallagher, M. "Electrode Wear in Resistance Spot Welding of Galvanized Steel Sheet". M.A. Sc. Thesis, University of Windsor, Windsor, ON.

2004. Peterson, W.A., Gould, J.E., Bowers, R., Santella, M., Babu, S. "Evaluation of Electrode Design and Materials for Improving Electrode Life," Sheet Metal Welding Conference XI, Paper 1-6. Sterling Heights, MI (May 11-14). AWS - Detroit Section.

2004. Gallagher, M., Athwal, K.S.B., Bowers, R., "Evaluation Wear Characterization in Resistance Spot Welding," Sheet Metal Welding Conference XI, Paper 1-5. Sterling Heights, MI (May 11-14). AWS - Detroit Section.

2004. Babu, S., Santella, M., Peterson, W.A., "Modeling of Resistance Spot Welding Electrode Life," Sheet Metal Welding Conference XI, Paper 7-2. Sterling Heights, MI (May 11-14). AWS - Detroit Section.

2005. Athwal, B. "Characterization of Electrode Wear Morphology via Sequential Life Testing". M.A. Sc. Thesis, University of Windsor, Windsor, ON.

Acknowledgements

The author would like to acknowledge the members of the AMD 302 project team for their hard work in successfully completing the work to date: Mike Santella of the Oak Ridge National Laboratory; Randy Bowers and Jeremy Caron of the University of Windsor; Jerry Gould, and Suresh Babu (previously ORNL) of the Edison Welding Institute; Eric Pakalnins of DaimlerChrysler; Mike Karagoulis and Peter Sun of General Motors; Arnon Wexler of Ford Motor Company; Brian Swank and Paul Ruess of Outokompu-Nippert; David Fleckenstein of CMW; Bill Brafford and Chuck Pfister of Tuffaloy; Nigel Scotchmer of Huys Industries; and Tom Natale of AK Steel.

The continuing support of our respective companies and the U.S. DOE is gratefully acknowledged.

[i] Denotes Project 302 of the Automotive Materials Division (AMD) of the United States Automotive Materials Partnership (USAMP), one of the formal consortia of the United States Council for Automotive Research set up by the "Big Three" traditionally U.S.-based automakers to conduct joint pre-competitive research and development.

F. Thermal-Drilling Application Development

Principal Investigators: Peter J. Blau
Oak Ridge National Laboratory (ORNL)
P.O. Box 2008, Oak Ridge, TN 37831-6063
(865) 574-5377; fax: (865) 574-6918; e-mail:blaupj@ornl.gov

Dean M. Paxton
Pacific Northwest National Laboratory (PNNL)
P.O. Box 999/K2-03,Richland, WA 99352
(509)375-2620; fax: (509)375-2186; e-mail:dean.paxton@pnl.gov

Technology Development Area Manager: Joseph A. Carpenter
(202)586-1022; fax: (202)587-1600; e-mail: joseph.carpenter@ee.doe.gov

Expert Technical Monitor: Philip S. Sklad
(865) 574-5069; fax: (865) 576-4963; e-mail: skladps@ornl.gov

Participants:
This project is being conducted as a partnership with USAMP-AMD[1] *that includes the following automotive company representatives:*
Bill Charron, Ford Motor Company
Larry Krawczak, Daimler-Chrysler Corporation
Ron Strong, General Motors Corporation

Contractor: Oak Ridge National Laboratory
Contract No.: DE-AC05-00OR22725

Objectives

- Determine the feasibility of using thermal drilling (ThD) to form fastener holes in high-strength steels and lightweight alloys in the form of castings, hydroformed parts, and sheet stock.
- Determine suitable ThD parameters for selected alloys if they prove to be amenable to the process.
- Thermally drill and tap fastener holes, measure their critical dimensions, and conduct clamp-load tests to compare ThD samples to those with traditionally-produced fastener holes.
- Develop a better understanding of the way in which the initial microstructure of the workpiece affects ThD hole quality, and in turn, the way in which ThD can affect microstructure.

Approach

- Alloys for ThD tests will be selected and provided by USAMP project team members. Thermal-drilling bits will be purchased or provided as in-kind contributions by tooling suppliers.
- ORNL will conduct ThD and tapping experiments on the selected alloys, noting which perform best. Hole dimensions and microstructures will be studied and documented.
- Where possible, methods will be developed to correct any observed hole defects. Needs for future process development will be documented.
- Maximum fastener clamp loads will be measured at PNNL and related to ThD parameters.

- The USAMP team will assess the feasibility of introducing ThD more widely in automotive component manufacturing and provide recommendations for further development.

Accomplishments

- Four high-strength steels and six non-ferrous alloys (Al and Mg-based) were obtained. Fixtures were fabricated to enable drilling of thin stock without excessive deflection or loss of frictional heat.
- Thermal-drilling conditions were found that avoid 'flower-petal' defects in Al alloys.
- Measurements were made to assess the extent to which the original stock thickness was increased by ThD.
- An improvement was made to a previous analytical model for thermal drilling and submitted for publication.
- A compilation of suitable ThD parameters for the selected alloys has begun. Alloys that worked well and those that require more process development are indicated.
- Metallographic cross-sections were prepared to study thermal-drilling-induced deformation and to investigate the differences between thread-cutting and thread-forming taps in Al.
- Clamp-load tests were begun on steels that had the best ThD response.

Future Directions

- Work will continue to complete the matrix of acceptable ThD parameters.
- Additional hole measurements and clamp-load tests are planned for hydro-formed steels.
- The drilling performance of tri-lobed thermal drills will be compared to those for four-lobed drills.
- ThD tests on M6 fasteners will be extended to include a limited number of M8 and M10 holes as well.
- Participants will identify ThD areas for future development, commercialization, and process optimization.

Introduction

Thermal drilling (ThD) is also known as "friction drilling." It is a member of a family of joining methods and surface conditioning processes that utilizes the frictional heat generated between a rotating tool and a metal part. Related processes include friction-stir welding and friction-stir processing. In ThD, a conically-tipped tool (usually metal-bonded tungsten carbide) spins against the surface of the part to be drilled, generating heat and softening the surface. It penetrates and then perforates the workpiece, as shown in Figure 1. Softened material is extruded to form a bush on the exit side of the workpiece. A small boss may also be formed on the entrance side, under the wide portion of the tool. Another version of the tool, having a cutter to remove the boss, is commercially available.

Advantages of ThD include the following:

- Unlike traditional drilling, ThD creates no chips.
- ThD does not require drilling fluid that must be handled and disposed of.
- By forming an extruded bush, ThD thickens the effective tappable thickness of thin workpieces, like sheet stock and thin-walled castings, so that weld nuts (with their added weight and assembly operations) may not be needed.
- ThD may enable designs that would be impossible due to the need to install nuts or get at the exit side of the hole.
- ThD could simplify manufacture of chassis components from lightweight materials.
- In cast materials, the ThD extrusion may eliminate the added mass of bolt bosses and thick flanges.

ThD is currently used in the manufacture of tubular hospital furniture and certain niche applications, but has not been adopted in the automotive industry where it has significant potential to enable more extensive use of lightweight, high-strength alloys.

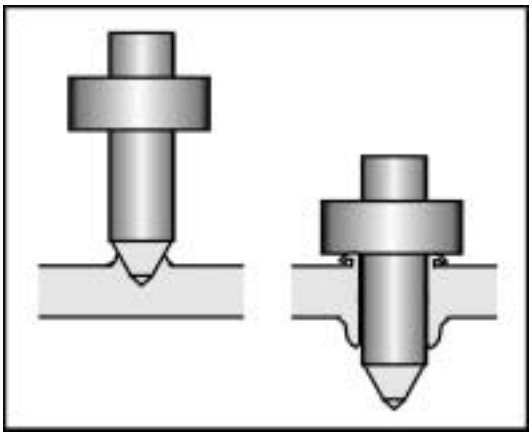

Figure 1. Schematic representation of thermal drilling. The spinning tool penetrates the workpiece to form a boss (inlet side) and bush (exit side).

The goal of this project is to demonstrate the feasibility of using ThD on ferrous and non-ferrous alloys of interest to the automotive industry. The alloys selected by the USAMP project team and provided for testing are listed in Table 1. They comprise a range of materials and product forms, and some materials were provided in more than one thickness.

Technical Approach

The technical approach draws on the strengths of USAMP team members and national laboratories. :

- Obtain alloys and determine fixturing requirements for workpiece materials.
- Obtain thermal-drilling bits from Formdrill™ and Flowdrill™.
- Determine criteria for ThD hole quality.
- Conduct and document systematic experiments on each alloy to determine suitable ThD conditions and their effects on hole quality.
- Determine which alloys can be effectively thermal drilled and which are problematic.
- Prepare ThD and tapped specimens of drillable alloys for clamp-load testing.
- Conduct clamp-load tests and compare results to traditionally-drilled holes and weld nuts.
- Assess metallurgical effects of ThD, considering both the initial condition of the stock material and the post-drilled and tapped conditions.

Table 1. Materials provided for thermal-drilling studies.

Alloy	Form
Al A380	Die casting
Al A319-T5	Die casting
Mg AZ91	Die casting
Mg AM60	Die casting
Mg AE44	Die casting
Mg AM50	Die casting
DP 600 HSS	Sheet
DP 780 HSS	Sheet
HSLA50 HSS	Sheet
TRIP 800 HSS	Sheet

The USAMP project team provides advice and critical evaluations of progress. Specifically, ORNL prepares ThD test specimens and conducts related metallurgical studies. For example, Figure 2 shows a polished cross-section of a Mg alloy in the as-drilled condition and before tapping.

PNNL conducts fastener clamp-load tests and analyses using their LabMaster Fastener Evaluation Test Cell. That unit can measure the clamp load from the installation of a fastener into a thermally-drilled hole. PNNL also determines the mode of clamp-load failure, such as thread stripping or fastener breakage.

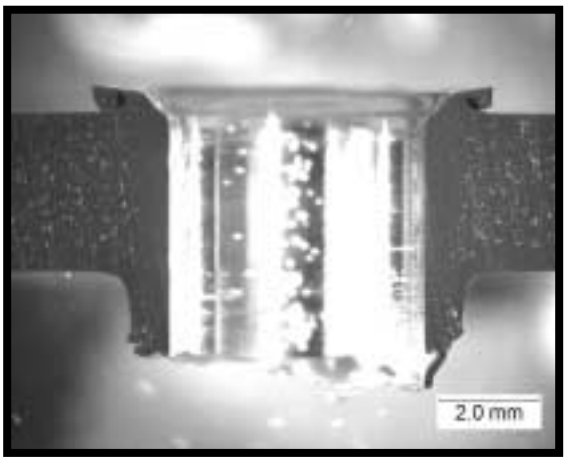

Figure 2. Polished cross-section of a thermally-drilled Mg alloy casting. The as-drilled hole interior has a bright, smooth surface finish. (The small white dots in the image are bubbles in the mounting medium and can be ignored).

Thermal-Drilling Results

In addition to the different alloys to be evaluated, the process variables used in these experiments included the following: (a) hole diameter (drill-bit diameter), (b) drill length, (c) spindle speed, (d) in-feed rate, (e) stock thickness, (f) use of drilling paste, (g) use of pre-heating or pilot holes, (h) use of several types of bits, and (i) use of thread-cutting or thread-forming taps.

A preliminary assessment was made of the ease of drilling the various materials provided. The assessment was based largely on visual observations of the quality of the bushes created using bits for M6-sized holes. Table 2 summarizes these assessments. The codes used in Table 2 to describe thermal drillability were:

- **Poor** (***P***) – not suitable (distorted or torn bushes)
- **Marginal** (***M***) – might work but requires additional studies and process enhancements
- **Special Procedures** (***SP***) – satisfactory results are obtained when using special procedures like pilot-hole drilling or pre-heating
- **Good** (***G***) – expected to work acceptably well, especially by optimizing standard process parameters like spindle speed and in-feed rate.

Most steels that were evaluated worked well for ThD, but not all. The *P* rating given the TRIP 800 was based on the formation of flower-petal-like features at the exit sides of the holes, rather than the smooth conically-shaped bushes needed for subsequent thread-forming operations.

For the steels, spindle speeds for M6-sized fastener holes ranged from about 2000 – 4000 rpm, but for the non-ferrous alloys, speeds could be as high as 10,000 rpm.

Table 2. Preliminary Assessment of Thermal-Drilling Response of Selected Alloys.

Alloy	**Form and Stock Thickness (mm)** (Note 1)	**'Thermal Drillability' Rating**
Al A380	DC (4.1)	*S P*
Al A319-T5	DC (4.1)	*S P*
Mg AZ91	DC (1.5, 3.0, 6.0)	*M*
Mg AM60	DC (3.0)	*M*
Mg AE44	DC (3.0)	*M*
Mg AM50	DC (3.0)	*M*
DP 600 steel	Sh (1.2 – 2.2)	*G*
DP 780 steel	Sh (1.15 – 2.0)	*G*
HSLA50 steel	Sh (1.14)	*G*
TRIP 800 steel	Sh (1.0)	*P*

Note 1) DC = die-cast, Sh = rolled sheet or plate

The thermal-drilling "extension factor" (EF) was used to express the additional length benefit of the tapped hole that results from the formation of an extruded bush by ThD. It can be defined as follows:

$$EF = (B + t) / t$$

where B = the length of the extruded bush on the exit side of the workpiece (in the final as-drilled and tapped condition) and t = the starting stock thickness. *EF* can also be expressed as a percentage.

Based on preliminary studies of steel and Al specimens, the EF values are given in Table 3. In general, thinner stock produces higher EF values. Values have yet to be determined for Mg alloys.

Table 3. Extension Factors for Aluminum Alloys and Steels for Thermal-Drilled and Tapped M6 Fastener Holes.

Alloy	**Form and Stock Thickness (mm)** (Note 1)	**Extension Factor**
Al A380	DC (4.1)	1.32
Al A319-T5	DC (4.1)	1.31
DP 600 steel	Sh (1.2)	2.70
DP 780 steel	Sh (1.15)	3.07
HSLA50 steel	Sh (1.14)	2.90

Note 1) DC = die-cast, Sh = rolled sheet or plate

By the conclusion of FY 2006, most of the steels on hand had been tested to provide a preliminary evaluation of their drilling characteristics. Also, ThD and tapped samples were sent to PNNL on a regular basis. Since the Mg alloys presented certain challenges, these will be further investigated in the early months of FY 2007 and suitable specimens will also be sent to PNNL. Initial clamp-load tests on the steel were promising, as the following section reveals.

Fastener Testing at PNNL

Torque-tension testing was performed using the LabMaster Fastener Evaluation Test Cell at PNNL. The Atlas-Copco nut-runner was programmed to drive the fasteners to failure and the Labmaster software recorded clamp load and input torque versus time and angular rotations of the fastener for each test. The failure mode was noted at the end of the test (break the fastener or strip the threads). A total of three tests at each combination of material and hole type has been completed and reported for traditional machine-screw fasteners with a Magni 565 coating.

Figure 3 shows the maximum clamp load and input torque at failure for both conventionally-drilled and thermally-drilled holes (both followed by tapping) in a range of alloys and plate thickness. Torque-tension testing of 1.2-mm-thick plates with conventionally-drilled and tapped holes resulted in stripped threads at ~9 Nm with a minimal amount of clamp load generated at ~6 kN. By thermally drilling the same thickness plates to increase the threadable thickness, the torque at thread stripping increased to ~17 Nm with corresponding clamp load of ~ 15 kN.

During similar testing of 2.2-mm-thick DP600 plate with conventionally-drilled and tapped holes, the holes stripped at ~16 Nm and generated ~ 12 kN of clamp load. However, after the thermal drilling and tapping of the 2.2-mm-thick DP600 plate, the fastener broke after ~17 kN of applied torque and generated ~17 kN of clamp load.

Future Work

Plans for the future include: (a) completing ThD and tapping of the ten selected alloys, (b) completing clamp-load testing, (c) determining what special processing might be required for the Mg alloys to improve their ThD response, (d) completing a compilation of suitable ThD conditions for all test materials, (e) evaluating results for four-lobed versus three-lobed ThD bits, and (f) preparing recommendations for further development of thermal drilling as a cost-savings and environmentally- friendly technology for manufacturing lightweight automotive parts.

Conclusions

Considerable progress has been made in several key areas due in part to enthusiastic collaboration among team members and by the ability to draw upon prior work at ORNL and the University of Michigan. The following conclusions were reached:

1. High-strength steels, such as DP 600, DP780, and HSLA50, seemed well-suited for thermal drilling, but TRIP800 was not.
2. The formation of extended bushes by thermal drilling can increase the tappable hole length in steel sheet products by as much as 300%.
3. Thermal-drilling conditions must be developed for the specific material being drilled and cannot be generalized for all metals and alloys in a particular class (e.g., steels).
4. Clamp-load data for thermally-drilled and tapped steels were encouraging and suggest the potential for using this method in assembling certain steel automotive components.
5. Additional research on the processing method is needed to improve the thermal-drilling results for die-cast Mg alloys, although results for cast Al are encouraging.

Publications

None this reporting period.

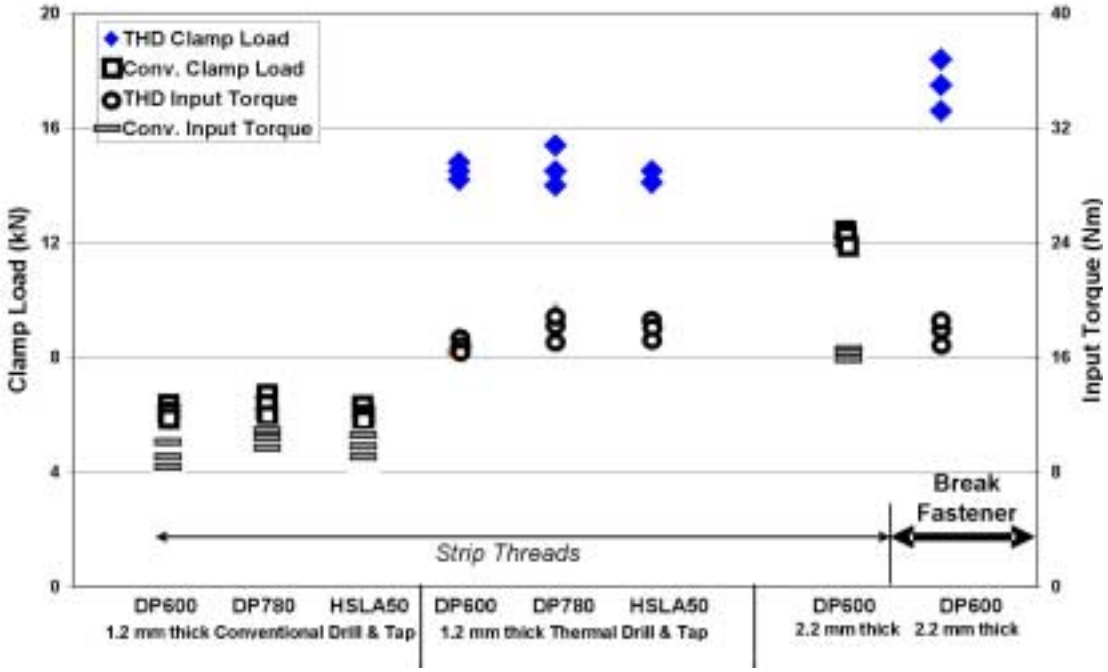

Figure 3. Torque-tension test results comparing conventional and thermally-drilled holes in a range of alloys and plate thickness.

[1] Denotes the Automotive Metals Division (AMD) of the United States Automotive Materials Partnership (USAMP), one of the formal consortia of the United States Council for Automotive Research (USCAR), set up by the "Big Three" traditionally USA-based automakers to conduct joint pre-competitive research and development.

6. NONDESTRUCTIVE EVALUATION

A. NDE Inspection of Resistance Spot-Welds in Automotive Structures Using an Ultrasonic Phased Array

Principal Investigator: Deborah Hopkins, Ph.D.
Lawrence Berkeley National Laboratory (LBNL)
1 Cyclotron Road, MS 46A-1123, Berkeley, CA 94720
(510) 486-4922; fax: (510) 486-4711; e-mail: dlhopkins@lbl.gov

Technology Area Development Manager: Joseph Carpenter
(202) 586-1022; fax: (202) 586-1600; e-mail: joseph.carpenter@ee.doe.gov

Expert Technical Monitor: Philip S. Sklad
(865) 574-5069; fax: (865) 576-4963; e-mail: skladps@ornl.gov

---

Contractor: Lawrence Berkeley National Laboratory (LBNL)
Contract No.: DE-AC03-765F0095

Objective

- Develop a cost-effective ultrasonic phased-array system that is sufficiently fast to inspect spot-welds in less than 4 seconds, that is also accurate and robust enough to be used in manufacturing environments.

Approach

- Work in conjunction with the U.S. Automotive Materials Partnership's Project AMD 409 (Contract No. DE-FC26-02OR22910).
- Develop a spot-weld inspection system that can be used by operators with minimal training by using state-of-the-art ultrasonic phased-array technology. The multi-element probe allows the ultrasonic energy to be focused at the interface between the welded sheets and electronically scanned through the weld.
- Design and fabricate a miniature mechanical scanner that will allow scanning in the direction perpendicular to the electronic scan to produce two-dimensional images of the weld. The portable system allows more than 4000 signals to be acquired in less than 4 seconds.
- Develop signal-processing and image-analysis software to distinguish satisfactory, undersized, and discrepant welds and provide dimensional analysis of the weld in a few seconds.
- Minimize the footprint of the probe assembly to ensure access to welds on complex components.
- Design and fabricate a probe housing that meets the size constraints while allowing mechanical scanning over a travel distance of 14+ mm. The housing must also maintain the probe in water and include an outer membrane that confines the water column and provides acoustic coupling to the part under inspection.
- Conduct trials on individual test specimens made under controlled conditions and on production parts to determine the resolution, repeatability, and accuracy of the prototype system.
- Conduct plant trials to demonstrate the system's ability to characterize welds with sufficient accuracy and repeatability in practice and to demonstrate that the integrated probe housing can be used successfully in a production environment by a trained operator.

Accomplishments

- Evaluated the performance and limitations of existing ultrasonic phased-array systems.
- Conducted a series of laboratory experiments to evaluate the performance of 5-, 10-, and 17-MHz phased-array probes for characterization of spot-welds in galvanized steel.
- Developed signal-processing algorithms to distinguish between satisfactory, undersized, and discrepant welds.
- Developed image-processing algorithms that allow three-dimensional analysis and dimensioning of welds.
- Demonstrated the ability to acquire more than 4000 signals per weld and analyze the resulting data in a few seconds to render an estimate of weld quality.
- Developed a difference-equation model that enables simulation as well as signal processing to recover reflectivity estimates, and to detect poor coupling and malfunctioning probe elements. Pre-processing algorithms are used to measure changes in thickness and to detect misalignment of the probe.
- Designed and fabricated a portable, integrated probe housing that maintains the phased-array probe in water, contains a miniature mechanical system that allows linear translation of the probe, and provides an outer membrane that confines the water column while also providing acoustic coupling to the part under inspection. Identified and tested coupling materials that allow satisfactory signals to be obtained outside of a water tank.
- Demonstrated good correlation between ultrasonic measurements and other measures of weld quality including measurements of weld buttons on peeled samples.

Future Direction

- Demonstrate technical feasibility by demonstrating good statistical correlation between ultrasonic measurements and weld buttons obtained by destructive teardown. Experiments are underway on production parts and specially-designed test coupons provided by industry partners that capture conditions found on production parts such as deep surface indentations and non-parallel sheets. Sample sizes are large enough to allow meaningful statistical analysis. Repeatability is being assessed by using three different operators to make measurements and by making repeat measurements.
- Conduct laboratory experiments to determine the concept feasibility of using ultrasonic phased arrays to inspect welds in advanced high-strength steels.
- Determine the diagnostic capability of measurable data including interface transmissivity, the spatial pattern of transmissivity, the number and spatial pattern of weak signals, and the depth of the surface indentation caused by the welding electrodes. Develop automated classifiers to determine weld quality and size, and to identify discrepant welds including cold welds.
- Develop a user interface in conjunction with end users to ensure ease of use and reporting of data in the most useful format for inspectors, welding engineers, and plant managers.
- Develop a fully-integrated prototype system suitable for deployment and testing in a manufacturing plant.
- Perform large-scale testing and measurement system analysis.

Introduction

Development of nondestructive evaluation (NDE) techniques is enabling for greater use of lightweight materials in the automotive industry where NDE methods to assure product quality are essential for industry and consumer acceptance of new materials and manufacturing methods. Recent studies have demonstrated cost savings associated with implementing NDE that derive from finding discrepancies early in the production process and reducing waste compared to destructive testing. One of the critical technical challenges in introducing lightweight materials is developing joining technologies and inspection strategies suitable for mass production. At present, the most common methods for inspecting spot-welds in automotive manufacturing are pry checks and physical teardown, during which spot-welded joints are pried apart and the resulting weld buttons are visually inspected or measured with calipers. Although these

methods have been used successfully for decades, destructive weld testing has several drawbacks including high costs associated with scrapped material, ergonomic injuries, and the time-lag between the onset and identification of problems. In addition, pry tests and teardowns do not allow quality-control personnel and engineers to easily collect inspection data that would allow them to identify trends and potential problems. Furthermore, these inspection techniques are not viable options for lightweight and high-strength materials, as well as non-pryable welds. For example, composite structures with adhesive-bonded joints cannot be pry checked, and aluminum is relatively expensive and more difficult to rework than steel making pry checks and teardown cost prohibitive.

Advances in sensors, computing, communication, and engineering technologies have all played a role in advancing the development of NDE methods with promising automotive applications. For example, ultrasonic phased-array systems have been available since the mid-1970s, but they were prohibitively expensive. In the past decade, prices have dropped dramatically, and increased competition promises additional price reductions in the future. A recent breakthrough is the availability of portable systems that are particularly attractive for use in production environments.

To best advance the adoption of lightweight materials while also serving the needs of the auto industry, the current project team has adopted a strategy that strives to develop platforms that add value immediately, minimize barriers to incorporating emerging technologies at a later date, and that are as modular as possible so that they can be easily modified or adapted for new applications. Consistent with that model, the current work is focused on development of a prototype spot-weld inspection platform that integrates the best available ultrasonic phased-array technology with custom-designed signal processing and analysis software, and hardware that will allow the system to be tested and implemented in manufacturing plants as a portable stand-alone unit.

Ultrasonic Phased-Array Technology

Most commercially-available spot-weld inspection systems use conventional high-frequency single-crystal ultrasonic probes working in pulse-echo mode. The output from these mono-probes is a single signal that is an integrated response over an area that depends on the diameter of the probe. Different probes must be used for different-sized welds. In contrast, a phased array is composed of many piezoelectric elements that are individually excited by electronic pulses at programmed delay times. As a result, phased arrays have several advantages over conventional ultrasonic probes that derive from the ability to dynamically control the acoustic beam transmitted into the structure under examination. An electronic delay can be applied separately to each channel when emitting and receiving the signal. These delay laws permit constructive and destructive interference of the acoustic wavefront transmitted into the structure, allowing predefined ultrasonic beams to be formed. The acoustic energy can be focused, and delay laws can be used to steer the acoustic beam. Electronic scanning is accomplished by firing successive groups of elements in the array.

Instead of assessing weld quality based on a single signal, as is the case with mono-probes, phased arrays allow thousands of signals to be obtained for individual welds in a few seconds. The ability to perform complex scanning of the acoustic beam through the weld allows greater accuracy in sizing, while also improving the flaw-characterization capability. These attributes of phased-array probes allow us to measure the size of welds, map the surface indentation caused by the welding electrodes, locate and image discrepancies, and identify misshapen and burnt welds. In addition, the same probe can be used to inspect different sized welds and welds in sheets with different thicknesses. It is also possible to electronically compensate for misalignment of the probe with respect to the sample.

Project Status

As described in detail below, the project is now in the second phase of assessing technical feasibility, having demonstrated concept feasibility and completed the first phase of technical feasibility. Concept feasibility was demonstrated using a phased-array probe in a water tank. Experiments were conducted with different probes to determine the optimal ultrasonic frequency. Work also

included a series of experiments performed on test specimens provided by DaimlerChrysler made from both mild and high-strength steel, with both equal-thickness and unequal-thickness stackups. The objective of these tests was to determine if the newly-acquired phased-array probe and LBNL's signal-processing software could be used without modification across the range of materials, sheet thicknesses and stackups tested. The probe and signal-processing algorithms performed as desired, and the resulting data were judged to be sufficient for demonstrating the concept feasibility of using a high-frequency phased-array probe to assess the size and quality of spot-welds.

The most challenging task in the first phase of technical feasibility was to design and fabricate a portable, integrated probe that allows ultrasonic measurements to be made outside of a water tank. As described in detail in the following section, this required not only a housing to maintain the phased-array probe in water, but also a miniature mechanical scanning system to provide lateral translation of the probe; to generate two-dimensional images of the welds, mechanical scanning is required in the direction perpendicular to the electronic scan. In the future, matrix phased-array probes may prove to be an attractive alternative to mechanical scanning if they can meet cost and robustness requirements.

As described below, the integrated probe was completed and tested in 2005. The miniature scanning system performed as designed, and the coupling membrane integrated into the probe housing was demonstrated to confine the water column and provide adequate acoustic coupling to welded assemblies. Along with the development of hardware, the first phase of technical feasibility also included further development of signal processing and analysis software that allows classifying and sizing welds. Experiments performed on test specimens provided by industry partners demonstrated the feasibility of imaging spot-welds using the portable phased-array probe assembly. More than 4000 signals were measured for each weld in a few seconds. Post-processing algorithms developed to analyze the signals demonstrated the capability of the system to qualitatively distinguish cold, undersized, satisfactory and burnt welds.

The second phase of demonstrating technical feasibility includes work underway to perform correlation studies to determine the accuracy and repeatability of measurements made with the integrated probe assembly. In addition to assessing the ability of the prototype system and the signal post-processing algorithms to classify welds, software developed to provide an estimate of the size of the weld nugget is also being assessed. Experiments are being performed on both production parts and specially-designed test coupons provided by industry.

Integrated Probe Unit

A plant-deployable unit requires a housing for the ultrasonic probe that maintains the probe in water and contains the miniature mechanical system for linear translation of the probe. The mechanical system designed and encapsulated into the probe housing allows the probe to travel a distance of 14.7 mm. A mechanical drawing of the scanning system is shown in Figure 1a. The small motor used to drive the system has a nominal speed of 4800 RPM and is coupled to a 1:16 gearbox. The drive assembly is separated from the water column containing the probe by two slider plates and O-rings that form a watertight seal. Pictures of the integrated probe housing are displayed in Figures 1b-1e.

One of the technical challenges in designing the miniature scanning system was in minimizing the size and weight of the integrated probe. In many cases, there is very limited access to spot-welds on production parts, making it essential to minimize the footprint of the probe assembly. Minimizing weight is important in designing an ergonomic tool that is relatively easy to position and hold on the part. The overall footprint of the first prototype, shown in Figure 1b, was 26 by 44 mm. This design works well on relatively flat components where there is easy access to the welds. In the next several iterations of the probe design, also shown in Figure 1, the bottom section of the housing was tapered to allow improved access to welds on production parts. As shown in Figure 1c, the bottom half of the housing in the latest designs is a cylinder with a diameter of approximately 2 cm. Several different designs of the end cap on the probe housing have

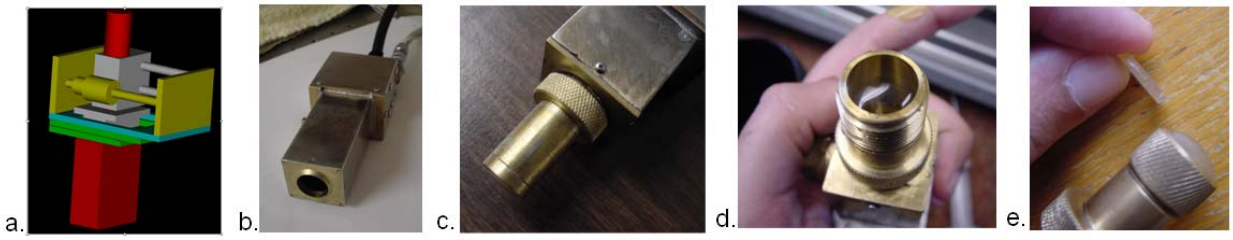

Figure 1. Mechanical drawing of the miniature scanning system (1a) encapsulated into the prototype probe housing (1b). In later prototypes, the lower section of the housing was redesigned to be much smaller for better accessibility to welds on production parts (1c). Figure 1d shows the end of the probe assembly after being filled with water, and Figure 1e shows one of the membranes tested.

also been tried, with two objectives: maximizing the ease of changing the membrane that confines the water column, and determining which design provides the best coupling between the membrane and the parts under inspection.

Figure 1d shows the end of the probe assembly after being filled with water, and Figure 1e shows one of the membranes tested. The optimal material for the outer membrane has also been investigated. The material must provide acoustic coupling to the part, which requires that it conform to the surface. Since many welds on production parts are associated with surface roughness and indentations caused by the welding electrodes, the membrane must be highly pliable, while also being durable enough to withstand thousands of measurements. With regard to its acoustic properties, the ideal membrane has an acoustic impedance equal to that of water, and does not attenuate the acoustic signal. Another important consideration in choosing a material is that it be relatively inexpensive. Experiments were performed with a variety of materials, and acceptable results were achieved even with inexpensive, off-the-shelf products. What has been shown to be important is the thickness of the material. Tests to date indicate that membranes thinner than 0.5 mm are necessary to achieve good coupling with the part. Tradeoffs between price, durability, and coupling will determine the best membrane option for any particular application.

Phased-Array Inspection Strategy

For all experiments performed to date, electronic scanning and focusing laws are combined to inspect the spot-welds. The acoustic energy is focused at the interface between the two sheets by applying symmetrical delay laws to the elements of the phased-array probe (see Figure 2). The results presented here were obtained using a 17-MHz focused probe. In contrast to the probes used for initial experiments that had flat elements, the 17-MHz probe has curved elements that focus the energy with a natural focal length of 37 mm. When used in conjunction with the delay laws described above that focus the energy from multiple elements, the acoustic beam at the interface between the welded sheets is a circular spot that is scanned across the weld. Using a portable phased-array controller, more than 4000 signals are recorded for each weld in approximately 4 seconds.

Signal Processing

The signals recorded while scanning through the weld are currently analyzed in the frequency and time domains with the goal of developing fast and accurate algorithms that work for the wide range of welds found on production parts. For a satisfactory weld, most of the ultrasonic energy is transmitted through the weld nugget and reflected off the back surface of the lower sheet (see Figure 2). In contrast, for a discrepant weld, incomplete fusion at the interface between the two sheets results in partial

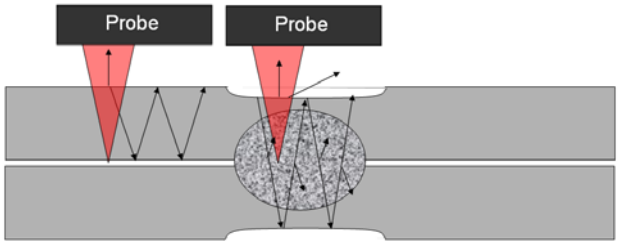

Figure 2. Schematic drawing illustrating focusing of the ultrasonic energy from several phased-array elements at the interface between welded sheets. The arrows indicate the travel paths of the acoustic waves in and outside of the welded area.

reflection of the ultrasonic energy at the interface. This affects the periodicity of the train of echoes; that is, signals that are reflected at the interface have a shorter travel path than signals that propagate through the weld, resulting in echoes in the time domain that are closer together than echoes off the back surface.

In the frequency domain, the power spectrum captures the periodicity of the ultrasonic echoes. The relative magnitude of the peaks in the spectra is indicative of the amount of energy reflected at the interface between the welded sheets. For a satisfactory weld, the ultrasonic wave propagates through the weld and reflects back and forth between the front and back surfaces resulting in a peak that corresponds to the travel path through both sheets. For discrepant welds, where most of the energy is reflected at the interface between the two sheets, there is a peak in the spectrum that corresponds to a travel path equal to twice the thickness of the upper sheet. For each of the 4000 signals that comprise each weld image, the ratio of the peaks in the power spectrum is calculated. To obtain a measure that can be directly compared to buttons and metallographic images, the frequency-ratio images are thresholded, and the largest contiguous area of high transmission is isolated and dimensioned.

The frequency-ratio images allow satisfactory and undersized welds to be distinguished according to the size of the area where there is significant transmission of energy into the lower sheet. Although discrepant welds such as cold welds can result in a large area of transmission into the second sheet, the frequency ratio often shows that the areas of high transmission are relatively sparse and dispersed compared to the well-defined and concentrated areas for the satisfactory and undersized welds. A drawback of this approach is that it requires setting a threshold, which tends to be arbitrary, and also results in ignoring some of the data. For these reasons, we have moved away from thresholding toward measures that use all of the available information. For our most recent study, the frequency ratio is integrated over the total area where there is ultrasonic transmission. In addition, the signals are amplified by the material attenuation rate, to make data obtained for different thickness sheets more comparable.

In addition to the signal processing based on Fourier peak ratios, a difference-equation model has been developed that describes the amplitude of the ultrasonic echoes in the time domain as a function of the *reflectivity* of the weld. At each measurement point, the reflectivity measures the share of acoustic energy incident on the interface between the sheets that is reflected. To create images of the welds, the signal obtained at each location during scanning is reduced to a single bounded value (reflectivity), and these values are plotted to create a reflectivity map of the weld.

The frequency-ratio method and difference-equation models have different advantages and disadvantages, making it valuable to have two approaches to signal processing. For example, the frequency-ratio method is very fast, whereas the difference-equation model enables simulations. Features of the reflectivity model also include the ability to detect and correct for weak signals that are almost always unavoidably present because the edge of the surface indentation tends to "scatter" the ultrasonic signals. Weak signals may also be present because of poor coupling or because of malfunction of one or more elements in the probe. The software identifies and, as far as possible, corrects for these cases as well.

An advantage of phased arrays is that the resulting signals provide an accurate measure of the surface indentation caused by the welding electrode. Knowing the depth and location of the top-surface indentation is necessary for signal processing when the indentation is deep, and is also important in analyzing the quality of the weld. The criteria used in the automotive industry for assessing weld quality include specifications for allowable indentation and loss of material. Although the relationship does not always hold, the depth of the indentation and the size of the weld nugget are often related; thus, the indentation depth may be of some value as a secondary criterion in evaluating quality for those welds that prove difficult to analyze. It is also possible to determine the shape and gradient of the indentation, which provides useful information on the state of the electrodes and may indicate problems in the fit between parts (see Figure 3). All of this information provides useful feedback to the welding process and is easily derived from the ultrasonic signals.

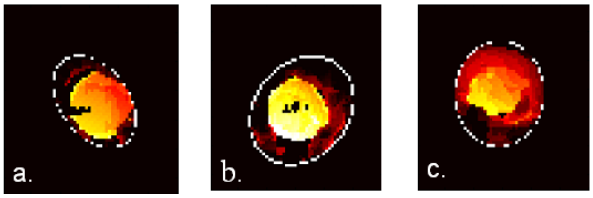

Figure 3. Maps of surface indentation caused by the welding electrodes derived from the ultrasonic signals. Figure 3a shows an indentation that is relatively uniform in depth compared to 3b, where there is a gradient that may indicate misaligned electrodes or parts. Figure 3c shows a relatively large area of surface distortion.

Measurements on Production Parts

To demonstrate the technical feasibility of phased arrays for spot-weld inspection, the recently completed prototype probe housing is being used to make measurements on production parts. This was not possible earlier, because it was necessary to design and build the miniature scanning system and the housing that allows the ultrasonic probe to be used outside of a water tank. To date, preliminary measurements have been made on package trays, apron assemblies, and a truck door. The pictures in Figure 4 show the prototype inspection system being used to make measurements on a truck door. For the

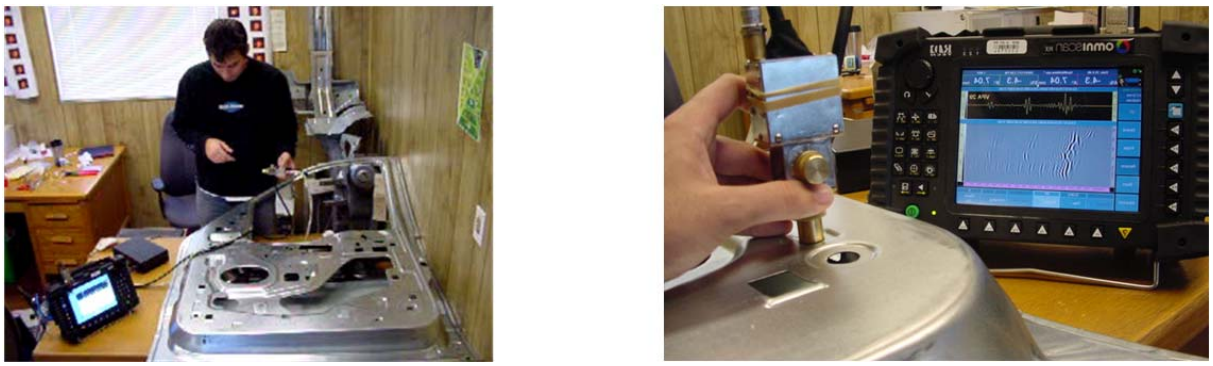

Figure 4. LBNL weld-inspection system being used to inspect a truck door provided by the Ford Motor Co. The right-hand image shows a close-up view of the portable, integrated probe positioned on a weld. The probe housing includes a miniature mechanical scanner, which allows two-dimensional images of the weld to be captured.

first set of measurements on the door, three different operators measured the welds. All three operators used a relatively thick membrane at the tip of the probe assembly, chosen because it has an acoustic impedance close to that of water. However, subsequent experiments have shown that better results are obtained with a thin-ner, much less expensive membrane.

Results for two of the welds on the door are displayed in Figure 5. After the welded joints were destructively torn down to reveal the weld buttons, two buttons were subsequently subjected to metallographic analysis. The welds were sectioned vertically, then polished and etched by RoMan Engineering Services. Pictures of the etched cross sections are shown in Figure 5 along with the ultrasonic images obtained for the same welds. Although the ultrasonic data for Weld 23 is noisy, and therefore difficult to analyze, there is an indication of a discrepancy inside the weld that may correspond to the void visible in the metallographic image.

In general, the quality of the measurements depends in large part on the surface conditions of the parts including the shape and roughness of the surface indentations. For example, very deep spherical indentations make it difficult to get enough energy into the parts to provide a dimensional analysis of the welds, and deep indentations make it more difficult to achieve good coupling with the probe. A practical solution for deep indentations is to fill the indentation with water. Another challenge arises when the welding electrodes are not aligned, creating non-parallel surfaces. In this case, some of the acoustic energy transmitted into the part is reflected away from the weld, and the reflected signals are not captured by the probe. Non-parallel surfaces and surface distortion occur most often in thin sheets. Many of these conditions are associated with burnt welds,

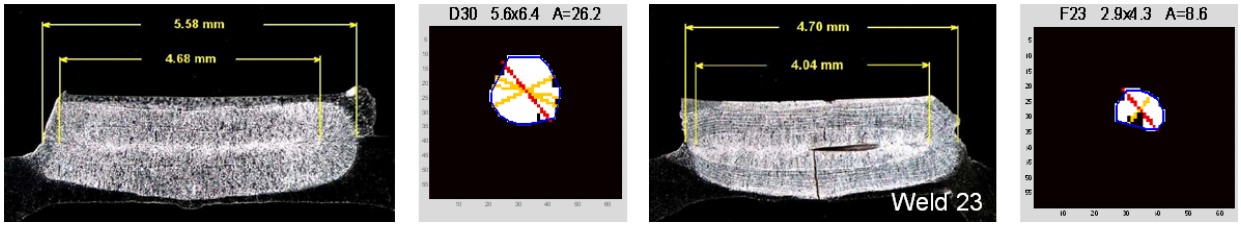

Figure 5. Metallographic images obtained for two of the weld buttons on the truck door pictured in Figure 4. A vertical crack and a void in the weld nugget are visible in the metallographic image of Weld 23 (right-hand image). Thresholded and dimensioned ultrasonic frequency-ratio images obtained for the same welds are also shown.

in which case it is easy to identify the welds as discrepant based on excessive material loss and indentation, which are easy to measure.

Correlation Studies

A fundamental problem with trying to use production parts for correlation studies is that almost all of the welds on these parts meet engineering specifications for size and are thus judged to be satisfactory welds. To have a meaningful correlation study, it is necessary to have sufficient numbers of welds in each of the many categories that the prototype system is expected to identify to allow statistical analysis of performance.

For spot-welds, this requires at a minimum statistical sample sizes of welds that are cold, undersized, satisfactory and burnt. It is also highly desirable to be able to test the ability of the signal-processing software under development to provide a dimensional analysis of the welds. In this case, a correlation study requires a range of sizes of weld nuggets that span the values observed in production.

The approach agreed upon in concert with industry partners is to perform well-controlled experiments on specially-made test specimens, in conjunction with measurements on production parts, to obtain the baseline correlation data required to assess technical feasibility. Both sets of experiments are deemed essential. The experiments on test coupons will make it possible to assess the accuracy and repeatability of the prototype system across the full range of weld sizes and qualities encountered in production. The measurements on production parts will address the reliability of the measurements under the wide variety of conditions encountered on production parts, including different surface conditions, stackups, and part geometries.

A series of laboratory experiments were conducted in collaboration with the Ford Motor Co. to better understand the relationships among ultrasonic measurements and other measures of weld quality including lap-shear strength, coach-peel strength, the dimensions of the weld buttons, and the dimensions of the weld nuggets determined from metallographic images. Ford's test specimens consisted of two different sheet-metal stackups: equal-thickness sheets that were 1-mm thick, and unequal-thickness stackups created by joining sheets that were 1-mm and 1.45-mm thick. Welds of varying quality were created by varying the applied force, current and number of cycles used during welding.

After LBNL made ultrasonic measurements on the 122 welds that comprised the sample set, Ford subjected the welds to strength testing or metallurgical analysis. Rather than taking vertical cross-sections through the welds, a methodology was developed to carefully grind and polish the weld in the plane of the sheet metal to create planar sections at the welding interface. These metallographic maps are particularly useful because they are in the same plane as the images created from the ultrasonic measurements (see Figure 6). For those welds that were sectioned, the size of the weld nugget was measured in the images and compared to the ultrasonic data (see Figure 7).

A new correlation study is underway using test coupons provided by General Motors with welds that span the size and quality of welds found on production parts. Samples have been made for three different sheet-metal stackups: thin-to-thin (sheet thickness equal to 0.8 mm); thick-to-thick (sheet thickness equal to 1.8 mm); and thin-to-thick. For each of the three stackups, there were five target

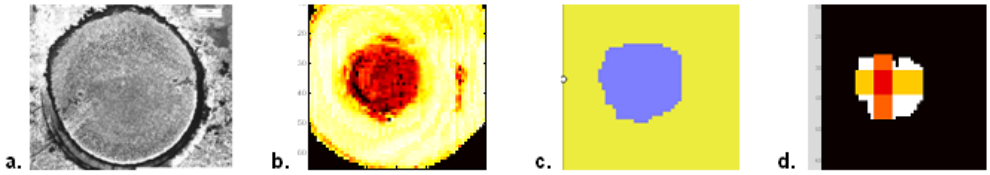

Figure 6. Metallographic planar section (6a), ultrasonic frequency-ratio plot (6b), and thresholded binary images for two different thresholds applied to the ultrasonic data (6c and 6d).

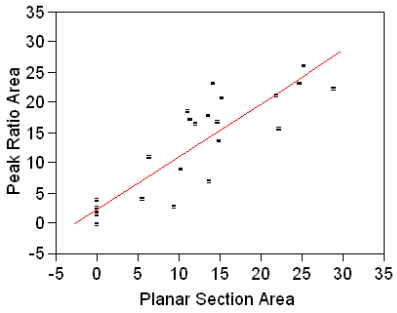

Figure 7. Best-fit line between weld area determined from processed ultrasonic data and weld nugget determined from planar metallographic images.

weld classes: stick, small, undersized, minimum acceptable, and large. The welds were inspected using the prototype phased-array system, by three different operators, from both sides of the coupons. An additional set of measurements was performed with the samples in a water tank, and many repeat measurements were also made. Following the ultrasonic inspections, the samples were peeled to determine the weld quality as indi- cated by the size of the weld button. Each of the samples was then sectioned, polished and etched.

The discernible weld classes are different for the three stackups, illustrating the variability that occurs even under nominally-identical welding conditions; i.e, welding schedules (current, pressure, number of cycles), cooling flow, presence of and distance from shunt weld were held constant.

Examples of the metallographic images, pictures of the buttons and ultrasonic frequency-ratio maps are shown in Figure 8. In general, there is good qualitative agreement between the ultrasonic images and the physical measurements. For example, good correspondence between the shape of weld button and the ultrasonic image can be seen in Figures 8h and 8m. The void in the nugget that can be seen in the metallographic image in 8d, is also evident in the ultrasonic image as a zone of weak signals in the center of the image (Figure 8n). The metallographic images show that for the thin-to-thick stackup, the weld nuggets in all cases formed at the geometric center of the stackup (see Figures 8a, 8c and 8d). An important observation is that, in some cases, it is possible to pull a weld button even when the nugget does not penetrate the thin sheet. This implies a strong bond at the interface that does not arise from development of a true spot -weld. Ultrasonic energy is transmitted across such bonds, but it was possible to identify these welds as discrepant.

Statistical modeling is being used to quantify the relationships between the ultrasonic data and the physical measurements. The best model fits to date are obtained via stepwise regression for a fully quadratic model. The ultrasonic data used thus far are the integrated amplified frequency ratio, the total area of ultrasonic transmission, and the surface-indentation area and depth. The models are stackup dependent, but in all cases the R^2 value is above 0.93 (see Figure 9), where R^2 is the percent share of the variation in the measured weld buttons that can be predicted by variation in the ultrasonic data.

It is a measure of the *goodness of fit* of the model that ranges between 0 and 1 (a perfect fit). The values reported here are adjusted slightly downward to account for the number of parameters in the model, allowing direct comparison of different models. R^2 values above 0.9 indicate excellent fits. When the surface indentation information is not used, the adjusted R^2 values are 0.95 for the thin-to-thin stackup, 0.87 for the thin-to-thick, and 0.89 for thick-to-thick.

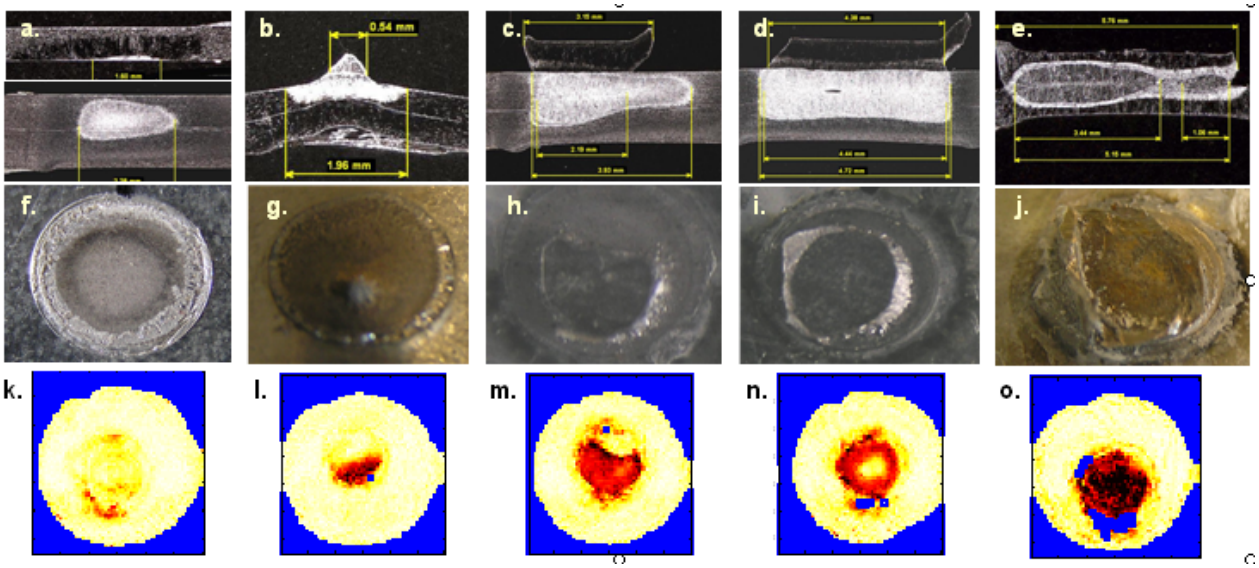

Figure 8. Metallographic cross-sections, pictures of weld buttons and ultrasonic amplified-frequency-ratio images for five welds with targeted qualities: stick, small, undersized, minimum acceptable, and large (left to right).

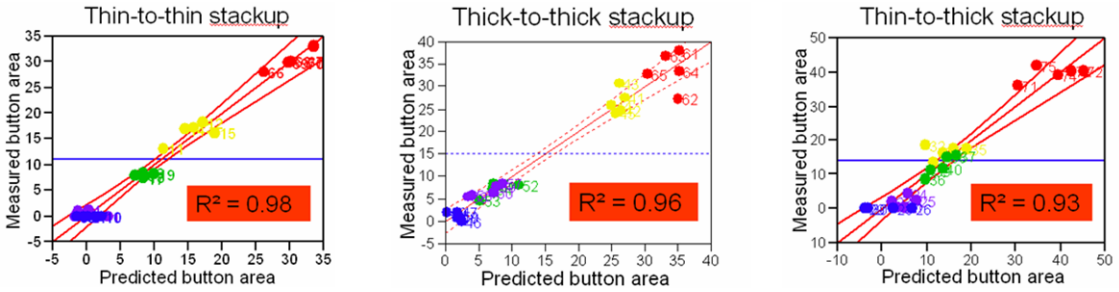

Figure 9. R^2 values for model fits and plots of measured versus ultrasonic-predicted weld-button areas.

Conclusions

There are substantial challenges in nondestructive testing of spot-welds on automotive parts such as surface roughness, indentations on the surface caused by the welding electrodes, expulsion, and complex geometries that make it difficult to access welds. There is also variability between parts that arises from variations in materials and differences that are inherent in products produced in any large-scale manufacturing operation. Previous work demonstrated the concept feasibility of inspecting spot-welds in steel using ultrasonic phased-array technology. To demonstrate the technical feasibility of phased arrays for spot-weld inspection, a portable, integrated probe assembly has been designed and fabricated that allows measurements to be made on production parts. This was not possible earlier, because it was necessary to design and build the miniature scanning system and the housing that allows the ultrasonic probe to be used outside of a water tank. Initial experiments were used to guide modifications made to improve accessibility to welds and coupling on production parts. The objective of experiments in progress is to validate the results obtained using the prototype probe assembly and LBNL's signal-processing algorithms. The focus is on determining the accuracy and repeatability of the ultrasonic measurements, as well as the resolution limits and the best diagnostic parameters for specific applications. Work under way will also yield integrated diagnostic tools amenable to programming in hardware with the goal of achieving processing speeds sufficient for assembly-line use. If these experiments are successful, the remaining challenge is to demonstrate robustness, accuracy, repeatability and cost-effectiveness for inspection of production parts in a manufacturing plant.

Presentations

1. D. Hopkins, "Strategic Plan for Nondestructive Evaluation Development in the North American Automotive Industry and Ultrasonic Phased-Array System for Resistance Spot-Weld Inspection," ASNT Automotive Industry Advancements with NDT, Birmingham, Alabama, June 7, 2006.

2. W.B. Davis, "Signal Processing to Measure Spot Weld Reflectivity with an Ultrasonic Phased Array." 33rd Annual Review of Progress in Quantitative Nondestructive Evaluation, Portland, *Oregon,* August1, 2006.

3. D. Hopkins, "Diagnostic Capability of Processed Phased-Array Images for Resistance-Spot-Weld Inspection," 33rd Annual Review of Progress in Quantitative Nondestructive Evaluation, Portland, Oregon, August 2, 2006.

4. D. Hopkins, "Development of an Ultrasonic Phased-Array System for Nondestructive Evaluation of Resistance Spot Welds," United States Automotive Materials Partnership (USAMP) ― Automotive Materials Division (AMD) Joining Offsite, December 2005, Southfield, Michigan.

Publications

1. W.B. Davis, "Simple Models and Methods for Estimating the Ultrasonic Reflectivity of Spot Welds," To appear in *Proc. 33rd Annual Review of Progress in Quantitative Nondestructive Evaluation*, Portland, 2007.

2. D. Hopkins, W.B. Davis and F. Reverdy, "Diagnostic Capability of Processed Phased-Array Images for Resistance-Spot-Weld Inspection," To appear *Proc. 33rd Annual Review of Progress in Quantitative Nondestructive Evaluation*, Portland, 2007.

3. T. Potter, B. Ghaffari, G. Mozurkewich, F. Reverdy and D. Hopkins, "Comparison of Metallurgical and Ultrasonic Inspections of Galvanized Steel Resistance Spot Welds," *Proc. 32nd Annual Review of Progress in Quantitative Nondestructive Evaluation*, 2006.

4. F. Reverdy, D. Hopkins, D. Turler, and K. Nihei, "Use of Ultrasonic Phased Arrays for Weld Inspection and Material Characterization," *Proc. Third US-Japan Symp. on Advancing Applications and Capabilities in NDE*, 2005.

B. Nondestructive Inspection of Adhesive Metal/Metal Bonds (NDE 601[i])

Principal Investigators: Joseph DiMambro and Dennis P. Roach
Sandia National Laboratories
3260 University SE
Albuquerque, NM 87106
(505) 843-8722 ext. 104; fax: (505) 843-8760; e-mail: jdimamb@sandia.gov

Principal Investigator: Cameron J. Dasch
General Motors Research & Development
30500 Mound Road, Warren MI 48090
(586) 986-0588, Fax (586) 986-3091, cameron.j.dasch@gm.com

Technology Area Development Manager: Joseph A. Carpenter
(202) 586-1022; fax: (202) 586-1600; e-mail: joseph.carpenter@ee.doe.gov

---

Contractor: U.S. Automotive Materials Partnership
Contract No.: DE-FC26-02OR22910

Objective

The goal of this project is to identify and develop a nondestructive inspection (NDI) method(s) for adhesive-bond evaluation to be used in an automotive manufacturing environment that would foster increased confidence and use in adhesive joining. The primary objective is to identify and validate an NDI method(s) which can 1) measure the adhesive area and thickness and 2) detect weak bonds having intimate contact but which have reduced strength ("kissing" bonds).

Approach

There are five major attributes which contribute to the strength of an adhesive bond on a metal flange: the width of the adhesive area, the thickness, the location of the bead relative to the edges of the flange, the state of cure, and the quality of the adhesion. The general approach is to develop a portfolio of methods that can be used on the plant floor which allow all these attributes to be measured nondestructively. These methods need to be single-side inspections that can follow a flange, deal with large changes in geometry and have resolution approaching 1 mm. To accomplish this, several sets of flat, adhesively-bonded specimens, representative of automobile flanges, have been generated by the OEMs and adhesive suppliers to test the feasibility of NDI techniques to assess bond area and bond-line thickness. The specimens vary in adhesive and adherent, type and thickness, stackup (2-3 layers), and cure state. A through-transmission ultrasound inspection was performed to characterize the specimens. The inspection images will be used as a gold standard to compare results from candidate inspection technologies such as pulse-echo ultrasound and pulsed thermography which can be deployed from one side of the flange. The specimens will be peeled destructively and photographs of the samples will also be compared with the inspection images. Similarly, weak-bond specimens will be manufactured for bond-strength quantification testing, which is the goal of the second and third years of the project. In addition, multiple automobile bodies-in-white (BIW) containing a number of adhesive joints were produced by the OEMs to determine whether complex geometry provides any inspection impediments and to provide a test-bed for the validation of promising inspection techniques.

Accomplishments

Pulsed-thermography and pulse-echo-ultrasound inspections of the adhesively-bonded specimens are currently in progress and preliminary results are encouraging. A pulse-echo ultrasonic linear-array scanning system is being developed and promises to reduce flange inspection time by deploying several small ultrasonic transducers placed in a single scanning probe. High-speed pulsing combined with rapid data capture permits the linear array to be quickly

moved over the structure. Several promising techniques for assessing weak bonds have been identified. They include vibrothermography, angle-beam ultrasonic spectroscopy, nonlinear ultrasonics, and laser shock peening.

Future Direction

Pulsed-thermography and pulse-echo-ultrasound inspection results will be compared with the through-transmission ultrasound inspection images and photographs of the samples after a destructive peel test. The inspection technologies will then be adapted to accommodate the complex geometry of production components, eliminate any surface treatments currently needed to improve inspectibility, and reduce overall system cost. Weak adhesive-bond specimens will be fabricated and testing of promising inspection techniques identified in the first year for assessing weak bonds, will follow.

Introduction

Adhesive bonding is increasing every year as automotive manufacturers strive to make bodies stiffer and stronger. Recent applications see as much as 30 to 100 m of adhesive per vehicle being used. Adhesive joining is already widely used in automotive production today for improving body stiffness and durability where needed. Current quality control of these joints relies primarily on the robust control of the adhesive preparation and application. These controls include machine-vision inspection of the applied adhesive bead. However, there is no method available to test the overall quality of the final joints other than destructive testing. This lack of verification especially limits adhesives being used to meet crash-performance requirements. Adhesives are also seen as a critical enabler for the joining of dissimilar materials in order to avoid corrosion.

Adhesive joining is seen as a major weight-saving technology. When adhesives are used in combination with spot-welds or rivets, the resulting joints are much stiffer and stronger. Almost a doubling of shear strength has been produced in weld-bonded joints when compared with spot-welds alone. Moreover, by enabling dissimilar materials to be used in close proximity to each other, assemblies can be constructed with optimized, lightweight materials such as magnesium and aluminum joined to lower-cost steels.

A major strategy of this project is to leverage the many decades of development in the aerospace sector devoted to the nondestructive inspection (NDI) of adhesive joints. NDI is now commonly used in aerospace manufacturing involving adhesive joints, especially for composite panel joining. Entire structures are being inspected. Some of the NDI methods are also being used in routine, in-service aircraft inspections.

Within the automotive manufacturing arena, the inspections are especially needed in the body shop before the adhesive is cured. This is the most likely place within the manufacturing process where discrepant joints would be repaired. However, inspections are also needed at the end of line to ensure the quality of the entire assembled, cured, and painted product. NDI inspections are also seen as a major cost savings for accelerating engineering and environmental testing, ramp-up to production, and monitoring the long-term performance of the joints.

Coupon Preparation and Characterization

Several sets of flat, adhesively-bonded specimens, representative of automobile flanges, have been generated by the automotive OEMs and adhesive suppliers to test the feasibility of NDI techniques to assess bond area and bond-line thickness. The specimens vary in adhesive and adherent, type and thickness, stack-up (2-3 layers), and cure state. These were designed to include many of the variations that can occur in production. Multiples of the same conditions are made to allow parallel testing with different nondestructive and destructive methods early on. An example of the coupons prior to assembly is shown in Figure 1 showing the wire spacers used to control the adhesive thickness, intentional skips, and a section of Teflon tape to simulate a kissing bond. Most of these have also been spot-welded using typical production equipment and weld schedules.

Figure 1. Coupons prior to assembly.

All the coupons have been nondestructively characterized using a lab-only method of ultrasonic through-transmission in an immersion tank. The transmitted signal strength allows the areas where all interfaces in the stack are wetted to be imaged (Figure 2a). Using the experimentally-measured speed-of-sound for each adhesive in its state-of-cure, a map of the adhesive thickness is simultaneously measured (Figure 2b).

a) Ultrasonic transmission intensity.

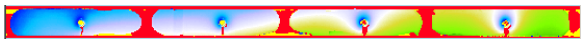

b) Ultrasonic thickness measurement.

Figure 2. Ultrasonic characterization of a 600-mm-long weld-bonded coupon.

The results of a destructive peel test on a 2-layer coupon are shown in Figure 3. This shows the effect of varying bead width on the strength of the bond.

a) Peeled coupons.

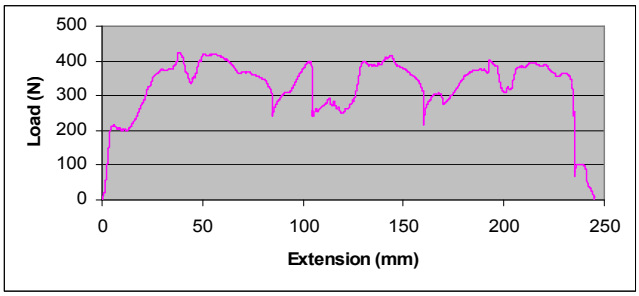

b) Peel force along coupon.

Figure 3. The peel-force trace and resulting sample faces for a 2-layer coupon with skips.

Determining Adhesive Area and Bond-Line Thickness

Candidate NDI technologies such as pulse-echo ultrasound and pulsed thermography, which can be deployed from one side of the flange, are currently being used to inspect the coupons described above and automobile bodies-in-white (BIW) containing a number of uncured adhesive joints.

Pulsed Thermography

Basic Description:

This technology uses thermal gradients to analyze the physical characteristics of a structure such as internal defects. This is done by converting a thermal gradient into a visible image by using a thermally-sensitive detector such as an infrared (IR) camera. A heat source, such as flash lamps, is used to raise the surface temperature of the structure. As the heat diffuses through the structure, the surface temperature is monitored for a period of time by an infrared camera. Areas that appear hotter or cooler than normal may indicate the presence of a flaw beneath the surface that is preventing or assisting heat diffusion into deeper layers. By using a computer to analyze the infrared data captured over time, subtle variations can be enhanced in the image. By plotting the log of temperature versus time, quantitative adhesive bond-line thickness measurements can be obtained.

Figure 4 illustrates a pulsed thermography inspection performed on a BIW truck-floor assembly having uncured adhesive areas. Note that the flash lamps which are not visible in Figure 1 are located within the rectangular shroud just below the IR camera.

Figure 5 is an infrared image indicating the presence of adhesive (adhesive area) from one location of the truck-floor assembly.

Temperature-versus-time plots were generated and shown in Figure 6 for each of the square cursors areas depicted in Figure 5. The cursor located at the top of Figure 5 is positioned in an area where adhesive was omitted. The middle and bottom cursors are located in the bond area.

Figure 4. Pulsed-thermography inspection of a BIW truck-floor assembly.

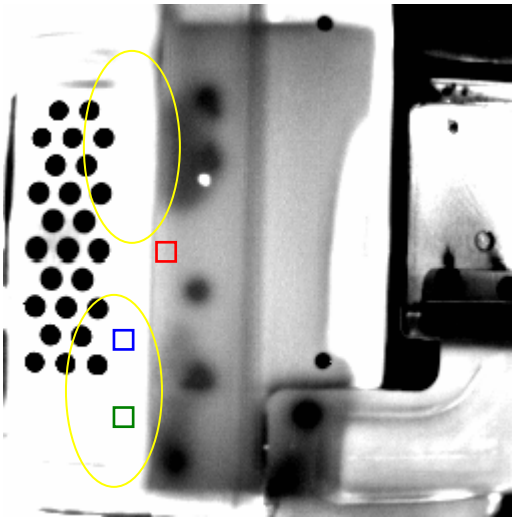

Figure 5. Pulsed-thermography-inspection image (0.868 sec after flash).

While Sandia National Laboratories is conducting pulsed-thermography inspections of BIW vehicles, similar inspections of the flat, adhesively-bonded specimens are being conducted concurrently at Thermal Wave Imaging Inc.

Unfortunately, the high optical reflectivity and low infrared emissivity of aluminum and steel typically prohibits a successful pulsed-thermography inspection. Only by the application of a surface treatment to the material (e.g., flat- black washable paint) will a pulsed thermography inspection become feasible. The painted material will improve the absorption of light (heat) from the flash lamps and the material will reradiate effectively as it cools. An investigation will be performed in the next few

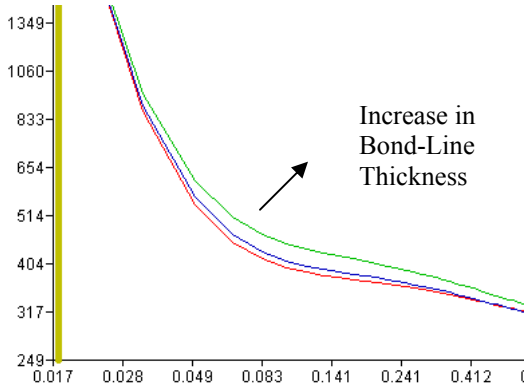

Figure 6. Log of temperature vs. log of time depicts thickness variations.

months to determine whether the technique can be modified to eliminate the surface-treatment step.

Pulse-Echo Ultrasonics

Basic Description

Short bursts of high-frequency sound waves are introduced into the material for the detection of surface and subsurface flaws in the material. The sound waves travel through the material with some attendant loss of energy (attenuations) and are reflected at interfaces. The reflected beam is displayed and then analyzed to define the presence and location of flaws. Complete reflection, partial reflection, scattering, or other detectable effects on the ultrasonic waves can be used as the basis of flaw detection. In addition to wave reflection, the time of transit through the test piece can be used to assess bond-line thickness.

Pulse-echo ultrasonic inspections of the flat adhesively bonded specimens are currently being performed at Lawrence Livermore National Laboratories, New Mexico State University, and Sandia National Laboratories.

Figure 7 illustrates a probe holder which houses a 17-MHz linear-array ultrasonic transducer. The probe holder has been designed specifically for the inspection of long and narrow flanges. The probe holder which is made of polycarbonate is approximately 1.5” wide by 3.5” long. Wheels facilitate the movement of the probe and probe holder over the flange and the holder can travel in both forward and backward directions. The angled inlet port is used to supply water below the probe to

couple the sound generated by the ultrasonic probe to the part. The two vertical ports are used to vacuum excess water from the part. An encoder is attached to the rear wheel and it is used to track the displacement of the probe. The linear array system is currently being tested at Sandia National Laboratories.

Figure 7. 17-MHz ultrasonic linear probe and custom probe holder.

[i] Denotes Project 601 of the Nondestructive Evaluation (NDE) Working Group of the United States Automotive Materials Partnership (USAMP), one of the formal consortia of the United States Council for Automotive Research set up by the "Big Three" traditionally U.S.-based automakers to conduct joint pre-competitive research and development.

7. RECYCLING

A. Recycling Assessments and Planning

Principal Investigator: Edward J. Daniels
Argonne National Laboratory (ANL)
9700 S. Cass Ave., Argonne, IL 60439
(630) 252-5279; fax: (630) 252-1342; e-mail: edaniels@anl.gov

Technology Area Development Manager: Joseph A. Carpenter
(202) 586-1022; fax: (202) 586-1600; e-mail: joseph.carpenter@ee.doe.gov

Expert Technical Monitor: Philip S. Sklad
(865) 574-5069; fax: (865) 576-4963; e-mail: skladps@ornl.gov

Participants:
This project is conducted as part of a Cooperative Research and Development Agreement (CRADA) among Argonne, USCAR's Vehicle Recycling Partnership[i], and the Plastics Division (formerly the American Plastics Council) of the American Chemistry Council.
CRADA Partner Principal Investigators:
Michael Fisher, American Chemistry Council, (703) 741-5599, e-mail: Mike_Fisher@americanchemistry.com
Gerald Winslow, VRP, DaimlerChrysler Corp., (248) 512-4802; e-mail: grwx@DCX.com
Claudia Duranceau, VRP, Ford Motor Co., (313) 390-0504; e-mail: cdurance@ford.com
Candace Wheeler, VRP, General Motors Corp., (586) 986-1674; e-mail: candace.s.wheeler@gm.com

---

Contractor: Argonne National Laboratory
Contract No.: W-31-109-Eng-38

Objectives

- Eliminate any real or perceived recycling barriers that might preclude the use of advanced automotive materials.
- Enable the optimum recycling of all automotive materials, current and future, thereby obviating the need for legislative recycling mandates.
- Assess the critical needs for cost-effective recycling of automotive materials and components.
- Establish research priorities to enable cost-effective recycling of advanced automotive materials and components.
- Communicate a collaborative industry/government approach to issues related to the recycling of automotive materials.
- Coordinate research with other agencies and stakeholders in the United States, Europe, and Asia.

Approach

- Consult with automotive manufacturers and recycling industries, USCAR and its affiliates, national laboratories, universities, and other relevant organizations to assess critical recycling needs/barriers.
- Develop a recycling research plan that will serve as a "working document" to guide the U.S. Department of Energy (DOE) in establishing priority goals, with an initial emphasis on lightweighting body and chassis materials.

- Establish an outreach/communication function to enable cooperation amongst, and leveraging of, resources with all stakeholders and the international community.
- Assist DOE in establishing advanced recycling research and development (R&D) initiatives and provide technical oversight to ensure that priority objectives/goals are accomplished.

Accomplishments During this Reporting Period (FY 2006)

- Conducted quarterly progress reviews with CRADA team.
- Conducted annual project review and gap analysis with CRADA team.
- Developed CRADA team presentation brochure (was prepared by Energetics) and one-pager.
- Conducted one-day peer review progress review. It was attended by experts in the field, in addition to the CRADA partners.
- Conducted one-day Roadmap workshop to update the 2001 Roadmap for Recycling End-of-Life Vehicles of the Future. The updated Roadmap will be issued in the first quarter of FY 2007.
- Launched US ELV CRADA Team website: http://www.es.anl.gov/Energy_Systems/ CRADA_Team_Link/ Index.html. It includes an overview of the CRADA team activities, downloadable CRADA team brochures, a bibliography of recycle literature and presentations and annual reports of the team.
- Presented papers outlining the industry/government collaboration at international conferences.
- The CRADA team held a media event for America Recycles Day. Press releases and related news stories are accessible through the CRADA team website.
- Continued liaison with the Institute of Scrap Recycling Industries (ISRI) and the Automotive Recycling Association (ARA) and held several meetings with the CRADA partners and representatives of ISRI and ARA.

Prior Accomplishments

FY 2005

- Conducted quarterly progress reviews with CRADA team.
- Conducted annual project review and gap analysis with CRADA team.
- Continued liaison with the Institute of Scrap Recycling Industries (ISRI) and held several meetings with the CRADA partners and representatives of ISRI.

FY 2004

- Conducted quarterly progress reviews with CRADA team.
- Conducted annual project review and gap analysis with CRADA team.
- Held a CRADA announcement event at Argonne on December 2, 2004 — the event was attended by representatives of the press, industry, and government.
- Established liaison with the Institute of Scrap Recycling Industries (ISRI) and held several meetings with the CRADA partners and representatives of ISRI.

FY 2003

- Developed 5-year project plan.
- Negotiated a CRADA with the VRP, the American Plastics Council (APC … now the Plastics Division of the American Chemistry Council) and ANL, as partners; effort under the CRADA was initiated in August 2003.

Future Direction

- Conduct gap analysis and continue development and management of the R&D plan with the CRADA partners consistent with the recommendations of the updated Roadmap. As appropriate, new recycle R&D needs that are identified will be incorporated into the plan and projects for conducting the requisite R&D will be developed.

- Conduct scheduled progress reviews.
- Maintain and update the US ELV CRADA team website.
- Continue ongoing efforts toward the milestones and objectives of the CRADA statement-of-work.
- Continue outreach efforts to broaden the basis for cooperation among stakeholders.
- Continue ongoing project efforts to assist DOE in preparation of planning documents, priority recycling R&D needs, proposal reviews, and related tasks.
- Update the ELV Roadmap as necessary.
- The team will prepare papers for presentation at the SAE Congress in FY 2007.

Summary

The objective of this project is to establish priorities and develop cost-effective recycling technologies and strategies in support of the U.S. Department of Energy (DOE's) FreedomCAR and Vehicle Technologies (FCVT) Program's long-term objectives and goals. The major goals of this research are to (1) enable the optimum recycling of all automotive materials, (2) ensure that advanced automotive materials that improve the life-cycle energy use of vehicles are not precluded from use as a result of a perception that those materials are not recyclable, and (3) continue to enable market-driven vehicle recycling.

Today, cars that reach the end of their useful service life in the United States are profitably processed for materials and parts recovery by an existing recycling infrastructure. That infrastructure includes automotive dismantlers, which recover useable parts for repair and reuse; automotive remanufacturers, which remanufacture a full range of components, including starters, alternators, and engines to replace defective parts; and, ultimately, the scrap processor, which recovers raw materials such as iron, steel, aluminum, and copper from the remaining auto "hulk" after components have been recovered for recycling. Today, more than 75% of the materials from obsolete cars are profitably recoverable for recycling.

The recyclability of the remaining 25% of the end-of-life vehicles (ELVs) is limited at present by the lack of (1) commercially-proven technologies to identify and cost-effectively separate materials and components and (2) profitable post-use markets. During the next 20 years, both the number and complexity of ELVs are expected to increase, posing significant challenges to the existing recycling infrastructure. The automobile of the future will use significantly greater amounts of lightweight materials (e.g., ultra-light steels, aluminum, plastics, and composites) and more sophisticated/complex components.

Roadmap Recommendations

A workshop to update the original roadmap, which was published in 2001, was held on September 14, 2005, at Argonne. Representatives from DOE, key stakeholders, universities and other experts attended the meeting (Exhibit 1). A draft of the new roadmap has been prepared and is being reviewed by the CRADA partners. The updated roadmap will be published during the first quarter of FY 2007. The workshop evaluated the original Roadmap and its recommendations.

The following were identified as some of the factors that can affect the recyclability of future shredder residue:

- Vehicles containing new materials of construction for lightweighting (composites, lightweight steel, aluminum alloys, and magnesium);
- Catalysts for better environmental control; and
- Vehicles powered by fuel cells, electric batteries, hydrogen, and hybrids.

The key recommendations from the original roadmap, which was developed with input from key stakeholders to guide DOE's recycle research, were:

- Come together as a unified recycling community to cost-share in the development of required new technology.

Exhibit 1. List of Roadmap Workshop Attendees.

Organization	Represented By
American Plastics Council	Trip Allen
Consultant	Richard Paul
American Plastics Council	Mike Fisher
Argonne	Ed Daniels
Argonne	Bassam Jody
Argonne	Pomykala Joe
Argonne	Jeff Spangenberger
Bayer Material Sciences	Don Schomer
DaimlerChrysler	James Frusti
DaimlerChrysler	James Ryan
DaimlerChrysler	Nakia Simon
DaimlerChrysler	Gerry Winslow
Energetics	Melissa Eichner
Energetics	Catherine Jereza
Ford	Claudia Duranceau
Georgia Tech	Bert Bras
Gesing Consultants	Adam Gesing
GM	Steve Cadle
GM	Candace Wheeler
ISRI	Dave Wagger
PURRC	Stephen Niemiec
Rochester Institute of Technology	Nabil Nasr
Steel Recycling Institute	Bill Heenan
Troy Polymers	Ibraham Sendijarevic
Troy Polymers	Vahid Sendijarevic
Univ. of Windsor	Edwin Tam
USCAR	Susan Bairsley
USCAR	Stacey Keast
USCAR	Mike Martin
USCAR	Virginia Smith
USDOE	Joseph Carpenter

- Incorporate reuse, remanufacturing, and recycling into the design phase for cars whenever possible.
- Recycle as early in the recycling stream as possible, while relying on the market to optimize the value and amount recycled at each step.
- Maintain a flexible recycling process that can adapt to diverse model lines fabricated with different techniques and materials from various suppliers.
- Develop automated ways to recover bulk materials.
- Emphasize R&D on post-shred material identification, sorting, and product recovery.
- Focus R&D efforts on materials not recycled today by sorters (e.g., post-shred glass, rubber, fluids, textiles, plastics).
- Develop uses for recovered materials (whether in the same or different applications) and testing specifications.
- Encourage investment in the infrastructure needed to achieve the recyclability goal. Build on the existing infrastructure.
- Develop a means to prevent the entry of polychlorinated biphenyls and other hazardous materials into the recycling stream and promote acceptable limits in shredder residues.
- Consider the recycling requirements of new technologies entering fleets as early as possible.

The Five-Year R&D Plan

On the basis of the roadmap and continuing discussions with key stakeholders, a five-year research plan was prepared. The plan includes three focus areas, as discussed below.

Area 1. Baseline Technology Assessment and Infrastructure Analysis

The focus of the work under this activity is to develop the tools and document the information necessary to make effective decisions relative to technology needs to facilitate sustainable future vehicle recycling and to make effective decisions regarding the allocation of R&D resources.

Area 2. Materials Recovery Technology Development and Demonstration

Research to be conducted in this area will initially focus on addressing technology needs for post-shred materials recovery, including mechanical recycling and conversion to fuels and chemicals. Projects that enhance pre-shred recovery — including disassembly for materials recovery and direct reuse and remanufacturing of components — will also be considered. In the long term, such components as fuel cells, advanced batteries, and onboard hydrogen reformers are more likely to enter the recycle stream through pre-shred recovery for remanufacturing, repair, and materials recovery. Research will be undertaken to determine the technology needs to

ensure the recyclability of these very advanced automotive components.

Area 3. Recovered Materials Performance and Market Evaluation

Understanding and enhancing recovered materials performance is an essential ingredient to a successful recycling program. This is especially true in automotive systems when the materials and components that are recovered have been in use for an average of from 10–15 years. Area 3 includes projects to quantify the relative performance of recovered materials vis-à-vis new or virgin materials; research on compatibilization of recovered polymers to improve performance properties; development of technologies to upgrade the recovered materials, such as separation of fibers from polymeric substrates; and development of applications for other recovered materials, such as rubber and glass.

CRADA Projects

A cooperative research and development agreement (CRADA) among Argonne, the VRP and the American Plastics Council (APC – now the Plastics Division of the American Chemistry Council) has been structured to provide a core team of expertise and the resources to enable the optimum recycling of all automotive materials.

The CRADA team's R&D agenda focuses on the following key objectives:

- Develop and demonstrate sustainable technologies and processes for ELV recycling.
- Demonstrate the feasibility of resource recovery from shredder residue, including materials recovery for reuse in automotive and other applications, chemical conversion of residue to fuels and chemicals, and energy recovery.
- Develop viable strategies for the control and minimization or the elimination of substances of concern.
- Benchmark recycling technology and provide data to stakeholders.
- Stimulate markets for reprocessed materials to support economic collection, processing, and transportation.
- Transfer technology to commercial practice.

This project (Recycling Assessments and Planning) provides for the overall management of the CRADA team activities and for communication and advocacy with other organizations. The other major projects that have been initiated under the CRADA include the following:

- Baseline Assessment of Recycling Systems and Technology (see 7.B).
- Post-Shred Materials Recovery Technology Development and Demonstration (see 7.E).
- Development of Technology for Removal of PCBs and Other Substances of Concern from Shredder Residue (see 7.C).
- Compatibilization/Compounding Evaluation of Recovered Polymers (see 7.D).

The objectives and progress on these projects are discussed in their respective sections of this report. Effort under the CRADA was initiated in the fourth quarter of FY 2003.

Outreach Efforts

While the CRADA team provides a core of expertise, cooperation with other organizations is the key to achieving the overall program objectives. In the United States, a market-driven recycling infrastructure is in place. The CRADA team is actively pursuing cooperation with the organizations and companies that are a part of that infrastructure. Cooperation with other stakeholders is also essential.

A website was launched in March of 2006 to provide for better communication and networking with stakeholders and other research teams: http://www.es.anl.gov/Energy_Systems/CRADA_Team_Link/Index.html. The website provides an update of the CRADA progress and provides access to relevant information and publications including a bibliography of mechanical, thermo-chemical conversion, and energy recovery technologies for recycling automotive materials.

The CRADA team held a media event at Argonne for *America Recycles Day*. It was attended by a number of media organizations. Articles featuring the work done by the CRADA team were written by the media members who attended. CRADA team

members were interviewed by several radio stations after the media event.

Several presentations and publications were made to further communicate with interested parties including a paper "Market Driven Technology Development for Sustainable End-of-Life Vehicle Recycling: A Perspective from the United States," presented by Edward Daniels at the 6th International Automobile Recycling Congress, Amsterdam, Netherlands, March 15-17, 2006. A joint DOE, USCAR, and APC paper on "Market Driven Recycling in North America" was presented as the keynote paper at the 2004 International Car Recycle Congress in Washington, D.C.

Several meetings with representatives of the Institute of Scrap Recycling Industries (ISRI) and the Automobile Recycling Association (ARA) were held to brief them on the CRADA objectives and projects and to elicit their participation.

To further communicate the U.S. approach to ELV recycling, a one-page CRADA summary and a CRADA brochure have been prepared and it is available at the CRADA website.
As previously mentioned, a review of the projects and ongoing efforts of the CRADA team was held September 13, 2005 and a workshop was also held on September 14, 2005, to review and update the ELV Roadmap. The updated roadmap will be issued during the first quarter of FY 2007.

Publications

1. *The R&D of the FreedomCAR Materials Program*, Carpenter, J.A., Jr., E.J. Daniels, P.S. Sklad, C.D. Warren and M.T. Smith, Proc. Of the International Auto Body Congress, Novi, MI, September 19, 2006.

2. *Market Driven Technology Development for Sustainable End-of-Life Vehicle Recycling: A Perspective from the United States*, Daniels, E.J., Jody, B. J., Pomykala, J. A. Jr., and Spangenberger, J. S., presented at the 6th International Automobile Recycling Congress, Amsterdam, Netherlands, March 15-17, 2006.

3. *Industry and Government Collaboration to Facilitate Sustainable End-of-Life Vehicle Recycling*, Daniels, E. J., 2005 ASME International Mechanical Engineering Congress & Exposition, BRTD-4: Sustainability Applications in Product Design and Manufacture, Orlando, Florida, November 5-11, 2005

4. *Market Driven Automotive Recycling in North America*, Duranceau, C., presented at the Institute of Scrap Recycling Industries Shredder Meeting, Dallas, TX (Oct. 30, 2004).

5. *Sustainable End-of-Life Vehicle Recycling: R&D Collaboration between Industry and the U.S. DOE*, Daniels, E.J., Carpenter, J.A. Jr., Duranceau, C., Fisher, M., Wheeler, C., and Winslow, G., JOM, The Mineral, Metals & Materials Society, vol. 56, no 8, pp 28-32 (Aug. 2004).

6. *Market Driven Automotive Recycling in North America*, Duranceau, C., USCAR, Carpenter, J., U.S. DOE, Fisher, M., American Plastics Council, keynote at the 2004 International Car Recycling Workshop, May 19, 2004, Washington D.C.

7. *Automotive Materials Recycling: A Status Report of U.S. DOE and Industry Collaboration*, Daniels, E. J., Ecomaterials and Ecoprocesses, Proc. of the International Symposium on Ecomaterials and Ecoprocesses, August 24-27, 2003, Vancouver, BC, Canada, pp 389-402.

8. *Effects of Transportation on the Ecosystem*, Carpenter, J.A., Jr., Ecomaterials and Ecoprocesses, Proc. of the International Symposium on Ecomaterials and Ecoprocesses, August 24-27, 2003, Vancouver, BC, Canada, pp 13-22.

9. *Automotive Technology: Looking Forward*, Sullivan, R., D. Hamilton and J.A. Carpenter, Jr., Ecomaterials and Ecoprocesses, Proc. of the International Symposium on Ecomaterials and Ecoprocesses, August 24-27, 2003, Vancouver, BC, Canada, pp 49-67.

10. *A Roadmap for Recycling End-of-Life Vehicles of the Future*, prepared by Energetics for the U.S. Department of Energy, Office of Advanced Automotive Technologies (May 2001).

[i] One of the formal consortia of the United States Council for Automotive Research (USCAR) set up by the "Big Three" traditionally U.S.-based automakers to conduct joint pre-competitive research and development.

B. Baseline Assessment of Recycling Systems and Technology

Principal Investigator: Edward J. Daniels
Argonne National Laboratory (ANL)
9700 S. Cass Ave., Argonne, IL 60439
(630) 252-5279; fax: (630) 252-1342; e-mail: edaniels@anl.gov

Technology Area Development Manager: Joseph A. Carpenter
(202) 586-1022; fax: (202) 586-1600; e-mail: joseph.carpenter@ee.doe.gov

Expert Technical Monitor: Philip S. Sklad
(865) 574-5069; fax: (865) 576-4963; e-mail: skladps@ornl.gov

Participants:
This project is conducted as part of a Cooperative Research and Development Agreement (CRADA) among Argonne, USCAR's Vehicle Recycling Partnershipiii, and the Plastics Division (formerly the American Plastics Council) of the American Chemistry Council.
CRADA Partner Principal Investigators:
Michael Fisher, American Chemistry Council, (703) 741-5599, e-mail: Mike_Fisher@americanchemistry.com
Gerald Winslow, VRP, DaimlerChrysler Corp., (248) 512-4802, e-mail: grwx@DCX.com
Claudia Duranceau, VRP, Ford Motor Co., (313) 390-0504, e-mail: cdurance@ford.com
Candace Wheeler, VRP, General Motors Corp., (586) 986-1674, e-mail: candace.s.wheeler@gm.com

---

Contractor: Argonne National Laboratory
Contract No.: W-31-109-Eng-38

Objective

- Establish the baseline or state-of-the-art for automotive-materials-recovery/recycling technology.

Approach

- Review the state-of-the-art of worldwide automotive-materials-recovery/recycling technologies.
- Develop technology profiles of emerging automotive materials recycling technologies.
- Review international, federal, and state regulatory information regarding vehicle recyclability, substances of concern, and recycle laws and mandates.
- Conduct life-cycle studies to quantify the environmental burdens associated with various end-of-life recycling technologies.
- Conduct reference-case end-of-life recyclability studies.

Accomplishments During this Reporting Period (FY 2006)

- Completed compilation of recycle bibliography, structured as a pull down PDF, posted on US ELV CRADA Team website, http://www.es.anl.gov/Energy_Systems/CRADA_Team_Link/Index.html.
- Completed Changing World Technologies (CWT) life-cycle case study.
- Completed life-cycle study of Argonne process technology.
- Completed second draft of state-of-the-art assessment in recycling of vehicles and automotive materials. The final document will be published in the first quarter of FY 2007.

Prior Accomplishments

FY 2005

- Conducted a literature search that identified mechanical, thermo-chemical conversion, and energy-recovery technologies and completed first draft of state-of-the-art assessment.
- Completed Salyp life-cycle case study, initiated CWT life-cycle case study.

FY 2004

- Compiled and structured recycle bibliography.
- Characterized North American recycle infrastructure.
- Conducted a review of U.S. regulatory issues.
- Initiated life-cycle studies of end-of-life recycle technologies (Salyp case study).
- Completed reference recyclability calculations for reference cases and three lightweight alternatives: lightweight steel, composite materials, and aluminum.

Future Direction

The focus of this task in FY 2007 will be on:

- Updating the database of recycle technologies
- Complete the life-cycle study of current shredding operations
- Update the document reviewing technologies for recycling shredder residue

---

Summary

The objectives of this project are to benchmark the automotive-materials recycling industry and to compile information in an accessible format regarding the status of existing and emerging recycling technology and research.

The focus of the work under this activity is (1) to develop the tools and document the information necessary to make effective decisions relative to technology needs to facilitate sustainable future vehicle recycling and (2) to make effective decisions regarding allocation of R&D resources.

The state-of-the-art of worldwide automotive-materials-recovery/recycling technologies and associated resource-recovery infrastructures have been reviewed to identify technology gaps and needs and to identify differences in automotive- recycling strategies among the North America, Europe, and Asia. Technologies in this review include, but are not limited to, post-shred materials- recovery technologies, pre-shred materials-recovery technologies, materials-identification technologies, automated dismantling technologies, technologies for the recycling of specific components of vehicles (such as bumpers), and thermochemical-conversion technologies.

Life-cycle analyses of alternative recycle technologies have also been conducted to identify differences between technologies, such as mechanical recycling vis-à-vis thermochemical recycling, relative to energy and environmental benefits.

Regulations at the international, federal, and state levels are examined to identify the impact that proposed and existing regulations may have regarding recycling of automotive materials. Reference-case recyclability calculations are made to quantify the expected recyclability of alternative vehicle designs.

Infrastructure

The North American recycling infrastructure has been characterized and a representative figure was shown in previous annual reports.

Technology Profiles

The recent literature has been reviewed, and summaries and profiles of available and emerging recycle technologies have been compiled into a draft working document and will be updated annually as new information becomes available.

A bibliography of abstracts of papers that discuss automotive-recycling issues has been compiled; see Table 1. The bibliography is organized into the fifteen sections shown.

The bibliography was compiled from an extensive literature search, which included the following sources:

1. Society of Automotive Engineers (International) World Congresses from 1997 to 2004
2. Environmental Sustainability Conference and Exhibition, 2001
3. Society of Plastics Engineers:
   - ARC '98 Conference
   - ARC '99 Conference
   - ARC '00 Conference
   - GPEC 2002 Conference
   - GPEC 2003 Conference
4. Other conference proceedings:
   - International Automobile Recycling Congress 2001, 2002, 2003, 2004
   - TMS Fourth International Symposium of Recycling of Metals and Engineered Materials, 2000.
   - Ecomaterials and Ecoprocesses, The Conference of Metallurgists, COM 2003

The complete bibliography has been posted on the US ELV CRADA Team website: http://www.es.anl.gov/Energy_Systems/CRADA_Team_Link/Index.html.

More references have been identified and will be added to the bibliography.

Table 1. Citations included in the recycling bibliography (as of September 2005).

Bibliography Section	Number of Citations
Recycling infrastructure	18
Design for recycling	4
Legal and regulatory issues	24
Life-cycle analysis	9
Research programs	10
Substances of concern	5
Disassembly technologies and case studies	9
Reuse of automotive parts and subassemblies	1
Remanufacturing	0
Mechanical separation technology	21
Thermochemical-conversion technology	12
Energy-recovery technology	16
Other technology	36
Advanced materials-recycle technology	7
Case studies of materials recycled for auto applications	24
Total citations	196

Recycling Technologies: State-of-the-Art

A draft document describing the state-of-the-art in recycling technologies for end-of-life vehicles, post-shred residue, and automotive materials has been prepared and it has been reviewed twice by the CRADA partners. The final document will be published in the 1st quarter of FY 2007. Because post-shred residue contains residue from shredded white goods and other obsolete items (in addition to vehicles), these were also discussed in the document. The table of contents of this document is shown in Table 2.

Regulatory Situation

The European Union has issued End-of-Life Vehicle Recycle Directives. The enforcement of these directives is, however, the responsibility of each member state. Although the United States has not developed a federal policy or mandate, regulations at the federal and state level can impact the technology needs for recycling automotive materials. For example, U.S. Environmental Protection Agency (EPA) regulations regarding polychlorinated

biphenyl (PCB) limits the concentration of PCBs on recycled materials to below the detectable limit (i.e., 2 ppm). State regulations regarding mercury and polybrominated diphenyl ethers (PBDEs) can also impede materials recycling.

Life-Cycle Studies

The objective is to use life-cycle analysis to assess the environmental impacts of various mechanical separation technologies and alternative end-of-life recycling technologies. This information will then be used to create a flexible, computerized, life-cycle inventory model, which is process-specific and yet can be modified to include additional recycling technologies and various material inputs. Life-cycle involves assessing all of the upstream burdens associated with the production of the materials and energies used in the process, including the transport of all materials to the facility.

PE Europe GmbH, a company that is experienced in conducting life-cycle assessments and in model development using its own GaBi (Ganzheitliche Bilanzerung) software, was contracted to perform these analyses. Three analyses have been completed for: (1) Salyp NV's mechanical separation process, (2) Changing World Technologies' (CWT's) thermal-conversion process, and (3) Argonne mechanical and froth-flotation process. PE Europe has developed a flexible end-of-life model, and the model was used to compare the two different approaches to recycling shredder residue. The model allows the user to run simulations on shredder-residue separation within different boundary conditions. The following boundary conditions can be modified: (1) shredder-residue composition, (2) location of the facility, (3) type and distance of transportation, (4) market values for the separated fractions, (5) new potential applications for separated fractions, and (6) utilization ratio of the facility.

Salyp's separation process combined equipment developed by ANL and several others to create a facility that separates shredder residue into discrete fractions of metals, foam, mixed plastics, and fiber-rich and fines streams. On the other hand, the CWT process converts organic materials into hydrocarbon fuels and other potential products.

Table 2. Draft state-of-the-art assessment table of contents.

1.0. Introduction and Background
2.0. The Process of Recycling Automobiles
— ***Dismantling for Direct Resale***
— ***Shredding***
3.0. The Process for Recycling White Goods
— ***Refurbishing of Units for Resale***
— ***De-Pollution of the Units***
— *Shredding*
4.0. Shredder Residue
— *Composition*
— *Recycling of Materials from Shredder Residue*
5.0. Technologies for Concentrating Recyclables from Shredder Residue
— *Mechanical Separation Systems*
— *Gravity Separators*
— *Electrostatic Separators*
6.0. Technologies for Separating and Recovering Products from Shredder Residue
— *Argonne's Separation and Recovery of Flexible Polyurethane Foam*
— *Separation and Recovery of Plastics from Shredder Residue*
- *Argonne's Froth Flotation Process*
- *The RPI Process*
- *The Salyp Process*
- *The VW/SiCon Process*
- *The Galloo Process*
- *The MBA Process*
- *The Toyota Process*

7.0. Thermochemical Processes for Recycling Shredder Residue
- *CWT Hydrolysis Process*
- *TPI Glycolysis Process*
- *Other*

8.0. Energy Recovery from Shredder Residue
9.0. Substances of Concern
— *Polychlorinated Biphenyls (PCBs)*
— *Heavy Metals*
— *Flame Retardants*
10.0. Recycling of Advanced Vehicles
— *Recycling of Fuel Cell vehicles*
— *Recycling of Electric and Hybrid Vehicles*
— *Recycling of Aluminum and Magnesium from New Generation vehicles*
— *Recycling of Composites*
11.0. Chemical Recycling of Shredder Residue
12.0. Conclusions

Data were collected for each of the three processes, including all energy, water, and material inputs, plus data on emissions to air and water, wastes, and products produced. The three sets of data were entered into the GaBi software to create a flexible model of the process.

In the case of the Salyp separation process, three different scenarios for handling the various materials recovered from shredder residue were determined. These scenarios included using specific material fractions as fuel for cement kilns (energy recovery), as well as using mixed plastics to replace such products as wood pallets and polypropylene (PP) pellets (material substitution). The various scenarios were assessed by using a variety of impact categories, including primary energy demand and CO_2 emissions. In the case of primary energy demand, all scenarios showed a net credit in total energy use. For the three scenarios studied, substituting recovered polypropylene/ polyethylene (PP/PE) in a new PP application had the greatest benefit. However, if the mixed plastic stream was used to replace wood (e.g., decking material, park benches, wood pallets, etc.), the benefits to primary energy demand were less than if the recovered materials were simply used for energy recovery. In terms of CO_2 emissions, the PP application again showed the greatest benefit. Substituting PP for wood applications was next with a lower benefit, while the energy-recovery scenario showed an increase in CO_2 emissions.

In the case of the CWT process, two basic scenarios were assessed. They involved using the light hydrocarbon oil generated by the process for fuel oil used in power plants to generate electricity and substituting light hydrocarbon oil for diesel oil (both with and without an added hot-oil processing step). While the oil product generated is more refined than an actual crude oil, it would require additional steps before it could be considered a true diesel oil. Therefore, reality is probably located somewhere between scenarios 1 and 2. In this study, the impact on primary energy demand resulted in a benefit in all cases. The benefits in the diesel-substitution case were slightly greater than in the fuel oil case. In the case of CO_2 emissions, all scenarios again showed an overall benefit. However, the diesel-substitution case had a greater benefit than the fuel-oil-substitution case.

Life-cycle analysis of the Argonne process considered both the mechanical separation of the shredder residue to produce a polymer concentrate and recover residual metals, followed by froth flotation to separate plastics from the polymer concentrate for recycling as plastics (material substitution). The analysis concluded both the mechanical and the froth-flotation processes resulted in environmental benefits, Figure 1. The environmental benefits of the Argonne process were also compared with those of Salyp (Table 3) and CWT processes (Table 4). The environmental benefits are higher for the Argonne process compared to the Salyp process except for the acidification potential and higher for the Argonne process compare to the CWT process except for the impact category EP and NO_x emissions. Energy-wise, the Argonne process was the most advantageous. Interestingly, the best results can be obtained by combining both (Argonne and CWT) processes, where organic fractions separated by Argonne which do not meet the requirements for material substitution (such as mixed plastics and rubber by-products) are processed by CWT for fuel production.

Recyclability Studies

Recyclability studies are being conducted to examine the effect of using automotive-lightweighting material on recyclability. A Toyota Prius hybrid was selected as a reference case. This vehicle is a second-generation hybrid with a gas/electric powertrain. Evaluating the recyclability of this vehicle and its new technology will be a step in identifying changes that will impact end-of-life recycling of vehicles of the future.

In collaboration with Johnson Controls, Inc. (JCI), the VRP dismantled the vehicle according to its procedures to single-material components and entered data for each part into a database. A material list that identified the breakdown of materials into separate classifications (such as ferrous and nonferrous metals, as well as composite materials and plastics) was prepared. The materials breakdown is summarized in Table 5. In comparison, the materials composition of a production Ford Taurus is summarized in Table 6.

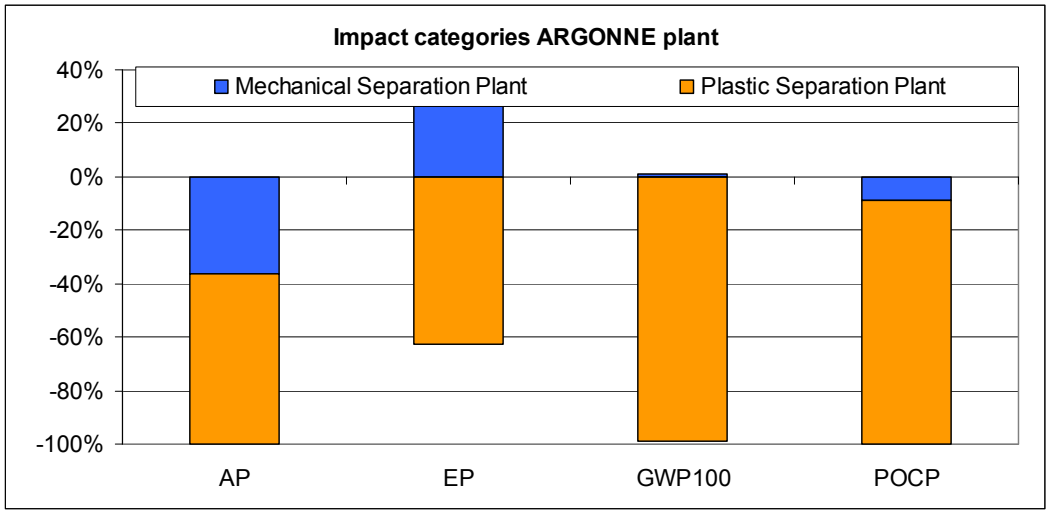

Figure 1. Impact categories of the Argonne plant. (AP is acidification potential, EP is eutrophication (depletion of oxygen in water) potential, GWP is global warning potential and POCP is photochemical ozone creation potential). (Y axis indicates increase (+) or decrease (-) in the impact of the different categories.

Table 3. Comparison of the Argonne and Salyp processes - Relative Environmental Impact. (A negative value indicates a reduction in the pollution category (an environmental benefit) while a positive value indicates an increase in the pollution category).

	ARGONNE process (mechanical and Froth Flotation)	**Salyp process**
AP [lb SO2-Equivalent.]	-0.0060	-0.0165
EP [lb Phosphate-Equivalent.]	-0.00011	0.00148
GWP100 [lb CO2-Equivalent.]	-1.354	0.861
POCP [lb Ethene-Equivalent.]	-0.0026	0.0126

Table 4. Comparison of the Argonne froth-flotation and CWT processes - Relative Environmental Impact. Both processes require mechanical separation of the inorganic fraction. (A negative value indicates a reduction in the pollution category (an environmental benefit) while a positive value indicates an increase in the pollution category).

	ARGONNE process (Froth Flotation*)	**CWT process**
AP [lb SO2-Equiv.]	-0.01103	-0.00662
EP [lb Phosphate-Equiv.]	-0.00055	-0.00079
GWP100 [lb CO2-Equiv.]	-4.167	-0.309
POCP [lb Ethene-Equiv.]	-0.0088	-0.0044

* Comparison is done here only with the froth-flotation process because both Argonne's froth-flotation process and CWT's process require mechanical separation of the inorganic materials.

Table 5. 2004 Toyota Prius materials breakdown.

Materials	Mass (lb)	Percent
Ferrous metals	1713	60.6
Nonferrous metals	507	17.9
Plastics	341	12.1
Elastomers	87	3.1
Inorganic material	77	2.7
Other	62	2.2
Organic materials	42	1.5
Vehicle mass (less fluids)	2829	100.0

Table 6. 2004 Ford Taurus materials breakdown.

Materials	Mass (lb)	Percent
Ferrous metals	2223	70.4
Plastics	340	10.8
Nonferrous metals	312	9.9
Elastomers	152	4.8
Inorganic material	90	2.9
Other	38	1.2
Organic materials	4	0.1
Vehicle mass (less fluids)	3159	100.0

Three different recyclability calculations were made (Table 7). The Federal Trade Commission (FTC) recyclability number is the percentage by weight of the material that is currently being recycled, and it includes metals, fluids less fuel, and batteries. The European guidelines include FTC materials plus fuel at 90% of a full tank, plastics that could be recycled, and up to 10% by weight energy recovery. Note that Europe requires 95% recyclability for new vehicles. The feasibility-to-recycle number includes the FTC materials plus plastics that can be recycled. Changes to the current infrastructure would be required to increase recycling beyond the current FTC percentage.

To establish an indication of the impact of lightweight materials on the reference-case recyclability calculations, the 2004 Toyota Prius is compared with a proposed aluminum-intensive lightweight vehicle and a proposed composite lightweight vehicle, both of which are also based on the 2004 Prius. The production 2004 Toyota Prius hybrid vehicle body was steel with an aluminum

Table 7. Reference case recyclability: 2004 Toyota Prius.

Calculation Method	Recyclability (%)
Federal Trade Commission	80.86
European	97.61
Feasibility of recycling	85.58
Ref. 2000 Ford Taurus	80.50

hood and decklid. The suspension was of steel, except for an aluminum steering knuckle on the front suspension. This vehicle was used as the base for this study.

The aluminum alternative is for a 2004 Toyota Prius with an aluminum body and a magnesium engine cradle and a rear axle substituted for the production parts. In addition, seat frames, body brackets, and the instrument panel cross car beam have been changed from steel to aluminum. As a result, the weight has been reduced by approximately 630 lb or 21%. Because the weight reduction is entirely in the currently recycled portion of the vehicle, the recyclability is adversely affected and is reduced from 80.86% to 76.10%. No changes were made to the currently non-recycled portion of the vehicle. Aluminum replaced steel at 50% by weight of the original steel.

The composite alternative is for a 2004 Toyota Prius that consists of (1) a carbon-fiber body with 40% carbon fiber and 60% thermoset polyurethane/urea resin by volume, 49.72% carbon, and 50.28% thermoset polyurethane/urea resin by weight and (2) a magnesium engine cradle and rear axle substituted for the production parts. In addition, seat frames, body brackets, and the instrument panel cross-car beam have been changed from steel to composite. As a result, the weight has been reduced by approximately 711 lb, or 24%. Because the weight reduction is entirely in the currently-recycled portion of the vehicle, the recyclability is adversely affected and is reduced from 80.86% to 57.20% if none of the composite is recycled or 74% if all of the composite material is recycled. No changes were made to the currently non-recycled portion of the vehicle. The composite material replaced steel at 40 wt% of the original steel.

There are reductions in all three recyclability calculations for lightweighted vehicles, even though the rest of the vehicle is not changed (Table 8). Where the aluminum and composite material is being recycled, the same amount of material would be disposed of in landfills in each of the three scenarios. The only difference is that the recycled portion of the lightweighted vehicles would be lighter. Although the recyclability would be less, there would be no difference in the amount of material disposed of in landfills, and the lighter vehicles would use less fuel during their life. As can be seen, lightweighting presents challenges in the European market. Note that these calculations do not take into account the downsizing of related components that would accompany any lightweight vehicle, such as powertrains, brakes, and tires. Because the downsized components are high in metallic content, downsizing will further reduce recyclability and make it difficult to meet the European 95% requirement.

In conjunction with this study, additional evaluations are planned by using these data as a starting point for assessing the recyclability of cars of the future. The impact of vehicle lightweighting and material selection on recyclability will be evaluated. In addition, the impact of powertrain changes in future vehicles (including hybrid and fuel-cell alternatives) on recyclability will be determined in comparison to powertrains in current vehicles. An assessment of various alternatives on recycling and the effect on the current recycling infrastructure will be produced. No downsizing of other components was included in this study. Future studies will reflect the downsizing of powertrains, brakes, tires, and other components in recyclability calculations. Items requiring further study resulting from these assessments will support future projects to determine the feasibility of various alternative vehicle configurations and choices of materials.

These results demonstrate the need for technology to recycle new automotive material if recycling mandates are to be met and to ensure that lightweighting materials are not excluded because of the inability to recycle them.

A seminar to address recyclability and recycled content in view of changing automotive materials has been planned.

Table 8. 2004 Toyota Prius recyclability, reference case vs. aluminum and composite body materials.

Calculation Method	As Produced (%)	Aluminum Body (%)	Composite Body (%)
FTC	80.9	76.1	74.0[a]
European	97.6	96.0	94.5[a]
Recycling feasibility	88.3	85.6	83.9[a]

[a] If the composite material were not recycled, then the numbers would be FTC, 57.2%; European, 78.2%; and feasibility of recycling, 67.1%. Recycling of the composite material would require significant changes in the current recycling infrastructure. In addition, a market for the recycled carbon fibers would need to be developed. Current technology for recycling carbon fibers results in a 20% loss in fiber properties and would limit their reuse to short fiber applications.

Publications

1. *A Life Cycle Look at Making Oil From End-of-Life Vehicles.,* Wheeler, C.S., Simon, N.L., Binder, M., Winslow, G.R., Duranceau, C.M., SAE 2006 World Congress, Detroit, Michigan, 2006. SAE-2006-01-0374.

2. *Modular Life Cycle Model — Basis for Analyzing the Environmental Performance of Different Vehicle End-of-Life Options*, Binder, M.; Simon, N.L.; Duranceau, C.M.; Wheeler, C.S.; Winslow, G.R., Proc. of the 5th International Automobile Recycling Congress, Amsterdam (Mar. 9-11, 2005).

3. *Modular Life Cycle Model of Vehicle End-of-Life Phase — Basis for Analysis of Environmental Performance,* Wheeler, C.S.; Simon, N.L.; Duranceau, C.M.; Winslow, G.R.; Binder, M., SAE Paper 2005-01-0847.

4. *United States National Life Cycle Inventory Database Project, A Status Report,* Sullivan, J.L.; Wheeler, C.S.; and Simon, N.L., SAE Paper 2005-01-0852.

[i] One of the formal consortia of the United States Council for Automotive Research (USCAR) set up by the "Big Three" traditionally U.S.-based automakers to conduct joint pre-competitive research and development.

C. Development of Technology for Removal of PCBs and Other Substances of Concern (SOCs) from Shredder Residue

Principal Investigator: Edward J. Daniels
Argonne National Laboratory (ANL)
9700 S. Cass Ave., Argonne, IL 60439
(630) 252-5279; fax: (630) 252-1342; e-mail: edaniels@anl.gov

Technology Area Development Manager: Joseph A. Carpenter
(202) 586-1022; fax: (202) 586-1600; e-mail: joseph.carpenter@ee.doe.gov
Expert Technical Monitor: Philip S. Sklad
(865) 574-5069; fax: (865) 576-4963; e-mail: skladps@ornl.gov

Participants:
This project is conducted as part of a Cooperative Research and Development Agreement (CRADA) among Argonne, USCAR's Vehicle Recycling Partnershipi, and the Plastics Division (formerly the American Plastics Council) of the American Chemistry Council.
CRADA Partner Principal Investigators:
Michael Fisher, American Chemistry Council, (703) 741-5599, e-mail: Mike_Fisher@americanchemistry.com
Gerald Winslow, VRP, DaimlerChrysler Corp., (248) 512-4802; e-mail: grwx@DCX.com
Claudia Duranceau, VRP, Ford Motor Co., (313) 390-0504; e-mail: cdurance@ford.com
Candace Wheeler, VRP, General Motors Corp., (586) 986-1674; e-mail: candace.s.wheeler@gm.com
Steve Niemic, The Polyurethane Recycle and Recovery Council (PURCC), (734) 479-4927; email: sfniemiec@wowway.com

---

Contractor: Argonne National Laboratory
Contract No.: W-31-109-Eng-38

Objective

- Develop viable strategies and technology for the control and minimization or elimination of polychlorinated biphenyls (PCBs) and other substances of concern (SOCs) from recycled automotive materials.

Approach

- Identify efficient and environmentally-acceptable process solutions for removal of contaminants, including PCBs, from materials recovered from shredder residue.
- Define variances in analytical procedures/test results for PCB analysis.
- Accomplishments During this Reporting Period (FY 2006)
- Argonne developed a two-stage cleaning process which in bench-scale tests has consistently produced plastics from the PP/PE product with <2 ppm PCBs.
- Completed tests in the commercial-solvent washing equipment using proprietary solvent-based solutions and in CO_2.
- Cooperated with the Bromine Science and Environmental Forum (BSEF) in preparing the BSEF brochure entitled "Deca-BDE Flame Retardant."

Prior Accomplishments

FY 2005

- Completed the study to explain discrepancies in PCBs analytical results.
- Initiated testing of commercial-solvent washing processes for cleaning plastics.
- Conducted a study to understand the interactions between PCBs and plastics.
- Identified and initiated testing of alternative methods for PCB removal.

FY 2004

- Completed the solvent/detergent screening study for removing PCBs and heavy metals from plastics.
- Completed aqueous cleaning tests in commercially-available equipment.
- Initiated a study to explain discrepancies in PCBs analytical results.

Future Direction

The FY 2007 plan includes:

- Develop experimental design and test Argonne's two-stage process at a larger scale (1-pound test) for the cleaning of the polyolefin concentrate.
- Develop a conceptual design and perform cost analysis of the process.
- Incorporate the process into the overall process design for recovering materials from shredder residue.

Argonne's two-stage process has successfully produced recovered plastics, at least PP/PE materials, with less than 2 ppm PCBs in multiple tests. However, this has been shown only in small-scale experiments. In FY 2007, larger-scale experiments will be conducted to investigate the scalability of the process including required residence time and operating temperatures.

Summary

The objective of this project is to develop techniques and/or technology to identify and/or cost-effectively remove polychlorinated biphenyls (PCBs) and other substances of concern (SOCs) from recycled automotive materials.

SOCs can impact the recyclability of automotive materials in a number of ways. Certainly, their presence in either recycled materials and/or materials source stream impact the overall costs of recovering recyclable materials. In some cases, their presence at parts-per-million levels, such as in the case of PCBs, can prevent the reuse of the recovered materials.

The strategy that is required for control of the SOCs may vary regionally. For example, requirements are different in Europe, North America, and Asia for various SOCs. Strategies for controlling SOCs can also depend on the technology used for recycling the automotive material.

The presence of SOCs in current vehicles and/or in other durable goods that are presently recycled with end-of-life vehicles is likely to impact the materials recycle stream for the foreseeable future. Consequently, the control of certain SOCs will require technology that will effectively remove the SOCs from recovered materials consistent with current regulatory requirements and consistent with the market requirement for the recovered material.

The focus of the work in this project is on the development of options and technology for the removal of PCBs from potentially recyclable materials recovered from shredder residue. PCBs, at parts-per-million levels, are routinely found in shredder residue. The source of the PCBs is not completely understood, but historically it has been associated with liquid PCB-containing capacitors and transformers that inadvertently escape the scrap inspections and control process at the shredders.

Development and Testing of a 2-Stage Process at Argonne

The work done so far on washing of polymers recovered from shredder residue suggests that different washing methods appear to reduce the PCBs concentration down to about 5-10 ppm in a reasonably short time. Further reduction in the concentration of PCBs requires more extensive and prolonged washing in fresh solution, Figure 1. The prolonged washing is further complicated by the adsorption of the cleaning solution by the plastics. This suggests that the PCBs on the plastics are adsorbed by two different mechanisms. First, some are in the oils and dirt that are on the plastics. Second, some of the PCBs are adsorbed on the plastics and they do not desorb easily during washing. We tested this hypothesis in the lab. We conducted washing tests using a non-flammable solvent to wash the plastics under conditions that minimized the absorption of the solvent by the plastics. This reduced the concentrations of PCBs from about 30 ppm to about 5 ppm under a range of operating conditions. The washed plastics were then processed in an environment that induces desorption. The PCBs concentration in several tests was reduced to below 2 ppm. Tests were also conducted where unwashed samples were exposed to the same environment that induces desorption. The PCBs concentration could not be reduced below 2 ppm. We are filing for a patent on the process.

A 2-stage process, based on this concept, has been developed and tested at Argonne which has repeatedly reduced the PCBs concentration in polypropylene/polyethylene samples recovered from shredder residue to less than 2 ppm. We are filing for a patent on the process.

Evaluation and Testing of Solvent-Based Washing Systems

Three companies with equipment and/or proprietary washing solvents and solutions that could potentially be used for non-aqueous removal of PCBs from plastics recovered from shredder residue were identified by Troy Polymers, Inc. (TPI):

- Environmental Technology Unlimited (Wilmington, North Carolina);
- Cool Clean Technologies, Inc. (Burnsville, Minnesota); and
- itec Environmental Group, Inc. (Oakdale, California).

Each company was supplied with a sample of plastics with the determined concentration of PCBs of 11 ppm. Samples were washed at the three companies, and the washed samples were evaluated for PCB levels.

Environmental Technology Unlimited uses a proprietary METHEX solvent-based system and aqueous-based systems. Environmental Technology Unlimited performed six treatments of shredder residue plastics, and five out of the six washed samples reduced the PCBs concentration to below 2 ppm. The METHEX solvent-based system was superior to the aqueous system. Unfortunately, the company does not have equipment to conduct large-scale testing of the process using plastics.

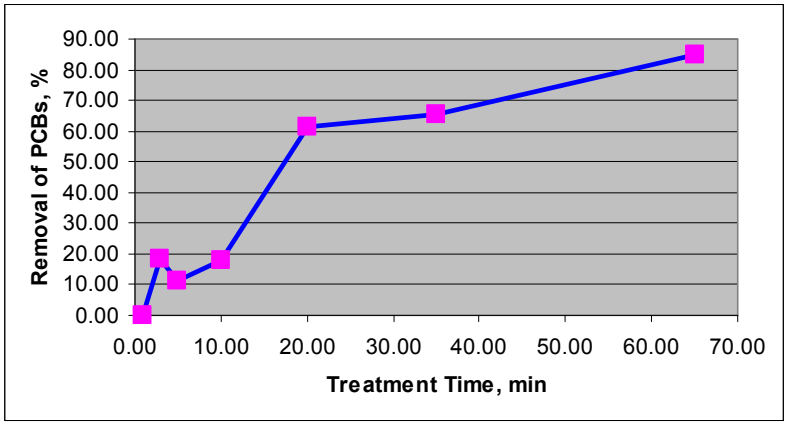

Figure 1. Removal of PCBs with time using a non-flammable organic solvent.

Cool Clean Technologies technology used CO_2 only. The washing failed to remove the PCBs. itec Environmental Group reduced PCB levels in the plastics from 11 ppm to 2.8 ppm via solvent washing; no CO_2 treatment, which normally follows the basic process, was used.

Further testing was conducted by itec in their new facilities in California, using plastics recovered by the Argonne process. The plastics were washed using itec's proprietary solvent and then with liquid CO_2. Two samples received by Argonne were analyzed and both showed residual PCBs concentration on the order of 5 ppm. Another series of trials were conducted at itec using different process conditions. Analysis showed the residual concentration of PCBs was still higher than 2 ppm.

Evaluation and Testing of Commercially-Available Aqueous-Based Washing Systems

Before testing the solvent-based systems, large-scale cleaning/washing tests were conducted using plastics from shredder residue by means of aqueous solutions and a surfactant previously identified earlier as the most promising from among many tested. The objective was to identify the limitations of the various types of existing washing equipment. Testing was done by using an ALMCO rotary-drum washer equipped with a dryer and SeKoN centrifuge equipment. The tests were carried out on about 100 lbs of plastic chips each. The particles were between 0.2 and 0.5 in. in size. Under a CRADA contract, GraPar Corporation built, for Troy Polymers, Inc. (TPI), and tested a specially-designed machine that has a design capacity of about 300 lbs/hour of plastics. TPI conducted further testing on this machine in its facilities.

In each of these tests, the washed material was "visually" clean. However, PCBs analyses were highly variable and indicated that, in some cases, the PCBs concentration had increased after washing. As a result, it was determined that the PCBs analysis procedures should be reexamined, as is discussed in the next section.

The results suggest that existing aqueous-based equipment, as is, is not likely to reduce the concentration of PCBs to acceptable levels. Modifications are necessary to wash small chips (1/8 to 1/2 in.) of plastics — such as what will be recovered from shredder residue.

Evaluation of the Variability of PCB Sampling and Analytical Procedures

The large variability in the analytical results raised questions about the analytical sampling and analyses procedures. Therefore, experiments were performed to develop an understanding of the variability in PCB analytical procedures, explain the variability in the results, and develop a consistent procedure for the determination of the concentration of PCBs.

The variability may be due to a number of factors including sample size, plastics particle size, PCBs extraction procedure, analytical procedures, and/or interference from other compounds. A one-day seminar was held and attended by analytical experts from the United States and overseas to develop recommendations for improved sampling and analysis techniques specific to plastics chips recovered from shredder residue.

To investigate the possible interference of phthalates in the PCBs analysis, a sample of plastics chips derived from shredder residue was thoroughly mixed and then divided into four parts. The first part was analyzed by using gas chromatography and an electron-capture detector (GC-ECD) and by using gas chromatography/mass spectroscopy (GC/MS). The other three parts were spiked with different quantities of phthalates, as shown in Table 1, and the spiked samples were analyzed by using the same two methods. The results show no interference of the phthalates in the PCBs analysis. Interestingly, the GC/MS results were always higher than the GC-ECD results.

Table 1. Effect of phthalates on PCBs analysis.

Weight-Percent of Phthalates added	PCBs Concentration (ppm) by GC/ECD	PCBs Concentrations (ppm) by GC/MS
0	4.6+/-0.3	7.9+/-1.0
0.5	4.7+/-0.3	7.4+/-0.2
1.0	5.1+/-0.6	7.0+/-0.4
2.5	4.8+/-0.3	7.4+/-0.3

To investigate the effects of plastics particle size on extraction efficiency of PCBs, a series of laboratory experiments were conducted at TPI on 300-g samples of plastics with two different particle sizes (one made of chips about 0.2 in. in size and the other was granulated to about 0.04 to 0.08 in. in size). Typically in PCBs analyses, extractions are done on a few grams of material, even though the dirt, oil, and the PCBs are not evenly distributed on the shredder-residue plastics.

Samples of the plastics before and after washing were analyzed directly by three different laboratories by using standard PCBs analytical procedures. Extracts from nine sonications of 300-g samples were also analyzed for PCBs by three laboratories. The results (Tables 2–5) show that:

1. The three labs are fairly consistent for each set of samples.

Table 2. Concentration of PCBs (ppm) in plastics before and after extraction with hexane (granulated and ungranulated) — analysis by standard PCBs analysis procedures.

	Aroclor 1232	Aroclor 1242	Aroclor 1254	Total
Designation	ppm	ppm	ppm	ppm
	Laboratory #1			
Ungranulated before extraction	10.34 +/-1.53	N/D	1.27 +/- 0.29	11.6 +/- 1.51
Ungranulated after extraction	1.06 +/- 0.32	N/D	0.07 +/- 0.01	1.13 +/- 0.32
Granulated before extraction	4.54 +/- 0.84	N/D	0.06 +/- 0.16	5.14 +/- 0.98
Granulated after extraction	0.54 +/- 0.33	N/D	0.07 +/- 0.01	0.60 +/- 0.34
	Laboratory #2			
Ungranulated before extraction	N/D	8.69 +/- 1.02	N/D	8.69 +/- 1.02
Ungranulated after extraction	N/D	2.8 +/- 0.98	N/D	2.8 +/- 0.98
Granulated before extraction	N/D	5.31 +/- 2.04	N/D	5.31 +/- 2.04
Granulated after extraction	N/D	0.75 +/- 0.18	N/D	0.75 +/- 0.18
	Laboratory #3			
Ungranulated before extraction	N/D	9.93 +/- 4.67	N/D	9.93 +/- 4.67
Ungranulated after extraction	N/D	1.57 +/- 0.17	N/D	1.57 +/- 0.17
Granulated before extraction	N/D	3.07 +/- 0.26	N/D	3.07 +/- 0.26
Granulated after extraction	N/D	0.68 +/- 0.27	N/D	0.68 +/- 0.27

Table 3. Concentration of PCBs in the ungranulated samples, as calculated from the analysis of the hexane solution extracts.

	Aroclor 1232	Aroclor 1242	Aroclor 1254	Total
Designation	ppm	ppm	ppm	ppm
	Laboratory #1			
Extract 1	8.67 +/- 0.87	N/D	1.02 +/- 0.29	9.69 +/- 0.99
Extract 2	4.59 +/- 1.52	N/D	0.28 +/- 0.05	4.86 +/- 1.49
Extract 3	0.51 +/- 0.09	N/D	0.14 +/- 0.01	0.65 +/- 0.10
Total	**13.76 +/- 2.47**	**N/D**	**1.43 +/- 0.34**	**15.19 +/- 2.57**
	Laboratory #2			
Extract 1	N/D	7.62 +/- 0.58	N/D	7.62 +/- 0.58
Extract 2	N/D	1.44 +/- 0.04	N/D	1.44 +/- 0.04
Extract 3	N/D	0.62 +/- 0.04	N/D	0.62 +/- 0.04
Total	**N/D**	**9.67 +/- 0.65**	**N/D**	**9.67 +/- 0.65**
	Laboratory #3			
Extract 1	N/D	6.56 +/- 0.67	N/D	6.56 +/- 0.67
Extract 2	N/D	1.52 +/- 0.23	N/D	1.52 +/- 0.23
Extract 3	N/D	0.64 +/- 0.03	N/D	0.64 +/- 0.03
Total	**N/D**	**8.71 +/- 0.92**	**N/D**	**8.71 +/- 0.92**

Table 4. Concentration of PCBs in the granulated samples, as calculated from the analysis of the hexane solution extracts.

	Aroclor 1232	Aroclor 1242	Aroclor 1254	Total
Designation	ppm	ppm	ppm	ppm
	Laboratory #1			
Extract 1	18.62 +/- 8.99	N/D	2.20 +/- 0.61	20.81 +/- 9.59
Extract 2	2.30 +/- 2.56	N/D	0.25 +/- 0.06	4.86 +/- 1.49
Extract 3	0.62 +/- 0.14	N/D	0.11 +/- 0.01	0.65 +/- 0.10
Total	**21.52 +/- 11.69**	**N/D**	**2.55 +/- 0.67**	**24.07 +/- 12.25**
	Laboratory #2			
Extract 1	N/D	7.24 +/- 0.34	N/D	7.24 +/- 0.34
Extract 2	N/D	1.01 +/- 0.03	N/D	1.01 +/- 0.03
Extract 3	N/D	0.42 +/- 0.03	N/D	0.42 +/- 0.03
Total	**N/D**	**8.67 +/- 0.40**	**N/D**	**8.67 +/- 0.40**
	Laboratory #3			
Extract 1	N/D	6.29 +/- 1.98	N/D	6.29 +/- 1.98
Extract 2	N/D	1.10 +/- 0.06	N/D	1.10 +/- 0.06
Extract 3	N/D	0.48 +/- 0.03	N/D	0.48 +/- 0.03
Total	**N/D**	**7.87 +/- 2.06**	**N/D**	**7.87 +/- 2.06**

Table 5. Comparison of PCBs concentration (ppm) in the starting plastics samples by direct analysis and by calculation based on the amounts in the hexane extracts.

Plastics Sample	PCB Concentration by Direct Analysis	PCB Concentration Calculated from PCBs in the Hexane Extracts
Ungranulated, Lab-1	11.6 +/- 1.51	15.19 +/- 2.57
Ungranulated, Lab-2	8.69 +/- 1.02	9.67 +/- 0.65
Ungranulated, Lab-3	9.93 +/- 4.67	8.71 +/- 0.92
Granulated, Lab-1	5.14 +/- 0.98	24.07 +/- 12.25
Granulated, Lab-2	5.31 +/- 2.04	8.67 +/- 0.4
Granulated, Lab-3	3.07 +/- 0.26	7.87 +/- 2.06

2. Direct analysis of the samples from the three labs showed that the concentration of PCBs in the granulated plastics was about 5 ppm, and for the un-granulated, it was 10 ppm. Obviously, the granulated samples have larger surface area per unit mass than the other samples. Therefore, more efficient extraction of PCBs from the plastics would be expected in the case of the granulated chips. Because this was not the case, the results indicate that the particle size does not affect the PCB results. Further, the results indicate that the PCBs are on the surface of the plastics and not absorbed in the plastics. After extraction, the samples all had less than 2 ppm of PCBs, except for one sample that showed 2.8 ppm.

3. Calculation of the concentration of PCBs in the original samples based on the determined PCBs in the hexane extracts (prepared via 9 sonications of 300-g samples) showed that the concentrations of PCBs in the granulated samples were comparable with those of the un-granulated samples. These results further indicate that the PCBs are predominantly on the surface of the plastics and not absorbed in the plastics, otherwise the granulated samples would have shown higher concentrations.

In addition, two of the laboratories identified Aroclor 1242 as the only PCB present, while the third laboratory identified Aroclors 1232 and 1254 as the only two present. TPI also conducted an analysis of various plastics samples by using GC-ECD and GC-MS methods. The results are compared in Table 6. Results from the two methods are in reasonable agreement, even though the GC-MS method showed higher values.

Evaluation of Soxhlet Method for PCBs Extraction

Successful commercialization of technology for recovering polymers from shredder residue depends on a reliable and inexpensive technique to analyze samples for PCBs in the field. The U.S. EPA and European protocols for PCBs analysis were reviewed and experiments were conducted to understand the requirements for on-site analysis. A Soxhlet-based method appears to be appropriate for testing because of its simplicity and because it is among the methods specified in both the U.S. EPA protocols and in the European protocols (Table 7). Limited experiments to define the operating conditions for the Soxhlet method were conducted. The results are discussed below.

Selection of a Solvent

Two solvents were tested: hexane and toluene. Three 120-g samples were extracted with hexane for 8 h, and another three 120-g samples were extracted with hexane for 24 hours. Similarly, three 120-g samples were extracted with toluene for 8 h, and another three 120-g samples were extracted with toluene for 24 hours. All extractions were carried out while maintaining the siphoning time at 8–10-min intervals. This procedure resulted in 24 samples of extracts and 12 samples of extracted plastics that were analyzed, Table 8. The results indicate that hexane is a better solvent than toluene.

Table 6. Comparison of PCBs analysis using GC-ECD and GC-MS methods (extraction was carried out using hexane at 2,000 PSIA and 100°C).

Sample Type	PCB Concentration, Using GC-ECD (ppm)	PCB Concentration, Using GC-MS (ppm)
Ungranulated Chips	7.55	9.67
Ungranulated Chips	3.70	5.07
Ungranulated Chips	1.50	3.3
Ungranulated Chips	1.35	2.66
Granulated Chips	7.56	9.37
Granulated Chips	0.93	1.82
Granulated Chips	0.82	2.11
Hexane Solution	9.93	9.50
Hexane Solution	8.3	11.13
Hexane Solution	1.41	1.72
Hexane Solution	0.78	0.92
Hexane Solution	0.53	0.65

Table 7. Protocols for PCBs analysis.

Parameter	European Protocols	U.S. EPA's Protocols	Recommended Protocols
Particle size (mm)	0.5	Not specified	1
Sample size for extraction (g)	3	30	30
Extraction equipment	Soxhlet	Sonication Soxhlet Pressurized fluid	Soxhlet
Extraction time	Not specified	Not specified	>/= 4 h Siphoning cycles at 8–10-min intervals
Solvent	Toluene	Hexane 50/50 Hexane/acetone 50/50 Methylene chloride/acetone	Hexane
Analytical method	MS	GC/ECD MS	MS
Quantification method	6 congeners multiplied by 5	Aroclors	Aroclors

Table 8. Results of the extractions of the 120-g samples with hexane and toluene.

Solvent	Extraction Time (h)	Average PCBs in Extract (ppm)	Standard Deviation (ppm)	Average PCBs in Extracted Plastics (ppm)	Standard Deviation(ppm)
Hexane	24	9.4	1.5	N.D	0
Hexane	8	9.3	0.8	N.D.	0
Toluene	24	9.8	2.4	1.4	0.2
Toluene	8	9.7	0.9	3.0	0.6
Hexane	4	14.5	2.9	N.D. in samples no. 1 and 2; 1.0 in no. 3	1.0

Determination of Extraction Time

Three additional 120-g samples were extracted with hexane for 4 hours each. This procedure resulted in six samples of extracts and three samples of extracted plastics that were analyzed. The results are given in Table 8 and indicate that a Soxhlet extraction time of 4 hours is adequate because it reduced the PCBs concentration in the extracted plastics to below the detectable limits in two of the three samples and reduced it in the third to 1 ppm, even though these samples apparently had more PCBs initially, as evidenced by the higher level of PCBs in the solvent.

Determination of Adequate Sample Size

In addition to the six 120-gram samples extracted for 24 hours discussed above, six additional 60-gram samples and six additional 30-g samples were processed and sampled in the same manner as before (24-hour extraction time and same siphoning intervals) by using hexane. The results are summarized in Table 9. The results indicate that a sample size of 30 g appears to be adequate.

Sample preparation was also investigated. The results indicated that a well-mixed plastics sample of at least one pound should be granulated to a size of 1 mm and mixed before sampling is done.

Comparison of the U.S. EPA and the European Quantification Methods

Four of the extracts from the 120-g samples that were extracted with hexane for 24 hours and two of the 120-g samples that were extracted with hexane for 8 hours were also quantified by using the European method. The results were essentially identical within analytical errors (Table 10). These results lead to the following conclusions:

1. A conventional Soxhlet extractor using hexane is effective for PCBs extraction from plastics.
2. A total extraction time of 4 hours with siphoning intervals of 8–10 min is adequate for complete extraction of the PCBs.
3. The EPA and the European quantification methodologies yield very close results.

Publications

Overview of Washing Systems for Commercial Cleaning of Plastics Separated from Automotive Shredder Residue, Sendijarevic, I.; Sendijarevic, V.; Winslow, G.R.; Duranceau, C.M.; Simon, N.L.; Niemiec, S. F.; and Wheeler, C.S., SAE Paper No. 2005-01-0851.

Screening Study to Evaluate Shredder Residue Materials, Sendijarevec, V.; Simon, N.; Duranceau, C.; Winslow, G.; Williams, R.; Wheeler, C.; Niemiec, S.; and Schomer, D., SAE Paper No. 2004-01-0468.

Table 9. Results of the 24-h extractions with hexane of different size samples.

Sample size (g)	Average PCBs in Extract (ppm)	Standard Deviation (ppm)	Average PCBs in Extracted Plastics (ppm)	Standard Deviation (ppm)
30	10.8	1.9	N.D	0
60	25.5	12.6	N.D.	0
120	9.4	1.5	N.D.	0

Table 10. Comparison of the U.S. EPA and the European quantification methods.

Extraction Time (h)	PCBs According to the EPA Method (ppm)	PCBs According to the European Method (ppm)
24	10.8	9.8
24	9.8	10.9
24	8.0	10.7
24	11.2	11.5
8	11.7	12.3
8	10.8	10.8

[i] One of the formal consortia of the United States Council for Automotive Research (USCAR) set up by the "Big Three" traditionally U.S.-based automakers to conduct joint pre-competitive research and development.

D. Compatibilization/Compounding Evaluation of Recovered Polymers

Principal Investigator: Bassam Jody
Argonne National Laboratory (ANL)
9700 S. Cass Ave., Argonne, IL 60439
(630) 252-5279; fax: (630) 252-1342; e-mail: bjody@anl.gov

Principal Investigator: Edward J. Daniels
ANL
9700 S. Cass Ave., Argonne, IL 60439
(630) 252-5279; fax: (630) 252-1342; e-mail: edaniels@anl.gov

Technology Area Development Manager: Joseph A. Carpenter
(202) 586-1022; fax: (202) 586-1600; e-mail: joseph.carpenter@ee.doe.gov

Expert Technical Monitor: Philip S. Sklad
(865) 574-5069; fax: (865) 576-4963; e-mail: skladps@ornl.gov

Participants:
This project is conducted as part of a Cooperative Research and Development Agreement (CRADA) among Argonne, USCAR's Vehicle Recycling Partnership[1], and the Plastics Division (formerly the American Plastics Council) of the American Chemistry Council.

CRADA Partner Principal Investigators:
Michael Fisher, American Chemistry Council, (703) 741-5599, e-mail: Mike_Fisher@americanchemistry.com
Gerald Winslow, VRP, DaimlerChrysler Corp., (248) 512-4802; e-mail: grwx@DCX.com
Claudia Duranceau, VRP, Ford Motor Co., (313) 390-0504; e-mail: cdurance@ford.com
Candace Wheeler, VRP, General Motors Corp., (586) 986-1674; e-mail: candace.s.wheeler@gm.com

---

Contractor: Argonne National Laboratory
Contract No.: W-31-109-Eng-38

Objectives

- Evaluate the market opportunity for polymers recovered from shredder residue.
- Identify limitations associated with the reuse of the materials as recovered and determine the need for post-processing technology to upgrade the recovered materials to meet the requirements of the market.

Approach

- Specify standard protocols for material testing, content characterization, and performance properties.
- Determine properties of recovered polymers.
- Conduct blending and pelletizing trials of the recovered polymers.
- Conduct mold trials using recovered polymers.

Accomplishments During this Reporting Period (FY 2006)

- Determined the physical properties of the 70% filled acrylonitrile-butadien-styrene (ABS) fraction .

- Determined the physical properties of two blends of the 70% filled ABS fraction with virgin ABS (10% recovered/90% virgin and 25% recovered/75% virgin).

Prior Accomplishments

FY 2005

- Midland Compounding developed a protocol for evaluating the physical properties of recovered plastics.
- Compiled a physical properties database for virgin plastics.
- Determined physical properties of the PP/PE product recovered from the Argonne froth-flotation process and from the polypropylene/polyethylene (PP/PE) fraction recovered by the Salyp process.
- Pelletized 1000 pounds of a blend of the Argonne recovered PP/PE product.
- Conducted mold trials of the recovered PP/PE product.

Future Direction

FY 2007 activities will focus on:

- Determine physical properties of the upgraded filled ABS fraction.
- Determine physical properties of the upgraded unfilled ABS and PS recovered from the unfilled ABS/PS concentrate.
- Determine physical properties of the 85% PC-ABS/PC alloy.
- Pelletize a blend of recovered filled ABS with virgin ABS and compare the properties of the blend with the properties of the virgin material.

Summary

The objectives of this project are (1) to characterize the properties of potentially recyclable automotive materials and (2) to confirm the technical and economic feasibility of using those materials in value-added applications.

The project will initially focus on establishing the properties of polymeric materials that are recovered as part of the Post-Shred Materials Recovery Technology Development project (see 7.E).

Regardless of the effectiveness of any automotive-materials recovery technology, the materials that will be recovered will be on average 10–15 years old and derived from different sources (automobiles, home appliances and others). In this project, the performance properties of recovered polymers will be compared vis-à-vis new or virgin materials to establish a database of the properties of recovered automotive polymers. At present, there are few data about the physical properties of polymers recovered from post-consumer durable goods. Absent such data, it is unlikely that sustainable applications for recycled materials will be either identified or developed.

Physical properties testing has been conducted by Midland Compounding, Inc. Midland also conducts composition testing, the results of which are compared with the results of compositional analysis done on recovered materials by Argonne.

Blending and pelletizing of the PP/PE recovered from shredder residue by Argonne has been tested by Palmer Plastics, Inc. More blending and compounding tests will be done, as required, to achieve the desired performance properties of the recovered materials for target applications.

Mold trials using the recovered PP/PE were also done by MGV Enterprises. More molding tests are planned to confirm the technical and economic feasibility of using recycled polymers in specific applications.

Three additional companies — Collins and Aikman Corporation, Enviro-Plas Corporation, and Mayco Plastics, Inc. — have agreed to evaluate, compound,

and run mold trials by using recovered materials, subject to the physical properties of the recovered materials.

Polymer Physical Properties and Materials Composition Analysis

Typically, 10-lb samples of recovered materials are used to define physical properties and to characterize the composition of the material.

To quantify the physical properties of the recovered material, a sample is extruded on a single-screw extruder, melt-screened through a 40-mesh screen, molded into American Society for Testing and Materials (ASTM) test bars and plaques, and tested. The molded parts and a random selection of regrind chips from each sample are evaluated for material identification by using infrared spectroscopy.

Common physical properties that are measured for each sample include the following:

- Melt flow rate (MFR),
- Izod impact,
- Flexural modulus,
- Tensile strength at yield,
- Tensile strength at rupture,
- Elongation at rupture,
- Deflection temperature under load (DTUL),
- Gardner impact, and
- Specific gravity (SG).

Physical Properties and Composition of the Recovered PP/PE

The physical properties of PP/PE recovered from different shredder residues by Argonne and by Salyp were determined for several samples. The results for the Argonne materials are given in Table 1. Properties of commercially-available PP and PE virgin resins and for PP from dismantled automobiles are presented in Table 2 for comparison. The Izod impact of the recovered material is about three times that of the virgin resins, while the tensile strength of the recovered material is lower than the tensile strength of the virgin resins by about 30%. This phenomenon may be attributed, at least in part, to the presence of thermoplastic olefins (TPO) and rubber in the recovered material, which act as impact modifiers. Recovered samples 8, 9, and 10 listed in Table 1 contained about 2% rubber, while samples 1 through 7 contained about 4% rubber.

The results for the more than 20 PP/PE samples recovered by Salyp from different European and U.S. shredder residues are given in Table 3. The properties of the Salyp recovered PP/PE are equivalent to the properties of the Argonne-recovered PP/PE.

Physical Properties and Composition of the Recovered Filled ABS

Filled ABS recovered by the Argonne froth-flotation process followed by removal of the rubber by the Argonne dry mechanical process contained 70% filled ABS (specific gravity greater than 1.07 and less than 1.1), 1.5% PS, 8% PPO, 3% rubber, 3% PP, 7% nylon and 7.5% others. The physical properties of this recovered filled ABS were determined. The results are given in Table 4 and are compared with properties of a commercially-available virgin ABS. Table 4 also shows the properties of two blends of the recovered ABS with virgin ABS (25% recovered/75% virgin and 10% recovered/90% virgin). Interestingly, except for elongation at rupture and Gardner impact, the properties of the blends were very close to the properties of the virgin material. Operating condition to upgrade the recovered filled ABS to over 90% has been determined. Properties of the upgraded material will also be established.

Polymer Physical Properties Database

A physical properties database has been compiled so that the physical properties of the recovered polymers can be compared with general purpose virgin polymers.

General purpose physical properties have been compiled for the following plastics:

- ABS,
- Nylon (6 cast, 6/6 extruded, 30% glass filled),
- PPO [polyphenylene oxide] (unfilled, 30% glass filled),
- Polycarbonate

Table 1. Properties of PP/PE recovered by Argonne from different shredder residues.

Property	Sample 1	Sample 2	Sample 3	Sample 4	Sample 5	Sample 6	Sample 7	Sample 8	Sample 9	Sample 10	Average
MFR, g/10min, 230°C, 2.16 kg	10.5	14.9	7.7	10.1	11.4	7.2	8.7	7.2	8.7	7.2	9.4
Izod impact, ft-lb/in., 73°F	12.3	10.5	11.9	10.8	9	10.7	13.2	1.7	2.8	3.3	8.6
Flex mod., 1% secant, 1,000 psi	83	73	89	84	82	101	112	126	127	113	99.0
Tensile strength at yield, 1,000 psi	2.6	2.2	2.7	2.6	2.4	2.8	3.1	3.4	3.3	3.1	2.8
Tensile strength at rupture, 1,000 psi	0.8	1.2	2.1	1.9	1.4	2.5	2.0	3.1	3.1	2.9	2.1
Elongation at yield, %	23.0	20.8	21.1	22.8	20. 6	20. 6	17.1	**	**	**	24.3
Elongation at rupture, %	132	78	233	154	82	251	229	12	14	13	119.8
DTUL, 66 psi, °F	131	131	134	134	138	147	155	**	171	160	145
Gardner impact, 73°F, in.- lb	104	88	136	96	56	144	184	20	32	40	90.0
SG, g/cc	0.94	0.95	0.94	0.95	0.94	0.93	0.93	0.94	0.94	0.94	0.94

** Not tested

Table 2. Comparison of recovered PP/PE with commercial grades of PP & PE (Boedeker) (http://www.boedeker.com/mtable.htm), unless specified otherwise.

Property	PP-Homo Polymer	PP-Co Polymer	PP-FR	Standard PP-Co	LDPE	HDPE
MFR, (g/10 min), 230°C	0.5-136*					
Izod impact, ft-lb/in.	1.9	7.5	0.65	0.7	No Break	3
Flex Mod, 1,000 psi	180	160	145	120	200	125
Tensile Strength, 1,000 psi	4.8	4.8	4.3	5.2	2.0	4.6
Elongation, %	12	23	28	600	600	900
DTUL, °F @66 psi	210	173	106	210	110	--
SG, g/cc	0.905	0.897	0.988	0.90	0.92	0.95
Gardner impact, 73°F, in.- lb	0.9-22*					

* Data from http://www.ed-cam.com/materials/propylene_molded.asp. Ranges are for with and without additives.

Table 3. Properties of PP/PE recovered by Salyp from different shredder residues.

Property	Salyp Data
MFR, (g/10 min), 230°C	2.3–4.6
Izod impact, (ft-lb/in.) 73°F	4.7–13.3
Flex mod., 1%, secant, 1,000 psi	81.7–116.5
Tensile strength at yield, 1,000 psi	2.4–2.9
Tensile strength at rupture, 1,000 psi	2.2–2.8
Elongation at rupture, %	19–57
DTUL, 66 psi, °F	150–169
Gardner impact, 73°F, in.-lb	190–240
Specific Gravity, g/cc	0.93

Table 4. Properties of recovered filled ABS, virgin ABS and blends of the two materials.

Property	Recovered Filled ABS	Virgin ABS (342 EZ)	90%Virgin/ 10% Recovered	75% Virgin/ 25% Recovered
MFR, g/10min, 230C, 3.8 kg	3.9	6.5	7.6	6.4
Izod Impact, ft.lbs./in., 73F	0.9	3.8	3.0	2.6
Flex Mod, 1% secant, ksi	324	296	299	302
Tensile strength at yield, psi	4982	5546	5392	5312
Tensile strength at rupture, psi	4956	4459	4544	4930
Elongation at rupture, %	2	56	9	6
DTUL, 264 psi, °F	162	165	166	164
Gardner Impact, 73F, in.lbs.	0	>320	32	8
SG, g/cc	1.08	1.05	1.05	1.06

- Polyethylene, low-density polyethylene [LDPE], high-density polyethylene [HDPE], ultra-high-molecular-weight [UHMW] polyethylene,
- Polypropylene,
- Polystyrene (general purpose, high impact), and
- Polyvinyl chloride (PVC).

The VRP had previously compiled physical properties data on selected polymers that were recovered during the U.S. field trials. These materials were recovered by disassembly. The data from these polymers are included in the database so that the physical properties of materials recovered by disassembly can be compared with those of materials that are recovered from post-shred operations, Table 5 ("USCAR U.S. Field Trial for Automotive Polymers Recycling," by W.W. Gallmeyer, C.M. Duranceau, R. L. Williams and G.R. Winslow, SAE Paper # 2003-01-0645, 2003).

Table 5 gives the properties of PP dismantled from automobiles as part of the USCAR U.S. field trial. The recovered PP was reported to have a specific gravity of 0.915 and it is made of 99.2% PP, 0.4% PE and 0.4% ABS. The differences in the properties of the dismantled PP and the PP/PE recovered from shredder residue are also compared in Table 5.

The differences are not significant and do not affect the usefulness of the material. For example the specific gravity of the material recovered at Argonne is about 0.94 compare to 0.915 for the dismantled material. The MFR reflects the largest difference: 17 for one of the two samples of the dismantled flakes versus about 9.4 for the material recovered from shredder residue. The USCAR study also found that the properties of the dismantled PP responded as expected when additives were added to the PP. For example, the Izod increased from less than 2 ft-lb/in.

Table 5. Properties of PP Dismantled of Cars as Part of the USCAR U.S. Trial. (SAE Paper # 2003-01-0645, "USCAR U.S. Field Trial for Automotive Polymers Recycling," by W.W. Gallmeyer, C.M. Duranceau, R.L. Williams and G.R. Winslow).

Property	Recovered, Extruded	Recovered Flakes, Sample #1	Average Properties of Recovered PP/PE*
MFR, (g/10 min), 230°C	19.9	17	9.4
Izod impact (ft-lb/in.) 73°F	1.8	1.8	8.6
Flx. Mod., 1%, secant, 1,000 psi	136.9	131.9	99
Tensile Strength at Yield, 1,000 psi	3.130	3.136	2.8
Elongation at Yield, %	19	18	24.3
Tensile Strength at Rupture, 1000 psi	2.388	2.384	2.1
Elongation at Rupture, %	59	60	119.8
DTUL, °F	129.7	136.5	145

* From Table 1

to about 11 when 10% of an impact modifier was added, and to about 14 when 20% were added (USCAR U.S. Field Trial for Automotive Polymers Recycling: Interim Findings", by W. W. Orr, SAE Paper # 2000-01-0735, 2000).

Blending and Pelletizing of Recovered PP/PE

250 lbs. of PP/PE recovered by Argonne were blended with 750 lbs. of supplemental PP copolymer regrind for 15 minutes. The blended material was then run through an extruder and pelletized. The general appearance of the final pellet was excellent (Figure 1). Properties of the recovered material used in blending and the properties of the regrind and of the resulting pellets are shown in Table 6. Standard pelletizing conditions were used. Barrel heats were set from 365°F at the rear barrel zone and increased progressively to 390°F at the front, with six heat zones in between. Screen- changer and breaker-plate heats were set at 405°F, and die heats were set at 395°F. Melt temperature was recorded as 460°F, and drive load and screw speed were set at 60% and 67.5% of the maximum values, respectively. Material output was recorded as 1,400 lb/h. Extra-fine screen packs were used (20/20/20/60/100/20 mesh screens) to remove impurities because this was the first time this material has been tried.

In addition, while screen changes are typically performed at pressure differences between 500 psi and 1,000 psi, in this test, changes were performed when the pressure exceeded 500 psi to safeguard against puncturing a screen pack and losing material. Because extra-fine screen packs were used in the test, screen changes were required approximately every five minutes. The results indicated that the recovered PP/PE can be blended with other olefinic regrind and pelletized by using standard processes and equipment.

Mold Trials

Three types of auto parts were molded by MGV Enterprises by using Argonne-recovered PP/PE from shredder residue: knee bolsters, battery trays, and steering column covers (Figure 2). A standard molding machine was used in these trails. No changes to the standard conditions were required to run the recovered material. The limited testing done on the recovered PP/PE fraction shows that quality products, including auto parts, may be produced from the recovered materials. Additives and/or modifiers may be added to meet the specifications of some products.

Figure 1. Pelletized PP/PE product recovered from shredder residue.

Table 6. Properties of recovered PP/PE when mixed with regrind.

Property	Argonne, As Recovered Sample 9 (see Table 1)	Regrind As Is	Pelletized Blend
MFR (g/10 min), 230°C	8.7	3.1	9.2
Izod impact (ft-lb/in.) 73°F	2.8	13.6	10.4
Flex mod., 1%, secant, 1,000 psi	127	157	136
Tensile strength at yield, 1,000 psi	3.3	3.7	3.4
Tensile strength at rupture, 1,000 psi	3.1	2.9	2.3
Elongation at rupture, %	14	125	57
DTUL,66 psi, °F	171	197	176
Gardner impact, 73°F, in.-lb	32	>320	132
SG, g/cc	0.94	0.91	0.92

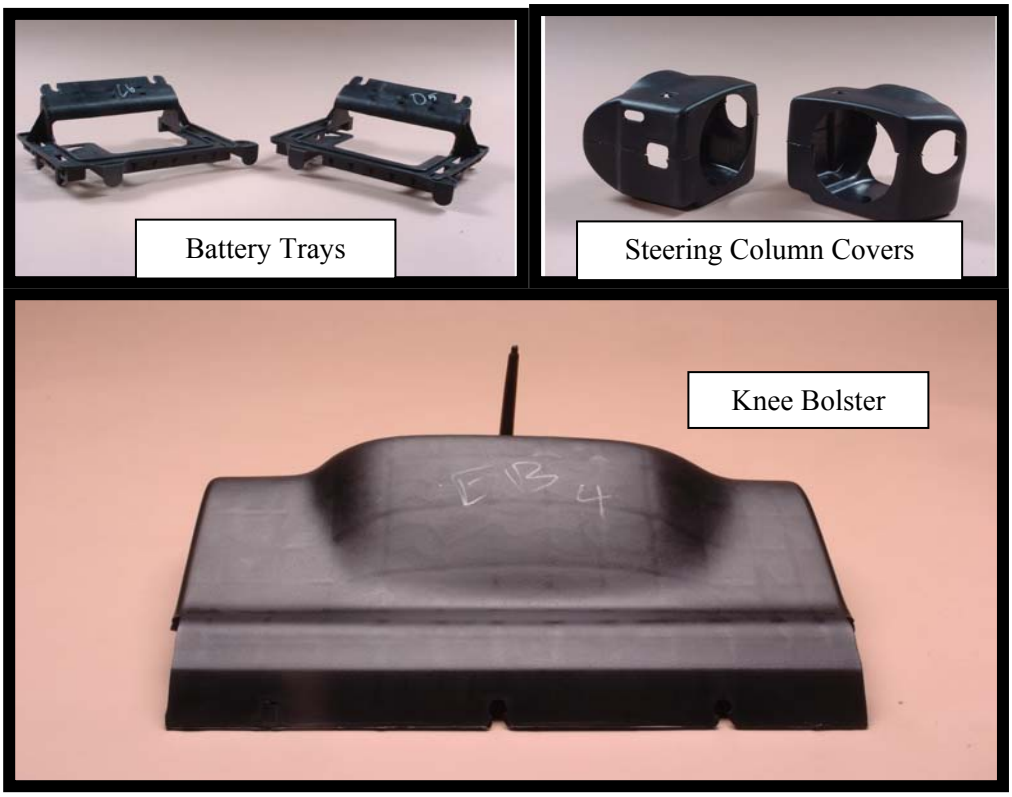

Figure 2. Auto parts molded from PP/PE recovered from shredder residue.

Recovered Rubber/Plastics Material

A mixed-rubber fraction with about 20% by weight mixed plastics was recovered. A sample of the recovered material was sent for testing by the "TireCycle" process used for recycling rubber. Preliminary tests done on the recovered material indicated that it may be suitable for making construction products, such as roofing shingles. The presence of the plastics in the mixed-rubber material appeared to improve its overall properties, especially its stiffness.

[1] One of the formal consortia of the United States Council for Automotive Research (USCAR) set up by the "Big Three" traditionally U.S.-based automakers to conduct joint pre-competitive research and development.

E. Post-Shred Materials-Recovery Technology Development

Principal Investigator: Edward J. Daniels
Argonne National Laboratory (ANL)
9700 S. Cass Ave., Argonne, IL 60439
(630) 252-5279; fax: (630) 252-1342; e-mail: edaniels@anl.gov

Technology Area Development Manager: Joseph A. Carpenter
(202) 586-1022; fax: (202) 586-1600; e-mail: joseph.carpenter@ee.doe.gov

Expert Technical Monitor: Philip S. Sklad
(865) 574-5069; fax: (865) 576-4963; e-mail: skladps@ornl.gov

Participants:
This project is conducted as part of a Cooperative Research and Development Agreement (CRADA) among Argonne, USCAR's Vehicle Recycling Partnership[i], and the Plastics Division (formerly the American Plastics Council) of the American Chemistry Council.

CRADA Partner Principal Investigators:
Michael Fisher, American Chemistry Council, (703) 741-5599, e-mail: Mike_Fisher@americanchemistry.com
Gerald Winslow, VRP, DaimlerChrysler Corp., (248) 512-4802; e-mail: grwx@DCX.com
Claudia Duranceau, VRP, Ford Motor Co., (313) 390-0504; e-mail: cdurance@ford.com
Candace Wheeler, VRP, General Motors Corp., (586) 986-1674; e-mail: candace.s.wheeler@gm.com
This project is conducted as part of the CRADA among Argonne, USCAR's Vehicle Recycling Partnership, and the

Changing World Technologies is cost-sharing on the evaluation of its thermal depolymerization process.
The Polyurethanes Recycle and Recovery Council (PURCC) is also participating and cost-sharing on the evaluation of the Troy Polymers, Inc., polyurethane glycolysis process.

Contractor: Argonne National Laboratory
Contract No.: W-31-109-Eng-38

Objective

- Develop technology for the cost-effective recovery of materials from post-shred residues.

Approach

- Characterize shredder residue from a number of sources to determine composition variability.
- Conduct bench-scale and large-scale process/technology tests to benchmark technology.
- Build and operate a pilot-plant for the separation of shredder residue to produce recovered materials for market evaluation and to provide "control" samples of materials for testing of alternative technologies, as appropriate.
- Conduct cost and performance analyses of alternative technologies to establish the business case for the technologies and to identify technology gaps.

Accomplishments During this Reporting Period (FY 2006)

Mechanical Separation of Shredder Residue

- Ran one 10-ton production campaign (fractions supplied to commercial equipment vendors for performance verification).
- Initiated engineering design for full-scale bulk-separation system--three process options in collaboration with a major shredder operator.
- Obtained budgetary quotes from vendors for major equipment.
- Confirmed performance of commercial equipment (including shredder and granulator) with field trials by vendors/Argonne of the as-is shredder residue and of the fractions generated in the Argonne pilot-plant.
- Designed, built and tested physical rubber separation system.
- Conducted preliminary investigation of costs and performance of commercial color sorters, electrostatic separators, and infrared (IR) sorters for removal of wood and rubber (also evaluated relative to plastics separation).

Froth-Flotation Process for Recovering Plastics

- Ran first campaign of the middling plastics fraction.
- Recovered a 60% unfilled acrylonitrile-butadiene-styrene/polystyrene (ABS/PS) concentrate and a 50% filled ABS concentrate from the middling plastics.
- Upgraded the filled ABS concentrate from 50% to 70% and defined process conditions to further upgrade this fraction to 90%.
- Defined process conditions for separating and recovering unfilled ABS and PS from the unfilled ABS/PS concentrate, to greater than 90% and 85%, respectively.
- Defined process conditions for separating and recovering an 85% polycarbonate (PC)-ABS/PC alloy from the middling plastics fraction.

Other Accomplishments

- Completed testing of Troy Polymer, Inc.'s (TPI's), glycolysis process for conversion of polyurethane (PU) foam to polyol initiators. Over 1,200 lbs. of foam were used, and over 100 gallons of polyol initiators were produced.
- Conducted pilot-scale testing of Changing World Technologies' (CWT's) thermal-depolymerization process for converting shredder residue to fuels. Pre-processed shredder residue from another shredder has been evaluated and shipped to CWT for further testing.
- Completed a large-scale plastics-separation test at MBA Polymers Inc. using a plastic concentrate produced by Salyp's mechanical separation system.
- Completed testing of the VW-SiCon plastics-separation process.

Prior Accomplishments

Argonne Pilot-Plant

- Construction of the pilot-plant at Argonne was initiated in FY 2003 and was completed in FY 2004. The pilot-plant consists of two major parts: a mechanical separation facility and a wet separation/froth-flotation facility.

Mechanical Separation Facility

FY 2005

- Ran four 15-ton production campaigns.
- Conducted complete materials loss analysis on all runs.

- Modified the bulk-separation operation resulting in an increase in polymer yield in concentrate from 40% (runs 1-2) to over 90% (runs 3-4).

FY 2004

- Completed construction, shakedown and start-up of the bulk-separation facility.
- Ran six (6) 5-ton trial campaigns, 4th quarter.

FY 2003 3rd quarter

- Initiated construction of bulk-separation facility.

Froth-Flotation Process for Recovering Plastics

FY 2005

- Conducted trials on gravity tables, mineral jigs, and a kinetic-density separator in the U.S. and Europe primarily for removal of wood and rubber.
- Conducted bench-scale research on settling velocities and density distributions of actual shredder-residue polymers including the wood and rubber.
- Ran a production campaign of the base process with shredder-residue polymer concentrate to yield three polymer fractions; the polyolefin fraction, middling plastic fraction, and the heavies plastic fraction.
- Developed a two-stage, wet-separation process for removal of wood and rubber from the recovered polyolefin fraction.
- Upgraded the polyolefin fraction, recovered 5000 pounds of polyethylene/polypropylene (PE/PP) product essentially free of wood and rubber.

FY 2004

- Completed construction and shakedown with electronics plastics, 2nd quarter.
- Redesigned and modified materials-handling equipment.
- Ran a shakedown campaign with shredder-residue polymer concentrate.

FY 2003, 3rd quarter

- Initiated construction of froth-flotation pilot-plant.

Other Accomplishments

- Conducted bench-scale tests and in a five-gallon reactor of Troy Polymer, Inc.'s (TPI's) glycolysis process for conversion of polyurethane (PU) foam to polyol initiators.
- Conducted bench- and pilot-scale testing of Changing World Technologies' (CWT's) thermal-depolymerization process for converting shredder residue to fuels.
- Completed large-scale tests of Salyp's "thermoplastics-sorting" technology by using residue from two European locations and one U.S. location as feed materials.
- Developed an Excel-based process cost model that incorporates two primary modules for the recovery of automotive plastics: the first module includes the unit operations required for recovering a plastics concentrate from shredder residues, and the second module includes the unit operations required to recover selected plastics from the mixed plastics concentrates.

Future Direction

- Efforts in FY 2007 will be as follows:
- Bulk Separation of Shredder Residue
- Complete engineering designs (3 process options) of bulk-separation system to include equipment specifications, equipment cost, operating requirements, and utility requirements (design basis 20 ton/hour, 1-shift, 2-shift, 3-shift).

- Conduct cost analysis including sensitivity of the cost of polymer concentrate as a function of: 1) yield per ton of shredder residue, 2) value of the by-products (ferrous, non-ferrous, and foam), 3) cost of utilities, 4) cost-of-capital, etc.
- Conduct performance trade-off and cost analyses of color sorter for wood and rubber removal vis-à-vis Argonne physical rubber separation and wet-wood separation; specify preferred process (dry or wet) for separation of wood and rubber from the polymer concentrate.

Froth-Flotation Separation of the Plastics

- Upgrade the filled ABS concentrate from 70% to greater than 90%.
- Upgrade the unfilled ABS and PS from the unfilled ABS/PS concentrate to greater than 90% and 85% respectively.
- Recover an 85% PC-ABS/PC alloy concentrate.
- Define process conditions for upgrading the PC-ABS/PC alloy concentrate to 90-95%.
- Initiate engineering designs of the froth-flotation process to include equipment specifications, equipment cost, operating requirements, and utility requirements (design basis 8 ton/hour of polymer concentrate, 1-shift, 2-shift, and 3-shift).
- Initiate development of a predictive simulation model for determining appropriate separation operating and solution conditions that can affect gravity and froth-flotation separation of selected polymer materials for separation and recovery of polymers from a shredder-residue concentrate.
- Development of bench-scale experimental design to provide requisite empirical data for the predictive simulation model.

CWT's Thermochemical Process for Producing Hydrocarbon Liquids

- Complete the 2000-lb sample run. Evaluation of the CWT technology will be completed and recommendations for path forward will be made.

Evaluation of Emerging Technologies for the Rapid Identification and Sorting of Plastics

- Evaluation of the applicability of color sorters and IR sortation technologies for further refinement of selected process streams from the Argonne physical separation and froth-flotation processes will be completed in FY 2007.

In FY 2007, evaluation of the following technologies will also be completed and recommendations for path-forward will be made.

- TPI's hydrolysis/glycolysis process for producing polyol initiators.
- VW-SiCon technology for separation of shredder residue.
- MBA Plastics separation technology.

Summary

The objective of this project is to develop technology for the cost-effective recovery of materials from post-shred residues. Research will provide data essential to establishing a business case for sustainable recycling of automotive materials from post-shred residue. Technologies specific to the recovery of materials from post-shred material streams are being evaluated and demonstrated to determine their commercial viability. The performance (e.g., yield, purity, efficiency, and cost) of these emerging technologies will be determined to enable the development of an integrated process for recovering materials from shredder residue.

Research has been completed on the Salyp process and on Argonne's physical separation process. Testing of the VW-Sicon and of the MBA Polymers processes were completed in FY 2006 and final reports will be prepared in FY 2007. Research is ongoing on the Argonne froth-flotation process, the Changing World Technologies (CWT) process, and the Troy Polymers process.

Characterization of Shredder Residue

Over 90 tons of shredder residues from five shredders were processed in Argonne's mechanical separation plant. Table 1 shows the composition of the different fractions that were produced. We observed:

- Large variations in non-plastic materials (e.g., fines, metals, rubber and wood) and
- Less-significant variation in the composition of the plastics fraction.

The mass fractions of the polymer concentrate separated from different shredder residues showed little variation, and the weight percent (wt%) of the polymer concentrate recovered from eight runs totaling 80,000 lbs of shredder residue from a given source conducted over a six-month period was reasonably consistent (41%, 26%, 36%, 39%, 45%, 37%, 43% and 45%,; average 40%). The composition of the different polymer concentrates was similar (Figure 1).

Argonne Pilot-Plant

Argonne's pilot-plant consists of two major facilities: a mechanical separation facility and a density/froth-flotation facility. The pilot -plant is used to:

1. Recover materials from shredder residue,
2. Conduct process improvement studies
3. Generate design and scale-up data
4. Produce samples of recovered materials for market evaluation,
5. Define the effectiveness of alternative separation technologies and systems, and
6. Serve as a user/demonstration facility.

Mechanical Separation Pilot-Plant

The mechanical separation facility processes raw shredder residue to yield a polymer concentrate, ferrous and non-ferrous concentrates and other fractions. Initially, the average yield of polymer concentrate recovered was only 17% of the weight of the shredder residue. The recovery of the

Table 1. Streams produced by mechanical separation of an average shredder residue.

	Shredder Residue	Oversized Heavies	Oversized Foam rich	Fines+	Ferrous Rich	Non-Ferrous Rich	Lights	Polymer Concentrate
Weight (lbs)	40,000	2,148	756	17,640	656	1,468	1,968	10,044
PP	1,075	0	0	0	17	33	129	897
PP (filled)	403	0	0	0	0	0	9	393
ABS	763	0	0	0	5	9	13	737
PE	941	0	0	0	9	18	85	830
HIPS	261	0	0	0	4	8	15	234
Nylon	379	0	0	0	4	9	19	347
PVC	512	0	0	0	0	0	0	511
PPO	139	0	0	0	0	0	4	135
PC-ABS	151	0	0	0	0	0	1	150
PC	212	0	0	0	0	0	12	200
Other Plastics	597	0	0	0	1	0	17	579
Rubber	4,505	20	0	0	6	172	61	4,246
PU	273	3	0	0	1	23	9	237
Wood	239	0	0	0	0	0	0	239
Metals	2,911	1,117	0	0	590	954	0	249
Foam, Fiber and others	21,320	1,008	756	17,640 +	19	241	1,597	59
Moisture	5,320	0	0	0	0	0	0	0
Total	40,000	2,148	756	17,640	656	1,468	1,968	10,044

+ Fines are material smaller than 0.25 inch in size and also contain some polymers and metals.
HIPS = high-impact polystyrene. PVC = polyvinyl chloride. PPO = polyphenylene oxide.

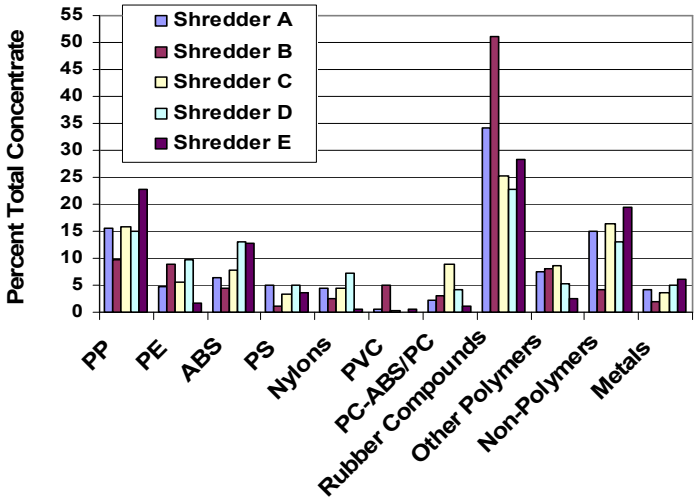

Figure 1. Composition of polymer concentrates from different shredder residues.

polymers in the polymer concentrate was also low (40–70%) for the different source materials. A loss analysis was undertaken including quantification of polymers in each of the fractions that are generated in the bulk processing of shredder residue.

On the basis of this analysis, process modifications were made, and some of the fractions were reprocessed. As a result, the yield of polymer concentrate more than doubled. The analyses also indicated that the recovery of polymers larger than 6 mm in size targeted for recovery in the polymer concentrate was over 90%.

The polymer concentrate included high and varying amounts of wood and rubber. Wood was about 1–4 wt%. In Figure 1, the wood is included in the "non-polymers."

Separation of Wood and Rubber

Trials were conducted by using commercially-available air aspirators, classifiers, air-gravity tables, and mineral jigs to remove wood and/or rubber from the polymer concentrate. This equipment did not yield satisfactory results. Conventional sink/float techniques did not work either. Trials using modified wet-separation approaches ultimately yielded a set of conditions to remove almost 100% of the wood and over 90% of the rubber with a nominal loss (~ 5%) of the plastics. This approach was integrated with the froth-flotation facility.

A dry process has been tested at Argonne, at a rate of up to 100 lb/hr of polymer concentrate, for separating the rubber in the polymer concentrate from recovered plastics concentrates. The process has been able to separate over 75% of the rubber and produce a rubber fraction containing less than 10% of non-rubber material. Further testing and scale-up of the process is on-going.

Froth-Flotation Pilot-Plant

This facility includes six continuous stages for the separation of targeted plastics from the polymer concentrate. A shakedown of the facility was conducted using 4,000 lb of post-consumer electronics and appliance mixed plastics and by using a mixture of colored plastics. These trials confirmed the effectiveness of the basic system.

Over 20,000 lbs of polymer concentrate from shredder residue have been processed in this facility. The recovered fractions include PP/PE, filled ABS and an unfilled ABS/PS concentrate. These are described below.

Recovered PP/PE Fraction: More than 5,000 lbs. of an unfilled PP/PE fraction that is over 95% PP/PE have been consistently produced. It contains less than 0.2% wood and less than 4% rubber. The recovered PP/PE has properties similar to those of some commercially-available PP materials. The recovered unfilled PP/PE product constituted about 5%–6% of the starting shredder-residue weight.

Table 2 summarizes the recoverable unfilled PP/PE and other plastics from 10,000 pounds of typical shredder residue.

Filled ABS Fraction: Filled ABS that has a specific gravity between 1.07 and 1.1 was isolated by the basic froth-flotation process as an ABS concentrate, Table 2. It contains 50% ABS, 20% rubber, 10% rigid urethane rubber, 8% PPO, 3% filled PP and 9% of other materials. Processing of this fraction to remove the wood and rubber increased the ABS concentration to 70% and reduced the rubber and urethane concentrations to 3% and 2%, respectively. When this material was blended with virgin ABS at 10% and 25% recovered material, the properties of the blends were slightly different from the properties of the virgin ABS. Laboratory tests have established process conditions to increase the ABS concentration to over 90%.

Unfilled ABS and PS: A fraction containing unfilled or slightly filled ABS, PS and PPO (43% ABS, 22% PS, 7% PPO, 12% rubber, 7% wood, 5% filled PP and 4% other materials) was produced by the basic process. This fraction is being used to recover the unfilled ABS and the PS/PPO. Laboratory tests defined process conditions to separate this fraction and produce fractions with over 90% ABS and over 85% PS/PPO.

PC-ABS/PC Alloy: Work is ongoing to isolate an ABS/PC-PC fraction. Laboratory tests produced a PC-ABS/PC fraction having a combined concentration of over 85%.

PVC: Recovery of these fractions leaves behind a fraction made of high specific-gravity materials. Rubber constitutes over 50% of the total and metals about 5%. After the rubber and the metals were separated, a PVC fraction having over 50% PVC and rich in glass-filled nylons can be produced.

Rubber: Recovered rubber concentrate was also evaluated by rubber recyclers. It was determined that the presence of thermoplastics in the rubber improves certain properties of the recycled rubber when used to make construction products (such as roofing shingles). The Argonne dry rubber separation process has been able to increase the rubber content of this fraction to over 90%.

Table 2. Composition of an average polymer concentrate and recovered polymer fractions.

	Polymer Concentrate	PP/PE Product	ABS Product	ABS/PC Product	Rubber Product	HIPS/ABS Concentrate	Mixed Plastics	Mixed Stream*
Weight (lbs)	10,044	1,736	141	108	689	856	1,203	5,311
PP	897	827	0	0	0	0	63	7
PP (filled)	393	0	0	0	11	43	194	146
ABS	737	0	105	2	0	365	176	88
PE	830	787	0	0	10	12	21	0
HIPS	234	0	2	0	0	186	25	21
Nylon	347	0	5	0	0	5	42	296
PVC	511	0	0	0	3	0	123	385
PPO	135	0	13	1	0	62	21	37
PC-ABS	150	0	0	6	0	0	0	143
PC	200	0	0	85	1	0	19	94
Other Plastics	579	0	9	2	2	12	8	547
Rubber	4,246	90	2	9	628	104	263	3,149
PU	237	21	4	2	18	0	96	96
Wood	239	0	1	0	17	66	146	8
Metals	249	0	0	0	0	0	0	249
Foam, Fiber and others	59	10	0	0	0	1	5	42
Total	10,044	1,736	141	108	689	856	1,203	5,311

* Rubber and metals are to be recovered from these streams

In summary, we have recovered the unfilled polyolefins as a potentially useable product, and isolated the filled ABS, unfilled ABS/PS, PC-ABS/PC and PVC into more manageable fractions. The objective now is to produce enough of these materials to determine their physical properties and conduct mold tests when warranted.

A 2000 lb/hr, continuous, flotation module has been designed and is being built. Testing of this module will provide valuable and necessary information for designing and building the first commercial plant.

Development of a Process Flowsheet

A process conceptual design for a 20 ton/ hr mechanical separation system has been developed. The key steps in the process include 1) a de-stoner to separate bulky components such as metal chunks and 2) a screen separator, such as a trommel, to separate pieces larger than 3 inches. This contains most of the foam as well as fabrics, tire-rubber pieces and some plastics, 3) a shredder to size reduce the material to 1 inch, 4) a vibrating screen or a trommel to separate "fines" that are smaller than ¼ inch, 5) a magnetic separator to recover ferrous metals, 6) an eddy current separator to recover non-ferrous metals, 7) a granulator to size-reduce the material to about 3/8 inch and 8) an air classifier to remove "lights" from the granulated material. Tests, using shredder residue, were conducted to evaluate the cost, performance and maintenance requirements of various equipment that was proposed for the conceptual design. The cost of a plant having a design capacity of 20 tons/hr of shredder residue is estimated, based on quotes from manufacturers, to be under a million dollars.

Processing of Polymer Concentrate at MBA

Salyp built a mechanical separation system that started with Argonne's original mechanical separation system. Salyp added an optical sorter to remove wood and a plastics-washing system that also separated heavy polymers from the polymer concentrate. Salyp's starting shredder residue also contained substantially less rubber and wood than the U.S. residue. It was decided to test the Salyp plastics concentrate using the MBA process. MBA processed the material on its pilot lines in Richmond, CA. Five materials grades were recovered: 1) Polyolefin "A", 2) Polyolefin "B", 3) filled PP, 4) ABS and 5) HIPS. The total yield of these products was estimated to be about 48.5% of the plastics-rich fraction. This yield is approximately 88% of the amounts of these plastics predicted from characterization of the feed material. The products were characterized and extruded on a small laboratory extruder, molded and tested. The purities and properties of the recovered plastics were reported to be "encouraging" and it is expected that most of the products could be used in some type of durable-good applications without modification. MBA also compounded modified versions of the recovered ABS and HIPS to enhance their properties. Their properties are being evaluated.

Changing World Technologies (CWT)

CWT has developed a thermal-conversion process that converts organic material into high-hydrocarbon oil. CWT built a pilot-scale apparatus to process a mixed shredder-residue waste stream. A 1/16-in. screen was used to separate the fines (~36% by weight). About 700 lbs. of the remaining material were processed along with 80 lbs. of tires and 1,700 lbs. of used motor oil. Thermal- cracking tests of the produced hydrocarbon fuel were performed. The products were hydrocarbon oil (84%), a fuel-gas (10%), and a solid carbon product (6%). Distillation of the oil generated gasoline (12%), diesel (32%), heavy hydrocarbon oils (15%), and (3%) as gas.

The products were analyzed to determine the fate of the inert solids and contaminants. Polychlorinated biphenyls (PCBs) in the input shredder residue was 21.8 ppm. PCBs in the products including the hydrolysis oils, cracked oil, distillates, hydrolysis water, wash water, and char were below the detection limits. This indicated that PCBs degrade during the CWT process.

Several heavy metals were found in the heavy-oil dissolver. Heavy metals decreased gradually in liquid output materials from the thermal-conversion processes. Cracked oil and distillates contained only traces of one or two metals. No measurable concentrations of heavy metals were found in distillate-cut #3. The char contained significant amounts of several metals and their salts.

The heavy oil from the dissolver contained about 3,200 parts per million (ppm) of total chlorine.

Chlorine decreased in the organic output products. No chlorine was found in the light distillates (Cuts #1 and #2), and only 14 ppm were found in the heavier distillate-cut #3 and 11 ppm in the distillate bottoms.

Bromine was found in the heavy oil from the dissolver (~135 ppm). No bromine was found in the output liquid products. Bromine was found in char (87 ppm).

The tire-rubber sample used with the shredder residue contained 17,200 ppm of sulfur. Total sulfur in the motor oil used in the dissolver was 1,600 ppm. Sulfur in the cracked oil was 621 ppm, and 2,696 ppm in the treated hydrolysis oil. This indicates that sulfur compounds degraded in the process.

The cracked oil contained 0.06% of ash and the treated hydrolysis oil contained 0.7% of ash.

A pre-processed organic fraction (about 2,000 pounds) derived from shredder residue has been characterized and shipped to CWT for next trials.

Troy Polymers Glycolysis Process (TPI)

TPI has developed a process for the conversion of mixed polyurethane (PU) foams into polyol initiators. Bench-scale testing demonstrated the technical feasibility of the process. Clean mixed foam and dirty foam from shredder residue were converted to polyol initiators at yields of about 88% and 72%, respectively. Commercially-available activated carbons reduced the concentration of PCBs in the products to < 2 ppm.

The process was scaled up in a 5-gal reactor. Over 1,200 lbs of foam separated from shredder residue have been processed, and over 100 gal of polyol initiator have been produced. By using optimized reaction conditions with diethylene glycol and potassium hydroxide, the yields were increased to over 90%.

Twenty gallons of the polyol initiator, (equivalent weight 163), was propoxylated and two lots of polyols were produced (equivalent weights 354 and 173). The recycled polyols were also tested in making rigid foams. The recycled polyols were more reactive in that they required less or no catalysts, and had better flame resistance than the foams made with virgin polyols.

Initial economic analysis of the process to produce polyol initiator indicated that the glycolysis process is potentially economical.

Recycling of Fines

As more lightweight materials are used in future vehicles, the amount and value of fines (<0.25 in.), which presently constitute about 50% of the weight of shredder residue, will increase. Therefore, recycling the fines is necessary to increase the recyclability of future vehicles.

Argonne conducted preliminary tests to recover metals and polymers from these fines. The results are summarized below.

1. The polymer concentrate recovered from the material in the 2-6 mm size range was 21 wt% of the starting shredder residue, or ~50 wt% of the weight of the fines fraction.
2. The composition of the recovered polymer concentrate is shown in Table 3.
3. 20 wt% of the plastics had specific gravity < 1.

Table 3. Composition of the 2-6 mm fines.

Fraction	Weight % of Polymer Concentrate
Rubber	52.1
Plastics	18.6
Non-Ferrous metals	8.3
Wood	6.7
Fibers	6.1
Foams	2.6
Ferrous metals	1.8
Glass	0.9
Others	2.9
Total	100.0

Evaluation of the plastics and the metals in this material will be conducted to decide if they should be recovered.

Trip Allen, a consultant to the Plastics Division of the American Chemistry Council, also conducted tests on 300 pound samples of fines (smaller than about 1 inch). In these tests, shredder residue was screened using a 7/8-in. (2.2-cm) screen. The material that passed the 2.2-cm screen was processed to yield organic- and inorganic-rich products. A combination of hydrocycloning, screening, rising current, wet tabling, magnet, and grinding technologies was utilized to give ferrous and non-ferrous metal, organic, and inorganic/sand separations at four different size distributions. Economic modeling of the process showed that recovery of the metal and sand may be viable.

Publications

1. *Scale Up Study on Converting and Recycling Shredder Residue Into a Fuel Oil*, Winslow, G.R. Appel, B.S., Adams, T.N., Simon, N.L., Duranceau, C.M., Wheeler, C.S., paper # SAE-2006-01-1580.

2. *Recycling of Polyurethane Foams Recovered From Shredder Residue Via Glycolysis Process Into Polyurethanes*, Sendijarevic, V., Sendijarevic, I., Mayne, K., Winslow, G.R., Duranceau, C.M., Simon, N.L. Wheeler, C.S., paper # SAE-2006-01-1579.

3. *Chemical Recycling of Mixed Polyurethane Foam Recovered from Shredder Residue into Polyurethane Polyols,* Sendijarevic, V.; Sendijarevic, I.; Winslow, G.R.; Duranceau, C.M.; Simon, N.I.; and Wheeler, C.S., SAE paper # 2005-01-0850.

4. *Recycling Shredder Residue Containing Plastics and Foam Using a Thermal Conversion Process,* Winslow, G.R.; Appel, B.S.; Adams, T.; Simon, N.I.; Duranceau, C.M.; Wheeler, C.S.; and Sendijarevic, V., SAE Paper #2005-01- 0848.

5. *Advanced Separation of Plastics from Shredder Residue,* Winslow, G.R., Simon, N.l., Duranceau, C.M., Williams, R., Wheeler, C.S., Fisher, M., Kistenmacher, A., and VanHerpe, I., SAE Paper No. 2004-01-0469.

6. *Recycling Automotive Shredder Residue and Plastics Using the CWT Thermal Process,* Winslow, G.R., and Adams, T., Proc. of the 10th Annual Global Plastics Environmental Conference (GPEC), Detroit, MI, February 18, 2004.

7. *Screening Study to Evaluate Shredder Residue Materials*, Winslow, G.R.; Wheeler, C.S.; Williams, R.L.; Duranceau, C.M.; Simon, N.L.; and Schomer, D.R., SAE paper # 2004-01-0468.

8. *Processes for Recycling the Non-Metallic Portion of Obsolete Automobiles*, Jody, B.J., Daniels, E.J., and Pomykala, J.A., Jr., U.S. Environment-2003 On-Line Conference, July 14-25, 2003.

9. *Cost Effective Recovery of Thermoplastics From Mixed Scrap*, Jody, B.J., Pomykala, J.A., Jr. and Daniels, E.J., Materials Technology, Volume 18 Number 1, March 2003, pp 18-24.

10. *Separation and Recovery of Thermoplastics From Mixed-Scrap Plastics*, Pomykala, J.A. Jr., Jody, B.J., Daniels, E.J., and Greminger, J., Proc. of the 9th Annual Global Plastics Environmental Conference (GPEC), Detroit, MI, February 26-27, 2003, pp 7-16.

[i] One of the formal consortia of the United States Council for Automotive Research (USCAR) set up by the "Big Three" traditionally U.S.-based automakers to conduct joint pre-competitive research and development.

8. MATERIALS CROSSCUTTING R&D

A. Technical Cost Modeling

Principal Investigator: Sujit Das
National Transportation Research Center
2360 Cherahala Boulevard
Knoxville, TN 37932-6472
(865) 946-1222; fax: (865) 946-1314; e-mail: dass@ornl.gov

Technology Area Development Manager: Joseph A. Carpenter
(202) 586-1022; fax: (202) 586-1600; e-mail: joseph.carpenter@ee.doe.gov

Expert Technical Monitor: Philip S. Sklad
(865) 574-5069; fax: (865) 576-4963; e-mail: skladps@ornl.gov

---

Contractor: Oak Ridge National Laboratory
Contract No.: DE-AC05-00OR22725

Objectives

- Address the economic viability of new and existing lightweight materials technologies.
- Develop technical cost models to estimate the cost of lightweight materials technologies.

Approach

- Address the economic viability of lightweight materials technologies supported by the ALM.
- Use cost modeling to estimate specific technology improvements and major cost drivers that are detrimental to the economic viability of these new technologies.
- Derive cost estimates based on a fair representation of the technical and economic parameters of each process step.
- Provide technical cost models and/or evaluations of the "realism" of cost projections of lightweight materials projects under consideration for ALM funding.
- Examine technical cost models of lightweight materials technologies that include (but are not limited to) aluminum sheet; carbon-fiber precursor and precursor-processing methods; fiber-reinforced polymer composites; and methods of producing primary aluminum, magnesium, and titanium and magnesium alloys with adequate high-temperature properties for powertrain applications.

Accomplishments

- The cost-benefit evaluation of the Phase II ALM projects funded during the fiscal year FY 2000-2004 period was completed by focusing on the remaining lightweight materials areas besides polymer composites.

Future Direction

- Provide specific assessments in support of the cost modeling and the life-cycle analysis tasks for the multinational magnesium front-end research and development project (see 2.K).

- Continue individual project-level cost modeling to identify specific technology improvements and major cost drivers that are detrimental to the economic viability of these technologies.

Benefit Evaluation of Non-Polymer Composites ALM Program Area

The focus during this fiscal year for this task has been to complete the benefit evaluation of the Phase II ALM projects (i.e., fiscal year 2000 -2004) started during the last fiscal year by evaluating the remaining ALM lightweight- materials areas. Only three remaining lightweight- materials areas have been considered during this fiscal year, i.e., aluminum, magnesium, and high-strength steel, since in other remaining lightweight materials areas, either the effort has been too limited or projects are still in their infancy. As before, the benefit evaluation of a specific lightweight-material area is based on a detailed evaluation of a few illustrative projects from that area. The following *four* illustrative projects (along with the specific lightweight-materials area represented and major partners listed within parenthesis for each case) were selected from the list of 32 non-polymer composites projects supported with a total funding level of around $60 million.

- Active flexible binder control system for robust stamping (aluminum – Ford)—see 2.B,
- Lightweighting front structures (advanced high-strength steel – Auto Steel Partnership)—see 2.W,
- Magnesium powertrain cast components (magnesium – General Motors)—see 2.H, and
- Structural cast magnesium development (magnesium – General Motors)—see 2.G.

These four projects complement five projects considered earlier in the polymer-composites area and mainly focus on the material application in a specific demanding area of automotive applications. The R&D project teams reflect multiple partners (including OEM suppliers and national laboratories) involved in the R&D effort, although these projects were led by a major OEM in most cases above. In choosing the four projects, we also took into consideration the level of funding (e.g., two of the largest funded projects in the magnesium area) and project status (e.g., projects completed and those on-going).

The magnesium projects selected not only are the two largest projects funded in this material area, but both are nearing completion and have had the greatest industry participation. Because aluminum is a relatively mature automotive material, the focus of the selected aluminum project has been on the stamping issue and the application of results to aluminum and other competing lightweighting materials. Despite the introduction of more advanced high-strength steels in light-duty vehicles, challenging areas such as joining, failure, and structural part manufacturing continue. Several ALM projects have been initiated to address these issues in coordination with the Auto/Steel Partnership. Only one project – lightweighting front structures – selected in this area is a technology-validation project and is the beneficiary of other projects supported in this area.

An evaluation framework developed earlier with the goal of evaluating both short-run outputs and long-run outcomes of the R&D projects was selected. The framework consists of four methods using both qualitative and quantitative measures and they are: qualitative assessment, National Research Council indicators, quantitative benefits, and benefit-cost analysis. The first three types of benefits information were collected from the project participants through surveys, which assessed their views about the benefits of projects, including the number of publications produced and graduate students supported by the end of a project and long-term benefits (knowledge level gained through the publications, human capital investment in graduate students' dissertations and theses produced, and increased international competitiveness of the Big 3 automakers). The benefit-cost analysis is used to monetize values for the benefits and costs of each project. The benefits are estimated based on the projected market penetration of a specific lightweight material in light-duty vehicles using a Delphi technique.

Table 1. Estimated Benefit-Cost (B-C) Ratios of Nine ALM Projects.

Table E.S.6: Benefit-cost Ratios				
Project	**Project Cost ($ millions)**	**B-C Ratio Base Case***	**B-C Ratio Moderate Case***	**B-C Ratio* High Case**
Composites				
DOE (carbon-fiber composites)	66.4	41 (35)	78 (60)	147 (104)
Composite-intensive body structure development for focal project 3	5.1	126 (108)	236 (183)	447 (318)
Durability of carbon-fiber composites	7.2	61 (52)	120 (93)	235 (168)
Low-cost carbon fiber from renewable resources	3.1	124 (106)	245 (190)	479 (341)
Low-cost carbon-fiber development program	3.6	188 (161)	341 (265)	631 (449)
Modeling of composite materials for energy absorption	4.4	73 (62)	150 (117)	301 (215)
Non-Composite Lightweighting Materials Projects				
DOE (aluminum)	32.9	425 (324)	669 (508)	1034 (794)
Active flexible binder control system for robust stamping	1.5	3217 (2360)	5207 (3950)	8540 (6563)
DOE (magnesium)	14.6	106 (90)	259 (199)	606 (417)
Magnesium powertrain cast components	4.3	156 (131)	424 (327)	1023 (696)
Structural cast magnesium development	8.2	34 (29)	86 (67)	198 (134)
DOE (High-strength steel)	10.5	472 (407)	818 (644)	1476 (1056)
Lightweighting Front Structures	3.1	804 (694)	1443 (1136)	2672 (1908)
*Numbers inside parenthesis indicate benefit-cost ratios without taking into account environmental and security benefits.				

These four methods complement the benefits matrix developed for DOE's reports to Congress mandated under the Government Performance and Results Act of 1993 (GPRA). Our framework, besides GPRA requirements, also includes realized knowledge benefits and costs, yet to be reported to Congress, through the qualitative assessment (knowledge gains) and through the coverage of publications and presentations, project deliverables, patents and graduate student support.

Overall, the results of the qualitative assessment are positive for the four projects considered. Nearly all respondents in three of the four non-composites projects believed his or her respective project had met its technical objectives with the exception of one case because the project was still on-going or the investigators were involved in only one task and could not speak for the entire project. Almost all investigators believed that their project yielded knowledge. One-third or fewer investigators believed that their respective projects would have occurred in the absence of DOE participation and/or funding, attesting to the crucial role of DOE. Several of these investigators noted that they would have had lower amounts of funding in the absence of DOE support. Respondents noted that DOE's participation fosters collaboration, attracts major participants, and is necessary because costs are too great for any single firm to bear. In two of the four projects—*lightweighting front structures* and *structural cast magnesium development*—participants agreed unanimously that collaboration was enhanced; while in the remaining projects, solid majorities of participants—83% and 93%—believed collaboration to have been enhanced. It is surprising to note that only 60% of participants in the *structural cast magnesium development* project believing the project results will be incorporated into product design, given that the 2006 model year Corvette Z06 already uses a magnesium engine cradle that emanated from the project. Cost of the material was identified as a barrier to wide-scale introduction of these lightweight materials, with the exception of the lightweighting front structures project which used advanced high-strength steel. Other prominent barriers were manufacturing/performance issues and the corporate culture of the Big Three automakers (e.g., a resistance to change).

Results of the National Academy of Sciences' indicators show numerous publications (in the range of (4-119) in each R&D effort where the number of publications is primarily dependent on the number of participants per research project. It is noteworthy that projects with heavy involvement from the private sector can publish extensively. Graduate students were involved in each project, including undergraduate students on both magnesium-focused projects. Only one patent has been sought to date, but respondents expect a number of patents and copyrights stemming from this research to be sought in 2006 or 2007. In most cases, the reaction of the Big Three automakers to the software packages or other deliverables finalized from the project was positive, particularly in the case of the magnesium powertrain cast components projects in their decision-making process for incorporating magnesium into automotive production. From the structural cast magnesium development R&D effort, there is potential for commercialization for the magnesium alloy database; radioscopic standard for magnesium castings; and failure model.

The results of the economic analyses, primarily the benefit-cost ratios for all nine projects (including five projects considered earlier under the polymer composites lightweight materials area), are shown in Table 1.

The benefit-cost analysis takes into account energy, environmental, and security benefits and the row designated as DOE in this table indicates the overall contribution of the U.S. Department Energy R&D programs in a specific lightweight material area. The project costs include both federal funding and private sector matching funds. The base, moderate, and high cases represent low, medium, and high monetary values for energy, environmental, and security savings in Table 1. Note that estimated benefits are based on the projected market penetration of a specific lightweight material in light-duty vehicles using a Delphi technique. In every case, the benefit-cost ratios indicate significant benefits for these projects. The estimated benefit-cost ratios of non-composite projects are significantly higher than for composite projects. The non-composite material areas--particularly the aluminum and high-strength steel areas--are comparatively more mature than the carbon-fiber polymer composite materials area. The selected projects under these two material areas are anticipated to aid in the significant penetration of these materials in light-duty vehicles, having significantly higher benefit-cost ratios than for overall material area. A significantly lower project cost in case of the flexible binder control project results in the most benefit-cost ratio in this case. The estimated benefit-cost ratios of magnesium are similar to carbon-fiber polymer composite projects, both indicating a relatively early stage of the use of these materials in light-duty vehicles. Person-year and cost savings from having access to federal R&D funds were also estimated and found to be quite substantial, in most project cases less than 20 person-years and $12 million, respectively.

Conclusions

There are two perspectives that can be taken from this evaluation. When considering an overwhelming majority of the indicators selected, the responses are outstanding. There remain questions about whether the results will be incorporated or whether a material is a viable option. What this evaluation has highlighted are the ongoing challenges to change in the automobile industry: there may remain a gap between establishing the technical feasibility of a material or process and making a business decisions to move forward with a lightweighting material.

The ALM effort helps to reduce the risks to the OEMs and suppliers by exploring new materials options. The program also facilitates discussion and collaborations among the OEMs and suppliers to help overcome the catch-22s such as when and which party (i.e., OEMs or suppliers) needs to invest in the R&D for lightweighting parts. The program is valuable in helping to identify next steps to developing new lightweighting parts. The ALM effort brings materials expertise found in national laboratories and universities that can get the discussions and R&D moving. It has also been shown that the projects help to build a critical mass of professional expertise needed to move the industry forward in these materials areas. This expertise could then direct future R&D in many new directions, not only in the directions represented by the ALM-funded projects.

Presentations/Publications/Patents

Das, S. Peretz, J. H. Tonn, B. E. (2006). "Automotive Lightweighting Materials Benefit Evaluation," ORNL/TM-2006/545, Oak Ridge National Laboratory, Oak Ridge, TN, November.

B. Intermediate-Rate Crush Response of Crash Energy Management Structures

Principal Investigator: J. Michael Starbuck
Oak Ridge National Laboratory (ORNL)
P.O. Box 2009, Oak Ridge, TN 37831-8048
(865) 576-3633; fax: (865)-574-8257; e-mail: starbuckjm@ornl.gov

Project Manager, Composites: C. David Warren
ORNL
P.O. Box 2008, Oak Ridge, TN 37831-6065
(865) 574-9693; fax: (865) 576-4963; e-mail: warrencd@ornl.gov

Technology Area Development Manager: Joseph A. Carpenter
(202) 586-1022; fax: (202) 586-1600; e-mail: joseph.carpenter@ee.doe.gov

Expert Technical Monitor: Philip S. Sklad
(865) 574-5069; fax: (865) 576-4963; e-mail: skladps@ornl.gov

---

Contractor: Oak Ridge National Laboratory
Contract No.: DE-AC05-00OR22725

Objective

- Develop a unique characterization facility for controlled progressive-crush experiments, at intermediate rates, of automotive materials (polymer composites, high-strength steels, and aluminum) and structures.
- Study the deformation and failure mechanisms of automotive materials subjected to crush forces as a function of impact velocity.
- Obtain specific-energy-absorption and strain data, and correlate with deformation and failure mechanisms to describe the unknown transitional effects from quasi-static to high loading rates for polymer composites.
- Characterize the strain-rate effects for metallic materials and components.
- Provide access to unique test capability to university, industry, and government users for collaborative research.

Approach

- Develop a unique, high-force (500 kN), high-velocity (8 m/s) servo-hydraulic machine to conduct progressive-crush experiments on structural components at intermediate rates.
- Use high-speed imaging to observe and document deformation and damage mechanism during the crush event.
- Conduct strain measurements at discrete locations and explore full-field measurements of strains and curvatures.
- Coordinate polymer composites investigations with the Automotive Composites Consortium (ACC) Energy Management Group (see 4.G).
- Coordinate steel investigations with the Auto/Steel Partnership.

Accomplishments

- Completed tube testing in support of Crash Analysis of Adhesively Bonded Structures (CAABS) project (see 4.H).
- Completed tube testing in support of the Auto/Steel Partnership Strain Rate Characterization project (see 2.U).
- Developed improved data-acquisition software for strain-gage measurements.
- Developed streamlined software for interfacing force-displacement data with high-speed video.
- Completed procurement and installation of a high-rate (18 meter/second) test machine for conducting complementary coupon-level testing.

Future Direction

- Explore techniques for full-field measurements of strains and curvatures.
- Develop User Interaction Plan.
- Support user collaboration as required.

Introduction

Progressive crush is an important mechanism by which the kinetic energy of a traveling automobile is dissipated in a collision to protect the safety of occupants. Unfortunately, the mechanisms governing the progressive-crush response of some emerging automotive materials are not well understood. Additionally, many of these materials are known to exhibit responses that are sensitive to rate of loading.

Understanding the influence of impact velocity on the crush response of materials and structures is critically important for crashworthiness modeling inasmuch as collisions occur at a range of velocities. Additionally, from a structural standpoint, the deformation (or strain) rate is generally not unique from either a spatial or temporal standpoint. Consequently, it is important to quantify the behavior of materials at various strain rates.

Test Machine for Automotive Crashworthiness (TMAC)

Typically, standard test machines are employed for experiments at quasi-static rates, whereas drop towers or impact sleds are the convention for dynamic rates. These two approaches bound a regime within which data for experiments at constant impact velocity are not available by conventional experimental practice. This regime is termed herein the "intermediate-rate" regime and is defined by impact velocities ranging from 1 m/s to 5 m/s. Investigation of rate effects within this regime requires experimental equipment that can supply a large force with constant velocity within these rates.

Using a drop tower or sled at intermediate rates, although technically possible, is problematic due to the prohibitively large mass required to maintain constant velocity during the crush. Consequently, ORNL and the ACC collaborated to define specifications for a unique experimental apparatus that mitigates the shortcomings of existing equipment. MTS Systems Corporation designed and built the servo-hydraulic test machine, referred to as the TMAC. TMAC is uniquely capable of conducting controlled progressive-crush tests at constant velocity in the intermediate velocity range (i.e., less than 5 m/s) because of the large energy available at those rates and to the sophisticated simulation and control software that permits velocity uniformity to within 10%.

The new experimental facility will be used to understand the crush behavior between the static and dynamic (8-m/s) conditions. The installation of the TMAC at its National Transportation Research Center (NTRC) Knoxville, Tennessee location is shown in Figure 1.

Figure 1. Installation of TMAC in the NTRC.

Status

Since the last reporting period, activities have focused on supporting users, developing and promoting user interactions, improving data acquisition, and expanding test capability for higher-rate coupon tests.

Interactions have taken place with Rutgers, Massachusetts Institute of Technology, SAE High Strain Rate Plastics Consortium, General Motors, Ford, Imperial College (London, England), Washington University, University of Utah, and L&L Products. Also, discussions continued with the University of South Carolina and Correlated Solutions towards developing a full-field dynamic strain measurement using digital image correlation techniques.

In addition to promoting user programs, continued support was provided to the development of a crashworthiness chapter for the military's composite design guide, MIL-HDBK-17, and the start of a technical division on the Dynamic Response of Materials within the Society for Experimental Mechanics.

Project Support Activities

Extensive testing was completed on TMAC in support of both the ACC Crash Analysis of Adhesively Bonded Structures (CAABS) project (see 4.H) and the Auto/Steel Partnership (A/S-P) Strain Rate Characterization project (see 2.U). For the CAABS project, 30 additional tubes were tested that quantified the effect that adhesive bonds have on energy absorption. In support of the A/S-P project, 30 tubes were tested for determining strain-rate sensitivities in high-strength low-alloy steels and dual-phase steels. Strain gages were used in these tests to locally measure the strains associated with plastic hinge formation in metal tubes undergoing progressive crushing (see Figure 2). Developing the full-field strain measurement technique using digital image correlation would eliminate the need for strain gages and their exact location for capturing the peak strains at the hinges.

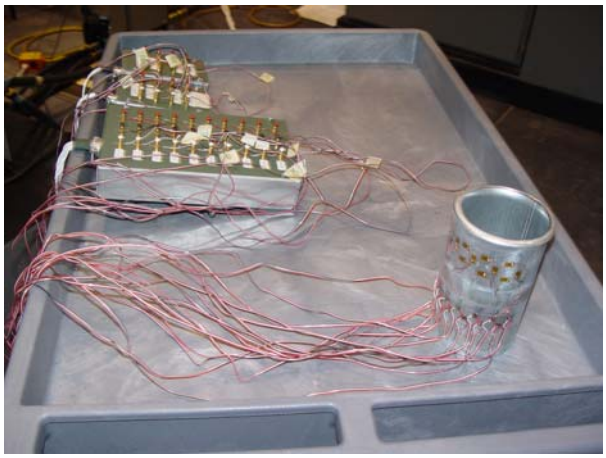

Figure 2. Strain gage pattern used for testing steel tubes.

High-Rate Coupon Test Machine

To complement the TMAC capability, a high-rate coupon test machine was designed, fabricated by MTS, and installed at ORNL. Where TMAC provides the capability for a large force (500 kN static) structural level test, this machine was designed to conduct low force (40 kN static) coupon-sized tests under primarily tensile loads. A typical-size coupon would be a dog-bone strip where

the gage section is 15 mm wide with a thickness of 3 mm. This type of test is ideal for generating rate-sensitive stress-strain curves in development of basic material constitutive laws. The machine has a maximum crosshead speed of 18 meters/second with a 400 mm total stroke capacity. The actually working stroke is reduced to 175 mm when installing a slack adapter to allow for the actuator to get up to constant speed before loading the specimen. These specifications were accomplished by a using a 400 gallon/minute (gpm) servo-valve and 50-gallon accumulators (see pictures 3 and 4). Another feature of the test machine is the use of low mass grips designed to reduce ringing in the system thereby minimizing inertial effects in the load signal. The grips were based on a Colorado School of Mine design and are shown in Figure 5.

Figure 3. High-rate (18 meter/second) coupon test machine.

Conclusions

TMAC provides a unique capability to measure the specific energy absorption on crush tubes and other specimen geometries as a function of (constant) impact velocity within a range from quasi-static to 8 meters/second. To complement this capability, a new machine was installed for conducting coupon-level tests up to 18 meters/second.

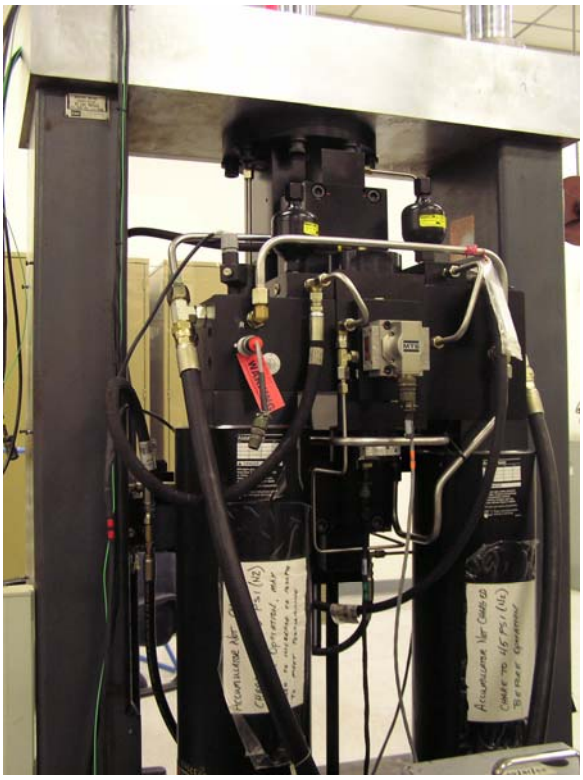

Figure 4. Accumulators and servo-valve for high-rate test machine.

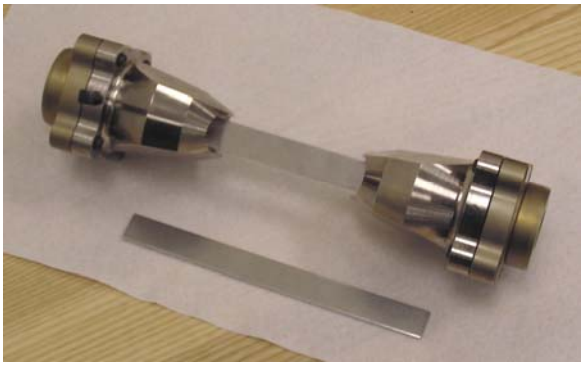

Figure 5. Low-mass grip used in high-rate test machine.

User interest in this equipment remains very high with three potential projects being in the draft stage. TMAC was also instrumental in meeting project objectives for the CAABS and A/S-P projects. In all of these tests, high-speed video was recorded to document the failure mechanisms using a state-of-the-art CMOS camera that was procured for the TMAC installation.

Presentations/Publications/Patents

Dynamic versus Static Energy Absorption in Carbon Fiber Reinforced Tubes, presented at the Society for the Advancement of Material and Process Engineering (SAMPE), 2006 Symposium, Long Beach, California, April 30-May 4, 2006.

APPENDIX A: ACRONYMS AND ABBREVIATIONS

2DTBC	two-dimensional triaxially-braided composite
2D-WAXS	two-dimensional wide-angle x-ray scattering
3D	three-dimensional
A/SP	Auto/Steel Partnership
ABS	acrylonitrile-butadiene-styrene
ACC	Automotive Composites Consortium
ACD	after concept design
ACDC	after concept design analysis check
ADCB	asymmetric double-cantilever beam
AF	anisotropy factor
AFM	atomic-force microscope(y)
AFO	after final optimization
AFS	American Foundry Society
AHSS	advanced high-strength steel
AISI	American Iron & Steel Institute
AKDQ	aluminum-killed draw-quality
Al	aluminum
ALM	Automotive Lightweighting Materials
AMD	Automotive Metals Division
ANL	Argonne National Laboratory
ANSI	American National Standards Institute
AO	after optimization
AP	acidification potential
APC	American Plastics Council
APGE	Arizona Proving Grounds Exposure
ARA	(International) Automotive Recycling Association
ARC	(International) Automobile Recycling Congress
ASTM	American Society for Testing and Materials
ATR	attenuated total reflection
AWS	American Welding Society
BCC	body center cubic
BDE	brominated diphenyl ethers
BET	Brunauer-Emmett-Teller
BFO	before final optimization
BH	bake hardenable
BIW	body(ies)-in-white
BL	black liquor
BLRT	bond-line read-through
BO	before optimization
BOF	body-on-frame
BSEF	Bromine Science and Environmental Forum
BT	bond-line thickness
BW	bond width
CAABS	crash analysis of adhesively bonded structures
CAD	computer-aided design

CAE	computer-aided engineering
CANMET	an R&D entity of the Minerals and Metals Sector of Natural Resources Canada
CB	cylinder block
CCD	charge-coupled device
CCHT	combinatorial, combi, high-throughput
CCT	cosmetic corrosion test
CDA	critical damage area
CF	carbon fiber
CFSI	carbon fiber systems integration
CLTE	coefficient of linear thermal expansion
CMM	coordinate measuring machine
CMOS	complementary metal oxide semi-conductor
COM	Conference of Metallurgists
CP	cold pressed / complex phase
CPU	central processing unit
CRADA	Cooperative Research and Development Agreement
CrN	chromium nitride
CRTM	compression resin-transfer molding
CT	compact tension / computerized tomography
CTE	coefficient of thermal expansion
CWT	Changing World Technologies
CZ	cohesive zone
DC	direct current
DCB	double cantilever beam
DCX	DaimlerChrysler
DCZM	discrete cohesive zone model
DFEP	Die Face Engineering Project
DHαMS	dihydroxy-α-methylstilbene
DIC	digital image correlation
D-LFT	direct long-fiber thermoplastic
DMA	dynamic mechanical analysis
DOE	Department of Energy
DoE	design of experiment
DP	dual phase
DP800	Dual Phase 800
DQ	drawing quality
DQSK	drawing-quality special-killed
DRIFT®	Direct Reinforcement Fabrication Technology
DSC	differential scanning calorimetry / dispersion-strengthened copper
DTA	differential thermal analysis
DTUL	deflection temperature under load
DW	driven wedge
ECD	electron capture detector
EDS	energy-dispersive spectrometer(ry)
EDX	energy-dispersive X-ray analysis
EF	(thermal-drilling) extension factor
EH&S	environmental, health and safety.
ELV	end-of-life vehicle(s)
EMF	electromagnetic forming

EP	eutrophication
EPA	Environmental Protection Agency
ERW	electric resistance welding
FCC	face-centered cubic
FCD	final concept design
FCVT	FreedomCAR and Vehicle Technologies
FE	finite element
FEA	finite-element analysis
FEC	front engine cover
FE/CV	finite-element/control volume
FEM	finite-element method/modeling
FGPC	Future Generation Passenger Compartment
FLD	fiber-length distribution or forming-limit diagram
FMBEM	Fast Multipole Boundary Element Method
FMVSS	Federal Motor Vehicle Safety Standard
FOP	fully-oxidized polyacrylonitrile
FP2	focal project 2
FP-3	focal project-3
FRP	fiber-reinforced plastic
FSSW	friction-stir spot welding
FSW	friction-stir welded
FTC	Federal Trade Commission
FT-IR	Fourier transform infrared
FY	fiscal year
GA	Galvaneeled
GaBi	Ganzheitliche Bilanzerung
GC	gas chromatography
GC/MS	gas chromatography/mass spectroscopy
GC-ECD	gas chromatography and electron-capture detector
GDIS	Great Designs in Steel
GF	glass fiber
GI	galvanized coating
GM	General Motors (Corporation)
GMAW	gas metal arc weld
GMT	glass-mat thermoplastic
GPEC	Global Plastics Environmental Conference
GPRA	Government Performance and Results Act of 1993
GWP	global warning potential
HAZ	heat-affected zone
HBA	hydroxybenzoic acid
HDG	heavy-duty galvanized / hot-dipped galvanized
HDPE	high-density polyethylene
HI-MAC	High-Integrity Magnesium Automotive Casting
HIPS	high-impact polystyrene
HNA	hydroxy-naphthoic acid
HPDC	high-pressure die casting
HSBS	hot-stamp(ed) boron steel
HSLA	high-strength low-alloy

HSS	high-strength steel
HTML	high-temperature materials laboratory
ICME	integrated computational materials engineering
IDDRG	International Deep Drawing Research Group
IF	interstitial free
IFU	University of Stuttgart
IIHS	Insurance Institute for Highway Safety
IISI	International Iron & Steel Institute
IP	instrument panel
IR	infrared
ISRI	Institute of Scrap Recycling Industries
ISV	internal state variable
ITP	International Titanium Powder (Inc.)
JCI	Johnson Controls, Inc
LBNL	Lawrence Berkeley National Laboratory
LC	liquid crystallines
LCM	liquid composite molding
LDH	limited dome height
LDPE	low-density polyethylene
LFT	long-fiber-reinforced injection-molded thermoplastics
LIMS	Liquid Injection Molding Simulation
LPPM	low-pressure permanent-mold
LW	laser-welded
LWB	laser-welded blanks
LWFS	lightweight front-end structure
MAP	microwave-assisted plasma
Mart	martensitic
MFE	magnesium front end
MFEDD	magnesium front end design and development
MFERD	magnesium front end research and development
MFR	melt flow rate
MHD	magnetohydrodynamic
MI	melt index
MIG	metal inert gas
Missu	Mississippi State University
M-K	Marciniak-Kuczynski
MLPD	magnesium low-pressure development
MMB	mixed-mode bending
MMV	multi-material vehicle
MOST	Ministry of Science and Technology (China)
MPCC	magnesium powertrain cast component
MS	martensitic steels / mass spectroscopy
MSS	mean/maximum shear strength
MTT	Materials Technical Team (FreedomCAR)
MW	Mead Westvaco
MWV	MeadWestvaco (Corporation)

N/D or N.D.	Not detected
NA	North America(n)
NANO	new application of nano obstacles
NC	numerical control
NCAP	New Car Assessment Program
NCC	National Composites Center
NCC-ET	North Carolina Central Campus—Emerging Technologies
NDE	non-destructive evaluation
NDI	non-destructive inspection
NEXAFS	near-edge x-ray absorption fine structure
NIST	National Institute for Standards and Technology
NMR	nuclear magnetic resonance
NSF	National Science Foundation
NSJS	normalized static joint strength
NTRC	National Transportation Research Center
NVH	noise, vibration, and harshness
OC	Owens Corning (Corporation)
OEM	original equipment manufacturer
ORNL	Oak Ridge National Laboratory
P/M	powder metallurgy
P4	programmable powdered preform process
PAN	polyacrylonitrile
PBDEs	polybrominated diphenyl ethers
PBT	polybutylene terephthalate
PC	polycarbonate
PCBN	polycrystalline cubic boron nitride
PCBs	polychlorinated biphenyls
PDE	partial differential equation
PE	polyethylene
PEY	partial electron yield
PI	principal investigator
PMC	polymer-matrix composite
PNNL	Pacific Northwest National Laboratory
POCP	photochemical ozone creation potential
PP	polypropylene
PP/PE	polypropylene/polyethylene
PPM	parts per million
PPO	polyphenylene oxide
PPS	post-peak softening
PS	polystyrene
PSC	Project Steering Committee
PTC	Project Technical Committee
PTT	Phan-Thien Tanner
PU	polyurethane
PVC	polyvinyl chloride
R&D	Research and Development
RFQ	request for quotes
RIS	radiographic inspection standards

RPM	revolutions per minute
RSC	rear seal cover / reduced strain closure
RSW	resistance spot-welding
RTM	resin-transfer molding
RUC	representative unit cell
RVE	representative volume element
RWD	rear-wheel drive
SAE	Society of Automotive Engineers
SAMPE	Society for the Advancement of Materials and Process Engineering
SCMD	structural cast magnesium development
SD	standard deviation
SDSM&T	South Dakota School of Mines and Technology
SEA	specific energy absorption
SEM	scanning election microcope(y)
SERR	strain-energy release rate
SFT	short-fiber-reinforced injection-molded thermoplastics
SG	specific gravity
SLB	single-leg bend
SLC	sub-liquidus casting
SMARTS	Spectrometer for MAterials Research at Temperature and Stress
SMC	sheet molding compound
SNL	Sandia National Laboratories
SOCs	substances of concern
SOP	standard operating procedure / structural oil pan
SORPAS	Simulation and Optimization of Resistance, Projection and Spot Welding Processes
SOW	statement of work
SRF	strain reduction factor
SRI	Southern Research Institute
SRIM	structural reaction-injection molding
SSM	semi-solid metal
ST	schapery-like, thermodynamically-based theory
SUV	sport utility vehicle
SWE	spot-weld element
SWSG	structural weld sub-group
TBD	to be determined
TC	transcrystalline region
TDM	Troy Design and Manufacturing
TFF	thread-forming fastener
TGA	thermo-gravimetric analysis
ThD	thermal drilling
TLCP	thermotropic liquid-crystalline polymer
TMAC	Test Machine for Automotive Crashworthiness
TMS	The Minerals, Metals, and Materials Society
TPI	Troy Polymers, Inc.
TPO	thermoplastic olefins
TP-P4	thermoplastic P4
TRIP	transformation-induced plasticity
TS	tensile strength
TTSP	time temperature superposition principle

TWB	tailor-welded blank
TWT	tailor welded tube
TYE	tensile, yield and elongation properties
UAB	University of Alabama-Birmingham
UD	unidirectional
UDRI	University of Dayton Research Institute
UEL	used-defined element
UHMW	ultra-high molecular weight
UHSS	ultra high strength steel
ULC	ultra-large casting
ULSAB-AVC	Ultralight Steel Auto Body-Advanced Vehicle Concepts
UPA	units per annum
UPE	unsaturated polyester
USAMP	United States Automotive Materials Partnership
USCAR	United States Council for Automotive Research
USPTO	United States Patent and Trademark Office
UT	University of Tennessee
UTK	University of Tennessee, Knoxville
UTS	ultimate tensile strength
UV	ultraviolet
VARTM	vacuum-assisted resin-transfer molding
VE	vinylester
VPB	viscous pressure bulge
VRP	Vehicle Recycling Partnership
VUMAT	vectorized user material
VW	Volkswagen
W25Re	25 wt% rhenium
WDS	wavelength-dispersive spectrometer(ry)
Wpm	welds per minute
XFEM	extended finite-element method
XRD	x-ray diffraction
YAG	yttrium-aluminum-garnet
YS	yield strength

A Strong Energy Portfolio for a Strong America

Energy efficiency and clean, renewable energy will mean a stronger economy, a cleaner environment, and greater energy independence for America. Working with a wide array of state, community, industry, and university partners, the U.S. Department of Energy's Office of Energy Efficiency and Renewable Energy invests in a diverse portfolio of energy technologies.

For more information contact:
EERE Information Center
1-877-EERE-INF (1-877-337-3463)
www.eere.energy.gov